Selective Ion Separations Using Shock Electrodialysis

by

Mohammad Ayman Alkhadra

Submitted to the Department of Chemical Engineering
in partial fulfillment of the requirements for the degree of

Doctor of Philosophy

at the

MASSACHUSETTS INSTITUTE OF TECHNOLOGY

September 2022

© Massachusetts Institute of Technology 2022. All rights reserved.

Author .....
Department of Chemical Engineering
September, 2022

Certified by .....
Martin Z. Bazant
Edwin G. Roos (1944) Professor of Chemical Engineering
Digital Learning Officer
Professor of Mathematics
Thesis Supervisor

Accepted by .....
Patrick S. Doyle
Robert T. Haslam (1911) Professor of Chemical Engineering
Singapore Research Professor
Graduate Officer

Selective Ion Separations Using Shock Electrodialysis

by

Mohammad Ayman Alkhadra

Submitted to the Department of Chemical Engineering
on September, 2022, in partial fulfillment of the
requirements for the degree of
Doctor of Philosophy

Abstract

Agricultural development, extensive industrialization, and rapid growth of the global population have inadvertently been accompanied by environmental pollution. At the same time, the chemicals and energy industries face a number of difficult challenges in the selective extraction of high-value ionic species from dilute aqueous solutions. Important examples include the selective removal of trace pollutants, such as toxic heavy metal ions, from industrial effluents; the fractionation of chemically and physically similar elements, such as lanthanides for catalytic processes; the extreme deionization of wastewaters, such as radioactive process water from nuclear power plants; and the recovery of lithium compounds and valuable metals for applications in mining and electronic waste recycling. These emerging trends have motivated the search for new principles and methods for improved ion separations. Electrochemical methods in particular have attractive features such as compact size, modularity, chemical selectivity, broad applicability, and reduced generation of secondary waste.

In this thesis, we investigate the emerging electrokinetic approach known as "shock electrodialysis" (shock ED) and its use in selective ion separations. Although the principles of deionization by shock ED have been established in previous work, the possibility of selective ion separations has only recently been discovered, and this capability is explored in depth in this thesis. The first major thrust is an extensive and comprehensive review of electrochemical methods for water purification, ion separations, and energy conversion. The review begins with an overview of conventional electrochemical methods, which drive chemical or physical transformations via Faradaic reactions at electrodes, and proceeds to a detailed examination of the two primary mechanisms by which contaminants are separated in non-destructive electrochemical processes, namely electrokinetics and electrosorption, with special attention given to emerging methods such as shock ED. The second major thrust is the design of processes and operating conditions to demonstrate the broad applicability of shock ED for selective ion removal from contaminated water. We developed several design concepts to control the selective separation of cations, anions, and small, charged hydrocarbons based on electric charge. The third major thrust is the examination of new types of materials in shock ED, including ceram-

ics, clays, and ion exchange resins, several of which enable operation under extreme conditions (e.g., high temperature, high radiation, chemically harsh or reactive contaminants). This study led to the development of shock ion extraction (shock IX), which is a new, hybrid process that combines shock ED and ion exchange and enables greater ion removal and selectivity, and for longer periods of time, compared to the use of either shock ED or ion exchange alone.

From a fundamental perspective, the novel electrokinetic mechanisms explored in this thesis are shown to have broader implications in deionization, water purification, and metals refining. For the field of chemical engineering, this work demonstrates shock-based methods as an energy-efficient and sustainable route to process intensification, and it paves their way for practical implementation in industry.

Thesis Supervisor: Martin Z. Bazant
Title: Edwin G. Roos (1944) Professor of Chemical Engineering
Digital Learning Officer
Professor of Mathematics

Acknowledgments

My journey through graduate school would not have been possible without the wonderful people who have inspired and encouraged me along the way.

I begin by thanking my advisor (and now co-founder of Lithios Technologies!), Prof. Martin Bazant, to whom no words are sufficient to express my gratitude. From the moment I joined his group, Martin has given me his unwavering support to all my scientific and professional endeavors. My thesis research has been an experience of independent inquiry, constant improvement, and exciting adventure into new and challenging topics. And throughout this rigorous journey, Martin was there to guide and support me. Martin also partly inspired my entrepreneurial spirit and believed in my potential to lead a successful business based on our backgrounds and research. With his help, I received the Activate Fellowship, a two-year entrepreneurial fellowship that supports scientists and engineers in turning technology concepts into useful products. Our vision is to establish new electrochemical processes for *Advanced Lithium Extraction* to scale the supply of lithium for our electric future. I sincerely thank Martin for his invaluable mentorship and friendship throughout my PhD, and I look forward to our journey together building and leading Lithios. I also thank the members of my thesis committee, Profs. T. Alan Hatton and John Lienhard V, for the enriching discussions during my our regular meetings.

During my time in Martin's group and at MIT in general, I had the privilege of developing many lifelong friendships and professional relationships. It would be difficult for me to name all of these amazing individuals in these pages, so I will list the ones whom have had the most significant impact on my experience over the past four years:

1. From Martin's lab: Huanhuan Tian, Kameron Conforti, Tao Gao, Supratim Das, Dimitrios Fraggedakis (he has perhaps the best taste in music of anyone that I met at MIT), Tingtao (Edmond) Zhou, Mohammad Amin Amooie, J. Pedro de Souza, Surya Effendy, Debbie Zhuang, and many others who have recently joined our group.

2. From chemical engineering: Flemming Holtorf, Brandon (nasty B) Johnston, Allen Jiang, Kevin Spiekermann, Lorenzo Milani, Husain Adamji, Aditya Limaye, Matthew VanBeek, Kelsey Reed, Charles Wan, Sam Park (from CS), Hyunhee (Rebecca) Lee, Amber Phillips, Chun Man Chow, Francesco Benedetti, Ali Kakhbod, the late Prof. Jim Swan, Prof. Daniel Blankschtein, and (very) many more.

3. From Practice School: Brian Baynes, Brian Stutts, Doug Harrison, Ram Ratnakar, and the Practice School crew (Lorenzo Milani, Hyunhee Lee, Lauren Clarke, Grace Noel, Keith Cheah, Billy Wang, Elvin Yang, Yuan Tian).

4. From the broader MIT community: Barbara Balkwill, Yolanda Rodriguez, Alejandro Jose Becerra, Prof. Hung Cheng, and others.

5. From outside of MIT (collaborators): Prof. Juan Santiago, Prof. Xiao Su, Prof. Matt Suss, Prof. I Gede Wenten, Prof. Chris Arges, Khoiruddin Ad-Damaki, Amit Shocron, Nayeong Kim, Michele Tedesco, Eric Guyes, Matthew Jordan, and others.

I also thank the Saudi Arabian Cultural Mission, the Chemical Engineering Department at MIT, and (in part) Mitsubishi Heavy Industries for funding my research.

Contents

List of Figures

List of Tables

Chapter 1

Electrochemical Methods for Water Purification, Ion Separations, and Energy Conversion

The work reported in this chapter has been published as "Electrochemical Methods for Water Purification, Ion Separations, and Energy Conversion," by Mohammad A. Alkhadra, Xiao Su, Matthew E. Suss, Huanhuan Tian, Eric N. Guyes, Amit N. Shocron, Kameron M. Conforti, J. Pedro de Souza, Nayeong Kim, Michele Tedesco, Khoiruddin Khoiruddin, I Gede Wenten, Juan G. Santiago, T. Alan Hatton, and Martin Z. Bazant. It has been adapted with permission from the American Chemical Society, 2022.

Abstract

Agricultural development, extensive industrialization, and rapid growth of the global population have inadvertently been accompanied by environmental pollution. Water pollution is exacerbated by the decreasing ability of traditional treatment methods to comply with tightening environmental standards. This review provides a comprehensive description of the principles and applications of electrochemical methods for water purification, ion separations, and energy conversion. Electrochemical methods have attractive features such as compact size, chemical selectivity, broad applicability, and reduced generation of secondary waste. Perhaps the greatest advantage of electrochemical methods, however, is that they remove contaminants directly from the water—while other technologies extract the water from

the contaminants—which enables efficient removal of trace pollutants. The review begins with an overview of conventional electrochemical methods, which drive chemical or physical transformations via Faradaic reactions at electrodes, and proceeds to a detailed examination of the two primary mechanisms by which contaminants are separated in nondestructive electrochemical processes, namely electrokinetics and electrosorption. In these sections, special attention is given to emerging methods, such as shock electrodialysis and Faradaic electrosorption. Given the importance of generating clean, renewable energy, which may sometimes be combined with water purification, the review also discusses inverse methods of electrochemical energy conversion based on reverse electrosorption, electrowetting, and electrokinetic phenomena. The review concludes with a discussion of technology comparisons, remaining challenges, and potential innovations for the field such as process intensification and technoeconomic optimization.

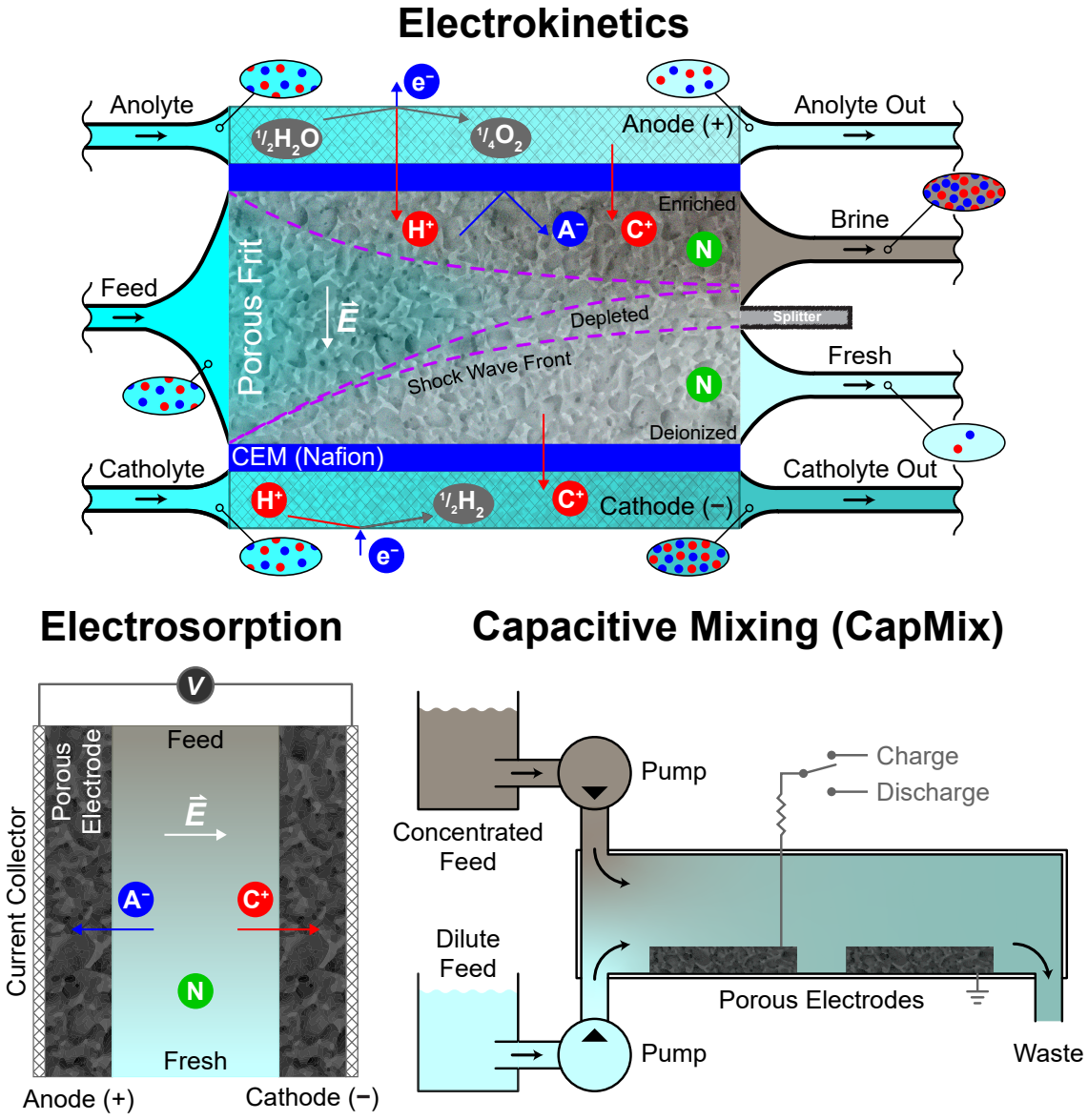

1.1 Introduction

1.1.1 Conventional Methods of Water Purification

It is estimated that four billion people live in localities which are, for at least one month of the year, under conditions of severe water scarcity.[1,2] One increasingly common method used to secure supplies of potable water is desalination, and so the development of desalination systems that are energy and infrastructure efficient is a critical technological challenge.[3] In the most general sense, desalination is a process that is used to remove ions, colloidal particles, chemical compounds, and organic matter—referred to hereafter by the single term contaminants—from saline water. Existing methods for desalination can be broadly categorized into physical methods and chemical methods.[3]

Physical methods include distillation,[4–6] freezing (or freeze–thaw) desalination,[7,8] (liquid-phase) solvent extraction,[9] membrane processes,[10–12] solar desalination,[13–15] and wave-powered desalination.[16] Distillation, a process which appears to have been used by early experimentalists of the classical era such as Aristotle,[17] involves separation of water from contaminants across the interface between a gas and a liquid by selective boiling and condensation. Modern implementations of this method include multistage flash distillation, multiple effect distillation, vapor compression, and humidification dehumidification, all of which are in essence a sequence of countercurrent heat exchangers.[5,18–24] In a similar way to distillation, freezing desalination also uses a phase change (freezing and melting) to separate water from contaminants.[25,26] Solvent extraction is used to separate contaminants based on their relative solubilities in two immiscible liquids, normally water (polar) and an organic solvent (nonpolar), where transport is driven by gradients in the chemical potential of the contaminants.[27] Membrane processes are diverse in that the kind of (semipermeable) membrane used can be tuned based on the target contaminant from which the water is to be removed. These processes include microfiltration, ultrafiltration, nanofiltration, reverse osmosis (RO), and forward

osmosis (FO), and they are distinct primarily in the pore sizes of the corresponding membrane.[11,28–38] During operation, water is driven across a membrane by an input of mechanical work (or by a gradient in osmotic pressure in the case of FO) to retain the contaminants in a concentrated brine. Like distillation, solar desalination is said to have been employed by humans for thousands of years, originally by Greek mariners and Persian alchemists.[39,40] The basis of this technology is not distinct from distillation or membrane processes; it is simply a means to generate the energy that these methods require: that is, heat for distillation or electricity for membrane processes. Wave-powered desalination is similar in principle to solar desalination methods in that it generates electricity (by the motion of submerged buoys in this case) to run a desalination process based on RO.[16] Although these technologies are mature and are cost effective for the desalination of seawater (as well as other concentrated solutions), they are inherently inefficient and energy intensive when used to treat dilute feeds or to selectively remove target contaminants from a concentrated feed, as explained in the following section. It is in these situations that selectively removing trace amounts of a desired species is preferable to indiscriminately concentrating all dissolved species in a brine.

Chemical methods, which tend to be selective in molecular separations, can be classified into two major types: the first, discussed in this section, involves no electrochemistry (these are the established chemical methods), and the second, introduced in Sections 1.1.3 and 1.2, is based on electrokinetic and electrochemical phenomena. Established chemical methods include precipitation,[41] coagulation flocculation,[42] adsorption,[43,44] ultraviolet, ozone, and chlorine disinfection,[45] aeration,[46] and ion exchange.[47,48] Precipitation involves the creation of a solid (the precipitate) from a solution using a chemical referred to as the precipitant.[49,50] Similarly, coagulation flocculation involves the addition of compounds (typically metallic salts) that promote the clumping of fines into larger floc which can be readily separated from water by sedimentation, filtration, or flotation.[51,52] Adsorption is a physicochemical phenomenon that is used to remove contaminants by binding them to the surfaces of an adsorbent material.[44,53] Disinfection technologies in gen-

eral are used to kill bacteria, viruses, and other disease-causing pathogens present in water. The most common disinfection treatments are based on ultraviolet radiation, chlorination, and ozonation, all of which inactivate the waterborne pathogen by disrupting its cellular functions.[45] Aeration of water is achieved by passing air through the liquid and is typically used to remove iron or organic matter, dispel certain dissolved gases, or oxidize dissolved or suspended compounds.[54,55] Ion exchange represents a broad class of processes where ions are exchanged between an electrolyte solution and a solid ion exchanger, such as polymeric resin, chelating agents, zeolites, clay, and montmorillonite.[47,48,56–62] Ion exchange is in general a reversible process, where the ion exchanger is regenerated using a wash solution. Altogether, these traditional chemical methods are based on either chemical reactivity (precipitation, adsorption, and chelation), affinity for charged or functionalized surfaces (coagulation flocculation and ion exchange), or susceptibility to oxidative degradation (disinfection and aeration) of the contaminants.

In practice, a water treatment process often combines several of the methods described above to improve the quality of water and make it suitable for a specific end use. Figure 1-1 shows the process diagram of a representative municipal water treatment facility, in which the water treated contains high levels of hardness and iron.[63] As described in ref 63, raw water is taken from wells and sent to an aerator, where contact with air removes volatile solutes (e.g., H_2S, CO_2, CH_4) and odorous substances (e.g., CH_3SH, bacterial metabolites). Contact with oxygen further promotes iron removal by oxidizing soluble Fe(II) to insoluble Fe(III). After aeration, lime is added (as CaO or $Ca(OH)_2$) to raise the pH and cause the precipitation of Ca^{2+} and Mg^{2+}. Precipitates of these hardness ions settle from the water in the primary basin, and much of the remaining solid material is suspended and requires the addition of coagulants (e.g., Fe(III), $Al_2(SO_4)_3$) to settle. Activated silica or synthetic polyelectrolytes (e.g., poly(sodium styrene sulfonate), polyacrylic acid) may also be added to induce coagulation or flocculation. Settling of colloidal particles occurs in the secondary basin after the addition of carbon dioxide to lower the pH. Sludge from both basins is then pumped to a lagoon, and the water is finally

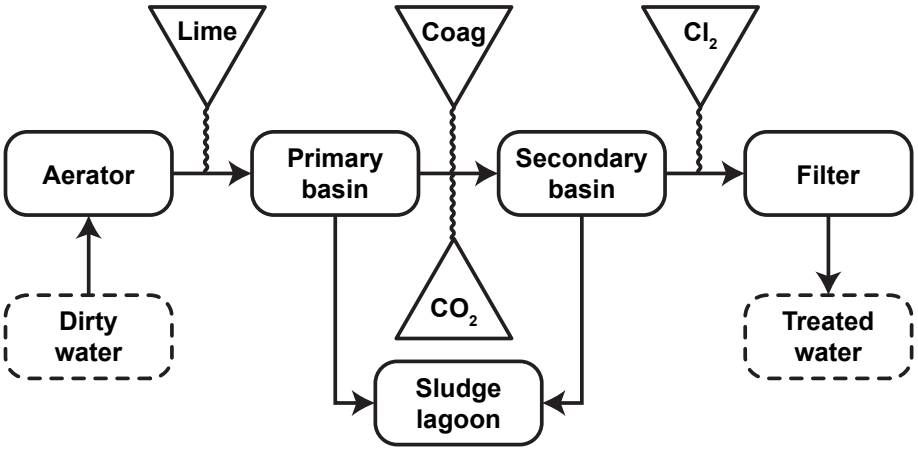

Figure 1-1. Process diagram of a representative municipal water treatment facility. This process combines several of the methods described in Section 1.1.1 to improve the quality of water and make it suitable for domestic use. Adapted with permission from ref 63. Copyright 2001, CRC Press.

chlorinated, filtered, and pumped to the water mains.

1.1.2 Limitations of Conventional Methods

Almost all of the methods introduced in Section 1.1.1 have seen commercial success for a range of applications across numerous industries. Each of these methods, however, has applications and operating constraints outside of which the use of an alternative process would be more practical. For example, thermal distillation has historically been the dominant means of seawater desalination, the most prevalent technology used today in large-scale desalination plants is RO because of its high energy efficiency and small footprint.[33,64] This technology works by pumping the feed at pressures above the osmotic pressure of the solution through a membrane permeable only to water molecules (3-5 MPa for seawater).[12] RO has been optimized over several decades of development for the desalination of concentrated feeds like seawater,[38,65] and modern seawater RO (SWRO) plants currently require under $3\,\mathrm{kWh\,m^{-3}}$ of fresh water produced when including all pre- and post-treatment steps.[66–69] While RO is the best available solution for city-scale seawater desalination, RO systems demonstrate poor scaling of energy demand with decreasing feed concentration, as demonstrated in Figure 1-2.[70] For example, brackish water RO

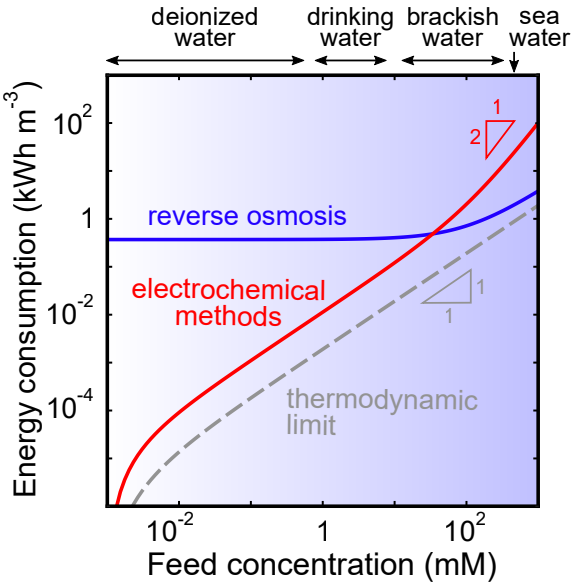

Figure 1-2. Estimates of the volumetric energy consumed by RO and a generic electrochemical process based on the analysis in Section 1.6.1, particularly Equations 1.18 and 1.19. These estimates assume that the feed is desalinated to a final concentration of 1 µM; here, $\gamma = 0.5$ (water recovery, defined as the fraction of the feed recovered as permeate) and $\mathscr{P} = 10\,\mathrm{L\,h^{-1}\,m^{-2}}$ (productivity). Energies are compared to the thermodynamic limit, represented by the dashed curve, and are reported in units of $\mathrm{kW\,h\,m^{-3}}$ of diluate.

(BWRO) plants require nearly the same energy input as SWRO plants ($1\text{-}3\,\mathrm{kW\,h\,m^{-3}}$), despite the fact that brackish water is less concentrated than seawater by about an order of magnitude.[71] According to the van't Hoff equation, osmotic pressure is linearly proportional to concentration for dilute solutions, which suggests that the energy demand for BWRO should be about an order of magnitude lower than for SWRO. Friction losses in RO systems, however, do not scale with salt concentration, but rather with the amount of water transported across the membrane. This intrinsic feature of RO thus explains the relatively high losses and poor energy efficiency of BWRO compared to SWRO.[72] Because desalination of brackish water is a promising solution for water scarcity, and because removal of trace contaminants from dilute feeds is an important capability, technologies whose energy demand scales with feed concentration would be more desirable than RO for these applications.

Another notable drawback of RO plants is that they require large capital expenditures and mature infrastructure, which limits their utility for small-scale appli-

cations or in remote locations.[66] Moreover, it is difficult to downscale RO systems because high-pressure pumps and resilient plumbing are required at any scale to pressurize the feed in excess of the osmotic pressure. Facile downscaling to smaller, less expensive plants that can be introduced into small residential areas and communities would help water treatment technologies further penetrate the market. Inexpensive, small-scale plants may in fact be the most appropriate solution for developing and off-grid locations, where water scarcity is severe and commonplace, and where infrastructure may be underdeveloped or nonexistent. Small-scale portable desalination units are also in demand by industrial facilities, by mobile military units and vessels, in recreational spaces, and in the travel industry.[73,74] To meet these growing and diverse needs for purified water, the technological focus should extend beyond RO by including scalable systems with lower energy demands and more flexible infrastructure requirements for treatment of brackish water and dilute feeds.

Many of the drawbacks of RO, particularly when used to treat dilute feeds, can be overcome by using the physicochemical methods introduced in Section 1.1.1. These methods, however, have their own limitations and often require nonreusable chemicals. Solvent extraction can be both efficient and cost effective in separating hazardous contaminants from benign feeds, but this process requires large volumes of organic extractants and sometimes toxic solvents, and the entrainment of phases yields low-quality effluents.[75,76] Precipitation is another simple and cost-effective process that is commonly used to remove toxic heavy metals from water, but it produces large amounts of sediment and sludge that is often difficult and expensive to dispose of. Precipitation is also ineffective at removing ions that are present at low concentration, and its utility may be limited when the water is contaminated with multiple metals.[76,77] Coagulation flocculation is often employed after precipitation to remove solid particulates from water, and this method could also be used to capture larger particles and inactivate biological agents.[78,79] The applicability of this method is limited, however, because it requires nonreusable inorganic coagulants which are usually toxic.[76,80] Ion exchange, on the other hand, offers a wider range

of simple and well-established commercial products, many of which can be regenerated for repeated use.[76,77,81] The performance of ion exchange resins and chelating agents, however, is sensitive to variations in pH, and some of these agents react with dissolved metal ions to form soluble metal complexes that lead to secondary pollution.[76,77,82]

1.1.3 Emerging Electrochemical Methods

A variety of innovative techniques based either on electrokinetics or electrosorption have been proposed for water purification, and these techniques have given rise to emerging electrochemical methods.[83–91] The recent discovery of deionization shock waves in microchannels[92,93] and porous media[87,94,95], for instance, inspired a new area of research in electrokinetic methods for deionization. Parallel developments in materials science have uncovered a wealth of novel electrode chemistries—where the electrosorption of ions is promoted by Faradaic reactions—to replace carbon, conventionally the material of choice in capacitive systems.[86,96] These innovations have not only enhanced deionization capacity but have also imparted molecular selectivity to the electrodes. Recent examples of Faradaic platforms for water purification are based on electrochemical reduction of target contaminants,[97,98] electrochemical switching of ion exchange,[99–101] and molecularly selective removal of ions,[86,96,102] uncharged compounds,[103,104] and biomolecules (e.g., proteins).[105] Many of these advances have relied on Faradaic compounds with immobilized surfaces to achieve superior electrochemical performance and chemical specificity. By modulating the binding interactions at the surfaces, the affinity of the electrodes can be tuned specifically for minority components in a feed, which in practice may be either highly valuable or seriously toxic.

Emerging electrochemical methods include electrodeionization (EDI, sometimes called hybrid ion exchange ED),[61,106–108] shock electrodialysis (shock ED),[87,109] capacitive deionization (CDI),[110,111] battery deionization (BDI),[112,113] and Faradaic electrosorption.[86,96] These technologies are unique from all of the others discussed so far in that removal of contaminants is based on their response to electric fields

in solution. Electrochemical systems use applied electrical currents to remove contaminants from the feed by either driving separations in bulk electrolytes,[61,114] electrostatically trapping them in electric double layers (EDLs),[90,110,115] or intercalating them in solid electrodes (e.g., materials composed of two-dimensional, layered structures).[116–118] The first of these mechanisms is governed by electrokinetics, and the second and third are forms of electrosorption, as explained in Figure 1-3. The primary input of energy to these systems is an applied electric potential, which makes these processes scalable without the need to be operated at extreme temperatures or pressures. Energy dissipation in electrochemical systems, however, arises from three general sources:[119,120] (i) ohmic resistance, due to hydrodynamic drag acting on moving ions in electrolytes or membranes,[72] as well as electronic resistance in porous electrodes and current collectors; (ii) Faradaic reaction resistance at electrodeâ€“electrolyte interfaces, leading to activation overpotential; and (iii) concentration polarization, associated with limitations in ion diffusion. These losses all scale with the number of ions removed rather than the amount of solution process, as shown in Figure 1-2. These systems therefore tend to be more energy efficient compared to physical methods (and are molecularly selective) when used to treat brackish water and dilute feeds.

Among the existing electrochemical methods, electrodialysis (ED) has been studied and used for water desalination for decades, and several ED desalination plants for treatment of brackish water are currently operational in the US.[114,123–127] The past decade, however, has seen the emergence of several novel electrochemical systems for water purification with unique functionalities and working principles compared to ED, and these are EDI,[128] shock ED,[87] CDI,[115,129,130] and Faradaic electrosorption.[86] This review summarizes the development of these novel technologies to form the basis for the emerging field of electrochemical systems for water purification and ion separations. For completeness, we also briefly discuss related microfluidic technologies, which have been reviewed in detail elsewhere.[131,132] Microfluidic systems, which are driven by electrical energy, have throughputs at the scale of nanoliters and may be difficult to scale up to the volumes needed for de-

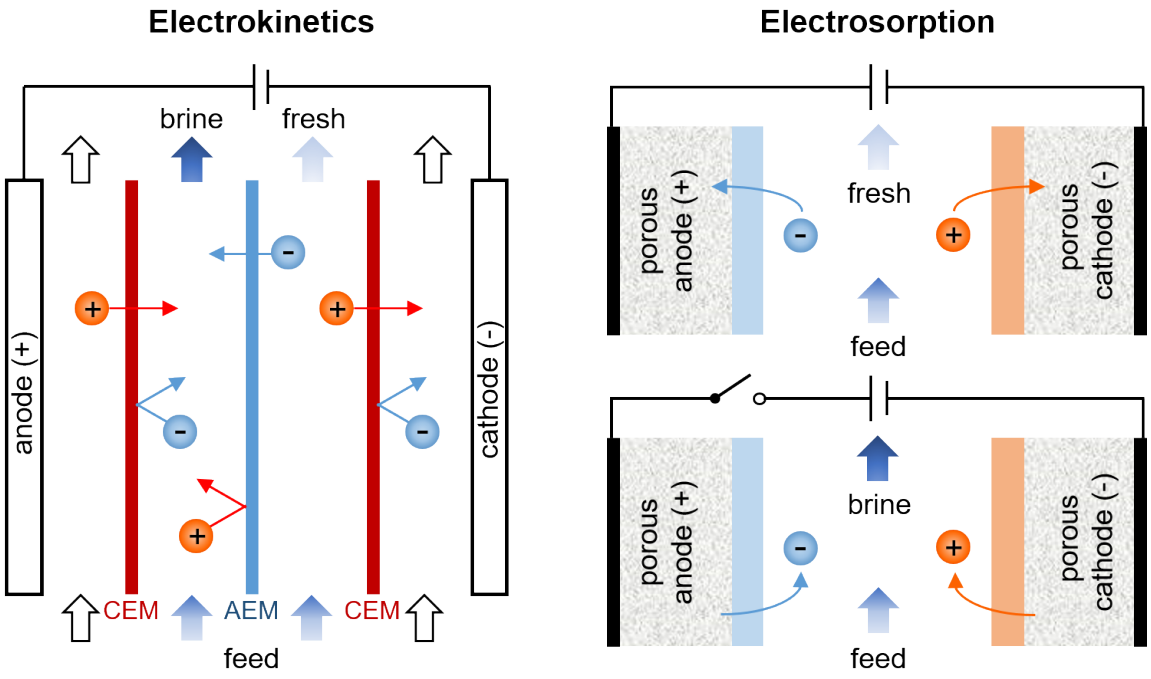

Figure 1-3. Electrokinetics and electrosorption are the two main mechanisms by which contaminants are separated in any nondestructive electrochemical process. Electrokinetic processes, which are typically continuous, involve transport of charged or uncharged but dielectric[121,122] species in an electrolyte in response to an applied electric field, and so removal of contaminants relies on effective mass transfer. Electrokinetic methods like EDI and shock ED use porous materials in the feed channels to increase the extent of deionization and to improve energy efficiency when the feed is dilute. Electrosorption processes are cyclic and encompass all phenomena in which the binding of contaminants is aided by an applied electric field. In addition to effective transport, electrosorption relies on favorable reaction kinetics and thermodynamics.

ployment for human consumption, agriculture, or industry. Electrochemical systems instead are based on cells and stacks made of components like ion exchange membranes (IEMs), porous dielectric separators, and porous electrodes that can be produced in large areas as flat sheets or films, and thus these systems naturally have clear pathways for scale up.

1.1.4 Outline of This Review

Conventional electrochemical methods, which exploit Faradaic electron transfer reactions at electrodes to drive chemical or physical transformations, have been previously reviewed, particularly in their use for removal of organic matter,[133] organic compounds,[134–139] inorganic contaminants,[140–144] and microorganisms[145–147] as well as for degradation of various contaminants and micropollutants.[125,148–151] The technologies on which many of these publications focus are well established and currently used in industry. We begin the review by introducing these established electrochemical transformation methods and the broad range of applications for which they are used (Section 1.2). We then build on the existing literature and related reviews[68,105,115,118,125,128,152–157] by emphasizing the principles and applications of emerging electrochemical methods for desalination, water purification, and ion separations (Sections 1.3 and 1.4). As shown in Figure 1-4, several of these emerging methods have developed only in the last ten years and have been reviewed either briefly or independently of other methods. To provide a foundation for our discussion, we examine recent developments in electrokinetic phenomena and electrosorption for water purification and selective ion separations. See refs 76,118 for tables that summarize the advantages and disadvantages of techniques used for water purification, including many of the emerging methods discussed here.

In Section 1.3, we explain (nondestructive) methods based on electrokinetics, which may either include or exclude membranes. Two methods in the class of membrane-based systems are ED and EDI, where the membrane plays a critical role in the removal of charged species. Ions can be separated from the bulk fluid

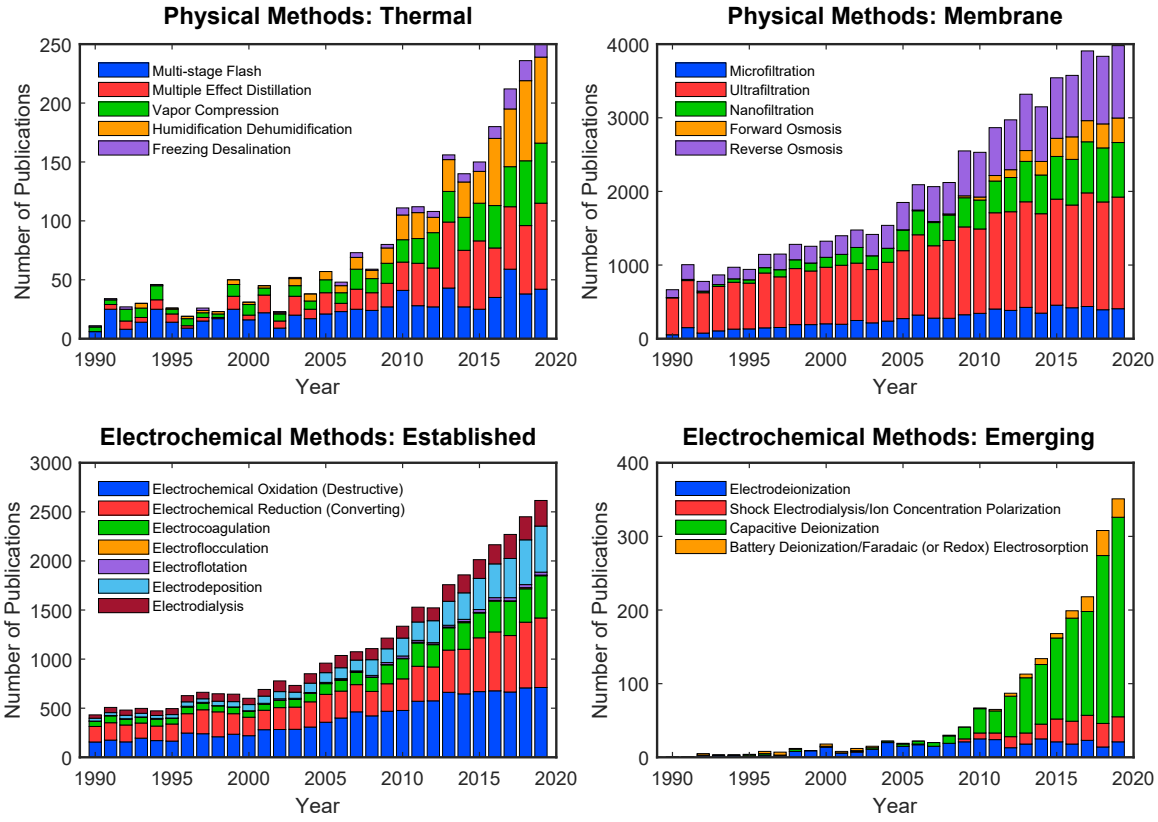

Figure 1-4. Number of publications per year for various methods used for desalination or ion separations. The technologies considered here are broadly classified as either physical (top row) or electrochemical (bottom row). This review focuses on electrochemical methods, and special attention is given to the emerging methods (marked by a double dagger), including shock ED, CDI, and Faradaic electrosorption. The literature search was performed using Elsevier's Scopus database with the search field TITLE-ABS(…).

directly, however, by virtue of the electrokinetic phenomena, without much contribution from the membrane itself. Key developments have also been made in the class of "semimembraneless" systems (i.e., systems in which the feed is partitioned into fresh and brine streams across a deionization shock wave that functions as a virtual interface), which include microfluidic (or nanofluidic) concentration polarization and shock ED. These methods are both based on the phenomenon of concentration polarization, which arises due to extreme gradients in the concentration of ions in solution. In Section 1.4, we describe electrosorption, the phenomenon that is responsible for sorption in electrochemical systems, and how this process is used for desalination and molecular separations. (These separations are often nondestructive, but in certain cases, they may involve electrochemical conversion or degradation of the contaminants.) This explanation is followed by an overview of CDI techniques as well as recent innovations in Faradaic (or redox-active) materials and their broad use in chemical and environmental processes. With these methods explained, we introduce inverse methods of energy conversion that convert gradients in salinity to energy (Section 1.5). We conclude by discussing the energetics, thermodynamic and technological challenges, and prospects of electrochemical methods for water purification and ion separations (Sections 1.6 and 1.7).

1.2 Electrochemical Transformations

In the general areas of water purification and wastewater treatment, a variety of electrochemical processes have been developed to remove contaminants ranging from ions to colloidal particles. For example, chemical coagulation flocculation, flotation, precipitation, and redox (reduction and oxidation) can be improved by applying electric fields.[158–160] In this section, we discuss nonelectrosorptive electrochemical methods that are well established and reviewed extensively in the literature, namely electrochemical oxidation, electrochemical reduction, electrocoagulation, electroflotation, and electrodeposition.[98,148,158–162] These processes involve Faradaic reactions at electrodes to drive chemical or physical transformations of ionic or molecular solutes. For example, electrochemical redox reactions are used

primarily when the objective is to degrade or convert nonbiodegradable organic contaminants and certain inorganic compounds (e.g., cyanides, thiocyanates, sulfides) and disinfect water. In Section 1.3, we examine both traditional and emerging electrokinetic methods based on ED, which rely on coupled transport phenomena in electrolyte solutions. We then discuss in Section 1.4 electrosorption systems (both capacitive and Faradaic) for selective ion removal based on various functional materials, including porous carbon, inorganic crystals, and polymers.[90,115]

1.2.1 Electrochemical Oxidation

Electrochemical oxidation is a chemical reaction involving the loss of one or more electrons by an atom or a molecule at the anode when an electrical current is passed through the system.[148,163,164] In the context of water treatment, electrochemical oxidation generates reactive oxidizing agents called free radicals that interact with the contaminants and degrade them, as explained in Figure 1-5.[125] Superoxide ($O_2 \cdot^-$), hydroperoxyl ($HO_2 \cdot$), hydroxyl ($HO \cdot$), and sulfate ($SO_4 \cdot^-$) radicals are examples of reactive agents that can degrade organic and organometallic contaminants by initiating a radical oxidation chain (see refs 125,148,165–169 for lists of common reaction pathways by which these radicals are formed).[138,170–172] Superoxide and hydroxyl are two of the most important radicals in free-radical chemistry, and they are both believed to be key species in oxidative processes.[165,166,173] While superoxide is normally a nucleophile and reducing agent,[166,174] it exists in equilibrium with the hydroperoxyl radical, which can behave as an oxidizing agent in various biological and chemical reactions.[175–179] (In general, superoxide is a weak reducing agent, but in the presence of solids or cosolvents that are less polar than water (e.g., H_2O_2), superoxide becomes reactive and can degrade halogenated aliphatic compounds,[180,181] including perfluorocarboxylic acids,[182,183] via nucleophilic attacks.[184]) The hydroxyl radical oxidizes both organic and inorganic compounds with high reaction rates, such that its action occurs only in the region where it is produced.[185] The degradation process begins with formation of the reactive oxidizer, followed by initial attacks on target molecules and their breakdown into

biodegradable intermediates. Subsequent attacks on these intermediates by the oxidizer can lead to their mineralization (i.e., production of water, carbon dioxide, and inorganic salts), as shown in Figure 1-5.[125,148] Another class of oxidizers is obtained by the oxidation of chloride ions to generate active chlorine (Cl_2), which may disproportionate to hypochloric acid (HClO) or hypochlorite (ClO^-) depending on the pH. Although these species can effectively oxidize various contaminants in real wastewaters (e.g., landfill leachates, textile effluents, olive oil wastewater, tannery wastewater),[97] this approach has the drawback of producing chlorinated organic compounds during the electrolysis, which is the main limitation of electrochemical oxidation.[97,186] These chlorinated byproducts increase the toxicity of the effluent since they tend to be much more persistent than what is initially present in the feed.[187–189] In the absence of chloride electrolytes, however, electrochemical oxidation can be reliably used for disinfection, wastewater treatment, groundwater treatment, soil remediation, wastewater sludge conditioning, and odor and taste removal.[148,190–192]

In the 1990s, researchers became increasingly aware that the anode material is an especially important parameter in the design and optimization of electrochemical oxidation processes.[195–198] (The cathodes are usually stainless steel plates, platinum meshes, or carbon felt electrodes.) The results obtained by several groups indeed demonstrated that the choice of anode influences the selectivity and efficiency of organic compound oxidation.[167,199] According to a model proposed by Comninellis,[196] anode materials are divided into active anodes (e.g., carbon, platinum, iridium oxides, ruthenium oxides) and nonactive anodes (e.g., antimony-doped tin oxide, lead dioxide, boron-doped diamond).[97] Active anodes have low oxygen evolution overpotential and are good electrocatalysts for oxygen evolution, while nonactive anodes have high oxygen evolution overpotential and are poor electrocatalysts for oxygen evolution. Anodes based on boron-doped diamond (BDD) have received considerable attention due to their chemical stability, high electrical conductivity, resistance to corrosion even in harsh environments, and wide window of electric potential.[200] As a result, BDD is generally viewed as one of the most effec-

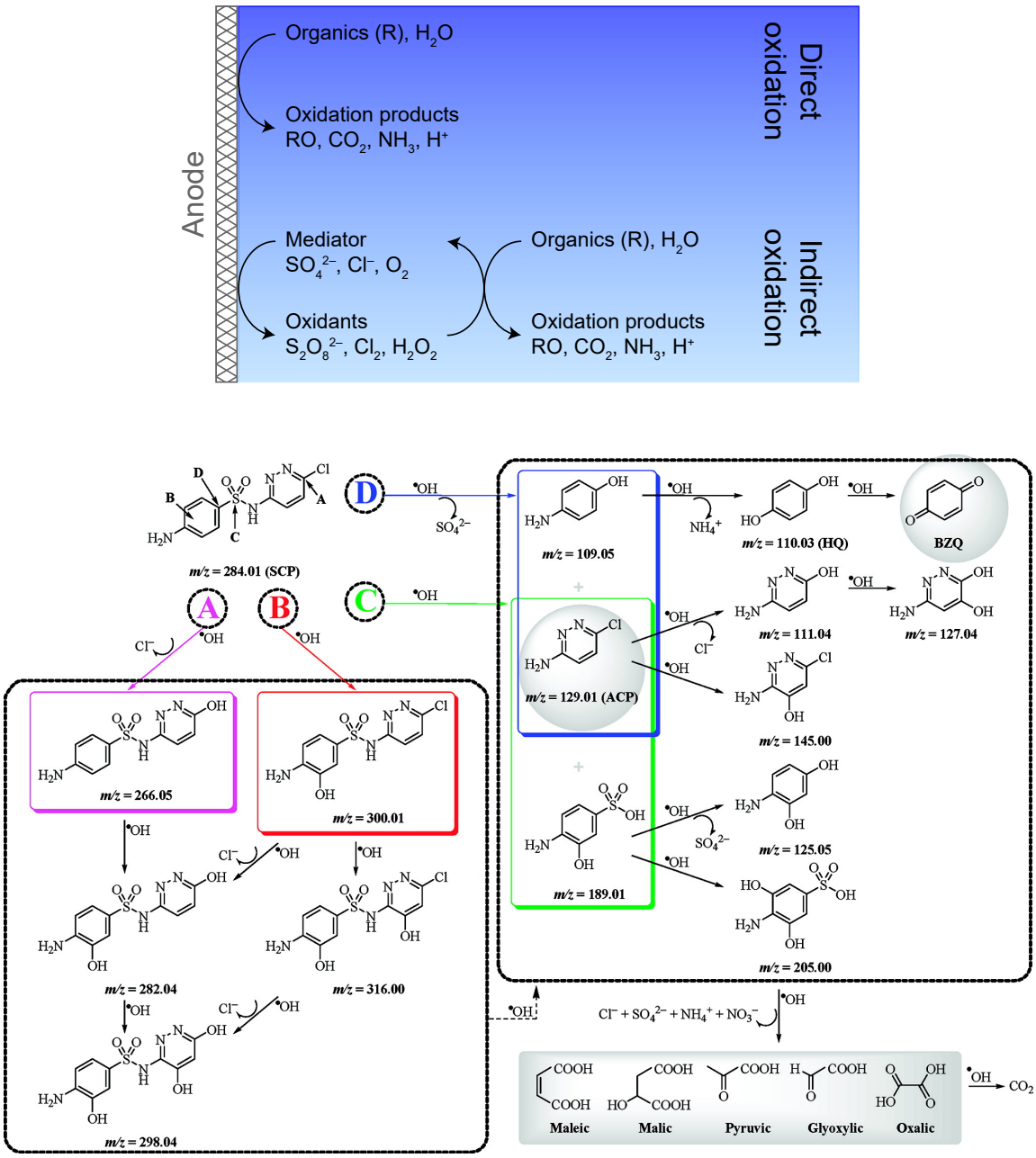

Figure 1-5. Electrochemical oxidation is an established destructive, nonelectrosorptive method that is used to degrade most organic contaminants and certain inorganic compounds. (top) The method involves formation of reactive oxidizers that interact with contaminants either at the anode surface (direct oxidation) or in the bulk (indirect, or mediated, oxidation).[125] Reproduced with permission from ref 193. Copyright 2017, Royal Society of Chemistry. (bottom) Complex organic compounds, such as the sulfonamide antibiotic sulfachloropyridazine, are degraded and mineralized by the attack of reactive oxidizers at key reaction sites (designated by the letters A-D). In this example, hydroxyl radicals can attack four unique sites on sulfachloropyridazine to yield different primary cyclic byproducts, all of which are eventually transformed into CO_2. Reproduced with permission from ref 194. Copyright 2012, American Chemical Society.

tive and energy efficient anodes for mineralization of organic contaminants, though its use in practice is limited to due high manufacturing costs.[200] Moreover, BDD (as well as other anodes) promotes the oxidation of chloride to chlorate (ClO_3^-) and perchlorate (ClO_4^-), which are water-soluble disinfection byproducts that are exceedingly mobile in aqueous solutions and are highly persistent under typical water conditions.[97,148] Since disinfection byproducts in drinking water are typically regulated, their concentrations should be monitored and controlled when performing in-line electrolysis.

Other prominent anodes include dimensionally stable anodes (DSAs, also called mixed metal oxide electrodes) and sub-stoichiometric titanium oxide anodes.[97,201,202] DSAs are fabricated by coating a substrate such as titanium with several kinds of metal oxides, including RuO_2, IrO_2, and PtO_2. These anodes exhibit high conductivity and corrosion resistance, and recent studies showed that doping DSAs with metal and non-metal elements can further improve their performance.[203–206] Moreover, the use of nanotechnology has gained traction in the field of electrode fabrication to increase the porosity and active surface area of the anodes.[207,208] Anodes based on sub-stoichiometric titanium oxide (Ti_nO_{2n-1}) also display high conductivity and corrosion resistance, and their many advantages and long service life have led to their broad use in fuel cells, lead-acid batteries, and, most recently, wastewater treatment.[209–212] Ganiyu et al. prepared a Magnéli-phase Ti_4O_7 electrode by plasma deposition and compared it to DSA and BDD anodes for the degradation of the beta-blocker propranolol[213] and the analgesic paracetamol.[214] These studies showed that the Ti_4O_7 electrode can achieve similar or better removal of organic carbon compared to DSA and BDD. Several methods have been reported in the literature to improve the performance of sub-stoichiometric titanium oxide electrodes, and these methods include plasma spraying,[215] which produces doped functional coatings, and high-temperature sintering, which produces an electrode with extensively interconnected macropores.[212]

Most anodes used in electrochemical oxidation produce highly active hydroxyl radicals on their surfaces,[216] and treatment of wastewater with these materials re-

quires adequate flow of the contaminants toward them. When the concentration of pollutants near the anode is low, the process rate is limited by mass transfer of these species to the surface of the electrode.[97] Common methods to overcome this limitation include gas sparging,[217] incorporation of turbulence promoters,[97] and use of nanoengineered materials.[218–220] Most importantly, the efficiency of electrochemical oxidation can be improved with the indirect (or mediated) oxidation method, which avoids the production of oxygen by generating precursors that are transformed to active oxidizers. Persulfate ($S_2O_8^{2-}$), percarbonate ($C_2O_6^{2-}$), and hydrogen peroxide (H_2O_2) are examples of precursors that can be produced using BDD anodes.[221–223] These species are relatively stable at ambient conditions and generate highly active inorganic radicals that enable mediated oxidation of organic contaminants.[97] Michaud et al. experimentally tested the production of precursors using BDD and observed that persulfate is produced with high current efficiency when the electrolyte is concentrated in sulfate (SO_4^{2-}) and the process temperature is low.[221] The persulfate precursor is activated to generate sulfate radicals, and this step requires a transition metal catalyst or sufficient energy.[224] Activated persulfate can then oxidize organic compounds, and this approach has been used to treat groundwater and soils contaminated with biorefractory organic species.[97]

In recent years, there have been significant advances in the design, synthesis, and use of nanostructured electrodes for electrochemical oxidation.[220] Nanoengineered materials exhibit new and improved properties, such as an increase in the number of active sites and an improvement in electrical conductivity, and these materials can promote heterogeneous catalysis at electrode surfaces.[220] According to Du et al., a wide range of nanostructured cathodes have been reported in literature, and they can be divided into four categories: cathodes based on carbon nanomaterials such as carbon nanotubes (CNTs) and graphene,[225,226] carbon cathodes doped with heteroatoms such as fluorine and nitrogen,[227,228] metals or metal oxides deposited on carbon,[229–231] and metal oxide cathodes.[232,233] In most studies, these electrodes are used for electrosynthesis of H_2O_2 via oxygen reduction, and the structural morphology and composition of functional groups largely affect cath-

ode performance.[226,234,235] Du et al. also explain that there exists a large variety of nanostructured anodes, which can be divided into four categories similar to those of the nanostructured cathodes: anodes based on carbon nanomaterials such as CNTs and nanostructured BDD,[236–239] anodes doped with heteroatoms such as fluorine and boron,[240,241] metals or metal oxides deposited on carbon,[242–244] and metal or metal oxide anodes.[245–248] Most articles published on nanostructured electrodes report improvements in the kinetics of HO· production and pollutant oxidation due to the synergistic effects of greater stability, electrical conductivity, electrochemical reactivity, and active-site exposure.[220] Although nanoengineering has enabled major advances in improving electrode stability, more efforts are needed to demonstrate stability for long-term use, and standard protocols must be established to assess the lifetime and reliability of these systems.[220]

Over the past two decades, scale up of anode systems has gained attention, where the focus has been on increasing the throughput of laboratory-scale systems while retaining performance and reliability.[249,250] At the same time, electrochemical advanced oxidation processes have been developed to improve the efficacy and applicability of conventional electrochemical oxidation.[148,251–253] These specialized variants of electrochemical oxidation introduce Fenton's reaction chemistry,[194,254,255] photoelectrocatalysis,[256] sonoelectrolysis,[148] and aerobic or anaerobic digestion (using microbial electrochemical technologies)[257–260] to the standard process.[261] In conventional electrochemical oxidation, the reactive oxidizers are often (but not always) produced at the anode surface; the advanced variants facilitate additional generation of oxidizers in the bulk.[148,199] Although these oxidative processes are more widely studied and used—since they usually lead to mineralization of the contaminants—treatments based on electrochemical reduction have been gaining interest because they enable partial recovery of chemicals as well as production of value-added substances.[97]

1.2.2 Electrochemical Reduction

Electrochemical reduction, the complementary process to electrochemical oxidation, is a chemical reaction involving the gain of one or more electrons by an atom or a molecule at the cathode when an electrical current is passed through the system.[125] Similar to electrochemical oxidation, electrochemical reduction can occur either directly on the surface of the cathode or indirectly in the bulk by the action of a reducing agent generated at one of the electrodes.[98] This process is typically used to treat water contaminated with heavy metal ions (see Section 1.2.5 also),[125,262] inorganic anions (e.g., bromate, perchlorate),[263,264] or halogenated organic compounds (e.g., organic volatile halides, chlorofluorocarbons, polychlorohydrocarbons, polyhalophenols)[97,98] by converting these species into more benign products. As shown in Figure 1-6, the mechanism of this conversion usually involves the removal of halogen atoms or the reduction of aldehydes and ketones to produces less toxic species.[97,125]

Among the major parameters that determine the efficiency of electrochemical reduction are catalyst loading, cathode potential, and water quality.[98] Generally, an increase in catalyst loading improves reduction activity, though only up to a limit beyond which activity either steadies or even decreases as the distance for electron transfer increases.[265] In the case of nanosized catalysts such as palladium, the particles can aggregate at higher loading, which results in excessive local evolution of hydrogen bubbles that restrict access of the contaminants to the catalyst.[266] As is the case for catalyst loading, a reaction will have an optimal operating cathode potential above which the abundance of hydrogen bubbles produced could inhibit adsorption of contaminants.[267,268] Electrochemical reduction is also sensitive to the quality and characteristics of the feed, which influence performance and electrode lifetime.[98] Performance typically improves at lower pH (due to increased formation of adsorbed hydrogen),[269,270] at higher ionic strength (due to smaller EDLs),[98] and in the absence of certain species (e.g., organic matter, electrocatalyst poisons, competing ions).[266,271]

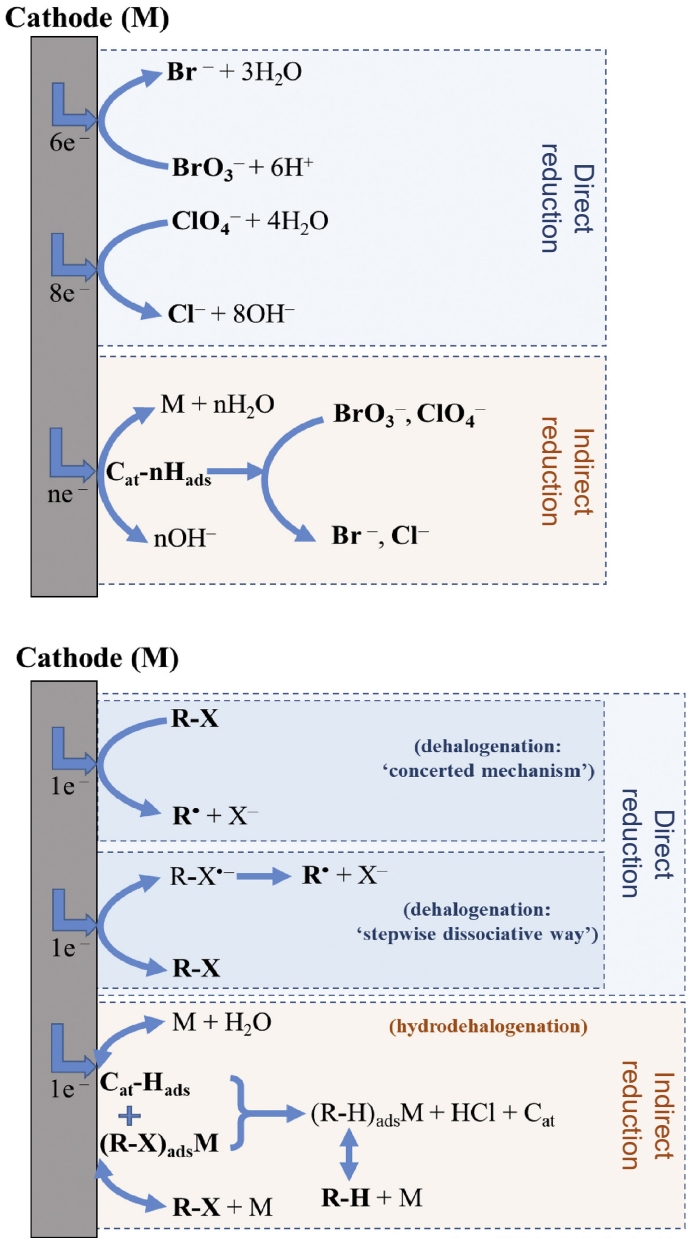

Figure 1-6. Electrochemical reduction is an established conversion method that is used to treat oxidized contaminants, such as (top) inorganic and (bottom) organic halides (R-X). The method involves formation of high energy electrons or reactive species that interact with contaminants either at the cathode surface (direct reduction) or in the bulk (indirect reduction). M refers to the cathode material (i.e., the catalyst, C_{at}); C_{at}-H_{ads}, $(R\text{-}X)_{ads}M$, and $(R\text{-}H)_{ads}M$ are the hydrogen atom, organic halide, and dehalogenated organic compound (R-H), respectively, adsorbed on the cathode. Reproduced with permission from ref 98. Copyright 2020, Elsevier.

The choice of electrode is another critical design parameter that influences the mechanism of electrochemical reduction, as it impacts the reaction pathway, selectivity, and energy consumption.[97,98] An effective catalyst enables strong bonding on the surface of the substrate.[98] From among the many materials investigated to date, electrodes based on silver, nickel, and carbon hold prominent positions due to their high electrocatalytic activity, robustness, and inexpensiveness with respect to conversion of halogenated contaminants.[97,98] Noble metals such as palladium, platinum, and ruthenium are also effective materials for electrocatalytic hydrodehalogenation,[265] especially when combined with other elements to produce bimetallic catalysts.[272–274] These bimetallic catalysts can even be modified by adding nanosized or anchored materials to further improve their electrocatalytic efficiency.[265,275,276] The main limitation of metallic catalysts, however, is their high cost, which makes the use of carbon-based materials an attractive alternative.[98,277] Some of the most effective carbon-based catalysts involve nanostructured polymer coatings that selectively adsorb halogenated compounds,[278,279] but the electrocatalytic activity of modified carbon materials in general is low.[280] Activity can be improved by combining nanostructured carbons such as reduced graphene oxide (RGO) with metallic electrodes.[266]

In general, electrochemical reduction is an effective method not only for treatment of pollutants, such as volatile organic halides and chlorofluorocarbons, but also for their transformation into value-added products.[97] This capability can be achieved by selective removal of halogens as well as by carboxylation or carbonylation of the organic compounds. The combination of electrochemical reduction and electrosynthesis is another way by which wastewater can be treated and upgraded for synthesis of value-added organic products.[281,282] Moving forward, it is important to assess and improve the stability and lifetime of electrocatalytic materials for use in practical applications.

1.2.3 Electrocoagulation and Electroflocculation

The two-step process of electrocoagulation and electroflocculation relies on the dissolution of metal anodes to induce formation of flocs, which trap contaminants and enable their removal by settling, sedimentation, precipitation, or flotation.[158,283–287] This method was patented in 1906 by Dieterich for treatment of sewage in London and bilge water from ships using iron and aluminum as sacrificial anodes.[288,289] As shown in Figure 1-7, the crucial electrochemically mediated step relies on in-situ oxidation of the appropriate metal surfaces (often aluminum or iron)[290] to produce metal ions which then form flocs that facilitate the removal of solids, organic species, and inorganic compounds.[160] What follows is essentially ordinary coagulation: the (typically negative) surface charge of the contaminants is neutralized, which destabilizes them and causes them to form aggregates that can be removed by settling, sedimentation, precipitation, or flotation.[291] Electrocoagulation is regularly used in industrial applications, such as removal of heavy metals, remediation of wastewater, and treatment of produced water.[292–294] To improve the performance of electrocoagulation for wastewater treatment, numerous studies have sought to integrate this technology with other processes, such as peroxidation or a more specialized biological process, both of which facilitate the removal of organic matter.[295]

Electrocoagulation has been extensively studied, often using iron electrodes, for specialty separations and wastewater treatment, particularly to remove light organic pollutants such as oils, dyes, and humic particles.[296] In addition, electrocoagulation can be used with aluminum electrodes to remove heavy metal ions, including Ag^{+}, Zn^{2+}, Cu^{2+}, Ni^{2+}, and Cr^{6+},[297–299] as well as halide ions.[300] Compared to classical coagulation, electrocoagulation has several advantages that lower its operating cost. For example, the cationic coagulant is generated in-situ by a chemical reaction on the sacrificial electrode, and this feature limits the introduction of counterions from chemical reactants that contribute to the formation of sludge.[301] Electrocoagulation thus requires no separation of unreacted counterions from the

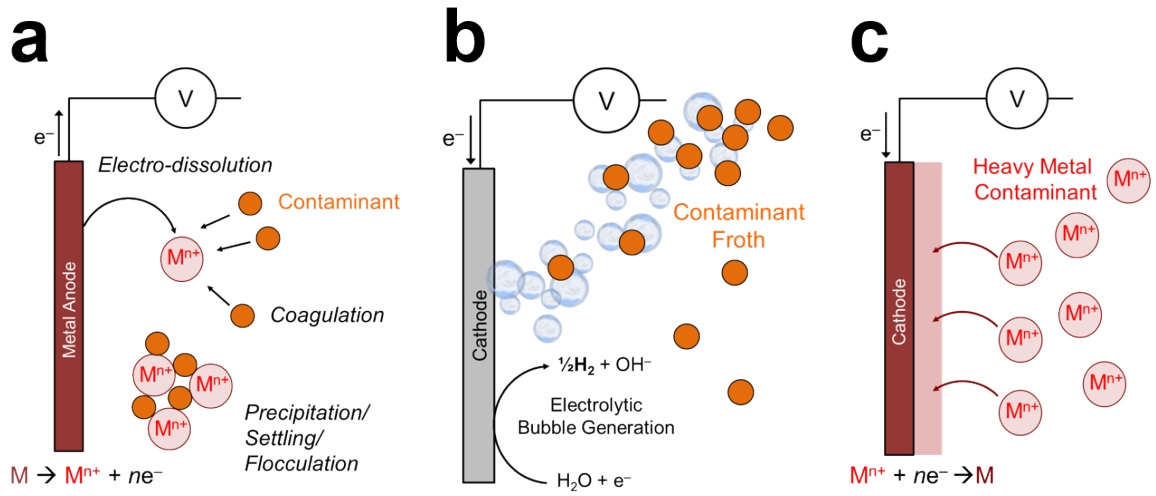

Figure 1-7. Established nondestructive, nonelectrosorptive methods of water purification. (a) Electrocoagulation and electroflocculation is a two-step process by which metal anodes are dissolved to induce formation of flocs that trap contaminants for removal by settling, sedimentation, precipitation, or flotation. (b) Electroflotation produces bubbles by water redox to transport lighter contaminants or flocs by flotation. (c) Electrodeposition is based on the electrochemical deposition of metal ions in solution onto an electrode.

chemical coagulant in solution, which are usually removed to meet discharge standards.[302] The reduced formation of sludge also lowers expenses associated with handling and disposal of this waste. Another advantage of electrocoagulation is that the electrochemical reactions that drive this process produce OH^-, which eliminates the need for external chemical agents to regulate pH.[303] These reactions also produce gaseous H_2, which could be captured and used subsequently as a fuel.[304]

In contrast to classical flocculation, which requires the input of large amounts of chemicals, electroflocculation relies on Faradaic (anodic) dissolution to dose the system with the coagulant, a property that enables finer control and easier handling of the process. Complexation of the released metal ions, such as Al^{3+} or Fe^{3+}, with hydroxides produces monomeric ($Al(OH)_2^+$ and $Al(OH)^{2+}$) or polymeric species ($Al_{13}(OH)_{34}^{5+}$) that then flocculate with organic compounds (e.g., dyes) and further promotes precipitation by either sedimentation or flotation.[305] Despite their advantages, however, electrocoagulation and electroflocculation exhibit operational challenges, such as electrode passivation, sludge deposition on the electrode, nonuniform dissolution of the anode, and inconsistent production

of the coagulant, all of which undermine performance under long-term, continuous operation.[306] The sacrificial anode is also consumed over time which necessitates periodic replacement of the electrode, and the high concentration of residual (metal) ions requires a post-treatment step prior to discharge.[307] But because of their operational simplicity, low cost, and versatility, electrocoagulation and electroflocculation remain active areas of research.[308]

1.2.4 Electroflotation

Electroflotation is often used in conjunction with electrocoagulation and electroflocculation for electrochemical–physical separations.[309–312] Electroflotation relies on the electrolytic process of water redox, in which bubbles are formed to transport lighter contaminants or flocs by flotation. The key driving Faradaic reaction for electroflotation is the electrolysis of water at both electrodes (O_2 evolves at the anode and H_2 at the cathode). The first proposed use of electroflotation is attributed to Elmore in a patent from 1905 for mining separations,[313] and this process has since been expanded to handle a range of contaminants, such as oils and low-density suspended particles in mining water and groundwater, among others.[309] The primary limitation of electroflotation is the difficulty of controlling the uniformity of bubble evolution.[160,314] Careful optimization of current densities and voltage windows is therefore crucial for effective performance.[141,284,311,315]

Electroflotation has several features that are attractive for applications in water treatment. For example, this process can be used to recover valuable components from wastewater without the need for chemical reagents.[316] The reason is that electroflotation generates gaseous O_2 and H_2 which are more active than the gases used in conventional flotation (e.g., natural gas, air, N_2). Electroflotation can also produce bubbles with diameters of 1-30μm, which leads to better dispersion, finer distribution, and longer residence times of the bubbles in solution.[317–319] This feature facilitates the flotation of fine particles in a way that is difficult to achieve by classical flotation. Finally, the energy consumption of electroflotation is in the range of $0.1\text{-}0.5\,\mathrm{kW\,h\,m^{-3}}$, and it decreases as the electrical conductivity of the solution in-

creases.[317]

1.2.5 Electrodeposition

The process of electrodeposition is synonymous with electroplating and is one of the earliest applications of electrochemistry, especially in metallurgical processing.[141,320–322] While many of these plating methods are major sources of heavy metal pollution, the same electrochemical principles have been used to treat industrial wastewater and sometimes even to recover and reuse discharged materials. As an example, copper electrodeposition is commonly used to print circuit boards and manufacture electronics. Recovery of copper from spent parts, however, has also been an application of electrochemical methods that combine leaching, ED, and electrodeposition from wastewater.[323,324]

Electrodeposition involves the application of cathodic overpotentials to induce the electrochemical deposition (or reduction) of metal ions in solution onto an electrode. In other words, this process is direct electrochemical reduction of metal ions adsorbed on an electrode surface. Electrodeposition can effectively handle both copper and arsenic wastes, often with the production of pure elemental copper depending on the electrochemical parameters.[325,326] This method has also been used for secondary recovery of residual copper from low-content tailings derived from waste electrical cable.[327] These applications of electrodeposition rely on the same principle of removing metal ions from aqueous solutions that is used to charge aqueous metal flow batteries, such as zinc–air,[328] zinc–bromine,[329] zinc–iron,[330] and lithium–air batteries.[331]

1.2.6 Challenges and Limitations

Established nonelectrosorptive processes exhibit irreversible side reactions that consume significant amounts of energy and reduce current efficiency.[289] Depending on the complexity of the electrochemical matrix, a number of byproducts can be produced, some of which passivate the electrodes and further diminish performance.[284,289,332] For example, even though there were attempts as early as the

late 1800s to implement electrocoagulation and electroflotation at scale, these processes never evolved into mainstream technologies because of their prohibitively high operating costs.[284] Electrocoagulation and electroflotation have also lacked systematic studies aimed at scaling up the processes and optimizing their operating parameters.[284,308] These methods, however, remain promising for localized and small-scale applications, and they continue to offer interesting avenues for scientific research in interfacial science, electrochemical engineering, and reactor design.

1.3 Electrokinetic Separations

When current is applied across a pair of electrodes, ions and larger particles in solution are transported by electromigration and electrokinetic phenomena,[91,333–335] such as surface conduction, electroosmosis, and electrophoresis. Water purification by electrokinetics is based on the transport of contaminants in an electrolyte, and methods of this kind can be used to remove both organic[161,336–338] and inorganic[68,115,155,339] ions from water. Electrokinetic methods such as ED, EDI, and shock ED are continuous and involve an electric field that is perpendicular to the direction of fluid flow. These methods also include IEMs to fractionate the feed into diluate and concentrate streams. EDI and shock ED are similar in that a porous material (e.g., ion exchange resin beads, ceramics, clays, porous glass) is used to enhance mass transfer across the liquid to the solid phase. This unique feature of EDI and shock ED allows for currents beyond the ideal diffusion limited current and makes these methods well suited to remove trace contaminants from dilute feeds. In this section, we briefly discuss the operating principles and basic physics of ED and EDI. We then focus on the emerging method known as shock ED which is being reviewed for the first time. Our discussion of shock ED is preceded by an examination of the key developments in microfluidics and electrokinetic modeling that inspired the invention of shock ED as a method for water purification and ion separations. We conclude this section with a discussion of fouling phenomena and methods to overcome them in electrokinetic systems.

1.3.1 Electrodialysis

Basic Principles of Electrodialysis

ED is a membrane-based electrochemical method that was developed in the 1950s[114,340] for desalination of brackish water and for ion separations.[341–346] The operating principles and underlying physics of this method are summarized in Figure 1-8 (see refs 154,155 for detailed reviews of membrane phenomena in ED). The process begins by passage of the feed through a stack of parallel, nonporous cation and anion exchange membranes (CEMs and AEMs; see refs 347,348 for detailed reviews of IEMs and the state of their development). At the same time, direct current (DC) is applied across the stack, perpendicular to the direction of flow to separate ions in alternating channels of fresh water (diluate) and brine (concentrate). In the sections where diluate is produced, cations pass through CEMs and anions through AEMs on the opposite side, which lowers the concentration of uncharged salt in a boundary layer that grows into the channel downstream. In the sections where concentrate is produced, anions are retained by CEMs and cations by AEMs, which results in boundary layers of increasing salt concentration.[341,349,350] Once the boundary layers span the entirety of the channels, a condition termed "fully developed" forced convection,[351] the dissolved salts have been effectively transported from diluate channels into neighboring concentrate channels for discharge.

Depletion and enrichment of salt in unsupported electrolytes lead to self-generated diffusional electric fields that impede the transport of active ionic species through the phenomenon of "ion concentration polarization" (ICP). These electric fields arise to maintain electroneutrality via redistribution of the inactive (typically oppositely charged) ionic species. The additional internal voltage drop associated with variations in salt concentration relative to that of electrical conduction in a uniform bulk electrolyte (Ohm's law) is termed the concentration overpotential. When the salt concentration tends to zero, the concentration overpotential diverges and leads to a diffusion limited current, as long as the transport is dominated by electrodiffusion in a neutral unsupported electrolyte without the creation of any ad-

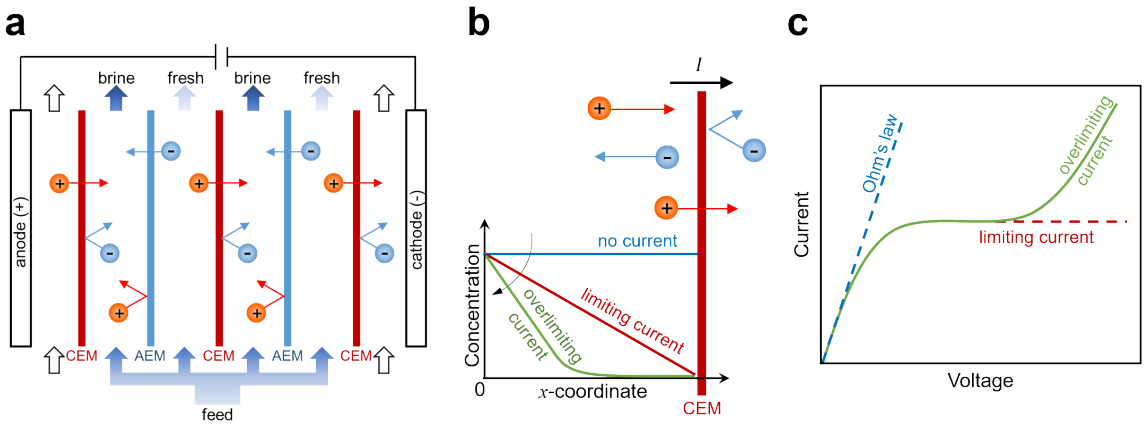

Figure 1-8. Operating principles and underlying physics of ED. (a) The feed flows through a stack of channels separated by alternating CEMs and AEMs, across which a current is applied. (These channels are filled with spacer material that physically separates the membranes, promotes turbulent mixing, and inhibits ICP and the formation of laminar boundary layers near the membranes.[352,353]) The concentration profiles of the ions exhibit axial growth of boundary layers of depletion and enrichment in the diluate and brine channels, respectively. Adapted with permission from ref 349. Copyright 1968, Elsevier. (b) Ion fluxes near a CEM and the associated convection–diffusion boundary layers, which become more strongly depleted with increasing current until the diffusion limit is reached. (c) The current–voltage relationship reaches a plateau at the limiting current, while overlimiting current, which results in an extended zone of ion depletion, is observed at higher voltages.

ditional ions.[334,354,355] For example, the mobilities of cations and anions in an electrolyte are comparable but may differ considerably in an IEM or a nanochannel with charged surfaces.[356] Salt depletion dramatically increases the electrical resistivity of the solution—which leads to significant departures from Ohm's law as shown in Figure 1-8—and limits the achievable rate of desalination by ED.[341–344,357] The current–voltage relationship for ICP in a symmetric ($z:z$) binary electrolyte resembles that of an ideal diode:

$$I = I_{\text{lim}} \left[1 - \exp\left(\frac{-zFV}{RT} \right) \right] \tag{1.1}$$

where I is current, I_{lim} is the diffusion limited current (or limiting current),[95] z is charge, V is voltage, F is Faraday's constant, R is the universal gas constant, and T is temperature. The maximum diffusion limited current, I_{lim}, is approached when a large potential difference (relative to the thermal voltage, $RT/F \approx 26\,\text{mV}$ at room temperature), V, is applied to the system, and as the salt concentration in the diluate sections approaches zero.

The theory of ED was pioneered by Peers[358], after which it was extended for arbitrary transference numbers by Rosenberg and Tirell[359] as well as for fully developed convection by Sonin and Probstein.[349] A useful approximation for the limiting current is given by the Peers equation,

$$I_{\text{lim}} = \frac{FDc_0}{\delta\left(\tau_\alpha - \tau_\beta\right)} \tag{1.2}$$

where c_0 is the bulk salt concentration, D is the effective salt diffusivity for coupled diffusion and electromigration (usually taken to be the ambipolar diffusivity in a dilute, binary electrolyte,[119,360] although concentration dependent corrections can be significant[361]), τ_α is an effective transference number for counterions that selectively cross the solution–membrane interface ($\tau_\alpha = 1$ for an ideal membrane or electrode),[342–344] τ_β is the transference number for counterions in the solution, and δ is the effective boundary layer thickness. This thickness scales as $\delta/H \sim \text{Pe}^{-1/3}$

in the Lévêque approximation,[341,349,351,362] where $\mathrm{Pe} = UH/D$ is the Péclet number, defined by the channel spacing, H, and characteristic fluid velocity, U. This theory is based on a boundary layer analysis of the steady convection–diffusion equation for an uncharged binary electrolyte,[341,351] where the flow is assumed to be fully developed and unidirectional and axial diffusion is neglected, as is usual for forced convection in straight pipes and channels.[351,363] Similar boundary layer approximations can be derived for membraneless flow batteries with forced convection over (selective) redox electrodes instead of IEMs.[364] Extensions for turbulent flow,[365] including effects of screen spacers to promote turbulent mixing,[366] were incorporated in a general equivalent circuit model of ED by Belfort and Guter.[367] Theoretical models were also used to calculate the pH profile[368] and analyze ion selectivity (e.g., K^+ versus Ca^{2+},[350] NO_3^- versus Cl^-[369]) in ED.

In practical systems, the ideal diffusion limited current is always exceeded when the applied voltage is sufficiently high, and possible mechanisms of this "overlimiting current" have been extensively studied in membrane science.[155,370] In bulk liquid electrolytes, there are two main kinds of mechanisms responsible for overlimiting current: electrochemical and electrokinetic.[371] Electrochemical mechanisms involve charge regulation[372–378] and self-ionization of water molecules,[72,358,379] both of which may lead to current induced membrane discharge[380] (i.e., loss of ion selectivity) and in turn passage of coions that would otherwise be repelled by the membrane. Electrokinetic mechanisms are based on the Rubinstein–Zaltzman electroconvective instability, where the EDL (either in[381] or out of equilibrium[382,383]) between the depleted solution and the membrane becomes hydrodynamically unstable to electroosmosis and in turn drives bulk vortices that transport ions to the membrane faster than diffusion would.[384–389] In ED, electroconvective mixing can enable overlimiting current and improve the transport of ions,[390] though at the expense of greater energy consumption compared to operating below the limiting current. These observations led the scientific community to develop ways to control electroconvection, including the use of topological heterogeneity—for example by patterning the surface of an IEM[389,391–394]—and pulsed electric fields.[395–399]

Phenomena resembling electroconvection also arise in metal electrodeposition, and they strongly influence the formation of patterns.[400,401] Understanding and controlling these instabilities in bulk electrolytes is a grand challenge, the solution to which could lead to novel electrochemical systems that benefit from operating in the exotic regime of overlimiting current, despite the higher energy demand.

The efficiency of ED depends on device structure (e.g., spacer thickness and geometry, number of cell pairs in the stack), membrane properties (e.g., material chemistry, concentration of the fixed ionic moiety),[366,402–406] electrode design (e.g., capacitive flow or membrane electrode, electrode redox couple),[407] operating conditions (e.g., electric potential, current density, hydrodynamics, temperature), and feed composition.[114,408] Based on their structure, commercial IEMs are classified as either homogeneous or heterogeneous.[409] A homogeneous IEM generally displays higher conductivity and permselectivity compared to a heterogeneous membrane because the latter comprises a larger insulating phase in its matrix as a result of the fabrication method.[410,411] A heterogeneous IEM, on the other hand, often has greater mechanical strength and is less expensive to manufacture.[412] The heterogeneous structure of such a membrane also promotes electroconvection and mass transfer by localizing the migration of ions through the conductive parts of the membrane.[389,413–417] Since a commercial ED stack may contain 300-500 cell pairs,[418] the conductivity of the membrane will largely determine the overall conductivity of the stack, which in turn influences the energy consumption of the process. Another critical feature of IEMs is their resistance to the formation of deposits (e.g., organic fouling, inorganic scaling) which degrade the performance of the membranes and negatively affect the quality of the water produced.[419,420] Much research has therefore been devoted to developing IEMs that have improved antifouling properties,[421–424] as discussed in Section 1.3.6.

Electrodialysis With Bipolar Membranes

One class of ED systems that remains an active area of research is based on bipolar membranes, which facilitate water dissociation without the need for chemi-

cals.[114,347,425–427] Bipolar membranes are fabricated by combining a CEM and an AEM, with a hydrophilic contact region separating the two IEMs. It is at this contact region where water is split into H^+ and OH^-, which migrate into acid and base compartments respectively, when an electric potential is applied. The primary benefits of using bipolar membranes with ED are that they catalyze the production of H^+ and OH^- at voltages lower than what is needed for standard electrolysis at an electrode, reduce the amount of brine generated, and increase the recyclability of the waste by recovering ions from the feed as their corresponding acids and bases.[58,428,429] The use of a bipolar membrane, however, also introduces an electrical resistance to the system that lowers the current efficiency. This decrease in efficiency is overcome by lowering layer resistance and incorporating weak ion exchange groups in the membrane.[430] As a result, the energy required to produce H^+ and OH^- with commercially available bipolar membranes is nearly equal to the theoretical minimum value.[430] (The theory of bipolar membranes is discussed extensively in refs 427,430–434.)

ED systems with bipolar membranes have several applications, one of which is the recovery of acids and bases from salts produced by chemical reactions or neutralization.[435–438] Because ions must first be separated to produce these acids and bases (e.g., Li^+ for LiOH, Na^+ for NaOH, SO_4^{2-} for H_2SO_4), this process desalinates a concentrated feed in the same way as conventional ED.[436,439–441] The first industrial process to employ ED with bipolar membranes was developed by Aqualytics to recover HF and HNO_3 from pickling baths in the steel industry.[436,442] Although commercial use of this technology remains limited due to the high cost, low permselectivity, and short lifetime of existing bipolar membranes,[114,436] novel applications are rapidly emerging, such as pH control, carbon capture, production and recovery of ammonia, and energy storage.[427]

Electrodialysis Driven by Chemical Energy

Recently, chemical energy was used in ED to simultaneously drive separations and generate electricity (Figure 1-9a).[443–446] Inspired by microbial desalination cells,[447,448]

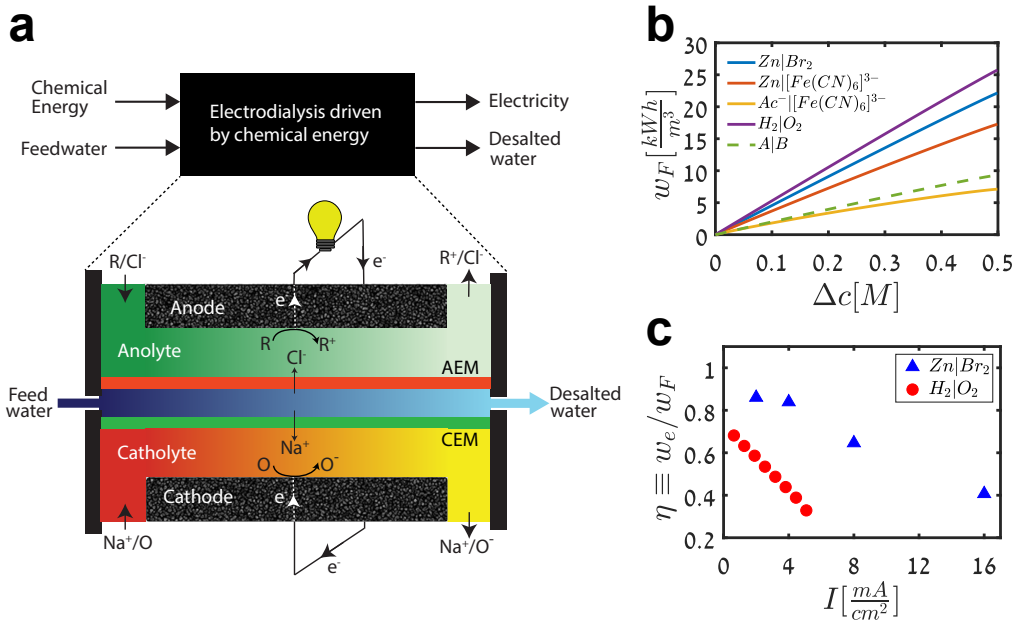

Figure 1-9. Operating principles of chemical energy ED. (a) Schematic of an ED cell driven by chemical energy, where a reductant R and oxidant O are used to drive desalination and generate electricity. Adapted with permission from ref 443. Copyright 2019, Elsevier. (b) Calculations of the maximum available energy from an ED cell driven by chemical energy for various redox couples. (c) Measured thermodynamic efficiency of ED cells driven by hydrogen–oxygen and zinc–bromine redox couples. Reproduced with permission from ref 449. Copyright 2020, The Electrochemical Society.

these ED systems are driven by inorganic redox couples, but they do not actually employ microbes as the use of microorganisms can limit electricity production and salt removal rates.[449] ED cells driven by chemical energy can simultaneously produce clean water and generate electricity by performing a combined reaction–separation process that is thermodynamically spontaneous. Atlas et al. calculated the maximum available energy from this combined process, as shown in Figure 1-9b, and quantified the thermodynamic efficiency of cells driven by chemical energy, as shown in Figure 1-9c.[449] The authors also found that, for certain chemistries, up to $25\,\mathrm{kWh\,m^{-3}}$ of electricity can be produced. This technology can thus generate significant excess electricity, well above what is that needed for pre- and post-treatment of the feed, which is approximately $1\,\mathrm{kWh\,m^{-3}}$ for seawater.[68]

The concept of chemical energy ED was tested with a variety of redox chemistries, including zinc–bromine[443], zinc–air[156], aluminum–air[445], hydrogen–oxygen[449–453]

and acid–base[454] couples. In particular, the hydrogen–oxygen couple is promising, as it relies on relatively inexpensive gas-phase reactants, and the product of the chemical reaction is simply water (Figure 1-9a); cells that use the hydrogen–oxygen chemistry are termed "desalination fuel cells."[446,449] Other chemistries that rely on liquid-phase reactants or that produce a waste product complicate disposal of the brine.[443,445] The hydrogen–oxygen chemistry, however, exhibits relatively low thermodynamic efficiency relative to other chemistries, such as zinc–bromine, mainly due to losses at electrodes attributed to (platinum) catalyst poisoning by halide ions in the brine (Figure 1-9c).[449,455] Therefore, a crucial area of research is the design and development of inexpensive catalyst materials tailored to long-term operation in desalination fuel cells. Asokan et al. demonstrated the use of chloride-tolerant, iron-based catalysts for oxygen reduction in a desalination fuel cell, which opens the field of non-platinum group metal catalysts for these systems.[456]

1.3.2 Electrodeionization

EDI, shown in Figure 1-10a, is typically used to generate highly pure products by processing feeds with low levels of dissolved solids (e.g., RO permeate).[128,457–461] This method originated in the late 1950s with the intent of enabling extreme deionization of contaminated feeds by packing the channels of an ED stack with charged porous media or conductive ion exchange resin beads.[61,106] The purpose of these conductive materials is to reduce the ICP observed in ED by enhancing transport of ions via electrokinetic phenomena (see Figure 1-11c and Figure 1-13). As in ED, ions are depleted in the diluate compartments of an EDI stack and are concentrated in the adjacent (concentrate) compartments because of the permselective properties of the IEMs. To deionize the electrolyte while maintaining reasonable conductivity across the stack, however, a conductive material (ion exchange resin, for example) is needed to lower the resistivity of the electrolyte in the diluate compartments.[61,462] As shown in Figure 1-10b, there is an optimal current density that is believed to coincide with the limiting current introduced in Section 1.3.1.[463] Another, more subtle reason ion exchange resin is used in the diluate compartments in

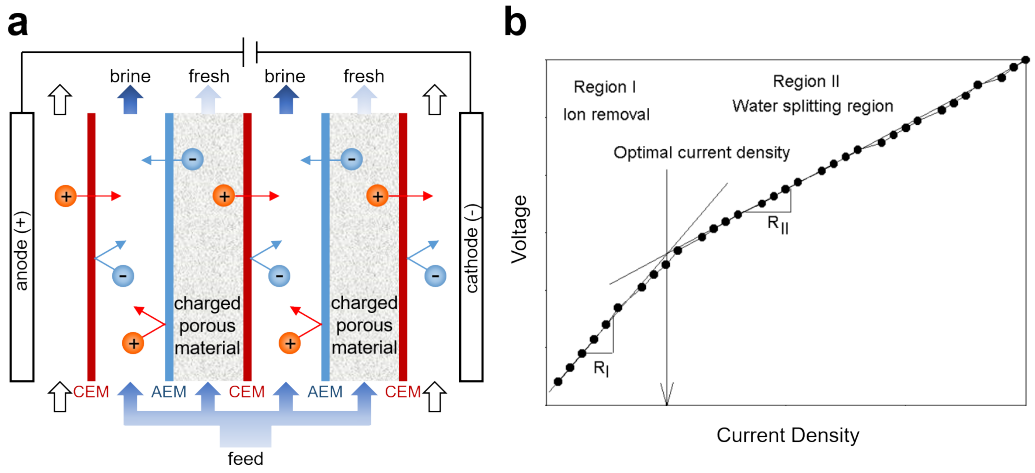

Figure 1-10. Design and operating principles of EDI. (a) As in ED, ions are depleted in the diluate compartments of an EDI stack and are concentrated in the adjacent (concentrate) compartments due to the permselective properties of the IEMs. In EDI, however, the use of a charged porous material (usually ion exchange resin) enables extreme deionization by boosting the conductivity of the electrolyte in the diluate compartments. (b) Typical current–voltage relationship in EDI, which reveals the existence of two regions with distinct resistivities (characterized by the slope of the graph). Reproduced with permission from ref 463. Copyright 2005, Springer.

EDI is to regulate the pH of the product streams by exploiting the relationship between the applied electrical current and the equilibrium concentrations of H^+ and OH^- in solution.[464]

As illustrated in Figure 1-8c, a typical ED cell exhibits a dramatic increase in electrical resistivity when salt is depleted from the diluate compartments. Because the concentration of ions in these compartments is smaller near the membranes than it is in the bulk, water dissociation occurs and reduces current efficiency.[465,466] The use of ion exchange resin (whether as loose beads or as a wafer[83,467,468]) in EDI mitigates this effect by promoting transport in a conductive medium, which functions as a bridge for ions between membrane pairs. The current–voltage curves in Figure 1-11 show that EDI maintains increasingly higher conductivity (or lower resistivity) than ED as a function of applied voltage.[128] Pathways of charge transfer in the ion exchange bed of an EDI cell are often studied using the porous plug model[469–471] introduced by Wyllie and coworkers.[472] The overall conductivity of the ion exchange bed is the sum of the conductivities of the ion exchange resin and

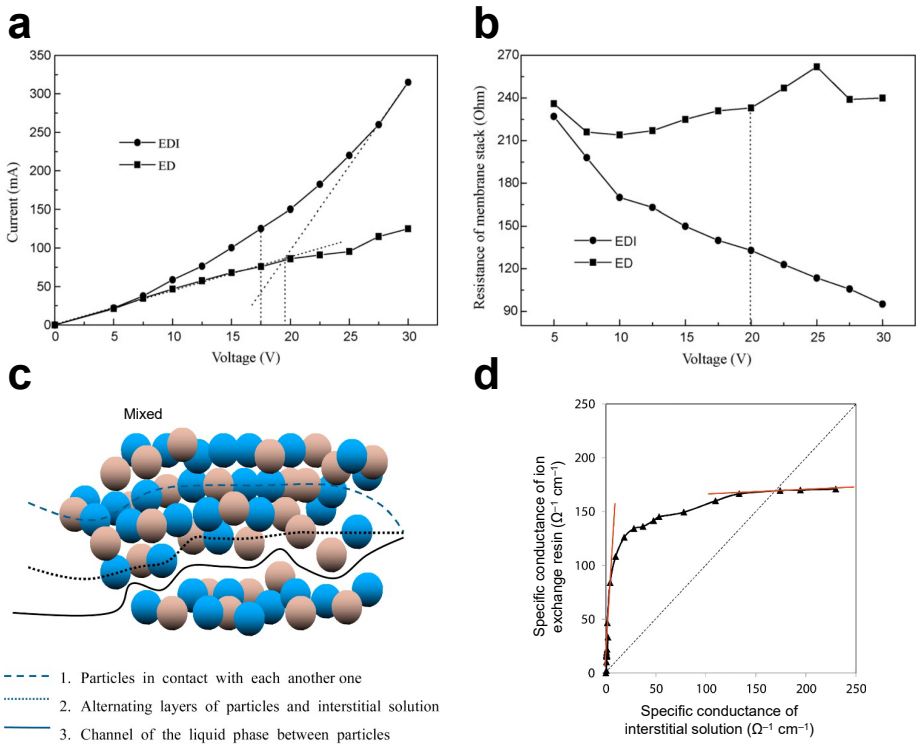

Figure 1-11. The role of ion exchange resin in EDI. Comparison of (a) current–voltage and (b) resistance–voltage relationships in ED and EDI. Reproduced with permission from ref 466. Copyright 2009, Elsevier. (c) Schematic of the three pathways for charge transport in a mixed bed. (d) Specific conductance of the ion exchange resin versus that of the interstitial solution. Reproduced with permission from ref 471. Copyright 2015, Elsevier.

interstitial solution. These conductivities are sustained via three different pathways, namely the resin (solid), the interstitial solution (liquid), or both (solid–liquid), as shown in Figure 1-11c. Alvarado et al. studied these pathways using an EDI cell as a mixed bed to treat a synthetic solution containing chromium at concentrations up to 250 mg L^{-1}.[471] In this system, nearly 82.9% of the electric charge was transported by the combined solid–liquid pathway, whereas only 0.6% was transported by the interstitial solution alone. In total, the ion exchange resin, alone or in combination with the interstitial solution, contributed to approximately 94% of ion transport, which underscores the crucial role of ion exchange in driving charge transfer in EDI (Figure 1-11d).

In addition to facilitating the migration of ions, ion exchange resin enables operation beyond the limiting current, at which diffusion of ions becomes the rate-

limiting step in electrochemical separations.[473] Operating in the regime of over-limiting current leads to water dissociation and exotic electrokinetic phenomena like the electroconvective instability,[370,474,475] as was microscopically visualized by Park and Kwak as well as Stockmeier et al.[476,477] In EDI, water dissociates due to the presence of bipolar zones formed at points of contact between resin particles and either other resin particles or IEMs.[26,467] As the ion exchange resin traps ions, H^+ and OH^- produced by water dissociation act as charge carriers and regenerate the resin through the process of electroregeneration.[106] Water dissociation is also important when complete removal of weakly ionized species, such as silicon and boron, is needed to produce ultrapure water. The OH^- generated by this dissociation reacts with silicon and boron as follows:[478]

$$SiO_2 + OH^- \longrightarrow HSiO_3{}^- \tag{1.3a}$$

$$HSiO_3{}^- + OH^- \longrightarrow SiO_3{}^{2-} + H_2O \tag{1.3b}$$

$$H_3BO_3 + OH^- \longrightarrow B(OH)_4{}^- \tag{1.3c}$$

Once the neutral species SiO_2 and H_3BO_3 become ionized, they are readily transported into the concentrate compartment and discharged.

Another useful function of the ion exchange resin in EDI is that, as a selective medium, it preferentially removes ions based on their affinity to the resin.[57] Selective separation of ions with similar charge and size can be achieved by controlling the mobility of these ions with a complexing agent.[479,480] For example, Taghdirian et al. used a complexing agent made of ethylenediaminetetraacetic acid (EDTA) to separate Ni^{2+} from Co^{2+}.[480] This complexing agent formed a strong bond with Ni^{2+}, which produced a negatively charged complex whose mobility was inhibited in the bed of cation exchange resin. On the other hand, Co^{2+} remained a free cation that could readily enter the gel phase of the resin. By removing Co^{2+}, the molar ratio of Ni^{2+} to Co^{2+} in the solution was increased from 3 to over 150.[480]

Although the microscopic mechanisms of EDI have received much less attention compared to those of ED, there have been several efforts to mathematically

model[107,461,481–484] and numerically simulate[485–488] the process of EDI. Early descriptions of EDI proposed that the removal of ions occurs in two steps.[489] First, ions diffuse from the bulk to the liquid–solid (resin) interface, where counterions are exchanged with mobile ions on the resin. Second, the adsorbed counterions are transported toward and across the corresponding IEM, where they are released into the concentrate compartments. Removal of ions is controlled by the rate of diffusion from the aqueous phase to the surface of the solid.[128,489] This rate is determined by the properties of the solid surface, the thickness of the liquid layer through which ions diffuse, and the concentration gradient between the two phases. When a current is applied beyond what is needed for the electromigration of ions to the surfaces of the resin, water molecules dissociate into H^+ and OH^-, which replace the ionic contaminants that have adsorbed on the resin.[128]

1.3.3 Electrokinetics in Nanochannels and Membranes

While nanofabricated devices are difficult to manufacture at scale, the scalable polymeric IEMs used in ED, EDI, and shock ED are essentially made of a network of nanoscale pores with high charge densities, as shown in Figure 1-12a.[340,347,490,491] This nanoscale structure promotes selectivity based on the charge of an ion and on chemical interactions between the ion and the pore walls.[492] IEMs are an integral component of many electrochemical methods of water purification, and this fact underpins the development of membrane properties like conductivity and selectivity.[340,347,493,494] There also exist exciting opportunities for enhanced separations as well as reduction in fluidic resistance using engineered nanoscale conduits like CNTs[495–498] and graphene,[499–501] but the success of these technologies in practice requires a high density of channels and a scalable and controlled fabrication process.

A membrane or surface in contact with an electrolyte solution either already has or will acquire a net charge, and under most circumstances, this surface charge is balanced (or screened) in the liquid by a diffuse layer of oppositely charged ions.[334,335] This concept of an “electric double layer” was originally proposed by

Helmholtz,[502] later refined by Gouy and Chapman,[503,504] and revised once more by Stern.[505] The local diffuse charge leads to electroosmosis and diffusioosmosis in response to an electric field and concentration gradient, respectively.[91] The equations that govern transport in charged nanoporous media are therefore coupled, such that gradients in pressure, concentration, or electric potential (Figure 1-12b) lead to combined fluxes in fluid flow, salt transport, or electrical current.[506] Gross and Osterle described the set of coupled transport phenomena by the Poisson–Nernst–Planck–Stokes (PNPS) equations, with assumptions of local equilibrium and electroneutrality in the cross sections of pores.[507] This approach presents a unified theoretical framework to describe ion and fluid transport in charged porous media down to the nanoscale, and it can be used to model ED, EDI, and shock ED. Recent work extended these results to numerically solve the PNPS equations[508] and describe nanofluidic transport in nanopores.[506] Systems modeled in this way include homogeneous networks with pores connected in series or in parallel as well as heterogeneous networks with pores of varying cross section.[509–511] The homogenization of the PNPS equations to heterogeneous porous media revealed complex flow patterns and vortices due to parallel connectivity in these materials.[512] Other models incorporated chemical interactions, mismatch in the diffusion coefficients,[513] multicomponent electrolytes,[514–516] electroviscous effects,[517] nonionic solutes,[513] salts with asymmetric valences,[518,519], reactions of fixed charges,[520,521] temperature gradients,[522] electron conducting[523] or polarizable nanopores,[524] and dielectric effects[514,515,525–527] to describe the distribution of ions and solvent molecules in the pores. Analytical approximations to the nonlinear transport equations are valid when the surface potentials are small[528] or when the EDLs are overlapping.[506]

Perhaps the most fundamental principle of nanofluidic transport is electroneutrality, which is an implicit assumption embedded in the models previously discussed that dictates that the charge within a pore must balance the charge on the pore walls. Indeed, in deionization processes such as EDI and shock ED, the strong tendency toward electroneutrality in charged nanopores allows for residual conductivity—even as the concentration of ions in the bulk goes to zero—because

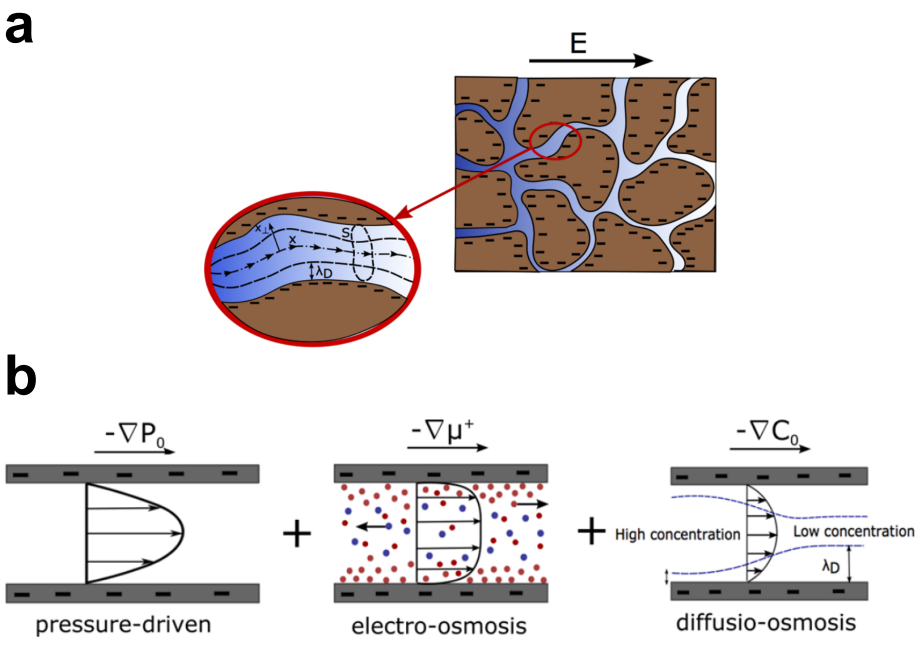

Figure 1-12. Electrokinetic transport in charged porous media. (a) Schematic of a charged porous medium with solid (brown) and porous (blue) domains. Ion and fluid transport occur along the center axes of pores. The thickness of the EDLs and the amount of surface charge influence the electrokinetic coupling. (b) Fluid can flow due to gradients in pressure, electric field, or electrolyte concentration. Ion separations use these modes of transport to impart selectivity based on electric charge. Reproduced with permission from ref 509. Copyright 2017, American Chemical Society.

counterions screening the surface charge are always present at a concentration determined by this charge.[94,356,529,530] Levy et al., however, recently showed that one-dimensional confinement of ions to an isolated nanochannel in a dielectric matrix can lead to breakdown of cross-sectional electroneutrality, as the screening length diverges exponentially with decreasing ion concentration.[531] Under these conditions, which are typical of biological ion channels,[532] the role of ion-specific chemical interactions becomes more significant than that of electroneutrality, although this order of importance is reversed in membranes where the distance between parallel channels becomes smaller than their lengths.[533] In addition to energy barriers to enter a pore, intrapore energy barriers can govern ion transport in one-dimensional pores, where ions are confined to the molecular scale.[534]

Other open questions exist about the structure and dynamics of ions and solvent molecules in the EDL, particularly at high ionic strength[535,536] or in the case of extreme confinement.[492] Discrepancies between molecular dynamics (MD) simulations and continuum electrokinetics predictions occur for channels with widths of $\sim 1\,\mathrm{nm}$.[492,537] As another example, overscreening of surface charge at high concentration can lead to reversal of electroosmotic flow,[538,539] and a high surface charge density can cause electric charge to crowd an interface.[536,540,541] A theoretical explanation of these phenomena requires consideration of electrostatic correlations in the EDL that go beyond the mean-field electrostatic potential.[538,542,543] Transport models of dense ionic solutions can account for these correlations as well as coupled transport modes due to friction between pairs of species. For example, transport equations based on the Stefan–Maxwell model have been used to describe the coupled fluxes of ions and solvent molecules passing through nanoporous membranes.[544–547] Regardless of the model, fixed surface charge influences the distribution of ions in a nanopore and in turn the observed transport properties. The regulation of surface charge via chemical reactions also affects transport dynamics.[374,377,548–551] While the surface charge is usually assumed to be in equilibrium, nonequilibrium reactions can participate in electrokinetic transport.[552,553]

1.3.4 Ion Concentration Polarization in Microfluidics

The physical phenomenon that enables shock ED—the deionization shock wave—was first discovered and studied in the seemingly distinct context of ICP in microfluidic devices.[92,93,356,554–560] What we now understand to be stationary deionization shock waves were observed by Wang et al. as early as 2005 in a microchannel near a nanochannel junction and used to trap and concentrate biomolecules in cross flow, albeit without a theoretical explanation of the mechanism.[561] In 2010, Kim et al. reported a microfluidic system that used ICP to desalinate seawater by applying current in the direction of flow and across a nanochannel junction,[558] albeit at very low efficiency and in nanoliter volumes.[559] A sharp, stationary depletion region was observed behind the nanojunction, and the deionized fluid below the shock was separated from the enriched brine into different microchannels. Separation of all charged solutes into the brine channel was also claimed,[562] although this would appear to contradict the theory of electrodiffusiophoresis,[563] which predicts the dominance of electrophoresis (motion in the direction of the Coulomb force) over diffusiophoresis (climbing salt concentration gradients, regardless of the charge sign) and suggests that fast-moving, positively charged particles in the deionized channel may not have been detected in the experiments.

The breakthrough in understanding microfluidic ICP that paved the way for shock ED occurred in 2009, when Mani, Zangle, and Santiago theoretically modeled[92] and experimentally observed[93] propagating ion concentration shock waves for the first time in a microchannel–nanochannel device with negatively charged surfaces. Two microchannels were filled with a stagnant electrolyte and were separated by a nanochannel with thick, overlapping EDLs, which behaved like a CEM to induce ICP and initiate a shock wave of salt depletion in one direction and salt enrichment in the other. Mathematical modeling revealed how the nonlinear drift arising from electromigration (competing with electrodiffusion) can create breaking waves of salt concentration and propagating shocks,[92] analogous to the shock waves that arise in isotachophoresis[564,565] and capillary electrophoresis.[566,567]

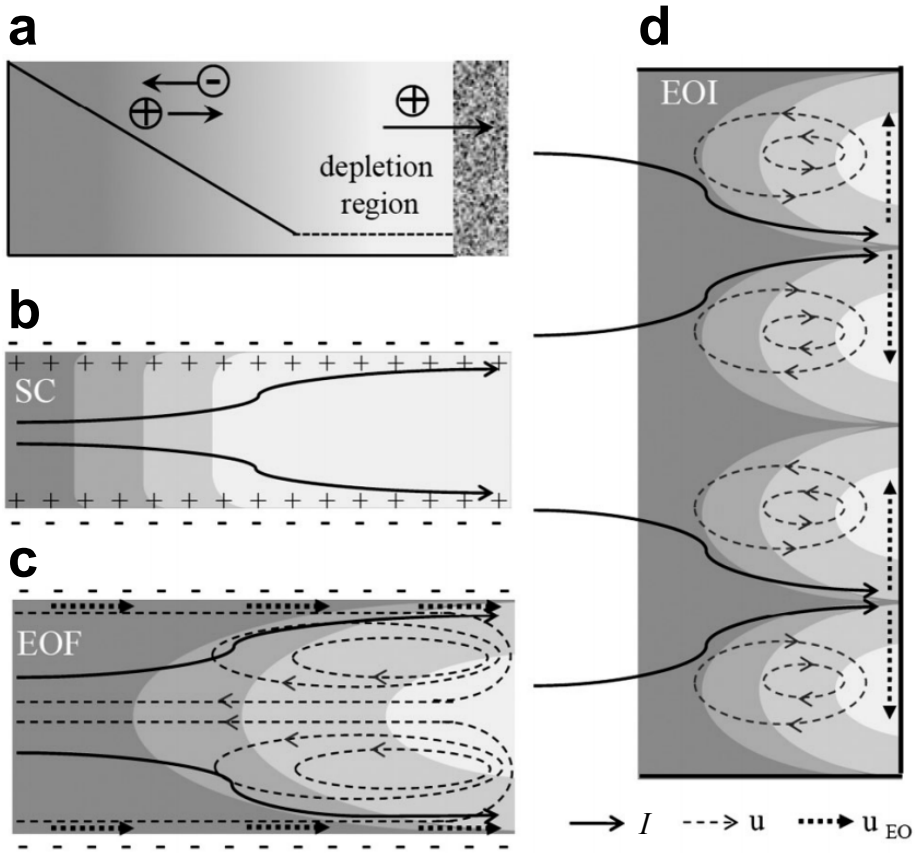

Figure 1-13. Cartoon representations of common mechanisms to sustain overlimiting current in a microchannel between a reservoir on the left and a CEM on the right. The volume average conductivity in (a) exhibits classical linear diffusion (continuous line) up to a region of depletion (dashed line), where charge carriers are transported by (b) surface conduction, (c) electroosmosis, or (d) electroconvection (visualized experimentally by Gu et al.[568]). The relative contributions of these effects depend on the width of the channel, such that surface conduction dominates in narrow channels and electroconvection in wide ones. Reproduced with permission from ref 529. Copyright 2011, American Physical Society.

1.3.5 Shock Electrodialysis

Deionization Shock Waves in Microstructures

While developments in microfluidics have been critical to advancing the scientific understanding of ICP under strong confinement, microfabricated lab-on-a-chip devices are neither scalable nor efficient for macroscopic ion separations and water treatment. To produce any meaningful volume of water, a prohibitively large number of channels or devices would need to be fabricated and operated in parallel. Porous media, on the other hand, represent a much more compact system of interconnected microchannels in parallel that can be manufactured at scale (consider ion exchange resin beads, ceramics, clays, and porous glass as examples). Moreover, theoretical and experimental work have demonstrated that overlimiting current can in fact be sustained in charged porous media.[94,95,569–572]

In 2011, Mani and Bazant demonstrated the propagation of deionization shock waves in porous microstructures by theory and simulation.[94] At the same time, Dydek et al. described the transport processes that enable overlimiting current in a charged microchannel, as shown in Figure 1-13.[529] This work explained that electroosmosis dominates the transport of ions when an electrolyte is confined to small pores ($\sim 100\mu$m). When the pores are even smaller ($\sim 1\mu$m), surface conduction becomes the dominant mechanism of overlimiting current. Experimental visualizations by Nam et al. later confirmed the theoretical predictions of the regimes in which surface conduction and electroosmosis sustain overlimiting current in a microchannel.[560,573] These observations and discoveries served as the foundation for developing a novel technology that can purify water by deionization shock waves in porous media. Deionization shocks have also proven useful in controlling the high-rate electrodeposition of metals in charged nanopores,[571] where shock electrodeposition can suppress dendritic growth[574] and enable resistive switching memory[575] and rechargeable metal batteries.[576]

In 2013, Deng et al. reported empirical evidence for overlimiting current—sustained by surface conduction and electroosmosis—and deionization shock waves

in a charged porous material.[95] This study was the first to observe these phenomena in porous media, and it demonstrated the feasibility of shock ED as a new platform to desalinate water and perform electrochemical separations.[95,577] The basic design of the original shock ED system used a silica glass frit (weakly charged porous material) sandwiched between two electrodes (which can be thought of as strongly charged porous material; recall the microchannel–nanochannel geometry of Mani et al.[92]), as shown in Figure 1-14. (Note that the porous material and the IEM must have surface charges of the same sign. This condition ensures the propagation of depleted and enriched regions.[93]) Since overlimiting current is sustained in shock ED to form a deionization shock wave near the cathodic CEM, as shown in Figure 1-14c, it is possible to deionize the feed to concentrations well below what could be achieved by standard ED. The experimental work by Deng et al. indeed demonstrated that shock ED can produce deionized water with concentrations of $\sim 10\mu$M (see Figure 1-14d).[95] In the same year, the nonlinear dynamics of ICP in porous media were mathematically described by Dydek et al. using a homogenized model (which assumes that the EDLs are thin relative to the nominal pore size), with emphasis on water treatment by shock ED.[530] These two publications also proposed a scalable shock ED system that would be operated continuously.

The original shock ED system by Deng et al. was a radially symmetric button cell that had to be operated in batch mode.[95] This geometry made it difficult to scale up the system, and it was clear to the authors at the time that a continuous process was more desirable. The second generation of shock ED devices, built by Schlumpberger et al. then improved by Conforti and Alkhadra, had a rectangular geometry and was shown to remove more than 99.9% of the salt present in solution.[87,578] This new system used a silica frit sandwiched between two CEMs and included a splitter at the outlet between the two membranes to partition the flow into a diluate and a concentrate, as shown in Figures 1-15 and 1-16a. In the range of concentrations tested using binary electrolytes of monovalent ions, Schlumpberger et al. showed

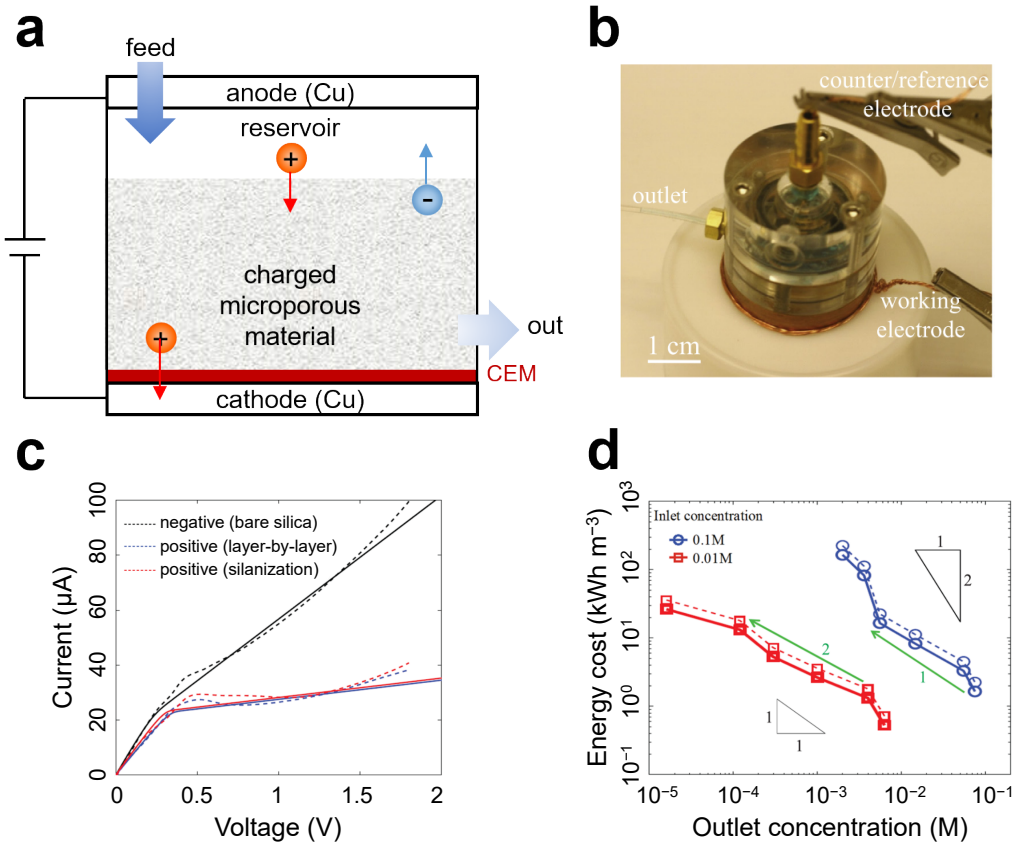

Figure 1-14. Prototype "button cell" used for shock ED. (a) Rectangular cross section and (b) photograph of the button cell prototype. This device is a cylindrical macroporous material submerged in an electrolyte and placed between copper electrodes. Electrical current is driven by the electrodeposition of copper onto the bottom electrode. (c) Current–voltage relationship in shock ED with 1 mM aqueous $CuSO_4$ as the electrolyte; the effect of the sign of surface charge is also shown. Dashed lines represent experimental data and solid lines represent the fit to a theoretical model. (d) Energy cost per unit volume of deionized water with (dashed lines) and without (solid lines) the series resistances due to the reservoir and electrodes. Reproduced with permission from ref 95. Copyright 2013, American Chemical Society.

that desalination was a function of only dimensionless current:

$$\widetilde{I} = \frac{I}{I_{\text{lim}}} \quad \text{with} \quad I_{\text{lim}} = z_+ c_+ F Q \tag{1.4}$$

where z_+ and c_+ correspond to the charge and concentration of the cation and Q is the volumetric flow rate of the feed. This definition of I_{lim} can be interpreted as the rate of advection of positive charge across the device; it is assumed that the flux of anions is zero across ideal CEMs. The authors also described the effect of electroosmosis on the fraction of liquid recovered as desalinated water from the contaminated feed, often referred to in the literature as the water recovery. Because the zeta potential of the glass frit is negative, the applied electric field induces electroosmosis in the same direction[351,579] (i.e., toward the depleted region near the cathode) and as a result increases water recovery (to above 80% at high current[87]). This effect resembles the function of an electroosmotic pump originally used in microfluidic devices[580,581] and later studied in relation to ICP in microchannels.[582]

To improve the mathematical model developed by Dydek et al. following these modifications,[530] Schlumpberger et al. considered the role of linear electroosmotic flow and captured some aspects of deionization and water recovery observed experimentally.[583] The model, however, significantly overestimates the extent of deionization and underestimates the overlimiting conductance. Recently, Tian et al. developed a more comprehensive model of shock ED that is valid for multicomponent electrolytes (irrespective of EDL thickness), captures the phenomena of electroosmosis, diffusioosmosis, and water dissociation, and incorporates more realistic boundary conditions.[584] This model also describes the role of electroosmotic vortices at the inlet and outlet of the system, and it considers the effect of hydronium transport. Figure 1-16c shows the profiles of concentration, electric potential, and velocity obtained from numerical simulations, which have enabled quantitative predictions of deionization and overlimiting conductance that agree with the experimental data in ref 87.

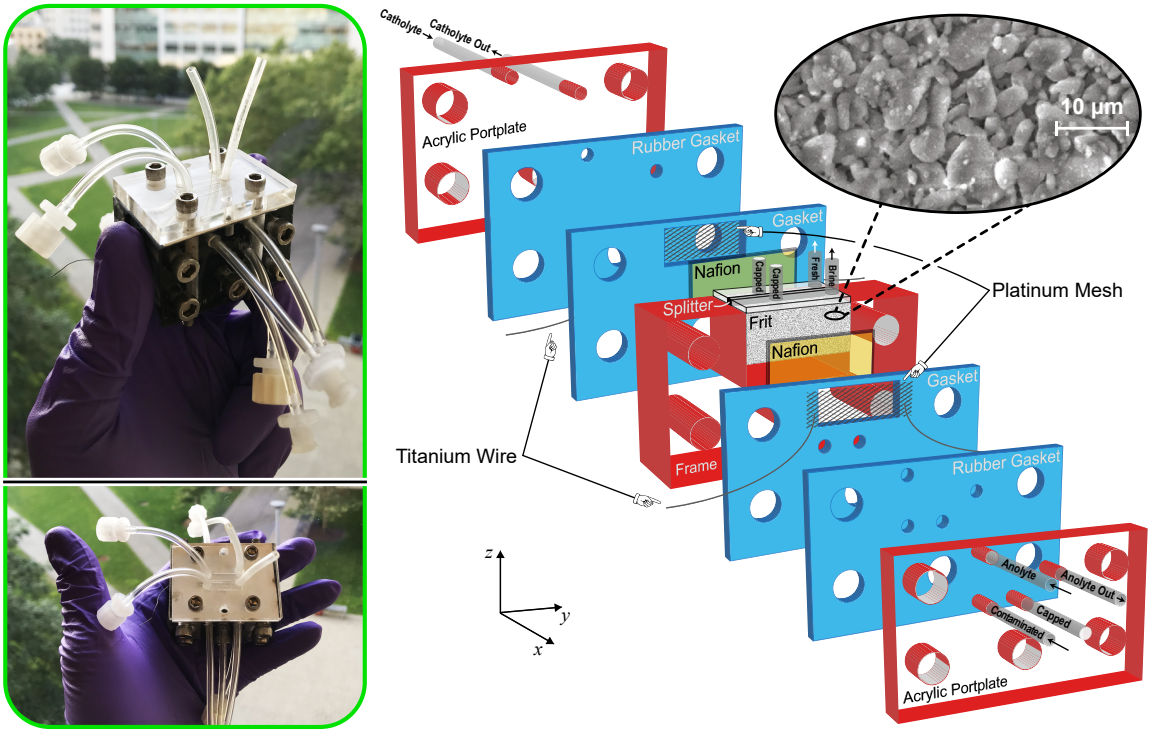

Figure 1-15. Shock ED as a continuous process. (left) Photographs and (right) illustration of the device that shows assembly: a working device consists of electrodes, wire, and a porous material sandwiched between identical IEMs. Inlet (outlet) streams are labeled contaminated, anolyte (anolyte out), and catholyte (catholyte out); fluid leaving the top edge of the porous material is split into fresh and brine streams. Reproduced with permission from ref 578. Copyright 2019, American Chemical Society.

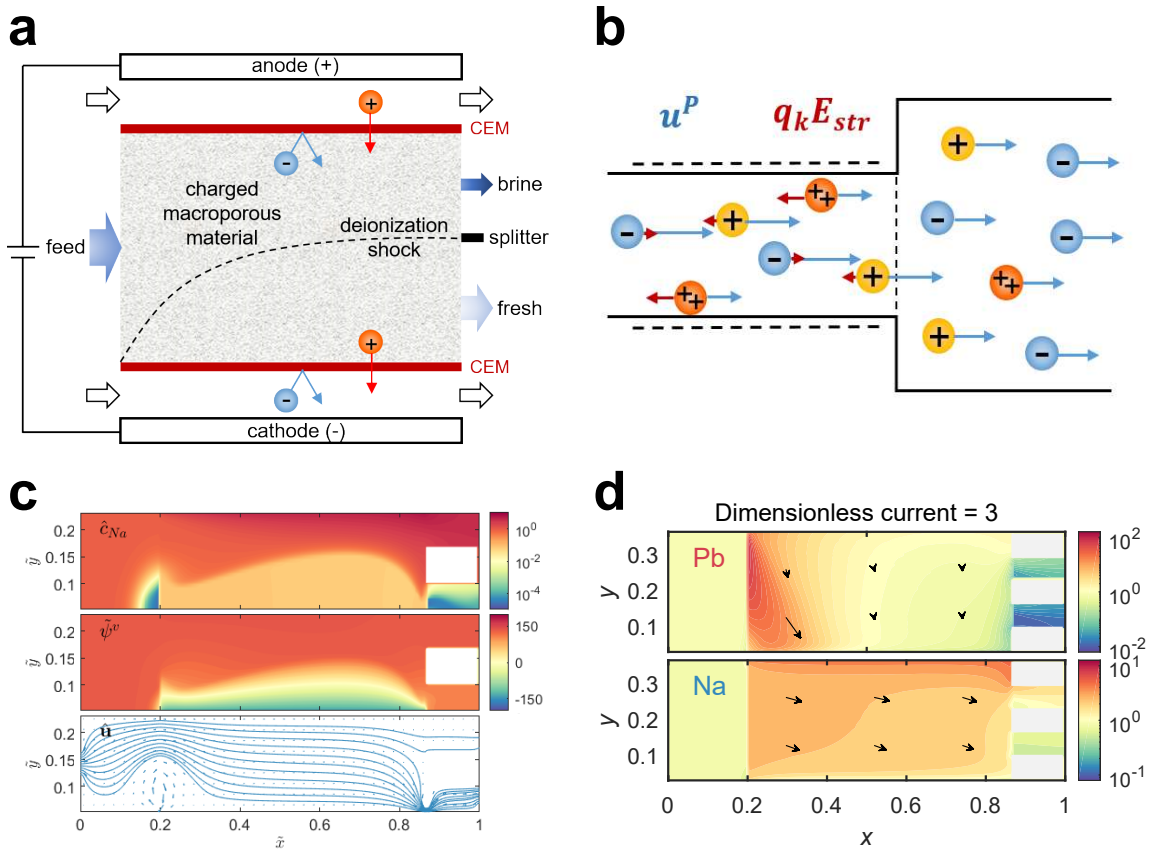

Figure 1-16. Operating principles and representative simulation results of shock ED. (a) Contaminants are transported by an electric field perpendicular to the flow, and the electrical current is driven by water redox at the electrodes. (b) Schematic to illustrate ion transport by advection (blue arrows) and streaming potential (red arrows) at the interface between a charged channel and the outlet. u^P is the hydrodynamic flow velocity and $q_k E_{\text{str}}$ is an electrostatic force generated by the streaming potential, where q_k is electric charge and E_{str} is electric field. Reproduced with permission from ref 585. Copyright 2021, American Chemical Society. (c) Steady-state profiles of concentration (c), electric potential (ψ), and velocity ($\mathbf{u}$) at a dimensionless current of 5. The velocity profile shows distortion of the depletion zone by electroosmotic vortices. The feed to all channels is $10\,\text{mM}$ NaCl aqueous solution at a pH of 7. Reproduced with permission from ref 584. Copyright 2021, Elsevier. (d) Contour plots of dimensionless, depth-averaged concentration and flux vectors for Na^+ and Pb^{2+} at six sample locations in the porous material. Reproduced with permission from ref 585. Copyright 2021, American Chemical Society.

Selective Separations by Shock Electrodialysis

The design introduced by Schlumpberger et al. was the first example of a scalable device that could be used for shock ED.[87] Recent work by Čížek et al. upgraded this design by using a multistack device with AEMs and various porous materials to remove Na^+.[586] In both studies, however, only binary electrolytes of monovalent ions were considered, which encouraged examination of selective removal of multivalent ions. This research began with a systematic study in which Mg^{2+} was selectively removed from an aqueous mixture of NaCl and $MgCl_2$.[109,587] For a feed with Na^+ and Mg^{2+} in molar proportions of nine to one, more than 99% of the Mg^{2+} was removed, even though the total desalination was only 68%. This outcome implied that the divalent ion was selectively removed in the presence of a competing monovalent ion. The results of this work inspired further research into the kinds of contaminants that can be targeted by shock ED in the presence of competing ions. The first of these studies used shock ED in two passes to desalinate artificial seawater (3.5 wt. %), from which 99.8% of the salt fed was rejected and more than 99.99% of the Mg^{2+} was removed, as shown in Figure 1-17a.[588] These results also revealed selectivity toward Mg^{2+}, which was preferentially removed relative to all other species by at least one (Mg^{2+}:K^+) and up to nearly two orders of magnitude (Mg^{2+}:Ca^{2+}). Scaled (retention) selectivity in the fresh stream was calculated as a function of dimensionless current between each pair of unique species i and j using the equation[109]

$$S_{j:i} \equiv j:i = \frac{c_{i_{\text{out}}}/c_{j_{\text{out}}}}{c_{i_{\text{in}}}/c_{j_{\text{in}}}} = \frac{c_{i_{\text{out}}}/c_{i_{\text{in}}}}{c_{j_{\text{out}}}/c_{j_{\text{in}}}} \tag{1.5}$$

For example, if $S_{j:i}$ was greater than one, then species j was selectively removed relative to species i. Despite the high rejection of salt and extreme selectivity toward Mg^{2+}, desalination of seawater by shock ED was energy intensive. It was therefore concluded that a more suitable application of this technology is to target trace contaminants in dilute feeds, such as toxic heavy metals in drinking water or radioactive ions in the process water of a nuclear reactor (i.e., water used in the boiler or for cooling).

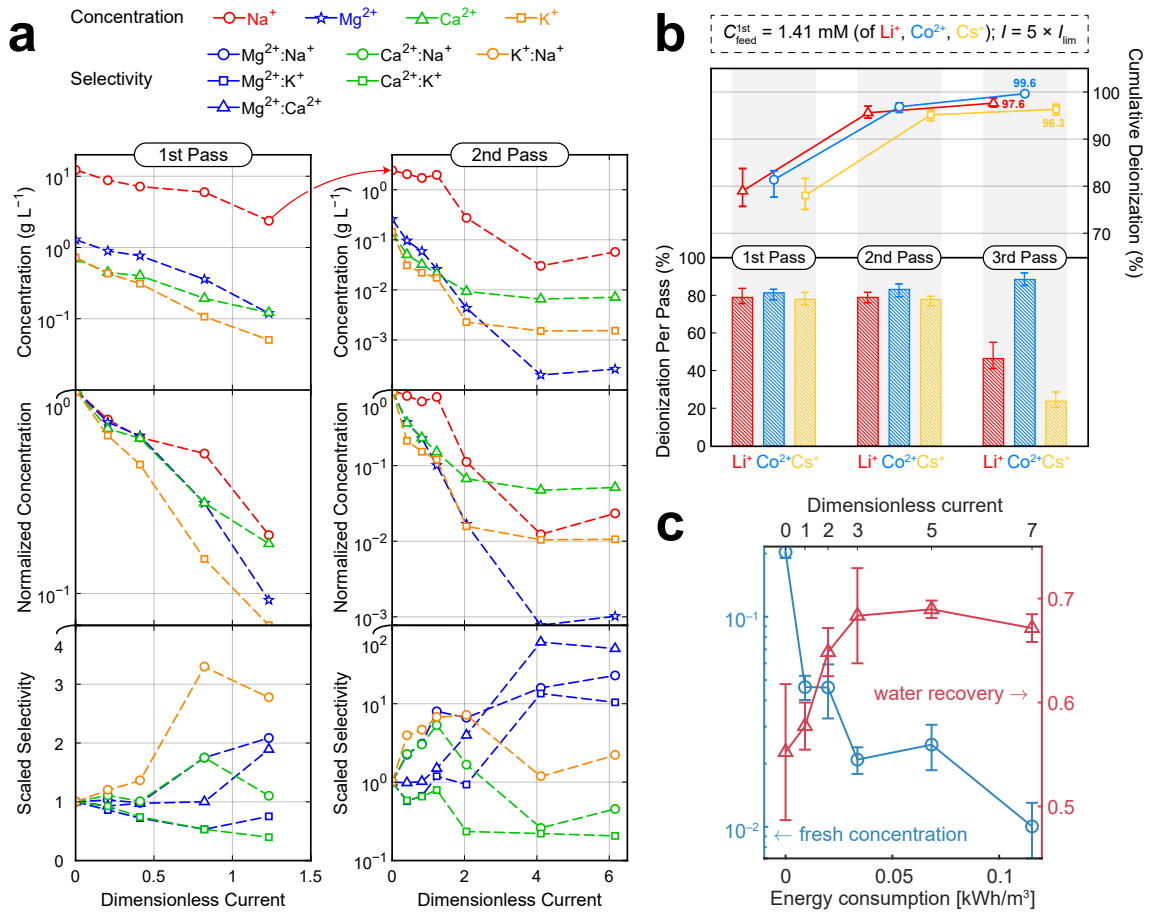

Figure 1-17. Representative experimental results of shock ED. (a) Concentration per pass (top and middle) and scaled selectivity (bottom) as functions of dimensionless current for the most abundant cations in seawater. Reproduced with permission from ref 588. Copyright 2020, Elsevier. (b) Deionization per pass (bottom) and cumulative deionization (top) at a dimensionless current of five for three cations normally present in the process water of light-water nuclear reactors. Reproduced with permission from ref 578. Copyright 2019, American Chemical Society. (c) Normalized concentration of Pb^{2+} and water recovery as functions of dimensionless current for removal of Pb^{2+} from water in the presence of excess competing Na^{+}. Reproduced with permission from ref 585. Copyright 2021, American Chemical Society.

Nuclear fission is a common method to produce energy in a nuclear reactor, though this process leads to contamination of the process water with several dissolved species, some of which are radioactive.[589,590] It is often desirable to selectively accumulate the radionuclides to reduce the volume of nuclear waste and facilitate its containment or disposal.[591–593] Shock ED was thus used to selectively and continuously remove cobalt and cesium from a feed of dissolved lithium, cobalt, cesium, and boric acid.[578] This formulation modeled the contaminated water normally found in light-water nuclear reactors and in other nuclear processes.[594–597] Figure 1-17b shows deionization per pass and cumulative deionization for each species (with the exception of boron which was present predominantly as the electrically neutral boric acid) in three passes. In each of the first two passes, all three species were removed in nearly equal proportions, but in the third pass, Co^{2+} was preferentially removed. Overall, the three-step process led to a high cumulative deionization for each species, ranging from 96.3% for Cs^{+} to 99.6% for Co^{2+}. Based on these results, a clear and consistent tradeoff was observed between the extent of purification (as well as water recovery) and the energy demand of the process. In general, however, the energy demand of this process (which has not yet been optimized) was low, ranging between $1.8\,kWh\,m^{-3}$ and $4.8\,kWh\,m^{-3}$, because only charged species were targeted and essentially no energy was expended removing boric acid, the most abundant species in the mixture.

Similar to radioactive species, heavy metals can damage normal functions of the human body and lead to heavy metal poisoning. Affordable and effective removal of toxic heavy metals from water, especially in the presence of excess competing ions, has been a longstanding goal in environmental science and engineering.[598] Tian et al. recently demonstrated low-cost, continuous, and selective removal of Pb^{2+} from simulated drinking water using shock ED.[585] As shown in Figure 1-17c, this process removed over 98% of Pb^{2+} (to safe levels[599] below 1 ppb) with a water recovery of 70% and at an energy cost of $0.1\,kWh\,m^{-3}$. At the same time, only 40% of Na^{+} was removed, which maintained electrolyte conductivity and lowered the energy demand of the process relative to nonselective methods.

Although these selective separations have been successfully demonstrated in practice, the basic physical mechanisms of selective ion removal by shock ED are still under investigation. Using the mathematical model of shock ED in ref 584, Tian et al. proposed several possible mechanisms for selective removal of multivalent cations. These mechanisms include greater separation of multivalent cations by the deionization shock wave, their high affinity to the negatively charged surfaces of the porous medium where transport is slow (due to the condition of no slip at solid surfaces), and a strong resistance to their emergence in the fresh product due to streaming potentials.[600] The last two of these mechanisms are shown schematically in Figure 1-16b. Tian et al. also used this model to explain the selective removal of Mg^{2+} relative to Na^{+} observed in refs 109,588. A recent publication adapted this model to simulate and interpret selective removal of Pb^{2+} in the presence of excess competing Na^{+} (see Figure 1-17c).[585] Figure 1-16d shows representative simulation results of concentration profiles and ion fluxes for both Pb^{2+} and Na^{+}. Indeed, the greater flux of Pb^{2+} relative to Na^{+} out of the feed and into the cathode stream (see Figure 1-16b) underpins the selective removal of Pb^{2+} by shock ED.

1.3.6 Fouling in Electrokinetic Systems

Fouling is the accumulation of unwanted material (known as foulant), such as mineral scale, organic compounds, colloids, and biomass, on solid surfaces. In electrokinetic systems, fouling typically occurs on the surfaces of membranes[419] and porous media (e.g., ion exchange resin),[601,602] which diminishes performance and increases electrical resistance. If left uncontrolled, fouling may introduce additional problems, such as increased pressure drop, flow blockages and instabilities, material fatigue, and premature system failure. In this section, we discuss how fouling occurs in electrokinetic systems as well as common methods used to prevent and control it.

Mineral scale is deposited on membrane surfaces (or within the membrane itself) when ions such as Ca^{2+}, Mg^{2+}, HCO_3^{-}, and SO_4^{2-} precipitate (or sometimes crystallize) from solution as solid salts.[419,603] Figure 1-18 shows scanning electron

microscopy (SEM) images of deposits of substrates on both CEM and AEM surfaces, particularly on the faces in contact with the concentrate.[604,605] In the concentrate compartments of ED and EDI cells, the concentration of an ion can approach or even exceed its saturation point, which leads to precipitation of the ion. Turek et al. developed a model to predict the formation of mineral scale by computing the saturation level of divalent cations in the concentrate compartment of an ED cell.[606] Precipitation of minerals also depends on the pH and temperature of the electrolyte.[419,605,607,608] For example, a basic electrolyte is concentrated in OH^-, which reacts with Ca^{2+} and Mg^{2+} as follows:[419]

$$Mg^{2+}\,(aq) + 2\,OH^-\,(aq) \rightleftharpoons Mg(OH)_2\,(s) \tag{1.6a}$$

$$Ca^{2+}\,(aq) + 2\,OH^-\,(aq) \rightleftharpoons Ca(OH)_2\,(s) \tag{1.6b}$$

As shown in Figure 1-19, these reactions may occur via several pathways, many of which begin with the dissociation of water into H^+ and OH^- in the boundary layers of the diluate compartment.[370,609] (See ref 610 for a more detailed explanation of the reaction pathways in Figure 1-19.) Cifuentes-Araya et al. demonstrated that scaling of the CEM can be reduced by using a modified cell configuration and pulsed electric fields to control water dissociation.[610–612]

Colloids, which are nondissolved suspended solids (e.g., silt granules, clay minerals, colloidal silica, metal nanoparticles, organic colloids), represent another common source of membrane fouling.[419] The key property of colloids that makes them potential foulants is their charged surfaces, which can lead to electrostatic interactions with oppositely charged IEMs.[613–615] For example, Lee et al.[613] and Mondor et al.[615] reported that colloidal silica deposits irreversibly on the surfaces of AEMs and forms so-called "cake" layers that cannot be removed by chemical cleaning.[616] Similar to colloids, organic compounds (e.g., humic substances, proteins, carbohydrates, organic acids) exhibit electrostatic interactions with the fixed charge of an IEM that can cause organic fouling.[617–621] Unlike colloidal fouling, however, organic fouling may also occur via hydrophobic interactions between the foulant and

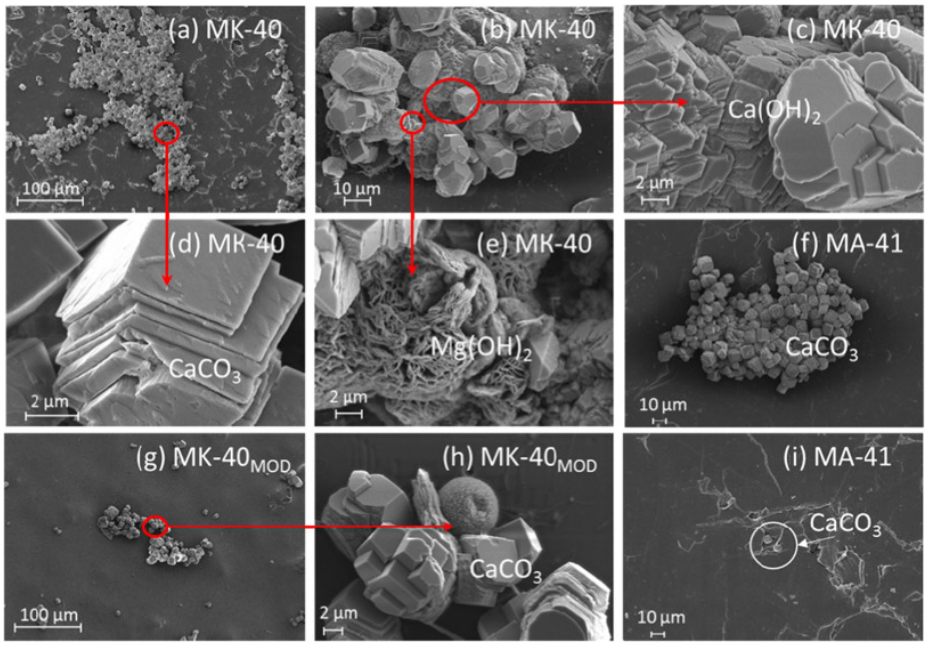

Figure 1-18. SEM images of deposits of $CaCO_3$, $Ca(OH)_2$, and $Mg(OH)_2$ on the surfaces of three IEMs (MK-40 and MK-40MOD are CEMs; MA-41 is an AEM). Reproduced with permission from ref 605. Copyright 2018, Elsevier.

membrane.[419,622–624]

Although chemical and mechanical procedures can be used to remove foulants from membrane surfaces,[620] cleaning protocols increase operating costs and user intervention. Frequent cleaning may also damage the membrane and shorten its lifetime. Several strategies have thus been developed to reduce the amount of cleaning and maintenance required, the earliest of which was to periodically reverse the electrical polarity in ED (electrodialysis reversal) and EDI (electrodeionization reversal) systems.[420,460,625–627] Membranes with intrinsic antifouling properties have also been explored as a means to reduce cleaning requirements.[421–424,628] Engineering membranes that are resistant to fouling requires careful design of chemical composition, surface hydrophobicity and roughness, and the surface charge of functional groups.[419] For instance, increasing the hydrophilicity of IEMs by modifying their surfaces with sulfonyl groups reduces the formation of mineral scale.[629] Similarly, the introduction of polyelectrolyte layers inhibits organic fouling by electrostatic repulsion.[630] Other methods to make membranes hydrophilic involve the use of additives such as inorganic particles,[421,422,629,631] some of which could even

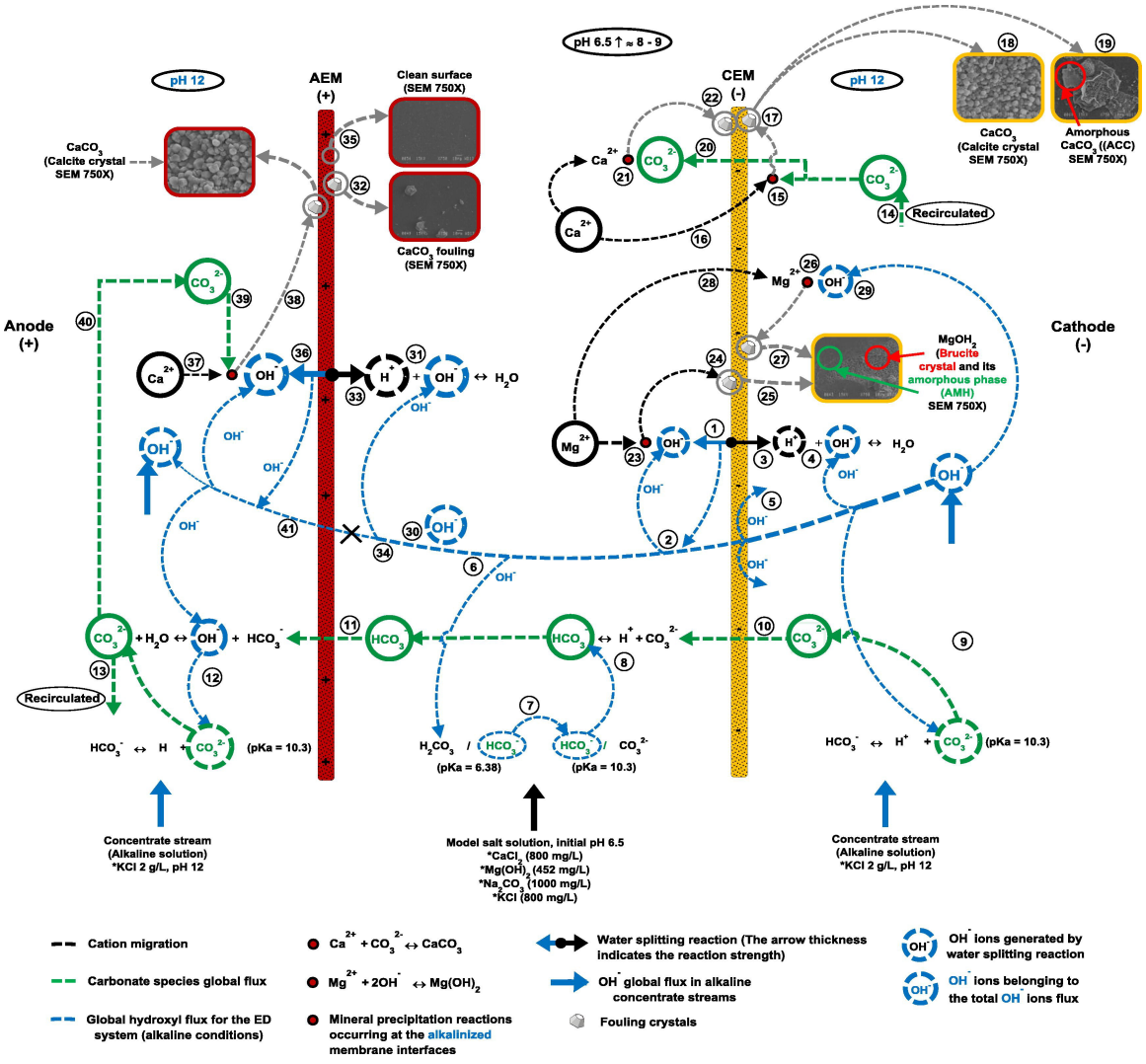

Figure 1-19. Pathways of mineral scaling on CEMs and AEMs in ED, many of which are initiated by water dissociation in the boundary layers of the diluate compartment. Reproduced with permission from ref 610. Copyright 2014, Elsevier.

be placed inside the membrane to modify its entire matrix. Membrane surfaces can also be made homogeneous to improve their resistance to fouling. For example, heterogeneous IEMs exhibit a dramatic reduction in scale deposition after being coated with a homogeneous layer of (hydrophobic) Nafion.[605] The improved resistance to scaling was attributed to enhanced electroconvective mixing, suppressed water dissociation, and decreased crystal growth at the membrane surfaces.[605,632]

1.4 Electrosorptive Separations

Electrosorption refers to the adsorption of dissolved species from a solvent onto the surfaces or into the bulk of a charged electrode and is driven by an applied voltage. The ability to cyclically trap and release ions without the need for chemical additives or swings in temperature and pressure is a major advantage of this process. The performance of devices that employ electrosorption depends on both effective transport of species to the electrode and adequate storage capacity by the electrode. When subjected to an electric potential, the surface of an electrode becomes polarized, and the mechanism by which electrosorption occurs depends on both the identity of the dissolved species and the electrode properties. For instance, ions in an electrolyte can be electrosorbed within the EDL that forms on a polarized surface, and they can be released by either attenuating or reversing the applied electric field. This mechanism is the basis of CDI with porous carbon electrodes, as shown in Figure 1-20a.[633] A number of emerging applications use CDI for water purification, including desalination of brackish water and selective electrosorption of target ions.[115,152,634–636] While electrosorption is generally limited to removal of charged species, porous carbons have a well-known ability to adsorb organic compounds which can enable simultaneous removal of salt and uncharged organic contaminants by CDI.[637] Many novel designs and cell architectures have been invented and characterized, such as membrane CDI (MCDI, see Figure 1-33)[70,638–641] and flow electrode CDI (FCDI, Figure 1-20b).[642–646] MCDI can improve cell cycle life and energy efficiency, and FCDI enables continuous desalination using a single CDI cell. Moreover, the structure of CDI cells can be categorized as either flow-

between (FB) or flow-through electrode (FTE), depending on the direction of the feed. In FB cells, the feed flows between the two porous electrodes, while in FTE cells, the feed flows directly through the electrodes.[647–649].

Selective ion electrosorption is an emerging and promising application of electrosorption technologies.[156,636,646] Compared to other methods such as RO and ED, standard CDI is membraneless and its active elements are the electrodes. These properties enable unique functionalities and mechanisms of selectivity not accessible to membrane-based systems. For example, the selectivity of inexpensive and widely available activated porous carbon electrodes in CDI can be tuned by various parameters such as electrode voltage, chemical charge, pore size, and cell charging time.[651–655] Through design and selection of functional materials, technologies for selective electrosorption are now well developed and can be used to separate both charged and neutral species from water.

Faradaic electrosorption, in particular, relies on the transfer of electrons to a distinct redox-active species bound to the electrode, which changes the oxidation state of that electrode and enables tunable binding of contaminants based on chemical affinity.[96,656,657] Systems for Faradaic electrosorption include crystalline intercalation materials, which operate on the same principles as lithium-ion batteries for charge storage, and redox-active polymers, which selectively interact with species through single-site binding. By changing the molecular structure of the functional material, the mechanism of binding can be adapted to a specific class of contaminants. In this section, we describe the general principles of electrosorption in CDI and provide a review of porous carbon, intercalation, and emerging redox-active electrodes for desalination and selective separations.

1.4.1 Capacitive Deionization With Porous Carbon Electrodes

Electrostatic Electrosorption in Electric Double Layers

The origins of CDI and electrosorption can be traced back to the work of Helmholtz, who in 1853 developed the first EDL theory to describe a monolayer of counterions at the surface of an electrode in terms of a mechanism of charge storage simi-

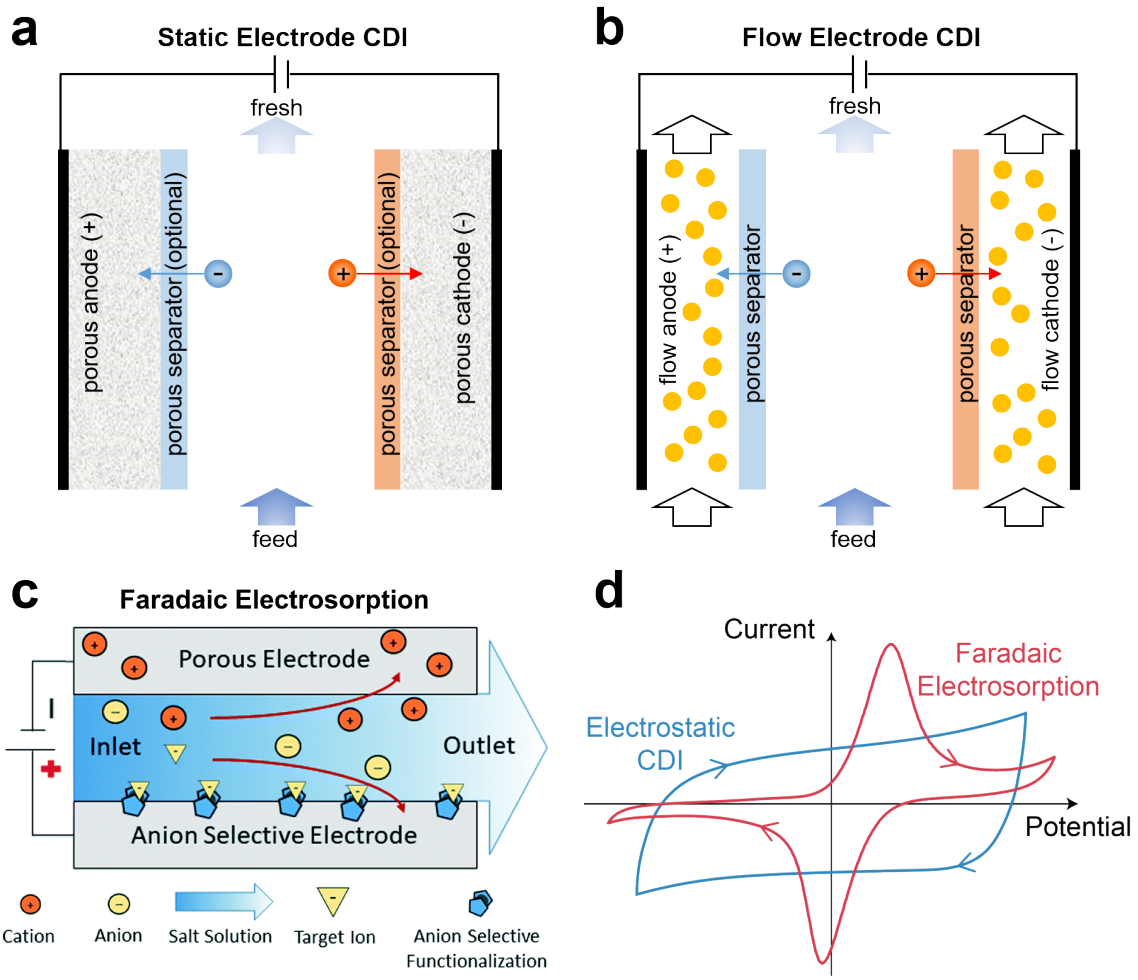

Figure 1-20. Schematics of various electrosorption processes. (a) Static electrode CDI has electrodes that are rigid solids, such as porous carbon and intercalation materials, whereas (b) flow electrode CDI has electrodes that are made of a suspension (or slurry) of carbon beads in an electrolyte. When oriented vertically, flow electrode CDI is often referred to as fluidized bed CDI, in which the flow of suspended carbon is impeded by gravity to establish a densely packed fluidized bed. (c) Faradaic electrosorption comprises redox-active electrodes that can selectively remove target ions. Reproduced with permission from ref 650. Copyright 2020, Royal Society of Chemistry. (d) Typical cyclic voltammograms for electrostatic electrosorption, where double-layer charging is associated with relatively constant capacitance over a wide range of potentials, versus Faradaic electrosorption (or electrochemical adsorption), where redox reactions that transfer electrons between certain ions and the electrode yield peaks in the voltammogram at specific potentials.

lar to a capacitor.[502] In the early 1900s, Gouy revised this theory by claiming the electrolyte in the EDL to be mostly diffuse and by allowing both coions and counterions to spread over a large distance.[503] Chapman further improved the model by deriving the EDL differential capacitance for a symmetric binary electrolyte,[504] and Stern introduced a series capacitance to account for surface solvation.[505] The Gouy–Chapman–Stern (GCS) theory emerging from these developments has become the most widely used model to understand EDLs, and it is relevant for many electrosorption systems, especially in the dilute limit. The theory of electrocapillarity and EDLs was extensively discussed by Grahame in 1947,[658] and there have since been several publications addressing the application of this theory to electrosorption and molecular separations.[152,659,660]

CDI models were first proposed by Johnson and Newman in 1971 based on an equivalent circuit for charging of EDLs in porous electrodes, and the models included an empirical factor for salt removal efficiency.[661] The first self-consistent microscopic theory for EDL charging and salt removal, however, was not developed until the work of Bazant, Thornton, and Ajdari in 2004.[662] This theory was motivated by the modeling of induced-charge electrokinetic phenomena,[122,536] where large applied voltages at blocking porous electrodes, including voltage steps[662] and alternating voltages,[663] lead to nonlinear double-layer responses such as transient salt depletion and space charge formation. From this work, the first mathematical model for CDI with porous carbon electrodes, which bridged EDL theory with applications in water purification and desalination, was developed in 2010[664] and validated by direct numerical simulations with corrections for surface conduction.[665] Further extensions of the theory include the addition of multicomponent asymmetric electrolytes, a generalized Frumkin–Butler–Volmer (FBV) model for parasitic Faradaic side reactions, a modified Donnan model for strongly overlapped EDLs, and a model for attractive ion image forces in metallic micropores.[666–669]

Storage of ions in EDLs for the purpose of water purification was first proposed and demonstrated in 1960. In the decades that followed, this area of research advanced slowly, though interest has grown quickly since 2010 with breakthroughs

in theoretical modeling, experimental methods, material performance, and surface modifications.[115,156,636,670] The most widely used materials for ion electrosorption are microporous carbons due to their broad commercial availability, electrochemical stability, and high electrical conductivity.[115] Prominent examples of microporous carbons include activated carbon, carbon aerogels, graphene, and CNTs.[633] Early theoretical frameworks of electrosorption in these materials are rooted in EDL models for planar surfaces (e.g., Helmholtz, GCS).[662,664,671] One of the main theoretical advances in the past decade was to treat the EDLs in carbon micropores as EDLs in an IEM, since geometric confinement in both cases leads to EDL overlapping. Current theories also assume a uniform potential in the liquid phase of a micropore as well as a Donnan potential drop between a micropore and its adjacent macropore. With these innovations, numerous modified Donnan-type models have been proposed and validated.[668,672–674] One benefit of such EDL models is their simplicity, which facilitates their integration into an electrode or cell-level transport theory.[675]

Ion Selectivity

Ions constitute a major subset of contaminants found in water. When present even at low concentration, ions like F^-, CrO_4^{2-}, AsO_4^{3-}, Hg^{2+}, and Pb^{2+} can pose a threat to the health of humans and animals.[676–678] For this reason, researchers have studied and developed platforms for targeted removal of ionic contaminants using CDI.[679–691] Selective adsorption by CDI can also be employed to recover valuable elements, such as lithium,[692–700] phosphorus,[701–706] and nitrogen.[705,707–714] In this section, we briefly review several experimental works that focus on selective separation of ions from multicomponent solutions using porous carbon electrodes. In particular, we focus on studies that involve either two monovalent ions or one monovalent and one divalent ion, and we exclude studies that involve mixtures of more than two competing ions because of the complexity of these systems.[715–724] We then discuss the quantification of ion selectivity via a separation factor. Next, we consider the use of composite and functionalized electrodes for enhanced of ion selectivity. Lastly, we present the foundations of selectivity modeling at equilibrium.

Several studies focus on theories that capture selectivity based on charge, size, or affinity, which are not reviewed in detail here.[653,655,668]

Early work by Avraham et al. reported the possibility of selective removal of ions by tuning the pore size of microporous carbons.[725] In this work, the electrodes were modified by chemical vapor deposition (CVD) using toluene as a precursor. This treatment influenced the outer surface of the micropores and reduced their size, so only small enough ions could access the pores. Results of this study demonstrated facile storage of the smaller, monovalent cation (Na^+) with reduced storage of larger, divalent cations (Ca^{2+} and Mg^{2+}). A follow-up study by Noked et al. also used this CVD approach for selective removal of NO_3^- from a mixture of NO_3^- and Cl^-.[726] NO_3^- and Cl^- are hydrated anions of similar size, but the openings of the pores were controlled for NO_3^- to preferentially enter by virtue of stereoselectivity. That is, the size and structure of unhydrated NO_3^- was what determined the capacity for electrosorption. Cerón et al. tuned the pore size of hierarchical carbon aerogel monolith electrodes by adjusting the activation time to toggle selectivity toward either Na^+ or Ca^{2+}.[727] In this study, Ca^{2+} was nearly completely excluded from the small pores of the electrode. In the large pores, however, MD simulations suggested that Ca^{2+} selectivity is limited at high applied potential due to the competition between volume exclusion and electrostatic forces as well as the more favorable desolvation of Na^+. Zhang et al. studied cation selectivity via pore sieving, charge, and desolvation effects, and they also examined time-dependent ion swapping.[654] Han et al. further explored the impact of ion size and pore characteristics on selectivity.[728] Eliad et al. showed that the capacity of an EDL can be independent of ion size when the pores are much larger than the ions, which effectively disables ion sieving.[729]

In addition to ion sieving, other widely employed strategies to selectively separate contaminants leverage the influence of ion charge and size on the EDL structure in micropores. Gabelich et al., for example, studied two different electrodes of aerogel carbon with relatively large nominal pore sizes (approximately 4 nm and 9 nm) and showed that charge had the greatest effect on electrosorption capac-

ity.[730] They also found that smaller, monovalent ions showed improved storage relative to larger, divalent ions. These results prompted additional research, for example by Hou et al. who combined Grand Canonical Monte Carlo (GCMC) simulations with experiments using electrodes made of carbon aerogel.[731] When two ions of the same charge but different sizes were present in solution (e.g., K^+ and Li^+), the smaller ions favorably screened the surface charge while occupying a smaller volume in the liquid phase. This result was also predicted using the closed-form Boublik–Mansoori–Carnahan–Starling–Leland (BMCSL) equation of state to model hydrated ions in the micropore EDLs as hard spheres,[653] building on earlier work using local-density approximations for ion crowding in thin EDLs[536] and the Carnahan–Starling equation for overlapping EDLs,[668] and consistent with later experimental observations.[687,694,732]

Ion separations in CDI are quite complicated, however, and cannot be fully explained by molecular or continuum models of equilibrium EDLs, especially in the presence of multivalent ions. For example, when a monovalent ion competes with a divalent ion (e.g., K^+ and Ca^{2+}), the GCMC simulations of Hou et al. predicted preferential electrosorption of the divalent ion (Ca^{2+}), but this result was not observed experimentally. This observation was later attributed to ion-specific electrosorption dynamics by Zhao et al.,[652] who developed a general theory of time-dependent ion-selectivity in CDI, based on the interplay of voltage-dependent adsorption capacities in the EDL and ion-specific transport resistances in the electrolyte. The theory was validated by experiments involving mixtures of Na^+ and Ca^{2+}, which also confirmed the prediction that selectivity toward Ca^{2+} would become high only after several hours of charging in their system.[652] To design more selective CDI electrodes for concentrated mixtures of multivalent ions, it may be important to extend these models to account for electrostatic correlations and hydration forces.[733] These effects can be incorporated using either local approximations based on the Bazant–Storey–Kornyshev (BSK) equation[538,539,542,543] or nonlocal weighted density approximations[734] based on fundamental measure theory[735] and charged-shell electrolyte models.[736]

Separations of anions using CDI have also been studied. Tang et al. observed moderate selectivity of Cl^- relative to F^- under constant voltage charging,[687] a result later observed and validated theoretically under constant current charging.[737] Selective removal of NO_3^- is a particularly common topic. Chen et al. studied a mixture of Cl^- and NO_3^- and showed that Cl^- is preferentially electrosorbed at early times, whereas Cl^- is displaced by NO_3^- in the EDLs at later times.[738] The time dependence of selectivity observed by Chen et al. was not observed for a mixture of SO_4^{2-} and Cl^-, from which neither anion was preferentially removed despite the difference in charge.[738] In contrast, Li et al. later observed dynamic replacement of Cl^- by both NO_3^- and SO_4^{2-} in separate experiments, and they suggested that selectivity and capacity are in fact determined by the hydration ratio, namely the ratio of the hydrated radius to the ionic radius.[739] This work reported that monovalent ions with lower hydration ratios exhibit greater electrosorption relative to other monovalent ions, and that divalent ions are preferentially stored over monovalent ions at equilibrium, which supports the results of Zhao et al.[652] Nonetheless, there appear to be multiple mechanisms at play for the selective separation of NO_3^- from Cl^-. In addition to the work by Chen et al. and Li et al.,[738,739] Oyarzun et al. modeled the intrinsic selectivity of electrodes treated with cetyltrimethylammonium bromide (CTAB) toward NO_3^- using surface group–ion equilibrium constants, and they obtained an observable NO_3^- selectivity factor of 6.5 relative to Cl^-.[655] Using MD simulations, Hawks et al. examined NO_3^- selectivity in slit-shaped, sub-nanometer pores with approximately the same size as the hydrated diameters of NO_3^- and Cl^-. This study attributed the high selectivity to the slit-like shape and low hydration energy of NO_3^-, which allows its hydration shell to be removed more readily than those of Cl^- and SO_4^{2-}.[720] Mubita et al. found that the high selectivity of NO_3^- relative to Cl^- was maintained even when the pore size exceeded that of the hydrated ion.[740]

Selectivity between competing ions can be quantified by a separation factor, defined as the ratio of the molar electrosorption of ion i (Γ_i) to that of ion j (Γ_j)

scaled by the respective feed concentrations, c_{i_0} and c_{j_0}:[653]

$$\beta_{i:j} = \frac{\Gamma_i / c_{i_0}}{\Gamma_j / c_{j_0}} \tag{1.7}$$

If $\beta_{i:j} > 1$, ion i is preferentially removed relative to ion j. We note that Equation 1.7, as it is written, does not hold for batch mode operation because the feed concentrations vary during charging and discharging. Considering the hydrated radii of the ions studied by Nightingale,[741] Figure 1-21 shows that $\beta_{i:j}$ for competing monovalent ions, with ion i being the smaller of the two, is typically between one and five. One exception is for NO_3^- which is larger than both Cl^- and Br^- but is selectively electrosorbed relative to these monatomic anions. For competing divalent (i) and monovalent (j) ions, $\beta_{i:j}$ is time dependent and can range from below one to more than ten.[652] Occasionally, selectivity is reported using a relation similar to the scaled retention selectivity introduced in Section 1.3.5 for shock ED (see Equation 1.5). The two definitions are related by rewriting the separation factor as

$$\beta_{i:j} = \frac{1 - c_i / c_{i_0}}{1 - c_j / c_{j_0}} \tag{1.8}$$

provided the system is operated in a single pass; here, c_i and c_j are the concentrations in the desalinated product (see ref 742 for details on sample collection). Unlike in shock ED, selectivity in (membraneless) CDI arises due to the storage of ions in electrode pores. It is therefore preferable in CDI to use Equation 1.7 since it explicitly accounts for ion electrosorption, and also since effluent concentrations can vary in time even if pore concentrations reach steady state.

In addition to examining the mechanisms of selective electrosorption, researchers have sought to increase electrode capacity toward a specific ion by using composite carbon electrodes embedded with materials like polymers and metal oxides.[682,684,751] Kim et al. demonstrated this concept by coating the surface of a carbon anode with anion exchange resin that is selective toward NO_3^-, which more than doubled the separation of NO_3^- to Cl^- compared to the commercial AEM Neosepta.[684] By applying a constant current to the device, the same group demon-

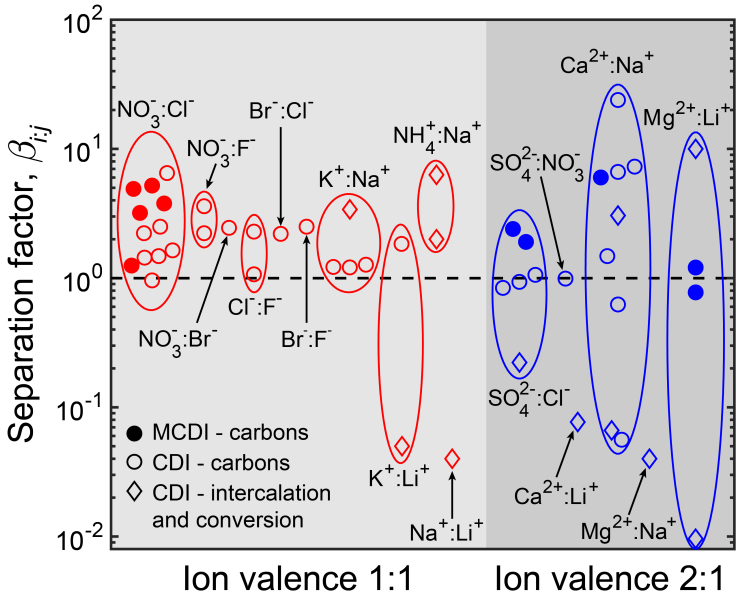

Figure 1-21. Separation factor $\beta_{i:j}$ calculated using Equation 1.7 in MCDI, CDI with porous carbons, and CDI with intercalation or conversion electrodes for pairs of competing anions and cations. $\beta_{i:j} > 1$ implies selectivity toward ion i, $\beta_{i:j} < 1$ implies selectivity toward ion j, and $\beta_{i:j} = 1$ (dashed line) corresponds to no selectivity. Competing monovalent ions (ion valence 1:1) typically display $\beta_{i:j}$ between one and ten. Competing divalent and monovalent ions (ion valence 2:1) display a wider range of $\beta_{i:j}$, typically between 0.01 and 24. References for valence 1:1 ion pairs in alphabetical order: Br^-:Cl^-,[739] Br^-:F^-,[739] Cl^-:F^-,[687,739] K^+:Li^+,[692,694] K^+:Na^+,[716,732,739,743] Na^+:Li^+,[692] NH_4^+:Na^+,[744] NO_3^-:Br^-,[739] NO_3^-:Cl^- (MCDI,[682,684] CDI[655,713,738,739]), and NO_3^-:F^-.[713,739] References for valence 2:1 ion pairs: Ca^{2+}:Li^+,[692] Ca^{2+}:Na^+ (MCDI,[745] CDI,[651,652,716,727] intercalation or conversion[746,747]) Mg^{2+}:Li^+,[692,693,748] Mg^{2+}:Na^+,[746] SO_4^{2-}:Cl^-,[738,749,750] and SO_4^{2-}:NO_3^-.[713]

strated even greater separation using the IEMs and composite electrodes reported by Kim and Choi.[682] Similarly, Tang et al. showed slight preferential removal of SO_4^{2-} by using an MCDI system operated at constant current.[752] It is important to distinguish composite electrodes, where materials are affixed directly to carbon, from MCDI, where free-standing membranes are layered onto the electrodes. MCDI can be used for selective removal of ions, as shown in Figure 1-21, but since ion selectivity in MCDI is primarily determined by the membranes rather than by the electrodes, we do not discuss this method further in this section. Besides using composites to tune selectivity, researchers have explored chemical treatments to functionalize electrode micropores for enhanced selectivity. Guyes et al. oxidized the negative electrode to add carboxylic groups to enhance ion selectivity based on size, which increased the selectivity factor of K^+ relative to Li^+ from approximately 1 to 1.84.[694] In a later study, Guyes et al. used a cell with a sulfonated cathode to increase the selective removal of Na^+ relative to Ca^{2+} at early charging times and high charging voltages.[651] Uwayid et al. then published the first demonstration of perfect Ca^{2+} selectivity relative to Na^+ in a CDI cell using a sulfonated cathode with long charging times and non-zero discharging voltages (i.e., only Ca^{2+} was removed during charging).[753]

The effects of ion size, chemical charge, and affinity can be mathematically modeled using continuum theories. Here, we briefly review the principles of modified Donnan (mD) EDL theory to describe some aspects of selectivity in porous carbon electrodes with micropores larger than the hydrated ions present in solution. In this framework, we spatially average over micropore volume to neglect the local pore structure and simplify the governing equations. We do not cover CDI models based on transport equations, which are needed to describe time-dependent electrosorption and selectivity.[651,754] An alternative yet related framework to the mD model, termed the amphoteric Donnan (amph-D) model, considers the electrodes to comprise separate regions of positive and negative surface charge.[755]

The mD model employs the Donnan approximation of spatially constant micropore potential and assumes equilibrium between the macropores and micropores,

which results in a Boltzmann distribution for concentration:

$$c_{i,k}^{\mathrm{mi}} = c_{i,k}^{\mathrm{mA}} \exp\left(-z_i \Delta\phi_{\mathrm{D},k} - \Delta\mu_{i,k}^{\mathrm{ex}}\right) \tag{1.9}$$

The terms $c_{i,k}^{\mathrm{mi}}$ and $c_{i,k}^{\mathrm{mA}}$ are the micropore and macropore concentrations, respectively, of ion i in electrode $k = \mathrm{A}$ (anode) or C (cathode), $\Delta\phi_{\mathrm{D},k}$ is the dimensionless difference in potential between the micropores and macropores, $\Delta\mu_{i,k}^{\mathrm{ex}}$ is the dimensionless difference in excess chemical potential between the micropores and macropores, and z_i is valence; all potentials are scaled by the thermal voltage (see Section 1.3.1). For single-pass operation and at cell equilibrium, it is usually assumed that the macropore concentration equals the feed concentration: $c_{i,k}^{\mathrm{mA}} = c_{i_0}$. The term $\Delta\mu_{i,k}^{\mathrm{ex}} = \mu_{i,k}^{\mathrm{ex,mi}} - \mu_{i,k}^{\mathrm{ex,mA}}$ accounts for nonideal effects, such as an affinity between the electrode surface and specific ions,[756] image forces acting on ions,[668] and hard-sphere interactions between ions.[653,694]

According to Equation 1.9, higher background (macropore) concentration of a particular ion increases its micropore concentration. In the case of two competing ions with equal valence and excess potential, the ion with higher background concentration will be stored in larger quantities. In a charged cell, $\Delta\phi_{\mathrm{D,C}}$ is negative and so cations are stored in the cathode, while $\Delta\phi_{\mathrm{D,A}}$ is positive and so anions are stored in the anode. Since the Donnan potential is multiplied by valence, multivalent ($|z_i| > 1$) counterions are preferentially stored relative to monovalent ($|z_i| = 1$) counterions. As captured by the term $\Delta\mu_{i,k}^{\mathrm{ex}}$, a larger excess potential reduces ion concentration in micropores. Considering effects of volume exclusion due to finite ion size, a small ion has a lower excess potential and is thus preferentially stored relative to a larger ion with equal valence.[653] The value of $\Delta\mu_{i,k}^{\mathrm{ex}}$ is also affected by electrode properties such as the chemical charge of surface groups, which can be tuned to improve selectivity toward target ions.[694] Moreover, it was recently demonstrated that volume exclusion may enhance selective removal of larger ions with higher valence due to the complex interplay between electrostatic forces and volume-exclusion effects.[753]

Energy Consumption

Energy consumption by CDI has been extensively studied over the past five years.[90,640,757–765] Recently, Hawks et al. proposed metrics and methodologies to compare energy consumption between different CDI systems and other desalination technologies.[742] They suggested that a target separation should be implemented across all systems being compared by specifying feed concentration, c_0, concentration reduction, Δc, and water recovery, γ. The systems can then be compared in terms of volumetric energy consumption (in units of $\mathrm{W\,h\,m^{-3}}$ of treated water) versus productivity, $\mathscr{P}$, defined as the throughput of fresh water scaled by the projected cross-sectional area of the electrode and multiplied by the number of cells (see Equation 1.25).[742] A related metric to quantify energy demand was used by Lin,[766] namely the specific energy consumption, SEC, scaled by either the amount of adsorbed salt[763,765]

$$\mathrm{SEC_{ion}} = \frac{E_{\mathrm{ch}}}{M_{\mathrm{salt}} Q t_{\mathrm{ch}} \Delta c} \tag{1.10}$$

or the volume of produced water[742,766]

$$\mathrm{SEC_{w}} = \frac{E_{\mathrm{ch}}}{Q t_{\mathrm{ch}}} \tag{1.11}$$

where E_{ch} is energy consumption during charging, M_{salt} is the molecular weight of the salt, Q is volumetric flow rate, and t_{ch} is charging time. Another common metric in the literature is energy normalized adsorbed salt (ENAS),[90,710,742] which equals $\mathrm{SEC_{ion}}^{-1}$. To ensure repeatable results, energy consumption should be determined from the CDI cycle after the cell has reached a dynamic steady state.[90] Dynamic steady state is usually reached after 3-5 cycles, after which the system exhibits steady behavior and the amount of salt adsorbed during charging equals the amount released during discharging.

In CDI, energy can be recovered from the discharging step to reduce the total energy consumption.[760] Energy recovery is often quantified as the ratio of energy recovered during discharging to energy consumed during charging.[767–771] Early

studies of energy recovery used either only the consumer unit, a CDI cell,[770] or only the storage unit, a buck-boost converter,[767–769] and reported recovery ratios of up to 83%. Kang et al. later examined a system comprising both a CDI cell and a buck-boost converter, which achieved recovery ratios of up to 50% that decreased with lower feed concentrations and faster desalination rates.[771] Oyarzun et al. emphasized the importance of utilization efficiency, defined as the recovery efficiency over a full cycle, including charging and discharging of the DC-DC converter used for energy storage.[772] The nature of the power source used to drive the CDI cell is also an important consideration. As demonstrated by Tan et al.,[773–775] photovoltaics are an adequate power source due the low applied voltage required for CDI cell charging ($< 1.2\,\mathrm{V}$), which makes CDI a candidate for off-grid desalination.

The energy efficiency of CDI systems is normally reported as a thermodynamic efficiency, η_{thermo} (see Equation 1.22),[90,152,761,765,766] defined as the ratio of the theoretical minimum energy needed to achieve a target separation (see Equation 1.20) to the energy consumed in practice. For comparisons of η_{thermo} to be meaningful, the systems being compared should have the same productivity and realized ion separation.[765,776] Porada et al. presented an MCDI cell with an efficiency of 16.04% at a productivity of $11.8\,\mathrm{L\,h^{-1}\,m^{-2}}$ and current density of $18.5\,\mathrm{mA\,m^{-2}}$.[640] Hemmatifar et al. analyzed a membraneless cell designed to achieve high efficiency with total recovery of the energy released during discharging.[90] This system achieved an efficiency of 8.89% at a productivity of $3\,\mathrm{L\,h^{-1}\,m^{-2}}$ and current density of $4\,\mathrm{mA\,m^{-2}}$; increasing productivity to $6\,\mathrm{L\,h^{-1}\,m^{-2}}$ and current density to $8\,\mathrm{mA\,m^{-2}}$ lowered the efficiency to 6.81%. Ramachandran et al. reported a cell with an efficiency of 8% when operated at constant current and 5% when operated at constant voltage, assuming total energy recovery.[764] A comprehensive review of CDI efficiencies was presented recently,[765,766] and it reported values of up to approximately 6%.[754,777]

Three efficiency indicators have been proposed to study mechanisms of charge and energy loss: Coulombic efficiency, charge efficiency,[90,742,778–780] and flow efficiency.[640,661,762,764] Coulombic efficiency quantifies the ratio of charge released during discharging to charge delivered to the cell during charging. Values below

one are due to parasitic Faradaic reactions that can occur during charging,[781] such as oxygen reduction at the cathode and carbon oxidation at the anode (see Equation 1.12). Parasitic reactions, which can degrade salt storage capacity in the electrodes, are more likely to occur when operating at higher charging voltages and for longer times.[759,760,782–785] Charge efficiency is defined as the ratio of moles of salt removed from the feed to moles of electrons transferred between the electrodes during discharging,[779,786,787] and typical charge efficiencies in CDI systems are in the range of 60-90%.[115,788] Many strategies have been explored to improve charge efficiency, such as using high discharge voltages (with 0.3 V as a minimum value),[760,789] chemically functionalizing electrodes,[788] or layering IEMs over the electrodes, as in MCDI.[70,790] Flow efficiency is defined as moles of salt removed from the feed divided by moles of salt adsorbed by the electrodes,[764] and it captures unwanted effects like direct mixing of diluate and concentrate when switching between charging and discharging. Hawks et al. demonstrated that flow efficiency can be improved by adding a high throughput flush step between charging and discharging.[762]

In addition to energy losses caused by electrons participating in side reactions, there are also resistive losses caused by electronic and ionic resistances.[757,758,765,791] Electronic losses arise mainly from resistances of the external circuit components, contact resistance between current collectors and electrodes, and resistances in the solid phase of the electrodes.[761,765] Electronic losses can be reduced by improving contact between the current collectors and electrodes,[765] which can be achieved by surface treatments of the current collectors and electrodes[761] or by using conductive epoxies.[757] Electronic losses are expected to be greater when the cell is operated at constant voltage, as current can be high at early times.[90,759,760] Ionic losses occur mainly due to the resistance of the electrolyte in the separator and electrode. Common methods to lower these losses are to reduce spacer thickness or increase spacer porosity.[761] Although operating at constant current is often considered more energy efficient than operating at constant voltage,[759,792] Dykstra et al. showed that the reverse can be true when operating at certain conditions.[760]

Qin et al. recently analyzed brackish water desalination by RO and by CDI, and they concluded that RO is much more energy efficient, with no expected change in the future.[793,794] However, several serious issues with this analysis were later identified, including unrealistic values of electrical resistance, unphysical trends in energy consumption, and inaccurate predictions of performance.[795] Porada et al. also highlighted that the comparison by Qin et al. was done using inconsistent definitions of salt rejection.[640] While the common definition given by $R_j = 1 - c_D/c_0$ (where c_D is diluate concentration) was used for CDI, salt rejection in RO was defined as $R_j = 1 - c_D/c_B$ (where c_B is brine concentration).[793] Porada et al. thus repeated the analysis with consistent definitions of salt rejection and demonstrated that CDI can indeed be competitive with RO for brackish water desalination, especially when water recovery is high.[640]

Many applications in desalination and water purification demand high water recovery to reduce the volume of waste generated.[640,640,761,764,765,793] It was recently shown that water recovery in CDI could be significantly improved, with only a small increase in energy consumption, by decreasing the discharging flow rate.[764,796] For example, Ramachandran et al. found that setting the discharging flow rate to 10% of the charging flow rate was most suitable in their study,[764] and Tan et al. used a stopped flow discharge process.[796] Water recovery can also be improved by adjusting the operating parameters, which include charging and discharging times as well as charging and discharging voltages (or currents).[760] Another method to increase water recovery is by flowing the brine product through the cell as a washing solution during discharging.[797]

Flow Electrode Capacitive Deionization

Research and commercialization efforts in CDI have grown significantly over the past ten years, and much of this growth has been catalyzed by the invention of new architectures and designs for CDI systems.[115,798,799] In 2011, Duduta et al. introduced semisolid lithium-ion flow batteries with flowable intercalation electrodes,[800] a concept that has since been applied to other rechargeable batteries[801–803]

as well as CDI. In 2013, Jeon et al. introduced flow electrodes for CDI, which were a suspension of carbon particles that are transported along with the flowing electrolyte, as shown in Figure 1-20a.[642] FCDI offers two major improvements to CDI with static electrodes, namely the ability to operate the system continuously rather than cyclically and an increased capacity for salt storage.[115] Transforming CDI into a continuous process requires discharge of the carbon particles (and formation of the brine) downstream, either in a mixing tank or in a second device.[645,804–811] FCDI has also demonstrated the possibility of desalinating feeds that are more concentrated than what is processed by static electrode CDI.[642,812]

FCDI is sometimes used to concentrate inorganic nutrients and organic molecules for later recovery.[703,704,813–816] Bian et al. introduced FCDI as an alternative to a complex and costly nutrient removal system for the extraction and up-concentration of inorganic nutrients, such as NH_4^+, NO_3^-, and PO_4^{3-}, from wastewater.[813] Although the system achieved a high recovery of NH_4^+ (89-99%), NO_3^- (83-99%), and PO_4^{3-} (49-91%), it required post-treatment to further separate inorganic nutrients from desalinated salts (e.g., NaCl). Several modifications of FCDI then enabled the recovery of inorganic nutrients, especially phosphorus. For instance, PO_4^{3-} was selectively recovered as H_3PO_4 by leveraging inevitable side reactions like the generation of H^+ by water splitting.[814] In this study, operating the system between 1.5 V and 2.1 V resulted in the dissociation of water, while both PO_4^{3-} and Cl^- were adsorbed by the positively charged carbon particles. As a result, both H_3PO_4 and H^+ were produced at the same electrode. During regeneration, the electrode released most of the adsorbed Cl^- back into the original chamber, whereas neutral H_3PO_4 remained in the electrolyte (with a selectivity factor of > 2 relative to Cl^-) to produce a solution rich in phosphorous.[814] Moreover, Zhang et al. recovered PO_4^{3-} with magnetic carbon particles (impregnated with Fe_3O_4) that showed strong affinity toward phosphorus.[704] This study proposed a two-step process for the recovery of highly purified PO_4^{3-} by concentrating the ion using FCDI and crystallizing it into vivianite (a hydrated iron phosphate mineral) using a fluidized bed crystallization column. The applications of FCDI have expanded to include recovery of carboxy-

lates, such as acetate and oxalate, downstream of advanced oxidation processes.[815]

In contrast to solid carbon electrodes which have electrical conductivities in excess of $1000\,\mathrm{mS\,cm^{-1}}$, flow electrodes have electrical conductivities mostly below $10\,\mathrm{mS\,cm^{-1}}$ because a suspension of carbon particles can form a largely discontinuous network for electron transport.[670,817] The electrical conductivity of flow electrodes is a function of the amount of suspended carbon, typically quantified by the weight fraction of carbon in the electrode (i.e., the dry weight of carbon particles divided by the total weight of the electrode). Increasing the fraction of carbon boosts electrical conductivity, though slurries used as flow electrodes become viscous and difficult to pump when the fraction of carbon exceeds about 20 wt%.[670] On the other hand, low electrical conductivity adversely impacts performance, particularly in the extreme case that the slurry does not percolate electric charge. In this limit, carbon particles through much of the network cannot be charged and do not store salt, and the mechanism of desalination reverts to that of an ED system driven by a steady Faradaic current.[643,818] This functionality is sometimes mistaken for capacitive storage of salt in carbon particles, which has led to spurious reports of unusually high salt adsorption capacities of flow electrodes.[818,819]

To overcome the limitations of weakly conductive flow electrodes, researchers have proposed new platforms that increase the loading of suspended carbon. These platforms include fluidized bed electrodes, a combination of these electrodes and slurry particles, conductive chemical additives, and redox electron mediators.[645,817,820–824] Fluidized bed electrodes are distinct from slurries used as flow electrodes because the former uses large ($\sim 100\,\mu$m), porous beads made of carbon that are pumped with the electrolyte vertically upward. The weight of the beads causes them to travel more slowly than the surrounding fluid, which leads to a densely packed electrode where the fraction of carbon can reach over 30 wt%.[645] Although these fluidized beds can be dense, the electrical conductivity often remains less than $1\,\mathrm{mS\,cm^{-1}}$.[817] One way to further increase the loading of carbon beads is to enrich the bed with a slurry of smaller particles, which feel a negligible force due to gravity. Cohen et al. showed that although this slurry itself could have a conduc-

tivity greater than $1\,\mathrm{mS\,cm^{-1}}$, the conductivity of the combined system would only just reach $1\,\mathrm{mS\,cm^{-1}}$.[817] This result suggests that a more detailed understanding is needed of the relationship between the properties of carbon particles and the conductivity of the electrolyte. Ma et al. found that by adding redox-active quinone to a flow electrode with carbon particles of $100\,\mu\mathrm{m}$ loaded at 1 wt%, the rate of salt removal can be increased in potentiostatic mode.[820] Similarly, other researchers have attempted to increase the conductivity of flow electrodes by introducing conductive additives such as multiwalled CNTs and carbon black.[821,822] Recently, Halfon and Suss demonstrated a system that comprised metal particles under two operating modes: the first was a static mode in which conductivity exceeded $10\,000\,\mathrm{mS\,cm^{-1}}$, and the second was a flow mode in which the particles were discharged.[825] In the future, this concept may be adapted to FCDI by replacing the metal particles with carbon.

The latest advances in the field of FCDI have focused on scaling up, discovering innovative alternate applications, and better understanding the overall process. Today, FCDI is scaled up by either fabricating a stack with multiple unit cells or using three-dimensional honeycomb cells with multiple channels that are interconnected by porous carbon supports.[826–829] At the same time, researchers have adapted FCDI for capacitive neutralization desalination, double displacement reactions,[830] ion separations,[708,711,831–836] and resource recovery.[703,704] To better understand the process, theoretical models have been proposed,[808,837,838] and the governing transport mechanisms have been studied.[839] Overall, FCDI has the potential to be used for water purification, but for this field to reach its potential, the community must develop ways to either improve or compensate for the low electrical conductivity of flow electrodes.

Parasitic Faradaic Reactions

Faradaic side reactions in an electrochemical system are often (but not always) undesirable and can limit the performance and stability of the process.[656,840] The two reactions that are believed to have the greatest impact on the performance

of CDI are carbon oxidation at the positive electrode and oxygen reduction at the negative electrode:[783,784]

$$\begin{aligned} &\text{Carbon oxidation:} \quad \mathrm{C(H) + 2H_2O \rightarrow COO^-(H^+) + 4H^+ + 4e^-} \\ &\text{Oxygen reduction:} \quad \mathrm{O_2 + 2H^+ + 2e^- \rightarrow H_2O_2} \end{aligned} \tag{1.12}$$

Managing the oxidative step in the corrosion of carbon plays a key role in the long-term stability of a CDI device, as the electrodes are repeatedly charged and discharged. While this reaction can lower Coulombic efficiency, reduce the conductivity of the electrode, and distort its microporous structure, the most severe effect is likely the production of carboxyl surface groups (COO^-).[656,782,786] As the concentration of these surface groups increases in the micropores of the positive electrode, so does the concentration of coions to compensate for the increased negative charge.[788] The result is that a larger fraction of the applied current is consumed during charging to expel coions from the positive electrode, which lowers charge efficiency. This phenomenon was observed in the form of "inversion peaks" in the effluent concentration profile during charging after several cycles.[782,788] In addition, X-ray photoelectron spectroscopy revealed that, after cycling, the positive electrode was oxidized to the point that its surface was highly oxygenated,[782] and measurements of pH indicated asymmetric electrosorption as well as irreversible consumption of charge.[783] Although salt removal significantly decreases due to corrosion of the positive electrode,[841] charge storage capacitance often remains largely unaffected.[842] For a cell with an oxidized cathode, it was found that the anode was relatively stable during cycling, but the cathode degraded due to loss of its negative chemical charge.[694,785] Uwayid et al. recently compared the lifetimes of oxidized cathodes and sulfonated cathodes, and they found that the sulfonic acid groups lead to a more stable cell.[843]

When no measures are taken to mitigate this corrosion, a CDI cell is often limited to fifty cycles before the capacity for salt adsorption exhibits a significant loss,[783,785,844] where FTE CDI cells are reported to degrade faster than FB cells.[644,845] Known strategies to mitigate corrosion include periodically reversing cell polar-

ity to slow the oxidation of carbon,[782,846] optimizing the voltage window to reduce electrode degradation,[847,848] reducing the concentration of dissolved oxygen (DO) by sparging with gaseous nitrogen,[782] decorating the electrodes with titania to enhance electrochemical reduction and prevent DO from participating in corrosion reactions,[844] treating the surfaces of the positive electrode to make it negatively charged (inverted CDI),[846,849,850] and reducing the charging time to inhibit Faradaic reactions.[651,785] Other proposed methods include recovering the electrodes by thermal treatment[842] and adding an AEM between the main channel and the positive electrode to both reduce corrosion and extend cycle life.[115,639,851] While the positive electrode may still corrode, its capacitance can be preserved, as the AEM is the active element in this desalination.

By measuring the concentration of DO in the product, researchers discovered that oxygen is reduced at the negative electrode during charging, while the concentration of DO recovers during discharging.[783,784] It was proposed that DO reduction at the cathode contributes to corrosion of the anode carbon because it causes asymmetry in the electric potential[782] and produces hydrogen peroxide (see Equation 1.12),[644,784,852] which accelerates oxidation of the positive electrode.[844] The reduction of oxygen, which dominates when the applied voltage is less than approximately 1 V, can severely diminish Coulombic efficiency under certain conditions.[783] The main approach to suppress this parasitic reaction is to dilute the DO by displacing it with gaseous nitrogen.[782] As with corrosion of carbon, the rate at which oxygen is reduced is lowered in MCDI systems,[639] since the membranes impede transport of DO inside the device.

Besides the two reactions in Equation 1.12, several other parasitic reactions may occur, though they usually have a minor impact on the performance of the cell.[656,690] One such reaction is electrolysis of water, which produces gaseous oxygen at the positive electrode and gaseous hydrogen at the negative electrode. The fact that this reaction is sluggish on carbon electrodes, however, reduces its impact on desalination by CDI. Moreover, electrolysis of water can be prevented by operating the system at or below the standard potential of water electrolysis (1.23 V).

Recent studies of Faradaic side reactions in CDI with carbon electrodes have enabled researchers to limit the destructive effects of these reactions.[785,845,847] While the use of IEMs can reduce the impact of side reactions and increase cycle life, future work in this area should focus on delivering stable electrodes without the need for potentially costly membranes.

Fouling in Capacitive Deionization with Porous Carbon Electrodes

CDI devices with porous carbon electrodes are susceptible to fouling, which may either occur on electrode surfaces or block electrode pores. In MCDI devices, fouling can also occur on membrane surfaces or inside the membrane structure. Here, we discuss common types of fouling and their mechanisms in CDI; we limit the discussion to fouling of electrodes, as membrane fouling was explained in Section 1.3.6. Fouling of electrodes by organic matter has received the most attention to date, and researchers generally report that salt capacity is reduced in the presence of organic matter.[562,730,853–859] Zhang et al. showed that the level of dissolved organic matter can determine the extent of fouling. In particular, treatment of lake water with low levels of organic matter led to little fouling and only a 13% loss in capacity over two weeks, whereas treatment of lake water with high levels of organic matter led to a 75% loss in capacity in the same amount of time.[854] Organic fouling also increases energy consumption due to adsorption of organic species that block active sites on the electrodes and inhibit fluid flow.[854,859] For example, Chen et al. found deposits of alginate gel and humic acid in the bulk electrode structure, and these deposits were more noticeable in the presence of Na^+ and Ca^{2+}.[859] The same authors observed similar deposits on the surfaces of IEMs in MCDI, though the alginate gels formed in the presence of Ca^{2+} were denser than those formed in the presence of Na^+. Organic foulants can also be adsorbed within carbon pores, though this adsorption may not significantly impact performance. Liu et al. found that while humic acid was adsorbed in both microporous and mesoporous activated carbons, salt capacity decreased by only 5% over thirty cycles.[856]

Mineral scale can form on the electrodes in CDI when ions such as Ca^{2+}, Mg^{2+},

HCO_3^-, and SO_4^{2-} are present in solution. Several studies found that scaling by Ca^{2+} and Mg^{2+} is minor,[853,854] though Mossad et al. observed that Fe^{3+}—even at concentrations as low as $2\,mg\,L^{-1}$—formed deposits which reduced salt removal by 7.4% and flow rate by 13% over thirty hours.[853] Moreover, Pb^{2+} and Cu^{2+} poorly desorb during cell discharging, which indicates that these species can remain bound to the electrode.[860]

A number of techniques have been studied to control fouling and prolong device lifetime, several of which are similar to the methods discussed in Section 1.3.6. Pretreatment involves removing foulants and scalants upstream of CDI using chemical additives and antiscaling compounds. Often, these compounds are added directly to the feed, though in some cases they may interfere with the electrosorption process. Special electrodes (e.g., TiO_2–RGO nanocomposites[861]) can also be designed to have intrinsic antifouling properties. Finally, cleaning solutions such as citric acid, NaOH, and HCl are used to regularly remove deposits and restore performance. A more detailed review of methods to control fouling in CDI can be found in ref 862.

1.4.2 Capacitive Deionization With Intercalation and Conversion Electrodes

Faradaic Electrosorption Involving Electron Transfer Reactions

CDI cells have historically relied on porous carbon electrodes[110] because carbons are inexpensive, widely available, and capable of reversible positive and negative polarization across a wide range of potentials.[863–866] Despite these advantages, however, carbon electrodes have several limitations. First, the extent to which a porous carbon can store salt (expressed as the mass of stored material per unit mass of material available for storage, often in $mg\,g^{-1}$) is limited and rarely exceeds $20\,mg\,g^{-1}$ for a typical salt like NaCl. Second, carbon electrodes must be charged to a relatively high voltage of 0.8-1.2 V for the amount of salt stored per unit charge to be meaningful. Third, the anode is unstable when exposed to water with a high concentration of DO, as discussed in Section 1.4.1.[845,867] Researchers have thus sought to develop novel materials that can address the shortcomings of porous car-

bons.[868,869]

One class of intercalation materials traps ions between the closely spaced layers of the electrode mainly by electrostatic forces, although these materials often exhibit redox reactions as well. Examples of such materials include the inorganic compounds MXene[130,870–872] and MoS_2 (shown in Figure 1-22a,b),[873–876] both of which can be used as a cathode and, to a lesser extent, as an anode in CDI cells. Intercalation in these materials is largely driven by the electrostatic attraction between the ions and electrode, with only limited influence of redox reactions, as signified by wide "box-like" cyclic voltammograms such as the one shown in Figure 1-22b. MXenes have so far demonstrated electrosorption capacities of NaCl of up to $45\,mg\,g^{-1}$ and charge efficiencies greater than 90%,[870,871] but degradation caused by oxidation and hydrolysis is a limiting factor.[877] Furthermore, these materials are susceptible to deformation (e.g., swelling) during operation because intercalation and ion exchange can alter the interlayer spacing,[878] as also observed in porous carbons adsorbing larger ions from room-temperature ionic liquids.[879] In MoS_2, salt capacity and charge efficiency have been shown to increase with increasing salt concentration in the feed, a trend opposite to what is observed in porous carbons.[874]

A second class of cells that do not use porous carbons involve asymmetric combinations of an electrostatic insertion cathode with a Faradaic conversion anode, such as Ag/AgCl,[882,883] Bi/BiOCl,[884] or MnO_2.[885,886] In this design, an important feature is that the metallic phase donates or accepts electrons in a redox reaction where ions are adsorbed from the liquid phase. The most familiar example of this process is the oxidation of Ag with Cl^-, which produces the solid salt AgCl on the surface of the electrode until the Ag is fully converted. As shown in Figure 1-22e-f, the reversible electron transfer reaction is associated with rate-dependent, symmetrically shifted peaks in the cyclic voltammograms, which are the most familiar waveforms observed in voltammetry.[887] Another such reaction is that of Bi with Cl^- to form

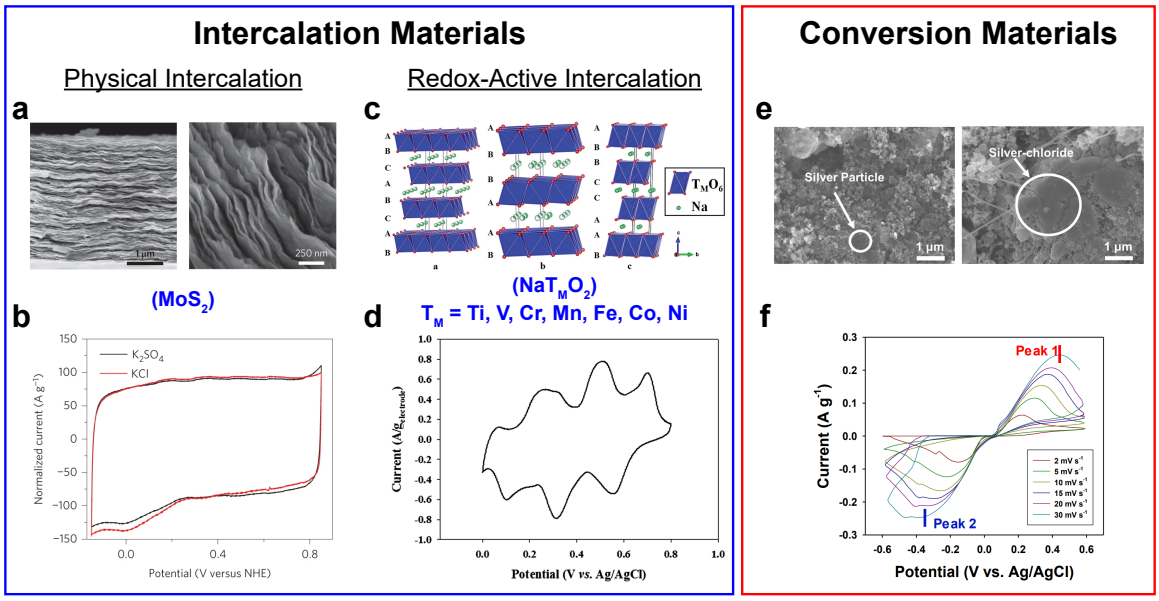

Figure 1-22. Representative intercalation and conversion electrodes used for electrochemical separations. Structural image and cyclic voltammetry of (a-b) MoS_2, (c-d) NMO, and (e-f) $Ag/AgCl$. Panels (a-b) reproduced with permission from ref 873. Copyright 2015, Springer Nature. Panel (c) reproduced with permission from ref 880. Copyright 2015, Royal Society of Chemistry. Panel (d) reproduced with permission from ref 851. Copyright 2014, Royal Society of Chemistry. Panels (e-f) reproduced with permission from ref 881. Copyright 2020, Elsevier.

BiOCl according to the chemical equation,[884]

$$\mathrm{Bi} + \mathrm{Cl}^- + \mathrm{H_2O} \rightleftharpoons \mathrm{BiOCl} + 2\,\mathrm{H}^+ + 3\,\mathrm{e}^- \tag{1.13}$$

and Bi-based electrodes enable high storage of Cl^- ($\sim 80\,\mathrm{mg\,g^{-1}}$).[884] MnO_2 is also used as an anode because of its stability, high capacity for storage, and inhibition of parasitic side reactions,[885] and the redox reaction in which MnO_2 participates is analogous to that observed for Prussian Blue Analogues (PBAs, discussed in more detail below).[888] Similarly, RuO_2 and TiO_2 increase electrosorption capacity when deposited onto a porous carbon electrode.[889,890] Overall, these inorganic materials are functional and selective, though they are limited in that only the primary atom in the host structure is reactive and that reactions of this kind can influence chemical structure.

Another class of intercalation materials is based on redox-active solid insertion electrodes, which enable ion storage throughout the (typically crystalline) solid bulk of the material.[868,891,892] (In this section, redox-active crystalline solids are distinguished from redox-active polymers, which are discussed as a separate class of materials for Faradaic electrosorption in Section 1.4.3.) The reactions that enable ion storage in these materials typically require less than 1 V.[719,851,888,893] Moreover, a high diffusivity of ions within the crystal structure is desirable to facilitate ion insertion into the electrode, which increases the capacity of adsorption and reduces energy consumption.[88] High rates can also be achieved using nanoparticles with small diffusion lengths, as in most intercalation batteries.[119,894,895] The enhanced salt capacity in redox electrodes was described theoretically by He et al., who generalized the EDL theory used for capacitive CDI electrodes to include redox-active groups.[896]

So far, three major classes of redox-active materials have been explored for use in CDI, namely $Na_2Mn_5O_{10}$ (NMO, shown in Figure 1-22c-d),[851,880,897] metal phosphates,[893,898] and PBAs.[99,888,899] PBAs are analogues of Prussian Blue in which a fraction of the iron is replaced by another metal like nickel or copper, and they are

widely investigated because of their potential longevity, high specific capacity, and facile intercalation of cations, particularly K^+.[719,743,900–904] Other materials have also been introduced in recent years, including V_2O_5,[905] TiS_2,[906] and sodium superionic conductors (NASICON), the last of which includes NMO. When subjected to an applied voltage, cations are selectively and reversibly inserted into the negatively charged crystal structure of these materials, whereas anions are electrostatically rejected. As the electrodes are charged more negatively (at increasingly positive cathodic potentials), the redox-active atoms are reduced further and more cations are drawn into the pores, which leads to desalination of the water surrounding the electrodes.[88] In practice, these materials are often combined with anodes such as Ag/AgCl and carbon to selectively adsorb the anions.[882,883,907,908]

Hybrid CDI (HCDI), first introduced by Lee et al.,[851] demonstrates this idea by pairing a redox-active electrode with a porous carbon anode.[698,885,889,904,909] Smith and Dmello discovered that redox-active materials can even be used as anodes as long as the two electrodes are separated by an IEM.[129] In the case of electrodes that selectively capture cations (e.g., NMO, metal phosphates, PBAs), the membrane must be an AEM which functions as the anion selective surface in the device.[116,129,743] The AEM in this symmetric design partitions the feed into two channels in a way that resembles ED, except the electric field is still cyclic. This mode of operation was mathematically modeled by Singh et al.[88]

Recent advances in electrosorption with intercalation materials have provided opportunities for combined theoretical and experimental studies,[86,96,129,635,896] which build on earlier models of ion intercalation in porous electrodes of lithium-ion batteries.[119,781,894,895] Redox-active systems have an electric charge that depends on the applied potential, and this variable charge yields storage capacity and ionic selectivity.[105,910] In 2017, Smith used nickel hexacyanoferrate (NiHCF) and NMO electrodes in an ED cell and developed the first model to account for two-dimensional ion transport in ED with intercalation electrodes.[116] In 2018, He et al. proposed the first model to account for the thermodynamics of electrosorption based on variable chemical charge at electrodes whose surfaces were decorated with redox-active

species.[896] This same framework was adapted to generate an equivalent circuit model to predict and validate the electroanalytical performance of intercalation materials.[911] He et al. further expanded the theory of electrosorption by redox-active materials by developing equivalent circuit models and a model based on coupled diffusion, convection, and electromigration with surface reaction kinetics.[911,912] Singh et al. also presented a theory for CDI with porous electrodes comprising nanoparticles made of a redox-active intercalation material, and the authors described the dynamics of this system in terms of concentration of the product, distribution of intercalated ions, cell potential, and energy consumption.[88] These models, however, neglect variations in ion concentration inside the particles and assume fast reactions with quasi-equilibrium adsorption isotherms. Inspired by recent progress in modeling intercalation batteries with multiphase layered materials,[781,894,895,913,914] it would be interesting to further consider the effects of coupled ion–electron transfer reactions, mechanical deformations, and phase transformations resulting from Faradaic electrosorption in porous electrodes.

Considering the many recent advances in intercalation materials, models, and cell designs summarized here, it is naturally useful to compare their desalination performances to those of traditional porous carbons. In a comparison of nine electrode materials, Pothanamkandathil et al. found that energy demands for NiHCF were lower than those of carbon materials when desalinating a 20 mM feed of NaCl without energy recovery; they were comparable, however, when assuming complete energy recovery.[915] Metzger et al. analyzed CDI with only intercalation electrodes and found that this CDI module costs approximately 27% of what a typical MCDI module does and is nearly four times smaller in volume due to the larger capacity of intercalation electrodes.[916] Liu et al. showed, however, that intercalation electrodes are more susceptible to declines in performance from organic fouling.[856]

The Role of Electron Transfer in Ion Intercalation

It is a common misconception that ion intercalation in solid host materials is a physical electroadsorption process, whenever the ion does not itself participate in redox

reactions. Indeed, lithium-ion batteries derive their name from the fact that Li^+ is inserted reversibly in each electrode without being reduced to metallic lithium, effectively shuttling back and forth during battery cycling like a “rocking chair.” This picture, reminiscent of physical adsorption, might appear to be inconsistent with peaked voltammograms for lithium-ion battery materials, which clearly signify redox reactions, similar to those shown in Figure 1-22d for intercalation electrodes used in electrochemical separations.

In the context of lithium-ion batteries, the resolution of this paradox began with the discovery of Bai and Bazant in 2014 that ion intercalation can be limited by solid–solid electron transfer reactions that reduce and oxidize nearby transition metal ions in the host crystal.[917] The authors constructed Tafel plots (logarithm of current versus overpotential) for the high-rate cathode material Li_xFePO_4 in quantitative agreement with those predicted by the quantum mechanical Marcus theory of electron transfer,[781,918,919] specifically the Marcus–Hush–Chidsey formula for electron transfer from a metallic electrode (Figure 1-23a),[920,921] and they postulated a rate-limiting step of electron transfer from the carbon coating to the iron redox site, $Fe^{2+} \rightleftharpoons Fe^{3+} + e^-$ (Figure 1-23b). They also showed that the temperature-independent curvature of the Tafel plot (Figure 1-23a) is controlled by the reorganization energy, λ, of the local “solvent" (dielectric solid environment), which is well approximated by the Marcus estimate for outer-sphere electron transfer:

$$\lambda_o = \frac{e^2}{8\pi\varepsilon_0 k_B T}\left(\frac{1}{a_0} - \frac{1}{2d}\right)\left(\frac{1}{\varepsilon_{op}} - \frac{1}{\varepsilon_s}\right) \tag{1.14}$$

based on the optical and static dielectric constants of the solid, ε_{op} and ε_s, respectively, as well as the effective radius of the reactant a_0 and the distance for electron transfer d, each set to the Fe–O bond distance, assuming direct contact of $FePO_4$ octahedra with a metallic (sufficiently thick) carbon coating.

The emerging understanding is that both mechanisms occur simultaneously, as ion intercalation in redox-active solids occurs by coupled ion–electron transfer (CIET).[922] In this new picture, classical transfer of an ion over the intercalation

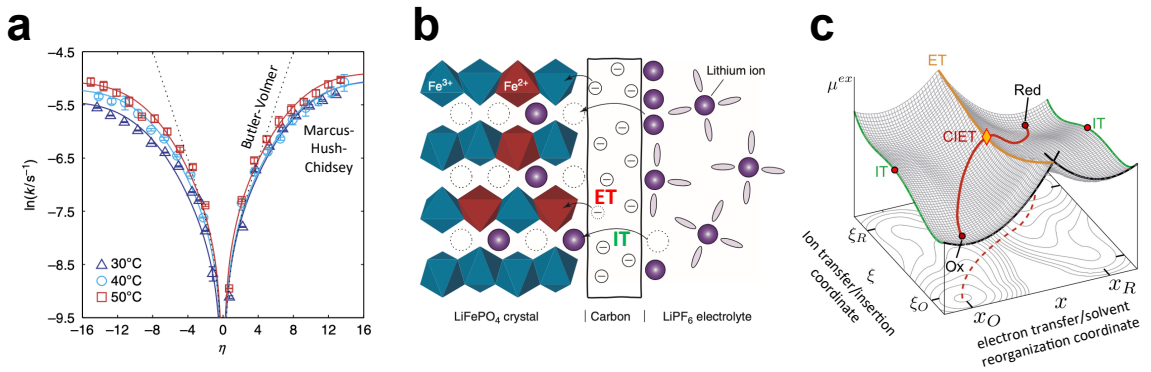

Figure 1-23. Coupled ion–electron transfer (CIET) mechanism for ion intercalation in redox-active solid electrodes. (a) Curved Tafel plots consistent with Marcus–Hush–Chidsey theory, indicating electron transfer limitation in $LiFePO_4$. (b) Sketch of lithium ion transfer (IT) coupled to electron transfer (ET) from the carbon coating to the nearest iron redox site. (c) Excess chemical potential landscape for coupled ion–electron transfer (CIET), combining the classical ion transfer coordinate with the solvent reorganization coordinate for quantum mechanical electron transfer. Panels (a-b) adapted with permission from ref 917. Copyright 2014, Nature Research. Panel (c) adapted with permission from ref 922. Copyright 2021, Elsevier.

energy barrier (dominated by the ion–electron Coulomb energy and the local dielectric response of the interface) facilitates the instantaneous quantum mechanical transfer of an electron tunneling between a localized state in the host crystal and a delocalized state in the electrode (Figure 1-23c). CIET theory is becoming widely used in modeling lithium-ion batteries,[895] and it could also be used to guide the design of Faradaic electrosorption systems from microscopic first principles. In contrast to the empirical Butler–Volmer equation, CIET theory predicts a reaction-limited current, which can be modified by tuning the electrostatic and dielectric properties of the electrode–electrolyte interface and the electronic structure of the electrode.[922,923] For example, the theory attributes the enhanced intercalation rate in Li_xFePO_4 achieved experimentally by anionic surface charge modification[924] to lowering of the ion-transfer barrier of lithium. CIET theory also reveals the roles of dielectric properties and crystal structure of the intercalation host, including generalizations of Equation 1.14 for the CIET barrier.[922]

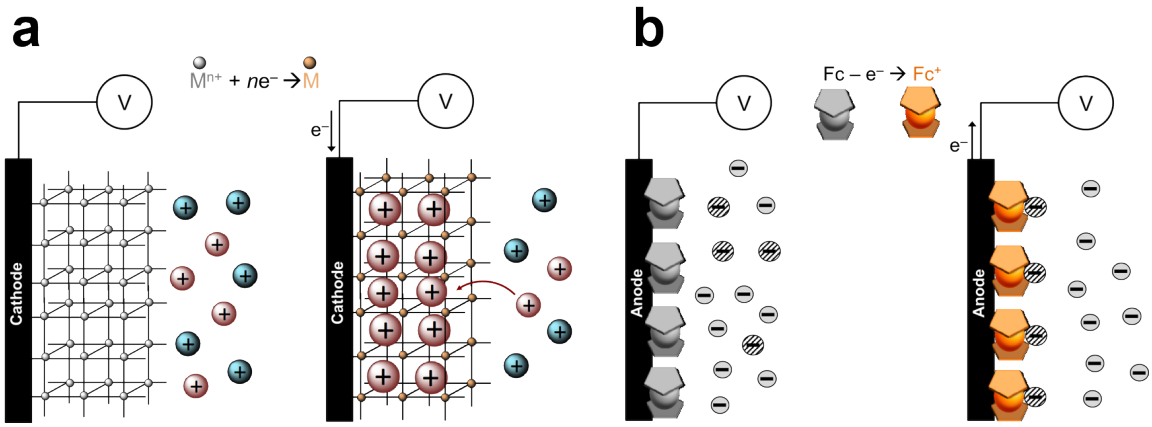

Figure 1-24. Overview of methods for water purification involving intercalation and conversion processes by (a) crystalline redox materials and (b) polymeric, single-site redox materials. Adapted with permission from ref 635. Copyright 2016 Wiley-VCH.

Ion Selectivity in Intercalation Materials

Unlike the selectivity in capacitive materials described in Section 1.4.1, selectivity in redox-active intercalation materials is achieved by insertion of specific ions into the crystalline structure, as shown in Figure 1-24a. Cyclic voltammetry of $NaTi_2(PO_4)_3$ and $Na_4Mn_9O_{18}$ indeed showed nearly one order of magnitude greater capacity for Na^+ compared to K^+, Ca^{2+}, and Al^{3+}. It was also concluded that the rate at which ions were removed from a dilute feed was limited by their transport from the bulk to the surfaces of the electrodes as well as by the concentration of noninserting (or electrochemically inert) ions.

In addition to the innovations already described in this section, several research groups developed novel device architectures and designs with the intent of selectively removing specific ions. For example, Pasta et al. created an asymmetric system in which one electrode was made of (redox-active) $Na_2Mn_5O_{10}$ and the other of (metallic) AgCl to desalinate seawater.[715] In contrast to carbon based electrodes which are slightly selective toward K^+, this system could selectively remove Na^+ with a separation factor of approximately 2.8 relative to K^+. Separation factors of more than ten were also reported for electrodes made of (redox-active) $LiMn_2O_4$ in electrolytes comprising Li^+ as well as the competing cations Na^+, K^+, Ca^{2+}, and Mg^{2+}.[692] Kim et al. reported an even higher separation factor of sixteen

for Na^+ relative to K^+ in the presence of competing ions such as Ca^{2+} and Mg^{2+} by using (redox-active) $Na_{0.44}MnO_2$ and AgCl electrodes.[925] Among the most extreme separations of Li^+, however, were those achieved by Trócoli et al.[926] who reported separation factors of 240 relative to Na^+ and 320 relative to K^+ by using (redox-active) $LiFePO_4$ and AgCl electrodes.[927,928] Recent studies that used PBAs for water desalination showed selectivity factors between 2.2 and 3.4 for K^+ relative to Na^+.[719,743,903] Although PBAs are usually selective toward monovalent cations, Singh et al. used the PBA vanadium hexacyanoferrate (VHCF) to preferentially remove Ca^{2+} in the presence of Na^+ with a selectivity factor of 3.5.[904]

Intercalation materials that are selective toward anions have also been examined in conventional CDI systems for the selective removal of PO_4^{3-} and F^-. For instance, Hong et al.[929] recently introduced ZnAl-layered double hydroxide (LDH, commonly used as an adsorbent for PO_4^{3-}) to an electrode material that is itself selective toward PO_4^{3-}.[930,931] LDH was composited with RGO to increase conductivity, and the LDH/RGO composite electrode (with activated carbon as the counter electrode) was used for selective separation of PO_4^{3-}. This composite electrode is selective toward PO_4^{3-} because as RGO boosts the conductivity of the composite electrode, the electron density of the transition metal sites in LDH is effectively reduced. The reduced metal sites then allow PO_4^{3-} to form inner-sphere complexations via an exchange reaction of ligands between the OH^- groups of the transition metal sites and PO_4^{3-}. As a result, the LDH/RGO composite electrode is selective toward PO_4^{3-} (with a selectivity factor of 6.1), even in the presence of Cl^- at ten times the concentration of PO_4^{3-}.[929] Similarly, hydroxyapatite (HA) was composited with RGO and used to selectively remove F^-:[932] as RGO boosts the conductivity, the RGO/HA composite electrode forms a region concentrated with anions near the electrode, where ion exchange occurs efficiently between OH^- in the HA metal sites and F^-.[932,933] With the HA/RGO composite electrode, the CDI system exhibited five times greater removal of F^- compared to an equivalent system with activated carbon electrodes when both were applied to an equimolar solution of F^-, Cl^-, and NO_3^-.[932]

Electrochemical Systems Design With Redox Reactions

Various cell architectures have been developed to use intercalation and conversion materials more efficiently. For instance, HCDI (shown in Figure 1-25a) is designed to increase the extent of desalination by using the Faradaic electrode as a working electrode. Since this design slows desalination, a capacitive carbon electrode is included to mitigate the reduction in the rate of ion removal.[851,893,934] HCDI systems usually comprise intercalation or conversion materials, such as $Na_4Mn_9O_{18}$[851] and $Na_2FeP_2O_7$,[893] as the negative electrode to selectively capture Na^+, along with porous carbon and an AEM as the positive electrode to capture the anions. $Na_4Mn_9O_{18}$ and $Na_2FeP_2O_7$ could be categorized as one-dimensional insertion materials that store and diffuse cations, especially Na^+, in their tunnel structures.[925,935] Compared to a system with ordinary capacitive electrodes (which had a capacity of $13.5\,mg\,g^{-1}$ and a maximum removal rate of $0.048\,mg\,g^{-1}\,s^{-1}$), Lee et al. demonstrated major improvements in the capacity ($31.2\,mg\,g^{-1}$) and maximum removal rate ($0.066\,mg\,g^{-1}\,s^{-1}$) by using HCDI with an NMO electrode, as shown in Figure 1-26a.[851] The HCDI system comprising $Na_2FeP_2O_7$ was also compared to an MCDI system based on capacity and rate capability using a CDI Ragone plot (see Figure 1-26b).[893] The Ragone plot of the HCDI system showed improvement in the capacity of ion removal by up to 150% relative to the MCDI system, which was attributed to the high capacity of $Na_2FeP_2O_7$. Moreover, the HCDI system achieved a rate capability comparable to that of its MCDI counterpart.[893] The hybrid use of electrodes has also been shown to enhance desalination performance in FCDI systems. As illustrated in Figure 1-25b, Chang et al. used copper hexacyanoferrate (CuHCF, a PBA) as the flow-negative electrode and activated carbon as the flow-positive electrode.[936] This system exhibited a higher rate of salt removal (up to $0.12\,mg\,cm^{-2}\,min^{-1}$) and a greater efficiency (up to 96%) compared to a system with only activated carbon electrodes.

Recently, several studies introduced dispersed redox species in various multi-channel architectures to further improve performance.[820,939–942] By using two IEMs

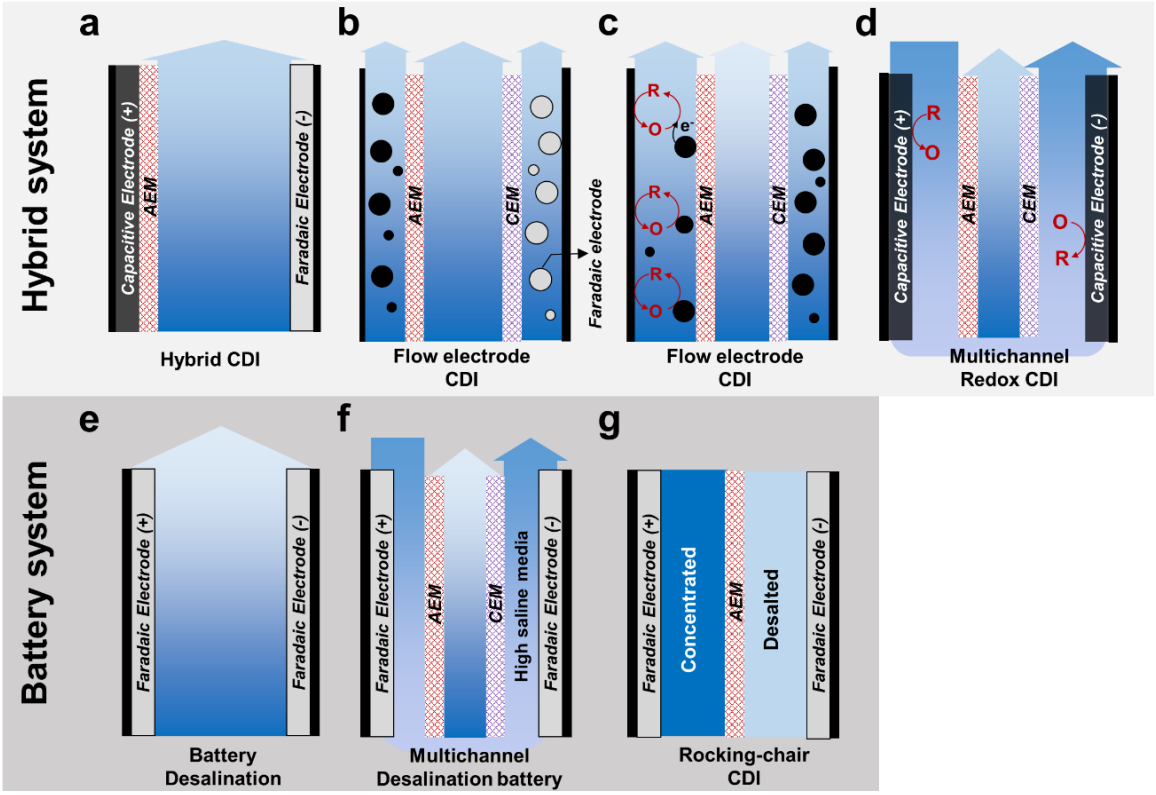

Figure 1-25. Schematic illustrations of CDI systems that use intercalation and conversion materials as electrodes. Adapted with permission from ref 937. Copyright 2020, Multidisciplinary Digital Publishing Institute.

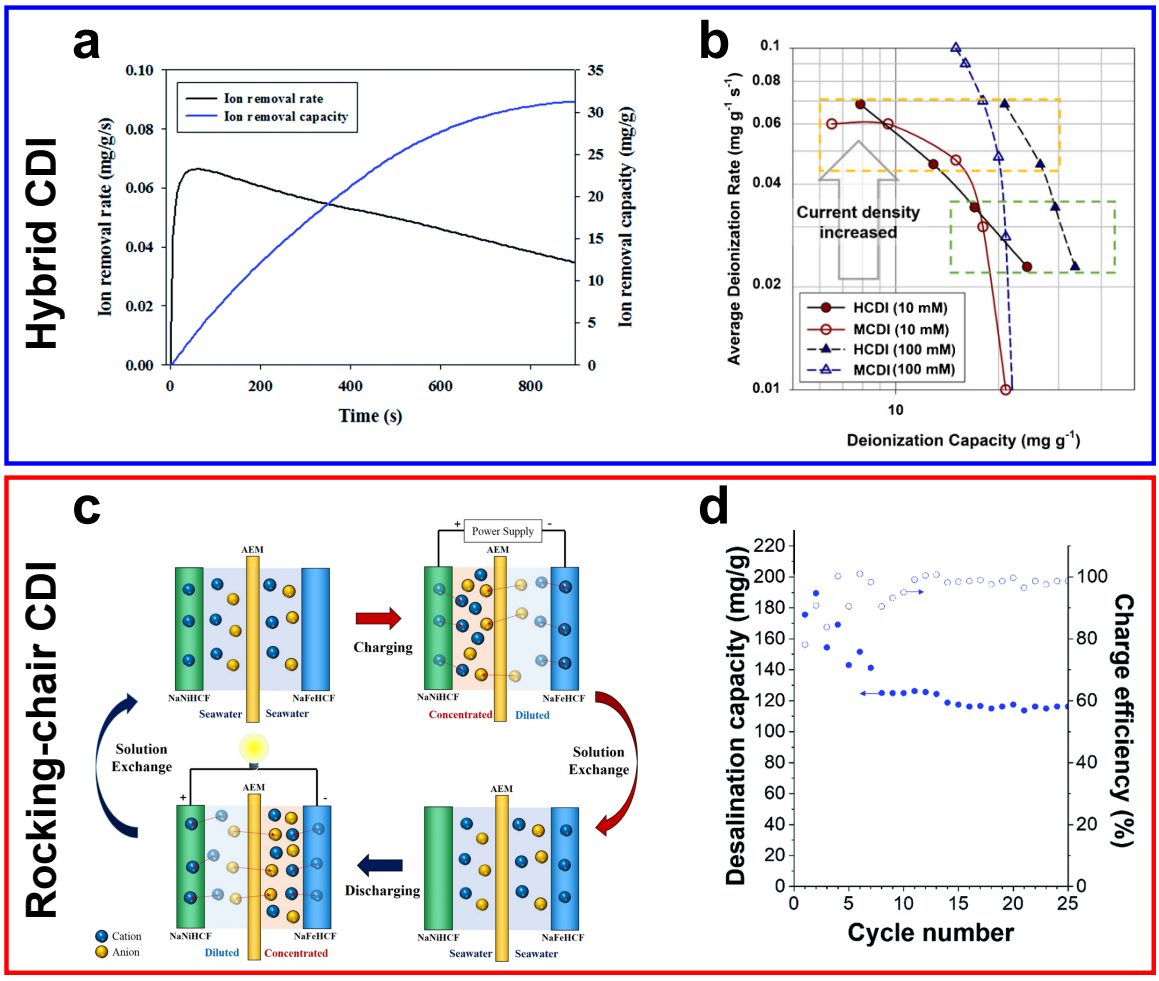

Figure 1-26. Representative results and mechanisms of CDI with intercalation and conversion electrodes. (a) Ion removal capacity and maximum removal rate in HCDI applied to a 10 mM solution of NaCl; the system is operated at 1.2 V for 15 min during the capture step and at −1.2 V for 15 min during the release step. Reproduced with permission from ref 851. Copyright 2014, Royal Society of Chemistry. (b) Ragone plot of HCDI (with $Na_2FeP_2O_7$) and MCDI for feed concentrations of 10 mM and 100 mM. Reproduced with permission from ref 893. Copyright 2016, Elsevier. (c) Mechanism and (d) performance metrics of RCDI applied to a 600 mM solution of NaCl; the system is operated at a cell voltage of 200 mV. Panel (c) reproduced with permission from ref 719. Copyright 2017, American Chemical Society. Panel (d) reproduced with permission from ref 938. Copyright 2019, Royal Society of Chemistry.

to provide different environmental conditions between the feed and electrolyte, the redox reaction can occur without contaminating the feed.[820,937,939–942] For instance, the use of redox-active species significantly improves charge transfer in FCDI by overcoming some of the limitations of charge transfer between current collectors and particles in the flow electrodes (see Figure 1-25c; details are provided in Section 1.4.1).[820,939] Although many studies have suggested increasing either carbon content or salt concentration to reduce the internal resistance of the electrode channels, the conductivity of these channels could be compromised if the carbon particles were to aggregate.[820,943] Ma et al. thus proposed the use of hydroquinone (H_2Q) as an electron mediator that shuttles electrons from the current collector to the particles in the flow electrodes.[820] As a result, the deionization system exhibited an increase of 131% in the average rate of salt removal compared to the same system in the absence of H_2Q.[820] Kim et al. used redox species as an additional means for salt removal in the multichannel redox system (see Figure 1-25d).[940] In this system, the redox reaction between $Fe(CN_6)^{3-}$ and $Fe(CN_6)^{4-}$ further remove ions from the feed to maintain bulk electroneutrality in the electrolyte,[937] and the redox species are continuously regenerated as the redox couple circulates the electrodes. Overall, the desalination performance of this system (with a capacity of $67.8\,mg\,g^{-1}$) was improved by more than a factor of three compared to the same system in the absence of the redox species (with a capacity of $20.0\,mg\,g^{-1}$).[940]

Another active area of research is on the development of various configurations of battery desalination,[715,719,881,884,938,944–947] where both capacitive electrodes are replaced by intercalation or conversion materials. This concept, shown in Figure 1-25e, was first introduced by Pasta et al. who used NMO to capture Na^+ and Ag to capture Cl^-.[715] Following this study, several intercalation and conversion materials have been used in desalination battery systems to overcome the limited capacity of capacitive electrodes. Electrodes used to capture Na^+ include NMO,[715] $NaTi_2(PO_4)_3$,[884,946] and PBAs,[948] and electrodes used to capture Cl^- include Ag and Bi. Since conversion electrodes have high theoretical specific capacities, they are typically used as counter electrodes.[715,884,946,948–950] Conversion reactions, how-

ever, can lead to poor electrode stability due to repeated volume expansion and contraction over many cycles.[951] Despite this drawback, battery desalination systems are regularly used to recover Li^+ using selective electrodes such as LMO[949] and $LiFePO_4$[950] because of the structural advantages these electrodes exhibit toward Li^+. For instance, the tetrahedral sites of LMO and $LiNi_{0.5}Mn_{1.5}O_4$ are narrowly spaced and enables selective removal of Li^+ relative to larger cations.[952–954] Although the use of Faradaic materials can significantly increase the capacity of salt removal, they tend to limit the rate at which salt is removed.[117,955] Initial studies showed that CDI with activated carbon permits an applied current greater than $1\,mA\,cm^{-2}$,[115] whereas intercalation electrodes limit the applied current to $\sim 100\,\mu A\,cm^{-2}$.[115,719,743]

Lee et al. recently proposed a multichannel desalination battery, as shown in Figure 1-25f, to overcome the mass transfer limitations of traditional desalination batteries.[947] The multichannel system was designed to have two independent channels (one for both electrodes and one for the feed) by placing an IEM at each interface.[947,956] The two electrodes (NaNiHCF and Ag) were exposed to a concentrated solution (1000 mM of NaCl) to reduce the resistance of the system, and the high salinity of the electrolyte significantly improve the capacity ($52.9\,mg\,g^{-1}$) and removal rate ($0.0576\,mg\,g^{-1}\,s^{-1}$).[947] Lee et al. also demonstrated the continuous battery desalination system known as "rocking-chair" CDI (RCDI; Figure 1-25g).[719] This configuration is usually made of two different PBAs, such as NaNiHCF and NaFeHCF, separated by an AEM. During the charging step, the working electrode (NaFeHCF) captures cations, while anions move to the counter electrode (NaNiHCF) to maintain bulk electroneutrality. During the discharging step, the working electrode is regenerated while the counter electrode captures cations, which enables continuous desalination with a removal capacity of $59.9\,mg\,g^{-1}$ (Figure 1-26c).[719,944,945] In the same manner, the cation selective electrodes can be replaced with anion selective conversion electrodes such as Ag/AgCl for even greater continuous desalination (85[881]-115[938] $mg\,g^{-1}$) at a low operating voltage ($\approx 200\,mV$; Figure 1-26d).[881,938] During oxidation of the Ag electrode, Ag reacts with Cl^- in solu-

tion to form AgCl by breaking Ag–Ag bonds. Since both the oxidation and reduction peaks of Ag/AgCl occur at a low cell potential (220 mV versus SHE), this Faradaic process requires only a small input of energy (ranging between $2.5\,k_BT\,\mathrm{ion}^{-1}$ [938] and $10\,\mathrm{kJ\,mol}^{-1}$ of salt[881]). By adapting these cell architectures to existing designs, the desalination performance of conventional systems can be greatly improved using intercalation and conversion electrodes.

1.4.3 Electrosorption by Redox-Active Polymers

As illustrated in Figure 1-24, Faradaic redox reactions occur when there is transfer of n electrons at the surface of an electrode that changes the oxidation state of a reactant[957,958]. The equilibrium thermodynamics of these reversible Faradaic reactions are governed by the Nernst equation.[781,959–961] In this review, the notion of a Faradaic process encompasses reactions at electrodes regardless of the phase in or across which the reactants are moving or are present. For instance, a Faradaic process could be either a redox event at a surface[86] or a variety of side reactions in which the electrons are transported across the electrolyte (e.g., water splitting, oxygen reduction).[89,962] Faradaic processes, combined with rich redox chemistry, have been extensively studied for a variety of applications, including energy storage,[963,964] bioelectrochemistry,[965] sensing,[966–968] and electrocatalysis.[969,970] As explained in Section 1.2, nonelectrosorptive electrochemical methods rely on Faradaic reactions, be it through dissolution of a metal electrode or changes in the oxidation state of a dissolved species for plating. In the context of water purification by capacitive electrosorption, electron transfer and redox reactions are common, even without the use of external electroactive species. If left unregulated, these reactions could be parasitic and in turn degrade the electrodes, produce undesired byproducts, and reduce the efficiency of the primary electrochemical process.[152,962]

In this section, we focus on electrosorption promoted by redox reactions at active polymer electrodes, which boost energy efficiency and, more importantly, enable molecular selectivity. Materials with intrinsic Faradaic properties have long been

studied and used for applications in energy storage.[971,972] Batteries, for example, store electric charge by Faradaic intercalation reactions and by changes in the oxidation state of a crystalline solid subjected to an electric field. These synthetic materials confine the redox reactions to within the solid electrode itself, without loss of electrons or transfer of ions across the electrolyte. Moreover, the surface reactions that occur usually promote specific binding of ions by creating sites of fixed charge that enable noncovalent interactions, such as hydrogen bonding, charge transfer processes, and hydrophobic transitions. From the perspective of electrochemical engineering, Faradaic materials also enable greater control of the window of operating voltages and suppress leakage currents and parasitic side reactions that would otherwise be detrimental to the longevity of the system.[910] The properties and applications of redox-active polymers are described in the sections below.

Overview of Redox-Active Polymers

Electrochemically tunable redox polymers, defined by the IUPAC as polymers with groups that can be either oxidized or reduced, play a key role as stimuli-responsive materials in many chemical and biochemical applications.[973] These materials have several properties that can be modulated electrochemically, such as reactivity,[974] mechanical actuation,[975] sensing,[976] and energy storage.[977] As shown in Figure 1-27, the redox group can exist either directly on the backbone of the polymer chain, as is the case of polyanilines, polypyrroles, and polyquinones, or in pendant groups like ferrocene.[978] Redox-active polymers with electroactive units in the main chain are often conjugated[979] and comprise π-bonds that enable semiconductivity. While some of these semiconducting polymers have linear backbones, such as polyacetylene, many have conjugated backbones made of aromatic groups, such as polyaniline (PANI) and polypyrrole (PPy). Both PANI and PPy have been used extensively in electrosorption, particularly for enhanced CDI.[96,980–984] Redox polymers with active units in pendant groups, like pendant-group metallopolymers, are charged by a combination of bounded diffusion and electron hopping (or free diffusion).[985] Although these materials are less electrically conductive, they exhibit unique elec-

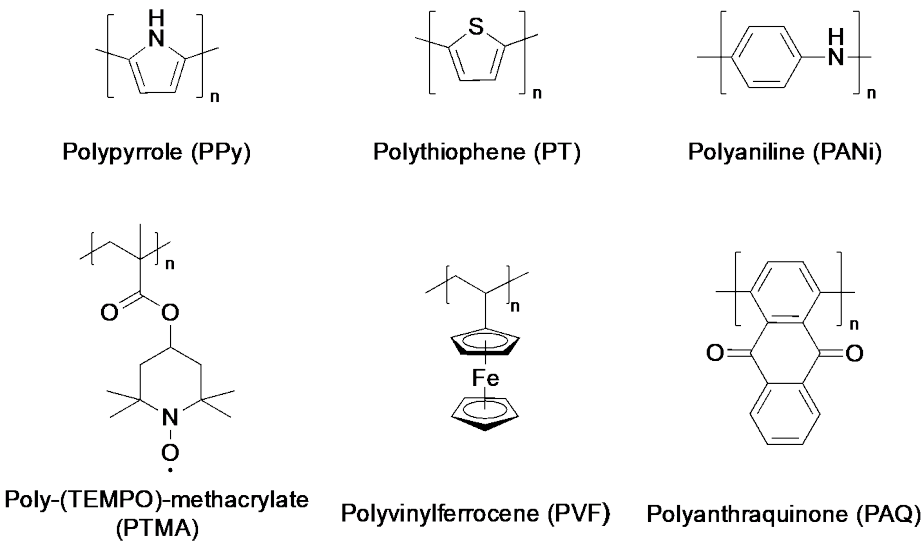

Figure 1-27. Chemical structures of representative redox-active and conducting polymers used to study selective electrochemical separations.

tronic properties and charge transfer interactions that make them highly selective toward target ions.[96,102,986]

Faradaic electrosorption relies on a change in the oxidation state of the electrode by electron transfer, which in turn influences the environment of the material. In a complementary manner, the solvent and immediate environment affect the behavior of redox polymers.[987,988] The oxidation or reduction of a redox polymer, for example, creates a fixed charge that selectively binds counterions by either ion exchange or insertion and release of the ions.[86,96,987–990] For redox systems that favor oxidation, the following chemical reactions are observed:

$$A^{n-} + n[P^+X^-] \rightleftharpoons [P_n{}^+A^{n-}] + nX^- \tag{1.15a}$$

$$A^{n-} + P_n \rightleftharpoons [P_n{}^+A^{n-}] + ne^- \tag{1.15b}$$

The first reaction describes a redox polymer P^+ (e.g., PPy) in which the weakly bound ion X^- is exchanged with the substituent ion A^{n-}. The second reaction describes a redox polymer P_n that is initially uncharged but, after undergoing oxidation (e.g., the transition from ferrocene to ferrocenium), can bind the counterion A^{n-} to a cationic group. In this process of binding, the affinity of the ions to the elec-

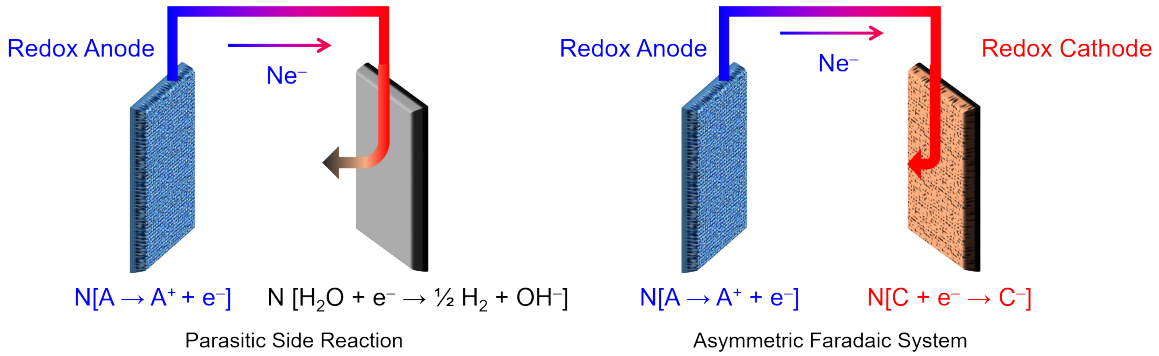

Figure 1-28. Suppression of side reactions using an asymmetric redox electrode configuration. Adapted with permission from ref 910. Copyright 2017, Royal Society of Chemistry.

trodes influences the electrochemical kinetics of adsorption. Ions that are strongly bound often facilitate electron transfer and shift the formal potentials, which makes the use of tunable redox polymers well suited for selective electrosorption and sensing.[986,991,992] Redox polymers, especially pendant-group metallopolymers, can also modulate electrode potentials, which prevents excursions in potential that would otherwise lead to side reactions. The suppression of parasitic side reactions (e.g., water splitting) improves performance and enables better control of water chemistry, as explained in Figure 1-28.[102,910,993] In the following sections, we describe recent advances in redox-active polymers for the separation of common pollutants like ions and uncharged contaminants.

Molecular Selectivity of Redox-Active Polymers

The main advantage of molecularly selective technologies is the ability to target a minority species in the presence of excess competing molecules. Redox-active polymers have facilitated the realization of this capability by enabling selective electrosorption and reversible release at fixed electric potentials. Because of their favorable electrochemical kinetics, electroactive polymers have been considered for various applications in analytical sensing.[994–997] The mechanisms of selective ion sorption onto conducting polymers have been studied since the advent of ion exchange voltammetry.[998–1000] For example, electroactive polymer films can be used as selective sensors by pre-concentrating them with a certain counterion from the contacting solution phase.[1001,1002] Conducting polymers (e.g., PANI, PPy),[1003,1004]

redox polymers,[990,1005–1007] and polymers entrapping redox units[1008–1010] have also been used for ion doping. These materials represent the archetypal systems of modified electrodes used during the development of electroanalytical chemistry.[959] The mechanisms of selectivity vary depending on the chemical structure of the redox monomer, the hydrophobicity of the polymer, and the electrostatic properties of the ions themselves. In general, the combination of controlled electric potentials and tailored molecular selectivity makes electroactive polymers a promising platform for energy efficient purification of water, recovery of valuable resources, and separation of fine chemicals.

Metallopolymers are one class of polymers that display electrochemically switchable properties, possess favorable electron transfer kinetics, and enable a diverse array of synthetic pathways for structural modification and tuning.[1011–1013] Recently, these materials were used as heterogeneous coatings on porous carbon to improve the capacity of energy storage. In particular, the noncovalent conjugation of polyvinylferrocene (denoted as PVF or PVFc) with CNTs was demonstrated by organic solution deposition and by electrodeposition.[1014,1015] The resulting systems displayed high capacitances ($1450\,\mathrm{F\,g^{-1}}$) and energy densities ($79.5\,\mathrm{W\,h\,kg^{-1}}$).[1015] Through similar electrochemical methods, the charged moieties of metallopolymers can be used to capture and release anions efficiently. Films of PVF are oxidized in water over a range of positive potentials near $0.3\,\mathrm{V}$ versus $\mathrm{Ag/AgCl}$,[1016] which is characteristic of stable electron transfer kinetics. Depending on the heterogeneity of the film, however, the applied voltage needed to fully charge all immobilized ferrocene units can be higher (in the range of 0.6-$0.8\,\mathrm{V}$ versus $\mathrm{Ag/AgCl}$), as was indicated by the large peak separation of different redox films in various electrolytes.

Redox-based electrosorption is cyclical and operates by electrochemical swings to capture target ions. During adsorption, electrodes become positively charged due to the formation of oxidized sites. Captured ions are then released by reversing the polarity due to the reduction of the redox adsorbent, as demonstrated in Figure 1-29a. The redox of PVF, for example, is used to selectively extract organic anions such as carboxylates, phosphonates, and sulfonates from water in the pres-

ence of excess ions and without the use of chemical additives.[96,910,986,1017] Since many organic micropollutants like pesticides (e.g., metolachlor-based pesticide), microplastics, and pharmaceuticals (e.g., ethinyloestradiol contraceptive, propranolol hydrochloride beta-blocker) are negatively charged,[1018–1020] electrosorption of negatively charged species is carried out in batches. In such a process, the functionalized redox electrode is immersed in an electrolyte comprising the minority organic anion (in concentrations ranging from 0.1 mM to 3 mM) as well as excess competing ions like ClO_4^- and Cl^- (in concentrations exceeding 100 mM). The transformation of ferrocene to ferrocenium results in a positively charged surface, which then electrostatically draws anions in solution to that surface. Systems based on PVF were also found to be stable over numerous cycles, and they generally display molecular selectivity, efficient use of energy, and a high capacity for uptake and storage of charge.[910] One example, shown in Figure 1-30a, is a system that paired a PVF anode with a polyanthraquinone (PAQ) cathode, which was effective compared to other systems at separating carboxylate, as quantified by an electrosorption capacity as high as 157 mg of anion per gram of adsorbent.[1017] Figure 1-30b reveals a relationship between the amount of oxidized species and the applied potential, and it shows that the utilization efficiency of ferrocene was lower than 100% during charging, which may be attributed to either active sites being inaccessible or redox units being kinetically trapped. In municipal wastewater, trace amounts of micropollutants usually exist in the range from micrograms to below a nanogram per liter.[1021] Demonstrating the effectiveness of electrochemical separations of trace micropollutants will thus provide insight into industrial feasibility.

As illustrated in Figure 1-29, redox-active electrodes made of PVF were recently used to selectively extract toxic heavy metal oxyanions, namely chromate (CrO_4^{2-}), arsenate (AsO_4^{3-}), and vanadate (VO_4^{3-}).[102,1022,1023] The concentrations of chromium and arsenic were as low as $100\,\mu g\,L^{-1}$, and the experiments were performed in the presence of secondary wastewater components and excess competing ions at 200 times the concentration of the target ions. This process displayed a high capacity for ion exchange ($>$ 100 mg of metal per gram of adsorbent; see

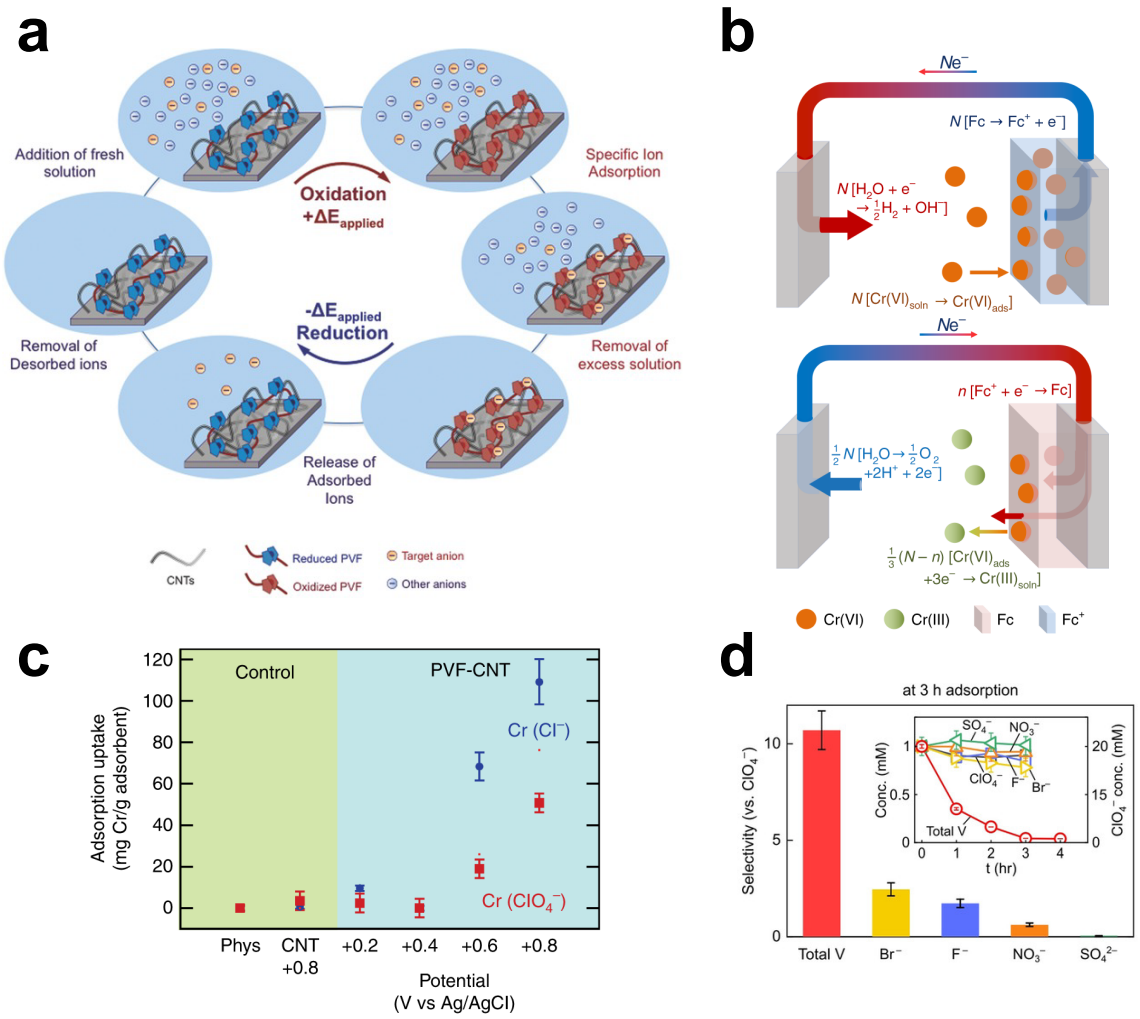

Figure 1-29. Electrochemical control of redox-active polymers for selective electrosorption. (a) Illustration of the concept of redox-based capture and release of a target anion. Reproduced with permission from ref 986. Copyright 2016, Wiley-VCH. (b) Selective separation of chromium at a PVFc electrode; the schematic shows both charging and discharging steps as well as the reactions that occur at each counter electrode. (c) Results of adsorption uptake of chromium on PVFc working electrodes as a function of potential. Reproduced with permission from ref 1022. Copyright 2018, Nature Research. (d) Calculated selectivity of individual anions (0.5 mM each) relative to a competing anion (20 mM of ClO_4^-) after three hours of adsorption on PVFc-CNT at 0.8 V (versus Ag/AgCl). Reproduced with permission from ref 1023. Copyright 2020, Wiley-VCH.

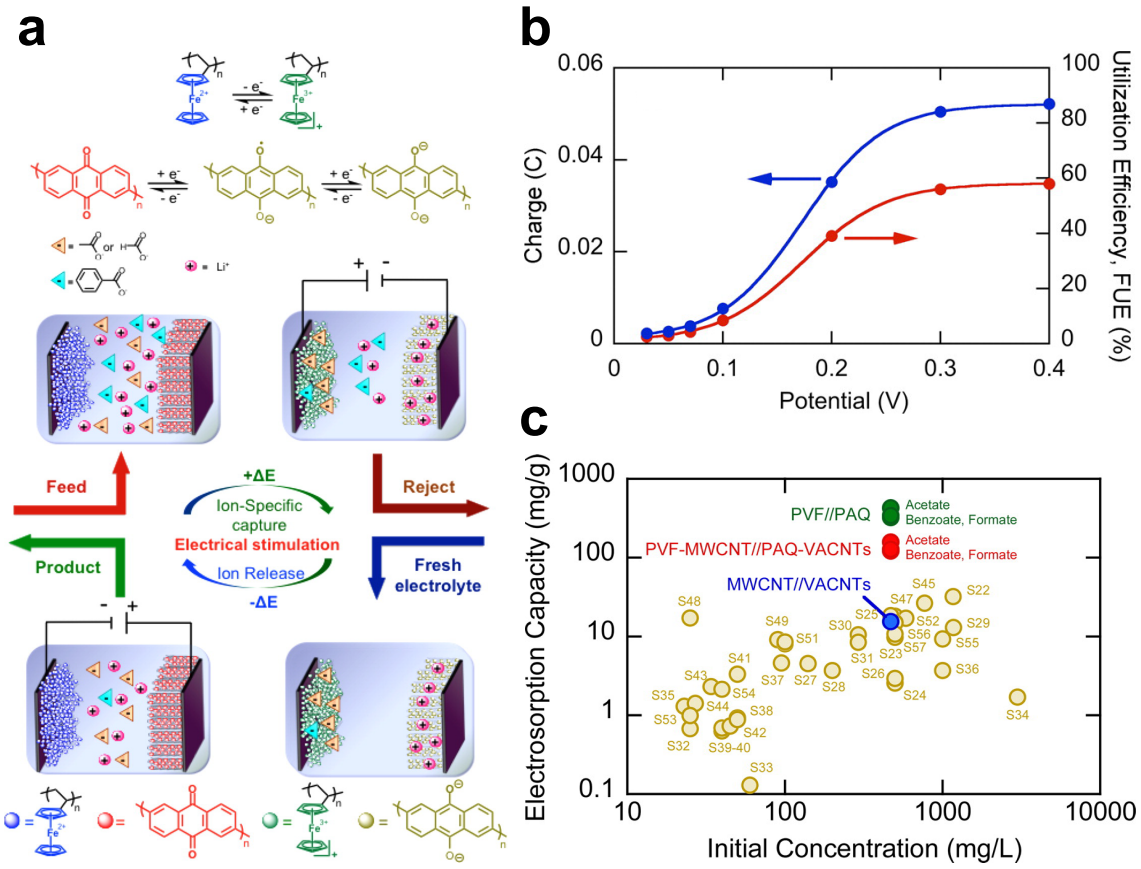

Figure 1-30. Operating principles of pseudocapacitive separation of ions. (a) Asymmetric PVFc/PAQ system for electroregulated, selective recovery of lithiated carboxylates. (b) Variations in charge and ferrocene utilization efficiency (FUE) as functions of the applied potential. (c) Electrosorption capacity of this system compared to other supercapacitors reported in the literature (denoted by the light colored symbols). Reproduced with permission from ref 1017. Copyright 2016, American Chemical Society.

Figure 1-29c), fast kinetics ($< 5\,\text{min}$ of equilibrium uptake) at moderate potentials ($\approx 0.8\,\text{V}$ versus Ag/AgCl), and nearly complete electrochemical reversibility. The redox-based mechanisms of electrosorption for PVF were inferred from its electrochemical behavior, where an increase in the uptake of anions was correlated with an increase in redox charging.[1022] In-situ measurements using transmission electron microscopy (TEM) supported the hypothesis that the insertion of ions into redox films was the main mechanism for selectivity, and there was no evidence of plating or phase changes of the transition metal during electrosorption.[1022] Further analysis revealed that Cr(VI) (hexavalent) was reduced to the less toxic Cr(III) (trivalent) during the release step due to thermodynamic speciation at the electrified surface, favored by regulation of solvent pH at the counter electrode.[1022] This Faradaic reaction worked to the benefit of water purification because Cr(VI)—often produced in industrial processes—is carcinogenic, unlike Cr(III) which is an essential element in the human diet.[1024–1026]

When using metallopolymers for electrosorption, one of the main mechanisms of selectivity is charge transfer. Quantum calculations of electronic structure have pointed to a strong correlation between charge transfer at the redox moieties and the binding energy of the participating anion.[986,1022] For example, the binding energies of Cl^-, $ClO_4{}^-$, $CrO_4{}^{2-}$, and $HAsO_4{}^{2-}$ with ferrocenium were calculated to be $2.90\,\text{kcal}\,\text{mol}^{-1}$, $3.47\,\text{kcal}\,\text{mol}^{-1}$, $5.53\,\text{kcal}\,\text{mol}^{-1}$, and $4.73\,\text{kcal}\,\text{mol}^{-1}$, respectively. These computations were performed using density functional theory (DFT) with corrections for entropic and solvation effects. Analysis of the binding of ferrocenium to anions, with supporting evidence from nuclear magnetic resonance (NMR) spectroscopy, has also underscored the role of cyclopentadienyl ligands on intermolecular binding. Once oxidized, ferrocenium (both the metal and the ligand) becomes a strong acceptor of charge that is selective toward anions. This selectivity was observed in both aqueous and organic solvents (e.g., acetonitrile), particularly during the removal of carboxylates in the presence of competing anions like hexafluorophosphate.[986,1017,1027,1028] The introduction of chemical interactions is thus what enables selective separations by redox electrodes made of metallopolymers.

More recently, radical-based redox polymers were also found to be highly effective at molecular separations for water purification. Kim et al. showed that TEMPO-based copolymers are effective at selective adsorption of per- and polyfluoroalkyl substances (PFAS) based on their affinity toward these polymers.[1029] PFAS contaminants are highly persistent and difficult to both capture and degrade due to their unique physicochemical properties. In the work by Kim et al., redox copolymers with amine functional groups and redox-active nitroxyl radical groups were used to achieve high selectivity and uptake of various PFAS compounds, with separation factors exceeding 500 relative to Cl^-. Furthermore, the use of BDD as the counter electrode reduced energy consumption and enabled degradation of PFAS—which was selectively adsorbed on the redox polymer electrode—in the electrode regeneration step. By tuning the ratio of amines to radical groups, the electrochemical regeneration and selectivity toward PFAS could be further improved.[1029]

Redox Separation of Uncharged Pollutants

Redox systems have recently been used to capture and release uncharged contaminants from water via hydrophilic-to-hydrophobic transitions. Many environmental micropollutants are uncharged pharmaceutical and personal care products (PPCPs) that are hazardous to humans and animals.[1030–1033] PPCPs have unique physicochemical properties and are often present in water in trace quantities, which complicates the removal of these contaminants by conventional methods such as adsorption, precipitation, biological treatment, and membrane filtration.[1032,1034–1036] As shown in Figure 1-31, Faradaic electrodes have been used to selectively capture uncharged micropollutants based on the electrochemically tunable affinity of these redox-active electrodes to the contaminants.

Prior work on chemical switching in redox-polymers, shown in Figure 1-31a, revealed the possibility of extracting an uncharged compound such as butanol from water based on its affinity to a copolymer of hydroxybutyl methacrylate (HBMA) and vinylferrocene (VF).[1037] The selectivity of the redox gel to butanol in the reduced state was reported in terms of a separation factor equal to the ratio of

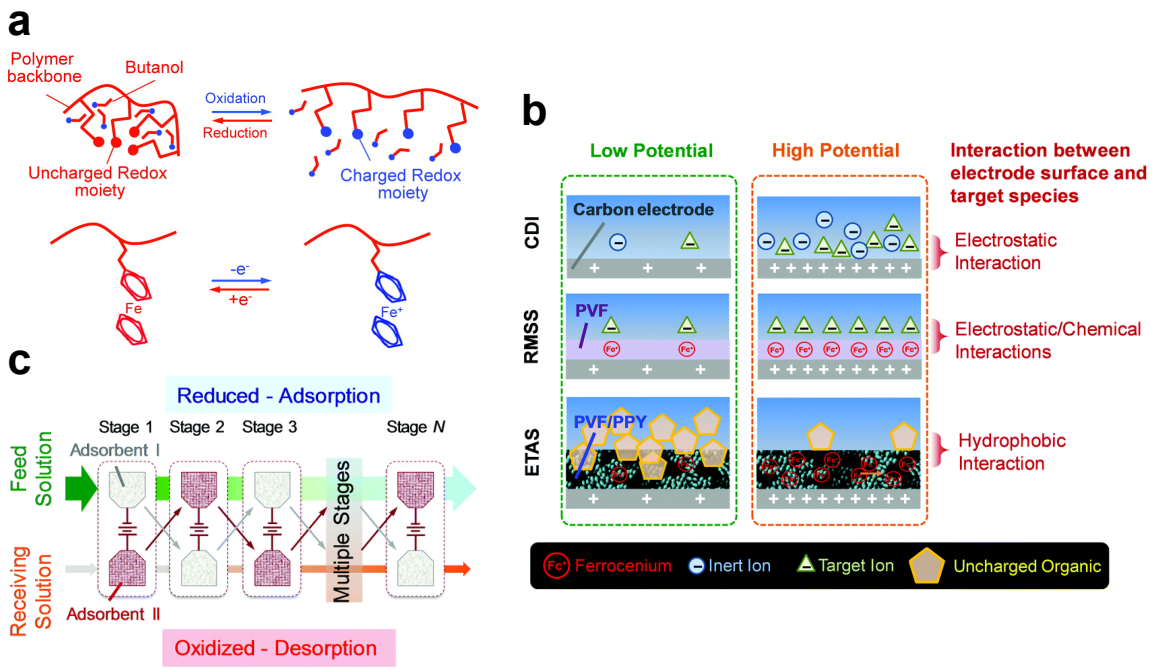

Figure 1-31. Faradaic systems with electrochemically tunable affinity for controlled capture of uncharged contaminants. (a) Redox of a ferrocene copolymer for separation of butanol from water. Reproduced with permission from ref 1037. Copyright 2011, American Chemical Society. (b) Comparison of the mechanisms of selectivity in CDI, RMSS, and ETAS. (c) Multistage electrochemical concentration of uncharged species using the ETAS process. Reproduced with permission from ref 103. Copyright 2018, Royal Society of Chemistry.

the equilibrium distribution coefficients (see Equation 1.16) of butanol and water, which was shown to exceed 5. This selectivity was attributed to the hydrophilic-to-hydrophobic transition and preferential swelling of the solvent within the gel.[1037] The concepts presented in this system served as the basis for electrochemically tunable affinity separations (ETAS), which leverage the redox switchable hydrophobicity of polymers to achieve targeted separations. Figure 1-31b compares the principles of electrostatic CDI, redox-mediated selective separations (RMSS), and ETAS.[103] In ETAS, a nanostructured blend of PVF and PPy was used to remove and concentrate a collection of uncharged organic pollutants, including dyes like methyl orange, endocrine disruptors like ethinylestradiol, and toxic chemicals like dichlorophenol and bisphenol. The PVF/PPy electrodes were synthesized by simultaneous electropolymerization of pyrrole and electrodeposition of PVF, which yielded a homogeneous coating of the PVF/PPy system onto a carbon cloth, as shown in Figure 1-32.[103,1038] These nanostructured hybrid materials also possess supercapacitive properties ($>500\,\mathrm{F\,g^{-1}}$) superior to those of their individual components (PVF with $79\,\mathrm{F\,g^{-1}}$ and PPy with $27.3\,\mathrm{F\,g^{-1}}$), without the use of carbon nanomaterials.[1038] Differential selectivity in ETAS was quantified using the distribution coefficient K_D:

$$K_D = \frac{Q_e}{c_e} \tag{1.16}$$

where Q_e is the adsorption capacity (in $\mathrm{mg\,g^{-1}}$) and c_e is the concentration of the target contaminant at equilibrium. The distribution coefficient is a function of the applied electric potential (see Figure 1-32f) and the physicochemical properties of the contaminants.[103] As shown in Figure 1-31c, ETAS was implemented in a multistage cyclic batch process to concentrate target uncharged species by several orders of magnitude. The principle of hydrophobic transitions was taken a step further by using complementary asymmetric electrodes.[104]

Electrode Design for Faradaic Electrosorption

As explained in Section 1.4.1, parasitic reactions compromise the performance of electrochemical systems.[782,1039] These unwanted side reactions lower current effi-

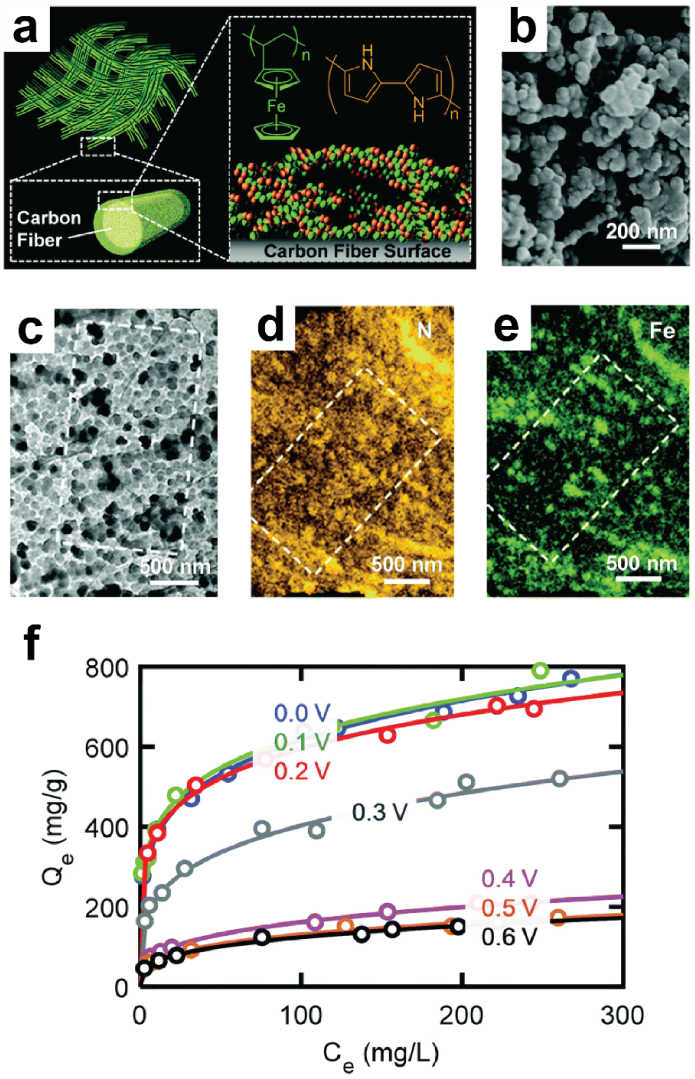

Figure 1-32. Imaging and analytical characterization of PVF/PPy coatings on a carbon cloth. (a) Schematic illustration of the ETAS adsorbent made of PVF/PPy coated on a flexible carbon substrate. Images of the PVF/PPy system using (b) SEM, (c) TEM, (d) energy dispersive X-ray spectroscopy (EDS) N mapping, and (e) EDS Fe mapping. (f) Adsorption isotherms of PVF/PPy at different potentials. Open circles represent experimental data and solid lines are fits based on the Freundlich adsorption model. Reproduced with permission from ref 103. Copyright 2018, Royal Society of Chemistry.

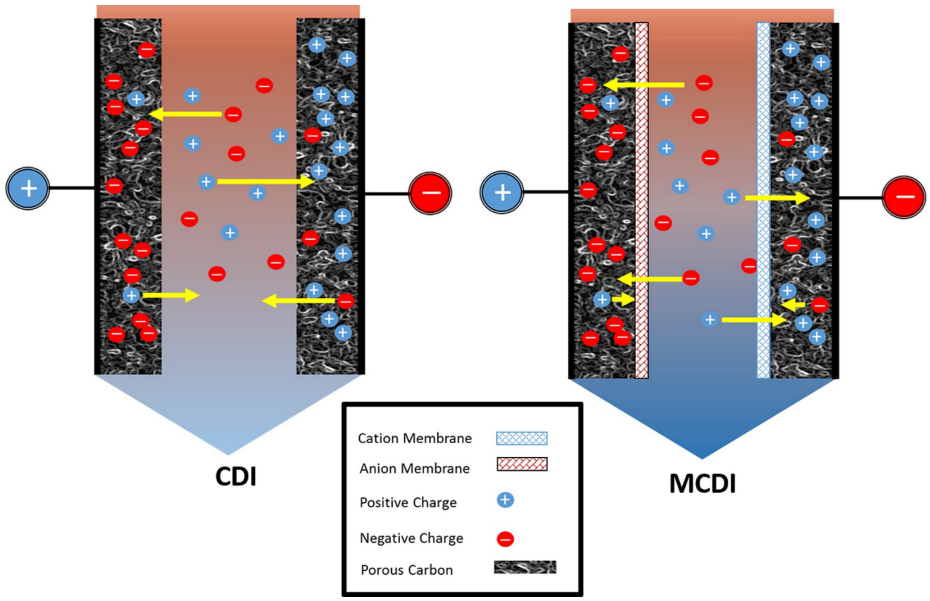

Figure 1-33. Comparison between the designs of conventional CDI and MCDI. Membranes in the latter repel coions and prevent them from escaping to the bulk, which in turn attracts more counterions to preserve electroneutrality. Reproduced with permission from ref 1040. Copyright 2014, American Chemical Society.

ciency and negatively impact the chemistry of the solution, for example by producing hydroxides which lower selectivity toward anions. Asymmetric configurations of the electrodes have thus been proposed to mitigate parasitic reactions and to improve efficiency. Innovations in this area encompass both Faradaic and nonFaradaic systems and involve the use of asymmetric membranes in CDI configurations,[1040] differential functionalization of the electrodes,[1041,1042] or implementation of asymmetric redox chemistries.[96,910,993] In one such example, the performance of CDI was improved by placing IEMs at the electrodes due to better adsorption of counterions and prevention of coions from escaping to the bulk, as shown in Figure 1-33.[672,1040]

Within the context of Faradaic systems, symmetric and asymmetric configurations have been proposed to improve charge storage in pseudocapacitors[1043–1045] and batteries.[1046–1048] Similar principles hold with regard to electroseparations: that is, the better the capacity for energy storage, the more ions will be separated and retained. Moreover, systems in which electron transfer occurs at a fixed, well-defined redox potential can help control the voltage window to limit side reactions

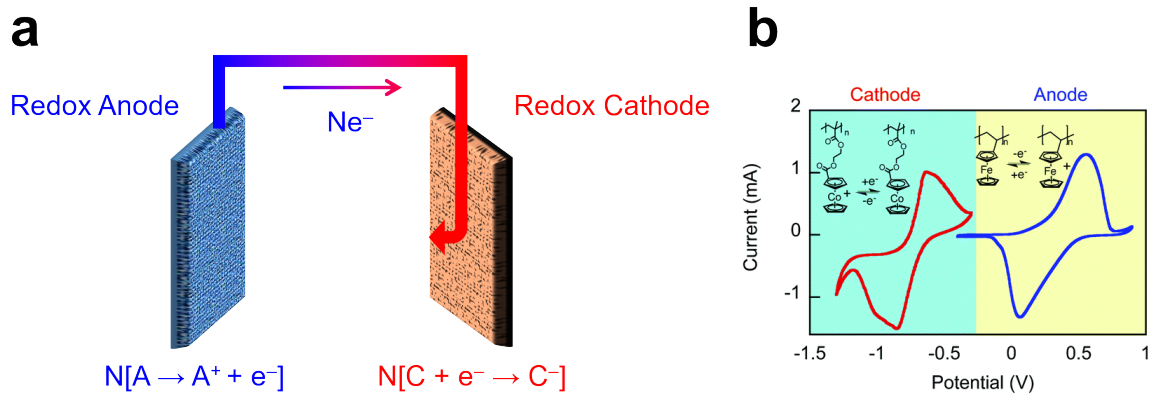

Figure 1-34. Asymmetric Faradaic systems for selective electrochemical separations. (a) Schematic of a Faradaic system with redox-active polymer electrodes, namely a ferrocene metallopolymer (PVF) for the anode and a cobaltocenium metallopolymer for the cathode. (b) Characterization of the electrochemical system and corresponding redox reactions by cyclic voltammetry. Reproduced with permission from ref 910. Copyright 2017, Royal Society of Chemistry.

and inhibit competing Faradaic reactions that result in current leakage.[910] These desirable properties can be achieved using asymmetric electrodes made of redox-active metallopolymers, as illustrated in Figure 1-34. Faradaic intercalation in crystalline systems can also be used to improve the efficiency of electrosorption. For example, symmetric electrodes of CuHCF have been used to reduce the amount of energy needed for desalination (down to $0.02\,\mathrm{kW\,h\,m^{-3}}$ for a feed with an initial concentration of 25 mM and a final concentration of 17 mM).[945] This system was operated at a much lower cell voltage (i.e., 0.6 V) compared to a standard CDI cell, which reduced parasitic side reactions.[945]

Asymmetric configurations have the advantage of increasing energy storage at each of the electrodes by promoting the appropriate electron transfer reactions, namely oxidation at the anode during charging and reduction at the cathode. In the case of electrosorption, asymmetric Faradaic designs have been used to capture anions at the anode and cations at the cathode.[86,96,156,715] One example of redox-active systems that enabled selective electrochemical separations was made of ferrocene (PVF) and cobaltocenium metallopolymers on opposite electrodes, respectively.[910] The two electrodes operated within the window of water stability, and more importantly, their redox reactions allowed for selective capture of anions

from solution and subsequent control of the voltage window with 96% current efficiency. By carrying out these redox reactions at low voltages (i.e., $0.4\,\mathrm{V}$ and $-0.6\,\mathrm{V}$ versus $\mathrm{Ag/AgCl}$ for the anode and cathode, respectively), the pH of the system was stable, and there was significant improvement in the efficiency with which anions were removed from dilute solutions. Furthermore, the selective properties of the PVF system were preserved upon capture of anions by preventing the formation of hydroxides.[910] In subsequent studies, it was shown that the organometallic cobalt center could be tuned using a tetraphenyl ligand,[1049] which enabled simultaneous recovery of cations and anions.[910]

More recently, hexacyanoferrate (HCF) electrodes were combined with redox-active polymers to achieve selective electrochemical separations that can be carried out with extremely small swings in voltage ($< 0.1\,\mathrm{V}$) by redox matching at the electrodes.[993] As shown in Figure 1-35a, both anions and cations were selectively captured by combining an electrode made of PVF with another made of HCF. The redox potential of the cathode was shown to be tunable based on the content of mixed metal (see Figure 1-35b), which enabled structural control of the window of operating voltages down to $\sim 0.1\,\mathrm{V}$ at a current density of $1\,\mathrm{A\,m^{-2}}$ for a two-cell system. This feature also improved anion selectivity and separation efficiency, as demonstrated in Figure 1-35c-d, which highlights the potential of hybrid redox polymers with crystal electrodes for efficient separations.[993]

In addition to their high efficiency, asymmetric redox systems combine separations and reactions to chemically transform a harmful contaminants into more benign species. By combining an electrosorption working electrode with an electrocatalytic counter electrode, Kim et al. found that $\mathrm{As(III)}$ (trivalent) can be captured and transformed into $\mathrm{As(V)}$ (pentavalent), as shown in Figure 1-36a.[102] The former is a naturally and artificially occurring contaminant in groundwater that is highly toxic, even though it is often present at low concentrations.[1050–1052] Capturing this contaminant in the presence of competing species and transforming it into $\mathrm{As(V)}$ is a major challenge in water purification. Because of the affinity of PVF for charge transfer anions, PVF-CNT composite electrodes were used to capture $\mathrm{AsO_4^{3-}}$ and

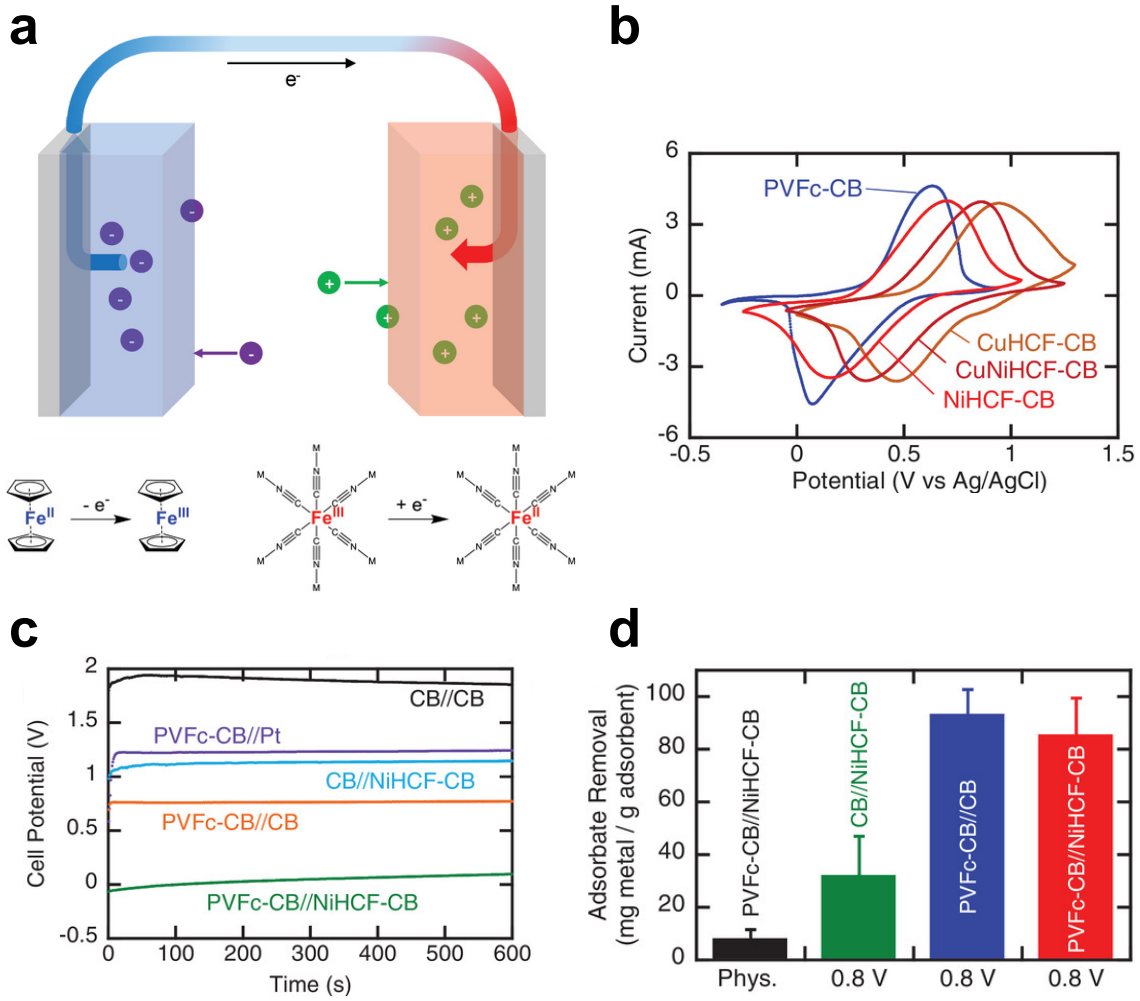

Figure 1-35. Asymmetric redox system using iron active centers for selective separations. (a) Schematic of the asymmetric Faradaic cell, in which a ferrocene metallopolymer is oxidized at the anode (blue) and an HCF crystal is reduced at the cathode (red). (b) Cyclic voltammetry shows that the HCF electrode can be structurally tuned to control the redox potential. (c) Cell potential during electrosorption and (d) recovery of molybdenum anions for different electrode chemistries. Reproduced with permission from ref 993. Copyright 2020, Wiley-VCH.

AsO_3^{3-} during oxidation of the working electrode.[986,1022] The counter electrode was coated with poly-TEMPO methacrylate (PTMA), which comprises stable nitroxide radicals that undergo oxidation by one-electron transfer. This system efficiently reduced the concentration of a contaminated solution from 100 ppb to below 10 ppb, the recommended maximum total exposure.[1053] Moreover, separation factors of over forty nine relative to competing Cl^- were achieved during the capture of these oxyanions. Upon release, the PVF electrode liberated As(III), and the counter electrode transformed the anions into As(V) in both batch and flow configurations. By taking advantage of these redox processes, contaminants were simultaneously separated and converted, as described in Figure 1-36. This dual process reduced energy consumption to $0.45\,kW\,h\,mol^{-1}$ of converted As and increased energy efficiency by one order of magnitude compared to systems that decouple separations from reactions.[102] This framework is similar to the use of PVF with a platinum counter electrode to capture and transform Cr(VI) into the less harmful Cr(III). In the latter process, however, the redox transformation occurs at a single PVF electrode which adsorbs Cr(VI) during oxidative charging and catalyzes its reduction during discharging, while water splitting occurs at the counter electrode to regulate pH.[1022] A study recently revealed the role of oxygen in ferrocene-mediated conversion of arsenic, where production of peroxide aided the regeneration of active ferrocenium units.[1054] The study also showed how PVF systems can be used for efficient remediation of groundwater contaminated with arsenic.

Asymmetric systems have been designed with complementary hydrophilic-to-hydrophobic transitions to increase the capacity of adsorption of uncharged organic contaminants.[104] As an example, one electrode was coated with the PVF/PPy hybrid introduced in Section 1.4.3 and the other with PPy containing the amphiphilic surfactant dioctyl sulfosuccinate (DOSS, known commercially as AOT). When paired, these two electrodes exhibit hydrophilic-to-hydrophobic transitions that are complementary and at opposite electrodes. That is, the PVF/PPy electrode becomes hydrophilic when oxidized and hydrophobic when reduced, whereas the PPy/AOT electrode becomes hydrophobic when oxidized and hydrophilic when reduced. As

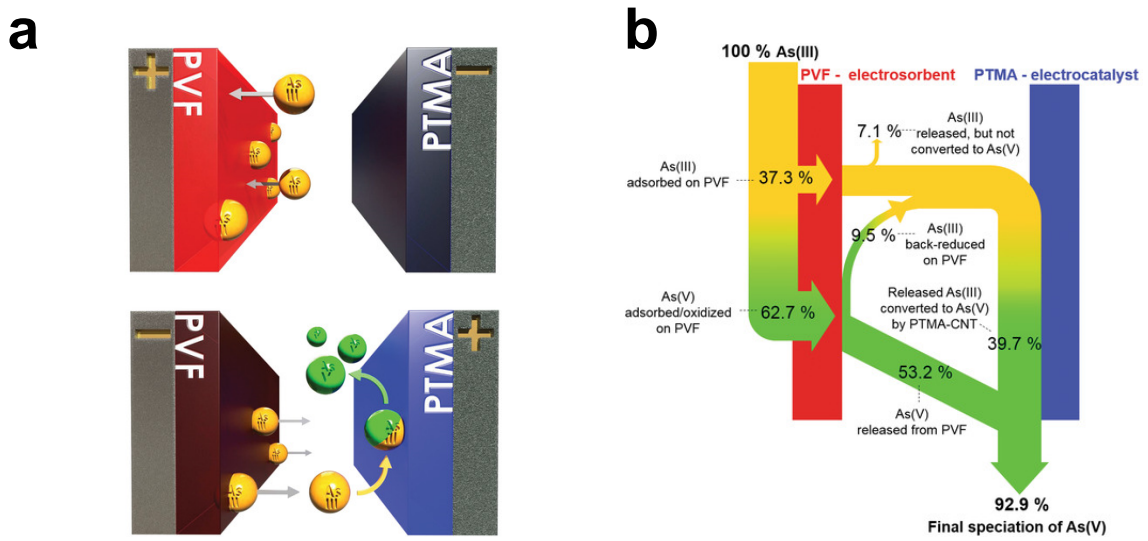

Figure 1-36. Simultaneous capture and conversion of $\mathrm{As(III)}$ into $\mathrm{As(V)}$ using redox-active electrodes. (a) Schematic of the asymmetric electrochemical system with electrodes made of PVF (electroadsorbent) and PTMA (electrocatalyst). (b) Flow diagram explaining the speciation of arsenic in this system. Reproduced with permission from ref 102. Copyright 2020, Wiley-VCH.

shown in Figure 1-37, this design enables capture of hydrophobic molecules like Sudan Orange G (SOG), which is released from both loaded electrodes during charging (oxidation at PVF/PPy and reduction at PPy/AOT).[104] The PPy/AOT electrode was developed to achieve superhydrophobic properties and strong $\pi - \pi$ interactions with uncharged aromatic species.[1055] During electrostatic charging, the surfactant dopants are reoriented to modulate hydrophobicity, an interaction that was explored in detail using DFT and MD simulations.[1055] While discharging, the asymmetric system of PVF/PPy and PPy/AOT was found to be nearly twenty times more energy efficient than systems based on activated carbon ($12\,\mathrm{J\,g^{-1}}$ of adsorbent for the asymmetric redox system and $235\,\mathrm{J\,g^{-1}}$ of adsorbent for activated carbon).

Finally, these asymmetric systems have been redesigned into flow configurations, in which CNTs coated with PVF and PPy (doped with the anionic surfactant dodecylbenzenesulfonate, DBS) were used as the electrodes to selectively remove organic contaminants.[1056] This system integrated in-situ ultraviolet, conductivity, and pH sensors for online monitoring, as shown in Figure 1-38, and it displayed a high capacity and rate of salt adsorption compared to CDI systems in the liter-

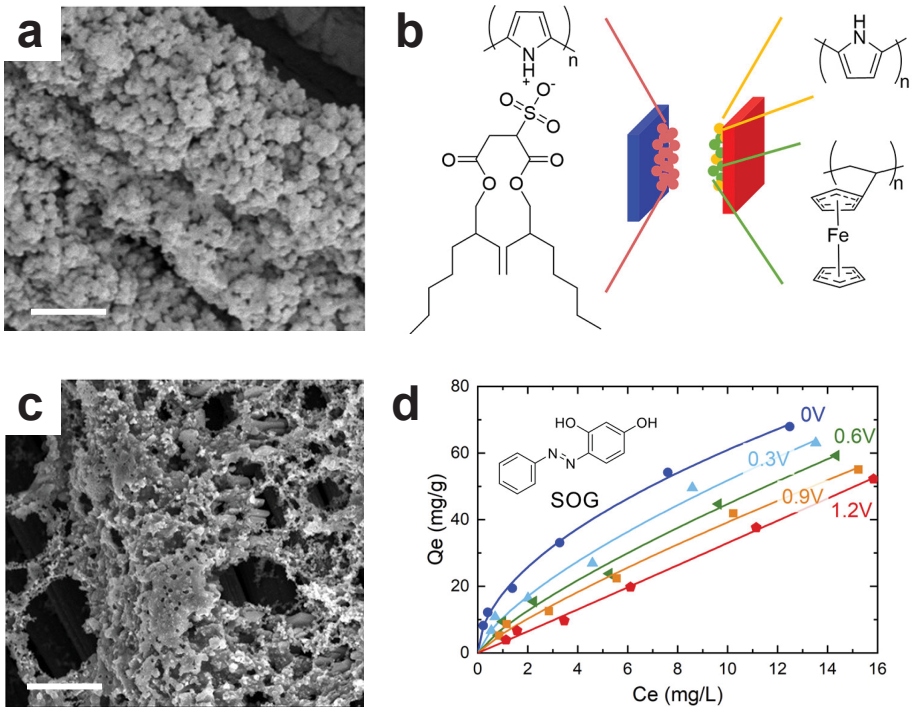

Figure 1-37. Asymmetric electrochemical system with tunable hydrophobicity. Complementary redox-active electrodes made of (a) PVF/PPy and (c) PPy/AOT nanostructures; scale bars are 10 µm. (b) Schematic of the asymmetric system with electrochemically modulated affinity toward uncharged organic molecules. (d) Adsorption isotherms of SOG for various applied potentials. Filled markers represent experimental data and solid lines are fits based on the Freundlich adsorption model. Reproduced with permission from ref 104. Copyright 2019, American Chemical Society.

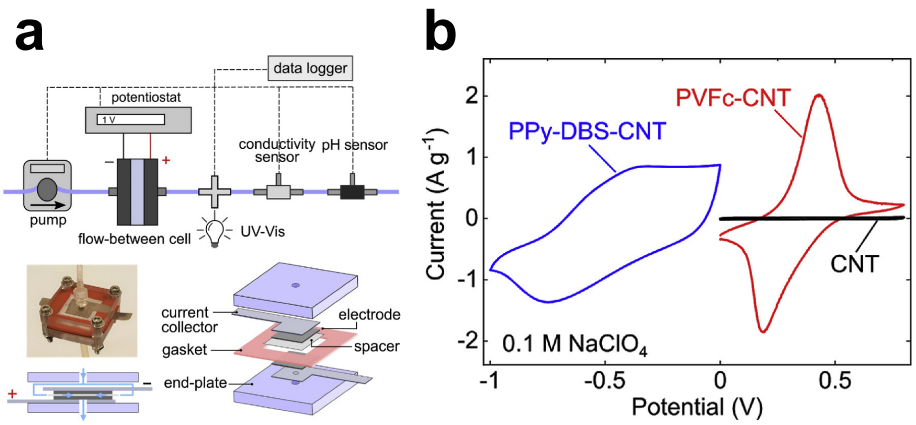

Figure 1-38. Selective adsorption of organic anions in a flow cell with asymmetric redox-active electrodes. (a) Schematic of the continuous electrosorption system with integrated sensing. (b) Cyclic voltammetry of carbon substrates functionalized with PVF-CNT, PPy-DBS-CNT, and CNT. Reproduced with permission from ref 1056. Copyright 2020, Elsevier.

ature.[1057] Based on dynamic measurements of adsorption and release, the flow platform was also selective toward benzoate—a compound representative of toxic carboxylates—in the presence of competing electrolytes, which were fifty times more concentrated than the target anion. This work demonstrated the feasibility of using asymmetric redox designs as on-site systems for water purification.

1.5 Inverse Methods of Energy Conversion

Generating clean, renewable energy is just as important as producing purified water for environmental sustainability. In this section, we introduce what are known as "inverse methods" of energy conversion and draw parallels between these systems and the methods of water purification discussed above. The electrochemical inverse methods that we describe here include reverse ED, capacitive mixing (CapMix), and battery mixing (BattMix). These technologies are similar in that they retrieve energy from the mixing of two streams between which there is a gradient in concentration (or more precisely in chemical potential), such as river water and seawater. They differ, however, in how they are designed and operated, but as we will show in this section, reverse ED, CapMix, and BattMix are in fact just ED, CDI, and Faradaic electrosorption, respectively, operated in reverse. For complete-

ness, we also review electrokinetic conversion of mechanical energy to electrical energy based on harvesting the streaming current produced by pressure-driven flow in charged microchannels or porous media.

Although the scope of this review is limited to electrochemical methods, we note that there exists a physical, membrane-based inverse method known as pressure-retarded osmosis (PRO), which converts the free energy of mixing into useful electrical power.[1058–1063] In this process, two streams of different concentrations are separated by a semipermeable membrane that allows only water to pass by osmosis. The imbalance in chemical potential across the membrane promotes transport of water from diluate to concentrate. This osmotic flow can be stopped if enough hydraulic pressure is applied to the concentrate. The applied pressure needed to maintain osmotic equilibrium is called osmotic pressure and is determined entirely by the composition of the solution. PRO thus occurs as long as the applied pressure is less than the osmotic pressure, and since water flows against this gradient in hydraulic pressure, the free energy of mixing can be converted into mechanical work.

1.5.1 Inverse Electrokinetic Methods

Reverse Electrodialysis

In reverse ED, the system is fed dilute and concentrated streams that are partitioned by alternating AEMs and CEMs. This stack is sandwiched between metal electrodes that are connected through an external load to which power is delivered, as shown in Figure 1-39.[1064,1065] Transport of cations across the CEMs and anions across the AEMs produces a flux of electric charge between the electrodes. The magnitude of the resulting electric potential is related to the difference in chemical potential of the salt in adjacent streams, and the voltages across each membrane are additive.[1064–1066] Natural runoffs and rivers in coastal areas are abundant sources of both dilute feed that is usually left to mix with seawater and energy that is produced without capture.[1067] It was estimated that 2.3 MJ of work could theoretically be extracted from each cubic meter of river water that flows into the

sea.[1064,1067,1068] With the typical discharges of all rivers combined, the net power produced by this unconventional source of energy was estimated to be between 2.4 TW and 2.6 TW.[1064,1069] Of course, not all of this energy could be harvested by reverse ED, but the question is exactly how much can be extracted? Forgacs conservatively predicted a yield of $0.35\,\mathrm{MJ\,m^{-3}}$ of river water,[1070] Audinos arrived at a similar yield and calculated an energy recovery of 21% (excluding losses due to pumping and power inversion),[1071] and Jagur-Grodzinski and Kramer experimentally determined a yield between $0.25\,\mathrm{MJ\,m^{-3}}$ and $0.6\,\mathrm{MJ\,m^{-3}}$ of river water.[1072] Długołęcki et al. then derived an equation to calculate the maximum power output $\mathscr{P}_{\max}$ based on the properties of the system and its components:[1073]

$$\mathscr{P}_{\max} = NA\frac{\left[\alpha_{\mathrm{avg}} RT/F \ln\left(a_c/a_d\right)\right]^2}{\mathscr{R}_{\mathrm{AEM}} + \mathscr{R}_{\mathrm{CEM}} + w_c/\kappa_c + w_d/\kappa_d} \tag{1.17}$$

where N is the number of membrane pairs, A is effective membrane area, α_{avg} is average membrane permselectivity, a is thermodynamic activity, $\mathscr{R}$ is membrane resistance (in $\Omega\,\mathrm{m^2}$), w is compartment width, κ is electrolyte conductivity, and subscripts "c" and "d" represent the concentrate and diluate, respectively.

Early studies of reverse ED showed that little energy is recovered relative to what is theoretically available. Post et al. later investigated how much energy can be recovered in reverse ED by distinguishing between internal and external losses of energy and by focusing exclusively on the former.[1067] (External losses arise due to pumping and power inversion and can only be quantified in a full-scale, optimized system.) In the literature, it is explained that internal losses arise due to ionic shortcut currents,[1078] internal resistances (e.g., friction losses, pumping requirements, electrochemical overpotentials),[1072,1079,1080] concentration polarization,[1064,1081] and osmotic transport.[1082] Internal losses must therefore be reduced to improve energy efficiency, which can be achieved by developing improved electrode systems (to lower electrochemical overpotentials),[1083] introducing air bubbles to the feed (to decrease ionic shortcut currents),[1067,1078] improving stack hydrodynamics and spacer design (to reduce concentration polarization),[1081] and de-

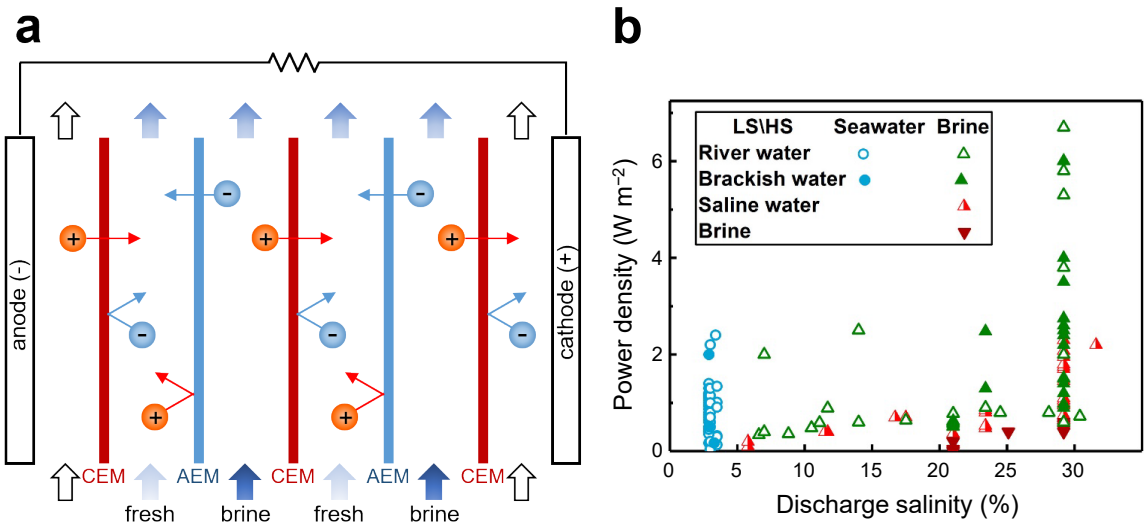

Figure 1-39. Operating principles and empirical results of reverse ED. (a) Dilute and concentrated streams are passed through a stack of alternating AEMs and CEMs. Differences in the chemical potentials of adjacent streams generate an electric potential across each membrane, and the total voltage is the sum of the potential differences across each membrane. In most reverse ED systems, reversible redox couples (e.g., Fe^{2+}/Fe^{3+}, $[Fe(CN)_6]^{4-}/[Fe(CN)_6]^{3-}$) in a supporting electrolyte (e.g., NaCl–HCl) are used as electrode streams to convert ion flux into electrical current.[1074–1076] (b) Power density versus discharge salinity for various pairs of low salinity (LS) and high salinity (HS) feeds. Reproduced with permission from ref 1077. Copyright 2018, Elsevier.

signing spiral wound modules (to decrease membrane area).[1084,1085] Using some of these principles, Post and Veerman et al. designed systems that, in the best case, recovered more than 80% of the work made available by mixing artificial river water and seawater.[1067,1078] Several other studies[1077] in the past decade also focused on optimizing the performance of reverse ED systems by modeling and developing new IEMs,[1086–1089] spacers,[1090] and electrodes.[1091] At the same time, researchers focused on improving the overall operation of the stack,[1092,1093] understanding the impact of fouling and mitigating it (see Section 1.3.6),[1094–1097] and combining reverse ED with desalination technologies.[1098–1103]

The fastest growing areas of research over the past five years, however, are related to applications for energy storage,[1104,1105] developing micro- and nanofluidic reverse ED systems,[1106,1107] and pilot studies for commercial use.[1108–1111] Pilot studies are essential to bridge the gap between experimentation at the laboratory scale and implementation at the industrial scale. So far, pilot plants for reverse ED exist in only few countries, including the Netherlands and Italy. The first of these plants was commissioned in 2014 in Afsluitdijk, a major dam in the Netherlands, and it features a dyke that is 32 km long which separates the IJssel Lake and the Wadden Sea.[1077] This plant produces electrical energy (the amount of which has not been made available to the public) from controlled mixing of fresh water with seawater. The pilot plant in Italy was commissioned near the Ettore e Infersa saltworks in Trapani, and it mixes saturated brine from the saltworks with brackish water from a nearby shoreline well to produce an average of $0.8\,\mathrm{W\,m^{-2}}$ of membrane in total.[1077,1108,1109] Future work in this area will largely focus on improving power density, performing complete cost analyses, and building plants with greater capacity.[1065,1082]

Electrokinetic Energy Conversion

Although this review focuses on the interplay of electrical and chemical energy, we discuss here how linear electrokinetic phenomena (see Section 1.3.3) can also be exploited to directly convert mechanical energy to electrical energy via the forced

motion of liquid electrolytes in charged microchannels and pores. In 1964, Osterle introduced the basic idea of mechanical electrokinetic energy conversion by harvesting the streaming current produced by pressure-driven flow in a charged capillary.[1112] Morrison and Osterle then estimated a maximum efficiency of 0.9% for ultrafine water–glass capillaries.[1113] Gross and Osterle comprehensively analyzed energy conversion by linear electrokinetic phenomena (recently extended by Peters et al.[506]) and estimated a maximum electroosmotic conversion efficiency of 4%.[507] This approach had attracted relatively little attention until its rediscovery in the context of microfluidics.[1114] The possibility of measuring and controlling the streaming potential in single nanochannels renewed interest in advancing this classical method through nanoscale engineering.[1115–1118] Indeed, van der Heyden et al. predicted theoretical conversion efficiencies of up to 12%[1116] and experimentally demonstrated 3% efficiency in 75 nm-thick silica glass nanochannels using dilute KCl electrolytes.[1117] Considering conduction through the Stern layer can further reduce the theoretically predicted efficiency.[1119] Recent advances with soft, flexible microchannels have allowed for practical applications of electrokinetic energy conversion in wearable and portable self-powered devices.[1120,1121]

Significant developments have also followed from theoretical predictions of massive enhancement of electrokinetic phenomena for charged surfaces with hydrodynamic slip.[1122–1124] Ren and Stein predicted that hydrodynamic slip could increase nanofluidic energy conversion up to 40% for hydrophobic surfaces with slip lengths on the order of tens of nanometers and up to 70% in CNTs or graphitic systems based on reported apparent slip lengths.[1125] These theoretical values have proven difficult to achieve in electrokinetic energy conversion with homogeneous solid–liquid interfaces, and there are lingering signs of knowledge gaps in our understanding of electrokinetic phenomena under nanoconfinement.[492] For example, the apparent slip observed for CNTs is absent in crystallographically similar boron nitride nanotubes with different electronic structures.[498] As a possible alternative to homogeneous surfaces, Bagha et al.[1126] predicted that micropatterned, superhydrophobic surfaces with high slip and charged liquid–gas interfaces could in-

crease efficiency at larger length scales, and this concept remains a subject of research.[1127–1129]

Reverse Electrowetting

Electrocapillary phenomena involve interactions between liquid electrolyte interfaces and charged solid surfaces or electrodes. The classical example is electrowetting, where an applied voltage changes the surface tension of a droplet via energy stored in EDL capacitors and thus manipulates the shape of an electrolyte droplet.[1130,1131] Krupenkin and Taylor first proposed the inverse effect of reverse electrowetting to convert mechanical energy to electrical energy, where immiscible electrolyte droplets were compressed by the motion of parallel-plate electrodes.[1132] Kolomeisky and Kornyshev suggested an alternative approach based on the reversible penetration of a liquid electrolyte into a solvophobic porous electrode, which could be used in a "double layer shoe" to harvest electricity from walking motion.[1133] Analogous to the use of moving wire electrodes in CDI for desalination,[863] capacitive rotors have been proposed to generate alternating current from mechanical motion by exploiting a time-varying EDL capacitance.[1134]

1.5.2 Inverse Electrosorption Methods

CapMix

In 2009, Brogioli proposed a method (later called "capacitive double layer expansion," or CDLE) to extract energy from the concentration gradient between two feeds, as shown in Figure 1-40.[1135] Unlike reverse ED and PRO, CDLE was founded on the concept of an electrochemical capacitor (obtained by immersing two electrodes in an electrolyte),[153,1136,1137] which is the basis of water purification in CDI technologies.[110] CDLE can therefore be described as CDI operated in reverse: current is applied to the capacitor when filled with salt water, coions are repelled and counterions are attracted at each electrode, and EDLs are formed to store electric charge. After the EDLs are charged—an input of energy—the cell is flushed with fresh water to increase the electric potential, and in turn the electrostatic energy,

of the system. The capacitor is then discharged—an output of energy—after which the cell is flushed with salt water to decrease the electric potential for a new cycle. This four-step cycle is demonstrated in Figure 1-40, and it reveals the possibility of extracting surplus energy due to a concentration gradient in the capacitor.

Brogioli explained the dynamics of EDLs in CDLE using the GCS theory[503–505,1138] and deduced that this process can achieve an energy output of $0.44\,\mathrm{kW\,h\,m^{-3}}$ of fresh water. By cycling the system at a rate of 1 Hz, the power output of CDLE would be comparable to that of membrane technologies for energy production. In 2011, Brogioli et al. assessed the performance of CDLE in a larger prototype and observed an efficiency of up to twenty times what was reported originally in ref 1135.[1139] To analyze the dynamics of CDLE and improve subsequent designs of these prototypes, Rica et al. mathematically modeled the electrodiffusion of ions as well as their adsorption and desorption in porous electrodes.[1140,1141] These models, which accounted for adsorption of both charge and salt, were based on a macroscopic formulation of ion diffusion and Ohm's law in porous media.

The original design by Brogioli had intrinsic technical deficiencies in that it was sensitive to impurities like DO and exhibited self-discharge.[1142] Several research groups improved the efficiency of energy conversion by introducing IEMs to the supercapacitor flow cell.[1143–1147] This system, which came to be known as capacitive Donnan potential (CDP), combined elements of reverse ED and Brogioli's capacitive method to both produce an electric potential across an IEM and store charge in the EDLs of porous electrodes.[1148] The method of Sales et al. was based on a fixed external resistance, and their work was followed by a study in which Liu et al. supplemented the charging cycle using an external power supply to ultimately draw more power.[1149] Shortly afterward, Brogioli et al. discovered that activated carbon behaves as a polarizable electrode on short time scales but reverts to its spontaneous (self) potential on long time scales, which limits the maximum power output of CapMix systems that use activated carbon as electrodes.[1150,1151] The authors attributed this effect to leakage of stored charge caused by unwanted electrochemical reactions.

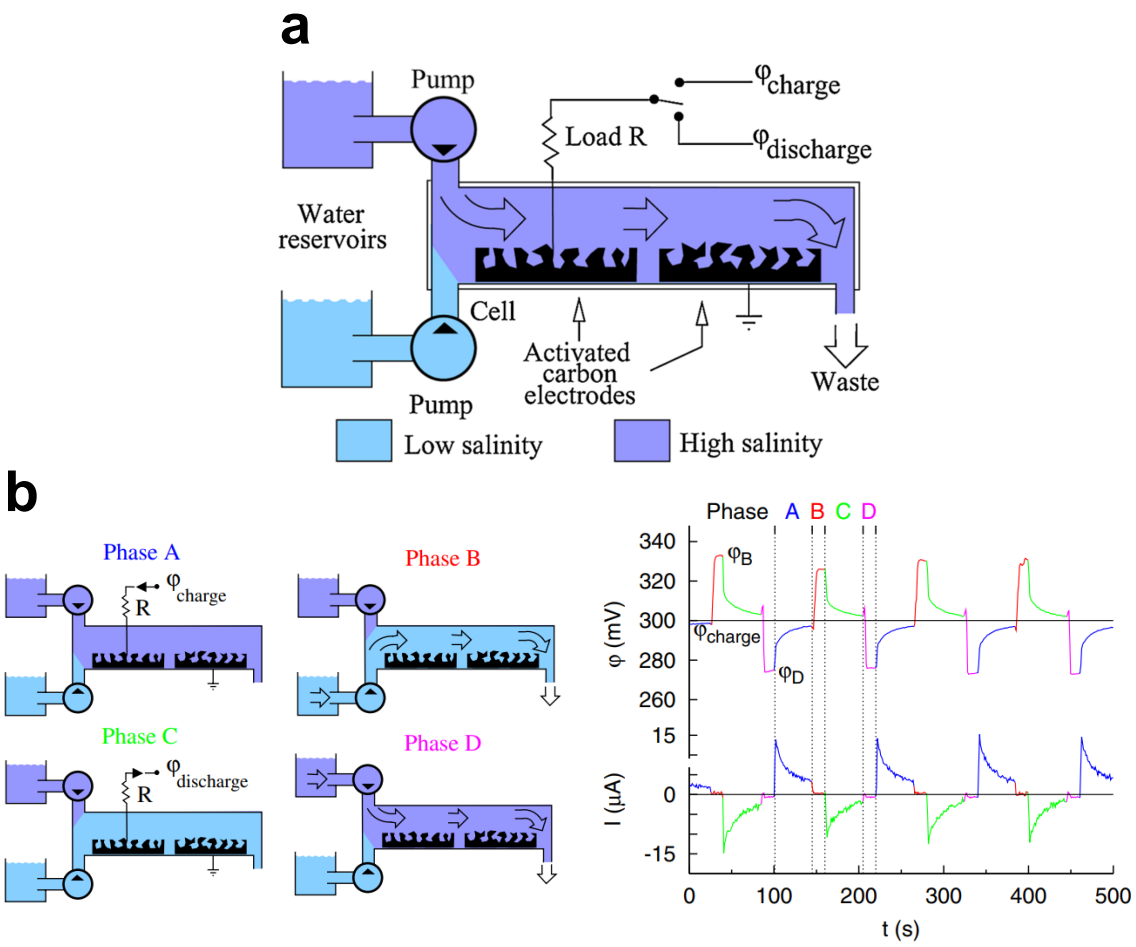

Figure 1-40. Schematic and operating procedure of CDLE, the original CapMix system. (a) The device comprises two electrodes made of porous activated carbon, and this pair of electrodes behaves as a capacitor that can be charged and discharged. Two reservoirs contain solutions with different concentrations that are pumped to the cell where they are mixed. (b) Graphical explanation of the four-step operating procedure of CDLE. In phase A, the electrical circuit is closed and the cell is charged; in phase B, the circuit is opened and the cell is flushed with fresh water to increase the electric potential; in phase C, the circuit is closed and the cell is discharged; and in phase D, the circuit is opened and the cell is flushed with salt water to decrease the electric potential. Reproduced with permission from ref 1135. Copyright 2009, American Physical Society.

To overcome the limitations of traditional carbon electrodes, researchers examined new geometries and arrangements for both the electrodes and IEMs, which enabled continuous operation[670,1152] and increased power output.[1153,1154] These advancements were accompanied by the use of novel materials for the electrodes, such as porous activated carbon coated with polyelectrolytes, to reduce the leakage current.[1155–1159] These so-called "soft electrodes" generate electrical energy in response to changes in both the capacitance of the EDL and the Donnan potential of the polyelectrolyte coat during exchange of electrolytes.

BattMix

In 2011, La Mantia et al. introduced a novel electrochemical system called the "mixing entropy battery" that extracted energy from a concentration gradient but then stored the energy in the bulk crystal structure of the electrodes.[897] The novelty of this BattMix system was in the use of a redox-active material, namely NMO, for the cathode (with Ag/AgCl for the anode), which improved the performance and efficiency of energy harvesting compared to supercapacitor electrodes made of activated carbon.[1160] The BattMix cell is first charged by applying an electric field that electrochemically transports Na^+ and Cl^- from the corresponding electrode into a dilute electrolyte. The cell is then discharged by exchanging this electrolyte for a concentrated one, which drives Na^+ to intercalate into the MnO_2 cathode and Ag to be oxidized to Ag^+ at the anode. Since the energy produced during discharging is greater than that expended during charging, net-positive energy can be harvested from this controlled mixing of two electrolytes. Following La Mantia et al., the scientific community developed and tested other redox-active materials (see Section 1.4.2), such as PBAs[1161–1165], inorganic compounds of metals,[1166–1168] and copper ammonia redox couples,[1169,1170] as well as conventional battery electrodes, such as zinc and silver.[1171,1172]

Like capacitive electrodes in CapMix, redox-active electrodes in BattMix are electrical accumulators that can store and release charge, and these two methods are broadly classified as accumulator mixing technologies.[1173] Marino et al. examined

the electrochemical kinetics of these technologies and determined that supercapacitors (CapMix) can deliver a larger specific power than batteries (BattMix).[1174] The authors also observed that the kinetics of capacitive electrodes are controlled by the diffusion of ions in the electrolyte,[1141] whereas the kinetics of redox-active electrodes are controlled by the diffusion of intercalated sodium.[1175] To limit the shortcomings of each class of materials, Lee et al. designed a hybrid accumulator mixing system that comprised a battery electrode (NMO), a capacitive electrode (activated carbon), and an AEM.[1176] This system extracted an amount of energy per unit membrane area three times greater than that achieved by previous CapMix designs, including those with IEMs. Tan and Zhu also built a hybrid accumulator mixing system using CuHCF for the cathode and Bi/BiOCl for the anode.[1157] Instead of including an IEM, however, Tan and Zhu coated the electrodes with a polyelectrolyte material to boost power output. Future work in the area of electrochemical energy harvesting includes creating better and more cost-effective materials, improving device configuration and assembly, and carrying out pilot studies.[1177]

1.6 Performance Comparisons and Process Intensification

Now that we have presented and discussed the basic principles of emerging electrochemical methods for water purification, we compare the performance of these technologies by quantifying energy demand, energy efficiency, and performance tradeoffs. A fair and comprehensive comparison of these metrics is generally difficult, and only few studies have been published which mainly compare one electrochemical method (typically ED or CDI) with RO. In this section, we expand the existing work on performance comparisons by quantifying similarities and differences between the electrochemical methods discussed in this review. From these comparisons, we highlight the kinds of applications where each technology could provide the greatest benefit. Finally, we conclude this section by discussing pathways and challenges associated with scale up as well as opportunities for process

intensification by combining electrochemical methods to achieve unique capabilities.

1.6.1 Energy Demand

Electrochemical methods have the potential to lower the cost of desalinating brackish water ($< 15\,\mathrm{g}$ of total dissolved solids per liter) as well as feeds that are dilute ($< 1\,\mathrm{g}$ of total dissolved solids per liter) but contaminated with hazardous substances.[125,1178] Unlike conventional desalination methods (e.g., distillation, RO), electrochemical processes are well suited for these tasks because their demand for electrical energy is proportional to the amount of salt removed (for instance by electrokinetics or electrosorption) and not the volume of water treated. To demonstrate how this distinction influences energy demand, Hemmatifar[1179] compared RO with a generic electrochemical process (EC) based on the analyses in refs 1178,1180. RO consumes energy, $\hat{E}_{\mathrm{RO}}$ (per unit volume of permeate), primarily in the form of mechanical work needed to overcome of the osmotic pressure of the feed:

$$\hat{E}_{\mathrm{RO}} \approx \frac{1}{\gamma}(\Delta P + \Delta\pi) \tag{1.18}$$

where ΔP and $\Delta\pi$ are the differences in hydrodynamic and osmotic pressures, respectively, and γ is water recovery. The hydrodynamic pressure difference is related to productivity, $\mathscr{P}$ (volumetric throughput normalized by active surface area, in units of $\mathrm{L\,h^{-1}\,m^{-2}}$), and membrane permeability, L_p (in units of $\mathrm{m\,s^{-1}\,Pa^{-1}}$), by Fick's law: $\Delta P = \mathscr{P}/L_p$. The osmotic pressure difference is related to the difference in salt concentration, Δc, across the membrane by the van't Hoff equation: $\Delta\pi = iRT\Delta c$, where i (≈ 2) is the van't Hoff factor.

In contrast to RO, electrochemical processes consume electrical energy to transport ions and activate electrochemical reactions. These processes are subject to losses in the form of overpotentials, which represent energy lost as heat to the surroundings. Overpotentials in electrochemical systems are grouped into three categories, namely activation (the potential difference above the equilibrium value

needed to produce a current in a redox event), concentration (the potential difference across a diffusion layer near the electrode), and resistance (the potential difference caused by resistances in conducting ions and electrons).[120] Hemmatifar showed that the energy demand, $\hat{E}_{\mathrm{EC}}$ (per unit volume of diluate), can be approximated based on ionic and Ohmic (resistive) losses:[90]

$$\hat{E}_{\mathrm{EC}} \approx \frac{I^2 \mathscr{R}_s}{\gamma Q} \tag{1.19}$$

where I is current (assumed to be constant under galvanostatic operation) and $\mathscr{R}_s$ is the equivalent resistance of ionic and Ohmic losses in series. This approximation holds unless the separation is slow and parasitic reactions dominate. Electrical current is related to the change in concentration as $I \approx FQ\Delta c/\Lambda$, where Λ is cycle efficiency. The quantity Λ equals the ratio of salt removed to electric charge fed (both in moles), and it is used to empirically account for coupled inefficiencies due to charge transfer, EDLs, and fluid flow.[1179,1181] Figure 1-2 presents estimates of the volumetric energy consumed by RO and EC using the equations above and the parameters in ref 1179.

These results confirm that although the energy required by RO is a linear function of concentration when the feed is salty (and $\Delta\pi$ is large compared to ΔP), it becomes nearly independent of concentration in the dilute limit. Thus, for feeds that would be classified as either brackish water or fresh water, $\hat{E}_{\mathrm{RO}}$ is bounded by the mechanical work needed to sustain the hydrodynamic pressure, which is independent of concentration. The energy demand of EC, on the other hand, scales approximately as $(\Delta c)^2$ over the entire range of concentrations, which implies that electrochemical processes should in theory be significantly less energy intensive than RO for desalination of dilute feeds. Although the estimates in this analysis are based on a specific set of parameters (e.g., water recovery, productivity, cycle efficiency), the general trend in energy consumption can be generalized to any electrochemical method that removes solute from solvent. Electrochemical processes offer a unique opportunity to efficiently purify brackish water and other dilute but

contaminated feeds.

1.6.2 Energy Efficiency

Although we have shown that electrochemical methods should theoretically be efficient in the dilute limit, the energy demand in practice has so far been tens or hundreds of times the thermodynamic minimum (see Figures 1-2 and 1-42). These values correspond to thermodynamic efficiencies, η_{thermo} (ratio of the free energy of separation to the input of electrical work), of only a few percent, which reveals the extent of dissipation (or energy loss) in state-of-the-art electrochemical systems. This gap between the thermodynamic limit and real efficiencies, however, is expected for emerging methods and presents an opportunity for the improvement of electrochemical technologies. In the early days of RO, for example, thermal distillation used to be the state-of-the-art method to desalinate seawater. But from the 1970s to 2008, the consumption of electrical power by RO systems was reduced by almost 90%, from approximately $16\,\mathrm{kWh\,m^{-3}}$ to $1.8\,\mathrm{kWh\,m^{-3}}$, which is near the theoretical minimum energy of $1.1\,\mathrm{kWh\,m^{-3}}$ needed to desalinate seawater with a water recovery of 50%.[68] These improvements resulted in the widespread implementation of RO, which today is considered the leading process for seawater desalination based on installed capacity and annual growth.[12]

Dissipation in electrochemical systems leads to inefficiency and may be caused by the dynamics of electrokinetics and electrosorption, ionic and Ohmic losses, parasitic losses due to charge transfer, hydrodynamic dispersion and fluid mixing, or mechanical work required to pump the electrolyte. We emphasize that all electrochemical processes exhibit a complex tradeoff between kinetics (measured in terms of productivity) and energetics.[90,742,761,763] As predicted by the simple model in Equation 1.19, a fast process (one that is operated at high current) consumes more energy but achieves the same level of separation as a slow process,[763] though this fact holds for all desalination processes because more entropy is generated when operating farther from equilibrium.[72,1182] Similarly, a slow process may be inefficient because of the dominance of parasitic side reactions,[90,761] and so it is critical

to understand these tradeoffs and quantify the kinetics and energetics of the separation method under consideration.[742]

With these general guidelines established, researchers have sought to develop efficient electrochemical processes by engineering improved systems, materials, and operating conditions. Systems to improve energy efficiency were designed, such as cyclic recovery of stored energy, reduction of series resistances,[757,761] and use of membranes in electrosorption methods.[754,1183] Materials to suppress parasitic reactions were developed, including redox-active electrodes[96] and intercalation materials.[116,129,945] And operating parameters were tuned, like flow rate, current, and voltage.[754,759–761,764,1184,1185] The use of IEMs directly adjacent to the electrodes in electrosorption was first reported by Andelman and Walker,[1186] and this approach was since pursued by many researchers.[638,754,1183,1187,1188] The selectivity introduced by these membranes increases charge efficiency by allowing for voltage reversal and increasing the capacity of adsorption.[1188] One disadvantage of using IEMs, however, is that they can incur additional capital costs that exceed those of all other components in an electrochemical device.[742]

To suppress parasitic side reactions, which often severely compromise efficiency,[90] researchers have developed and used redox-active electrodes that guide the transfer of electrons toward redox groups.[96] For example, organometallic and metallopolymeric electrodes were used in an asymmetric Faradaic CDI system and led to no appreciable changes in the pH of the treated solution, which indicated that water reactions were indeed suppressed.[910] The authors also demonstrated stability of pH when the system was operated in batch mode, before complete oxidation of the electrodes. A second class of materials that has been developed to control parasitic side reactions are intercalation electrodes.[945] For instance, Kim et al. developed a battery desalination system using identical sodium intercalation electrodes, namely CuHCF, with one or more IEMs to partition successive channels of diluate and concentrate. A triple-stack device with five IEMs showed a tenfold reduction in energy consumption compared to an MCDI device operated under the same conditions. Again, these improvements in performance must be weighed against the capital

cost incurred by using additional membranes.

The third standard approach to improve energy efficiency is to optimize the operating conditions of the process. One example is reported by Hemmatifar et al. who showed that careful selection of the operating conditions in CDI can increase the thermodynamic efficiency up to 9%.[761] These high efficiencies were achieved by operating the system at constant current, recovering energy during discharging, balancing the rates of charge and fluid transport (which represent the rates of adsorption and ion advection, respectively), limiting the window of voltages to between $0.4\,\mathrm{V}$ and $1\,\mathrm{V}$ (higher voltages trigger side reactions and smaller ones diminish charge efficiency), and lowering series resistances by using current collectors made of titanium mesh separated by thin (30μm) spacers. In another study, Ramachandran et al. proposed the use of alternating electrical current and successfully removed much of the salt fed without compromising energy efficiency.[1185] The alternating current was sustained at the intrinsic resonant frequency of the system (equivalent to the time constant of an RC circuit), which was shown to be inversely proportional to the geometric mean of residence time and charging time. In a similar way to electrical current, the flow profile can be better controlled to improve performance, particularly in systems that are cyclic like CDI and Faradaic electrosorption. The main issue that arises in systems with uncontrolled flow profiles is hydrodynamic dispersion, which inadvertently mixes diluate (produced during adsorption) and concentrate (produced during desorption). A recent study showed that hydrodynamic dispersion (a phenomenon that increases mass diffusivity by an amount proportional to the square of the average fluid velocity) can be inhibited by reducing the flow rate during the discharging step.[764] Using this approach, water recovery was increased to about 90% (compared to 50% with the flow rate fixed) without compromising desalination, productivity, or energy efficiency. In fact, the increase in water recovery enhanced the thermodynamic efficiency by up to a factor of 3. Management of electrical input and fluid flow can thus improve existing electrochemical systems at minimal cost.

1.6.3 Performance Tradeoffs

Our discussion in the previous section would be incomplete without quantifying the performance of electrochemical methods because there are underlying tradeoffs between kinetics and energetics in any separation process. For this reason, the desalination community uses productivity and energy consumption (per unit volume of diluate) as the two core measures to both quantify performance[128,1189,1190] and estimate the capital and operating costs of a plant.[742,763] In this section, we examine the relationship between these two parameters and how they collectively influence thermodynamic efficiency.

Constraining the extent of desalination, productivity and (volumetric) energy consumption reveal complex coupling, as shown in Figure 1-41. This plot condenses data obtained from thirty CDI experiments reported in ref 1179 into a single graph of energy versus productivity. As noted by Hawks et al.[742] and Wang et al.,[763] these quantities depend on conditions like water recovery, feed concentration, and average reduction in concentration. The data in Figure 1-41 are interpolated to obtain a curve that corresponds to the following conditions: water recovery is 50%, feed concentration is 20 mM, and product concentration is 15.5 mM. The free energy of separation, $\Delta\hat{G}$ (per unit volume of diluate), is known and given by

$$\Delta\hat{G} = RT\sum_i \left[\frac{c_{i_0}}{\gamma}\ln\left(\frac{c_{i_B}}{c_{i_0}}\right) - c_{i_D}\ln\left(\frac{c_{i_B}}{c_{i_D}}\right)\right] \tag{1.20}$$

where the summation is taken over all ions in solution, c_{i_0} is the feed concentration of ion i, and $c_{i_D} = c_{i_0} - \Delta c_i$ and $c_{i_B} = c_{i_0} + \gamma\Delta c_i/(1-\gamma)$ are the concentrations of ion i in the diluate and concentrate (brine), respectively. For a univalent binary electrolyte of a single salt, Equation 1.20 can be rewritten as[761]

$$\Delta\hat{G} = 2RT\left[\frac{c_0}{\gamma}\ln\left(\frac{c_B}{c_0}\right) - c_D\ln\left(\frac{c_B}{c_D}\right)\right] \tag{1.21}$$

The free energy of separation can then be used to determine the thermodynamic

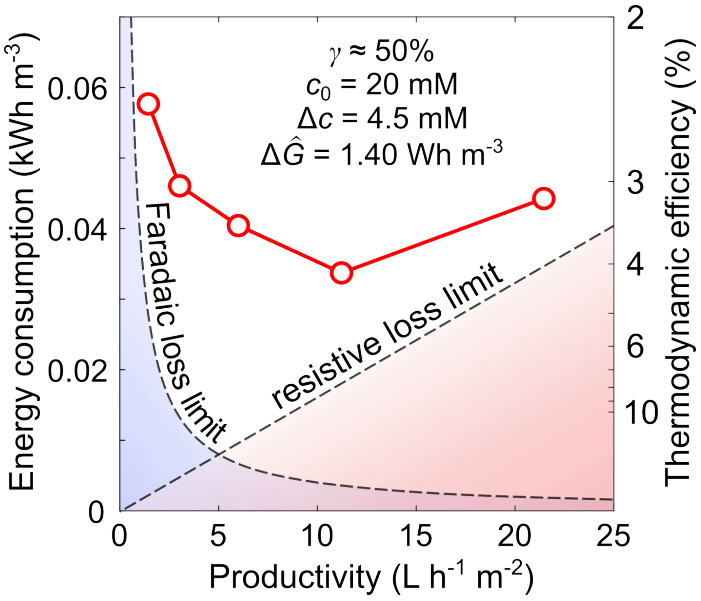

Figure 1-41. Graphical explanation of the relationship between productivity, energy consumption, and thermodynamic efficiency. Values were obtained by interpolation of data from thirty CDI experiments reported in ref 1179. In this plot, water recovery (γ), feed concentration (c_0), and average reduction in concentration (Δc) are prescribed. The dashed straight line and dashed curved line show qualitative lower limits imposed by resistive and Faradaic losses, respectively.

efficiency of a given desalination process:

$$\eta_{\text{thermo}} = \Delta\hat{G}/\hat{E} \tag{1.22}$$

where $\hat{E}$ is the energy consumed per unit volume of treated water.

Figure 1-41 shows the relationship between productivity and energy consumption in a general electrosorption process. This nonmonotonic behavior can be explained by the fact that energy consumption is governed primarily by resistive losses at high current and can be approximated as

$$\hat{E}_{\text{EC}} \approx A\mathscr{R}_s \left(\frac{F\Delta c}{\gamma\Lambda}\right)^2 \mathscr{P} \tag{1.23}$$

where A is total active surface area and $\mathscr{P} = \gamma Q/A$. If cycle efficiency and total resistance are constant, energy consumption and productivity would be directly proportional (see refs 742,763 for similar conclusions). The dashed straight line in

Figure 1-41 shows a qualitative lower limit imposed by resistive losses that dominates when productivity is high. At low current, on the hand, energy consumption is determined mainly by Faradaic losses[90] and can be approximated as

$$\hat{E}_{\mathrm{EC}} \approx \frac{\mathscr{R}_s I_F^2}{A} \mathscr{P}^{-1} \tag{1.24}$$

where the charging current was replaced by the Faradaic leakage current, I_F. This simple model, represented by the dashed curved line in Figure 1-41, shows that energy consumption is inversely proportional to productivity. With the extent of desalination fixed, thermodynamic efficiency can be improved by carefully balancing the counteracting resistive and Faradaic losses.[90]

1.6.4 Desalination

In this section, we quantify the energy consumed by various electrochemical methods for desalination based on data reported in the literature. Figure 1-42 shows that the energy needed to desalinate brackish water by these methods ranges mostly between ten and one hundred times the theoretical minimum requirement. In contrast, optimized SWRO systems come within a factor of two (excluding pre- and post-treatment steps) of the thermodynamic limit.[68] As a result, much research is focused on improving electrochemical systems to reliably desalinate brackish water and remove trace contaminants from dilute feeds with energy inputs closer to the thermodynamic limit. Accomplishment of this task requires innovation and optimization of advanced technologies for water purification. Electrochemical methods are well positioned to be at the forefront of this effort because, as shown in Figures 1-2 and 1-42, they can efficiently desalinate brackish water and dilute feeds under a broad range of operating conditions.

Figure 1-42 plots the thermodynamic efficiency (Equation 1.22) versus productivity for several electrochemical systems used for desalination. Here, we use the definition of productivity given by Hawks et al.:[742]

$$\mathscr{P} = \frac{V_D}{nA}, \tag{1.25}$$

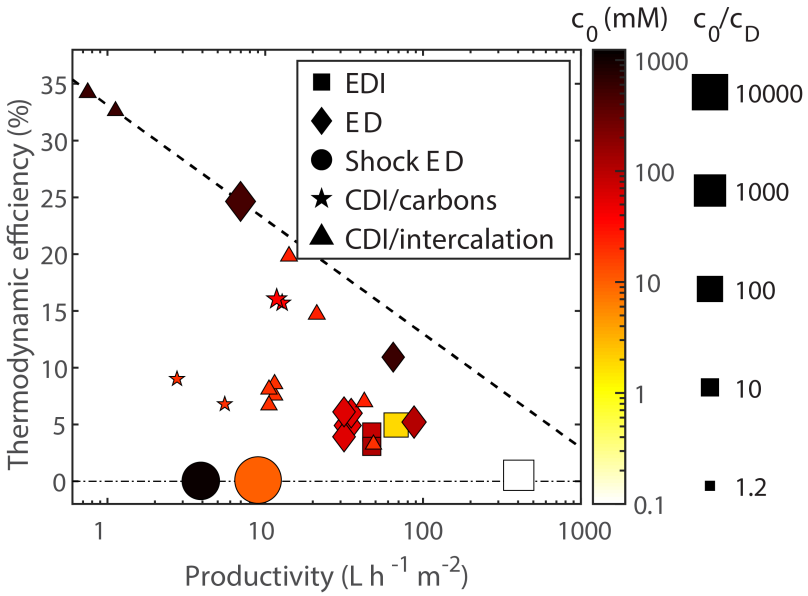

Figure 1-42. Thermodynamic energy efficiency as a function of productivity for various electrochemical methods performing laboratory-scale desalination of brackish and dilute water. Representative data are presented for EDI (squares),[627,1191,1192] ED (diamonds),[345,1193–1196] shock ED (circles),[87,588] and CDI with either carbon electrodes (stars)[640,761] or intercalation electrodes (triangles).[719,915,945] The color and size of each data marker represent feed concentration and the ratio c_0/c_D (see Equation 1.20), respectively. The dashed line represents an (approximate) empirical efficiency limit and is given by $\eta_{\text{thermo}} = 0.331 - 0.101 \log_{10}(\mathscr{P})$, where $\mathscr{P}$ is in units of $\text{L}\,\text{h}^{-1}\,\text{m}^{-2}$.

where V_D is the volume of diluate, A is the projected membrane or electrode area of a single cell or a cell pair, and n is the number of cells or cell pairs. (An alternative definition, which is not used here, is based on total membrane area and sets $n = 1$; this definition differs from Equation 1.25 by a factor of 2.) The methods considered in Figure 1-42 include EDI (squares), ED (diamonds), shock ED (circles), and CDI with either carbon (stars) or intercalation (triangles) electrodes. The color of each marker represents feed concentration, and marker size corresponds to the ratio c_0/c_D, which quantifies salt rejection. The data in Figure 1-42 reveal a tradeoff between energy consumption and productivity, where systems with higher productivity generally exhibit lower efficiency. We also observe a quantitative trend where all data points fall below a straight line, which we argue is an empirical efficiency limit at this time for desalination by the electrochemical methods considered in this review. Devices near this line are among the most efficient electrochemical systems currently used for desalination. In the future, further development and optimization will lead to devices that can surpass this empirical limit.

Based on Figure 1-42, CDI with membranes and intercalation electrodes as well as ED are the most efficient electrochemical systems for desalination, with maximum values of 34.2% for CDI ($\mathscr{P} < 1\,\mathrm{L\,h^{-1}\,m^{-2}}$) and 24.6% for ED ($\mathscr{P} = 7\,\mathrm{L\,h^{-1}\,m^{-2}}$). At the same time, these systems have primarily been used to remove small quantities of salt (c_0/c_D equals up to 5.6 for carbon CDI, 1.5 for intercalation CDI, and 44 for ED). In contrast, methods like EDI and shock ED display lower energy efficiency but have mainly been used to deionize water (c_0/c_D equals up to 500 for EDI and 10^4 for shock ED). For nearly all the systems presented in Figure 1-42, water recovery ranges between 31% and 86%. (In this context, water recovery is defined as the ratio of diluate volume to total feed volume, including electrode streams.) One ED system, however, achieved only 4% water recovery ($\eta_{\mathrm{thermo}} = 4.91\%$ and $\mathscr{P} = 33.3\,\mathrm{L\,h^{-1}\,m^{-2}}$) due to the high flow rate of the electrode streams, which were not recycled.[1194]

1.6.5 Scale Up and Optimization

Electrodialysis

As explained in Section 1.3.1, the cost of desalination by ED depends on the concentration of ions in the feed. In electromembrane processes, ion concentration determines current density and membrane area, both of which contribute to capital and operating costs and influence process efficiency. For example, a more conductive membrane results in faster ion transport, lower stack resistance, and less energy consumption. Faster ion transport also reduces the membrane area required by the device. Meanwhile, to separate the various components of a feed, the system needs a selective membrane. Numerous studies have focused on preparing IEMs with improved electrochemical properties, such as by employing functional nanomaterials and advanced surface modifications.[346,1197–1199] These efforts have shown noticeable improvements in the electrochemical properties of IEMs and ultimately in the performance of ED systems.[126] Today, ED stacks can operate at industrial throughputs and are commercially available from many companies, including PCCell, Suez Water Technologies & Solutions, Pure Water Group, and Hydro Volta. These ED systems have been deployed for a variety of applications, including brine desalination, wastewater treatment, nutrient recovery (e.g., nitrogen, phosphorus), whey and sugar demineralization, juice deacidification, and wine stabilization.[127,418,436,1200–1205]

In most of these applications, ED systems are subject to organic fouling, as discussed in Section 1.3.6.[1206] Strong hydrophobic interactions between the membrane and organic species can lead to irreversible adsorption and an increase in membrane resistance.[1205,1206] Surface modifications with polyelectrolytes have thus attracted much interest in the design of fouling-resistant IEMs.[347,630,1207,1208] These modifications significantly increase the hydrophilicity of membrane surfaces and are simple to perform. Today, IEMs are manufactured by several companies, including DuPont (Nafion), Chemours (Nafion), ASTOM (Neosepta), AGC Chemicals (Selemion), and FUMATECH BWT (Fumasep), and much research has been de-

voted to improving the durability and lowering lowering the cost of these membranes.[419,424,1209,1210]

In practice, an ED stack may comprise hundreds of membrane pairs to achieve a sufficient membrane area when operating at high throughput.[418] A large number of membrane pairs and compartments, however, increases the resistance of the stack, and so ED is usually built with thin spacers and gaskets (thicknesses are commonly in the range of 0.5-$2.0\,\mathrm{mm}$) to lower this resistance.[1211] The narrow channels and compartments created by these thin spacers also induce a high cross-flow velocity, which elevates the pressure difference between the diluate and concentrate compartments. This pressure difference must be controlled to prevent excessive stress on the membranes.[1212] Another effective way to decrease stack resistance and improve performance is to use thinner membranes.[1073,1213] Reducing the thickness of the membranes, however, must be accompanied by improving their mechanical properties, as thinner membranes can become mechanically delicate. Profiled (or patterned) membranes are some of the latest developed IEMs that are used to boost the performance of electromembrane processes. With their nonflat, patterned surfaces, profiled membranes enhance fluid mixing at interfaces and in turn improve ion transport.[1214] In the future, ED may even require no spacer, which would further reduce the stack resistance and fabrication cost of ED.

Electrodeionization

One aspect of EDI that remains an important research topic is resin configuration.[484] Devices with mixed-bed configurations are commonly used to boost the removal of ions present at low concentrations by exploiting water dissociation. Random contact between cation and anion exchange resins in this configuration, however, may negatively impact ion transport due to reverse junction leakage.[1215] Separated and layered beds are alternative configurations that improve current efficiency by providing more pathways for ion transport,[1215] though the stack may need additional compartments or special spacer designs to maintain the resin in layers.

The loose resin beads in EDI can accumulate at the end of compartments or near the electrolyte outlets, which increases the pressure drop across the device.[1216] Accumulation of resin beads can also lead to an uneven distribution of current and suboptimal ion transport. One solution to this problem is to introduce ion exchange resin wafers, which are made of resin beads bound and immobilized into a porous matrix.[83,458,467,1217–1219] These wafers ensure a mechanically stable distribution of the resin and prevent accumulation of resin beads. The binder material used in resin wafers could be either insulating[83] or conducting,[468] and water splitting could be promoted by incorporating a catalyst in Janus bipolar resin wafers.[467]

Additional design features have been introduced to EDI systems to further improve their performance. One example, known as fractional EDI, involves the division of an EDI cell into a sequence of stages to optimize the distribution of electrical current.[483,1220] A fractional EDI cell comprises two or more separated pairs of electrodes to divide the power supply into amounts appropriate for each pair. In this way, the energy consumption can be lowered, and selective separations based on the charge of the impurities can be achieved.[1220] Moreover, this design is better at limiting the formation of mineral scale since concentrates from different fractions are separated, which prevents interaction between multivalent ions from one fraction and the OH^- generated in another.

Shock Electrodialysis

The principles discussed in Section 1.6.5 are also relevant to the engineering of shock ED, although scaled-up commercial systems have yet to be demonstrated. As in ED or EDI, stacks of repeated layers may serve to lower the energy cost of driving electrical current at the electrodes relative to that of driving separations in all the layers,[1221] though it may be possible to achieve similar efficiency at lower cost and complexity by using fewer but thicker porous layers at the centimeter scale.[87,95] Performance of shock ED may also be improved by varying the charge and microstructure of the porous material.[530,586,1222] Similar hierarchical porous media as in EDI, such as immobilized beds of ion exchange resin,[83,467,468] could be

used to boost electromigration (compared to surface conduction in a glass frit) and promote shock formation and ion separations in the depletion zone. It may also be possible to lower capital costs and improve performance by replacing the IEMs used to initiate shock waves with thin, nanoporous ceramic or polymer layers analogous to the nanochannel junctions used in microfluidic ICP.[93,93,554,558]

Capacitive Deionization

Today, CDI systems are available from several water technology companies. The first to develop a commercial CDI system was Voltea (founded in 2006), and it was followed by other companies including Ur-Water, Atlantis Technologies, Idropan dell'Orto Depuratori, EST Water Technologies, Siontech, and InnoDI Water Technologies.[1223,1224] As discussed in Section 1.4.1, energy consumption by CDI has been extensively studied, and recent research demonstrated the possibility of combining photovoltaics and batteries to power a pilot CDI plant for remote applications.[796] Since pumping also contributes to the total energy demand, there has been growing interest in process design to reduce pumping costs.[796] For example, Nordstrand et al. recently designed a parallel arrangement of cells with symmetrically distributed flows to maintain a low pressure drop across the system.[649] Another challenge during scale up of CDI is to make the process continuous, which has been the focus of FCDI[810,826,827,1225] and multichannel MCDI[937,956,1226,1227] systems. The latter enables continuous production of both fresh and brine streams by periodically switching the products of the middle and side channels.[1226] Technoeconomic analyses of CDI also show the importance of achieving long system lifetimes, as capital costs (e.g., electrodes, membranes, frames, current collectors) are expected to outweigh operating costs (e.g., electricity, materials, labor).[776,1228,1229] In particular, it is necessary to understand and mitigate electrode degradation[656,786] (see Section 1.4.1) and cell fouling (see Section 1.4.1). Several other publications on CDI optimization and pilot systems provide additional design rules and principles for scale up.[649,775,796,826,1224,1225,1227,1230–1233]

Faradaic Electrosorption

Redox based separation technologies remain an emerging area of research, and there are only a few preliminary studies on scale up and technoeconomic analysis. In one example, Joo et al. demonstrated a pilot electrochemical system using $LiMn_2O_4$ to selectively recover lithium from the desalination concentrate produced by RO and membrane distillation.[1234] This continuous system comprised fourteen pairs of λ-MnO_2 and Ag electrodes arranged in parallel, and it was sequentially submerged in solutions for capturing, washing, and cleaning to recover the lithium. The system processed the desalination concentrate at a flow rate of $250\,L\,h^{-1}$ and produced an up-concentrated lithium solution with 88% purity and an enrichment factor of 1800. Metzger et al. conducted a comprehensive technoeconomic analysis on MCDI, HCDI, and intercalation CDI.[916] This analysis showed that, compared to MCDI, intercalation CDI can achieve higher removal capacity and is more cost effective and energy efficient.[916,1235] To treat equal volumes of water with similar performance, for example, an intercalation CDI module would cost only 27% of an MCDI module and would be four times smaller in size.

It has been shown, for certain applications, that electrochemical systems with redox reactions can be more cost effective than conventional desalination methods. Kim et al. designed a system with redox-active electrodes to valorize proteins from whey waste and performed a preliminary technoeconomic analysis.[1236] To produce equal volumes of whey protein, the redox desalination system consumed up to 72% less energy than ED by driving redox reactions rather than water splitting. Moreover, the use of fewer IEMs in the redox system relative to ED lowered capital costs by 62%.[1236] Further progress in redox separation technologies requires a focus on device scale up, uncomplicated and economical synthesis of electrodes, long-term stability, and innovative stacking methods.[1237]

1.6.6 Process Intensification

Many of the methods discussed in this review are still under development, and it is anticipated that innovations in materials science, device engineering, and process

design will continue to advance these technologies. In addition to these advancements, process intensification can be undertaken to achieve more holistic (or global) improvements in electrochemical methods for water purification. Process intensification is any integration of unit operations, functions, and phenomena that leads to a smaller, cleaner, safer, and more efficient technology.[1238,1239] Emerging electrochemical methods provide new opportunities for process intensification by combining these systems with either other emerging methods or established technologies that are complementary in function.[578,1240,1241] In an electrochemical method, the electric field enables selectivity and interfacial control, promotes fast reaction rates, and reduces energy consumption.[1240,1242] Advances in electrocatalysis have revealed that existing thermal and chemical methods can in fact be replaced by novel electrochemical processes.[1243,1244] Due to the importance of product purification, waste processing, and materials recycling, separations based on electrokinetics and electrosorption can play a key role in process intensification. Examples of process intensification for electroseparations include integration of reaction and separation using redox interfaces (as shown in Figure 1-29)[102,1022] as well as selective recovery of target species from waste streams using shock ED.[578]

The dual nature of electrochemical systems, highlighted by cells with asymmetrically configured electrodes, provides a new conceptual platform for process intensification.[102,910,1022] Although some Faradaic reactions are unwanted and can compromise efficiency, others can drive separations and promote catalysis.[96,656] In Section 1.4.3, we explained that molecular design of Faradaic processes enables electrosorptive removal of heavy metal oxyanions and simultaneous redox transformation at the counter electrode. In one such example, As(III) was captured and transformed into As(V) using PVF and PTMA as electrodes,[102] and in another, Cr(VI) was captured and transformed into the less harmful Cr(III) using PVF and platinum as electrodes.[1022] Both of these systems involved electron transfer, which activated the redox units, and Faradaic reactions, which transformed the target metals into more benign products. Asymmetric combinations of intercalation systems and BDD electrodes have also been proposed for removal of both lithium and or-

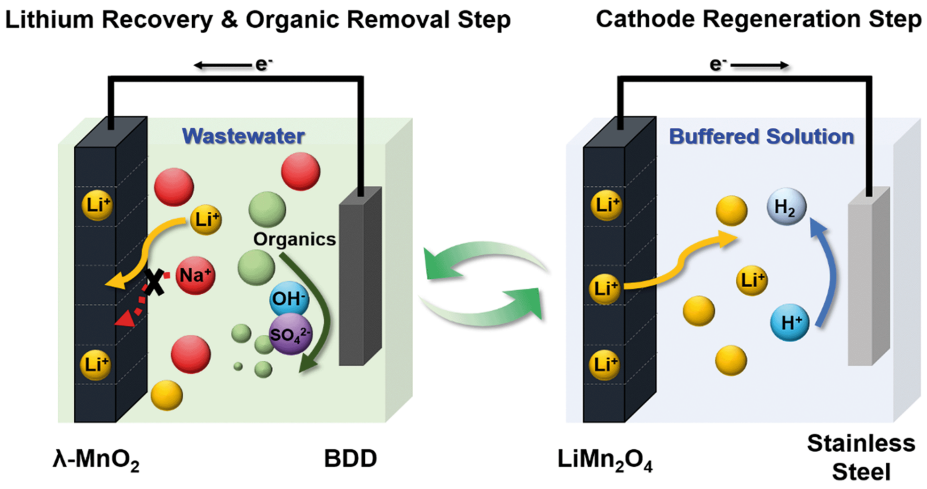

Figure 1-43. Schematic of an electrochemical system with $LiMn_2O_4$ and BDD as electrodes for removal of both lithium and organic pollutants from industrial wastewater. Reproduced with permission from ref 1245. Copyright 2018, Royal Society of Chemistry.

ganic pollutants from industrial wastewater, as shown in Figure 1-43.[1245] Li^+ was recovered (in excess of 98%) using an MnO_2 electrode with high selectivity toward Li^+ relative to Na^+, and more than 65% of the organic pollutant was decomposed at the stainless steel counter electrode. Kim et al. observed a tradeoff, however, between the utilization efficiency of $LiMn_2O_4$ and the rate at which Li^+ could be recovered.[1245] Moving forward, we expect a growing set of concepts that combine separations and reactions for water purification.

Electrokinetic methods can also be used for molecular separations to effectively remove harmful contaminants or recover valuable targets.[480,578] For example, Li^+ can be selectively captured from a multicomponent mixture and recycled (or reused elsewhere) by integrating CDI with intercalation materials[88,656] as a second step following shock ED.[578] As shown in Figure 1-44, process intensification of this kind can in principle be achieved in two steps. In the first step, shock ED is used to concentrate waste in the brine, from which Li^+ is selectively captured in the CDI unit by intercalation into an appropriate electrode such as $LiFePO_4$ or $LiMn_2O_4$.[692,927,1246–1248] During this process, all cations are driven toward the intercalation electrode, but Li^+ will be predominantly inserted into its crystal lattice because the vacancies in $FePO_4$ are well fitted for this small monovalent cation.

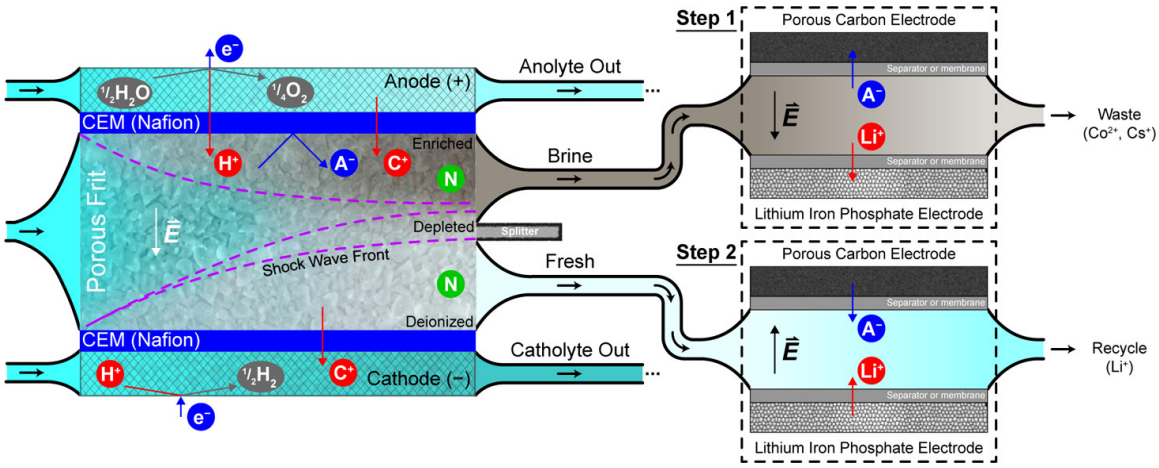

Figure 1-44. Process intensification of shock ED (left) by integrating CDI (right) to recycle Li^+ in two steps. The first step is selective capture of Li^+ in the intercalation electrode of a CDI unit from the brine discharged by shock ED. The second step is release of Li^+ into the fresh stream produced by shock ED by reversing the direction of the applied field. Cations other than Li^+ and H^+ are labeled C^+, anions are labeled A^-, and neutral species (unaffected by the electric fields) are labeled N; streams are colored based on the relative concentration of ions. Reproduced with permission from ref 578. Copyright 2019, American Chemical Society.

Moreover, the anions are inserted into a porous carbon electrode, so fluid leaving the device will be depleted of Li^+ and its counterion(s). In the second step, Li^+ and its counterion(s) are released from the electrodes by reversing the direction of the applied electric field, and the fresh stream produced by shock ED is passed through the CDI unit to collect these ions.

Process intensification of electrochemical methods not only enables targeted separations but also dramatically reduces energy consumption. By comparing the energetics of sequential and coupled Faradaic processes, Kim et al. lowered the energy needed to remove arsenic from $2.2\,kW\,h\,mol^{-1}$ to $0.45\,kW\,h\,mol^{-1}$, as shown in Figure 1-45.[102] The basis of this energy integration was to reduce parasitic side reactions and improve current efficiency by using asymmetric redox systems. Relative to systems with nonselective electrodes (e.g., CDI with porous carbon electrodes), energy efficiency was improved by nearly an order of magnitude. Similarly, in recent work on PFAS capture by electrochemical mediation with TEMPO-based polymers, an asymmetric system of TEMPO copolymers with a BDD counter electrode achieved reactive separation of PFAS.[1029] During release of the PFAS

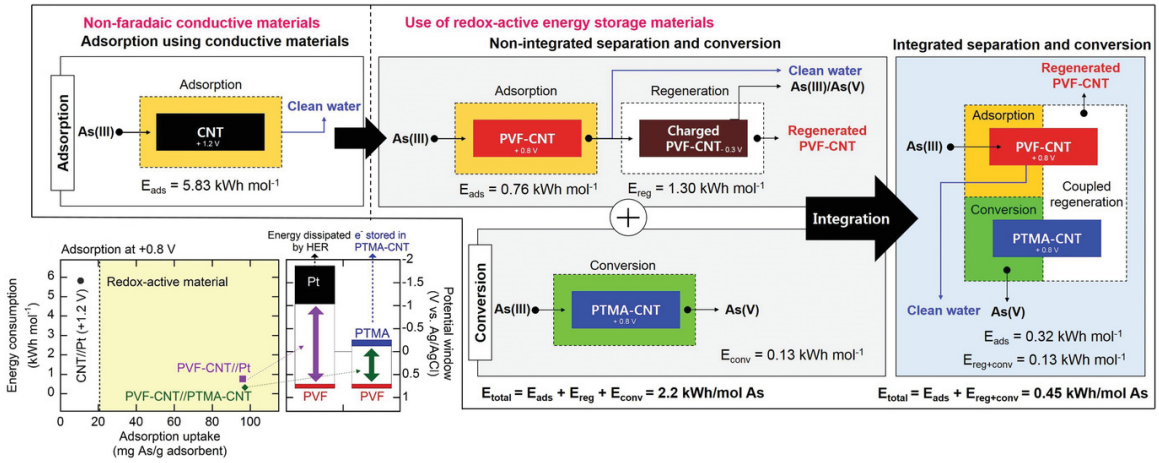

Figure 1-45. Description of energy integration and process intensification using redox electrochemistry with coated electrodes for reactive separations. Reproduced with permission from ref 102. Copyright 2020, Wiley-VCH.

by the redox polymer, the BDD electrode simultaneously broke down PFAS with low energy consumption and a defluorination efficiency over 50%. Electroseparations can therefore enable processes that would otherwise be prohibitively expensive or complex, such as purification of dilute feeds, recovery of metals, valorization of wastes, and isomeric separations of biochemicals and pharmaceutical compounds.[105,156,1241,1249] As shown in this review, electrokinetics and electrochemistry can improve energy efficiency and reduce secondary waste, which enables cleaner and more sustainable processes for water purification.

1.7 Conclusions and Outlook

Electrochemical methods for water purification use applied electric fields to remove contaminants by either degrading or converting them through redox reactions, driving their separations in a bulk electrolyte, electrostatically trapping them in an EDL (where they may undergo electrochemical reactions), or intercalating them in solid electrodes. The ability to remove contaminants directly from water—as opposed to removing the water from the contaminants—is the property that enables most advantages of these methods. Nondestructive electrochemical methods, which are based on electrokinetic (ED, EDI, ICP, shock ED) and electrosorption (CDI, Faradaic electrosorption) processes, tend to be more energy efficient compared to physical

methods when used for molecular separations or purification of dilute feeds. These systems have other attractive features including compactness, molecular selectivity, versatility, decreased generation of secondary waste, and the ability to combine reactions and separations. The selectivity and versatility of electrochemical systems enables unique combinations of technologies for exotic separations and recovery of high-value elements. In particular, the dual nature of these systems provides a new conceptual platform for process intensification of existing methods. Significant advances, however, are still needed both at the fundamental level (e.g., to impart higher molecular selectivity to electrodes for emerging applications) and in process engineering through the development of new hybrid systems for higher energy efficiency. Comprehensive work on technoeconomic analysis is also needed for these emerging methods to provide a comparative evaluation against other treatment technologies and identify limitations, areas of opportunity, and protocols for optimal operation. Here, we highlight emerging research directions, challenges, and opportunities in electrochemical methods for water purification, ion separations, and energy conversion.

1.7.1 Materials Design for Multicomponent Separations

Despite advances in redox-active materials, which have enabled new selectivity and higher uptake, there remain significant challenges in both fundamental studies and new areas of application.

Multifunctional redox materials. To enhance selectivity and overcome existing limitations, one promising approach has been to combine several distinct chemical groups. While redox homopolymers are efficient for applications that demand ion selectivity,[96] redox copolymers extend these capabilities by combining orthogonal properties. For example, redox copolymers have enhanced electrochemical regeneration, chemical binding of rare-earth elements,[1250] and control of hydrophobicity, affinity, and electrostatics within redox adsorbents for PFAS molecules and other micropollutants.[1029,1251,1252] Nanostructured combination of two distinct redox polymers has also enabled the reversible electrochemical binding and control of neu-

tral molecules through redox-tunable hydrophobicity.[103] Similar concepts of hybrid materials may be generalized to redox crystals and various multicomponent separations, in which reversibility or selectivity could be enhanced through hybridization to achieve properties beyond the base chemical structure. Moving forward, we envision these multifunctional materials will provide a versatile platform for extraction of multiple desired elements simultaneously.

Computational design and operando electrochemical tools for understanding interactions. To guide the bottom-up design of materials, computational studies play a key role in the selection of chemistry and tuning of morphology. Tools such as MD[720] and electronic structure calculations[1253] have been critical in understanding selectivity in ultramicroporous carbon and redox-active materials, respectively. We envision molecular simulation tools will increase in utility due to the need for a greater understanding of selective interactions and their underlying mechanisms. In addition to computational tools, we expect that the integration of operando electrochemical tools such as vibrational spectroscopy will elucidate interfacial structure and binding mechanisms. These molecular tools, along with macroscopic transport modeling, can help advance the performance of electrochemical separation methods at multiple scales.

Advances in membrane materials. Advances in membrane materials can improve the efficiency of electrokinetic processes. Membrane fouling and poor stability under certain operating conditions remain longstanding challenges in electrokinetic systems. Besides, redox materials in electrokinetic systems could pass the membranes and contaminate the treated water. The introduction of more durable, cost-effective, and selective membranes is thus needed for more efficient and reliable electrokinetic systems. Structured nanomaterials are expected to play an important role in improving membrane performance.[1254,1255] Moreover, ion selectivity can be modulated through fine control of the structure, pore size, water permeability, and functional groups of the membranes.[1255,1256]

Multicomponent mixtures for separations. Many of the recent studies on selective removal and resource recovery have been performed using idealized sim-

ulated solutions. Real industrial and municipal effluents, however, involve complex speciation of ions and organic compounds, which affects both the selectivity and the lifetime of electrodes and membranes. Municipal effluents are often complex multicomponent mixtures that comprise organic substances, inorganic ions, and sometimes biological species,[147,1257] many of which could form unwanted deposits. Groundwater often contains significant organic matter, and it can exhibit a range of ionic strengths and pHs. As a result, there is a need to evaluate the performance of functional materials when exposed to real samples[1258] to quantify reliability and stability (e.g., electrochemical, chemical, mechanical). At a fundamental level, these studies may reveal the need for materials modification such as the use of antifouling coatings, which can provide a tunable balance between uptake, selectivity, and stability.

Nutrient recovery and metal recovery are two areas of emerging interest in the development of molecularly selective materials. There have been significant advances in the design of selective materials for nutrient recovery, especially using nanostructured porous carbons.[720] Improving selectivity further requires a deeper understanding of solvation, sterics, and electronic structure interactions due to the similarity in electric charge between nutrient species (particularly NO_3^-) and competing ions. At the same time, many electrosorption systems are still highly dependent on pH during separations,[1259,1260] and since many oxyanions have complex speciations that depend on pH, there have been approaches that leverage electrochemical swings in pH for the recovery of nutrients such as PO_4^{3-}.[814,1260]

The recovery of critical elements from mining, recycling, and industrial wastewater streams is another area of emerging importance for selective separations. Many of these transition metals are present in small amounts and are surrounded by excess competing species of similar valence and structure, which makes ion-selective electrosorption a “needle-in-a-haystack” challenge.[1253,1261] Functionalized carbons and redox-active electrodes have made significant strides toward efficient metal recovery and heavy metal removal.[650,1262,1263] However, there are key challenges still to be overcome, such as achieving higher selectivity between different transi-

tion metals within multicomponent mixtures. Rare-earth elements, for example, are often found in the presence of each other as well as other transition metals,[1264] which makes their separation a difficult and costly task. Many competing metals are electroactive at moderate potentials (e.g., copper, lead), and they can often interfere with selective electrosorption processes. Therefore, pretreatment and tuning of electrochemical potentials will be needed to selectively purify multicomponent mixtures.

1.7.2 Intensifying Water Treatment Processes Through Hybrid Approaches

Electrochemical methods can assist in process intensification by decreasing waste, lowering solvent use, and reducing the number of unit operations. In particular, areas for integration include the direct combination of electrochemical methods with renewable energy sources as well as the development of single-cell reactive separations.

Integration of renewable energy sources and electrochemical methods. Coupled with global environmental crises, the development of sustainable manufacturing processes has become a major goal for industries. In this regard, combining electrochemical processes with renewable energy sources (e.g., solar panels) can reduce energy consumption and carbon intensity.[1265] Recently, electrochemical methods for water purification have been hybridized with dye-sensitized solar cells for direct conversion of light to electricity.[1266,1267] The photoanode uses desalinated chloride to generate reactive chlorine species, which can treat wastewater, while the cathode produces molecular hydrogen.[1268] The combination of photoelectrochemistry and redox-flow desalination enables continuous treatment, even in the absence of an external energy source. These systems demonstrate opportunities for the development of processes that integrate energy conversion and electrochemical separations.

Coupling reaction and separation. For persistent contaminants, degradation of these species is as important as their removal from water. The coupling of re-

action and separation can be a powerful approach for providing modular water treatment, as in the case of capture and breakdown of PFAS.[993,1269] The integration of membrane technologies and electrochemical advanced oxidation processes has gained much attention for treatment of organic pollutants in wastewater. In these hybrid processes, a conductive membrane serves as a flow-through anode, which filters the wastewater and drives oxidation of the organic contaminants and pharmaceutical residues.[1270] Moreover, integration of redox processes and magnetic nanoparticles enables selective separation of various organic and inorganic micropollutants.[1252] We envision that emerging electrosorption and electrokinetic systems coupled with advanced oxidation processes can provide efficient process intensification for wastewater treatment.

1.7.3 Translation to Practical Applications

While there have been extensive studies of carbon electrode stability,[1271,1272] many of the emerging Faradaic materials have only been examined at a basic level using idealized solutions. Demonstration of stability and reliability using real samples with relevant electrolyte concentrations is essential. For desalination, electrode stability can be improved by doping the carbon and creating hybrid materials.[1272,1273] It is also important to design materials that suppress parasitic reactions and function at lower potentials, especially when the side reactions involve chloride or oxygen which often produce unwanted byproducts.[656] Proof of economic feasibility is also critical for commercialization of electrochemical systems. Recently, there has been an increase in the number of publications on life cycle assessment and technoeconomic analysis.[1228,1274,1275] These technoeconomic analyses show that the costs of electrodes and membranes are key contributors to the overall capital and operating costs.[916,1228] In practice, technoeconomic analysis will provide a comprehensive framework for assessing feasible electrochemical approaches for water treatment.

In summary, electrochemical systems for water purification and resource recovery are already commercialized in many industries to treat water contaminated with various kinds of waste. Whether or not the emerging purification methods

meet their expectations in the areas of water desalination, remediation, and separations, it seems likely that several of these methods will eventually be employed. In the near term, we expect that a deeper knowledge of the transport phenomena and electrochemical kinetics that govern these methods will facilitate their engineering and optimization. In the long term, work directed toward understanding and improving the design of these processes at scale may guide how commercial prototypes should be built for a given application.

1.8 Acknowledgments

Part of this work was performed in the cooperation framework of Wetsus, European Centre of Excellence for Sustainable Water Technology. Wetsus is cofunded by the Dutch Ministry of Economic Affairs and Ministry of Infrastructure and Environment, the Province of Fryslân, and the Northern Netherlands Provinces (www.wetsus.eu). I Gede Wenten acknowledges financial support from the Indonesian Ministry of Research and Technology/National Agency for Research and Innovation and the Indonesian Ministry of Education and Culture under the World Class University program managed by ITB. J. Pedro de Souza acknowledges support from the National Science Foundation Graduate Research Fellowship. The authors thank Dr. Ali Hemmatifar for his significant contribution to the writing of this manuscript.

1.9 References

[1] Mesfin M Mekonnen and Arjen Y Hoekstra. Four billion people facing severe water scarcity. *Science advances*, 2(2):e1500323, 2016.

[2] Arjen Y Hoekstra. *The water footprint of modern consumer society*. Routledge, 2019.

[3] Jane Kucera. *Desalination: water from water*. John Wiley & Sons, 2019.

[4] M Al-Shammiri and M Safar. Multi-effect distillation plants: state of the art. *Desalination*, 126(1-3):45–59, 1999.

[5] Akili D Khawaji, Ibrahim K Kutubkhanah, and Jong-Mihn Wie. Advances in seawater desalination technologies. *Desalination*, 221(1-3):47–69, 2008.

[6] Doriano Brogioli, Fabio La Mantia, and Ngai Yin Yip. Thermodynamic analysis and energy efficiency of thermal desalination processes. *Desalination*, 428:29–39, 2018.

[7] John Eugene Boysen and Bradley G Stevens. *Demonstration of the Natural Freeze-thaw Process for the Desalination of Water from the Devils Lake Chain to Provide Water for the City of Devils Lake*. US Department of the Interior, Bureau of Reclamation, Technical Service Center, 2004.

[8] Chungang Xie, Lingpin Zhang, Yanhui Liu, Qingchun Lv, Guoling Ruan, and Seyed Saeid Hosseini. A direct contact type ice generator for seawater freezing desalination using lng cold energy. *Desalination*, 435:293–300, 2018.

[9] PR Kiezyk and D Mackay. Waste water treatment by solvent extraction. *The Canadian Journal of Chemical Engineering*, 49(6):747–752, 1971.

[10] Bart Van der Bruggen and Carlo Vandecasteele. Distillation vs. membrane filtration: overview of process evolutions in seawater desalination. *Desalination*, 143(3):207–218, 2002.

[11] Tzahi Y Cath, Amy E Childress, and Menachem Elimelech. Forward osmosis: principles, applications, and recent developments. *Journal of membrane science*, 281(1-2):70–87, 2006.

[12] Clemens Fritzmann, Jonas Löwenberg, Thomas Wintgens, and Thomas Melin. State-of-the-art of reverse osmosis desalination. *Desalination*, 216(1-3):1–76, 2007.

[13] Lourdes Garcia-Rodriguez, Ana I Palmero-Marrero, and Carlos Gómez-Camacho. Comparison of solar thermal technologies for applications in seawater desalination. *Desalination*, 142(2):135–142, 2002.

[14] John H Lienhard, Gregory P Thiel, David M Warsinger, and Leonardo D Banchik. *Low carbon desalination: Status and research, development, and demonstration needs, report of a workshop conducted at the Massachusetts Institute of Technology in association with the Global Clean Water Desalination Alliance*. Massachusetts Institute of Technology, 2016.

[15] Peter Godart. Design and simulation of a heat-driven direct reverse osmosis device for seawater desalination powered by solar thermal energy. *Applied Energy*, 284:116039, 2021.

[16] PA Davies. Wave-powered desalination: resource assessment and review of technology. *Desalination*, 186(1-3):97–109, 2005.

[17] Alfred J Liebmann. History of distillation. *Journal of Chemical Education*, 33(4):166, 1956.

[18] SE Aly. Energy savings in distillation plants by using vapor thermocompression. *Desalination*, 49(1):37–56, 1984.

[19] Adil Al-Radif. Review of various combinations of a multiple effect desalination plant (med) and a thermal vapour compression unit. *Desalination*, 93(1-3):119–125, 1993.

[20] Najem M Al-Najem, MA Darwish, and FA Youssef. Thermovapor compression desalters: energy and availability—analysis of single-and multi-effect systems. *Desalination*, 110(3):223–238, 1997.

[21] Sandeep Parekh, MM Farid, JR Selman, and Said Al-Hallaj. Solar desalination with a humidification-dehumidification technique—a comprehensive technical review. *Desalination*, 160(2):167–186, 2004.

[22] G Prakash Narayan, Mostafa H Sharqawy, Edward K Summers, John H Lienhard, Syed M Zubair, and Mohamed A Antar. The potential of solar-driven humidification–dehumidification desalination for small-scale decentralized water production. *Renewable and Sustainable Energy Reviews*, 14(4):1187–1201, 2010.

[23] G Prakash Narayan, Mostafa H Sharqawy, John H Lienhard V, and Syed M Zubair. Thermodynamic analysis of humidification dehumidification desalination cycles. *Desalination and water treatment*, 16(1-3):339–353, 2010.

[24] Khedidja Dahmani, Djamal Eddine Kherroub, and Mohamed Belloul. Pretreatment of seawater using precipitation agents to retard scale formation in multi-stage flash evaporators. In *Materials Research and Applications*, pages 251–261. Springer, 2021.

[25] Anouar Rich, Youssef Mandri, Nourimane Bendaoud, Denis Mangin, Souad Abderafi, Christine Bebon, Naoual Semlali, Jean-Paul Klein, Tijani Bounahmidi, and Ahmed Bouhaouss. Freezing desalination of sea water in a static layer crystallizer. *Desalination and Water Treatment*, 13(1-3):120–127, 2010.

[26] Z Lu and L Xu. Freezing desalination process. *Thermal desalination processes*, 2, 2010.

[27] Vinod Kumar Gupta, Imran Ali, Tawfik A Saleh, Arunima Nayak, and Shilpi Agarwal. Chemical treatment technologies for waste-water recycling—an overview. *Rsc Advances*, 2(16):6380–6388, 2012.

[28] Georges Belfort, Robert H Davis, and Andrew L Zydney. The behavior of suspensions and macromolecular solutions in crossflow microfiltration. *Journal of membrane science*, 96(1-2):1–58, 1994.

[29] R Rautenbach, K Vossenkaul, T Linn, and T Katz. Waste water treatment by membrane processes—new development in ultrafiltration, nanofiltration and reverse osmosis. *Desalination*, 108(1-3):247–253, 1997.

[30] Andrea Schaefer, Anthony G Fane, and T David Waite. *Nanofiltration: principles and applications*. Elsevier, 2005.

[31] Baltasar Peñate and Lourdes García-Rodríguez. Current trends and future prospects in the design of seawater reverse osmosis desalination technology. *Desalination*, 284:1–8, 2012.

[32] Jane Kucera. *Reverse Osmosis: Industrial Processes and Applications*. John Wiley & Sons, 2015.

[33] IG Wenten and K Khoiruddin. Reverse osmosis applications: prospect and challenges. *Desalination*, 391:112–125, 2016.

[34] Joseph Imbrogno and Georges Belfort. Membrane desalination: where are we, and what can we learn from fundamentals? *Annual review of chemical and biomolecular engineering*, 7:29–64, 2016.

[35] Leos J Zeman and Andrew Zydney. *Microfiltration and ultrafiltration: principles and applications*. CRC Press, 2017.

[36] PTP Aryanti, AN Hakim, S Widodo, IN Widiasa, and IG Wenten. Prospect and challenges of tight ultrafiltration membrane in drinking water treatment. In *IOP Conference Series: Materials Science and Engineering*, volume 395, page 012012. IOP Publishing, 2018.

[37] Bart Van der Bruggen. Microfiltration, ultrafiltration, nanofiltration, reverse osmosis, and forward osmosis. In *Fundamental Modelling of Membrane Systems*, pages 25–70. Elsevier, 2018.

[38] PM Biesheuvel, S Porada, M Elimelech, and JE Dykstra. Tutorial review of reverse osmosis and electrodialysis. *Journal of Membrane Science*, page 120221, 2022.

[39] Hazim Mohameed Qiblawey and Fawzi Banat. Solar thermal desalination technologies. *Desalination*, 220(1-3):633–644, 2008.

[40] Soteris A Kalogirou. *Solar energy engineering: processes and systems*. Academic Press, 2013.

[41] Lawrence K Wang, David A Vaccari, Yan Li, and Nazih K Shammas. Chemical precipitation. In *Physicochemical treatment processes*, pages 141–197. Springer, 2005.

[42] Jia-Qian Jiang. The role of coagulation in water treatment. *Current Opinion in Chemical Engineering*, 8:36–44, 2015.

[43] Purnendu Bose, M Aparna Bose, and Sunil Kumar. Critical evaluation of treatment strategies involving adsorption and chelation for wastewater containing copper, zinc and cyanide. *Advances in Environmental Research*, 7(1):179–195, 2002.

[44] Samuel D Faust and Osman M Aly. *Adsorption processes for water treatment*. Elsevier, 2013.

[45] Maria Cristina Collivignarelli, Alessandro Abbà, Ilaria Benigna, Sabrina Sorlini, and Vincenzo Torretta. Overview of the main disinfection processes for wastewater and drinking water treatment plants. *Sustainability*, 10(1):86, 2018.

[46] Diego Rosso, Lory E Larson, and Michael K Stenstrom. Aeration of large-scale municipal wastewater treatment plants: state of the art. *Water Science and Technology*, 57(7):973–978, 2008.

[47] Azpe Dąbrowski, Z Hubicki, P Podkościelny, and E Robens. Selective removal of the heavy metal ions from waters and industrial wastewaters by ion-exchange method. *Chemosphere*, 56(2):91–106, 2004.

[48] Junfeng Li and Jianlong Wang. Advances in cement solidification technology for waste radioactive ion exchange resins: A review. *Journal of hazardous materials*, 135(1-3):443–448, 2006.

[49] GR Choppin and A Morgenstern. Radionuclide separations in radioactive waste disposal. *Journal of Radioanalytical and Nuclear Chemistry*, 243(1):45–51, 2000.

[50] Nicholas V Ashley and Daniel JW Roach. Review of biotechnology applications to nuclear waste treatment. *Journal of Chemical Technology & Biotechnology*, 49(4):381–394, 1990.

[51] Badiaa Ghernaout, Djamel Ghernaout, and Ali Saiba. Algae and cyanotoxins removal by coagulation/flocculation: A review. *Desalination and Water Treatment*, 20(1-3):133–143, 2010.

[52] Akshaya Kumar Verma, Rajesh Roshan Dash, and Puspendu Bhunia. A review on chemical coagulation/flocculation technologies for removal of colour from textile wastewaters. *Journal of environmental management*, 93(1):154–168, 2012.

[53] Vinod K Gupta, PJM Carrott, MML Ribeiro Carrott, and Suhas. Low-cost adsorbents: growing approach to wastewater treatment—a review. *Critical reviews in environmental science and technology*, 39(10):783–842, 2009.

[54] Hyun Dong Kim and Kyu Han Kim. Water purification using aeration techniques in the lagoon. In *Applied Mechanics and Materials*, volume 675, pages 602–607. Trans Tech Publ, 2014.

[55] Dareen Dardor, Joel Minier-Matar, Arnold Janson, Eman AlShamari, and Samer Adham. The effect of hydrogen sulfide oxidation with ultraviolet light and aeration on sour water treatment via membrane contactors. *Separation and Purification Technology*, 236:116262, 2020.

[56] Khalid Z Elwakeel. Environmental application of chitosan resins for the treatment of water and wastewater: a review. *Journal of dispersion science and technology*, 31(3):273–288, 2010.

[57] Zbigniew Hubicki and Dorota Kołodyńska. Selective removal of heavy metal ions from waters and waste waters using ion exchange methods. *Ion exchange technologies*, 7:193–240, 2012.

[58] Atsushi Iizuka, Yasunobu Yamashita, Hiroki Nagasawa, Akihiro Yamasaki, and Yukio Yanagisawa. Separation of lithium and cobalt from waste lithium-ion batteries via bipolar membrane electrodialysis coupled with chelation. *Separation and Purification Technology*, 113:33–41, 2013.

[59] Maninder Kaur, Huijin Zhang, Leigh Martin, Terry Todd, and You Qiang. Conjugates of magnetic nanoparticle–actinide specific chelator for radioactive waste separation. *Environmental science & technology*, 47(21):11942–11959, 2013.

[60] Viktor Shkolnikov, Supreet S Bahga, and Juan G Santiago. Desalination and hydrogen, chlorine, and sodium hydroxide production via electrophoretic ion exchange and precipitation. *Physical Chemistry Chemical Physics*, 14(32):11534–11545, 2012.

[61] Özgür Arar, Ümran Yüksel, Nalan Kabay, and Mithat Yüksel. Various applications of electrodeionization (edi) method for water treatment—a short review. *Desalination*, 342:16–22, 2014.

[62] Tung Cao Thanh Pham, Son Docao, In Chul Hwang, Mee Kyung Song, Dohyun Moon, Peter Oleynikov, and Kyung Byung Yoon. Capture of iodine and organic iodides using silica zeolites and the semiconductor behaviour of iodine in a silica zeolite. *Energy & Environmental Science*, 9(3):1050–1062, 2016.

[63] Stanley E Manahan. Water treatment. In *Fundamentals of Environmental Chemistry*, pages 1–42. CRC Press, 2001.

[64] Muhammad Qasim, Mohamed Badrelzaman, Noora N Darwish, Naif A Darwish, and Nidal Hilal. Reverse osmosis desalination: A state-of-the-art review. *Desalination*, 459:59–104, 2019.

[65] Mark A Shannon, Paul W Bohn, Menachem Elimelech, John G Georgiadis, Benito J Marinas, and Anne M Mayes. Science and technology for water purification in the coming decades. In *Nanoscience and technology: a collection of reviews from nature Journals*, pages 337–346. World Scientific, 2010.

[66] B. Sauvet-Goichon. Ashkelon desalination plant - a successful challenge. *Desalination*, 203(1-3):75–81, 2007.

[67] R. Semiat. Energy issues in desalination processes. *Environmental Science & Technology*, 42(22):8193–8201, 2008.

[68] M. Elimelech and W. A. Phillip. The future of seawater desalination: Energy, technology, and the environment. *Science*, 333(6043):712–717, 2011.

[69] Jungbin Kim, Kiho Park, Dae Ryook Yang, and Seungkwan Hong. A comprehensive review of energy consumption of seawater reverse osmosis desalination plants. *Applied Energy*, 254:113652, 2019.

[70] R. Zhao, S. Porada, P. M. Biesheuvel, and A. Van der Wal. Energy consumption in membrane capacitive deionization for different water recoveries and flow rates, and comparison with reverse osmosis. *Desalination*, 330:35–41, 2013.

[71] J. Zhou, V. W. C. Chang, and A. G. Fane. Environmental life cycle assessment of brackish water reverse osmosis desalination for different electricity production models. *Energy & Environmental Science*, 4(6):2267–2278, 2011.

[72] K. S. Spiegler and Y. M. El-Sayed. The energetics of desalination processes. *Desalination*, 134(1-3):109–128, 2001.

[73] J Ayoub and R Alward. Water requirements and remote arid areas: the need for small-scale desalination. *Desalination*, 107(2):131–147, 1996.

[74] Jie Song, Tian Li, Lucía Wright-Contreras, and Adrian Wing-Keung Law. A review of the current status of small-scale seawater reverse osmosis desalination. *Water international*, 42(5):618–631, 2017.

[75] NN Azwanida. A review on the extraction methods use in medicinal plants, principle, strength and limitation. *Med Aromat Plants*, 4(196):2167–0412, 2015.

[76] Grégorio Crini and Eric Lichtfouse. Advantages and disadvantages of techniques used for wastewater treatment. *Environmental Chemistry Letters*, 17(1):145–155, 2019.

[77] Yuzhe Zhang, Tingting Bian, Yi Zhang, Xudong Zheng, and Zhongyu Li. Chelation resin efficient removal of cu (ii), cr (iii), ni (ii) in electroplating wastewater. *Fullerenes, Nanotubes and Carbon Nanostructures*, 26(11):765–776, 2018.

[78] Mary Drikas, Christopher WK Chow, Jenny House, and Michael D Burch. Using coagulation, flocculation, and settling to remove toxic cyanobacteria. *Journal-American Water Works Association*, 93(2):100–111, 2001.

[79] Shixin Zhang, Huaili Zheng, Xiaomin Tang, Chun Zhao, Chaofan Zheng, and Baoyu Gao. Sterilization by flocculants in drinking water treatment. *Chemical Engineering Journal*, 382:122961, 2020.

[80] Chee Yang Teh, Pretty Mori Budiman, Katrina Pui Yee Shak, and Ta Yeong Wu. Recent advancement of coagulation–flocculation and its application in wastewater treatment. *Industrial & Engineering Chemistry Research*, 55(16):4363–4389, 2016.

[81] CA De Wolf, E Bang, A Bouwman, W Braun, E De Oliveira, and H Nasr-El-Din. Evaluation of environmentally friendly chelating agents for applications in the oil and gas industry. In *SPE International Symposium and Exhibition on Formation Damage Control*. Society of Petroleum Engineers, 2014.

[82] Jiaping Paul Chen. *Decontamination of heavy metals: processes, mechanisms, and applications*. Crc Press, 2012.

[83] Shu-Yuan Pan, Seth W Snyder, Hwong-Wen Ma, Yupo J Lin, and Pen-Chi Chiang. Development of a resin wafer electrodeionization process for impaired water desalination with high energy efficiency and productivity. *Acs Sustainable Chemistry & Engineering*, 5(4):2942–2948, 2017.

[84] William A Tarpeh, James M Barazesh, Tzahi Y Cath, and Kara L Nelson. Electrochemical stripping to recover nitrogen from source-separated urine. *Environmental science & technology*, 52(3):1453–1460, 2018.

[85] Linchao Mu, Yichong Wang, and William A Tarpeh. Validation and mechanism of a low-cost graphite carbon electrode for electrochemical brine valorization. *ACS Sustainable Chemistry & Engineering*, 8(23):8648–8654, 2020.

[86] X. Su and T. A. Hatton. Electrosorption at functional interfaces: from molecular-level interactions to electrochemical cell design. *Physical Chemistry Chemical Physics*, 19(35):23570–23584, 2017.

[87] S. Schlumpberger, N. B. Lu, M. E. Suss, and M. Z. Bazant. Scalable and continuous water deionization by shock electrodialysis. *Environmental Science & Technology Letters*, 2(12):367–372, 2015.

[88] K Singh, HJM Bouwmeester, LCPM De Smet, MZ Bazant, and PM Biesheuvel. Theory of water desalination with intercalation materials. *Physical review applied*, 9(6):064036, 2018.

[89] D. He, C. E. Wong, W. W. Tang, P. Kovalsky, and T. D. Waite. Faradaic reactions in water desalination by batch-mode capacitive deionization. *Environmental Science & Technology Letters*, 3(5):222–226, 2016.

[90] Ali Hemmatifar, James W. Palko, Michael Stadermann, and Juan G. Santiago. Energy breakdown in capacitive deionization. *Water Research*, 104:303–311, 2016.

[91] Todd M Squires. Particles in electric fields. *Fluids, Colloids and Soft Materials: An Introduction to Soft Matter Physics*, pages 59–79, 2016.

[92] Ali Mani, Thomas A Zangle, and Juan G Santiago. On the propagation of concentration polarization from microchannel-nanochannel interfaces part i: analytical model and characteristic analysis. *Langmuir*, 25(6):3898–3908, 2009.

[93] Thomas A Zangle, Ali Mani, and Juan G Santiago. On the propagation of concentration polarization from microchannel-nanochannel interfaces part ii: numerical and experimental study. *Langmuir*, 25(6):3909–3916, 2009.

[94] Ali Mani and Martin Z Bazant. Deionization shocks in microstructures. *Physical Review E*, 84(6):061504, 2011.

[95] Daosheng Deng, E Victoria Dydek, Ji-Hyung Han, Sven Schlumpberger, Ali Mani, Boris Zaltzman, and Martin Z Bazant. Overlimiting current and shock electrodialysis in porous media. *Langmuir*, 29(52):16167–16177, 2013.

[96] X. Su and T. A. Hatton. Redox-electrodes for selective electrochemical separations. *Advances in Colloid and Interface Science*, 244:6–20, 2017.

[97] Christos Comninellis and Guohua Chen. *Electrochemistry for the Environment*, volume 2015. Springer, 2010.

[98] Emmanuel Mousset and Kyle Doudrick. A review of electrochemical reduction processes to treat oxidized contaminants in water. *Current Opinion in Electrochemistry*, 22:221–227, 2020.

[99] Michael A Lilga, Rick J Orth, JPH Sukamto, SM Haight, and DT Schwartz. Metal ion separations using electrically switched ion exchange. *Separation and purification technology*, 11(3):147–158, 1997.

[100] Kavita M Jeerage and Daniel T Schwartz. Characterization of cathodically deposited nickel hexacyanoferrate for electrochemically switched ion exchange. *Separation Science and Technology*, 35(15):2375–2392, 2000.

[101] Hang Dong, Lingze Wei, and William A Tarpeh. Electro-assisted regeneration of ph-sensitive ion exchangers for sustainable phosphate removal and recovery. *Water Research*, 184:116167, 2020.

[102] Kwiyong Kim, Stephen Cotty, Johannes Elbert, Raylin Chen, Chia-Hung Hou, and Xiao Su. Asymmetric redox-polymer interfaces for electrochemical reactive separations: Synergistic capture and conversion of arsenic. *Advanced Materials*, 32(6):1906877, 2020.

[103] Xianwen Mao, Wenda Tian, Yinying Ren, Dexin Chen, Sarah E Curtis, Marjorie T Buss, Gregory C Rutledge, and T Alan Hatton. Energetically efficient electrochemically tunable affinity separation using multicomponent polymeric nanostructures for water treatment. *Energy & Environmental Science*, 11(10):2954–2963, 2018.

[104] Yinying Ren, Xianwen Mao, and T Alan Hatton. An asymmetric electrochemical system with complementary tunability in hydrophobicity for selective separations of organics. *ACS Central Science*, 5(8):1396–1406, 2019.

[105] Xiao Su, Jonas Hübner, Monique J Kauke, Luiza Dalbosco, Jonathan Thomas, Christopher C Gonzalez, Eric Zhu, Matthias Franzreb, Timothy F Jamison, and T Alan Hatton. Redox interfaces for electrochemically controlled protein–surface interactions: Bioseparations and heterogeneous enzyme catalysis. *Chemistry of Materials*, 29(13):5702–5712, 2017.

[106] Jonathan Wood, Joseph Gifford, John Arba, and Michael Shaw. Production of ultrapure water by continuous electrodeionization. *Desalination*, 250(3):973–976, 2010.

[107] AN Hakim and IG Wenten. Mechanism of ion transfer in electrodeionization (edi) system. *Advanced Science Letters*, 23(6):5640–5642, 2017.

[108] B Senthil Rathi, P Senthil Kumar, and R Parthiban. A review on recent advances in electrodeionization for various environmental applications. *Chemosphere*, 289:133223, 2022.

[109] Kameron M Conforti and Martin Z Bazant. Continuous ion-selective separations by shock electrodialysis. *AIChE Journal*, 66(1):e16751, 2020.

[110] Yoram Oren. Capacitive deionization (cdi) for desalination and water treatment—past, present and future (a review). *Desalination*, 228(1-3):10–29, 2008.

[111] C Huyskens, J Helsen, and AB de Haan. Capacitive deionization for water treatment: Screening of key performance parameters and comparison of performance for different ions. *Desalination*, 328:8–16, 2013.

[112] L. Guo, Y. X. Huang, M. Ding, Z. Y. Leong, S. Vafakhah, and H. Y. Yang. A high performance electrochemical deionization method to desalinate brackish water with an fepo4/rgo nanocomposite. *Journal of Materials Chemistry A*, 6(19):8901–8908, 2018.

[113] L. Guo, R. W. Mo, W. H. Shi, Y. X. Huang, Z. Y. Leong, M. Ding, F. M. Chen, and H. Y. Yang. A prussian blue anode for high performance electrochemical deionization promoted by the faradaic mechanism. *Nanoscale*, 9(35):13305–13312, 2017.

[114] H. Strathmann. Electrodialysis, a mature technology with a multitude of new applications. *Desalination*, 264(3):268–288, 2010.

[115] ME Suss, Slawomir Porada, Xiaowei Sun, PM Biesheuvel, Jeyong Yoon, and Volker Presser. Water desalination via capacitive deionization: what is it and what can we expect from it? *Energy & Environmental Science*, 8(8):2296–2319, 2015.

[116] Kyle C. Smith. Theoretical evaluation of electrochemical cell architectures using cation intercalation electrodes for desalination. *Electrochimica Acta*, 230:333–341, 2017.

[117] Matthew E Suss and Volker Presser. Water desalination with energy storage electrode materials. *Joule*, 2(1):10–15, 2018.

[118] Adarsh Suresh, Grant T Hill, Eli Hoenig, and Chong Liu. Electrochemically mediated deionization: a review. *Molecular Systems Design & Engineering*, 6(1):25–51, 2021.

[119] John Newman and Karen E Thomas-Alyea. *Electrochemical systems*. John Wiley & Sons, 2012.

[120] R O'Hayre, SW Cha, W Colella, and FB Prinz. Fuel cell reaction kinetics. In *Fuel Cell Fundamentals*, pages 59–92. Wiley New York, 2006.

[121] Martin Z Bazant and Todd M Squires. Induced-charge electrokinetic phenomena: theory and microfluidic applications. *Physical Review Letters*, 92(6):066101, 2004.

[122] Martin Z Bazant and Todd M Squires. Induced-charge electrokinetic phenomena. *Current Opinion in Colloid & Interface Science*, 15(3):203–213, 2010.

[123] Arthur L Goldstein. Electrodialysis on the american continent. *Desalination*, 30(1):49–58, 1979.

[124] Andrea Bernardes, MarcoAntônioSiqueira Rodrigues, and JaneZoppas Ferreira. *Electrodialysis and water reuse*. Springer, 2016.

[125] Mika Sillanpää and Marina Shestakova. *Electrochemical water treatment methods: fundamentals, methods and full scale applications*. Butterworth-Heinemann, 2017.

[126] A Campione, L Gurreri, M Ciofalo, G Micale, As Tamburini, and A Cipollina. Electrodialysis for water desalination: A critical assessment of recent developments on process fundamentals, models and applications. *Desalination*, 434:121–160, 2018.

[127] Luigi Gurreri, Alessandro Tamburini, Andrea Cipollina, and Giorgio Micale. Electrodialysis applications in wastewater treatment for environmental protection and resources recovery: A systematic review on progress and perspectives. *Membranes*, 10(7):146, 2020.

[128] Lucía Alvarado and Aicheng Chen. Electrodeionization: Principles, strategies and applications. *Electrochimica Acta*, 132:583–597, 2014.

[129] K. C. Smith and R. Dmello. Na-ion desalination (nid) enabled by na-blocking membranes and symmetric na-intercalation: Porous-electrode modeling. *Journal of the Electrochemical Society*, 163(3):A530–A539, 2016.

[130] P. Srimuk, F. Kaasik, B. Kruner, A. Tolosa, S. Fleischmann, N. Jackel, M. C. Tekeli, M. Aslan, M. E. Suss, and V. Presser. Mxene as a novel intercalation-type pseudocapacitive cathode and anode for capacitive deionization. *Journal of Materials Chemistry A*, 4(47):18265–18271, 2016.

[131] Olgica Balcajin, Alelcsandr Noy, Francesco Fornasiero, Costas P Grigoropoulos, Jason K Holt, Jung Bin In, Sangil Kim, and Hyung Gyu Park. Nanofluidic carbon nanotube membranes: applications for water purification and desalination. In *Nanotechnology Applications for Clean Water*, pages 77–93. Elsevier, 2009.

[132] S. H. Roelofs, A. van den Berg, and M. Odijk. Microfluidic desalination techniques and their potential applications. *Lab on a Chip*, 15(17):3428–3438, 2015.

[133] Heikki Särkkä, Mikko Vepsäläinen, and Mika Sillanpää. Natural organic matter (nom) removal by electrochemical methods—a review. *Journal of Electroanalytical Chemistry*, 755:100–108, 2015.

[134] Carlos A Martínez-Huitle, Manuel A Rodrigo, Ignasi Sirés, and Onofrio Scialdone. Single and coupled electrochemical processes and reactors for the abatement of organic water pollutants: a critical review. *Chemical reviews*, 115(24):13362–13407, 2015.

[135] Brian P Chaplin. Critical review of electrochemical advanced oxidation processes for water treatment applications. *Environmental Science: Processes & Impacts*, 16(6):1182–1203, 2014.

[136] Marco Panizza, Cristina Bocca, and Giacomo Cerisola. Electrochemical treatment of wastewater containing polyaromatic organic pollutants. *Water Research*, 34(9):2601–2605, 2000.

[137] Carlos A Martínez-Huitle and Enric Brillas. Decontamination of wastewaters containing synthetic organic dyes by electrochemical methods: a general review. *Applied Catalysis B: Environmental*, 87(3-4):105–145, 2009.

[138] Ignasi Sirés and Enric Brillas. Remediation of water pollution caused by pharmaceutical residues based on electrochemical separation and degradation technologies: a review. *Environment international*, 40:212–229, 2012.

[139] Enric Brillas and Carlos A Martínez-Huitle. Decontamination of wastewaters containing synthetic organic dyes by electrochemical methods. an updated review. *Applied Catalysis B: Environmental*, 166:603–643, 2015.

[140] J Grimm, D Bessarabov, and R Sanderson. Review of electro-assisted methods for water purification. *Desalination*, 115(3):285–294, 1998.

[141] GH Chen. Electrochemical technologies in wastewater treatment. *Separation and purification Technology*, 38(1):11–41, 2004.

[142] Susanna Pulkka, Mika Martikainen, Amit Bhatnagar, and Mika Sillanpää. Electrochemical methods for the removal of anionic contaminants from water–a review. *Separation and Purification Technology*, 132:252–271, 2014.

[143] Mohammad Alsheyab, Jia-Qian Jiang, and Cecile Stanford. On-line production of ferrate with an electrochemical method and its potential application for wastewater treatment–a review. *Journal of Environmental Management*, 90(3):1350–1356, 2009.

[144] Heikki Särkkä, Amit Bhatnagar, and Mika Sillanpää. Recent developments of electro-oxidation in water treatment—a review. *Journal of Electroanalytical Chemistry*, 754:46–56, 2015.

[145] Carlos A Martínez-Huitle and Enric Brillas. Electrochemical alternatives for drinking water disinfection. *Angewandte Chemie International Edition*, 47(11):1998–2005, 2008.

[146] Alexander Kraft. Electrochemical water disinfection: a short review. *Platinum metals review*, 52(3):177–185, 2008.

[147] Sergi Garcia-Segura, Joey D Ocon, and Meng Nan Chong. Electrochemical oxidation remediation of real wastewater effluents—a review. *Process Safety and Environmental Protection*, 113:48–67, 2018.

[148] Ignasi Sirés, Enric Brillas, Mehmet A Oturan, Manuel A Rodrigo, and Marco Panizza. Electrochemical advanced oxidation processes: today and tomorrow. a review. *Environmental Science and Pollution Research*, 21(14):8336–8367, 2014.

[149] David B Miklos, Christian Remy, Martin Jekel, Karl G Linden, Jörg E Drewes, and Uwe Hübner. Evaluation of advanced oxidation processes for water and wastewater treatment–a critical review. *Water research*, 139:118–131, 2018.

[150] Marek Trojanowicz, Anna Bojanowska-Czajka, Iwona Bartosiewicz, and Krzysztof Kulisa. Advanced oxidation/reduction processes treatment for aqueous perfluorooctanoate (pfoa) and perfluorooctanesulfonate (pfos)–a review of recent advances. *Chemical Engineering Journal*, 336:170–199, 2018.

[151] Sanaullah Khan, Murtaza Sayed, M Sohail, Luqman Ali Shah, and Mazhar Ali Raja. Advanced oxidation and reduction processes. *Advances in Water Purification Techniques*, pages 135–164, 2019.

[152] S. Porada, R. Zhao, A. van der Wal, V. Presser, and P. M. Biesheuvel. Review on the science and technology of water desalination by capacitive deionization. *Progress in Materials Science*, 58(8):1388–1442, 2013.

[153] Ngai Yin Yip, Doriano Brogioli, Hubertus VM Hamelers, and Kitty Nijmeijer. Salinity gradients for sustainable energy: primer, progress, and prospects. *Environmental science & technology*, 50(22):12072–12094, 2016.

[154] Laurent Bazinet and Thibaud R Geoffroy. Electrodialytic processes: Market overview, membrane phenomena, recent developments and sustainable strategies. *Membranes*, 10(9):221, 2020.

[155] IG Wenten, K Khoiruddin, Mohammad A Alkhadra, Huanhuan Tian, and Martin Z Bazant. Novel ionic separation mechanisms in electrically driven membrane processes. *Advances in Colloid and Interface Science*, page 102269, 2020.

[156] Pattarachai Srimuk, Xiao Su, Jeyong Yoon, Doron Aurbach, and Volker Presser. Charge-transfer materials for electrochemical water desalination, ion separation and the recovery of elements. *Nature Reviews Materials*, pages 517–538, 2020.

[157] Jaromír Marek. State-of-the-art water treatment in czech power sector: Industry-proven case studies showing economic and technical benefits of membrane and other novel technologies for each particular water cycle. *Membranes*, 11(2):98, 2021.

[158] JPF Koren and U Syversen. State-of-the-art electroflocculation. *Filtration and Separation*, 32(2):153–156, 1995.

[159] A Alinsafi, M Khemis, Marie-Noëlle Pons, Jean-Pierre Leclerc, A Yaacoubi, A Benhammou, and A Nejmeddine. Electro-coagulation of reactive textile dyes and textile wastewater. *Chemical engineering and processing: Process intensification*, 44(4):461–470, 2005.

[160] M. Y. A. Mollah, R. Schennach, J. R. Parga, and D. L. Cocke. Electrocoagulation (ec) - science and applications. *Journal of Hazardous Materials*, 84(1):29–41, 2001.

[161] MA Rodrigo, Nihal Oturan, and Mehmet A Oturan. Electrochemically assisted remediation of pesticides in soils and water: a review. *Chemical reviews*, 114(17):8720–8745, 2014.

[162] Arezoo Azimi, Ahmad Azari, Mashallah Rezakazemi, and Meisam Ansarpour. Removal of heavy metals from industrial wastewaters: a review. *ChemBioEng Reviews*, 4(1):37–59, 2017.

[163] Chong Liu, Tong Wu, Po-Chun Hsu, Jin Xie, Jie Zhao, Kai Liu, Jie Sun, Jinwei Xu, Jing Tang, and Ziwen Ye. Direct/alternating current electrochemical method for removing and recovering heavy metal from water using graphene oxide electrode. *ACS nano*, 13(6):6431–6437, 2019.

[164] Fei Wang and Shannon S Stahl. Electrochemical oxidation of organic molecules at lower overpotential: Accessing broader functional group compatibility with electron-proton transfer mediators. *Accounts of chemical research*, 53(3):561–574, 2020.

[165] Jian Long Wang and Le Jin Xu. Advanced oxidation processes for wastewater treatment: formation of hydroxyl radical and application. *Critical reviews in environmental science and technology*, 42(3):251–325, 2012.

[166] Maan Hayyan, Mohd Ali Hashim, and Inas M AlNashef. Superoxide ion: generation and chemical implications. *Chemical reviews*, 116(5):3029–3085, 2016.

[167] Carlos Alberto Martínez-Huitle, Manuel A Rodrigo, and Onofrio Scialdone. *Electrochemical water and wastewater treatment*. Butterworth-Heinemann, 2018.

[168] Xinhui Xia, Fengyi Zhu, Jianju Li, Haizhou Yang, Liangliang Wei, Qiaoyang Li, Junqiu Jiang, Guangshan Zhang, and Qingliang Zhao. A review study on sulfate-radical-based advanced oxidation processes for domestic/industrial wastewater treatment: degradation, efficiency, and mechanism. *Frontiers in Chemistry*, page 1092, 2020.

[169] Sanghyeon Kim, Aebin Sin, Heeyeon Nam, Yeji Park, Haesung Lee, and Changseok Han. Advanced oxidation processes for microplastics degradation: A recent trend. *Chemical Engineering Journal Advances*, 9:100213, 2022.

[170] Francisca C Moreira, Rui AR Boaventura, Enric Brillas, and Vítor JP Vilar. Electrochemical advanced oxidation processes: a review on their application to synthetic and real wastewaters. *Applied Catalysis B: Environmental*, 202:217–261, 2017.

[171] Junqun Du, Baogang Zhang, Jiaxin Li, and Bo Lai. Decontamination of heavy metal complexes by advanced oxidation processes: A review. *Chinese Chemical Letters*, 31(10):2575–2582, 2020.

[172] Salatiel Wohlmuth da Silva, Julia Bitencourt Welter, Louidi Lauer Albornoz, Alan Nelson Arenhart Heberle, Jane Zoppas Ferreira, and Andrea Moura Bernardes. Advanced electrochemical oxidation processes in the treatment of pharmaceutical containing water and wastewater: a review. *Current Pollution Reports*, pages 1–14, 2021.

[173] C Sen, Lester Packer, and Osmo Hänninen. *Handbook of oxidants and antioxidants in exercise*. Elsevier, 2000.

[174] Barry Halliwell and John MC Gutteridge. *Free radicals in biology and medicine*. Oxford university press, USA, 2015.

[175] Benon HJ Bielski, Diane E Cabelli, Ravindra L Arudi, and Alberta B Ross. Reactivity of ho2/o- 2 radicals in aqueous solution. *Journal of physical and chemical reference data*, 14(4):1041–1100, 1985.

[176] Hui Zhang, Jie Wu, Zhongqiong Wang, and Daobin Zhang. Electrochemical oxidation of crystal violet in the presence of hydrogen peroxide. *Journal of Chemical Technology & Biotechnology*, 85(11):1436–1444, 2010.

[177] Garry R Buettner. Superoxide dismutase in redox biology: the roles of superoxide and hydrogen peroxide. *Anti-Cancer Agents in Medicinal Chemistry (Formerly Current Medicinal Chemistry-Anti-Cancer Agents)*, 11(4):341–346, 2011.

[178] Zhihui Ai, Zhiting Gao, Lizhi Zhang, Weiwei He, and Jun Jie Yin. Core–shell structure dependent reactivity of fe@ fe2o3 nanowires on aerobic degradation of 4-chlorophenol. *Environmental science & technology*, 47(10):5344–5352, 2013.

[179] Dušan S Dimić, Dejan A Milenković, Edina H Avdović, Đura J Nakarada, Jasmina M Dimitrić Marković, and Zoran S Marković. Advanced oxidation processes of coumarins by hydroperoxyl radical: An experimental and theoretical study, and ecotoxicology assessment. *Chemical Engineering Journal*, 424:130331, 2021.

[180] Richard J Watts, Brett C Bottenberg, Thomas F Hess, Mark D Jensen, and Amy L Teel. Role of reductants in the enhanced desorption and transformation of chloroaliphatic compounds by modified fenton's reactions. *Environmental science & technology*, 33(19):3432–3437, 1999.

[181] Amy L Teel and Richard J Watts. Degradation of carbon tetrachloride by modified fentonâ€™s reagent. *Journal of Hazardous Materials*, 94(2):179–189, 2002.

[182] Shannon M Mitchell, Mushtaque Ahmad, Amy L Teel, and Richard J Watts. Degradation of perfluorooctanoic acid by reactive species generated through catalyzed h2o2 propagation reactions. *Environmental Science & Technology Letters*, 1(1):117–121, 2014.

[183] Lu Bai, Ying Jiang, Deming Xia, Zongsu Wei, Richard Spinney, Dionysios D Dionysiou, Daisuke Minakata, Ruiyang Xiao, Hong-Bin Xie, and Liyuan Chai. Mechanistic understanding of superoxide radical-mediated degradation of perfluorocarboxylic acids. *Environmental science & technology*, 2021.

[184] Richard J Watts and Amy L Teel. Hydroxyl radical and non-hydroxyl radical pathways for trichloroethylene and perchloroethylene degradation in catalyzed h2o2 propagation systems. *Water research*, 159:46–54, 2019.

[185] George V Buxton, Clive L Greenstock, W Phillips Helman, and Alberta B Ross. Critical review of rate constants for reactions of hydrated electrons, hydrogen atoms and hydroxyl radicals ($\cdot$OH/$\cdot$O$^-$ in aqueous solution. *Journal of physical and chemical reference data*, 17(2):513–886, 1988.

[186] J Naumczyk, L Szpyrkowicz, and F Zilio-Grandi. Electrochemical treatment of textile wastewater. *Water Science and Technology*, 34(11):17–24, 1996.

[187] Ch Comninellis and A Nerini. Anodic oxidation of phenol in the presence of nacl for wastewater treatment. *Journal of applied electrochemistry*, 25(1):23–28, 1995.

[188] Carlos A Martinez-Huitle and Sergio Ferro. Electrochemical oxidation of organic pollutants for the wastewater treatment: direct and indirect processes. *Chemical Society Reviews*, 35(12):1324–1340, 2006.

[189] Hongna Li and Jinren Ni. Electrogeneration of disinfection byproducts at a boron-doped diamond anode with resorcinol as a model substance. *Electrochimica acta*, 69:268–274, 2012.

[190] Hongna Li, Yujiao Long, Xiuping Zhu, Yunlong Tian, and Jing Ye. Influencing factors and chlorinated byproducts in electrochemical oxidation of bisphenol a with boron-doped diamond anodes. *Electrochimica Acta*, 246:1121–1130, 2017.

[191] María Belén Carboneras, Pablo Cañizares, Manuel Andrés Rodrigo, José Villaseñor, and Francisco Jesus Fernandez-Morales. Improving biodegradability of soil washing effluents using anodic oxidation. *Bioresource technology*, 252:1–6, 2018.

[192] Ane Urtiaga, Ana Rueda, Ángela Anglada, and Inmaculada Ortiz. Integrated treatment of landfill leachates including electrooxidation at pilot plant scale. *Journal of Hazardous Materials*, 166(2-3):1530–1534, 2009.

[193] Hanspeter Zöllig, Annette Remmele, Eberhard Morgenroth, and Kai M Udert. Removal rates and energy demand of the electrochemical oxidation of ammonia and organic substances in real stored urine. *Environmental science: water research & technology*, 3(3):480–491, 2017.

[194] Ahmad Dirany, Ignasi Sirés, Nihal Oturan, Ali Özcan, and Mehmet A Oturan. Electrochemical treatment of the antibiotic sulfachloropyridazine: kinetics, reaction pathways, and toxicity evolution. *Environmental science & technology*, 46(7):4074–4082, 2012.

[195] Ch Comninellis and C Pulgarin. Electrochemical oxidation of phenol for wastewater treatment using sno2, anodes. *Journal of applied electrochemistry*, 23(2):108–112, 1993.

[196] Christos Comninellis. Electrocatalysis in the electrochemical conversion/combustion of organic pollutants for waste water treatment. *Electrochimica Acta*, 39(11-12):1857–1862, 1994.

[197] Didier Gandini, Eric Mahé, Pierre Alain Michaud, Werner Haenni, André Perret, and Ch Comninellis. Oxidation of carboxylic acids at boron-doped diamond electrodes for wastewater treatment. *Journal of Applied Electrochemistry*, 30(12):1345–1350, 2000.

[198] Marta Wala and Wojciech Simka. Effect of anode material on electrochemical oxidation of low molecular weight alcohols—a review. *Molecules*, 26(8):2144, 2021.

[199] Carlos Alberto Martínez-Huitle and Marco Panizza. Electrochemical oxidation of organic pollutants for wastewater treatment. *Current Opinion in Electrochemistry*, 11:62–71, 2018.

[200] Marco Panizza and Giacomo Cerisola. Direct and mediated anodic oxidation of organic pollutants. *Chemical reviews*, 109(12):6541–6569, 2009.

[201] Nihal Oturan, Soliu O Ganiyu, Stephane Raffy, and Mehmet A Oturan. Substoichiometric titanium oxide as a new anode material for electro-fenton process: application to electrocatalytic destruction of antibiotic amoxicillin. *Applied Catalysis B: Environmental*, 217:214–223, 2017.

[202] Jing Qiao and Yuzhu Xiong. Electrochemical oxidation technology: A review of its application in high-efficiency treatment of wastewater containing persistent organic pollutants. *Journal of Water Process Engineering*, 44:102308, 2021.

[203] RE Palma-Goyes, J Vazquez-Arenas, RA Torres-Palma, C Ostos, F Ferraro, and I González. The abatement of indigo carmine using active chlorine electrogenerated on ternary sb2o5-doped ti/ruo2-zro2 anodes in a filter-press fm01-lc reactor. *Electrochimica Acta*, 174:735–744, 2015.

[204] Xiaoyue Duan, Cuimei Zhao, Wei Liu, Xuesong Zhao, and Limin Chang. Fabrication of a novel pbo2 electrode with a graphene nanosheet interlayer for electrochemical oxidation of 2-chlorophenol. *Electrochimica Acta*, 240:424–436, 2017.

[205] Juan Zuo, Junqiu Zhu, Mingzhou Zhang, Qiming Hong, Jie Han, and Jianfu Liu. Synergistic photoelectrochemical performance of la-doped ruo2-tio2/ti electrodes. *Applied Surface Science*, 502:144288, 2020.

[206] Weida Wang, Ke Wang, Wenting Hao, Tingting Zhang, Yijie Liu, Linghong Yu, and Weiping Li. Preparation of ti-based yb-doped sno2–ruo2 electrode and electrochemical oxidation treatment of coking wastewater. *Journal of Rare Earths*, 40(5):763–771, 2022.

[207] Chunhui Zhang, Jiawei Tang, Chen Peng, and Minying Jin. Degradation of perfluorinated compounds in wastewater treatment plant effluents by electrochemical oxidation with nano-zno coated electrodes. *Journal of Molecular Liquids*, 221:1145–1150, 2016.

[208] Shuaishuai Man, Hebin Bao, Haifeng Yang, Ke Xu, Anqi Li, Yuting Xie, Yan Jian, Wenjing Yang, Zhihong Mo, and Xueming Li. Preparation and characterization of nano-sic doped pbo2 electrode for degradation of toluene diamine. *Journal of Alloys and Compounds*, 859:157884, 2021.

[209] OI Kasian, TV Lukâ€™Yanenko, P Demchenko, RE Gladyshevskii, R Amadelli, and AB Velichenko. Electrochemical properties of thermally treated platinized ebonex® with low content of pt. *Electrochimica Acta*, 109:630–637, 2013.

[210] Ping Geng, Jingyang Su, Caroline Miles, Christos Comninellis, and Guohua Chen. Highly-ordered magnéli ti4o7 nanotube arrays as effective anodic material for electro-oxidation. *Electrochimica Acta*, 153:316–324, 2015.

[211] Tsutomu Ioroi and Kazuaki Yasuda. Highly reversal-tolerant anodes using ti4o7-supported platinum with a very small amount of water-splitting catalyst. *Journal of Power Sources*, 450:227656, 2020.

[212] Hui Lin, Junfeng Niu, Shangtao Liang, Chong Wang, Yujuan Wang, Fangyuan Jin, Qi Luo, and Qingguo Huang. Development of macroporous magnéli phase ti4o7 ceramic materials: As an efficient anode for mineralization of poly-and perfluoroalkyl substances. *Chemical Engineering Journal*, 354:1058–1067, 2018.

[213] Soliu O Ganiyu, Nihal Oturan, Stéphane Raffy, Giovanni Esposito, Eric D van Hullebusch, Marc Cretin, and Mehmet A Oturan. Use of substoichiometric titanium oxide as a ceramic electrode in anodic oxidation and electro-fenton degradation of the beta-blocker propranolol: degradation kinetics and mineralization pathway. *Electrochimica Acta*, 242:344–354, 2017.

[214] Soliu O Ganiyu, Nihal Oturan, Stéphane Raffy, Marc Cretin, Cristel Causserand, and Mehmet A Oturan. Efficiency of plasma elaborated substoichiometric titanium oxide (ti4o7) ceramic electrode for advanced elec-

trochemical degradation of paracetamol in different electrolyte media. *Separation and Purification Technology*, 208:142–152, 2019.

[215] Zhaohui Han, Yang Xu, Shenggang Zhou, and Peixian Zhu. Preparation and electrochemical properties of al-based composite coating electrode with ti4o7 ceramic interlayer for electrowinning of nonferrous metals. *Electrochimica Acta*, 325:134940, 2019.

[216] J Iniesta, PA Michaud, M Panizza, G Cerisola, A Aldaz, and Ch Comninellis. Electrochemical oxidation of phenol at boron-doped diamond electrode. *Electrochimica Acta*, 46(23):3573–3578, 2001.

[217] Angela Anglada, Ane Urtiaga, and Inmaculada Ortiz. Contributions of electrochemical oxidation to waste-water treatment: fundamentals and review of applications. *Journal of Chemical Technology & Biotechnology*, 84(12):1747–1755, 2009.

[218] Ch Venkata Reddy, Kakarla Raghava Reddy, VVN al Harish, Jaesool Shim, MV Shankar, Nagaraj P Shetti, and Tejraj M Aminabhavi. Metal-organic frameworks (mofs)-based efficient heterogeneous photocatalysts: synthesis, properties and its applications in photocatalytic hydrogen generation, co2 reduction and photodegradation of organic dyes. *International Journal of Hydrogen Energy*, 45(13):7656–7679, 2020.

[219] Ahmed M Elgarahy, Khalid Z Elwakeel, Abdullah Akhdhar, and Mohammed F Hamza. Recent advances in greenly synthesized nanoengineered materials for water/wastewater remediation: an overview. *Nanotechnology for Environmental Engineering*, 6(1):1–24, 2021.

[220] Xuedong Du, Mehmet A Oturan, Minghua Zhou, Nacer Belkessa, Pei Su, Jingju Cai, Clément Trellu, and Emmanuel Mousset. Nanostructured electrodes for electrocatalytic advanced oxidation processes: From materials preparation to mechanisms understanding and wastewater treatment applications. *Applied Catalysis B: Environmental*, 296:120332, 2021.

[221] P-A Michaud, Eric Mahé, Werner Haenni, André Perret, and Ch Comninellis. Preparation of peroxodisulfuric acid using boron-doped diamond thin film electrodes. *Electrochemical and Solid-state letters*, 3(2):77, 1999.

[222] K Serrano, PA Michaud, Ch Comninellis, and A Savall. Electrochemical preparation of peroxodisulfuric acid using boron doped diamond thin film electrodes. *Electrochimica Acta*, 48(4):431–436, 2002.

[223] Madhu Sudan Saha, Tsuneto Furuta, and Yoshinori Nishiki. Electrochemical synthesis of sodium peroxycarbonate at boron-doped diamond electrodes. *Electrochemical and solid-state letters*, 6(7):D5, 2003.

[224] Jianlong Wang and Shizong Wang. Activation of persulfate (ps) and peroxymonosulfate (pms) and application for the degradation of emerging contaminants. *Chemical Engineering Journal*, 334:1502–1517, 2018.

[225] Aliyeh Hasanzadeh, Alireza Khataee, Mahmoud Zarei, and Yifeng Zhang. Two-electron oxygen reduction on fullerene c60-carbon nanotubes covalent hybrid as a metal-free electrocatalyst. *Scientific reports*, 9(1):1–13, 2019.

[226] Zhihong Zhang, Hongshan Meng, Yujing Wang, Limin Shi, Xue Wang, and Shouning Chai. Fabrication of graphene@ graphite-based gas diffusion electrode for improving h2o2 generation in electro-fenton process. *Electrochimica Acta*, 260:112–120, 2018.

[227] Pei Su, Minghua Zhou, Xiaoye Lu, Weilu Yang, Gengbo Ren, and Jingju Cai. Electrochemical catalytic mechanism of n-doped graphene for enhanced h2o2 yield and in-situ degradation of organic pollutant. *Applied Catalysis B: Environmental*, 245:583–595, 2019.

[228] Wei Wang, Xiaoye Lu, Pei Su, Yawei Li, Jingju Cai, Qizhan Zhang, Minghua Zhou, and Omotayo Arotiba. Enhancement of hydrogen peroxide production by electrochemical reduction of oxygen on carbon nanotubes modified with fluorine. *Chemosphere*, 259:127423, 2020.

[229] Jussara F Carneiro, Robson S Rocha, Peter Hammer, R Bertazzoli, and MRV Lanza. Hydrogen peroxide electrogeneration in gas diffusion electrode nanostructured with ta2o5. *Applied Catalysis A: General*, 517:161–167, 2016.

[230] Jussara F Carneiro, Fernando L Silva, Alysson S Martins, Rafael MP Dias, Guilherme M Titato, Alvaro J Santos-Neto, Rodnei Bertazzoli, and Marcos RV Lanza. Simultaneous degradation of hexazinone and diuron using zro2-nanostructured gas diffusion electrode. *Chemical Engineering Journal*, 351:650–659, 2018.

[231] Edson C Paz, Luci R Aveiro, Victor S Pinheiro, Felipe M Souza, Verônica B Lima, Fernando L Silva, Peter Hammer, Marcos RV Lanza, and Mauro C Santos. Evaluation of h2o2 electrogeneration and decolorization of orange ii azo dye using tungsten oxide nanoparticle-modified carbon. *Applied Catalysis B: Environmental*, 232:436–445, 2018.

[232] Songhu Yuan, Na Gou, Akram N Alshawabkeh, and April Z Gu. Efficient degradation of contaminants of emerging concerns by a new electro-fenton process with ti/mmo cathode. *Chemosphere*, 93(11):2796–2804, 2013.

[233] Yingying He, Yali Ma, Jiang Meng, Xiaoyu Zhang, and Yuzhou Xia. Dual electrochemical catalysis of bi2mo3o12/ti cathode for hydrogen peroxide production in electro-fenton system. *Journal of catalysis*, 373:297–305, 2019.

[234] Ragupathy Pitchai, Velmurugan Thavasi, Subodh G Mhaisalkar, and Seeram Ramakrishna. Nanostructured cathode materials: a key for better performance in li-ion batteries. *Journal of Materials Chemistry*, 21(30):11040–11051, 2011.

[235] Chellakannu Rajkumar, Pitchaimani Veerakumar, Shen-Ming Chen, Balamurugan Thirumalraj, and King-Chuen Lin. Ultrathin sulfur-doped graphitic carbon nitride nanosheets as metal-free catalyst for electrochemical sensing and catalytic removal of 4-nitrophenol. *ACS Sustainable Chemistry & Engineering*, 6(12):16021–16031, 2018.

[236] Zizhen Li, Chensi Shen, Yanbiao Liu, Chunyan Ma, Fang Li, Bo Yang, Manhong Huang, Zhiwei Wang, Liming Dong, and Sand Wolfgang. Carbon nanotube filter functionalized with iron oxychloride for flow-through electro-fenton. *Applied Catalysis B: Environmental*, 260:118204, 2020.

[237] Gustavo dos Santos Cunha, Bianca Miguel de Souza-Chaves, Daniele Maia Bila, João Paulo Bassin, Chad David Vecitis, and Márcia Dezotti. Insights into estrogenic activity removal using carbon nanotube electrochemical filter. *Science of the Total Environment*, 678:448–456, 2019.

[238] Yu V Pleskov, MD Krotova, VV Elkin, VP Varnin, IG Teremetskaya, AV Saveliev, and VG Ralchenko. Benzene oxidation at diamond electrodes: Comparison of microcrystalline and nanocrystalline diamonds. *ChemPhysChem*, 13(12):3047–3052, 2012.

[239] Chad D Vecitis, Guandao Gao, and Han Liu. Electrochemical carbon nanotube filter for adsorption, desorption, and oxidation of aqueous dyes and anions. *The Journal of Physical Chemistry C*, 115(9):3621–3629, 2011.

[240] Jianglin Cao, Haiyan Zhao, Fahe Cao, Jianqing Zhang, and Chunan Cao. Electrocatalytic degradation of 4-chlorophenol on f-doped pbo2 anodes. *Electrochimica Acta*, 54(9):2595–2602, 2009.

[241] Guilherme Garcia Bessegato, Juliano Carvalho Cardoso, and Maria Valnice Boldrin Zanoni. Enhanced photoelectrocatalytic degradation of an acid dye with boron-doped tio2 nanotube anodes. *Catalysis Today*, 240:100–106, 2015.

[242] Yu Chen, Guojie Zhang, Juan Ma, Yiming Zhou, Yawen Tang, and Tianhong Lu. Electro-oxidation of methanol at the different carbon materials supported pt nano-particles. *international journal of hydrogen energy*, 35(19):10109–10117, 2010.

[243] Shu-Hong Li, Yue Zhao, Jian Chu, Wen-Wei Li, Han-Qing Yu, and Gang Liu. Electrochemical degradation of methyl orange on pt–bi/c nanostructured electrode by a square-wave potential method. *Electrochimica Acta*, 92:93–101, 2013.

[244] Dong Li, Xiaolei Guo, Haoran Song, Tianyi Sun, and Jiafeng Wan. Preparation of ruo2-tio2/nano-graphite composite anode for electrochemical degradation of ceftriaxone sodium. *Journal of hazardous materials*, 351:250–259, 2018.

[245] Xin Chang, Sapanbir S Thind, and Aicheng Chen. Electrocatalytic enhancement of salicylic acid oxidation at electrochemically reduced tio2 nanotubes. *ACS Catalysis*, 4(8):2616–2622, 2014.

[246] Choonsoo Kim, Seonghwan Kim, Jusol Choi, Jaehan Lee, Jin Soo Kang, Yung-Eun Sung, Jihwa Lee, Wonyong Choi, and Jeyong Yoon. Blue tio2 nanotube array as an oxidant generating novel anode material fabricated by simple cathodic polarization. *Electrochimica Acta*, 141:113–119, 2014.

[247] Jang-Hee Yoon, Yoon-Bo Shim, Byoung-seob Lee, Se-Yong Choi, and Mi-Sook Won. Electrochemical degradation of phenol and 2-chlorophenol using pt/ti and boron-doped diamond electrodes. *Bulletin of the Korean Chemical Society*, 33(7):2274–2278, 2012.

[248] Linlin Huang, Da Li, Junfeng Liu, Lisha Yang, Changchao Dai, Nanqi Ren, and Yujie Feng. Construction of tio2 nanotube clusters on ti mesh for immobilizing sb-sno2 to boost electrocatalytic phenol degradation. *Journal of Hazardous Materials*, 393:122329, 2020.

[249] Elisama Vieira Dos Santos, Shirley Feitosa Machado Sena, Djalma Ribeiro da Silva, Sergio Ferro, Achille De Battisti, and Carlos A Martínez-Huitle. Scale-up of electrochemical oxidation system for treatment of produced water generated by brazilian petrochemical industry. *Environmental Science and Pollution Research*, 21(14):8466–8475, 2014.

[250] Brian P Chaplin. The prospect of electrochemical technologies advancing worldwide water treatment. *Accounts of chemical research*, 52(3):596–604, 2019.

[251] Robert Stirling, W Shane Walker, Paul Westerhoff, and Sergi Garcia-Segura. Techno-economic analysis to identify key innovations required for electrochemical oxidation as point-of-use treatment systems. *Electrochimica Acta*, 338:135874, 2020.

[252] Marco Coha, Giulio Farinelli, Alberto Tiraferri, Marco Minella, and Davide Vione. Advanced oxidation processes in the removal of organic substances from produced water: Potential, configurations, and research needs. *Chemical Engineering Journal*, 414:128668, 2021.

[253] Soliu Oladejo Ganiyu, Shailesh Sable, and Mohamed Gamal El-Din. Advanced oxidation processes for the degradation of dissolved organics in produced water: A review of process performance, degradation kinetics and pathway. *Chemical Engineering Journal*, 429:132492, 2022.

[254] Enric Brillas, Ignasi Sirés, and Mehmet A Oturan. Electro-fenton process and related electrochemical technologies based on fentonâ€™s reaction chemistry. *Chemical reviews*, 109(12):6570–6631, 2009.

[255] PV Nidheesh and R Gandhimathi. Trends in electro-fenton process for water and wastewater treatment: an overview. *Desalination*, 299:1–15, 2012.

[256] Josué Daniel García-Espinoza, Irma Robles, Alfonso Durán-Moreno, and Luis A Godínez. Photo-assisted electrochemical advanced oxidation processes for the disinfection of aqueous solutions: A review. *Chemosphere*, page 129957, 2021.

[257] Abdul Hakeem Anwer, Mohammad Danish Khan, Mohammad Zain Khan, and Rajkumar Joshi. Microbial electrochemical cell: an emerging technology for waste water treatment and carbon sequestration. In *Modern Age Waste Water Problems*, pages 339–360. Springer, 2020.

[258] Jesús Alberto Pérez-García, Francisco Javier Bacame-Valenzuela, Arnold Palomares Hernández, Federico Castañeda-Zaldivar, Fabricio Espejel-Ayala, and Yolanda Reyes-Vidal. Microbial electrochemical technologies for wastewater treatment. In *The Future of Effluent Treatment Plants*, pages 287–306. Elsevier, 2021.

[259] Shaoan Cheng, Zhengzhong Mao, Yi Sun, Jiawei Yang, Zhen Yu, and Ruonan Gu. A novel electrochemical oxidation-methanogenesis system for simultaneously degrading antibiotics and reducing co2 to ch4 with low energy costs. *Science of The Total Environment*, 750:141732, 2021.

[260] Carlos A Ramírez-Vargas, Amanda Prado, Carlos A Arias, Pedro N Carvalho, Abraham Esteve-Núñez, and Hans Brix. Microbial electrochemical technologies for wastewater treatment: principles and evolution from microbial fuel cells to bioelectrochemical-based constructed wetlands. *Water*, 10(9):1128, 2018.

[261] Mehmet A Oturan and Jean-Jacques Aaron. Advanced oxidation processes in water/wastewater treatment: principles and applications. a review. *Critical Reviews in Environmental Science and Technology*, 44(23):2577–2641, 2014.

[262] Hao Peng and Jing Guo. Removal of chromium from wastewater by membrane filtration, chemical precipitation, ion exchange, adsorption electrocoagulation, electrochemical reduction, electrodialysis, electrodeionization, photocatalysis and nanotechnology: a review. *Environmental Chemistry Letters*, pages 1–14, 2020.

[263] Qi Yang, Fubing Yao, Yu Zhong, Dongbo Wang, Fei Chen, Jian Sun, Shan Hua, Sibei Li, Xiaoming Li, and Guangming Zeng. Catalytic and electrocatalytic reduction of perchlorate in water–a review. *Chemical Engineering Journal*, 306:1081–1091, 2016.

[264] Sergi Garcia-Segura, Mariana Lanzarini-Lopes, Kiril Hristovski, and Paul Westerhoff. Electrocatalytic reduction of nitrate: Fundamentals to full-scale water treatment applications. *Applied Catalysis B: Environmental*, 236:546–568, 2018.

[265] Chen Sun, Shams Ali Baig, Zimo Lou, Jin Zhu, Zhuoxing Wang, Xia Li, Jiahan Wu, Yifu Zhang, and Xinhua Xu. Electrocatalytic dechlorination of 2, 4-dichlorophenoxyacetic acid using nanosized titanium nitride doped palladium/nickel foam electrodes in aqueous solutions. *Applied Catalysis B: Environmental*, 158:38–47, 2014.

[266] Ran Mao, Xu Zhao, Huachun Lan, Huijuan Liu, and Jiuhui Qu. Graphene-modified pd/c cathode and pd/gac particles for enhanced electrocatalytic removal of bromate in a continuous three-dimensional electrochemical reactor. *Water research*, 77:1–12, 2015.

[267] Emmanuel Mousset, Marta Puce, and Marie-Noëlle Pons. Advanced electro-oxidation with boron-doped diamond for acetaminophen removal from real wastewater in a microfluidic reactor: Kinetics and mass-transfer studies. *ChemElectroChem*, 6(11):2908–2916, 2019.

[268] Ran Mao, Xu Zhao, Huachun Lan, Huijuan Liu, and Jiuhui Qu. Efficient electrochemical reduction of bromate by a pd/rgo/cfp electrode with low applied potentials. *Applied Catalysis B: Environmental*, 160:179–187, 2014.

[269] MR Gennero De Chialvo and AC Chialvo. Kinetics of hydrogen evolution reaction with frumkin adsorption: re-examination of the volmer–heyrovsky and volmer–tafel routes. *Electrochimica acta*, 44(5):841–851, 1998.

[270] Fubing Yao, Qi Yang, Jian Sun, Fei Chen, Yu Zhong, Huanyu Yin, Li He, Ziletao Tao, Zhoujie Pi, and Dongbo Wang. Electrochemical reduction of bromate using noble metal-free nanoscale zero-valent iron immobilized activated carbon fiber electrode. *Chemical Engineering Journal*, 389:123588, 2020.

[271] Chen Sun, Zimo Lou, Yu Liu, Ruiqi Fu, Xiaoxin Zhou, Zhen Zhang, Shams Ali Baig, and Xinhua Xu. Influence of environmental factors on the electrocatalytic dechlorination of 2,4-dichlorophenoxyacetic acid on ntin doped pd/ni foam electrode. *Chemical Engineering Journal*, 281:183–191, 2015.

[272] Michael S Wong, Pedro JJ Alvarez, Yu-lun Fang, Nurgül Akçin, Michael O Nutt, Jeffrey T Miller, and Kimberly N Heck. Cleaner water using bimetallic nanoparticle catalysts. *Journal of Chemical Technology & Biotechnology: International Research in Process, Environmental & Clean Technology*, 84(2):158–166, 2009.

[273] Michael O Nutt, Joseph B Hughes, and Michael S Wong. Designing pd-on-au bimetallic nanoparticle catalysts for trichloroethene hydrodechlorination. *Environmental science & technology*, 39(5):1346–1353, 2005.

[274] Huachun Lan, Ran Mao, Yating Tong, Yanzhen Liu, Huijuan Liu, Xiaoqiang An, and Ruiping Liu. Enhanced electroreductive removal of bromate by a supported pd–in bimetallic catalyst: kinetics and mechanism investigation. *Environmental Science & Technology*, 50(21):11872–11878, 2016.

[275] Zimo Lou, Jiasheng Zhou, Mei Sun, Jiang Xu, Kunlun Yang, Dan Lv, Yaping Zhao, and Xinhua Xu. MnO_2 enhances electrocatalytic hydrodechlorination by pd/ni foam electrodes and reduces pd needs. *Chemical Engineering Journal*, 352:549–557, 2018.

[276] Shuang Song, Qiuxiang Liu, Jinhui Fang, and Weiting Yu. Enhanced electrocatalytic dechlorination of 2,4-dichlorophenoxyacetic acid on in situ prepared pd-anchored $Ni(OH)_2$ bifunctional electrodes: synergistic effect between $H\cdot$ formation on $Ni(OH)_2$ and dechlorination steps on pd. *Catalysis Science & Technology*, 9(18):5130–5141, 2019.

[277] Armando Gennaro, Abdirisak A Isse, Claudia L Bianchi, Patrizia R Mussini, and Manuela Rossi. Is glassy carbon a really inert electrode material for the reduction of carbon–halogen bonds? *Electrochemistry communications*, 11(10):1932–1935, 2009.

[278] Ya Zhang, Shaolin Mu, Baolin Deng, and Jianzhong Zheng. Electrochemical removal and release of perchlorate using poly (aniline-co-o-aminophenol). *Journal of Electroanalytical Chemistry*, 641(1-2):1–6, 2010.

[279] Liang Ding, Qin Li, Hao Cui, Rong Tang, Hui Xu, Xianchuan Xie, and Jianping Zhai. Electrocatalytic reduction of bromate ion using a polyaniline-modified electrode: An efficient and green technology for the removal of BrO_3^- in aqueous solutions. *Electrochimica acta*, 55(28):8471–8475, 2010.

[280] C Bellomunno, D Bonanomi, L Falciola, M Longhi, PR Mussini, LM Doubova, and G Di Silvestro. Building up an electrocatalytic activity scale of cathode materials for organic halide reductions. *Electrochimica acta*, 50(11):2331–2341, 2005.

[281] Christoph Gütz, Markus Bänziger, Christoph Bucher, Tomás R Galvão, and Siegfried R Waldvogel. Development and scale-up of the electrochemical dehalogenation for the synthesis of a key intermediate for ns5a inhibitors. *Organic Process Research & Development*, 19(10):1428–1433, 2015.

[282] Sabine Möhle, Michael Zirbes, Eduardo Rodrigo, Tile Gieshoff, Anton Wiebe, and Siegfried R Waldvogel. Modern electrochemical aspects for the synthesis of value-added organic products. *Angewandte Chemie International Edition*, 57(21):6018–6041, 2018.

[283] Eilen A Vik, Dale A Carlson, Arild S Eikum, and Egil T Gjessing. Electrocoagulation of potable water. *Water research*, 18(11):1355–1360, 1984.

[284] P. K. Holt, G. W. Barton, and C. A. Mitchell. The future for electrocoagulation as a localised water treatment technology. *Chemosphere*, 59(3):355–367, 2005.

[285] Irena Ljubomir Mickova. Advanced electrochemical technologies in wastewater treatment part i: electrocoagulation. *American Scientific Research Journal for Engineering, Technology, and Sciences (ASRJETS)*, 14(2):233–257, 2015.

[286] Irena Ljubomir Mickova. Advanced electrochemical technologies in wastewater treatment. part ii: Electro-flocculation and electro-flotation. *American Scientific Research Journal for Engineering, Technology, and Sciences (ASRJETS)*, 14(2):273–294, 2015.

[287] PV Nidheesh, Abhijeet Kumar, D Syam Babu, Jaimy Scaria, and M Suresh Kumar. Treatment of mixed industrial wastewater by electrocoagulation and indirect electrochemical oxidation. *Chemosphere*, 251:126437, 2020.

[288] Albert E Dieterich. Electric water-purifier., June 19 1906. US Patent 823,671.

[289] Hector A Moreno C, David L Cocke, Jewel AG Gomes, Paul Morkovsky, JR Parga, Eric Peterson, and Cristina Garcia. Electrochemical reactions for electrocoagulation using iron electrodes. *Industrial & Engineering Chemistry Research*, 48(4):2275–2282, 2009.

[290] P. Canizares, M. Carmona, J. Lobato, F. Martinez, and M. A. Rodrigo. Electrodissolution of aluminum electrodes in electrocoagulation processes. *Industrial & Engineering Chemistry Research*, 44(12):4178–4185, 2005.

[291] E. Ofir, Y. Oren, and A. Adin. Electroflocculation: the effect of zeta-potential on particle size. *Desalination*, 204(1-3):33–38, 2007.

[292] Siva RS Bandaru, Case M van Genuchten, Arkadeep Kumar, Sara Glade, Dana Hernandez, Mohit Nahata, and Ashok Gadgil. Rapid and efficient arsenic removal by iron electrocoagulation enabled with in situ generation of hydrogen peroxide. *Environmental science & technology*, 54(10):6094–6103, 2020.

[293] AK Darban, A Shahedi, F Taghipour, and A Jamshidi-Zanjani. A review on industrial wastewater treatment via electrocoagulation processes. *Current Opinion in Electrochemistry*, 2:154–169, 2020.

[294] AY Bagastyo. Electrocoagulation for drinking water treatment: a review. In *IOP Conference Series: Earth and Environmental Science*, volume 623, page 012016. IOP Publishing, 2021.

[295] Amina Tahreen, Mohammed Saedi Jami, and Fathilah Ali. Role of electrocoagulation in wastewater treatment: A developmental review. *Journal of Water Process Engineering*, 37:101440, 2020.

[296] S. Mahesh, B. Prasad, I. D. Mall, and I. M. Mishra. Electrochemical degradation of pulp and paper mill wastewater. part 1. cod and color removal. *Industrial & Engineering Chemistry Research*, 45(8):2830–2839, 2006.

[297] I. Heidmann and W. Calmano. Removal of zn(ii), cu(ii), ni(ii), ag(i) and cr(vi) present in aqueous solutions by aluminium electrocoagulation. *Journal of Hazardous Materials*, 152(3):934–941, 2008.

[298] B. Merzouk, B. Gourich, A. Sekki, K. Madani, and M. Chibane. Removal turbidity and separation of heavy metals using electrocoagulation-electroflotation technique a case study. *Journal of Hazardous Materials*, 164(1):215–222, 2009.

[299] I. Zongo, J. P. Leclerc, H. A. Maiga, J. Wethe, and F. Lapicque. Removal of hexavalent chromium from industrial wastewater by electrocoagulation: A comprehensive comparison of aluminium and iron electrodes. *Separation and Purification Technology*, 66(1):159–166, 2009.

[300] F. Shen, X. M. Chen, P. Gao, and G. H. Chen. Electrochemical removal of fluoride ions from industrial wastewater. *Chemical Engineering Science*, 58(3-6):987–993, 2003.

[301] Tugba Ölmez. The optimization of cr (vi) reduction and removal by electrocoagulation using response surface methodology. *Journal of Hazardous Materials*, 162(2-3):1371–1378, 2009.

[302] Maria A Mamelkina, Salvador Cotillas, Engracia Lacasa, Cristina Sáez, Ritva Tuunila, Mika Sillanpää, Antti Häkkinen, and Manuel A Rodrigo. Removal of sulfate from mining waters by electrocoagulation. *Separation and Purification Technology*, 182:87–93, 2017.

[303] Chih-Ta Wang, Wei-Lung Chou, and Yi-Ming Kuo. Removal of cod from laundry wastewater by electrocoagulation/electroflotation. *Journal of hazardous materials*, 164(1):81–86, 2009.

[304] Chantaraporn Phalakornkule, Pisut Sukkasem, and Chinnarat Mutchimsattha. Hydrogen recovery from the electrocoagulation treatment of dye-containing wastewater. *International Journal of Hydrogen Energy*, 35(20):10934–10943, 2010.

[305] O. T. Can, M. Bayramoglu, and M. Kobya. Decolorization of reactive dye solutions by electrocoagulation using aluminum electrodes. *Industrial & Engineering Chemistry Research*, 42(14):3391–3396, 2003.

[306] Markus Ingelsson, Nael Yasri, and Edward PL Roberts. Electrode passivation, faradaic efficiency, and performance enhancement strategies in electrocoagulation—a review. *Water Research*, page 116433, 2020.

[307] Sergi Garcia-Segura, Maria Maesia SG Eiband, Jailson Vieira de Melo, and Carlos Alberto Martínez-Huitle. Electrocoagulation and advanced electrocoagulation processes: A general review about the fundamentals, emerging applications and its association with other technologies. *Journal of Electroanalytical Chemistry*, 801:267–299, 2017.

[308] Jean Nepo Hakizimana, Bouchaib Gourich, Mohammed Chafi, Youssef Stiriba, Christophe Vial, Patrick Drogui, and Jamal Naja. Electrocoagulation process in water treatment: A review of electrocoagulation modeling approaches. *Desalination*, 404:1–21, 2017.

[309] X. M. Chen, G. H. Chen, and P. L. Yue. Novel electrode system for electroflotation of wastewater. *Environmental Science & Technology*, 36(4):778–783, 2002.

[310] J. T. Ge, J. H. Qu, P. J. Lei, and H. J. Liu. New bipolar electrocoagulation-electroflotation process for the treatment of laundry wastewater. *Separation and Purification Technology*, 36(1):33–39, 2004.

[311] M. Y. A. Mollah, P. Morkovsky, J. A. G. Gomes, M. Kesmez, J. Parga, and D. L. Cocke. Fundamentals, present and future perspectives of electrocoagulation. *Journal of Hazardous Materials*, 114(1-3):199–210, 2004.

[312] VA Kolesnikov, VI Ilâ€™in, and AV Kolesnikov. Electroflotation in wastewater treatment from oil products, dyes, surfactants, ligands, and biological pollutants: a review. *Theoretical Foundations of Chemical Engineering*, 53(2):251–273, 2019.

[313] Alexander Stanley Elmore. Apparatus for concentrating ores., September 3 1907. US Patent 865,334.

[314] NK Khosla, S Venkatachalam, and P Somasundaran. Pulsed electrogeneration of bubbles for electroflotation. *Journal of Applied Electrochemistry*, 21(11):986–990, 1991.

[315] Mohammad M Emamjomeh and Muttucumaru Sivakumar. Review of pollutants removed by electrocoagulation and electrocoagulation/flotation processes. *Journal of environmental management*, 90(5):1663–1679, 2009.

[316] KA Matis and EN Peleka. Alternative flotation techniques for wastewater treatment: focus on electroflotation. *Separation Science and Technology*, 45(16):2465–2474, 2010.

[317] Reza Mohtashami and Julie Q Shang. Electroflotation for treatment of industrial wastewaters: A focused review. *Environmental Processes*, 6(2):325–353, 2019.

[318] Efrosyni N Peleka, George P Gallios, and Kostas A Matis. A perspective on flotation: a review. *Journal of Chemical Technology & Biotechnology*, 93(3):615–623, 2018.

[319] Bogale Tadesse, Boris Albijanic, Fidele Makuei, and Richard Browner. Recovery of fine and ultrafine mineral particles by electroflotation–a review. *Mineral Processing and Extractive Metallurgy Review*, 40(2):108–122, 2019.

[320] A. Agrawal, S. Kumari, and K. K. Sahu. Iron and copper recovery/removal from industrial wastes: A review. *Industrial & Engineering Chemistry Research*, 48(13):6145–6161, 2009.

[321] S. Vasudevan and M. A. Oturan. Electrochemistry: as cause and cure in water pollution-an overview. *Environmental Chemistry Letters*, 12(1):97–108, 2014.

[322] Mohammad Rahimi, Zachary Schoener, Xiuping Zhu, Fang Zhang, Christopher A Gorski, and Bruce E Logan. Removal of copper from water using a thermally regenerative electrodeposition battery. *Journal of hazardous materials*, 322:551–556, 2017.

[323] Changsheng Peng, Yanyan Liu, Jingjing Bi, Huizhen Xu, and Abou-Shady Ahmed. Recovery of copper and water from copper-electroplating wastewater by the combination process of electrolysis and electrodialysis. *Journal of hazardous materials*, 189(3):814–820, 2011.

[324] Yuri F Guimaraes, Iranildes D Santos, and Achilles JB Dutra. Direct recovery of copper from printed circuit boards (pcbs) powder concentrate by a simultaneous electroleaching–electrodeposition process. *Hydrometallurgy*, 149:63–70, 2014.

[325] A. Janin, F. Zaviska, P. Drogui, J. F. Blais, and G. Mercier. Selective recovery of metals in leachate from chromated copper arsenate treated wastes using electrochemical technology and chemical precipitation. *Hydrometallurgy*, 96(4):318–326, 2009.

[326] M. L. K. Sulonen, M. E. Kokko, A. M. Lakaniemi, and J. A. Puhakka. Simultaneous removal of tetrathionate and copper from simulated acidic mining water in bioelectrochemical and electrochemical systems. *Hydrometallurgy*, 176:129–138, 2018.

[327] Georgios N Anastassakis, Paolo Bevilacqua, and Lorenzo De Lorenzi. Recovery of residual copper from low-content tailings derived from waste electrical cable treatment. *International Journal of Mineral Processing*, 143:105–111, 2015.

[328] S Müller, F Holzer, and O Haas. Optimized zinc electrode for the rechargeable zinc–air battery. *Journal of applied electrochemistry*, 28(9):895–898, 1998.

[329] Qinzhi Lai, Huamin Zhang, Xianfeng Li, Liqun Zhang, and Yuanhui Cheng. A novel single flow zinc–bromine battery with improved energy density. *Journal of Power Sources*, 235:1–4, 2013.

[330] Ke Gong, Xiaoya Ma, Kameron M Conforti, Kevin J Kuttler, Jonathan B Grunewald, Kelsey L Yeager, Martin Z Bazant, Shuang Gu, and Yushan Yan. A zinc–iron redox-flow battery under $100 per kw h of system capital cost. *Energy & Environmental Science*, 8(10):2941–2945, 2015.

[331] Birger Horstmann, Timo Danner, and Wolfgang G Bessler. Precipitation in aqueous lithium–oxygen batteries: a model-based analysis. *Energy & Environmental Science*, 6(4):1299–1314, 2013.

[332] D Gilroy and BE Conway. Kinetic theory of inhibition and passivation in electrochemical reactions. *The Journal of Physical Chemistry*, 69(4):1259–1267, 1965.

[333] J Lyklema and M Minor. On surface conduction and its role in electrokinetics. *Colloids and Surfaces A: Physicochemical and Engineering Aspects*, 140(1-3):33–41, 1998.

[334] Johannes Lyklema. *Fundamentals of interface and colloid science: soft colloids*, volume 5. Elsevier, 2005.

[335] Jacob N Israelachvili. *Intermolecular and surface forces*. Academic press, 2015.

[336] MT Ricart, M Pazos, S Gouveia, C Cameselle, and MA Sanroman. Removal of organic pollutants and heavy metals in soils by electrokinetic remediation. *Journal of Environmental Science and Health Part A*, 43(8):871–875, 2008.

[337] Alexandra B Ribeiro, Eduardo P Mateus, and José-Miguel Rodríguez-Maroto. Removal of organic contaminants from soils by an electrokinetic process: the case of molinate and bentazone. experimental and modeling. *Separation and Purification Technology*, 79(2):193–203, 2011.

[338] L Handojo, AK Wardani, D Regina, C Bella, MTAP Kresnowati, and IG Wenten. Electro-membrane processes for organic acid recovery. *RSC advances*, 9(14):7854–7869, 2019.

[339] Dongdong Wen, Rongbing Fu, and Qian Li. Removal of inorganic contaminants in soil by electrokinetic remediation technologies: A review. *Journal of Hazardous Materials*, 401:123345, 2021.

[340] Heiner Strathmann. *Ion-exchange membrane separation processes*. Elsevier, 2004.

[341] R. Probstein. *Physicochemical Hydrodynamics: An Introduction*. John Wiley & Sons, New York, 1994.

[342] F. Hellferich. *Ion Exchange*. McGraw-Hill, New York, 1962.

[343] S.-T. Hwang and K. Kammermeyer. *Membranes in Separation*. Wiley, New York, 1975.

[344] V.V. Nikonenko, A.B. Yaroslavtsev, and G. Pourcelly. *Ion transfer in and through charged membranes*. John Wiley & Sons Inc, 2012.

[345] Qing-Bai Chen, Jianyou Wang, Yu Liu, Jinli Zhao, and Pengfei Li. Novel energy-efficient electrodialysis system for continuous brackish water desalination: Innovative stack configurations and optimal inflow modes. *Water Research*, page 115847, 2020.

[346] Mayur R Ladole, Sujata S Patil, Pavan M Paraskar, Pravin B Pokale, and Pravin D Patil. Desalination using electrodialysis. In *Sustainable Materials and Systems for Water Desalination*, pages 15–38. Springer, 2021.

[347] Tongwen Xu. Ion exchange membranes: State of their development and perspective. *Journal of membrane science*, 263(1-2):1–29, 2005.

[348] Tao Luo, Said Abdu, and Matthias Wessling. Selectivity of ion exchange membranes: A review. *Journal of membrane science*, 555:429–454, 2018.

[349] A.A. Sonin and R.F. Probstein. A hydrodynamic theory of desalination by electrodialysis. *Desalination*, 5:293–329, 1968.

[350] Younggy Kim, W Shane Walker, and Desmond F Lawler. Competitive separation of di-vs. mono-valent cations in electrodialysis: Effects of the boundary layer properties. *water research*, 46(7):2042–2056, 2012.

[351] W.M. Deen. *Analysis of Transport Phenomena*. Oxford University Press, Oxford, 2 edition, 2012.

[352] S Geissler, H Heits, and U Werner. Description of fluid flow through spacers in flat-channel filtration systems. *Filtration & separation*, 32(6):538–544, 1995.

[353] J Balster, DF Stamatialis, and Matthias Wessling. Membrane with integrated spacer. *Journal of membrane science*, 360(1-2):185–189, 2010.

[354] Stanislav Samuilovich Dukhin and Boris Vladimirovich Deri̯agin. *Electrokinetic phenomena*. 1974.

[355] Stanislav S Dukhin. Electrokinetic phenomena of the second kind and their applications. *Advances in colloid and interface science*, 35:173–196, 1991.

[356] Andriy Yaroshchuk. What makes a nano-channel? a limiting-current criterion. *Microfluidics and nanofluidics*, 12(1-4):615–624, 2012.

[357] Kamel-Eddine Bouhidel and Salah Benslimane. Ion exchange membrane modification by weak electrolytes and glycine: reduction and elimination of the concentration polarization plateau in electrodialysis. *Desalination*, 199(1-3):67–69, 2006.

[358] A.M. Peers. Disc faraday soc 21, 1956.

[359] NW Rosenberg and CE Tirrell. Limiting currents in membrane cells. *Industrial & Engineering Chemistry*, 49(4):780–784, 1957.

[360] R Byron Bird, Warren E Stewart, Edwin N Lightfoot, and Daniel J Klingenberg. *Introductory transport phenomena*, volume 1. Wiley New York, 2015.

[361] S.A. Mareev, DYu Butylskii, A.V. Kovalenko, A.V. Petukhova, N.D. Pismenskaya, L. Dammak, C. Larchet, and V.V. Nikonenko. Accounting for the concentration dependence of electrolyte diffusion coefficient in the sand and the peers equations. *Electrochimica Acta*, 195:85–93, 2016.

[362] M.A. LÃ©vÃªque. Les lois de la transmission de chaleur par convection, 1928. Doctoral Dissertation.

[363] Pijush K Kundu and Ira M Cohen. *Fluid mechanics*. Elsevier, 2001.

[364] William A Braff, Cullen R Buie, and Martin Z Bazant. Boundary layer analysis of membraneless electrochemical cells. *Journal of The Electrochemical Society*, 160(11):A2056–A2063, 2013.

[365] Donald A Cowan and Jerry H Brown. Effect of turbulence on limiting current in electrodialysis cells. *Industrial & Engineering Chemistry*, 51(12):1445–1448, 1959.

[366] Georges Belfort and Gerald A Guter. An experimental study of electrodialysis hydrodynamics. *Desalination*, 10(3):221–262, 1972.

[367] Georges Belfort and GA Guter. An electrical analogue for electrodialysis. *Desalination*, 5(3):267–291, 1968.

[368] I. Atlas, J. Wu, A. N. Shocron, and M. E. Suss. Spatial variations of pH in electrodialysis stacks: Theory. *Electrochimica Acta*, 413:140151, may 2022.

[369] T.M. Mubita, S. Porada, P.M. Biesheuvel, A. van der Wal, and J.E. Dykstra. Strategies to increase ion selectivity in electrodialysis. *Separation and Purification Technology*, 292:120944, mar 2022.

[370] Victor V Nikonenko, Anna V Kovalenko, Mahamet K Urtenov, Natalia D Pismenskaya, Jongyoon Han, Philippe Sistat, and Gérald Pourcelly. Desalination at overlimiting currents: State-of-the-art and perspectives. *Desalination*, 342:85–106, 2014.

[371] V.V. Nikonenko, N.D. Pismenskaya, E.I. Belova, P.Huguet Ph. Sistat, G. Pourcelly, and C. Larchet. Intensive current transfer in membrane systems: Modelling, mechanisms and application in electrodialysis. *Advances in Colloid and Interface Science*, 160(1):101–123, 2010.

[372] John Westall and Herbert Hohl. A comparison of electrostatic models for the oxide/solution interface. *Advances in Colloid and Interface Science*, 12(4):265–294, 1980.

[373] KG Marinova, RG Alargova, ND Denkov, OD Velev, DN Petsev, IB Ivanov, and RP Borwankar. Charging of oil- water interfaces due to spontaneous adsorption of hydroxyl ions. *Langmuir*, 12(8):2045–2051, 1996.

[374] Sven H Behrens and David G Grier. The charge of glass and silica surfaces. *The Journal of Chemical Physics*, 115(14):6716–6721, 2001.

[375] Rikkert J Nap, Anže Lošdorfer Božič, Igal Szleifer, and Rudolf Podgornik. The role of solution conditions in the bacteriophage pp7 capsid charge regulation. *Biophysical journal*, 107(8):1970–1979, 2014.

[376] Cyrus R Safinya and Joachim Radler. *Handbook of Lipid Membranes: Molecular, Functional, and Materials Aspects*. CRC Press, 2018.

[377] Gregor Trefalt, Sven Holger Behrens, and Michal Borkovec. Charge regulation in the electrical double layer: ion adsorption and surface interactions. *Langmuir*, 32(2):380–400, 2016.

[378] Huanhuan Tian and Moran Wang. Electrokinetic mechanism of wettability alternation at oil-water-rock interface. *Surface Science Reports*, 72(6):369–391, 2017.

[379] Yu I Kharkats and AV Sokirko. Theory of the effect of migration current exaltation taking into account dissociation-recombination reactions. *Journal of electroanalytical chemistry and interfacial electrochemistry*, 303(1-2):27–44, 1991.

[380] M.B. Andersen, M. Soestbergen, A. Mani, H. Bruus, P.M. Biesheuvel, and M.Z. Bazant. Current-induced membrane discharge. *Phys. Rev. Lett*, 109:108301, 2012.

[381] I. Rubinstein and B. Zaltzman. Equilibrium electroconvective instability. *Phys. Rev. Lett*, 114:114502, 2015.

[382] Isaak Rubinstein and Boris Zaltzman. Extended space charge in concentration polarization. *Advances in colloid and interface science*, 159(2):117–129, 2010.

[383] B. Zaltzman and I. Rubinstein. Electro-osmotic slip and electroconvective instability. *J. Fluid Mech*, 579:173–226, 2007.

[384] S.M. Rubinstein, G. Manukyan, A. Staicu, I. Rubinstein, B. Zaltzman, R.G.H. Lammertink, F. Mugele, and M. Wessling. Direct observation of a nonequilibrium electro-osmotic instability. *Phys. Rev. Lett*, 101:236101, 2008.

[385] G. Yossifon and H.-C. Chang. Selection of nonequilibrium overlimiting currents: universal depletion layer formation dynamics and vortex instability. *Phys. Rev. Lett*, 101:254501, 2008.

[386] S.V. Pham, Z. Li, K.M. Lim, J.K. White, and J. Han. Direct numerical simulation of electroconvective instability and hysteretic current-voltage response of permselective membrane. *Phys. Rev. E*, 86:046310, 2012.

[387] R. Kwak, V.S. Pham, K.M. Lim, and J. Han. Shear flow of an electrically charged fluid by ion concentration polarization: scaling laws for convection vortices. *Phys. Rev. Lett*, 110:114501, 2013.

[388] Hsueh-Chia Chang, Gilad Yossifon, and Evgeny A Demekhin. Nanoscale electrokinetics and microvortices: How microhydrodynamics affects nanofluidic ion flux. *Annual review of fluid mechanics*, 44:401–426, 2012.

[389] Scott M Davidson, Matthias Wessling, and Ali Mani. On the dynamical regimes of pattern-accelerated electroconvection. *Scientific reports*, 6(1):22505, 2016.

[390] Bingrui Xu, Zhibo Gu, Wei Liu, Peng Huo, Yueting Zhou, SM Rubinstein, MZ Bazant, B Zaltzman, I Rubinstein, and Daosheng Deng. Electro-osmotic instability of concentration enrichment in curved geometries for an aqueous electrolyte. *Physical Review Fluids*, 5(9):091701, 2020.

[391] M Wessling, L Garrigós Morcillo, and S Abdu. Nanometer-thick lateral polyelectrolyte micropatterns induce macrosopic electro-osmotic chaotic fluid instabilities. *Scientific reports*, 4:4294, 2014.

[392] Florian Roghmans, Elizaveta Evdochenko, Felix Stockmeier, Sven Schneider, Amel Smailji, Rahul Tiwari, Annabel Mikosch, Elif Karatay, Alexander Kühne, and Andreas Walther. 2d patterned ion-exchange membranes induce electroconvection. *Advanced Materials Interfaces*, 6(1):1801309, 2019.

[393] Svetlana Zyryanova, Semyon Mareev, Violetta Gil, Elizaveta Korzhova, Natalia Pismenskaya, Veronika Sarapulova, Olesya Rybalkina, Evgeniy Boyko, Christian Larchet, and Lasaad Dammak. How electrical heterogeneity parameters of ion-exchange membrane surface affect the mass transfer and

water splitting rate in electrodialysis. *International journal of molecular sciences*, 21(3):973, 2020.

[394] Dmitrii Butylskii, Ilya Moroz, Kseniya Tsygurina, and Semyon Mareev. Effect of surface inhomogeneity of ion-exchange membranes on the mass transfer efficiency in pulsed electric field modes. *Membranes*, 10(3):40, 2020.

[395] NA Mishchuk. Perspectives of the electrodialysis intensification. *Desalination*, 117(1-3):283–295, 1998.

[396] NA Mishchuk, LK Koopal, and F Gonzalez-Caballero. Intensification of electrodialysis by applying a non-stationary electric field. *Colloids and Surfaces A: Physicochemical and Engineering Aspects*, 176(2-3):195–212, 2001.

[397] Noémie Lemay, Sergey Mikhaylin, and Laurent Bazinet. Voltage spike and electroconvective vortices generation during electrodialysis under pulsed electric field: Impact on demineralization process efficiency and energy consumption. *Innovative food science & emerging technologies*, 52:221–231, 2019.

[398] Noémie Lemay, Sergey Mikhaylin, Semen Mareev, Natalia Pismenskaya, Victor Nikonenko, and Laurent Bazinet. How demineralization duration by electrodialysis under high frequency pulsed electric field can be the same as in continuous current condition and that for better performances? *Journal of Membrane Science*, page 117878, 2020.

[399] Alvaro Gonzalez-Vogel and Orlando J Rojas. Exploiting electroconvective vortices in electrodialysis with high-frequency asymmetric bipolar pulses for desalination in overlimiting current regimes. *Desalination*, 474:114190, 2020.

[400] J.M. Huth, H.L. Swinney, W.D. Mccormick, A. Kuhn, and F. Argoul. *Phys Rev E*, 51:3444–3458, 1995.

[401] Peng Bai, Ju Li, Fikile R Brushett, and Martin Z Bazant. Transition of lithium growth mechanisms in liquid electrolytes. *Energy & Environmental Science*, 9(10):3221–3229, 2016.

[402] Yubin He, Liang Ge, ZiJuan Ge, Zhang Zhao, Fangmeng Sheng, Xiaohe Liu, Xiaolin Ge, Zhengjin Yang, Rongqiang Fu, and Zhaomin Liu. Monovalent cations permselective membranes with zwitterionic side chains. *Journal of membrane science*, 563:320–325, 2018.

[403] Anusha Chandra, E Bhuvanesh, Priyabrata Mandal, and Sujay Chattopadhyay. Surface modification of anion exchange membrane using layer-by-layer polyelectrolytes deposition facilitating monovalent organic acid transport. *Colloids and Surfaces A: Physicochemical and Engineering Aspects*, 558:579–590, 2018.

[404] Ivan Merino-Garcia, Francis Kotoka, Carla AM Portugal, João G Crespo, and Svetlozar Velizarov. Characterization of poly (acrylic) acid-modified heterogenous anion exchange membranes with improved monovalent permselectivity for red. *Membranes*, 10(6):134, 2020.

[405] Yvana D Ahdab, Danyal Rehman, and John H Lienhard. Brackish water desalination for greenhouses: Improving groundwater quality for irrigation using monovalent selective electrodialysis reversal. *Journal of Membrane Science*, 610:118072, 2020.

[406] Yvana D Ahdab, Danyal Rehman, Georg Schücking, Maria Barbosa, and John H Lienhard. Treating irrigation water using high-performance membranes for monovalent selective electrodialysis. *ACS ES&T Water*, 1(1):117–124, 2020.

[407] Hailong Tian, Ying Wang, Yuansheng Pei, and John C Crittenden. Unique applications and improvements of reverse electrodialysis: A review and outlook. *Applied Energy*, 262:114482, 2020.

[408] Lin Liu and Qing Cheng. Mass transfer characteristic research on electrodialysis for desalination and regeneration of solution: A comprehensive review. *Renewable and Sustainable Energy Reviews*, 134:110115, 2020.

[409] IG Wenten, K Khoiruddin, Anita K Wardani, and IN Widiasa. Synthetic polymer-based membranes for heavy metal removal. In *Synthetic Polymeric Membranes for Advanced Water Treatment, Gas Separation, and Energy Sustainability*, pages 71–101. Elsevier, 2020.

[410] D Ariono and IG Wenten. Heterogeneous structure and its effect on properties and electrochemical behavior of ion-exchange membrane. *Materials Research Express*, 4(2):024006, 2017.

[411] MA Andreeva, VV Gil, ND Pismenskaya, VV Nikonenko, L Dammak, C Larchet, D Grande, and NA Kononenko. Effect of homogenization and hydrophobization of a cation-exchange membrane surface on its scaling in the presence of calcium and magnesium chlorides during electrodialysis. *Journal of Membrane Science*, 540:183–191, 2017.

[412] SM Hosseini, N Rafiei, A Salabat, and A Ahmadi. Fabrication of new type of barium ferrite/copper oxide composite nanoparticles blended polyvinylchloride based heterogeneous ion exchange membrane. *Arabian Journal of Chemistry*, 13(1):2470–2482, 2020.

[413] SA Mareev, D Yu Butylskii, ND Pismenskaya, C Larchet, L Dammak, and VV Nikonenko. Geometric heterogeneity of homogeneous ion-exchange neosepta membranes. *Journal of membrane science*, 563:768–776, 2018.

[414] V Vasil'eva, E Goleva, N Pismenskaya, A Kozmai, and V Nikonenko. Effect of surface profiling of a cation-exchange membrane on the phenylalanine and nacl separation performances in diffusion dialysis. *Separation and Purification Technology*, 210:48–59, 2019.

[415] Tomáš Belloň and Zdeněk Slouka. Overlimiting behavior of surface-modified heterogeneous anion-exchange membranes. *Journal of Membrane Science*, page 118291, 2020.

[416] Violetta Gil, Mikhail Porozhnyy, Olesya Rybalkina, Dmitrii Butylskii, and Natalia Pismenskaya. The development of electroconvection at the surface of a heterogeneous cation-exchange membrane modified with perfluorosulfonic acid polymer film containing titanium oxide. *Membranes*, 10(6):125, 2020.

[417] EM Akberova and VI Vasil'eva. Effect of the resin content in cation-exchange membranes on development of electroconvection. *Electrochemistry Communications*, 111:106659, 2020.

[418] Sajjad Al-Amshawee, Mohd Yusri Bin Mohd Yunus, Abdul Aziz Mohd Azoddein, David Geraint Hassell, Ihsan Habib Dakhil, and Hassimi Abu Hasan. Electrodialysis desalination for water and wastewater: A review. *Chemical Engineering Journal*, 380:122231, 2020.

[419] Sergey Mikhaylin and Laurent Bazinet. Fouling on ion-exchange membranes: Classification, characterization and strategies of prevention and control. *Advances in colloid and interface science*, 229:34–56, 2016.

[420] MACK Hansima, Madhubhashini Makehelwala, KBSN Jinadasa, Yuansong Wei, KGN Nanayakkara, Ajith C Herath, and Rohan Weerasooriya. Fouling of ion exchange membranes used in the electrodialysis reversal advanced water treatment: A review. *Chemosphere*, page 127951, 2020.

[421] Xin Tong, Bopeng Zhang, and Yongsheng Chen. Fouling resistant nanocomposite cation exchange membrane with enhanced power generation for reverse electrodialysis. *Journal of Membrane Science*, 516:162–171, 2016.

[422] Yujiao Li, Shaoyuan Shi, Hongbin Cao, Zhijuan Zhao, Chunlei Su, and Hao Wen. Improvement of the antifouling performance and stability of an anion exchange membrane by surface modification with graphene oxide (go) and polydopamine (pda). *Journal of Membrane Science*, 566:44–53, 2018.

[423] Yuanwei Liu, Shanshan Yang, Yu Chen, Junbin Liao, Jiefeng Pan, Arcadio Sotto, and Jiangnan Shen. Preparation of water-based anion-exchange membrane from pva for anti-fouling in the electrodialysis process. *Journal of Membrane Science*, 570:130–138, 2019.

[424] Myriam Bdiri, Christian Larchet, and Lasâad Dammak. A review on ion-exchange membranes fouling and antifouling during electrodialysis used in food industry: Cleanings and strategies of prevention. *Chemistry Africa*, pages 609–633, 2020.

[425] Chuanhui Huang and Tongwen Xu. Electrodialysis with bipolar membranes for sustainable development. *Environmental science & technology*, 40(17):5233–5243, 2006.

[426] Victor Nikonenko, Mahamet Urtenov, Semyon Mareev, and Gérald Pourcelly. Mathematical modeling of the effect of water splitting on ion transfer in the depleted diffusion layer near an ion-exchange membrane. *Membranes*, 10(2):22, 2020.

[427] R Pärnamäe, S Mareev, V Nikonenko, S Melnikov, N Sheldeshov, V Zabolotskii, HVM Hamelers, and M Tedesco. Bipolar membranes: A review on principles, latest developments, and applications. *Journal of Membrane Science*, page 118538, 2020.

[428] K Nagasubramanian, FP Chlanda, and Kang-Jen Liu. Use of bipolar membranes for generation of acid and base—an engineering and economic analysis. *Journal of Membrane Science*, 2:109–124, 1977.

[429] Gülay Bayramoğlu, Ilhami Tuzun, Gokce Celik, Meltem Yilmaz, and M Yakup Arica. Biosorption of mercury (ii), cadmium (ii) and lead (ii) ions from aqueous system by microalgae chlamydomonas reinhardtii immobilized in alginate beads. *International Journal of Mineral Processing*, 81(1):35–43, 2006.

[430] FG Wilhelm, I Pünt, NFA Van Der Vegt, Matthias Wessling, and H Strathmann. Optimisation strategies for the preparation of bipolar membranes with reduced salt ion leakage in acid–base electrodialysis. *Journal of Membrane Science*, 182(1-2):13–28, 2001.

[431] Salvador Mafé, Patricio Ramırez, and Antonio Alcaraz. Electric field-assisted proton transfer and water dissociation at the junction of a fixed-charge bipolar membrane. *Chemical Physics Letters*, 294(4-5):406–412, 1998.

[432] VI Zabolotskii, MV Sharafan, and NV Shelâ€™deshov. Influence of the nature of membrane ionogenic groups on water dissociation and electrolyte ion transport: A rotating membrane disk study. *Russian Journal of Electrochemistry*, 44(10):1127–1134, 2008.

[433] Victor Zabolotskii, Nicolay Sheldeshov, and Stanislav Melnikov. Heterogeneous bipolar membranes and their application in electrodialysis. *Desalination*, 342:183–203, 2014.

[434] SA Mareev, E Evdochenko, M Wessling, OA Kozaderova, SI Niftaliev, ND Pismenskaya, and VV Nikonenko. A comprehensive mathematical model of water splitting in bipolar membranes: Impact of the spatial distribution of fixed charges and catalyst at bipolar junction. *Journal of Membrane Science*, 603:118010, 2020.

[435] Xu Zhang, Chuanrun Li, Yaoming Wang, Jingyi Luo, and Tongwen Xu. Recovery of acetic acid from simulated acetaldehyde wastewaters: Bipolar membrane electrodialysis processes and membrane selection. *Journal of membrane science*, 379(1-2):184–190, 2011.

[436] Karel Ghyselbrecht, Marie Huygebaert, Bart Van der Bruggen, Rob Ballet, Boudewijn Meesschaert, and Luc Pinoy. Desalination of an industrial saline water with conventional and bipolar membrane electrodialysis. *Desalination*, 318:9–18, 2013.

[437] Fatih Ilhan, Harun Akif Kabuk, Ugur Kurt, Yasar Avsar, and M Talha Gonullu. Recovery of mixed acid and base from wastewater with bipolar membrane electrodialysis—a case study. *Desalination and Water Treatment*, 57(11):5165–5173, 2016.

[438] Xiaohan Sun, Huixia Lu, and Jianyou Wang. Recovery of citric acid from fermented liquid by bipolar membrane electrodialysis. *Journal of Cleaner Production*, 143:250–256, 2017.

[439] Samuel Bunani, Muserref Arda, Nalan Kabay, Kazuharu Yoshizuka, and Syouhei Nishihama. Effect of process conditions on recovery of lithium and boron from water using bipolar membrane electrodialysis (bmed). *Desalination*, 416:10–15, 2017.

[440] Miyuki Noguchi, Yurina Nakamura, Tadashi Shoji, Atsushi Iizuka, and Akihiro Yamasaki. Simultaneous removal and recovery of boron from waste water by multi-step bipolar membrane electrodialysis. *Journal of Water Process Engineering*, 23:299–305, 2018.

[441] Jiuyang Lin, Fang Lin, Xiangyu Chen, Wenyuan Ye, Xiaojuan Li, Huiming Zeng, and Bart Van der Bruggen. Sustainable management of textile wastewater: A hybrid tight ultrafiltration/bipolar-membrane electrodialysis process for resource recovery and zero liquid discharge. *Industrial & Engineering Chemistry Research*, 58(25):11003–11012, 2019.

[442] A Ti Cherif, J Molenat, and A Elmidaoui. Nitric acid and sodium hydroxide generation by electrodialysis using bipolar membranes. *Journal of applied electrochemistry*, 27(9):1069–1074, 1997.

[443] S Abu Khalla and ME Suss. Desalination via chemical energy: An electrodialysis cell driven by spontaneous electrode reactions. *Desalination*, 467:257–262, 2019.

[444] I Atlas and ME Suss. Theory of simultaneous desalination and electricity generation via an electrodialysis cell driven by spontaneous redox reactions. *Electrochimica Acta*, 319:813–821, 2019.

[445] M Ghahari, S Rashid-Nadimi, and H Bemana. Metal-air desalination battery: Concurrent energy generation and water desalination. *Journal of Power Sources*, 412:197–203, 2019.

[446] Lei Wang, Yuan Zhang, Karsten Moh, and Volker Presser. From capacitive deionization to desalination batteries and desalination fuel cells. *Current Opinion in Electrochemistry*, page 100758, 2021.

[447] Xi Chen, Xue Xia, Peng Liang, Xiaoxin Cao, Haotian Sun, and Xia Huang. Stacked microbial desalination cells to enhance water desalination efficiency. *Environmental science & technology*, 45(6):2465–2470, 2011.

[448] Youpeng Qu, Yujie Feng, Xin Wang, Jia Liu, Jiangwei Lv, Weihua He, and Bruce E Logan. Simultaneous water desalination and electricity generation in a microbial desalination cell with electrolyte recirculation for ph control. *Bioresource technology*, 106:89–94, 2012.

[449] I Atlas, S Abu Khalla, and ME Suss. Thermodynamic energy efficiency of electrochemical systems performing simultaneous water desalination and electricity generation. *Journal of The Electrochemical Society*, 167(13):134517, 2020.

[450] Yuan Zhang, Lei Wang, and Volker Presser. Electrocatalytic fuel cell desalination for continuous energy and freshwater generation. *Cell Reports Physical Science*, 2(5):100416, 2021.

[451] Shada Abu Khalla, Imri Atlas, Shawn Litster, and Matthew E Suss. Desalination fuel cells with high thermodynamic energy efficiency. *Environmental science & technology*, 2021.

[452] Gidon Amikam, Naama Manor-Korin, Paz Nativ, and Youri Gendel. Separation of ions from water and wastewater using micro-scale capacitive-faradaic fuel cells (cffcs), powered by h2 (g) and air. *Separation and Purification Technology*, 253:117494, 2020.

[453] Matthew E Suss, Y Zhang, I Atlas, Youri Gendel, EB Ruck, and Volker Presser. Emerging, hydrogen-driven electrochemical water purification. *Electrochemistry Communications*, 136:107211, 2022.

[454] Zahid Manzoor Bhat, Deepraj Pandit, Shane Ardo, Ravikumar Thimmappa, Alagar Raja Kottaichamy, Neethu Christudas Dargily, Mruthunjayachari Chattanahalli Devendrachari, and Musthafa Ottakam Thotiyl. An electrochemical neutralization cell for spontaneous water desalination. *Joule*, 4(8):1730–1742, 2020.

[455] Salman Abdalla, Shada Abu Khalla, and Matthew E Suss. Voltage loss breakdown in desalination fuel cells. *Electrochemistry Communications*, 132:107136, 2021.

[456] Arunchander Asokan, Shada Abu-Khalla, Salman Abdalla, and Matthew E Suss. Chloride-tolerant, inexpensive fe/n/c catalysts for desalination fuel cell cathodes. *ACS Applied Energy Materials*, 5(2):1743–1754, 2022.

[457] Kamel-Eddine Bouhidel and Aicha Lakehal. Influence of voltage and flow rate on electrodeionization (edi) process efficiency. *Desalination*, 193(1-3):411–421, 2006.

[458] Shu-Yuan Pan, Seth W Snyder, Hwong-Wen Ma, Yupo J Lin, and Pen-Chi Chiang. Energy-efficient resin wafer electrodeionization for impaired water reclamation. *Journal of Cleaner Production*, 174:1464–1474, 2018.

[459] Chunxia Zhao, Lifang Zhang, Rongshu Ge, Ailin Zhang, Chunhui Zhang, and Xiaoxin Chen. Treatment of low-level cu (ii) wastewater and regeneration through a novel capacitive deionization-electrodeionization (cdi-edi) technology. *Chemosphere*, 217:763–772, 2019.

[460] Hong-Joo Lee, Jung-Hoon Song, and Seung-Hyeon Moon. Comparison of electrodialysis reversal (edr) and electrodeionization reversal (edir) for water softening. *Desalination*, 314:43–49, 2013.

[461] B Senthil Rathi and P Senthil Kumar. Electrodeionization theory, mechanism and environmental applications. a review. *Environmental Chemistry Letters*, 18(4):1209–1227, 2020.

[462] Özgür Arar, Ümran Yüksel, Nalan Kabay, and Mithat Yüksel. Demineralization of geothermal water reverse osmosis (ro) permeate by electrodeionization (edi) with layered bed configuration. *Desalination*, 317:48–54, 2013.

[463] Jung-Hoon Song, Min-Chul Song, Kyeong-Ho Yeon, Jung-Bae Kim, Kun-Jai Lee, and Seung-Hyeon Moon. Purification of a primary coolant in a nuclear power plant using a magnetic filter–electrodeionization hybrid separation system. *Journal of radioanalytical and nuclear chemistry*, 262(3):725–732, 2005.

[464] GC Ganzi, Y Egozy, AJ Giuffrida, and AD Jha. High purity water by electrodeionization performance of the ionpure continuous deionization system. *Ultrapure Water*, 4(3):43–50, 1987.

[465] VA Shaposhnik, VA Kuzminykh, OV Grigorchuk, and VI Vasil'eva. Analytical model of laminar flow electrodialysis with ion-exchange membranes. *Journal of membrane science*, 133(1):27–37, 1997.

[466] Lin Fu, Jianyou Wang, and Yulong Su. Removal of low concentrations of hardness ions from aqueous solutions using electrodeionization process. *Separation and Purification Technology*, 68(3):390–396, 2009.

[467] Matthew L Jordan, Lauren Valentino, Nargiza Nazyrynbekova, Varada Menon Palakkal, Subarna Kole, Deepra Bhattacharya, Yupo J Lin, and Christopher G Arges. Promoting water-splitting in janus bipolar ion-exchange resin wafers for electrodeionization. *Molecular Systems Design & Engineering*, 5(5):922–935, 2020.

[468] Varada Menon Palakkal, Lauren Valentino, Qi Lei, Subarna Kole, Yupo J Lin, and Christopher G Arges. Advancing electrodeionization with conductive ionomer binders that immobilize ion-exchange resin particles into porous wafer substrates. *npj Clean Water*, 3(1):5, 2020.

[469] KH Yeon, JH Seong, S Rengaraj, and SH Moon. Electrochemical characterization of ion-exchange resin beds and removal of cobalt by electrodeionization for high purity water production. *Separation Science and Technology*, 38(2):443–462, 2003.

[470] Akrama Mahmoud, Laurence Muhr, Georges Grévillot, Gérard Valentin, and François Lapicque. Ohmic drops in the ion-exchange bed of cationic electrodeionisation cells. *Journal of applied electrochemistry*, 36(3):277–285, 2006.

[471] Lucía Alvarado, Israel Rodríguez-Torres, and Patricia Balderas. Investigation of current routes in electrodeionization system resin beds during chromium removal. *Electrochimica Acta*, 182:763–768, 2015.

[472] MC Sauer, PF Southwick, KS Spiegler, and MRJ Wyllie. Electrical conductance of porous plugs-ion exchange resin-solution systems. *Industrial & Engineering Chemistry*, 47(10):2187–2193, 1955.

[473] H Strathmann, JJ Krol, H-J Rapp, and G Eigenberger. Limiting current density and water dissociation in bipolar membranes. *Journal of Membrane Science*, 125(1):123–142, 1997.

[474] VV Nikonenko, SA Mareev, ND Pisâ€™menskaya, AM Uzdenova, AV Kovalenko, M Kh Urtenov, and G Pourcelly. Effect of electroconvection and its use in intensifying the mass transfer in electrodialysis. *Russian Journal of Electrochemistry*, 53(10):1122–1144, 2017.

[475] Ali Mani and Karen May Wang. Electroconvection near electrochemical interfaces: Experiments, modeling, and computation. *Annual Review of Fluid Mechanics*, 52:509–529, 2020.

[476] Sudong Park and Rhokyun Kwak. Microscale electrodeionization: In situ concentration profiling and flow visualization. *Water research*, 170:115310, 2020.

[477] Felix Stockmeier, Michael Schatz, Malte Habermann, John Linkhorst, Ali Mani, and Matthias Wessling. Direct 3d observation and unraveling of electroconvection phenomena during concentration polarization at ion-exchange membranes. *Journal of Membrane Science*, page 119846, 2021.

[478] Ruimei Wen, Shouquan Deng, and Yafeng Zhang. The removal of silicon and boron from ultra-pure water by electrodeionization. *Desalination*, 181(1-3):153–159, 2005.

[479] A Lounis, L Setti, A Djennane, and R Melikchi. Separation of molybdenum-uranium by a process combining ion exchange resin and membranes. *J. Appl. Sci*, 7(14):1963–1967, 2007.

[480] Hamid Reza Taghdirian, Ahmad Moheb, and Mohsen Mehdipourghazi. Selective separation of ni (ii)/co (ii) ions from dilute aqueous solutions using continuous electrodeionization in the presence of edta. *Journal of Membrane Science*, 362(1-2):68–75, 2010.

[481] Yohanes Ervan and I Gede Wenten. Study on the influence of applied voltage and feed concentration on the performance of electrodeionization. *Songklanakarin J. Sci. Technol*, 24:955–963, 2002.

[482] Isabelle Monzie, Laurence Muhr, François Lapicque, and Georges Grévillot. Mass transfer investigations in electrodeionization processes using the microcolumn technique. *Chemical engineering science*, 60(5):1389–1399, 2005.

[483] AN Hakim, K Khoiruddin, D Ariono, and IG Wenten. Ionic separation in electrodeionization system: Mass transfer mechanism and factor affecting separation performance. *Separation & Purification Reviews*, pages 294–316, 2019.

[484] Carolina Otero, Adriana Urbina, Eligio P Rivero, and Francisca A Rodríguez. Desalination of brackish water by electrodeionization: Experimental study and mathematical modeling. *Desalination*, 504:114803, 2021.

[485] HM Verbeek, L Fürst, and H Neumeister. Digital simulation of an electrodeionization process. *Computers & chemical engineering*, 22:S913–S916, 1998.

[486] Jun Lu, Yu-Xin Wang, and Jia Zhu. Numerical simulation of the electrodeionization (edi) process accounting for water dissociation. *Electrochimica acta*, 55(8):2673–2686, 2010.

[487] Jun Lu, Xiao-Yun Ma, and Yu-Xin Wang. Numerical simulation of the electrodeionization (edi) process with layered resin bed for deeply separating salt ions. *Desalination and Water Treatment*, 57(23):10546–10559, 2016.

[488] F Zahakifar, AR Keshtkar, E Zamani Souderjani, and MA Moosavian. Use of response surface methodology for optimization of thorium (iv) removal from aqueous solutions by electrodeionization (edi). *Progress in Nuclear Energy*, 124:103335, 2020.

[489] E Glueckauf. Electro-deionization through a packed bed. *Brit. Chem. Eng.*, 4:646–651, 1959.

[490] I Dobrevsky and A Zvezdov. Investigation of pore structure of ion exchange membranes. *Desalination*, 28(3):283–289, 1979.

[491] Andrei B Yaroslavtsev, Viktor V Nikonenko, and Viktor I Zabolotsky. Ion transfer in ion-exchange and membrane materials. *Russian chemical reviews*, 72(5):393–421, 2003.

[492] Samuel Faucher, Narayana Aluru, Martin Z Bazant, Daniel Blankschtein, Alexandra H Brozena, John Cumings, J Pedro de Souza, Menachem Elimelech, Razi Epsztein, and John T Fourkas. Critical knowledge gaps in mass transport through single-digit nanopores: a review and perspective. *The Journal of Physical Chemistry C*, 123(35):21309–21326, 2019.

[493] NP Berezina, NA Kononenko, OA Dyomina, and NP Gnusin. Characterization of ion-exchange membrane materials: properties vs structure. *Advances in colloid and interface science*, 139(1-2):3–28, 2008.

[494] RK Nagarale, GS Gohil, and Vinod K Shahi. Recent developments on ion-exchange membranes and electro-membrane processes. *Advances in colloid and interface science*, 119(2-3):97–130, 2006.

[495] PS Goh, AF Ismail, and BC Ng. Carbon nanotubes for desalination: performance evaluation and current hurdles. *Desalination*, 308:2–14, 2013.

[496] Rasel Das, Md Eaqub Ali, Sharifah Bee Abd Hamid, Seeram Ramakrishna, and Zaira Zaman Chowdhury. Carbon nanotube membranes for water purification: a bright future in water desalination. *Desalination*, 336:97–109, 2014.

[497] Jason K Holt, Hyung Gyu Park, Yinmin Wang, Michael Stadermann, Alexander B Artyukhin, Costas P Grigoropoulos, Aleksandr Noy, and Olgica Bakajin. Fast mass transport through sub-2-nanometer carbon nanotubes. *Science*, 312(5776):1034–1037, 2006.

[498] Eleonora Secchi, Sophie Marbach, Antoine Niguès, Derek Stein, Alessandro Siria, and Lydéric Bocquet. Massive radius-dependent flow slippage in carbon nanotubes. *Nature*, 537(7619):210–213, 2016.

[499] Evelyn N Wang and Rohit Karnik. Graphene cleans up water. *Nature nanotechnology*, 7(9):552–554, 2012.

[500] Arash Aghigh, Vahid Alizadeh, Hin Yong Wong, Md Shabiul Islam, Nowshad Amin, and Mukter Zaman. Recent advances in utilization of graphene for filtration and desalination of water: a review. *Desalination*, 365:389–397, 2015.

[501] Luda Wang, Michael SH Boutilier, Piran R Kidambi, Doojoon Jang, Nicolas G Hadjiconstantinou, and Rohit Karnik. Fundamental transport mechanisms, fabrication and potential applications of nanoporous atomically thin membranes. *Nature nanotechnology*, 12(6):509–522, 2017.

[502] H von Helmholtz. Ueber einige gesetze der vertheilung elektrischer ströme in körperlichen leitern, mit anwendung auf die thierisch-elektrischen versuche (schluss.). *Annalen der Physik*, 165(7):353–377, 1853.

[503] M Gouy. Sur la constitution de la charge électrique à la surface d'un électrolyte. *J. Phys. Theor. Appl.*, 9(4):457–468, 1910.

[504] David Leonard Chapman. A contribution to the theory of electrocapillarity. *The London, Edinburgh, and Dublin philosophical magazine and journal of science*, 25(148):475–481, 1913.

[505] Otto Stern. Zur theorie der elektrolytischen doppelschicht. *Zeitschrift für Elektrochemie und angewandte physikalische Chemie*, 30(21-22):508–516, 1924.

[506] PB Peters, R Van Roij, Martin Z Bazant, and PM Biesheuvel. Analysis of electrolyte transport through charged nanopores. *Physical review E*, 93(5):053108, 2016.

[507] Richard J Gross and JF Osterle. Membrane transport characteristics of ultrafine capillaries. *The Journal of chemical physics*, 49(1):228–234, 1968.

[508] Christoffer P Nielsen and Henrik Bruus. Concentration polarization, surface currents, and bulk advection in a microchannel. *Physical Review E*, 90(4):043020, 2014.

[509] Shima Alizadeh and Ali Mani. Multiscale model for electrokinetic transport in networks of pores, part i: model derivation. *Langmuir*, 33(25):6205–6219, 2017.

[510] Shima Alizadeh and Ali Mani. Multiscale model for electrokinetic transport in networks of pores, part ii: computational algorithms and applications. *Langmuir*, 33(25):6220–6231, 2017.

[511] Shima Alizadeh, Martin Z Bazant, and Ali Mani. Impact of network heterogeneity on electrokinetic transport in porous media. *Journal of colloid and interface science*, 553:451–464, 2019.

[512] Mohammad Mirzadeh, Tingtao Zhou, Mohammad Amin Amooie, Dimitrios Fraggedakis, Todd R Ferguson, and Martin Z Bazant. Vortices of electro-osmotic flow in heterogeneous porous media. *Physical Review Fluids*, 5(10):103701, 2020.

[513] Varanasi Sasidhar and Eli Ruckenstein. Electrolyte osmosis through capillaries. *Journal of colloid and interface science*, 82(2):439–457, 1981.

[514] Andriy Yaroshchuk, Merlin L Bruening, and Emiliy Zholkovskiy. Modelling nanofiltration of electrolyte solutions. *Advances in Colloid and Interface Science*, 268:39–63, 2019.

[515] Y Lanteri, A Szymczyk, and P Fievet. Membrane potential in multi-ionic mixtures. *The Journal of Physical Chemistry B*, 113(27):9197–9204, 2009.

[516] Yahan Yang and Peter N Pintauro. Multicomponent space-charge transport model for ion-exchange membranes. *AIChE journal*, 46(6):1177–1190, 2000.

[517] Ingmar H Huisman, Pedro Prádanos, José Ignacio Calvo, and Antonio Hernández. Electroviscous effects, streaming potential, and zeta potential in polycarbonate track-etched membranes. *Journal of Membrane Science*, 178(1-2):79–92, 2000.

[518] Varanasi Sasidhar and Eli Ruckenstein. Anomalous effects during electrolyte osmosis across charged porous membranes. *Journal of Colloid and Interface Science*, 85(2):332–362, 1982.

[519] Wei-Juan Shang, Xiao-Lin Wang, and Yang-Xin Yu. Theoretical calculation on the membrane potential of charged porous membranes in 1-1, 1-2, 2-1 and 2-2 electrolyte solutions. *Journal of membrane science*, 285(1-2):362–375, 2006.

[520] P Ramirez, M Aguilella-Arzo, A Alcaraz, J Cervera, and VM Aguilella. Theoretical description of the ion transport across nanopores with titratable fixed charges. *Cell biochemistry and biophysics*, 44(2):287–312, 2006.

[521] Manoel Manghi, John Palmeri, Khadija Yazda, François Henn, and Vincent Jourdain. Role of charge regulation and flow slip in the ionic conductance of nanopores: An analytical approach. *Physical Review E*, 98(1):012605, 2018.

[522] Wenyao Zhang, Qiuwang Wang, Min Zeng, and Cunlu Zhao. Thermoelectric effect and temperature-gradient-driven electrokinetic flow of electrolyte solutions in charged nanocapillaries. *International Journal of Heat and Mass Transfer*, 143:118569, 2019.

[523] L Zhang, PM Biesheuvel, and II Ryzhkov. Theory of ion and water transport in electron-conducting membrane pores with ph-dependent chemical charge. *Physical Review Applied*, 12(1):014039, 2019.

[524] Ilya I Ryzhkov, Denis V Lebedev, Vera S Solodovnichenko, Andrey V Minakov, and Mikhail M Simunin. On the origin of membrane potential in membranes with polarizable nanopores. *Journal of membrane science*, 549:616–630, 2018.

[525] JR Bontha and Peter N Pintauro. Water orientation and ion solvation effects during multicomponent salt partitioning in a nafion cation exchange membrane. *Chemical engineering science*, 49(23):3835–3851, 1994.

[526] Yannick Lanteri, Anthony Szymczyk, and Patrick Fievet. Influence of steric, electric, and dielectric effects on membrane potential. *Langmuir*, 24(15):7955–7962, 2008.

[527] Anthony Szymczyk, Mohammed Sbaï, Patrick Fievet, and Alain Vidonne. Transport properties and electrokinetic characterization of an amphoteric nanofilter. *Langmuir*, 22(8):3910–3919, 2006.

[528] E Hawkins Cwirko and RG Carbonell. Transport of electrolytes in charged pores: analysis using the method of spatial averaging. *Journal of colloid and interface science*, 129(2):513–531, 1989.

[529] E Victoria Dydek, Boris Zaltzman, Isaak Rubinstein, DS Deng, Ali Mani, and Martin Z Bazant. Overlimiting current in a microchannel. *Physical review letters*, 107(11):118301, 2011.

[530] E Victoria Dydek and Martin Z Bazant. Nonlinear dynamics of ion concentration polarization in porous media: The leaky membrane model. *AIChE Journal*, 59(9):3539–3555, 2013.

[531] Amir Levy, J Pedro de Souza, and Martin Z Bazant. Breakdown of electroneutrality in nanopores. *Journal of Colloid and Interface Science*, 579:162–176, 2020.

[532] Christopher Maffeo, Swati Bhattacharya, Jejoong Yoo, David Wells, and Aleksei Aksimentiev. Modeling and simulation of ion channels. *Chemical reviews*, 112(12):6250–6284, 2012.

[533] J Pedro de Souza, Amir Levy, and Martin Z Bazant. Electroneutrality breakdown in nanopore arrays. *Physical Review E*, 104(4):044803, 2021.

[534] Xuechen Zhou, Zhangxin Wang, Razi Epsztein, Cheng Zhan, Wenlu Li, John D Fortner, Tuan Anh Pham, Jae-Hong Kim, and Menachem Elimelech. Intrapore energy barriers govern ion transport and selectivity of desalination membranes. *Science advances*, 6(48):eabd9045, 2020.

[535] Alexei A Kornyshev. Double-layer in ionic liquids: paradigm change?, 2007.

[536] Martin Z Bazant, Mustafa Sabri Kilic, Brian D Storey, and Armand Ajdari. Towards an understanding of induced-charge electrokinetics at large applied voltages in concentrated solutions. *Advances in colloid and interface science*, 152(1-2):48–88, 2009.

[537] R Qiao and Narayana R Aluru. Ion concentrations and velocity profiles in nanochannel electroosmotic flows. *The Journal of chemical physics*, 118(10):4692–4701, 2003.

[538] Brian D Storey and Martin Z Bazant. Effects of electrostatic correlations on electrokinetic phenomena. *Physical Review E*, 86(5):056303, 2012.

[539] Robert F Stout and Aditya S Khair. A continuum approach to predicting electrophoretic mobility reversals. *Journal of Fluid Mechanics*, 752:R1, 2014.

[540] Mustafa Sabri Kilic, Martin Z Bazant, and Armand Ajdari. Steric effects in the dynamics of electrolytes at large applied voltages. i. double-layer charging. *Physical review E*, 75(2):021502, 2007.

[541] Mustafa Sabri Kilic, Martin Z Bazant, and Armand Ajdari. Steric effects in the dynamics of electrolytes at large applied voltages. ii. modified poisson-nernst-planck equations. *Physical review E*, 75(2):021503, 2007.

[542] Martin Z Bazant, Brian D Storey, and Alexei A Kornyshev. Double layer in ionic liquids: Overscreening versus crowding. *Physical Review Letters*, 106(4):046102, 2011.

[543] J Pedro de Souza and Martin Z Bazant. Continuum theory of electrostatic correlations at charged surfaces. *The Journal of Physical Chemistry C*, 124(21):11414–11421, 2020.

[544] JA Wesselingh, P Vonk, and G Kraaijeveld. Exploring the maxwell-stefan description of ion exchange. *The Chemical Engineering Journal and The Biochemical Engineering Journal*, 57(2):75–89, 1995.

[545] WB Samuel de Lint and Nieck E Benes. Predictive charge-regulation transport model for nanofiltration from the theory of irreversible processes. *Journal of membrane science*, 243(1-2):365–377, 2004.

[546] M Tedesco, HVM Hamelers, and PM Biesheuvel. Nernst-planck transport theory for (reverse) electrodialysis: Ii. effect of water transport through ion-exchange membranes. *Journal of Membrane Science*, 531:172–182, 2017.

[547] YS Oren and PM Biesheuvel. Theory of ion and water transport in reverse-osmosis membranes. *Physical Review Applied*, 9(2):024034, 2018.

[548] PM Biesheuvel and MZ Bazant. Analysis of ionic conductance of carbon nanotubes. *Physical Review E*, 94(5):050601, 2016.

[549] Eleonora Secchi, Antoine Niguès, Laetitia Jubin, Alessandro Siria, and Lydéric Bocquet. Scaling behavior for ionic transport and its fluctuations in individual carbon nanotubes. *Physical review letters*, 116(15):154501, 2016.

[550] R Vangara, DCR Brown, F van Swol, and DN Petsev. Electrolyte solution structure and its effect on the properties of electric double layers with surface charge regulation. *Journal of colloid and interface science*, 488:180–189, 2017.

[551] Patricio Ramirez, José A Manzanares, Javier Cervera, Vicente Gomez, Mubarak Ali, Saima Nasir, Wolfgang Ensinger, and Salvador Mafe. Surface charge regulation of functionalized conical nanopore conductance by divalent cations and anions. *Electrochimica Acta*, 325:134914, 2019.

[552] BL Werkhoven, Jeffrey Christopher Everts, S Samin, and R Van Roij. Flow-induced surface charge heterogeneity in electrokinetics due to stern-layer conductance coupled to reaction kinetics. *Physical review letters*, 120(26):264502, 2018.

[553] BL Werkhoven, S Samin, and René van Roij. Dynamic stern layers in charge-regulating electrokinetic systems: three regimes from an analytical approach. *The European Physical Journal Special Topics*, 227(18):2539–2557, 2019.

[554] Sung Jae Kim, Ying-Chih Wang, Jeong Hoon Lee, Hongchul Jang, and Jongyoon Han. Concentration polarization and nonlinear electrokinetic flow near a nanofluidic channel. *Physical review letters*, 99(4):044501, 2007.

[555] Sung Jae Kim, Leon D Li, and Jongyoon Han. Amplified electrokinetic response by concentration polarization near nanofluidic channel. *Langmuir*, 25(13):7759–7765, 2009.

[556] Sung Jae Kim, Yong-Ak Song, and Jongyoon Han. Nanofluidic concentration devices for biomolecules utilizing ion concentration polarization: theory, fabrication, and applications. *Chemical Society Reviews*, 39(3):912–922, 2010.

[557] Thomas A Zangle, Ali Mani, and Juan G Santiago. Theory and experiments of concentration polarization and ion focusing at microchannel and nanochannel interfaces. *Chemical Society Reviews*, 39(3):1014–1035, 2010.

[558] Sung Jae Kim, Sung Hee Ko, Kwan Hyoung Kang, and Jongyoon Han. Direct seawater desalination by ion concentration polarization. *Nature nanotechnology*, 5(4):297–301, 2010.

[559] Sung Jae Kim, Sung Hee Ko, Kwan Hyoung Kang, and Jongyoon Han. Erratum: Direct seawater desalination by ion concentration polarization. *Nature nanotechnology*, 8:609, 2013.

[560] Sungmin Nam, Inhee Cho, Joonseong Heo, Geunbae Lim, Martin Z Bazant, Dustin Jaesuk Moon, Gun Yong Sung, and Sung Jae Kim. Experimental verification of overlimiting current by surface conduction and electro-osmotic flow in microchannels. *Physical review letters*, 114(11):114501, 2015.

[561] Ying-Chih Wang, Anna L Stevens, and Jongyoon Han. Million-fold preconcentration of proteins and peptides by nanofluidic filter. *Analytical chemistry*, 77(14):4293–4299, 2005.

[562] Yu-Jin Kim, Jin Hur, Wisup Bae, and Jae-Hwan Choi. Desalination of brackish water containing oil compound by capacitive deionization process. *Desalination*, 253(1-3):119–123, 2010.

[563] Raúl A. Rica and Martin Z Bazant. Electrodiffusiophoresis: Particle motion in electrolytes under direct current. *Physics of Fluids*, 22(11):112109, 2010.

[564] Ludmila Křivánková, Pavla Pantůčková, and Petr Boček. Isotachophoresis in zone electrophoresis. *Journal of Chromatography A*, 838(1-2):55–70, 1999.

[565] Byoungsok Jung, Rajiv Bharadwaj, and Juan G Santiago. On-chip millionfold sample stacking using transient isotachophoresis. *Analytical chemistry*, 78(7):2319–2327, 2006.

[566] Sandip Ghosal and Zhen Chen. Nonlinear waves in capillary electrophoresis. *Bulletin of mathematical biology*, 72(8):2047–2066, 2010.

[567] Supreet S Bahga and Juan G Santiago. Coupling isotachophoresis and capillary electrophoresis: a review and comparison of methods. *Analyst*, 138(3):735–754, 2013.

[568] Zhibo Gu, Bingrui Xu, Peng Huo, Shmuel M Rubinstein, Martin Z Bazant, and Daosheng Deng. Deionization shock driven by electroconvection in a circular channel. *Physical Review Fluids*, 4(11):113701, 2019.

[569] Andriy Yaroshchuk, Emiliy Zholkovskiy, Sergey Pogodin, and Vladimir Baulin. Coupled concentration polarization and electroosmotic circulation near micro/nanointerfaces: Taylor–aris model of hydrodynamic dispersion and limits of its applicability. *Langmuir*, 27(18):11710–11721, 2011.

[570] Andriy Yaroshchuk. Over-limiting currents and deionization "shocks" in current-induced polarization: Local-equilibrium analysis. *Advances in colloid and interface science*, 183:68–81, 2012.

[571] Ji-Hyung Han, Edwin Khoo, Peng Bai, and Martin Z Bazant. Over-limiting current and control of dendritic growth by surface conduction in nanopores. *Scientific reports*, 4:7056, 2014.

[572] Markus Schmuck and Martin Z Bazant. Homogenization of the poisson–nernst–planck equations for ion transport in charged porous media. *SIAM Journal on Applied Mathematics*, 75(3):1369–1401, 2015.

[573] Jihye Choi, Seongho Baek, Hee Chan Kim, Jong-Hee Chae, Youngil Koh, Sang Woo Seo, Hyomin Lee, and Sung Jae Kim. Nanoelectrokinetic selective preconcentration based on ion concentration polarization. *BioChip Journal*, pages 100–109, 2020.

[574] Ji-Hyung Han, Miao Wang, Peng Bai, Fikile R Brushett, and Martin Z Bazant. Dendrite suppression by shock electrodeposition in charged porous media. *Scientific reports*, 6:28054, 2016.

[575] Ji-Hyung Han, Ramachandran Muralidhar, Rainer Waser, and Martin Z Bazant. Resistive switching in aqueous nanopores by shock electrodeposition. *Electrochimica acta*, 222:370–375, 2016.

[576] Jian Zhi, Shengkai Li, Mei Han, and P Chen. Biomolecule-guided cation regulation for dendrite-free metal anodes. *Science advances*, 6(32):eabb1342, 2020.

[577] Daosheng Deng, Wassim Aouad, William A Braff, Sven Schlumpberger, Matthew E Suss, and Martin Z Bazant. Water purification by shock electrodialysis: Deionization, filtration, separation, and disinfection. *Desalination*, 357:77–83, 2015.

[578] Mohammad A Alkhadra, Kameron M Conforti, Tao Gao, Huanhuan Tian, and Martin Z Bazant. Continuous separation of radionuclides from contaminated water by shock electrodialysis. *Environmental Science & Technology*, 54(1):527–536, 2019.

[579] Egon Matijevic and Robert J Good. *Surface and colloid science*, volume 12. Springer Science & Business Media, 2012.

[580] Christopher T Culbertson, Roswitha S Ramsey, and J Michael Ramsey. Electroosmotically induced hydraulic pumping on microchips: differential ion transport. *Analytical Chemistry*, 72(10):2285–2291, 2000.

[581] Timothy E McKnight, Christopher T Culbertson, Stephen C Jacobson, and J Michael Ramsey. Electroosmotically induced hydraulic pumping with integrated electrodes on microfluidic devices. *Analytical Chemistry*, 73(16):4045–4049, 2001.

[582] Matthew E Suss, Ali Mani, Thomas A Zangle, and Juan G Santiago. Electroosmotic pump performance is affected by concentration polarizations of both electrodes and pump. *Sensors and Actuators A: Physical*, 165(2):310–315, 2011.

[583] Sven Schlumpberger, Raymond B. Smith, Huanhuan Tian, Ali Mani, and Martin Z. Bazant. Deionization shocks in crossflow. *AIChE Journal*, 67:e17274, 2021.

[584] Huanhuan Tian, Mohammad A Alkhadra, and Martin Z Bazant. Theory of shock electrodialysis i: Water dissociation and electrosmotic vortices. *Journal of Colloid and Interface Science*, 589:605–615, 2021.

[585] Huanhuan Tian, Mohammad A Alkhadra, Kameron Conforti, and Martin Z Bazant. Continuous and selective removal of lead from drinking water by shock electrodialysis. *Environment Science & Technology Water*, 2021.

[586] Jan Čížek, Petr Cvejn, Jaromír Marek, and David Tvrzník. Desalination performance assessment of scalable, multi-stack ready shock electrodialysis unit utilizing anion-exchange membranes. *Membranes*, 10(11):347, 2020.

[587] Kameron Michael Conforti. *Continuous ion-selective separation by shock electrodialysis*. PhD thesis, Massachusetts Institute of Technology, 2019.

[588] Mohammad A Alkhadra, Tao Gao, Kameron M Conforti, Huanhuan Tian, and Martin Z Bazant. Small-scale desalination of seawater by shock electrodialysis. *Desalination*, 476:114219, 2020.

[589] Kojo Menyah and Yemane Wolde-Rufael. Co2 emissions, nuclear energy, renewable energy and economic growth in the us. *Energy Policy*, 38(6):2911–2915, 2010.

[590] Kais Saidi and Mounir Ben Mbarek. Nuclear energy, renewable energy, co2 emissions, and economic growth for nine developed countries: Evidence from panel granger causality tests. *Progress in Nuclear Energy*, 88:364–374, 2016.

[591] DH Lister. The transport of radioactive corrosion products in high-temperature water ii. the activation of isothermal steel surfaces. *Nuclear Science and Engineering*, 59(4):406–426, 1976.

[592] Takashi Honda, Masakiyo Izumiya, Akira Minato, Katsumi Ohsumi, and Hideo Matsubayashi. Radiation buildup on stainless steel in a boiling water reactor environment. *Nuclear Technology*, 64(1):35–42, 1984.

[593] Kwang-Ho Choo, Dae-Joong Kwon, Kwang-Won Lee, and Sang-June Choi. Selective removal of cobalt species using nanofiltration membranes. *Environmental science & technology*, 36(6):1330–1336, 2002.

[594] M Kikuchi, E Ga, K Funabashi, H Yusa, S Uchida, and K Fujita. Removal of radioactive cobalt ion in high temperature water using titanium oxide. *Nuclear Engineering and Design*, 53(3):387–392, 1979.

[595] B Cox and C Wu. Transient effects of lithium hydroxide and boric acid on zircaloy corrosion. *Journal of nuclear materials*, 224(2):169–178, 1995.

[596] S K Sengupta, E Hooper, and E Dubost. Processing of nuclear power plant waste streams containing boric acid. *International Atomic Energy Agency (Technical Report)*, page 49, 2019.

[597] Xiaojing Liu, Jinling Wu, and Jianlong Wang. Removal of cs (i) from simulated radioactive wastewater by three forward osmosis membranes. *Chemical Engineering Journal*, 344:353–362, 2018.

[598] P Barry Ryan, Natalie Huet, and David L MacIntosh. Longitudinal investigation of exposure to arsenic, cadmium, and lead in drinking water. *Environmental health perspectives*, 108(8):731–735, 2000.

[599] Lead in drinking water. Technical report, 2012.

[600] Huanhuan Tian, Mohammad A Alkhadra, and Martin Z Bazant. Theory of shock electrodialysis ii: Mechanisms of selective ion removal. *Journal of Colloid and Interface Science*, 589:616–621, 2021.

[601] IM Abrams. Organic fouling of ion exchange resins. In *Studies in Environmental Science*, volume 19, pages 213–224. Elsevier, 1982.

[602] B Anupkumar, TS Rao, and KK Satpathy. Microbial fouling of an anion exchange resin. *Current science*, 80(9):1104–1107, 2001.

[603] Meital Asraf-Snir, Jack Gilron, and Yoram Oren. Gypsum scaling of anion exchange membranes in electrodialysis. *Journal of Membrane Science*, 520:176–186, 2016.

[604] Dandan Zhao, Lai Yoke Lee, Say Leong Ong, Prannoy Chowdhury, Keng Boon Siah, and How Yong Ng. Electrodialysis reversal for industrial reverse osmosis brine treatment. *Separation and Purification Technology*, 213:339–347, 2019.

[605] MA Andreeva, VV Gil, ND Pismenskaya, L Dammak, NA Kononenko, C Larchet, Daniel Grande, and VV Nikonenko. Mitigation of membrane scaling in electrodialysis by electroconvection enhancement, ph adjustment and pulsed electric field application. *Journal of Membrane Science*, 549:129–140, 2018.

[606] Marian Turek, Joanna Waś, and Krzysztof Mitko. Scaling prediction in electrodialytic desalination. *Desalination and Water Treatment*, 44(1-3):255–260, 2012.

[607] Christophe Casademont, Monica Araya Farias, Gérald Pourcelly, and Laurent Bazinet. Impact of electrodialytic parameters on cation migration kinetics and fouling nature of ion-exchange membranes during treatment of solutions with different magnesium/calcium ratios. *Journal of membrane Science*, 325(2):570–579, 2008.

[608] Ilhem Ben Salah Sayadi, Philippe Sistat, Mohamed Ben Amor, and Mohamed Tlili. Brackish water desalination by electrodialysis: Caco3 scaling monitoring during batch recirculation operation. *International Journal of Chemical Reactor Engineering*, 11(1):517–525, 2013.

[609] Yoshinobu Tanaka. Water dissociation in ion-exchange membrane electrodialysis. *Journal of Membrane Science*, 203(1-2):227–244, 2002.

[610] Nicolás Cifuentes-Araya, Carolina Astudillo-Castro, and Laurent Bazinet. Mechanisms of mineral membrane fouling growth modulated by pulsed modes of current during electrodialysis: Evidences of water splitting implications in the appearance of the amorphous phases of magnesium hydroxide and calcium carbonate. *Journal of colloid and interface science*, 426:221–234, 2014.

[611] Sergey Mikhaylin, Victor Nikonenko, Gérald Pourcelly, and Laurent Bazinet. Intensification of demineralization process and decrease in scaling by application of pulsed electric field with short pulse/pause conditions. *Journal of membrane science*, 468:389–399, 2014.

[612] Guillaume Dufton, Sergey Mikhaylin, Sami Gaaloul, and Laurent Bazinet. Positive impact of pulsed electric field on lactic acid removal, demineralization and membrane scaling during acid whey electrodialysis. *International journal of molecular sciences*, 20(4):797, 2019.

[613] Hong-Joo Lee, Jin-Soo Park, Moon-Sung Kang, and Seung-Hyeon Moon. Effects of silica sol on ion exchange membranes: Electrochemical characterization of anion exchange membranes in electrodialysis of silica sol containing-solutions. *Korean Journal of Chemical Engineering*, 20(5):889–895, 2003.

[614] E Korngold. Prevention of colloidal-fouling in electrodialysis by chlorination. *Desalination*, 9(3):213–216, 1971.

[615] M Mondor, D Ippersiel, F Lamarche, and L Masse. Fouling characterization of electrodialysis membranes used for the recovery and concentration of ammonia from swine manure. *Bioresource technology*, 100(2):566–571, 2009.

[616] SG Yiantsios and AJ Karabelas. The effect of colloid stability on membrane fouling. *Desalination*, 118(1-3):143–152, 1998.

[617] Nobuyuki Tanaka, Minami Nagase, and Mitsuru Higa. Organic fouling behavior of commercially available hydrocarbon-based anion-exchange membranes by various organic-fouling substances. *Desalination*, 296:81–86, 2012.

[618] Bram De Jaegher, Eneko Larumbe, Wim De Schepper, Arne Verliefde, and Ingmar Nopens. Data on ion-exchange membrane fouling by humic acid during electrodialysis. *Data in Brief*, 31:105763, 2020.

[619] Bram De Jaegher, Eneko Larumbe, Wim De Schepper, Arne Verliefde, and Ingmar Nopens. Colloidal fouling in electrodialysis: A neural differential equations model. *Separation and Purification Technology*, 249:116939, 2020.

[620] Sahar Talebi, George Q Chen, Benny Freeman, Francisco Suarez, Adrian Freckleton, Karren Bathurst, and Sandra E Kentish. Fouling and in-situ cleaning of ion-exchange membranes during the electrodialysis of fresh acid and sweet whey. *Journal of Food Engineering*, 246:192–199, 2019.

[621] Mathieu Persico, Sergey Mikhaylin, Alain Doyen, Loubna Firdaous, Victor Nikonenko, Natalia Pismenskaya, and Laurent Bazinet. Prevention of peptide fouling on ion-exchange membranes during electrodialysis in overlimiting conditions. *Journal of Membrane Science*, 543:212–221, 2017.

[622] Arne RD Verliefde, Emile R Cornelissen, Sebastiaan GJ Heijman, Eric MV Hoek, Gary L Amy, Bart Van der Bruggen, and Johannis C Van Dijk. Influence of solute- membrane affinity on rejection of uncharged organic solutes by nanofiltration membranes. *Environmental science & technology*, 43(7):2400–2406, 2009.

[623] Hong-Joo Lee, Min-Kyoung Hong, Sang-Don Han, Seung-Hee Cho, and Seung-Hyeon Moon. Fouling of an anion exchange membrane in the electrodialysis desalination process in the presence of organic foulants. *Desalination*, 238(1-3):60–69, 2009.

[624] Haicheng Guo, Lan Xiao, Shuili Yu, Haijun Yang, Jun Hu, Guicai Liu, and Yulin Tang. Analysis of anion exchange membrane fouling mechanism caused by anion polyacrylamide in electrodialysis. *Desalination*, 346:46–53, 2014.

[625] William E Katz. The electrodialysis reversal (edr) process. *Desalination*, 28(1):31–40, 1979.

[626] Yu-Mei Chao and TM Liang. A feasibility study of industrial wastewater recovery using electrodialysis reversal. *Desalination*, 221(1-3):433–439, 2008.

[627] Xiaohan Sun, Huixia Lu, and Jianyou Wang. Brackish water desalination using electrodeionization reversal. *Chemical Engineering and Processing: Process Intensification*, 104:262–270, 2016.

[628] Sabrina Tamersit, Kamel-Eddine Bouhidel, and Zakaria Zidani. Investigation of electrodialysis anti-fouling configuration for desalting and treating tannery unhairing wastewater: Feasibility of by-products recovery and water recycling. *Journal of environmental management*, 207:334–340, 2018.

[629] Jinli Zhao, Qingbai Chen, Luyao Ren, and Jianyou Wang. Fabrication of hydrophilic cation exchange membrane with improved stability for electrodialysis: An excellent anti-scaling performance. *Journal of Membrane Science*, 617:118618, 2021.

[630] Sri Mulyati, Ryosuke Takagi, Akihiro Fujii, Yoshikage Ohmukai, Tatsuo Maruyama, and Hideto Matsuyama. Improvement of the antifouling potential of an anion exchange membrane by surface modification with a polyelectrolyte for an electrodialysis process. *Journal of Membrane Science*, 417:137–143, 2012.

[631] K Khoiruddin, D Ariono, S Subagjo, and IG Wenten. Improved anti-organic fouling of polyvinyl chloride-based heterogeneous anion-exchange membrane modified by hydrophilic additives. *Journal of Water Process Engineering*, 41:102007, 2021.

[632] VV Gil, MA Andreeva, L Jansezian, J Han, ND Pismenskaya, VV Nikonenko, C Larchet, and L Dammak. Impact of heterogeneous cation-exchange membrane surface modification on chronopotentiometric and current–voltage characteristics in nacl, cacl2 and mgcl2 solutions. *Electrochimica Acta*, 281:472–485, 2018.

[633] Yutuo Cheng, Zhiqi Hao, Changrun Hao, Yu Deng, Xingying Li, Kexun Li, and Yubo Zhao. A review of modification of carbon electrode material in capacitive deionization. *RSC advances*, 9(42):24401–24419, 2019.

[634] Tung-Yu Ying, Kun-Lin Yang, Sotira Yiacoumi, and Costas Tsouris. Electrosorption of ions from aqueous solutions by nanostructured carbon aerogel. *Journal of colloid and interface science*, 250(1):18–27, 2002.

[635] Xiao Su and T Alan Hatton. Electrosorption. *Kirk-Othmer Encyclopedia of Chemical Technology*, pages 1–11, 2016.

[636] JG Gamaethiralalage, K Singh, S Sahin, J Yoon, M Elimelech, ME Suss, P Liang, PM Biesheuvel, R Linzmeyer Zornitta, and LCPM de Smet. Recent advances in ion selectivity with capacitive deionization. *Energy & Environmental Science*, 14(3):1095–1120, 2021.

[637] Yaal Lester, Evyatar Shaulsky, Razi Epsztein, and Ines Zucker. Capacitive deionization for simultaneous removal of salt and uncharged organic contaminants from water. *Separation and Purification Technology*, 237:116388, 2020.

[638] Jae Bong Lee, Kwang Kyu Park, Hee Moon Eum, and Chi Woo Lee. Desalination of a thermal power plant wastewater by membrane capacitive deionization. *Desalination*, 196:125–134, 2006.

[639] Wangwang Tang, Di He, Changyong Zhang, Peter Kovalsky, and T David Waite. Comparison of faradaic reactions in capacitive deionization (cdi) and membrane capacitive deionization (mcdi) water treatment processes. *Water research*, 120:229–237, 2017.

[640] S Porada, Li Zhang, and JE Dykstra. Energy consumption in membrane capacitive deionization and comparison with reverse osmosis. *Desalination*, 488:114383, 2020.

[641] Jialin Yang, Ya Bu, Fangyuan Liu, Wenqing Zhang, Dandi Cai, Aodi Sun, Yuqi Wu, Rui Zhou, and Chunpeng Zhang. Potential application of membrane capacitive deionization for heavy metal removal from water: A minireview. *Int. J. Electrochem. Sci*, 15:7848–7859, 2020.

[642] Sung-il Jeon, Hong-ran Park, Jeong-gu Yeo, SeungCheol Yang, Churl Hee Cho, Moon Hee Han, and Dong Kook Kim. Desalination via a new membrane capacitive deionization process utilizing flow-electrodes. *Energy & Environmental Science*, 6(5):1471–1475, 2013.

[643] Jinxing Ma, Calvin He, Di He, Changyong Zhang, and T David Waite. Analysis of capacitive and electrodialytic contributions to water desalination by flow-electrode cdi. *Water research*, 144:296–303, 2018.

[644] Changyong Zhang, Di He, Jinxing Ma, Wangwang Tang, and T David Waite. Comparison of faradaic reactions in flow-through and flow-by capacitive deionization (cdi) systems. *Electrochimica Acta*, 299:727–735, 2019.

[645] G J Doornbusch, J E Dykstra, P M Biesheuvel, and M E Suss. Fluidized bed electrodes with high carbon loading for water desalination by capacitive deionization. *Journal of Materials Chemistry A*, 4(10):3642–3647, 2016.

[646] Xudong Zhang, Kuichang Zuo, Xiaori Zhang, Changyong Zhang, and Peng Liang. Selective ion separation by capacitive deionization (cdi) based technologies: a state-of-the-art review. *Environmental Science: Water Research & Technology*, 6(2):243–257, 2020.

[647] Matthew E Suss, Theodore F Baumann, William L Bourcier, Christopher M Spadaccini, Klint A Rose, Juan G Santiago, and Michael Stadermann. Capacitive desalination with flow-through electrodes. *Energy & Environmental Science*, 5(11):9511–9519, 2012.

[648] E Marielle Remillard, Amit N Shocron, John Rahill, Matthew E Suss, and Chad D Vecitis. A direct comparison of flow-by and flow-through capacitive deionization. *Desalination*, 444:169–177, 2018.

[649] Johan Nordstrand and Joydeep Dutta. Design principles for enhanced upscaling of flow-through capacitive deionization for water desalination. *Desalination*, 500, 2021.

[650] Raylin Chen, Thomas Sheehan, Jing Lian Ng, Matthew Brucks, and Xiao Su. Capacitive deionization and electrosorption for heavy metal removal. *Environmental Science: Water Research & Technology*, 6(2):258–282, 2020.

[651] Eric N Guyes, Amit N Shocron, Yinke Chen, Charles E Diesendruck, and Matthew E Suss. Long-lasting, monovalent-selective capacitive deionization electrodes. *npj Clean Water*, 4(1):22, 2021.

[652] R Zhao, M Van Soestbergen, HHM Rijnaarts, A Van der Wal, MZ Bazant, and PM Biesheuvel. Time-dependent ion selectivity in capacitive charging of porous electrodes. *Journal of colloid and interface science*, 384(1):38–44, 2012.

[653] Matthew E Suss. Size-based ion selectivity of micropore electric double layers in capacitive deionization electrodes. *Journal of The Electrochemical Society*, 164(9):E270, 2017.

[654] Yuan Zhang, Jiaxing Peng, Guang Feng, and Volker Presser. Hydration shell energy barrier differences of sub-nanometer carbon pores enable ion sieving and selective ion removal. *Chemical Engineering Journal*, 419:129438, 2021.

[655] Diego I. Oyarzun, Ali Hemmatifar, James W. Palko, Michael Stadermann, and Juan G. Santiago. Ion selectivity in capacitive deionization with functionalized electrode: Theory and experimental validation. *Water Research X*, 1:100008, 2018.

[656] Changyong Zhang, Di He, Jinxing Ma, Wangwang Tang, and T David Waite. Faradaic reactions in capacitive deionization (cdi)-problems and possibilities: A review. *Water research*, 128:314–330, 2018.

[657] Hansun Yoon, Jiho Lee, Seoni Kim, and Jeyong Yoon. Review of concepts and applications of electrochemical ion separation (eions) process. *Separation and Purification Technology*, 215:190–207, 2019.

[658] David C Grahame. The electrical double layer and the theory of electrocapillarity. *Chemical reviews*, 41(3):441–501, 1947.

[659] Robert De Levie. On porous electrodes in electrolyte solutions: I. capacitance effects. *Electrochimica acta*, 8(10):751–780, 1963.

[660] Ryan Burt, Greg Birkett, and XS Zhao. A review of molecular modelling of electric double layer capacitors. *Physical Chemistry Chemical Physics*, 16(14):6519–6538, 2014.

[661] A. M. Johnson and John Newman. Desalting by Means of Porous Carbon Electrodes. *Journal of The Electrochemical Society*, 118(3):510, 1971.

[662] Martin Z Bazant, Katsuyo Thornton, and Armand Ajdari. Diffuse-charge dynamics in electrochemical systems. *Physical review E*, 70(2):021506, 2004.

[663] Laurits Højgaard Olesen, Martin Z Bazant, and Henrik Bruus. Strongly nonlinear dynamics of electrolytes in large ac voltages. *Physical Review E*, 82(1):011501, 2010.

[664] PM Biesheuvel and MZ Bazant. Nonlinear dynamics of capacitive charging and desalination by porous electrodes. *Physical review E*, 81(3):031502, 2010.

[665] Mohammad Mirzadeh, Frederic Gibou, and Todd M Squires. Enhanced charging kinetics of porous electrodes: Surface conduction as a short-circuit mechanism. *Physical review letters*, 113(9):097701, 2014.

[666] PM Biesheuvel, Yeqing Fu, and Martin Z Bazant. Diffuse charge and faradaic reactions in porous electrodes. *Physical Review E*, 83(6):061507, 2011.

[667] PM Biesheuvel, Yeqing Fu, and MZ Bazant. Electrochemistry and capacitive charging of porous electrodes in asymmetric multicomponent electrolytes. *Russian Journal of Electrochemistry*, 48(6):580–592, 2012.

[668] PM Biesheuvel, S Porada, M Levi, and Martin Z Bazant. Attractive forces in microporous carbon electrodes for capacitive deionization. *Journal of solid state electrochemistry*, 18(5):1365–1376, 2014.

[669] Amit N Shocron and Matthew E Suss. The effect of surface transport on water desalination by porous electrodes undergoing capacitive charging. *Journal of Physics: Condensed Matter*, 29(8):084003, 2017.

[670] S Porada, D Weingarth, H V M Hamelers, M Bryjak, V Presser, and P M Biesheuvel. Carbon flow electrodes for continuous operation of capacitive deionization and capacitive mixing energy generation. *Journal of Materials Chemistry A*, 2(24):9313–9321, 2014.

[671] Jorge Gabitto and Costas Tsouris. Volume averaging study of the capacitive deionization process in homogeneous porous media. *Transport in Porous Media*, 109(1):61–80, 2015.

[672] P.M. Biesheuvel, R Zhao, S Porada, and A Van der Wal. Theory of membrane capacitive deionization including the effect of the electrode pore space. *Journal of colloid and interface science*, 360(1):239–248, 2011.

[673] S Porada, M Bryjak, A Van Der Wal, and PM Biesheuvel. Effect of electrode thickness variation on operation of capacitive deionization. *Electrochimica Acta*, 75:148–156, 2012.

[674] Li Wang, PM Biesheuvel, and Shihong Lin. Reversible thermodynamic cycle analysis for capacitive deionization with modified donnan model. *Journal of colloid and interface science*, 512:522–528, 2018.

[675] A N Shocron and M E Suss. Should we pose a closure problem for capacitive charging of porous electrodes? *EPL (Europhysics Letters)*, 130(3):34003, jun 2020.

[676] Akpor OB and M Muchie. Remediation of heavy metals in drinking water and wastewater treatment systems: Processes and applications. *Int. J. Phys. Sci.*, 5(12):1807–1817, 2010.

[677] Veena Chaudhary, Mukesh Kumar, Mukesh Sharma, and BS Yadav. Fluoride, boron and nitrate toxicity in ground water of northwest rajasthan, india. *Environmental monitoring and assessment*, 161(1-4):343–348, 2010.

[678] Chaitali V Mohod and Jayashree Dhote. Review of heavy metals in drinking water and their effect on human health. *International Journal of Innovative Research in Science, Engineering and Technology*, 2(7):2992–2996, 2013.

[679] Pei Xu, JÃ¶rg E. Drewes, Dean Heil, and Gary Wang. Treatment of brackish produced water using carbon aerogel-based capacitive deionization technology. *Water Research*, 42(10):2605–2617, 2008.

[680] Romain Broséus, John Cigana, Benoit Barbeau, Catherine Daines-Martinez, and HervÃ© Suty. Removal of total dissolved solids, nitrates and ammonium ions from drinking water using charge-barrier capacitive deionisation. *Desalination*, 249(1):217–223, 2009.

[681] Haibo Li, Linda Zou, Likun Pan, and Zhuo Sun. Using graphene nano-flakes as electrodes to remove ferric ions by capacitive deionization. *Separation and Purification Technology*, 75(1):8–14, 2010.

[682] Yu-Jin Kim and Jae-Hwan Choi. Selective removal of nitrate ion using a novel composite carbon electrode in capacitive deionization. *Water Research*, 46(18):6033–6039, 2012.

[683] Mohamed Mossad and Linda Zou. A study of the capacitive deionisation performance under various operational conditions. *Journal of Hazardous Materials*, 213–214(0):491–497, 2012.

[684] Yu-Jin Kim, Jin-Hyun Kim, and Jae-Hwan Choi. Selective removal of nitrate ions by controlling the applied current in membrane capacitive deionization (mcdi). *Journal of Membrane Science*, 429(0):52–57, 2013.

[685] C. Macías, P. Lavela, G. Rasines, M. C. Zafra, J. L. Tirado, and C. O. Ania. Improved electro-assisted removal of phosphates and nitrates using mesoporous carbon aerogels with controlled porosity. *Journal of Applied Electrochemistry*, 44(8):963–976, 2014.

[686] Haitao Wang and Chongzheng Na. Binder-free carbon nanotube electrode for electrochemical removal of chromium. *ACS Applied Materials & Interfaces*, 6(22):20309–20316, 2014.

[687] Wangwang Tang, Peter Kovalsky, Baichuan Cao, and T. David Waite. Investigation of fluoride removal from low-salinity groundwater by single-pass constant-voltage capacitive deionization. *Water Research*, 99:112–121, 2016.

[688] Wangwang Tang, Peter Kovalsky, Di He, and T. David Waite. Fluoride and nitrate removal from brackish groundwaters by batch-mode capacitive deionization. *Water Research*, 84(Supplement C):342–349, 2015.

[689] Zhe Huang, Lu Lu, Zhenxiao Cai, and Zhiyong Jason Ren. Individual and competitive removal of heavy metals using capacitive deionization. *Journal of Hazardous Materials*, 302:323–331, 2016.

[690] Julio J. Lado, Rodolfo E. PÃ©rez-Roa, Jesse J. Wouters, M. Isabel Tejedor-Tejedor, Cade Federspill, Juan M. Ortiz, and Marc A. Anderson. Removal of nitrate by asymmetric capacitive deionization. *Separation and Purification Technology*, 183(Supplement C):145–152, 2017.

[691] Chengzhi Hu, Jingjing Dong, Ting Wang, Ruiping Liu, Huijuan Liu, and Jiuhui Qu. Nitrate electro-sorption/reduction in capacitive deionization using a novel pd/nial-layered metal oxide film electrode. *Chemical Engineering Journal*, 335(Supplement C):475–482, 2018.

[692] Dong-Hee Lee, Taegong Ryu, Junho Shin, Jae Chun Ryu, Kang-Sup Chung, and Young Ho Kim. Selective lithium recovery from aqueous solution using a modified membrane capacitive deionization system. *Hydrometallurgy*, 173:283–288, 2017.

[693] Wenhui Shi, Xiaoyue Liu, Chenzeng Ye, Xiehong Cao, Congjie Gao, and Jiangnan Shen. Efficient lithium extraction by membrane capacitive deionization incorporated with monovalent selective cation exchange membrane. *Separation and Purification Technology*, 210:885–890, 2019.

[694] Eric N. Guyes, Tahel Malka, and Matthew E. Suss. Enhancing the ion-size-based selectivity of capacitive deionization electrodes. *Environmental Science & Technology*, 53:8447–8454, 2019.

[695] Yuncheol Ha, Hye Bin Jung, Hyunseung Lim, Pil Sung Jo, Hana Yoon, Chung Yul Yoo, Tuan Kiet Pham, Wook Ahn, and Younghyun Cho. Continuous lithium extraction from aqueous solution using flow-electrode capacitive deionization. *Energies*, 12(15), 2019.

[696] Anna Siekierka, Barbara Tomaszewska, and Marek Bryjak. Lithium capturing from geothermal water by hybrid capacitive deionization. *Desalination*, 436:8–14, 2018.

[697] Anna Siekierka and Marek Bryjak. Novel anion exchange membrane for concentration of lithium salt in hybrid capacitive deionization. *Desalination*, 452:279–289, 2019.

[698] Anna Siekierka and Marek Bryjak. Selective sorbents for recovery of lithium ions by hybrid capacitive deionization. *Desalination*, 520:115324, 2021.

[699] Byeongkyu Kim, Jung Yong Seo, and Chan-Hwa Chung. Electrochemical Desalination and Recovery of Lithium from Saline Water upon Operation of a Capacitive Deionization Cell Combined with a Redox Flow Battery. *ACS ES&T Water*, 1(4):1047–1054, apr 2021.

[700] Bin Hu, Xiaohong Shang, Pengfei Nie, Boshuang Zhang, Jianmao Yang, and Jianyun Liu. Lithium ion sieve modified three-dimensional graphene electrode for selective extraction of lithium by capacitive deionization. *Journal of Colloid and Interface Science*, 612:392–400, apr 2022.

[701] Xin Huang, Di He, Wangwang Tang, Peter Kovalsky, and T. David Waite. Investigation of pH-dependent phosphate removal from wastewaters by membrane capacitive deionization (MCDI). *Environmental Science: Water Research and Technology*, 3(5), 2017.

[702] Jiaxi Jiang, David Inhyuk Kim, Pema Dorji, Sherub Phuntsho, Seungkwan Hong, and Ho Kyong Shon. Phosphorus removal mechanisms from domestic wastewater by membrane capacitive deionization and system optimization for enhanced phosphate removal. *Process Safety and Environmental Protection*, 126, 2019.

[703] Changyong Zhang, Xiang Cheng, Min Wang, Jinxing Ma, Richard Collins, Andrew Kinsela, Ying Zhang, and T. David Waite. Phosphate recovery as vivianite using a flow-electrode capacitive desalination (FCDI) and fluidized bed crystallization (FBC) coupled system. *Water Research*, 194, 2021.

[704] Changyong Zhang, Min Wang, Wei Xiao, Jinxing Ma, Jingyi Sun, Hengliang Mo, and T. David Waite. Phosphate selective recovery by magnetic iron oxide impregnated carbon flow-electrode capacitive deionization (FCDI). *Water Research*, 189, 2021.

[705] A.N. Shocron, E.N. Guyes, P.M. Biesheuvel, H.H.M. Rijnaarts, M.E. Suss, and J.E. Dykstra. Electrochemical removal of amphoteric ions. *Proceedings of the National Academy of Sciences*, 118(40):e2108240118, 2021.

[706] Rafael L. Zornitta, Luis A.M. Ruotolo, and Louis C.P.M. de Smet. High-Performance Carbon Electrodes Modified with Polyaniline for Stable and Selective Anion Separation. *Separation and Purification Technology*, 290:120807, jun 2022.

[707] Yu Jin Kim, Jin Hyun Kim, and Jae Hwan Choi. Selective removal of nitrate ions by controlling the applied current in membrane capacitive deionization (MCDI). *Journal of Membrane Science*, 429:52–57, feb 2013.

[708] Changyong Zhang, Jinxing Ma, Jingke Song, Calvin He, and T. David Waite. Continuous Ammonia Recovery from Wastewaters Using an Integrated Capacitive Flow Electrode Membrane Stripping System. *Environmental Science and Technology*, 52(24):14275–14285, 2018.

[709] Kuo Fang, Hui Gong, Wenyan He, Fei Peng, Conghui He, and Kaijun Wang. Recovering ammonia from municipal wastewater by flow-electrode capacitive deionization. *Chemical Engineering Journal*, 348, 2018.

[710] Diego I. Oyarzun, Ali Hemmatifar, James W. Palko, Michael Stadermann, and Juan G. Santiago. Adsorption and capacitive regeneration of nitrate using inverted capacitive deionization with surfactant functionalized carbon electrodes. *Separation and Purification Technology*, 194:410–415, apr 2018.

[711] Changyong Zhang, Jinxing Ma, and T. David Waite. Ammonia-Rich Solution Production from Wastewaters Using Chemical-Free Flow-Electrode Capacitive Deionization. *ACS Sustainable Chemistry and Engineering*, 7(7):6480–6485, 2019.

[712] Hacer Sakar, Isıl Celik, Cigdem Balcik-Canbolat, Bulent Keskinler, and Ahmet Karagunduz. Ammonium removal and recovery from real digestate wastewater by a modified operational method of membrane capacitive deionization unit. *Journal of Cleaner Production*, 215:1415–1423, 2019.

[713] Ling Gan, Yifan Wu, Haiou Song, Shupeng Zhang, Chang Lu, Shuang Yang, Zheng Wang, Bicun Jiang, Changming Wang, and Aimin Li. Selective removal of nitrate ion using a novel activated carbon composite carbon electrode in capacitive deionization. *Separation and Purification Technology*, 212:728–736, 2019.

[714] Kuo Fang, Wenyan He, Fei Peng, and Kaijun Wang. Ammonia recovery from concentrated solution by designing novel stacked FCDI cell. *Separation and Purification Technology*, 250, 2020.

[715] M. Pasta, C.D. Wessells, Y. Cui, and F. La Mantia. A desalination battery. *Nano letters*, 12(2):839–843, 2012.

[716] Chia-Hung Hou and Cheng-Ye Huang. A comparative study of electrosorption selectivity of ions by activated carbon electrodes in capacitive deionization. *Desalination*, 314(0):124–129, 2013.

[717] Jin-Hee Yeo and Jae-Hwan Choi. Enhancement of nitrate removal from a solution of mixed nitrate, chloride and sulfate ions using a nitrate-selective carbon electrode. *Desalination*, 320(0):10–16, 2013.

[718] Seonghwan Kim, Hansun Yoon, Dongyoon Shin, Jaehan Lee, and Jeyong Yoon. Electrochemical selective ion separation in capacitive deionization with sodium manganese oxide. *Journal of Colloid and Interface Science*, 506(Supplement C):644–648, 2017.

[719] J. Lee, S. Kim, and J. Yoon. Rocking chair desalination battery based on prussian blue electrodes. *Acs Omega*, 2(4):1653–1659, 2017.

[720] Steven A Hawks, Maira R Cerón, Diego I Oyarzun, Tuan Anh Pham, Cheng Zhan, Colin K Loeb, Daniel Mew, Amanda Deinhart, Brandon C Wood, Juan G Santiago, Michael Stadermann, and Patrick G Campbell. Using ultramicroporous carbon for the selective removal of nitrate with capacitive deionization. *Environmental Science & Technology*, 53(18):10863–10870, sep 2019.

[721] Qianqian Dong, Xiaoru Guo, Xingkang Huang, Lianjun Liu, Rebecca Tallon, Bruce Taylor, and Junhong Chen. Selective removal of lead ions through capacitive deionization: Role of ion-exchange membrane. *Chemical Engineering Journal*, 361:1535–1542, 2019.

[722] Seok Jun Seo, Hongrae Jeon, Jae Kwang Lee, Gha Young Kim, Daewook Park, Hideo Nojima, Jaeyoung Lee, and Seung Hyeon Moon. Investigation on removal of hardness ions by capacitive deionization (CDI) for water softening applications. *Water Research*, 44(7):2267–2275, 2010.

[723] Armineh Hassanvand, George Q. Chen, Paul A. Webley, and Sandra E. Kentish. A comparison of multicomponent electrosorption in capacitive deionization and membrane capacitive deionization. *Water Research*, 131:100–109, mar 2018.

[724] Sevil Sahin, Han Zuilhof, Rafael L. Zornitta, and Louis C.P.M. de Smet. Enhanced monovalent over divalent cation selectivity with polyelectrolyte multilayers in membrane capacitive deionization via optimization of operational conditions. *Desalination*, 522:115391, jan 2022.

[725] Eran Avraham, Bouhadana Yaniv, Abraham Soffer, and Doron Aurbach. Developing ion electroadsorption stereoselectivity, by pore size adjustment

with chemical vapor deposition onto active carbon fiber electrodes. case of ca2+/na+ separation in water capacitive desalination. *The Journal of Physical Chemistry C*, 112(19):7385–7389, 2008.

[726] Malachi Noked, Eran Avraham, Yaniv Bohadana, Abraham Soffer, and Doron Aurbach. Development of anion stereoselective, activated carbon molecular sieve electrodes prepared by chemical vapor deposition. *The Journal of Physical Chemistry C*, 113(17):7316–7321, 2009.

[727] Maira R. Cerón, Fikret Aydin, Steven A. Hawks, Diego I. Oyarzun, Colin K. Loeb, Amanda Deinhart, Cheng Zhan, Tuan Anh Pham, Michael Stadermann, and Patrick G. Campbell. Cation Selectivity in Capacitive Deionization: Elucidating the Role of Pore Size, Electrode Potential, and Ion Dehydration. *ACS Applied Materials and Interfaces*, 12(38):42644–42652, 2020.

[728] Linchen Han, K. G. Karthikeyan, Marc A. Anderson, and Kelvin B. Gregory. Exploring the impact of pore size distribution on the performance of carbon electrodes for capacitive deionization. *Journal of Colloid and Interface Science*, 430(Supplement C):93–99, 2014.

[729] Linoam Eliad, Gregory Salitra, Abraham Soffer, and Doron Aurbach. Ion sieving effects in the electrical double layer of porous carbon electrodes: Estimating effective ion size in electrolytic solutions. *The Journal of Physical Chemistry B*, 105(29):6880–6887, 2001.

[730] Christopher J. Gabelich, Tri D. Tran, and I. H. Suffet. Electrosorption of inorganic salts from aqueous solution using carbon aerogels. *Environmental Science & Technology*, 36(13):3010–3019, 2002.

[731] Chia-Hung Hou, Taboada-Serrano Patricia, S. Yiacoumi, and C. Tsouris. Electrosorption selectivity of ions from mixtures of electrolytes inside nanopores. *The Journal of Chemical Physics*, 129:224703–224709, 2008.

[732] J.E. Dykstra, J. Dijkstra, A. van der Wal, H.V.M. Hamelers, and S. Porada. On-line method to study dynamics of ion adsorption from mixtures of salts in capacitive deionization. *Desalination*, 390:47–52, jul 2016.

[733] Rahul Prasanna Misra, J Pedro de Souza, Daniel Blankschtein, and Martin Z Bazant. Theory of surface forces in multivalent electrolytes. *Langmuir*, 35(35):11550–11565, 2019.

[734] Yan Levin. Electrostatic correlations: from plasma to biology. *Reports on progress in physics*, 65(11):1577, 2002.

[735] Roland Roth. Fundamental measure theory for hard-sphere mixtures: a review. *Journal of Physics: Condensed Matter*, 22(6):063102, 2010.

[736] J Pedro de Souza, Zachary AH Goodwin, Michael McEldrew, Alexei A Kornyshev, and Martin Z Bazant. Interfacial layering in the electric double layer of ionic liquids. *Physical Review Letters*, 125(11):116001, 2020.

[737] Wangwang Tang, Peter Kovalsky, Baichuan Cao, Di He, and T David Waite. Fluoride removal from brackish groundwaters by constant current capacitive deionization (cdi). *Environmental Science & Technology*, 50(19):10570–10579, 2016.

[738] Zhaolin Chen, Hongtao Zhang, Chunxu Wu, Yushuang Wang, and Wei Li. A study of electrosorption selectivity of anions by activated carbon electrodes in capacitive deionization. *Desalination*, 369:46–50, 2015.

[739] Yingzhen Li, Chang Zhang, Yanping Jiang, Ting-Jie Wang, and Haifeng Wang. Effects of the hydration ratio on the electrosorption selectivity of ions during capacitive deionization. *Desalination*, 399(Supplement C):171–177, 2016.

[740] T M Mubita, J E Dykstra, P M Biesheuvel, A van der Wal, and S Porada. Selective adsorption of nitrate over chloride in microporous carbons. *Water Research*, 164:114885, 2019.

[741] E R Nightingale. Phenomenological Theory of Ion Solvation. Effective Radii of Hydrated Ions. *Journal of Physical Chemistry*, 63(9):1381–1387, 1959.

[742] Steven A. Hawks, Ashwin Ramachandran, Slawomir Porada, Patrick G. Campbell, Matthew E. Suss, P. M. Biesheuvel, Juan G. Santiago, and Michael Stadermann. Performance Metrics for the Objective Assessment of Capacitive Deionization Systems. *Water Research*, pages 126–137, 2019.

[743] Slawomir Porada, Aniruddh Shrivastava, Pamela Bukowska, P. M. Biesheuvel, and Kyle C. Smith. Nickel hexacyanoferrate electrodes for continuous cation intercalation desalination of brackish water. *Electrochimica Acta*, 255(Supplement C):369–378, 2017.

[744] Taeyoung Kim, Christopher A Gorski, and Bruce E Logan. Ammonium Removal from Domestic Wastewater Using Selective Battery Electrodes. *Environmental Science & Technology Letters*, 5(9):578–583, sep 2018.

[745] Jongmoon Choi, Hyunkyung Lee, and Seungkwan Hong. Capacitive deionization (CDI) integrated with monovalent cation selective membrane for producing divalent cation-rich solution. *Desalination*, 400:38–46, 2016.

[746] Kaustub Singh, Zexin Qian, P.M. Biesheuvel, Han Zuilhof, Slawomir Porada, and Louis C.P.M. de Smet. Nickel hexacyanoferrate electrodes for high mono/divalent ion-selectivity in capacitive deionization. *Desalination*, 481(November 2019):114346, 2020.

[747] Yingsheng Xu, Hongjian Zhou, Guozhong Wang, Yunxia Zhang, Haimin Zhang, and Huijun Zhao. Selective Pseudocapacitive Deionization of Calcium Ions in Copper Hexacyanoferrate. *ACS Applied Materials & Interfaces*, 12(37):41437–41445, sep 2020.

[748] Xiaohong Shang, Bin Hu, Pengfei Nie, Wei Shi, Taimoor Hussain, and Jianyun Liu. LiNi0.5Mn1.5O4-based hybrid capacitive deionization for highly selective adsorption of lithium from brine. *Separation and Purification Technology*, 258:118009, 2021.

[749] Kuichang Zuo, Jun Kim, Amit Jain, Tianxiao Wang, Rafael Verduzco, Mingce Long, and Qilin Li. Novel Composite Electrodes for Selective Removal of Sulfate by the Capacitive Deionization Process. *Environmental Science & Technology*, 52(16):9486–9494, aug 2018.

[750] Junjun Chang, Yuping Li, Feng Duan, Chunlei Su, Yujiao Li, and Hongbin Cao. Selective removal of chloride ions by bismuth electrode in capacitive deionization. *Separation and Purification Technology*, 240:116600, 2020.

[751] Ji Sun Kim, Yi Seul Jeon, and Ji Won Rhim. Application of poly(vinyl alcohol) and polysulfone based ionic exchange polymers to membrane capacitive deionization for the removal of mono- and divalent salts. *Separation and Purification Technology*, 157(Supplement C):45–52, 2016.

[752] Wangwang Tang, Di He, Changyong Zhang, and T. David Waite. Optimization of sulfate removal from brackish water by membrane capacitive deionization (mcdi). *Water Research*, 121(Supplement C):302–310, 2017.

[753] Rana Uwayid, Eric N. Guyes, Amit N. Shocron, Jack Gilron, Menachem Elimelech, and Matthew E. Suss. Perfect divalent cation selectivity with capacitive deionization. *Water Research*, 210:117959, feb 2022.

[754] R. Zhao, P. M. Biesheuvel, and a. van der Wal. Energy consumption and constant current operation in membrane capacitive deionization. *Energy & Environmental Science*, 5(11):9520–9527, 2012.

[755] Complementary surface charge for enhanced capacitive deionization. *Water Research*, 92:275–282, 2016.

[756] Ali Hemmatifar, Michael Stadermann, and Juan G. Santiago. Two-Dimensional Porous Electrode Model for Capacitive Deionization. *Journal of Physical Chemistry C*, 119(44):24681–24694, 2015.

[757] Yatian Qu, Theodore F. Baumann, Juan G. Santiago, and Michael Stadermann. Characterization of Resistances of a Capacitive Deionization System. *Environmental Science & Technology*, 49(16):9699–9706, aug 2015.

[758] J.E. Dykstra, R. Zhao, P.M. Biesheuvel, and A. van der Wal. Resistance identification and rational process design in Capacitive Deionization. *Water Research*, 88:358–370, jan 2016.

[759] Yatian Qu, Patrick G. Campbell, Lei Gu, Jennifer M. Knipe, Ella Dzenitis, Juan G. Santiago, and Michael Stadermann. Energy consumption analysis of constant voltage and constant current operations in capacitive deionization. *Desalination*, 400:18–24, 2016.

[760] J. E. Dykstra, S. Porada, A. van der Wal, and P. M. Biesheuvel. Energy consumption in capacitive deionization – Constant current versus constant voltage operation. *Water Research*, 143:367–375, 2018.

[761] Ali Hemmatifar, Ashwin Ramachandran, Kang Liu, Diego I. Oyarzun, Martin Z. Bazant, and Juan G. Santiago. Thermodynamics of Ion Separation by Electrosorption. *Environmental Science and Technology*, 52:10196–10204, 2018.

[762] Steven A. Hawks, Jennifer M. Knipe, Patrick G. Campbell, Colin K. Loeb, McKenzie A. Hubert, Juan G. Santiago, and Michael Stadermann. Quantifying the flow efficiency in constant-current capacitive deionization. *Water Research*, 129:327–336, feb 2018.

[763] Li Wang and Shihong Lin. Intrinsic tradeoff between kinetic and energetic efficiencies in membrane capacitive deionization. *Water Research*, 129:394–401, feb 2018.

[764] Ashwin Ramachandran, Diego I Oyarzun, Steven A Hawks, Michael Stadermann, and Juan G Santiago. High water recovery and improved thermodynamic efficiency for capacitive deionization using variable flowrate operation. *Water research*, 155:76–85, 2019.

[765] Li Wang, J. E. Dykstra, and Shihong Lin. Energy Efficiency of Capacitive Deionization. *Environmental Science & Technology*, 53(7):3366–3378, apr 2019.

[766] Shihong Lin. Energy Efficiency of Desalination: Fundamental Insights from Intuitive Interpretation. *Environmental Science and Technology*, 54(1):76–84, dec 2020.

[767] Mohammad Alkuran and Mohamed Orabi. Utilization of a buck boost converter and the method of segmented capacitors in a CDI water purification system. In *2008 12th International Middle-East Power System Conference*, pages 470–474. IEEE, mar 2008.

[768] A. M. Pernía, J. G. Norniella, J. A. Martín-Ramos, J. Díaz, and J. A. Martínez. Up–Down Converter for Energy Recovery in a CDI Desalination System. *IEEE Transactions on Power Electronics*, 27(7):3257–3265, jul 2012.

[769] A. M. Pernía, F. J. Alvarez-Gonzalez, Miguel A. J. Prieto, Pedro J. Villegas, and F. Nuno. New Control Strategy of an Up–Down Converter for Energy Recovery in a CDI Desalination System. *IEEE Transactions on Power Electronics*, 29(7):3573–3581, jul 2014.

[770] Piotr Długołęcki and Albert Van Der Wal. Energy recovery in membrane capacitive deionization. *Environmental Science and Technology*, 47(9):4904–4910, 2013.

[771] Junil Kang, Taeyoung Kim, Hojoon Shin, Jiho Lee, Jung-Ik Ha, and Jeyong Yoon. Direct energy recovery system for membrane capacitive deionization. *Desalination*, 398:144–150, nov 2016.

[772] Diego I. Oyarzun, Steve A. Hawks, Patrick G. Campbell, Ali Hemmatifar, Ashish Krishna, Juan G. Santiago, and Michael Stadermann. Energy transfer for storage or recovery in capacitive deionization using a DC-DC converter. *Journal of Power Sources*, 448:227409, 2020.

[773] Wei Zhang, Mohamed Mossad, Javad Sadoghi Yazdi, and Linda Zou. A statistical experimental investigation on arsenic removal using capacitive deionization. *Desalination and Water Treatment*, 57(7):3254–3260, feb 2014.

[774] Tingting Wu, Gang Wang, Qiang Dong, Fei Zhan, Xu Zhang, Shaofeng Li, Huiying Qiao, and Jieshan Qiu. Starch Derived Porous Carbon Nanosheets for High-Performance Photovoltaic Capacitive Deionization. *Environmental Science and Technology*, 51(16):9244–9251, aug 2017.

[775] Cheng Tan, Calvin He, Wangwang Tang, Peter Kovalsky, John Fletcher, and T. David Waite. Integration of photovoltaic energy supply with membrane capacitive deionization (MCDI) for salt removal from brackish waters. *Water Research*, 147, 2018.

[776] Steven Hand, Jeremy S. Guest, and Roland D. Cusick. Technoeconomic Analysis of Brackish Water Capacitive Deionization: Navigating Tradeoffs between Performance, Lifetime, and Material Costs. *Environmental Science & Technology*, 53(22):13353–13363, nov 2019.

[777] Junil Kang, Taeyoung Kim, Kyusik Jo, and Jeyong Yoon. Comparison of salt adsorption capacity and energy consumption between constant current and constant voltage operation in capacitive deionization. *Desalination*, 352:52–57, nov 2014.

[778] Eran Avraham, Malachi Noked, Yaniv Bouhadana, Abraham Soffer, and Doron Aurbach. Limitations of charge efficiency in capacitive deionization: Ii. on the behavior of cdi cells comprising two activated carbon electrodes. *Journal of the Electrochemical Society*, 156(10):P157, 2009.

[779] Eran Avraham, Malachi Noked, Yaniv Bouhadana, Abraham Soffer, and Doron Aurbach. Limitations of charge efficiency in capacitive deionization processes III: The behavior of surface oxidized activated carbon electrodes. *Electrochimica Acta*, 56(1):441–447, dec 2010.

[780] S. Shanbhag, J. F. Whitacre, and M. S. Mauter. The Origins of Low Efficiency in Electrochemical De-Ionization Systems. *Journal of The Electrochemical Society*, 163(14):E363–E371, oct 2016.

[781] Martin Z Bazant. Theory of chemical kinetics and charge transfer based on nonequilibrium thermodynamics. *Accounts of chemical research*, 46(5):1144–1160, 2013.

[782] Yaniv Bouhadana, Eran Avraham, Malachi Noked, Moshe Ben-Tzion, Abraham Soffer, and Doron Aurbach. Capacitive deionization of NaCl solutions at non-steady-state conditions: Inversion functionality of the carbon electrodes. *Journal of Physical Chemistry C*, 115(33):16567–16573, 2011.

[783] Nicolas Holubowitch, Ayokunle Omosebi, Xin Gao, James Landon, and Kunlei Liu. Quasi-Steady-State Polarization Reveals the Interplay of Capacitive and Faradaic Processes in Capacitive Deionization. *ChemElectroChem*, 4:2404–2413, 2017.

[784] Di He, Chi Eng Wong, Wangwang Tang, Peter Kovalsky, and T. David Waite. Faradaic Reactions in Water Desalination by Batch-Mode Capacitive Deionization. *Environmental Science & Technology Letters*, 3(5):222–226, 2016.

[785] Rana Uwayid, Nicola M Seraphim, Eric N Guyes, David Eisenberg, and Matthew E Suss. Characterizing and mitigating the degradation of oxidized cathodes during capacitive deionization cycling. *Carbon*, 173:1105–1114, 2021.

[786] Izaak Cohen, Eran Avraham, Malachi Noked, Abraham So, and Doron Aurbach. Enhanced Charge Efficiency in Capacitive Deionization Achieved by Surface-Treated Electrodes and by Means of a Third Electrode. *Journal of Physical Chemistry C*, 115(40):19856–19863, 2011.

[787] Xin Gao, Ayokunle Omosebi, James Landon, and Kunlei Liu. Enhancement of charge efficiency for a capacitive deionization cell using carbon xerogel with modified potential of zero charge. *Electrochemistry Communications*, 39:22–25, feb 2014.

[788] P. M. Biesheuvel, H. V M Hamelers, and M. E. Suss. Theory of Water Desalination by Porous Electrodes with Immobile Chemical Charge. *Colloids and Interface Science Communications*, 9(2015):1–5, 2015.

[789] T. Kim, J.E. Dykstra, S. Porada, A. van der Wal, J. Yoon, and P.M. Biesheuvel. Enhanced charge efficiency and reduced energy use in capacitive deionization by increasing the discharge voltage. *Journal of Colloid and Interface Science*, 446:317–326, may 2015.

[790] Robert McNair, Gyorgy Szekely, and Robert AW Dryfe. Ion-exchange materials for membrane capacitive deionization. *ACS ES&T Water*, 1(2):217–239, 2020.

[791] Xitong Liu, Sneha Shanbhag, Sittichai Natesakhawat, Jay F Whitacre, and Meagan S Mauter. Performance loss of activated carbon electrodes in capacitive deionization: Mechanisms and material property predictors. *Environmental Science & Technology*, 54(23):15516–15526, 2020.

[792] Linchen Han, K. G. Karthikeyan, and Kelvin B. Gregory. Energy Consumption and Recovery in Capacitive Deionization Using Nanoporous Activated Carbon Electrodes. *Journal of The Electrochemical Society*, 162(12):E282–E288, sep 2015.

[793] Mohan Qin, Akshay Deshmukh, Razi Epsztein, Sohum K Patel, Oluwaseye M Owoseni, W Shane Walker, and Menachem Elimelech. Comparison of energy consumption in desalination by capacitive deionization and reverse osmosis. *Desalination*, 455:100–114, 2019.

[794] Mohan Qin, Akshay Deshmukh, Razi Epsztein, Sohum K. Patel, Oluwaseye M. Owoseni, W. Shane Walker, and Menachem Elimelech. Response to comments on "comparison of energy consumption in desalination by capacitive deionization and reverse osmosis". *Desalination*, 462:48–55, 2019.

[795] Ashwin Ramachandran, Diego I Oyarzun, Steven A Hawks, Patrick G Campbell, Michael Stadermann, and Juan G Santiago. Comments on "comparison of energy consumption in desalination by capacitive deionization and reverse osmosis". *Desalination*, 461:30–36, 2019.

[796] Cheng Tan, Calvin He, John Fletcher, and T. David Waite. Energy recovery in pilot scale membrane CDI treatment of brackish waters. *Water Research*, 168:115146, 2020.

[797] Enrique García-Quismondo, Cleis Santos, Jorge Soria, Jesús Palma, and Marc A. Anderson. New Operational Modes to Increase Energy Efficiency in Capacitive Deionization Systems. *Environmental Science and Technology*, 50(11):6053–6060, 2016.

[798] Arun Subramani and Joseph G Jacangelo. Emerging desalination technologies for water treatment: a critical review. *Water research*, 75:164–187, 2015.

[799] Baoping Jia and Wei Zhang. Preparation and application of electrodes in capacitive deionization (cdi): a state-of-art review. *Nanoscale research letters*, 11(1):64, 2016.

[800] Mihai Duduta, Bryan Ho, Vanessa C Wood, Pimpa Limthongkul, Victor E Brunini, W Craig Carter, and Yet-Ming Chiang. Semi-solid lithium rechargeable flow battery. *Advanced Energy Materials*, 1(4):511–516, 2011.

[801] Minjoon Park, Jaechan Ryu, Wei Wang, and Jaephil Cho. Material design and engineering of next-generation flow-battery technologies. *Nature Reviews Materials*, 2(1):1–18, 2016.

[802] Hongning Chen and Yi-Chun Lu. A high-energy-density multiple redox semi-solid-liquid flow battery. *Advanced Energy Materials*, 6(8):1502183, 2016.

[803] Thaneer Malai Narayanan, Yun Guang Zhu, Emre Gençer, Gareth McKinley, and Yang Shao-Horn. Low-cost manganese dioxide semi-solid electrode for flow batteries. *Joule*, 5(11):2934–2954, 2021.

[804] Sung-il Jeon, Jeong-gu Yeo, SeungCheol Yang, Jiyeon Choi, and Dong Kook Kim. Ion storage and energy recovery of a flow-electrode capacitive deionization process. *Journal of Materials Chemistry A*, 2(18):6378–6383, 2014.

[805] Kelsey B Hatzell, Etsuro Iwama, Anais Ferris, Barbara Daffos, Koki Urita, Theodore Tzedakis, Fabien Chauvet, Pierre-Louis Taberna, Yury Gogotsi, and Patrice Simon. Capacitive deionization concept based on suspension electrodes without ion exchange membranes. *Electrochemistry Communications*, 43:18–21, 2014.

[806] Alexandra Rommerskirchen, Youri Gendel, and Matthias Wessling. Single module flow-electrode capacitive deionization for continuous water desalination. *Electrochemistry Communications*, 60:34–37, 2015.

[807] Changyong Zhang, Lei Wu, Jinxing Ma, A. Ninh Pham, Min Wang, and T. David Waite. Integrated Flow-Electrode Capacitive Deionization and Microfiltration System for Continuous and Energy-Efficient Brackish Water Desalination. *Environmental Science and Technology*, 53:13364–13373, 2019.

[808] Alexandra Rommerskirchen, Christian J. Linnartz, Daniel Müller, Lisa Kathrin Willenberg, and Matthias Wessling. Energy Recovery and Process Design in Continuous Flow-Electrode Capacitive Deionization Processes. *ACS Sustainable Chemistry and Engineering*, 6(10):13007–13015, 2018.

[809] Junjun Ma, Peng Liang, Xueliang Sun, Helan Zhang, Yanhong Bian, Fan Yang, Junfei Bai, Qianming Gong, and Xia Huang. Energy recovery from the

flow-electrode capacitive deionization. *Journal of Power Sources*, 421:50–55, 2019.

[810] Changyong Zhang, Jinxing Ma, Lei Wu, Jingyi Sun, Li Wang, Tianyu Li, and T. David Waite. Flow Electrode Capacitive Deionization (FCDI): Recent Developments, Environmental Applications, and Future Perspectives. *Environmental Science and Technology*, 55(8), 2021.

[811] Fan Yang, Yunfei He, Leon Rosentsvit, Matthew E. Suss, Xiaori Zhang, Tie Gao, and Peng Liang. Flow-electrode capacitive deionization: A review and new perspectives. *Water Research*, 200:117222, jul 2021.

[812] Alexandra Rommerskirchen, Christian J Linnartz, Franziska Egidi, Sefkan Kendir, and Matthias Wessling. Flow-electrode capacitive deionization enables continuous and energy-efficient brine concentration. *Desalination*, 490:114453, 2020.

[813] Yanhong Bian, Xi Chen, Lu Lu, Peng Liang, and Zhiyong Jason Ren. Concurrent nitrogen and phosphorus recovery using flow-electrode capacitive deionization. *ACS Sustainable Chemistry & Engineering*, 7(8):7844–7850, 2019.

[814] Longqian Xu, Chao Yu, Shiyu Tian, Yunfeng Mao, Yang Zong, Xiaomeng Zhang, Bing Zhang, Changyong Zhang, and Deli Wu. Selective recovery of phosphorus from synthetic urine using flow-electrode capacitive deionization (fcdi)-based technology. *ACS ES&T Water*, 1(1):175–184, 2020.

[815] Chao Yu, Longqian Xu, Yunfeng Mao, Yang Zong, and Deli Wu. Efficient recovery of carboxylates from the effluents treated by advanced oxidation processes using flow-electrode capacitive deionization in short-circuited closed-cycle operation. *Separation and Purification Technology*, page 119151, 2021.

[816] Kuo Fang, Fei Peng, Erfu San, and Kaijun Wang. The impact of concentration in electrolyte on ammonia removal in flow-electrode capacitive deionization system. *Separation and Purification Technology*, 255:117337, jan 2021.

[817] Hagai Cohen, Shaked Ein Eli, Morten Jõgi, and Matthew E. Suss. Suspension Electrodes Combining Slurries and Upflow Fluidized Beds. *ChemSusChem*, 9(21):3045–3048, 2016.

[818] Paz Nativ, Yuval Badash, and Youri Gendel. New insights into the mechanism of flow-electrode capacitive deionization. *Electrochemistry Communications*, 76:24–28, 2017.

[819] Youri Gendel, Alexandra Klara Elisabeth Rommerskirchen, Oana David, and Matthias Wessling. Batch mode and continuous desalination of water using

flowing carbon deionization (FCDI) technology. *Electrochemistry Communications*, 46:152–156, 2014.

[820] J. Ma, D. He, W. Tang, P. Kovalsky, C. He, C. Zhang, and T.D. Waite. Development of redox-active flow electrodes for high-performance capacitive deionization. *Environmental science & technology*, 50(24):13495–13501, 2016.

[821] SeungCheol Yang, Hong-ran Park, Jungjoon Yoo, Hanki Kim, Jiyeon Choi, Moon Hee Han, and Dong Kook Kim. Plate-Shaped Graphite for Improved Performance of Flow-Electrode Capacitive Deionization. *Journal of The Electrochemical Society*, 164(13):E480–E488, 2017.

[822] Peng Liang, Xueliang Sun, Yanhong Bian, Helan Zhang, Xufei Yang, Yong Jiang, Panpan Liu, and Xia Huang. Optimized desalination performance of high voltage flow-electrode capacitive deionization by adding carbon black in flow-electrode. *Desalination*, 420:63–69, 2017.

[823] Bilen Akuzum, Lutfi Agartan, J Locco, and EC Kumbur. Effects of particle dispersion and slurry preparation protocol on electrochemical performance of capacitive flowable electrodes. *Journal of Applied Electrochemistry*, 47(3):369–380, 2017.

[824] Bilen Akuzum, Pushpendra Singh, Devon A Eichfeld, Lutfi Agartan, Simge Uzun, Yury Gogotsi, and E Caglan Kumbur. Percolation characteristics of conductive additives for capacitive flowable (semi-solid) electrodes. *ACS applied materials & interfaces*, 12(5):5866–5875, 2020.

[825] Elad B. Halfon and Matthew E. Suss. Measurements of the electric conductivity of an electrode as it transitions between static and flowable modes. *Electrochemistry Communications*, 99:61–64, 2019.

[826] Seungcheol Yang, Sung Il Jeon, Hanki Kim, Jiyeon Choi, Jeong Gu Yeo, Hong Ran Park, and Dong Kook Kim. Stack Design and Operation for Scaling Up the Capacity of Flow-Electrode Capacitive Deionization Technology. *ACS Sustainable Chemistry and Engineering*, 4(8):4174–4180, 2016.

[827] Younghyun Cho, Ki Sook Lee, SeungCheol Yang, Jiyeon Choi, Hong-ran Park, and Dong Kook Kim. A novel three-dimensional desalination system utilizing honeycomb-shaped lattice structures for flow-electrode capacitive deionization. *Energy Environ. Sci.*, 10:1746–1750, 2017.

[828] Jinxing Ma, Junjun Ma, Changyong Zhang, Jingke Song, Wenjia Dong, and T David Waite. Flow-electrode capacitive deionization (fcdi) scale-up using a membrane stack configuration. *Water research*, 168:115186, 2020.

[829] Christian J. Linnartz, Alexandra Rommerskirchen, Joanna Walker, Janis Plankermann-Hajduk, Niklas Köller, and Matthias Wessling. Membrane-electrode assemblies for flow-electrode capacitive deionization. *Journal of Membrane Science*, 605:118095, 2020.

[830] Christian J. Linnartz, Alexandra Rommerskirchen, Matthias Wessling, and Youri Gendel. Flow-Electrode Capacitive Deionization for Double Displacement Reactions. *ACS Sustainable Chemistry and Engineering*, 5(5):3906–3912, 2017.

[831] Miao Wang, Shujin Hou, Yong Liu, Xingtao Xu, Ting Lu, Ran Zhao, and Likun Pan. Capacitive neutralization deionization with flow electrodes. *Electrochimica Acta*, 216:211–218, 2016.

[832] Paz Nativ, Ori Lahav, and Youri Gendel. Separation of divalent and monovalent ions using flow-electrode capacitive deionization with nanofiltration membranes. *Desalination*, 425(July 2017):123–129, 2018.

[833] Calvin He, Jinxing Ma, Changyong Zhang, Jingke Song, and T. David Waite. Short-Circuited Closed-Cycle Operation of Flow-Electrode CDI for Brackish Water Softening. *Environmental Science and Technology*, 52(16):9350–9360, 2018.

[834] Jingke Song, Jinxing Ma, Changyong Zhang, Calvin He, and T. David Waite. Implication of non-electrostatic contribution to deionization in flow-electrode CDI: Case study of nitrate removal from contaminated source waters. *Frontiers in Chemistry*, 7(MAR):146, 2019.

[835] Jinxing Ma, Yumeng Zhang, Richard N. Collins, Sergey Tsarev, Noboru Aoyagi, Andrew S. Kinsela, Adele M. Jones, and T. David Waite. Flow-Electrode CDI Removes the Uncharged Ca-UO2-CO3 Ternary Complex from Brackish Potable Groundwater: Complex Dissociation, Transport, and Sorption. *Environmental Science and Technology*, 53(5):2739–2747, 2019.

[836] Huan Jiang, Zhang Jing, Kunyue Luo, Wenle Xing, Jiaxin Du, Yi Dong, Xiaoting Li, and Wangwang Tang. Effective fluoride removal from brackish groundwaters by flow-electrode capacitive deionization (FCDI) under a continuous-flow mode. *Science of The Total Environment*, 804:150166, jan 2022.

[837] Alexandra Rommerskirchen, Michael Alders, Florian Wiesner, Christian J. Linnartz, Anna Kalde, and Matthias Wessling. Process model for high salinity flow-electrode capacitive deionization processes with ion-exchange membranes. *Journal of Membrane Science*, 616:118614, 2020.

[838] Li Wang, Changyong Zhang, Calvin He, T. David Waite, and Shihong Lin. Equivalent film-electrode model for flow-electrode capacitive deionization: Experimental validation and performance analysis. *Water Research*, 181:115917, 2020.

[839] Alexandra Rommerskirchen, Anna Kalde, Christian J. Linnartz, Leon Bongers, Georg Linz, and Matthias Wessling. Unraveling charge transport in carbon flow-electrodes: Performance prediction for desalination applications. *Carbon*, 145:507–520, 2019.

[840] L. Eifert, Z. Jusys, R.J. Behm, and R. Zeis. Side reactions and stability of pre-treated carbon felt electrodes for vanadium redox flow batteries: A dems study. *Carbon*, 158:580–587, 2020.

[841] Izaak Cohen, Eran Avraham, Yaniv Bouhadana, Abraham Soffer, and Doron Aurbach. Long term stability of capacitive de-ionization processes for water desalination: The challenge of positive electrodes corrosion. *Electrochimica Acta*, 106:91–100, 2013.

[842] Bei Li, Tianye Zheng, Sijia Ran, Mingzhe Sun, Jin Shang, Haibo Hu, Po Heng Lee, and Steven T. Boles. Performance Recovery in Degraded Carbon-Based Electrodes for Capacitive Deionization. *Environmental Science and Technology*, 54(3):1848–1856, 2020.

[843] Rana Uwayid, Charles E. Diesendruck, and Matthew E. Suss. Emerging investigator series: a comparison of strong and weak-acid functionalized carbon electrodes in capacitive deionization. *Environmental Science: Water Research & Technology*, 8(5):949–956, may 2022.

[844] Pattarachai Srimuk, Marco Zeiger, Nicolas Jäckel, Aura Tolosa, Benjamin Krüner, Simon Fleischmann, Ingrid Grobelsek, Mesut Aslan, Boris Shvartsev, Matthew E Suss, and Volker Presser. Enhanced performance stability of carbon / titania hybrid electrodes during capacitive deionization of oxygen saturated saline water. *Electrochimica Acta*, 224:314–328, 2017.

[845] Izaak Cohen, Eran Avraham, Yaniv Bouhadana, Abraham Soffer, and Doron Aurbach. The effect of the flow-regime, reversal of polarization, and oxygen on the long term stability in capacitive de-ionization processes. *Electrochimica Acta*, 153:106–114, 2015.

[846] X. Gao, A. Omosebi, J. Landon, and K. Liu. Voltage-Based Stabilization of Microporous Carbon Electrodes for Inverted Capacitive Deionization. *Journal of Physical Chemistry C*, 122(2):1158–1168, 2018.

[847] Ding Lu, Wangfeng Cai, and Yan Wang. Optimization of the voltage window for long-term capacitive deionization stability. *Desalination*, 424:53–61, 2017.

[848] Jae-Hun Lee, Wi-Sup Bae, and Jae-Hwan Choi. Electrode reactions and adsorption/desorption performance related to the applied potential in a capacitive deionization process. *Desalination*, 258(1-3):159–163, 2010.

[849] Xin Gao, Ayokunle Omosebi, James Landon, and Kunlei Liu. Surface charge enhanced carbon electrodes for stable and efficient capacitive deionization using inverted adsorption–desorption behavior. *Energy Environ. Sci.*, 8(3):897–909, 2015.

[850] X. Gao, A. Omosebi, N. Holubowitch, J. Landon, and K. Liu. Capacitive Deionization Using Alternating Polarization: Effect of Surface Charge on Salt Removal. *Electrochimica Acta*, 233:249–255, 2017.

[851] Jaehan Lee, Seoni Kim, Choonsoo Kim, and Jeyong Yoon. Hybrid capacitive deionization to enhance the desalination performance of capacitive techniques. *Energy & Environmental Science*, 7(11):3683–3689, 2014.

[852] Taeyoung Kim, Jihyun Yu, Choonsoo Kim, and Jeyong Yoon. Hydrogen peroxide generation in fl ow-mode capacitive deionization. *Jeac*, 776:101–104, 2016.

[853] Mohamed Mossad and Linda Zou. Study of fouling and scaling in capacitive deionisation by using dissolved organic and inorganic salts. *Journal of hazardous materials*, 244:387–393, 2013.

[854] Wei Zhang, Mohamed Mossad, and Linda Zou. A study of the long-term operation of capacitive deionisation in inland brackish water desalination. *Desalination*, 320:80–85, 2013.

[855] Changming Wang, Haiou Song, Quanxing Zhang, Baijun Wang, and Aimin Li. Parameter optimization based on capacitive deionization for highly efficient desalination of domestic wastewater biotreated effluent and the fouled electrode regeneration. *Desalination*, 365:407–415, 2015.

[856] Xitong Liu, Jay F Whitacre, and Meagan S Mauter. Mechanisms of humic acid fouling on capacitive and insertion electrodes for electrochemical desalination. *Environmental science & technology*, 52(21):12633–12641, 2018.

[857] Tianyu Wang, Changyong Zhang, Langming Bai, Binghan Xie, Zhendong Gan, Jiajian Xing, Guibai Li, and Heng Liang. Scaling behavior of iron in capacitive deionization (cdi) system. *Water research*, 171:115370, 2020.

[858] Tianyu Wang, Langming Bai, Changyong Zhang, Xuewu Zhu, Jiajian Xing, Yuanqing Guo, Jinlong Wang, Dachao Lin, Guibai Li, and Heng Liang. Formation mechanism of iron scale in membrane capacitive deionization (mcdi) system. *Desalination*, 495:114636, 2020.

[859] Lin Chen, Chengyi Wang, Shanshan Liu, Qinzheng Hu, Liang Zhu, and Chuqing Cao. Investigation of the long-term desalination performance of membrane capacitive deionization at the presence of organic foulants. *Chemosphere*, 193:989–997, 2018.

[860] Yanting Li, Ty C Stewart, and Hao L Tang. A comparative study on electrosorptive rates of metal ions in capacitive deionization. *Journal of water process engineering*, 26:257–263, 2018.

[861] Wei Zhang and Baoping Jia. Toward anti-fouling capacitive deionization by using visible-light reduced tio2/graphene nanocomposites. *MRS Communications*, 5(4):613–617, 2015.

[862] Enyu Liu, Lai Yoke Lee, Say Leong Ong, and How Yong Ng. Treatment of industrial brine using capacitive deionization (cdi) towards zero liquid discharge–challenges and optimization. *Water Research*, 183:116059, 2020.

[863] S Porada, L Weinstein, R Dash, A Van Der Wal, M Bryjak, Y Gogotsi, and PM Biesheuvel. Water desalination using capacitive deionization with microporous carbon electrodes. *ACS applied materials & interfaces*, 4(3):1194–1199, 2012.

[864] S Porada, L Borchardt, M Oschatz, M Bryjak, JS Atchison, KJ Keesman, S Kaskel, PM Biesheuvel, and V Presser. Direct prediction of the desalination performance of porous carbon electrodes for capacitive deionization. *Energy & Environmental Science*, 6(12):3700–3712, 2013.

[865] Zheng-Hong Huang, Zhiyu Yang, Feiyu Kang, and Michio Inagaki. Carbon electrodes for capacitive deionization. *Journal of Materials Chemistry A*, 5(2):470–496, 2017.

[866] Paula Ratajczak, Matthew E Suss, Friedrich Kaasik, and François Béguin. Carbon electrodes for capacitive technologies. *Energy Storage Materials*, 16:126–145, 2019.

[867] Bei Li, Tianye Zheng, Sijia Ran, Po-Heng Lee, Baojun Liu, and Steven T Boles. Role of metastable-adsorbed charges in the stability degradation of carbon-based electrodes for capacitive deionization. *Environmental Science: Water Research & Technology*, 4(8):1172–1180, 2018.

[868] K Singh, S Porada, HD de Gier, PM Biesheuvel, and LCPM de Smet. Timeline on the application of intercalation materials in capacitive deionization. *Desalination*, 455:115–134, 2019.

[869] Bing Han, Gong Cheng, Yunkai Wang, and Xiangke Wang. Structure and functionality design of novel carbon and faradaic electrode materials for high-performance capacitive deionization. *Chemical Engineering Journal*, 360:364–384, 2019.

[870] Pattarachai Srimuk, Joseph Halim, Juhan Lee, Quanzheng Tao, Johanna Rosen, and Volker Presser. Two-dimensional molybdenum carbide (mxene) with divacancy ordering for brackish and seawater desalination via cation and anion intercalation. *ACS Sustainable Chemistry & Engineering*, 6(3):3739–3747, 2018.

[871] Weizhai Bao, Xiao Tang, Xin Guo, Sinho Choi, Chengyin Wang, Yury Gogotsi, and Guoxiu Wang. Porous cryo-dried mxene for efficient capacitive deionization. *Joule*, 2(4):778–787, 2018.

[872] Xiaojie Shen, Yuecheng Xiong, Reti Hai, Fei Yu, and Jie Ma. An all-mxene-based integrated membrane electrode constructed using $ti_3c_2t_x$ as an intercalating agent for high performance desalination. *Environmental Science & Technology*, 54:4554–4563, 2020.

[873] Muharrem Acerce, Damien Voiry, and Manish Chhowalla. Metallic 1t phase MoS_2 nanosheets as supercapacitor electrode materials. *Nature nanotechnology*, 10(4):313–318, 2015.

[874] P. Srimuk, J. Lee, S. Fleischmann, S. Choudhury, N. Jackel, M. Zeiger, C. Kim, M. Aslan, and V. Presser. Faradaic deionization of brackish and sea water via pseudocapacitive cation and anion intercalation into few-layered molybdenum disulfide. *Journal of Materials Chemistry A*, 5(30):15640–15649, 2017.

[875] Fei Xing, Tao Li, Junye Li, Huarui Zhu, Ning Wang, and Xia Cao. Chemically exfoliated mos2 for capacitive deionization of saline water. *Nano Energy*, 31:590–595, 2017.

[876] Yanmeng Cai, Wen Zhang, Rongli Fang, Dongdong Zhao, Yue Wang, and Jixiao Wang. Well-dispersed few-layered mos2 connected with robust 3d conductive architecture for rapid capacitive deionization process and its specific ion selectivity. *Desalination*, 520:115325, 2021.

[877] Shuohan Huang and Vadym N Mochalin. Hydrolysis of 2D Transition-Metal Carbides (MXenes) in Colloidal Solutions. *Inorganic Chemistry*, 58(3):1958–1966, feb 2019.

[878] Louisiane Verger, Varun Natu, Michael Ghidiu, and Michel W Barsoum. Effect of Cationic Exchange on the Hydration and Swelling Behavior of $Ti_3C_2T_z$ MXenes. *The Journal of Physical Chemistry C*, 123(32):20044–20050, 2019.

[879] Friedrich Kaasik, Tarmo Tamm, Moritz M Hantel, Emilie Perre, Alvo Aabloo, Enn Lust, Martin Z Bazant, and Volker Presser. Anisometric charge dependent swelling of porous carbon in an ionic liquid. *Electrochemistry communications*, 34:196–199, 2013.

[880] Man Huon Han, Elena Gonzalo, Gurpreet Singh, and Teófilo Rojo. A comprehensive review of sodium layered oxides: powerful cathodes for na-ion batteries. *Energy & Environmental Science*, 8(1):81–102, 2015.

[881] Jaewuk Ahn, Jiho Lee, Seoni Kim, Choonsoo Kim, Jaehan Lee, PM Biesheuvel, and Jeyong Yoon. High performance electrochemical saline

water desalination using silver and silver-chloride electrodes. *Desalination*, 476:114216, 2020.

[882] Fuming Chen, Yinxi Huang, Lu Guo, Meng Ding, and Hui Ying Yang. A dual-ion electrochemistry deionization system based on agcl-$na_{0.44}mno_2$ electrodes. *Nanoscale*, 9(28):10101–10108, 2017.

[883] Weiyun Zhao, Lu Guo, Meng Ding, Yinxi Huang, and Hui Ying Yang. Ultrahigh-desalination-capacity dual-ion electrochemical deionization device based on $na_3v_2(po_4)_3$@c–agcl electrodes. *ACS applied materials & interfaces*, 10(47):40540–40548, 2018.

[884] D.-H. Nam and K.-S. Choi. Bismuth as a new chloride-storage electrode enabling the construction of a practical high capacity desalination battery. *Journal of the American Chemical Society*, 139(32):11055–11063, 2017.

[885] Tingting Wu, Gang Wang, Shiyong Wang, Fei Zhan, Yu Fu, Huiying Qiao, and Jieshan Qiu. Highly stable hybrid capacitive deionization with a MnO_2 anode and a positively charged cathode. *Environmental Science & Technology Letters*, 5(2):98–102, 2018.

[886] Juan Yang, Linda Zou, Huaihe Song, and Zhengping Hao. Development of novel mno2/nanoporous carbon composite electrodes in capacitive deionization technology. *Desalination*, 276(1-3):199–206, 2011.

[887] Richard Guy Compton and Craig E Banks. *Understanding Voltammetry*. World Scientific, 2018.

[888] Arkady A Karyakin. Prussian blue and its analogues: electrochemistry and analytical applications. *Electroanalysis: An International Journal Devoted to Fundamental and Practical Aspects of Electroanalysis*, 13(10):813–819, 2001.

[889] Xu Ma, Yi-An Chen, Kefu Zhou, Po-Chang Wu, and Chia-Hung Hou. Enhanced desalination performance via mixed capacitive-Faradaic ion storage using RuO2-activated carbon composite electrodes. *Electrochimica Acta*, 295:769–777, 2019.

[890] Meng Ding, Shuang Fan, Shaozhuan Huang, Mei Er Pam, Lu Guo, Yumeng Shi, and Hui Ying Yang. Tunable Pseudocapacitive Behavior in Metal–Organic Framework-Derived TiO 2 @Porous Carbon Enabling High-Performance Membrane Capacitive Deionization. *ACS Applied Energy Materials*, 2(3):1812–1822, mar 2019.

[891] Fei Yu, Lei Wang, Ying Wang, Xiaojie Shen, Yujuan Cheng, and Jie Ma. Faradaic reactions in capacitive deionization for desalination and ion separation. *Journal of Materials Chemistry A*, 7(27):15999–16027, 2019.

[892] Aditya Sood, Andrey D. Poletayev, Daniel A. Cogswell, Peter M. Csernica, J. Tyler Mefford, Dimitrios Fraggedakis, Michael F. Toney, Aaron M. Lindenberg, Martin Z. Bazant, and William C. Chueh. Electrochemical ion insertion: From atoms to devices. *Nature Reviews Materials*, 2021.

[893] S. Kim, J. Lee, C. Kim, and J. Yoon. $Na_2FeP_2O_7$ as a novel material for hybrid capacitive deionization. *Electrochimica Acta*, 203:265–271, 2016.

[894] Todd R Ferguson and Martin Z Bazant. Nonequilibrium thermodynamics of porous electrodes. *Journal of The Electrochemical Society*, 159(12):A1967, 2012.

[895] Raymond B Smith and Martin Z Bazant. Multiphase porous electrode theory. *Journal of The Electrochemical Society*, 164(11):E3291, 2017.

[896] Fan He, PM Biesheuvel, Martin Z Bazant, and T Alan Hatton. Theory of water treatment by capacitive deionization with redox active porous electrodes. *Water research*, 132:282–291, 2018.

[897] Fabio La Mantia, Mauro Pasta, Heather D. Deshazer, Bruce E. Logan, and Yi Cui. Batteries for efficient energy extraction from a water salinity difference. *Nano Letters*, 11(4):1810–1813, 2011.

[898] Sneha Shanbhag, Yousuf Bootwala, Jay F. Whitacre, and Meagan S. Mauter. Ion transport and competition effects on $nati_2(po_4)_3$ and $na_4mn_9o_{18}$ selective insertion electrode performance. *Langmuir*, 33:12580–12591, 2017.

[899] Tamio Ikeshoji. Separation of alkali metal ions by intercalation into a prussian blue electrode. *Journal of The Electrochemical Society*, 133(10):2108, 1986.

[900] Andrew B. Bocarsly and Sujit Sinha. Effects of surface structure on electrode charge transfer properties: Induction of ion selectivity at the chemically derivatized interface. *Journal of Electroanalytical Chemistry and Interfacial Electrochemistry*, 140(1):167–172, 1982.

[901] Mark R. Deakin and Houston Byrd. Prussian blue coated quartz crystal microbalance as a detector for electroinactive cations in aqueous solution. *Analytical Chemistry*, 61(4):290–295, 1989.

[902] S. D. Rassat, J. H. Sukamto, R. J. Orth, M. A. Lilga, and R. T. Hallen. Development of an electrically switched ion exchange process for selective ion separations. *Separation and Purification Technology*, 15(3):207–222, 1999.

[903] Collins Erinmwingbovo, Maria Sofia Palagonia, Doriano Brogioli, and Fabio La Mantia. Intercalation into a prussian blue derivative from solutions containing two species of cations. *ChemPhysChem*, 18(8):917–925, 2017.

[904] Kaustub Singh, Guanna Li, Juhan Lee, Han Zuilhof, Beata L Mehdi, Rafael L Zornitta, and Louis CPM de Smet. Divalent ion selectivity in capacitive deionization with vanadium hexacyanoferrate: Experiments and quantum-chemical computations. *Advanced Functional Materials*, page 2105203, 2021.

[905] Juhan Lee, Pattarachai Srimuk, Katherine Aristizabal, Choonsoo Kim, Soumyadip Choudhury, Yoon-Chae Nah, Frank Mücklich, and Volker Presser. Pseudocapacitive Desalination of Brackish Water and Seawater with Vanadium-Pentoxide-Decorated Multiwalled Carbon Nanotubes. *ChemSusChem*, 10(18):3611–3623, sep 2017.

[906] Pattarachai Srimuk, Juhan Lee, Aura Tolosa, Choonsoo Kim, Mesut Aslan, and Volker Presser. Titanium Disulfide: A Promising Low-Dimensional Electrode Material for Sodium Ion Intercalation for Seawater Desalination. *Chemistry of Materials*, 29(23):9964–9973, dec 2017.

[907] Xiao Tang, Hao Liu, Dawei Su, Peter HL Notten, and Guoxiu Wang. Hierarchical sodium-rich prussian blue hollow nanospheres as high-performance cathode for sodium-ion batteries. *Nano Research*, 11(8):3979–3990, 2018.

[908] Yinxi Huang, Fuming Chen, Lu Guo, Jun Zhang, Tupei Chen, and Hui Ying Yang. Low energy consumption dual-ion electrochemical deionization system using nati2 (po4) 3-agnps electrodes. *Desalination*, 451:241–247, 2019.

[909] B. W. Byles, D. A. Cullen, K. L. More, and E. Pomerantseva. Tunnel structured manganese oxide nanowires as redox active electrodes for hybrid capacitive deionization. *Nano Energy*, 44:476–488, 2018.

[910] X. Su, K. J. Tan, J. Elbert, C. Ruttiger, M. Gallei, T. F. Jamison, and T. A. Hatton. Asymmetric faradaic systems for selective electrochemical separations. *Energy & Environmental Science*, 10(5):1272–1283, 2017.

[911] Fan He, Martin Z Bazant, and T Alan Hatton. Equivalent circuit model for electrosorption with redox active materials. *arXiv preprint arXiv:2101.00091 (under review)*, 2020.

[912] Fan He, Martin Z Bazant, and T Alan Hatton. Theory of faradaically modulated redox active electrodes for electrochemically mediated selective adsorption processes. *Journal of The Electrochemical Society*, 168(5):053501, 2021.

[913] Todd R Ferguson and Martin Z Bazant. Phase transformation dynamics in porous battery electrodes. *Electrochimica Acta*, 146:89–97, 2014.

[914] Raymond B Smith, Edwin Khoo, and Martin Z Bazant. Intercalation kinetics in multiphase-layered materials. *The Journal of Physical Chemistry C*, 121(23):12505–12523, 2017.

[915] Vineeth Pothanamkandathil, Jenelle Fortunato, and Christopher A. Gorski. Electrochemical Desalination Using Intercalating Electrode Materials: A Comparison of Energy Demands. *Environmental Science and Technology*, 54(6):3653–3662, 2020.

[916] Michael Metzger, Münir M Besli, Saravanan Kuppan, Sondra Hellstrom, Soo Kim, Elias Sebti, Chinmayee V Subban, and Jake Christensen. Techno-economic analysis of capacitive and intercalative water deionization. *Energy & Environmental Science*, 13(6):1544–1560, 2020.

[917] Peng Bai and Martin Z Bazant. Charge transfer kinetics at the solid–solid interface in porous electrodes. *Nature communications*, 5(1):1–7, 2014.

[918] Rudolph A Marcus. Electron transfer reactions in chemistry. theory and experiment. *Reviews of Modern Physics*, 65(3):599, 1993.

[919] Alexander M Kuznetsov and Jens Ulstrup. *Electron transfer in chemistry and biology: an introduction to the theory*. John Wiley & Sons Ltd, 1999.

[920] C. E. D. Chidsey. Free-energy and temperature-dependence of electron-transfer at the metal-electrolyte interface. *Science*, 251(4996):919–922, 1991.

[921] Yi Zeng, Raymond B Smith, Peng Bai, and Martin Z Bazant. Simple formula for marcus–hush–chidsey kinetics. *Journal of Electroanalytical Chemistry*, 735:77–83, 2014.

[922] Dimitrios Fraggedakis, Michael McEldrew, Raymond B Smith, Yamini Krishnan, Yirui Zhang, Peng Bai, William C Chueh, Yang Shao-Horn, and Martin Z Bazant. Theory of coupled ion-electron transfer kinetics. *Electrochimica Acta*, 367:137432, 2021.

[923] Dimitrios Fraggedakis and Martin Z Bazant. Tuning the stability of electrochemical interfaces by electron transfer reactions. *The Journal of chemical physics*, 152(18):184703, 2020.

[924] Kyu-Sung Park, Penghao Xiao, So-Yeon Kim, Anthony Dylla, Young-Min Choi, Graeme Henkelman, Keith J Stevenson, and John B Goodenough. Enhanced charge-transfer kinetics by anion surface modification of $LiFePO_4$. *Chemistry of Materials*, 24(16):3212–3218, 2012.

[925] Heejin Kim, RA Shakoor, Chansun Park, Soo Yeon Lim, Joo-Seong Kim, Yong Nam Jo, Woosuk Cho, Keiichi Miyasaka, Ramazan Kahraman, Yousung Jung, and Jang Wook Choi. $Na_2FeP_2O_7$ as a promising iron-based pyrophosphate cathode for sodium rechargeable batteries: a combined experimental and theoretical study, 2013.

[926] Rafael Trócoli, Alberto Battistel, and Fabio La Mantia. Selectivity of a lithium-recovery process based on lifepo$_4$. *Chemistry – A European Journal*, 20(32):9888–9891, 2014.

[927] Chong Liu, Yanbin Li, Dingchang Lin, Po-Chun Hsu, Bofei Liu, Gangbin Yan, Tong Wu, Yi Cui, and Steven Chu. Lithium extraction from seawater through pulsed electrochemical intercalation. *Joule*, 4:1459–1469, 2020.

[928] Xin He, Sumanjeet Kaur, and Robert Kostecki. Mining lithium from seawater. *Joule*, 4(7):1357–1358, 2020.

[929] S.P. Hong, H. Yoon, J. Lee, C. Kim, S. Kim, J. Lee, C. Lee, and J. Yoon. Selective phosphate removal using layered double hydroxide/reduced graphene oxide (ldh/rgo) composite electrode in capacitive deionization. *Journal of Colloid and Interface Science*, 564:1–7, 2020.

[930] E. Seftel, R. Ciocarlan, B. Michielsen, V. Meynen, S. Mullens, and P. Cool. Insights into phosphate adsorption behavior on structurally modified znal layered double hydroxides. *Applied Clay Science*, 165:234–246, 2018.

[931] H. He, H. Kang, S. Ma, Y. Bai, and X. Yang. High adsorption selectivity of znal layered double hydroxides and the calcined materials toward phosphate. *Journal of colloid and interface science*, 343(1):225–231, 2010.

[932] G. Park, S.P. Hong, C. Lee, J. Lee, and J. Yoon. Selective fluoride removal in capacitive deionization by reduced graphene oxide/hydroxyapatite composite electrode. *Journal of Colloid and Interface Science*, 581:396–402, 2020.

[933] X. Yu, S. Tong, M. Ge, and J. Zuo. Removal of fluoride from drinking water by cellulose@ hydroxyapatite nanocomposites. *Carbohydrate polymers*, 92(1):269–275, 2013.

[934] Lutfi Agartan, Brendan Hayes-Oberst, Bryan W Byles, Bilen Akuzum, Ekaterina Pomerantseva, and E Caglan Kumbur. Influence of operating conditions and cathode parameters on desalination performance of hybrid cdi systems. *Desalination*, 452:1–8, 2019.

[935] F. Sauvage, E. Baudrin, and J.-M. Tarascon. Study of the potentiometric response towards sodium ions of $Na_{0.44-x}MnO_2$ for the development of selective sodium ion sensors. *Sensors and Actuators B: Chemical*, 120(2):638–644, 2007.

[936] J. Chang, F. Duan, H. Cao, K. Tang, C. Su, and Y. Li. Superiority of a novel flow-electrode capacitive deionization (fcdi) based on a battery material at high applied voltage. *Desalination*, 468:114080, 2019.

[937] Nayeong Kim, Jiho Lee, Seonghwan Kim, Sung Pil Hong, Changha Lee, Jeyong Yoon, and Choonsoo Kim. Short review of multichannel membrane capacitive deionization: Principle, current status, and future prospect. *Applied Sciences*, 10(2):683, 2020.

[938] Pattarachai Srimuk, Samantha Husmann, and Volker Presser. Low voltage operation of a silver/silver chloride battery with high desalination capacity in seawater. *RSC advances*, 9(26):14849–14858, 2019.

[939] Nguyen Anh Thu Tran, Ngo Minh Phuoc, Hana Yoon, Euiyeon Jung, Young-Woo Lee, Beom-Goo Kang, Hong Suk Kang, Chung-Yul Yoo, and Younghyun Cho. Improved desalination performance of flow-and fixed-capacitive deionization using redox-active quinone. *ACS Sustainable Chemistry & Engineering*, 8(44):16701–16710, 2020.

[940] Nayeong Kim, Sung Pil Hong, Jiho Lee, Choonsoo Kim, and Jeyong Yoon. High-desalination performance via redox couple reaction in the multichannel capacitive deionization system. *ACS Sustainable Chemistry & Engineering*, 7(19):16182–16189, 2019.

[941] Jinhong Dai, Jian Wang, Xianhua Hou, Qiang Ru, Qingyu He, Pattarachai Srimuk, Volker Presser, and Fuming Chen. Dual-zinc electrode electrochemical desalination. *ChemSusChem*, 13(10):2792, 2020.

[942] Fuming Chen, Jian Wang, Chunhua Feng, Jinxing Ma, and T David Waite. Low energy consumption and mechanism study of redox flow desalination. *Chemical Engineering Journal*, 401:126111, 2020.

[943] S. Yang, J. Choi, J.-g Yeo, S.-i Jeon, H.-r Park, and D.K. Kim. Flow-electrode capacitive deionization using an aqueous electrolyte with a high salt concentration. *Environmental science & technology*, 50(11):5892–5899, 2016.

[944] Jaewuk Ahn, Seongsoo Kim, Sung-il Jeon, Changha Lee, Jaehan Lee, and Jeyong Yoon. Nafion-coated prussian blue electrodes to enhance the stability and efficiency of battery desalination system. *Desalination*, 500:114778, 2021.

[945] T. Kim, C.A. Gorski, and B.E. Logan. Low energy desalination using battery electrode deionization. *Environmental Science & Technology Letters*, 4(10):444–449, 2017.

[946] L. Wang, C. Mu, H. Li, and F. Li. A dual-function battery for desalination and energy storage. *Inorganic Chemistry Frontiers*, 5(10):2522–2526, 2018.

[947] J. Lee, J. Lee, J. Ahn, K. Jo, S.P. Hong, C. Kim, C. Lee, and J. Yoon. Enhancement in desalination performance of battery electrodes via improved mass transport using a multichannel flow system. *ACS applied materials & interfaces*, 11(40):36580–36588, 2019.

[948] D.-H. Nam, M.A. Lumley, and K.-S. Choi. A desalination battery combining $Cu_3[Fe(CN)_6]_2$ as a na-storage electrode and bi as a cl-storage electrode enabling membrane-free desalination. *Chemistry of Materials*, 31(4):1460–1468, 2019.

[949] S. Kim, H. Joo, T. Moon, S.-H. Kim, and J. Yoon. Rapid and selective lithium recovery from desalination brine using an electrochemical system. *Environmental Science: Processes & Impacts*, 21(4):667–676, 2019.

[950] M. Pasta, A. Battistel, and F. La Mantia. Batteries for lithium recovery from brines. *Energy & Environmental Science*, 5(11):9487–9491, 2012.

[951] Q. Li, Y. Zheng, D. Xiao, T. Or, R. Gao, Z. Li, M. Feng, L. Shui, G. Zhou, and X. Wang. Faradaic electrodes open a new era for capacitive deionization. *Advanced Science*, 7(22):2002213, 2020.

[952] H. Shiiba, N. Zettsu, M. Nakayama, S. Oishi, and K. Teshima. Defect formation energy in spinel $LiNi_{0\cdot5}Mn_{1\cdot5}O_4-\delta$ using ab initio dft calculations. *The Journal of Physical Chemistry C*, 119(17):9117–9124, 2015.

[953] C.P. Lawagon, G.M. Nisola, R.A.I. Cuevas, R.E.C. Torrejos, H. Kim, S.-P. Lee, and W.-J. Chung. $Li_{1-x}Ni_{0.5}Mn_{1.5}O_4/Ag$ for electrochemical lithium recovery from brine and its optimized performance via response surface methodology. *Separation and Purification Technology*, 212:416–426, 2019.

[954] J.-S. Kim, Y.-H. Lee, S. Choi, J. Shin, H.-C. Dinh, and J.W. Choi. An electrochemical cell for selective lithium capture from seawater. *Environmental science & technology*, 49(16):9415–9422, 2015.

[955] W. Tang, J. Liang, D. He, J. Gong, L. Tang, Z. Liu, D. Wang, and G. Zeng. Various cell architectures of capacitive deionization: Recent advances and future trends. *Water research*, 150:225–251, 2019.

[956] N. Kim, J. Lee, S.P. Hong, C. Lee, C. Kim, and J. Yoon. Performance analysis of the multi-channel membrane capacitive deionization with porous carbon electrode stacks. *Desalination*, 479:114315, 2020.

[957] John Thomas Stock and Mary Virginia Orna. *Electrochemistry, past and present*, volume 390. ACS Publications, 1989.

[958] Steven S Zumdahl and Donald J DeCoste. *Chemical principles*. Nelson Education, 2012.

[959] A. J. Bard and L. R. Faulkner. *Electrochemical Methods: Fundamentals and Applications*. John Wiley & Sons, In, Hoboken, NJ, 2001.

[960] Roland R Netz and Henri Orland. Beyond poisson-boltzmann: Fluctuation effects and correlation functions. *The European Physical Journal E*, 1(2-3):203–214, 2000.

[961] Phil Attard. *Thermodynamics and statistical mechanics: equilibrium by entropy maximisation*. Academic Press, 2002.

[962] C. Y. Zhang, D. He, J. X. Ma, W. W. Tang, and T. D. Waite. Faradaic reactions in capacitive deionization (cdi) - problems and possibilities: A review. *Water Research*, 128:314–330, 2018.

[963] AK Shukla, S Sampath, and K Vijayamohanan. Electrochemical supercapacitors: Energy storage beyond batteries. *Current science*, 79(12):1656–1661, 2000.

[964] Abdul Muqsit Khattak, Zahid Ali Ghazi, Bin Liang, Niaz Ali Khan, Azhar Iqbal, Lianshan Li, and Zhiyong Tang. A redox-active 2d covalent organic framework with pyridine moieties capable of faradaic energy storage. *Journal of Materials Chemistry A*, 4(42):16312–16317, 2016.

[965] Fraser A Armstrong, H Allen O Hill, and Nicholas J Walton. Direct electrochemistry of redox proteins. *Accounts of Chemical Research*, 21(11):407–413, 1988.

[966] P. H. Chen and R. L. McCreery. Control of electron transfer kinetics at glassy carbon electrodes by specific surface modification. *Analytical Chemistry*, 68(22):3958–3965, 1996.

[967] T. G. Drummond, M. G. Hill, and J. K. Barton. Electrochemical dna sensors. *Nature Biotechnology*, 21(10):1192–1199, 2003.

[968] X. H. Kang, J. Wang, H. Wu, I. A. Aksay, J. Liu, and Y. H. Lin. Glucose oxidase-graphene-chitosan modified electrode for direct electrochemistry and glucose sensing. *Biosensors & Bioelectronics*, 25(4):901–905, 2009.

[969] C. Costentin, M. Robert, and J. M. Saveant. Catalysis of the electrochemical reduction of carbon dioxide. *Chemical Society Reviews*, 42(6):2423–2436, 2013.

[970] B. H. Solis and S. Hammes-Schiffer. Proton-coupled electron transfer in molecular electrocatalysis: Theoretical methods and design principles. *Inorganic Chemistry*, 53(13):6427–6443, 2014.

[971] M. R. Lukatskaya, B. Dunn, and Y. Gogotsi. Multidimensional materials and device architectures for future hybrid energy storage. *Nature Communications*, 7:12647, 2016.

[972] T. Brousse, D. Belanger, and J. W. Long. To be or not to be pseudocapacitive? *Journal of the Electrochemical Society*, 162(5):A5185–A5189, 2015.

[973] Raquel Gracia and David Mecerreyes. Polymers with redox properties: materials for batteries, biosensors and more. *Polymer Chemistry*, 4(7):2206–2214, 2013.

[974] Michael EG Lyons. Electrocatalysis using electroactive polymers, electroactive composites and microheterogeneous systems. *Analyst*, 119(5):805–826, 1994.

[975] Rachel D Harris, Jeffrey T Auletta, S Amin Mohaghegh Motlagh, Matthew J Lawless, Nicholas M Perri, Sunil Saxena, Lisa M Weiland, David H Waldeck, William W Clark, and Tara Y Meyer. Chemical and electrochemical manipulation of mechanical properties in stimuli-responsive copper-cross-linked hydrogels. *ACS Macro Letters*, 2(12):1095–1099, 2013.

[976] Jeonghun Kim, Jung Ho Kim, and Katsuhiko Ariga. Redox-active polymers for energy storage nanoarchitectonics. *Joule*, 1(4):739–768, 2017.

[977] Tobias Janoschka, Norbert Martin, Udo Martin, Christian Friebe, Sabine Morgenstern, Hannes Hiller, Martin D Hager, and Ulrich S Schubert. An aqueous, polymer-based redox-flow battery using non-corrosive, safe, and low-cost materials. *Nature*, 527(7576):78–81, 2015.

[978] K Horie, Máximo Barón, RB Fox, J He, M Hess, J Kahovec, T Kitayama, P Kubisa, E Maréchal, and W Mormann. Definitions of terms relating to reactions of polymers and to functional polymeric materials (iupac recommendations 2003). *Pure and Applied Chemistry*, 76(4):889–906, 2004.

[979] Alan J Heeger. Semiconducting polymers: the third generation. *Chemical Society Reviews*, 39(7):2354–2371, 2010.

[980] Caijuan Yan, Linda Zou, and Rob Short. Single-walled carbon nanotubes and polyaniline composites for capacitive deionization. *Desalination*, 290:125–129, 2012.

[981] Caijuan Yan, Yasodinee Wimalasiri Kanaththage, Rob Short, Christopher T Gibson, and Linda Zou. Graphene/polyaniline nanocomposite as electrode material for membrane capacitive deionization. *Desalination*, 344:274–279, 2014.

[982] Yue Wang, Liwen Zhang, Yafei Wu, Shichang Xu, and Jixiao Wang. Polypyrrole/carbon nanotube composites as cathode material for performance enhancing of capacitive deionization technology. *Desalination*, 354:62–67, 2014.

[983] Xiaoyu Gu, Yu Yang, Yang Hu, Meng Hu, Jian Huang, and Chaoyang Wang. Facile fabrication of graphene–polypyrrole–mn composites as high-performance electrodes for capacitive deionization. *Journal of Materials Chemistry A*, 3(11):5866–5874, 2015.

[984] Rafael L Zornitta, Francisco J García-Mateos, Julio J Lado, José Rodríguez-Mirasol, Tomás Cordero, Peter Hammer, and Luis AM Ruotolo. High-performance activated carbon from polyaniline for capacitive deionization. *Carbon*, 123:318–333, 2017.

[985] Abhinav Akhoury, Lev Bromberg, and T Alan Hatton. Interplay of electron hopping and bounded diffusion during charge transport in redox polymer electrodes. *The Journal of Physical Chemistry B*, 117(1):333–342, 2013.

[986] X. Su, H. J. Kulik, T. F. Jamison, and T. A. Hatton. Anion-selective redox electrodes: Electrochemically mediated separation with heterogeneous organometallic interfaces. *Advanced Functional Materials*, 26(20):3394–3404, 2016.

[987] S. Bruckenstein, A. T. Fensore, and A. R. Hillman. Time-resolved mono-anion, di-anion, and solvent transfers into a poly(vinylferrocene)-modified electrode. *Journal of the Electrochemical Society*, 145(2):L24–L26, 1998.

[988] I. Jureviciute, S. Bruckenstein, and A. R. Hillman. Counter-ion specific effects on charge and solvent trapping in poly(vinylferrocene) films. *Journal of Electroanalytical Chemistry*, 488(1):73–81, 2000.

[989] Gilberto Schiavon, Gianni Zotti, Nicola Comisso, Anna Berlin, and Giorgio Pagani. Ion exchange in the electrochemical switching of polypyrroles in acetonitrile by the electrochemical quartz crystal microbalance. electrolyte incorporation by hydrogen bonding of anions to pyrrole. *The Journal of Physical Chemistry*, 98(18):4861–4864, 1994.

[990] Meral Arca, Michael V Mirkin, and Allen J Bard. Polymer films on electrodes. 26. study of ion transport and electron transfer at polypyrrole films by scanning electrochemical microscopy. *The Journal of Physical Chemistry*, 99(14):5040–5050, 1995.

[991] P. D. Beer, P. A. Gale, and G. Z. Chen. Mechanisms of electrochemical recognition of cations, anions and neutral guest species by redox-active receptor molecules. *Coordination Chemistry Reviews*, 185-6:3–36, 1999.

[992] P. D. Beer and P. A. Gale. Anion recognition and sensing: The state of the art and future perspectives. *Angewandte Chemie-International Edition*, 40(3):486–516, 2001.

[993] Kai-Jher Tan, Xiao Su, and T Alan Hatton. An asymmetric iron-based redox-active system for electrochemical separation of ions in aqueous media. *Advanced Functional Materials*, 30(15):1910363, 2020.

[994] Peter G Pickup. Conjugated metallopolymers. redox polymers with interacting metal based redox sites. *Journal of Materials Chemistry*, 9(8):1641–1653, 1999.

[995] A Ramanavičius, A Ramanavičienė, and A Malinauskas. Electrochemical sensors based on conducting polymer–polypyrrole. *Electrochimica acta*, 51(27):6025–6037, 2006.

[996] Ulrich Lange, Nataliya V Roznyatovskaya, and Vladimir M Mirsky. Conducting polymers in chemical sensors and arrays. *Analytica chimica acta*, 614(1):1–26, 2008.

[997] Lijia Pan, Guihua Yu, Dongyuan Zhai, Hye Ryoung Lee, Wenting Zhao, Nian Liu, Huiliang Wang, Benjamin C-K Tee, Yi Shi, and Yi Cui. Hierarchical nanostructured conducting polymer hydrogel with high electrochemical activity. *Proceedings of the National Academy of Sciences*, 109(24):9287–9292, 2012.

[998] M. W. Espenscheid, A. R. Ghatakroy, R. B. Moore, R. M. Penner, M. N. Szentirmay, and C. R. Martin. Sensors from polymer modified electrodes. *Journal of the Chemical Society-Faraday Transactions I*, 82:1051–1070, 1986.

[999] R. Toniolo, N. Comisso, and G. Bontempelli. Potential shifts at electrodes coated with ion-exchange polymeric films. *Talanta*, 41(3):473–478, 1994.

[1000] P. Ugo and L. M. Moretto. Ion-exchange voltammetry at polymer-coated electrodes: Principles and analytical prospects. *Electroanalysis*, 7(12):1105–1113, 1995.

[1001] C. R. Martin and M. W. Espenscheid. Electroactive ion-exchange polymers. *Journal of the Electrochemical Society*, 131(8):C328–C328, 1984.

[1002] C. R. Martin, M. W. Espenscheid, and A. R. Ghatakroy. The electrochemistry of electroactive ionomers. *Journal of the Electrochemical Society*, 133(3):C128–C128, 1986.

[1003] E. T. Kang, K. G. Neoh, and K. L. Tan. Polyaniline: A polymer with many interesting intrinsic redox states. *Progress in Polymer Science*, 23(2):277–324, 1998.

[1004] Y. H. Lin, X. L. Cui, and J. Bontha. Electrically controlled anion exchange based on polypyrrole and carbon nanotubes nanocomposite for perchlorate removal. *Environmental Science & Technology*, 40(12):4004–4009, 2006.

[1005] F. C. Anson, T. Ohsaka, and J. M. Saveant. Kinetics of electron-transfer cross-reactions within redox polymers - coatings of a protonated polylysine co-polymer with incorporated electroactive anions. *Journal of the American Chemical Society*, 105(15):4883–4890, 1983.

[1006] M. Watanabe, M. L. Longmire, and R. W. Murray. A study of ferrocene diffusion dynamics in network poly (ethylene oxide) polymer electrolyte by solid-state voltammetry. *Journal of Physical Chemistry*, 94(6):2614–2619, 1990.

[1007] A. R. Hillman, N. A. Hughes, and S. Bruckenstein. Solvation phenomena in polyvinylferrocene films - effect of history and redox state. *Journal of the Electrochemical Society*, 139(1):74–77, 1992.

[1008] J. A. Bruce and M. S. Wrighton. Electrostatic binding of electroactive and non-electroactive anions in a surface-confined, electroactive polymer - selectivity of binding measured by auger-spectroscopy and cyclic voltammetry. *Journal of the American Chemical Society*, 104(1):74–82, 1982.

[1009] Charles R Martin, Israel Rubinstein, and Allen J Bard. Polymer films on electrodes. 9. electron and mass transfer in nafion films containing tris (2, 2'-bipyridine) ruthenium (2+). *Journal of the American Chemical Society*, 104(18):4817–4824, 1982.

[1010] M. L. Shi and F. C. Anson. High sensitivity of electron transfer rates within nafion coatings saturated with os(bpy)(3)(2+) to the extent of hydration of the coating. *Journal of the Electrochemical Society*, 142(12):4205–4214, 1995.

[1011] Christopher G Hardy, Jiuyang Zhang, Yi Yan, Lixia Ren, and Chuanbing Tang. Metallopolymers with transition metals in the side-chain by living and controlled polymerization techniques. *Progress in polymer science*, 39(10):1742–1796, 2014.

[1012] Markus Gallei and Johannes Elbert. Recent advances in immobilized ferrocene-containing polymers. In *Functional Metallosupramolecular Materials*, pages 120–148. Royal Society of Chemistry, 2015.

[1013] Markus Gallei and Christian Rüttiger. Recent trends in metallopolymer design: Redox-controlled surfaces, porous membranes, and switchable optical materials using ferrocene-containing polymers. *Chemistry–A European Journal*, 24(40):10006–10021, 2018.

[1014] Xianwen Mao, Gregory C Rutledge, and T Alan Hatton. Polyvinylferrocene for noncovalent dispersion and redox-controlled precipitation of carbon nanotubes in nonaqueous media. *Langmuir*, 29(31):9626–9634, 2013.

[1015] Xianwen Mao, Fritz Simeon, Demetra S Achilleos, Gregory C Rutledge, and T Alan Hatton. Metallocene/carbon hybrids prepared by a solution process for supercapacitor applications. *Journal of Materials Chemistry A*, 1(42):13120–13127, 2013.

[1016] Huangxian Ju and Dónal Leech. Electrochemistry of poly(vinylferrocene) formed by direct electrochemical reduction at a glassy carbon electrode. *Journal of the Chemical Society, Faraday Transactions*, 93(7):1371–1375, 1997.

[1017] Demetra S Achilleos and T Alan Hatton. Selective molecularly mediated pseudocapacitive separation of ionic species in solution. *ACS applied materials & interfaces*, 8(48):32743–32753, 2016.

[1018] Kalliopi N Fotopoulou and Hrissi K Karapanagioti. Surface properties of beached plastic pellets. *Marine environmental research*, 81:70–77, 2012.

[1019] Tamara S Galloway, Matthew Cole, and Ceri Lewis. Interactions of microplastic debris throughout the marine ecosystem. *Nature ecology & evolution*, 1(5):1–8, 2017.

[1020] Alaaeddin Alsbaiee, Brian J Smith, Leilei Xiao, Yuhan Ling, Damian E Helbling, and William R Dichtel. Rapid removal of organic micropollutants from water by a porous β-cyclodextrin polymer. *nature*, 529(7585):190–194, 2016.

[1021] Manfred Clara, Birgit Strenn, Oliver Gans, Elena Martinez, Norbert Kreuzinger, and Helmut Kroiss. Removal of selected pharmaceuticals, fragrances and endocrine disrupting compounds in a membrane bioreactor and conventional wastewater treatment plants. *Water research*, 39(19):4797–4807, 2005.

[1022] Xiao Su, Akihiro Kushima, Cameron Halliday, Jian Zhou, Ju Li, and T Alan Hatton. Electrochemically-mediated selective capture of heavy metal chromium and arsenic oxyanions from water. *Nature communications*, 9(1):4701, 2018.

[1023] Ali Hemmatifar, Nil Ozbek, Cameron Halliday, and T Alan Hatton. Electrochemical selective recovery of heavy metal vanadium oxyanion from continuously flowing aqueous streams. *ChemSusChem*, 13(15):3865–3874, 2020.

[1024] V Dimos, KJ Haralambous, and S Malamis. A review on the recent studies for chromium species adsorption on raw and modified natural minerals. *Critical reviews in environmental science and technology*, 42(19):1977–2016, 2012.

[1025] Jolanta Skowron and Katarzyna Konieczko. Occupational exposure to chromium (vi) compounds. *Medycyna Pracy*, 66(3):407–427, 2015.

[1026] Adam Pawełczyk, František Božek, and Kazimierz Grabas. Impact of military metallurgical plant wastes on the population's health risk. *Chemosphere*, 152:513–519, 2016.

[1027] G. R. Whittell and I. Manners. Metallopolymers: New multifunctional materials. *Advanced Materials*, 19(21):3439–3468, 2007.

[1028] M. A. Vorotyntsev and S. V. Vasilyeva. Metallocene-containing conjugated polymers. *Advances in Colloid and Interface Science*, 139(1-2):97–149, 2008.

[1029] Kwiyong Kim, Paola Baldaguez Medina, Johannes Elbert, Emmanuel Kayiwa, Roland D Cusick, Yujie Men, and Xiao Su. Molecular tuning of redox-copolymers for selective electrochemical remediation. *Advanced Functional Materials*, page 2004635, 2020.

[1030] Beate I Escher and Kathrin Fenner. Recent advances in environmental risk assessment of transformation products. *Environmental science & technology*, 45(9):3835–3847, 2011.

[1031] Vasiliki S Thomaidi, Athanasios S Stasinakis, Viola L Borova, and Nikolaos S Thomaidis. Is there a risk for the aquatic environment due to the existence of emerging organic contaminants in treated domestic wastewater? greece as a case-study. *Journal of hazardous materials*, 283:740–747, 2015.

[1032] Jimoh O Tijani, Ojo O Fatoba, Omotola O Babajide, and Leslie F Petrik. Pharmaceuticals, endocrine disruptors, personal care products, nanomaterials and perfluorinated pollutants: a review. *Environmental chemistry letters*, 14(1):27–49, 2016.

[1033] Yin Xu, Tingjiao Liu, Ying Zhang, Fei Ge, Rachel M Steel, and Luyi Sun. Advances in technologies for pharmaceuticals and personal care products removal. *Journal of materials chemistry A*, 5(24):12001–12014, 2017.

[1034] Jonathan T Alexander, Faisal I Hai, and Turki M Al-aboud. Chemical coagulation-based processes for trace organic contaminant removal: Current state and future potential. *Journal of environmental management*, 111:195–207, 2012.

[1035] Jessica Benner, Damian E Helbling, Hans-Peter E Kohler, Janneke Wittebol, Elena Kaiser, Carsten Prasse, Thomas A Ternes, Christian N Albers, Jens Aamand, and Benjamin Horemans. Is biological treatment a viable alternative for micropollutant removal in drinking water treatment processes? *Water Research*, 47(16):5955–5976, 2013.

[1036] Abreham Tesfaye Besha, Abaynesh Yihdego Gebreyohannes, Ramato Ashu Tufa, Dawit Nega Bekele, Efrem Curcio, and Lidietta Giorno. Removal of emerging micropollutants by activated sludge process and membrane bioreactors and the effects of micropollutants on membrane fouling: A review. *Journal of environmental chemical engineering*, 5(3):2395–2414, 2017.

[1037] Abhinav Akhoury, Lev Bromberg, and T Alan Hatton. Redox-responsive gels with tunable hydrophobicity for controlled solubilization and release of organics. *ACS applied materials & interfaces*, 3(4):1167–1174, 2011.

[1038] Wenda Tian, Xianwen Mao, Paul Brown, Gregory C Rutledge, and T Alan Hatton. Electrochemically nanostructured polyvinylferrocene/polypyrrole hybrids with synergy for energy storage. *Advanced Functional Materials*, 25(30):4803–4813, 2015.

[1039] Barak Shapira, Eran Avraham, and Doron Aurbach. Side reactions in capacitive deionization (cdi) processes: the role of oxygen reduction. *Electrochimica Acta*, 220:285–295, 2016.

[1040] Ayokunle Omosebi, Xin Gao, James Landon, and Kunlei Liu. Asymmetric electrode configuration for enhanced membrane capacitive deionization. *ACS applied materials & interfaces*, 6(15):12640–12649, 2014.

[1041] Xin Gao, James Landon, James K Neathery, and Kunlei Liu. Modification of carbon xerogel electrodes for more efficient asymmetric capacitive deionization. *Journal of The Electrochemical Society*, 160(9):E106–E112, 2013.

[1042] Hanjoo Jo, Kyung Hoon Kim, Min-Jung Jung, Jae Hyun Park, and Young-Seak Lee. Fluorination effect of activated carbons on performance of asymmetric capacitive deionization. *Applied Surface Science*, 409:117–123, 2017.

[1043] HB Li, MH Yu, FX Wang, P Liu, Y Liang, J Xiao, CX Wang, YX Tong, and GW Yang. Amorphous nickel hydroxide nanospheres with ultrahigh capacitance and energy density as electrochemical pseudocapacitor materials. *Nature communications*, 4(1):1894, 2013.

[1044] Bo Liu, Dezhi Kong, Jun Zhang, Ye Wang, Tupei Chen, Chuanwei Cheng, and Hui Ying Yang. 3d hierarchical Co_3O_4@Co_3S_4 nanoarrays as cathode materials for asymmetric pseudocapacitors. *Journal of Materials Chemistry A*, 4(9):3287–3296, 2016.

[1045] Muhammad Boota and Yury Gogotsi. Mxene–conducting polymer asymmetric pseudocapacitors. *Advanced Energy Materials*, 9(7):1802917, 2019.

[1046] Glenn G Amatucci, Fadwa Badway, Aurelien Du Pasquier, and Tao Zheng. An asymmetric hybrid nonaqueous energy storage cell. *Journal of the Electrochemical Society*, 148(8):A930–A939, 2001.

[1047] Qunting Qu, Peng Zhang, Bin Wang, Yuhui Chen, Shu Tian, Yuping Wu, and Rudolf Holze. Electrochemical performance of mno2 nanorods in neutral aqueous electrolytes as a cathode for asymmetric supercapacitors. *The Journal of Physical Chemistry C*, 113(31):14020–14027, 2009.

[1048] Yonggang Wang, Yanfang Song, and Yongyao Xia. Electrochemical capacitors: mechanism, materials, systems, characterization and applications. *Chemical Society Reviews*, 45(21):5925–5950, 2016.

[1049] C Rüttiger, V Pfeifer, V Rittscher, D Stock, D Scheid, S Vowinkel, F Roth, H Didzoleit, B Stühn, and J Elbert. One for all: cobalt-containing polymethacrylates for magnetic ceramics, block copolymerization, unexpected electrochemistry, and stimuli-responsiveness. *Polymer Chemistry*, 7(5):1129–1137, 2016.

[1050] W Douglass Shaw, Mark Walker, and Marnee Benson. Treating and drinking well water in the presence of health risks from arsenic contamination: results from a us hot spot. *Risk Analysis: An International Journal*, 25(6):1531–1543, 2005.

[1051] D Pokhrel, BS Bhandari, and T Viraraghavan. Arsenic contamination of groundwater in the terai region of nepal: an overview of health concerns and treatment options. *Environment International*, 35(1):157–161, 2009.

[1052] Lucy Mar Camacho, Mélida Gutiérrez, Maria Teresa Alarcón-Herrera, Maria de Lourdes Villalba, and Shuguang Deng. Occurrence and treatment of arsenic in groundwater and soil in northern mexico and southwestern usa. *Chemosphere*, 83(3):211–225, 2011.

[1053] World Health Organization. Arsenic in drinking water: Background document for development of who guidelines for drinking water quality. Technical report, World Health Organization, 2011.

[1054] Zhao Song, Shikha Garg, Jinxing Ma, and T David Waite. Selective arsenic removal from groundwaters using redox-active polyvinylferrocene-functionalized electrodes: Role of oxygen. *Environmental Science & Technology*, 54(19):12081–12091, 2020.

[1055] Yinying Ren, Zhou Lin, Xianwen Mao, Wenda Tian, Troy Van Voorhis, and T Alan Hatton. Superhydrophobic, surfactant-doped, conducting polymers for electrochemically reversible adsorption of organic contaminants. *Advanced Functional Materials*, 28(32):1801466, 2018.

[1056] Fan He, Ali Hemmatifar, Martin Z Bazant, and T Alan Hatton. Selective adsorption of organic anions in a flow cell with asymmetric redox active electrodes. *Water Research*, page 115963, 2020.

[1057] Fan He. *Theoretical and experimental study of electrochemically mediated adsorption processes*. PhD thesis, Massachusetts Institute of Technology, 2019.

[1058] Sidney Loeb, F Van Hessen, J Levi, and M Ventura. The osmotic power plant. In *11th Intersociety Energy Conversion Engineering Conference*, pages 51–57, 1976.

[1059] Sidney Loeb. One hundred and thirty benign and renewable megawatts from great salt lake? the possibilities of hydroelectric power by pressure-retarded osmosis. *Desalination*, 141(1):85–91, 2001.

[1060] Andrea Achilli and Amy E Childress. Pressure retarded osmosis: from the vision of sidney loeb to the first prototype installation. *Desalination*, 261(3):205–211, 2010.

[1061] Bruce E Logan and Menachem Elimelech. Membrane-based processes for sustainable power generation using water. *Nature*, 488(7411):313–319, 2012.

[1062] Fernanda Helfer, Charles Lemckert, and Yuri G Anissimov. Osmotic power with pressure retarded osmosis: theory, performance and trends–a review. *Journal of Membrane Science*, 453:337–358, 2014.

[1063] Tai-Shung Chung and Chun Feng Wan. *Membrane Technology for Osmotic Power Generation by Pressure Retarded Osmosis*. CRC Press, 2020.

[1064] John N Weinstein and Frank B Leitz. Electric power from differences in salinity: the dialytic battery. *Science*, 191(4227):557–559, 1976.

[1065] Masahiro Yasukawa, Tasuma Suzuki, and Mitsuru Higa. Salinity gradient processes: Thermodynamics, applications, and future prospects. In *Membrane-based salinity gradient processes for water treatment and power generation*, pages 3–56. Elsevier, 2018.

[1066] M Turek and B Bandura. Renewable energy by reverse electrodialysis. *Desalination*, 205(1-3):67–74, 2007.

[1067] Jan W Post, Hubertus VM Hamelers, and Cees JN Buisman. Energy recovery from controlled mixing salt and fresh water with a reverse electrodialysis system. *Environmental science & technology*, 42(15):5785–5790, 2008.

[1068] Richard S Norman. Water salination: a source of energy. *Science*, 186(4161):350–352, 1974.

[1069] GL Wick and Schmitt WR. Prospects for renewable energy from the sea. *Mar. Technol. Soc. J.*, 11:16–21, 1977.

[1070] C Forgacs. Recent developments in the utilization of salinity power. *Desalination*, 40(1-2):191–195, 1982.

[1071] R Audinos. Electric power produced from two solutions of unequal salinity by reverse electrodialysis. *Indian Journal of Chemistry*, 31 A:348–354, 1992.

[1072] Joseph Jagur-Grodzinski and Riry Kramer. Novel process for direct conversion of free energy of mixing into electric power. *Industrial & Engineering Chemistry Process Design and Development*, 25(2):443–449, 1986.

[1073] Piotr Długołęcki, Kitty Nymeijer, Sybrand Metz, and Matthias Wessling. Current status of ion exchange membranes for power generation from salinity gradients. *Journal of Membrane Science*, 319(1-2):214–222, 2008.

[1074] Joost Veerman, Michel Saakes, Sybrand J Metz, and GJ Harmsen. Reverse electrodialysis: evaluation of suitable electrode systems. *Journal of Applied Electrochemistry*, 40(8):1461–1474, 2010.

[1075] O Scialdone, C Guarisco, S Grispo, A Dâ€™Angelo, and A Galia. Investigation of electrode material–redox couple systems for reverse electrodialysis processes. part i: Iron redox couples. *Journal of Electroanalytical Chemistry*, 681:66–75, 2012.

[1076] O Scialdone, A Albanese, A Dâ€™Angelo, A Galia, and C Guarisco. Investigation of electrode material–redox couple systems for reverse electrodialysis processes. part ii: Experiments in a stack with 10–50 cell pairs. *Journal of electroanalytical chemistry*, 704:1–9, 2013.

[1077] Ying Mei and Chuyang Y Tang. Recent developments and future perspectives of reverse electrodialysis technology: A review. *Desalination*, 425:156–174, 2018.

[1078] J Veerman, JW Post, M Saakes, SJ Metz, and GJ Harmsen. Reducing power losses caused by ionic shortcut currents in reverse electrodialysis stacks by a validated model. *Journal of Membrane Science*, 310(1-2):418–430, 2008.

[1079] RE Lacey. Energy by reverse electrodialysis. *Ocean engineering*, 7:1–47, 1980.

[1080] Jan W Post, Joost Veerman, Hubertus VM Hamelers, Gerrit JW Euverink, Sybrand J Metz, Kitty Nymeijer, and Cees JN Buisman. Salinity-gradient power: Evaluation of pressure-retarded osmosis and reverse electrodialysis. *Journal of membrane science*, 288(1-2):218–230, 2007.

[1081] Piotr Długołęcki, Antoine Gambier, Kitty Nijmeijer, and Matthias Wessling. Practical potential of reverse electrodialysis as process for sustainable energy generation. *Environmental science & technology*, 43(17):6888–6894, 2009.

[1082] Jordi Moreno, Simon Grasman, Ronny Van Engelen, and Kitty Nijmeijer. Upscaling reverse electrodialysis. *Environmental science & technology*, 52(18):10856–10863, 2018.

[1083] Odne S Burheim, Frode Seland, Jon G Pharoah, and Signe Kjelstrup. Improved electrode systems for reverse electro-dialysis and electro-dialysis. *Desalination*, 285:147–152, 2012.

[1084] Tong Wen, GS Solt, and YF Sun. Spirally wound electrodialysis (sped) modules. *Desalination*, 101(1):79–91, 1995.

[1085] Natasha C Wright. Design of spiral-wound electrodialysis modules. *Desalination*, 458:54–65, 2019.

[1086] David A Vermaas, Michel Saakes, and Kitty Nijmeijer. Power generation using profiled membranes in reverse electrodialysis. *Journal of membrane science*, 385:234–242, 2011.

[1087] Jin Gi Hong and Yongsheng Chen. Evaluation of electrochemical properties and reverse electrodialysis performance for porous cation exchange membranes with sulfate-functionalized iron oxide. *Journal of membrane science*, 473:210–217, 2015.

[1088] Luigi Gurreri, Michele Ciofalo, Andrea Cipollina, Alessandro Tamburini, Willem Van Baak, and Giorgio Micale. Cfd modelling of profiled-membrane channels for reverse electrodialysis. *Desalination and water treatment*, 55(12):3404–3423, 2015.

[1089] Esra Altıok, Tuğçe Zeynep Kaya, Enver Güler, Nalan Kabay, and Marek Bryjak. Performance of reverse electrodialysis system for salinity gradient energy generation by using a commercial ion exchange membrane pair with homogeneous bulk structure. *Water*, 13(6):814, 2021.

[1090] Zhaolong He, Xueli Gao, Yushan Zhang, Yuhong Wang, and Jian Wang. Revised spacer design to improve hydrodynamics and anti-fouling behavior in reverse electrodialysis processes. *Desalination and Water Treatment*, 57(58):28176–28186, 2016.

[1091] Su-Yoon Lee, Ye-Jin Jeong, So-Ryong Chae, Kyeong-Ho Yeon, Yunkyu Lee, Chan-Soo Kim, Nam-Jo Jeong, and Jin-Soo Park. Porous carbon-coated graphite electrodes for energy production from salinity gradient using reverse electrodialysis. *Journal of Physics and Chemistry of Solids*, 91:34–40, 2016.

[1092] Xiuping Zhu, Weihua He, and Bruce E Logan. Influence of solution concentration and salt types on the performance of reverse electrodialysis cells. *Journal of membrane science*, 494:154–160, 2015.

[1093] M Tedesco, E Brauns, A Cipollina, G Micale, P Modica, G Russo, and J Helsen. Reverse electrodialysis with saline waters and concentrated brines: a laboratory investigation towards technology scale-up. *Journal of Membrane Science*, 492:9–20, 2015.

[1094] Heinz B Winzeler and Georges Belfort. Enhanced performance for pressure-driven membrane processes: the argument for fluid instabilities. *Journal of Membrane Science*, 80(1):35–47, 1993.

[1095] Mahboobeh Vaselbehagh, Hamed Karkhanechi, Ryosuke Takagi, and Hideto Matsuyama. Biofouling phenomena on anion exchange membranes under the reverse electrodialysis process. *Journal of Membrane Science*, 530:232–239, 2017.

[1096] T Rijnaarts, J Moreno, M Saakes, WM de Vos, and K Nijmeijer. Role of anion exchange membrane fouling in reverse electrodialysis using natural feed waters. *Colloids and surfaces A: Physicochemical and engineering aspects*, 560:198–204, 2019.

[1097] EJ Bodner, M Saakes, T Sleutels, CJN Buisman, and HVM Hamelers. The red fouling monitor: A novel tool for fouling analysis. *Journal of membrane science*, 570:294–302, 2019.

[1098] Xi Luo, Xiaoxin Cao, Yinghui Mo, Kang Xiao, Xiaoyuan Zhang, Peng Liang, and Xia Huang. Power generation by coupling reverse electrodialysis and ammonium bicarbonate: Implication for recovery of waste heat. *Electrochemistry communications*, 19:25–28, 2012.

[1099] Younggy Kim and Bruce E Logan. Hydrogen production from inexhaustible supplies of fresh and salt water using microbial reverse-electrodialysis electrolysis cells. *Proceedings of the National Academy of Sciences*, 108(39):16176–16181, 2011.

[1100] Weiyi Li, William B Krantz, Emile R Cornelissen, Jan W Post, Arne RD Verliefde, and Chuyang Y Tang. A novel hybrid process of reverse electrodialysis and reverse osmosis for low energy seawater desalination and brine management. *Applied energy*, 104:592–602, 2013.

[1101] Roland D Cusick, Younggy Kim, and Bruce E Logan. Energy capture from thermolytic solutions in microbial reverse-electrodialysis cells. *Science*, 335(6075):1474–1477, 2012.

[1102] Qing Chen, Yuan-Yuan Liu, Chang Xue, Yu-Ling Yang, and Wei-Ming Zhang. Energy self-sufficient desalination stack as a potential fresh water supply on small islands. *Desalination*, 359:52–58, 2015.

[1103] Qun Wang, Xueli Gao, Yushan Zhang, Zhaolong He, Zhiyong Ji, Xinyan Wang, and Congjie Gao. Hybrid red/ed system: Simultaneous osmotic energy recovery and desalination of high-salinity wastewater. *Desalination*, 405:59–67, 2017.

[1104] WJ Van Egmond, M Saakes, S Porada, T Meuwissen, CJN Buisman, and HVM Hamelers. The concentration gradient flow battery as electricity storage system: Technology potential and energy dissipation. *Journal of Power Sources*, 325:129–139, 2016.

[1105] Ramato Ashu Tufa, Sylwin Pawlowski, Joost Veerman, Karel Bouzek, Enrica Fontananova, Gianluca di Profio, Svetlozar Velizarov, João Goulão Crespo, Kitty Nijmeijer, and Efrem Curcio. Progress and prospects in reverse electrodialysis for salinity gradient energy conversion and storage. *Applied energy*, 225:290–331, 2018.

[1106] Wei Guo, Liuxuan Cao, Junchao Xia, Fu-Qiang Nie, Wen Ma, Jianming Xue, Yanlin Song, Daoben Zhu, Yugang Wang, and Lei Jiang. Energy harvesting with single-ion-selective nanopores: a concentration-gradient-driven nanofluidic power source. *Advanced functional materials*, 20(8):1339–1344, 2010.

[1107] Liuxuan Cao, Wei Guo, Wen Ma, Lin Wang, Fan Xia, Shutao Wang, Yugang Wang, Lei Jiang, and Daoben Zhu. Towards understanding the nanofluidic

reverse electrodialysis system: well matched charge selectivity and ionic composition. *Energy & Environmental Science*, 4(6):2259–2266, 2011.

[1108] Michele Tedesco, Claudio Scalici, Davide Vaccari, Andrea Cipollina, Alessandro Tamburini, and Giorgio Micale. Performance of the first reverse electrodialysis pilot plant for power production from saline waters and concentrated brines. *Journal of Membrane Science*, 500:33–45, 2016.

[1109] Michele Tedesco, Andrea Cipollina, Alessandro Tamburini, and Giorgio Micale. Towards 1 kw power production in a reverse electrodialysis pilot plant with saline waters and concentrated brines. *Journal of Membrane Science*, 522:226–236, 2017.

[1110] Eanna Farrell, Mohamed I Hassan, Ramato A Tufa, Arttu Tuomiranta, Ahmet H Avci, Antonio Politano, Efrem Curcio, and Hassan A Arafat. Reverse electrodialysis powered greenhouse concept for water-and energy-self-sufficient agriculture. *Applied Energy*, 187:390–409, 2017.

[1111] A Tamburini, M Tedesco, A Cipollina, G Micale, M Ciofalo, M Papapetrou, W Van Baak, and A Piacentino. Reverse electrodialysis heat engine for sustainable power production. *Applied Energy*, 206:1334–1353, 2017.

[1112] J. F. Osterle. Electrokinetic Energy Conversion. *Journal of Applied Mechanics*, 31(2):161–164, 06 1964.

[1113] FA Morrison Jr and JF Osterle. Electrokinetic energy conversion in ultrafine capillaries. *The Journal of Chemical Physics*, 43(6):2111–2115, 1965.

[1114] Jun Yang, Fuzhi Lu, Larry W Kostiuk, and Daniel Y Kwok. Electrokinetic microchannel battery by means of electrokinetic and microfluidic phenomena. *Journal of Micromechanics and Microengineering*, 13(6):963, 2003.

[1115] Frank HJ van der Heyden, Derek Stein, and Cees Dekker. Streaming currents in a single nanofluidic channel. *Physical review letters*, 95(11):116104, 2005.

[1116] Frank HJ Van der Heyden, Douwe Jan Bonthuis, Derek Stein, Christine Meyer, and Cees Dekker. Electrokinetic energy conversion efficiency in nanofluidic channels. *Nano letters*, 6(10):2232–2237, 2006.

[1117] Frank HJ van der Heyden, Douwe Jan Bonthuis, Derek Stein, Christine Meyer, and Cees Dekker. Power generation by pressure-driven transport of ions in nanofluidic channels. *Nano letters*, 7(4):1022–1025, 2007.

[1118] Lydéric Bocquet and Elisabeth Charlaix. Nanofluidics, from bulk to interfaces. *Chemical Society Reviews*, 39(3):1073–1095, 2010.

[1119] Christian Davidson and Xiangchun Xuan. Effects of stern layer conductance on electrokinetic energy conversion in nanofluidic channels. *Electrophoresis*, 29(5):1125–1130, 2008.

[1120] Jian Zhang, Kan Zhan, Shuli Wang, and Xu Hou. Soft interface design for electrokinetic energy conversion. *Soft matter*, 16(12):2915–2927, 2020.

[1121] Kai Xiao, Lei Jiang, and Markus Antonietti. Ion transport in nanofluidic devices for energy harvesting. *Joule*, 3(10):2364–2380, 2019.

[1122] Laurent Joly, Christophe Ybert, Emmanuel Trizac, and Lydéric Bocquet. Hydrodynamics within the electric double layer on slipping surfaces. *Physical review letters*, 93(25):257805, 2004.

[1123] Laurent Joly, Christophe Ybert, Emmanuel Trizac, and Lydéric Bocquet. Liquid friction on charged surfaces: From hydrodynamic slippage to electrokinetics. *The Journal of chemical physics*, 125(20):204716, 2006.

[1124] Elena F Silkina, Evgeny S Asmolov, and Olga I Vinogradova. Electro-osmotic flow in hydrophobic nanochannels. *Physical Chemistry Chemical Physics*, 21(41):23036–23043, 2019.

[1125] Yongqiang Ren and Derek Stein. Slip-enhanced electrokinetic energy conversion in nanofluidic channels. *Nanotechnology*, 19(19):195707, 2008.

[1126] Supreet S Bahga, Olga I Vinogradova, and Martin Z Bazant. Anisotropic electro-osmotic flow over super-hydrophobic surfaces. *Journal of fluid mechanics*, 644:245–255, 2010.

[1127] Aleksey V Belyaev and Olga I Vinogradova. Electro-osmosis on anisotropic superhydrophobic surfaces. *Physical review letters*, 107(9):098301, 2011.

[1128] B Fan and PR Bandaru. Tensorial modulation of electrokinetic streaming potentials on air and liquid filled surfaces. *Langmuir*, 35(46):14812–14817, 2019.

[1129] Olga I Vinogradova, Elena F Silkina, Naren Bag, and Evgeny S Asmolov. Achieving large zeta-potentials with charged porous surfaces. *Physics of Fluids*, 32(10):102105, 2020.

[1130] Frieder Mugele and Jean-Christophe Baret. Electrowetting: from basics to applications. *Journal of physics: condensed matter*, 17(28):R705, 2005.

[1131] Frieder Mugele and Jason Heikenfeld. *Electrowetting: fundamental principles and practical applications*. John Wiley & Sons, 2018.

[1132] Tom Krupenkin and J Ashley Taylor. Reverse electrowetting as a new approach to high-power energy harvesting. *Nature communications*, 2(1):1–8, 2011.

[1133] Anatoly B Kolomeisky and Alexei A Kornyshev. Current-generating â€˜double layer shoeâ€™ with a porous sole. *Journal of Physics: Condensed Matter*, 28(46):464009, 2016.

[1134] Ehud Haimov, Aidan Chapman, Fernando Bresme, Andrew S Holmes, Tom Reddyhoff, Michael Urbakh, and Alexei A Kornyshev. Theoretical demonstration of a capacitive rotor for generation of alternating current from mechanical motion. *Nature Communications*, 12(1):1–13, 2021.

[1135] Doriano Brogioli. Extracting renewable energy from a salinity difference using a capacitor. *Physical review letters*, 103(5):058501, 2009.

[1136] AS Aricò, P Bruce, B Scrosati, JM Tarascon, and W van Schalkwijk. Nanostructured materials for advanced energy conversion and storage devices. *Nature materials*, 4(5):366–377, 2005.

[1137] Patrice Simon and Yury Gogotsi. Materials for electrochemical capacitors. In *Nanoscience and technology: a collection of reviews from Nature journals*, pages 320–329. World Scientific, 2010.

[1138] Robert J Hunter. *Introduction to modern colloid science*, volume 7. Oxford University Press Oxford, 1993.

[1139] D Brogioli, R Zhao, and PM Biesheuvel. A prototype cell for extracting energy from a water salinity difference by means of double layer expansion in nanoporous carbon electrodes. *Energy & Environmental Science*, 4(3):772–777, 2011.

[1140] Raúl A Rica, Doriano Brogioli, Roberto Ziano, Domenico Salerno, and Francesco Mantegazza. Ions transport and adsorption mechanisms in porous electrodes during capacitive-mixing double layer expansion (cdle). *The Journal of Physical Chemistry C*, 116(32):16934–16938, 2012.

[1141] Raúl A Rica, Roberto Ziano, Domenico Salerno, Francesco Mantegazza, Martin Z Bazant, and Doriano Brogioli. Electro-diffusion of ions in porous electrodes for capacitive extraction of renewable energy from salinity differences. *Electrochimica Acta*, 92:304–314, 2013.

[1142] Doriano Brogioli and Fabio La Mantia. Capacitive energy extraction from double layer expansion (cdle). fundamentals of the method. In *Interface Science and Technology*, volume 24, pages 87–117. Elsevier, 2018.

[1143] BB Sales, M Saakes, JW Post, CJN Buisman, PM Biesheuvel, and HVM Hamelers. Direct power production from a water salinity difference in a membrane-modified supercapacitor flow cell. *Environmental science & technology*, 44(14):5661–5665, 2010.

[1144] O Burheim, B Sales, O Schaezle, F Liu, and HVM Hamelers. Auto generative capacitive mixing of sea and river water by the use of membranes. In *ASME 2011 International Mechanical Engineering Congress and Exposition (IMECE2011)(Denver, Colorado, USA) p*, pages 483–492, 2011.

[1145] Bruno B Sales, Fei Liu, Olivier Schaetzle, Cees JN Buisman, and Hubertus VM Hamelers. Electrochemical characterization of a supercapacitor flow cell for power production from salinity gradients. *Electrochimica acta*, 86:298–304, 2012.

[1146] O Burheim, BB Sales, O Schaetzle, F Liu, and HVM Hamelers. Auto generative capacitive mixing for power conversion of sea and river water by the use of membranes. *Journal of Energy Resources Technology*, 135(1):011601, 2013.

[1147] Katarzyna Smolinska-Kempisty, Anna Siekierka, and Marek Bryjak. Interpolymer ion exchange membranes for capmix process. *Desalination*, 482:114384, 2020.

[1148] MFM Bijmans, OS Burheim, M Bryjak, A Delgado, P Hack, F Mantegazza, S Tenisson, and HVM Hamelers. Capmix-deploying capacitors for salt gradient power extraction. *Energy Procedia*, 20:108–115, 2012.

[1149] Fei Liu, Olivier Schaetzle, Bruno Bastos Sales, Michel Saakes, Cees JN Buisman, and Hubertus VM Hamelers. Effect of additional charging and current density on the performance of capacitive energy extraction based on donnan potential. *Energy & environmental science*, 5(9):8642–8650, 2012.

[1150] D Brogioli, R Ziano, RA Rica, D Salerno, O Kozynchenko, HVM Hamelers, and F Mantegazza. Exploiting the spontaneous potential of the electrodes used in the capacitive mixing technique for the extraction of energy from salinity difference. *Energy & environmental science*, 5(12):9870–9880, 2012.

[1151] Raúl A Rica, Roberto Ziano, Domenico Salerno, Francesco Mantegazza, Renéa Van Roij, and Doriano Brogioli. Capacitive mixing for harvesting the free energy of solutions at different concentrations. *Entropy*, 15(4):1388–1407, 2013.

[1152] Marta C Hatzell, Kelsey B Hatzell, and Bruce E Logan. Using flow electrodes in multiple reactors in series for continuous energy generation from capacitive mixing. *Environmental Science & Technology Letters*, 1(12):474–478, 2014.

[1153] Guillermo R Iglesias, María M Fernández, Silvia Ahualli, María L Jiménez, Oleksander P Kozynchenko, and Ángel V Delgado. Materials selection for optimum energy production by double layer expansion methods. *Journal of Power Sources*, 261:371–377, 2014.

[1154] AV Delgado, S Ahualli, MM Fernández, MA González, GR Iglesias, JF Vivo-Vilches, and ML Jiménez. Geometrical properties of materials for energy production by salinity exchange. *Environmental Chemistry*, 14(5):279–287, 2017.

[1155] Silvia Ahualli, ML Jimenez, Maria M Fernández, Guillermo Iglesias, Doriano Brogioli, and Angel V Delgado. Polyelectrolyte-coated carbons used in the generation of blue energy from salinity differences. *Physical Chemistry Chemical Physics*, 16(46):25241–25246, 2014.

[1156] MM Fernandez, RM Wagterveld, Silvia Ahualli, Fei Liu, AV Delgado, and HVM Hamelers. Polyelectrolyte-versus membrane-coated electrodes for energy production by capmix salinity exchange methods. *Journal of Power Sources*, 302:387–393, 2016.

[1157] Guangcai Tan and Xiuping Zhu. Polyelectrolyte-coated copper hexacyanoferrate and bismuth oxychloride electrodes for efficient salinity gradient energy recovery in capacitive mixing. *Energy Technology*, page 1900863, 2019.

[1158] Silvia Ahualli, Sergio Orozco-Barrera, María del Mar Fernández, Ángel V Delgado, and Guillermo R Iglesias. Assembly of soft electrodes and ion exchange membranes for capacitive deionization. *Polymers*, 11(10):1556, 2019.

[1159] GR Iglesias, S Ahualli, AV Delgado, PM Arenas-Fernández, and MM Fernández. Combining soft electrode and ion exchange membranes for increasing salinity difference energy efficiency. *Journal of Power Sources*, 453:227840, 2020.

[1160] Meng Ye, Mauro Pasta, Xing Xie, Yi Cui, and Craig S Criddle. Performance of a mixing entropy battery alternately flushed with wastewater effluent and seawater for recovery of salinity-gradient energy. *Energy & Environmental Science*, 7(7):2295–2300, 2014.

[1161] Zhijun Jia, Baoguo Wang, Shiqiang Song, and Yongsheng Fan. A membraneless na ion battery-based capmix cell for energy extraction using water salinity gradients. *RSC advances*, 3(48):26205–26209, 2013.

[1162] Samira Haj Mohammad Hosein Tehrani, Seyed Abolfazl Seyedsadjadi, and Ali Ghaffarinejad. Application of electrodeposited cobalt hexacyanoferrate film to extract energy from water salinity gradients. *RSC Advances*, 5(38):30032–30037, 2015.

[1163] Wellington JAS Gomes, CainaÌƒ de Oliveira, and Fritz Huguenin. Energy harvesting by nickel prussian blue analogue electrode in neutralization and mixing entropy batteries. *Langmuir*, 31(31):8710–8717, 2015.

[1164] Xiuping Zhu, Taeyoung Kim, Mohammad Rahimi, Christopher A Gorski, and Bruce E Logan. Integrating reverse-electrodialysis stacks with flow batteries for improved energy recovery from salinity gradients and energy storage. *ChemSusChem*, 10(4):797–803, 2017.

[1165] Meng Ye, Mauro Pasta, Xing Xie, Kristian L Dubrawski, Jianqaio Xu, Chong Liu, Yi Cui, and Craig S Criddle. Charge-free mixing entropy battery enabled by low-cost electrode materials. *ACS omega*, 4(7):11785–11790, 2019.

[1166] Taeyoung Kim, Mohammad Rahimi, Bruce E Logan, and Christopher A Gorski. Evaluating battery-like reactions to harvest energy from salinity differences using ammonium bicarbonate salt solutions. *ChemSusChem*, 9(9):981–988, 2016.

[1167] Taeyoung Kim, Mohammad Rahimi, Bruce E Logan, and Christopher A Gorski. Harvesting energy from salinity differences using battery electrodes in a concentration flow cell. *Environmental science & technology*, 50(17):9791–9797, 2016.

[1168] Taeyoung Kim, Bruce E Logan, and Christopher A Gorski. High power densities created from salinity differences by combining electrode and donnan potentials in a concentration flow cell. *Energy & Environmental Science*, 10(4):1003–1012, 2017.

[1169] Fang Zhang, Jia Liu, Wulin Yang, and Bruce E Logan. A thermally regenerative ammonia-based battery for efficient harvesting of low-grade thermal energy as electrical power. *Energy & Environmental Science*, 8(1):343–349, 2015.

[1170] Fang Zhang, Nicole LaBarge, Wulin Yang, Jia Liu, and Bruce E Logan. Enhancing low-grade thermal energy recovery in a thermally regenerative ammonia battery using elevated temperatures. *ChemSusChem*, 8(6):1043–1048, 2015.

[1171] Massimo Marino, Lorenza Misuri, Andrea Carati, and Doriano Brogioli. Proof-of-concept of a zinc-silver battery for the extraction of energy from a concentration difference. *Energies*, 7(6):3664–3683, 2014.

[1172] M Marino, L Misuri, A Carati, and D Brogioli. Boosting the voltage of a salinity-gradient-power electrochemical cell by means of complex-forming solutions. *Applied Physics Letters*, 105(3):033901, 2014.

[1173] Andrea Cipollina and Giorgio Micale. *Sustainable energy from salinity gradients*. Woodhead Publishing, 2016.

[1174] M Marino, L Misuri, R Ruffo, and D Brogioli. Electrode kinetics in the "capacitive mixing" and "battery mixing" techniques for energy production from salinity differences. *Electrochimica Acta*, 176:1065–1073, 2015.

[1175] Dong Jun Kim, Rubha Ponraj, Aravindaraj G Kannan, Hyun-Wook Lee, Reza Fathi, Riccardo Ruffo, Claudio M Mari, and Do Kyung Kim. Diffusion behavior of sodium ions in $na_{0.44}mno_2$ in aqueous and non-aqueous electrolytes. *Journal of Power Sources*, 244:758–763, 2013.

[1176] Jiho Lee, Hongsik Yoon, Jaehan Lee, Taeyoung Kim, and Jeyong Yoon. Extraction of salinity-gradient energy by a hybrid capacitive-mixing system. *ChemSusChem*, 10(7):1600–1606, 2017.

[1177] Khairul Nisak Md Hasan, Tian Xian Khai, Ramani Kannan, and Zainul Azhar Zakaria. Harnessing â€˜blue energyâ€™: A review on techniques and preliminary analysis. In *MATEC Web of Conferences*, volume 131, page 04013. EDP Sciences, 2017.

[1178] Shu Yuan Pan, Seth W. Snyder, Yupo J. Lin, and Pen Chi Chiang. Electrokinetic desalination of brackish water and associated challenges in the water and energy nexus. *Environmental Science: Water Research and Technology*, 4(5):613–638, 2018.

[1179] Ali Hemmatifar. *Energy Consumption and Salt Adsorption in Capacitive Deionization*. PhD thesis, 2018.

[1180] Matthew Suss. *Capacitive water desalination with hierarchical porous electrodes*. PhD thesis, 2013.

[1181] Ashwin Ramachandran, Ali Hemmatifar, Steven A. Hawks, Michael Stadermann, and Juan G. Santiago. Self similarities in desalination dynamics and performance using capacitive deionization. *Water Research*, 140:323–334, 2018.

[1182] Karan H Mistry, Ronan K McGovern, Gregory P Thiel, Edward K Summers, Syed M Zubair, and John H Lienhard. Entropy generation analysis of desalination technologies. *Entropy*, 13(10):1829–1864, 2011.

[1183] Yajing Zhao, Yue Wang, Ruguo Wang, Yafei Wu, Shichang Xu, and Jixiao Wang. Performance comparison and energy consumption analysis of capacitive deionization and membrane capacitive deionization processes. *Desalination*, 324:127–133, sep 2013.

[1184] Jae-Hwan Choi. Comparison of constant voltage (CV) and constant current (CC) operation in the membrane capacitive deionisation process. *Desalination and Water Treatment*, 56(4):921–928, oct 2015.

[1185] Ashwin Ramachandran, Steven A. Hawks, Michael Stadermann, and Juan G. Santiago. Frequency analysis and resonant operation for efficient capacitive deionization. *Water Research*, 144:581–591, 2018.

[1186] Mark D Andelman and Gregory S Walker. Charge barrier flow-through capacitor, 2004.

[1187] Haibo Li, Yang Gao, Likun Pan, Yanping Zhang, Yiwei Chen, and Zhuo Sun. Electrosorptive desalination by carbon nanotubes and nanofibres electrodes and ion-exchange membranes. *Water Research*, 42(20):4923–4928, 2008.

[1188] P.M. Biesheuvel and A Van der Wal. Membrane capacitive deionization. *Journal of Membrane Science*, 346(2):256–262, 2010.

[1189] David Cohen-Tanugi, Ronan K. McGovern, Shreya H. Dave, John H. Lienhard, and Jeffrey C. Grossman. Quantifying the potential of ultra-permeable membranes for water desalination. *Energy and Environmental Science*, 7:1134–1141, 2014.

[1190] Ho Bum Park, Jovan Kamcev, Lloyd M Robeson, Menachem Elimelech, and Benny D Freeman. Maximizing the right stuff: The trade-off between membrane permeability and selectivity, 2017.

[1191] Lucía Alvarado, Israel Rodríguez Torres, and Aicheng Chen. Integration of ion exchange and electrodeionization as a new approach for the continuous treatment of hexavalent chromium wastewater. *Separation and Purification Technology*, 105:55–62, 2013.

[1192] Ying Liu, Jianyou Wang, Yong Xu, and Bin Wu. A deep desalination and anti-scaling electrodeionization (EDI) process for high purity water preparation. *Desalination*, 468:114075, 2019.

[1193] J. M. Ortiz, E. Expósito, F. Gallud, V. García-García, V. Montiel, and V. A. Aldaz. Desalination of underground brackish waters using an electrodialysis system powered directly by photovoltaic energy. *Solar Energy Materials and Solar Cells*, 92(12):1677–1688, 2008.

[1194] Natasha C Wright, Sahil R Shah, and Susan E Amrose. A robust model of brackish water electrodialysis desalination with experimental comparison at different size scales. *Desalination*, 443:27–43, 2018.

[1195] GJ Doornbusch, M Tedesco, JW Post, Z Borneman, and K Nijmeijer. Experimental investigation of multistage electrodialysis for seawater desalination. *Desalination*, 464:105–114, 2019.

[1196] Haiyang Yan, Yaoming Wang, Liang Wu, Muhammad A Shehzad, Chenxiao Jiang, Rongqiang Fu, Zhaoming Liu, and Tongwen Xu. Multistage-batch electrodialysis to concentrate high-salinity solutions: Process optimisation, water transport, and energy consumption. *Journal of Membrane Science*, 570:245–257, 2019.

[1197] Xin Tong, Bopeng Zhang, Yilin Fan, and Yongsheng Chen. Mechanism exploration of ion transport in nanocomposite cation exchange membranes. *ACS applied materials & interfaces*, 9(15):13491–13499, 2017.

[1198] Hanqing Fan, Yuxuan Huang, and Ngai Yin Yip. Advancing the conductivity-permselectivity tradeoff of electrodialysis ion-exchange membranes with sulfonated cnt nanocomposites. *Journal of Membrane Science*, 610:118259, 2020.

[1199] Adetunji Alabi, Levente Cseri, Ahmed Al Hajaj, Gyorgy Szekely, Peter Budd, and Linda Zou. Electrostatically-coupled graphene oxide nanocomposite cation exchange membrane. *Journal of Membrane Science*, 594:117457, 2020.

[1200] Marcello Fidaleo and Mauro Moresi. Electrodialysis applications in the food industry. *Advances in food and nutrition research*, 51:265–360, 2006.

[1201] Edwin Vera, Jacqueline Sandeaux, Françoise Persin, Gérald Pourcelly, Manuel Dornier, and Jenny Ruales. Deacidification of passion fruit juice by electrodialysis with bipolar membrane after different pretreatments. *Journal of food engineering*, 90(1):67–73, 2009.

[1202] Hana Šímová, Vladimír Kysela, and Aleš Černín. Demineralization of natural sweet whey by electrodialysis at pilot-plant scale. *Desalination and Water Treatment*, 14(1-3):170–173, 2010.

[1203] L Bazinet, A Doyen, and C Roblet. Electrodialytic phenomena, associated electromembrane technologies and applications in the food, beverage and nutraceutical industries. In *Separation, Extraction and Concentration Processes in the Food, Beverage and Nutraceutical Industries*, pages 202–218. Elsevier, 2013.

[1204] Yaoming Wang, Chenxiao Jiang, Laurent Bazinet, and Tongwen Xu. Electrodialysis-based separation technologies in the food industry. In *Separation of Functional Molecules in Food by Membrane Technology*, pages 349–381. Elsevier, 2019.

[1205] Nayeong Kim, Jemin Jeon, Raylin Chen, and Xiao Su. Electrochemical separation of organic acids and proteins for food and biomanufacturing. *Chemical Engineering Research and Design*, 178:267–288, 2022.

[1206] Viktoria Lindstrand, Göran Sundström, and Ann-Sofi Jönsson. Fouling of electrodialysis membranes by organic substances. *Desalination*, 128(1):91–102, 2000.

[1207] Le Han. Current strategies for the design of anti-fouling ion-exchange membranes. *Membrane Technology Enhancement for Environmental Protection and Sustainable Industrial Growth*, pages 13–25, 2021.

[1208] Mahboobeh Vaselbehagh, Hamed Karkhanechi, Sri Mulyati, Ryosuke Takagi, and Hideto Matsuyama. Improved antifouling of anion-exchange membrane by polydopamine coating in electrodialysis process. *Desalination*, 332(1):126–133, 2014.

[1209] Wenyun Wang, Rongqiang Fu, Zhaoming Liu, and Haizeng Wang. Low-resistance anti-fouling ion exchange membranes fouled by organic foulants in electrodialysis. *Desalination*, 417:1–8, 2017.

[1210] Jin Ran, Liang Wu, Yubin He, Zhengjin Yang, Yaoming Wang, Chenxiao Jiang, Liang Ge, Erigene Bakangura, and Tongwen Xu. Ion exchange membranes: New developments and applications. *Journal of Membrane Science*, 522:267–291, 2017.

[1211] Yoshinobu Tanaka. Electrodialysis. In *Progress in Filtration and Separation*, pages 207–284. Elsevier, 2015.

[1212] Rubaba Mohammadi, Walter Tang, and Mika Sillanpää. A systematic review and statistical analysis of nutrient recovery from municipal wastewater by electrodialysis. *Desalination*, 498:114626, 2021.

[1213] Etienne Brauns. Salinity gradient power by reverse electrodialysis: effect of model parameters on electrical power output. *Desalination*, 237(1-3):378–391, 2009.

[1214] Sylwin Pawlowski, João G Crespo, and Svetlozar Velizarov. Profiled ion exchange membranes: A comprehensible review. *International journal of molecular sciences*, 20(1):165, 2019.

[1215] Andrej Grabowski, Guiqing Zhang, Heiner Strathmann, and Gerhart Eigenberger. Production of high-purity water by continuous electrodeionization with bipolar membranes: influence of concentrate and protection compartment. *Separation and purification technology*, 60(1):86–95, 2008.

[1216] I Gede Wenten and Fany Arfianto. Bench scale electrodeionization for high pressure boiler feed water. *Desalination*, 314:109–114, 2013.

[1217] Xin-Yu Zheng, Shu-Yuan Pan, Po-Chih Tseng, Huai-Li Zheng, and Pen-Chi Chiang. Optimization of resin wafer electrodeionization for brackish water desalination. *Separation and Purification Technology*, 194:346–354, 2018.

[1218] Christa N Hestekin, Jamie A Hestekin, Sadia Paracha, Grace Morrison, Efecan Pakkaner, John Moore, Leticia Santos de Souza, Sam Stephens, Catey Atchley, and Ira Kurtz. Simulating nephron ion transport function using activated wafer electrodeionization. *Communications Materials*, 1(1):1–10, 2020.

[1219] Humeyra B Ulusoy Erol, Christa N Hestekin, and Jamie A Hestekin. Effects of resin chemistries on the selective removal of industrially relevant metal ions using wafer-enhanced electrodeionization. *Membranes*, 11(1):45, 2021.

[1220] Devesh Mittal, Venkat Jagannathan, and Narender Singh Bisht. Use of unique fractional electrodeionization in power plant applications. *Power Plant Chemistry*, 11, 2009.

[1221] Karim M Chehayeb, Daniel M Farhat, and Kishor G Nayar. Optimal design and operation of electrodialysis for brackish-water desalination and for high-salinity brine concentration. *Desalination*, 420:167–182, 2017.

[1222] Jaromír Marek, Jan Čížek, and D Tvrzník. Optimizing porous material in shock electrodialysis unit. *Desalin. Water Treat.*, 170:38–45, 2019.

[1223] Soujit Sen Gupta, Md Rabiul Islam, and Thalappil Pradeep. Chapter 7 - Capacitive Deionization (CDI): An Alternative Cost-Efficient Desalination Technique. In *Advances in Water Purification Techniques: Meeting the Needs of Developed and Developing Countries*. 2018.

[1224] Wenle Xing, Jie Liang, Wangwang Tang, Di He, Ming Yan, Xiangxi Wang, Yuan Luo, Ning Tang, and Mei Huang. Versatile applications of capacitive deionization (CDI)-based technologies. *Desalination*, 482, 2020.

[1225] Calvin He, Boyue Lian, Jinxing Ma, Changyong Zhang, Yuan Wang, Hengliang Mo, and T. David Waite. Scale-up and Modelling of Flow-electrode CDI Using Tubular Electrodes. *Water Research*, 203:117498, sep 2021.

[1226] Choonsoo Kim, Pattarachai Srimuk, Juhan Lee, Mesut Aslan, and Volker Presser. Semi-continuous capacitive deionization using multi-channel flow stream and ion exchange membranes. *Desalination*, 425, 2018.

[1227] Jiho Lee, Jaehan Lee, Seok Won Hong, Choonsoo Kim, and Jeyong Yoon. Parametric study of multichannel desalination battery for low-energy electrochemical deionization of brackish water. *Desalination*, 515, 2021.

[1228] Tristan D. Hasseler, Ashwin Ramachandran, William A. Tarpeh, Michael Stadermann, and Juan G. Santiago. Process design tools and techno-economic analysis for capacitive deionization. *Water Research*, 183:116034, 2020.

[1229] Xitong Liu, Sneha Shanbhag, Timothy V. Bartholomew, Jay F. Whitacre, and Meagan S. Mauter. Cost Comparison of Capacitive Deionization and Reverse Osmosis for Brackish Water Desalination. *ACS ES&T Engineering*, 1(2):261–273, 2021.

[1230] Clare Bales, Peter Kovalsky, John Fletcher, and T. David Waite. Low cost desalination of brackish groundwaters by Capacitive Deionization (CDI) â€“ Implications for irrigated agriculture. *Desalination*, 453, 2019.

[1231] Yu-Yi Shen, Shih-Han Sun, Shao-Wei Tsai, Tsai-Hsuan Chen, and Chia-Hung Hou. Development of a membrane capacitive deionization stack for domestic wastewater reclamation: A pilot-scale feasibility study. *Desalination*, 500:114851, 2021.

[1232] Qi Wang, Kuo Fang, Conghui He, and Kaijun Wang. Ammonia removal from municipal wastewater via membrane capacitive deionization (mcdi) in pilot-scale. *Separation and Purification Technology*, page 120469, 2022.

[1233] Sung-il Jeon, Nayeong Kim, Kyusik Jo, Jaewuk Ahn, Hwajoo Joo, Changha Lee, Choonsoo Kim, and Jeyong Yoon. Improvement in the desalination performance of membrane capacitive deionization with a bipolar electrode via an energy recovery process. *Chemical Engineering Journal*, 439:135603, 2022.

[1234] Hwajoo Joo, Seoni Kim, Seongsoo Kim, Minjune Choi, Seung-Hyun Kim, and Jeyong Yoon. Pilot-scale demonstration of an electrochemical system for lithium recovery from the desalination concentrate. *Environmental Science: Water Research & Technology*, 6(2):290–295, 2020.

[1235] Erik R Reale, Lyle Regenwetter, Adreet Agrawal, Brian Dardon, Nicholas Dicola, Sathvik Sanagala, and Kyle C Smith. Low porosity, high areal-capacity prussian blue analogue electrodes enhance salt removal and thermodynamic efficiency in symmetric faradaic deionization with automated fluid control. *Water Research X*, page 100116, 2021.

[1236] Nayeong Kim, Jemin Jeon, Johannes Elbert, Choonsoo Kim, and Xiao Su. Redox-mediated electrochemical desalination for waste valorization in dairy production. *Chemical Engineering Journal*, 428:131082, 2022.

[1237] Steven Hand and Roland D Cusick. Emerging investigator series: capacitive deionization for selective removal of nitrate and perchlorate: impacts of ion selectivity and operating constraints on treatment costs. *Environmental Science: Water Research & Technology*, 6(4):925–934, 2020.

[1238] Michael Baldea. From process integration to process intensification. *Computers & Chemical Engineering*, 81:104–114, 2015.

[1239] Frerich J Keil. Process intensification. *Reviews in Chemical Engineering*, 34(2):135–200, 2018.

[1240] Yong-ha Kim, Lydia K Park, Sotira Yiacoumi, and Costas Tsouris. Modular chemical process intensification: a review. *Annual review of chemical and biomolecular engineering*, 8:359–380, 2017.

[1241] Xiao Su. Electrochemical interfaces for chemical and biomolecular separations. *Current Opinion in Colloid & Interface Science*, 46:77–93, 2020.

[1242] Zachary J Schiffer and Karthish Manthiram. Electrification and decarbonization of the chemical industry. *Joule*, 1(1):10–14, 2017.

[1243] Sumit Verma, Shawn Lu, and Paul JA Kenis. Co-electrolysis of co_2 and glycerol as a pathway to carbon chemicals with improved technoeconomics due to low electricity consumption. *Nature Energy*, 4(6):466–474, 2019.

[1244] John L Barton. Electrification of the chemical industry. *Science*, 368(6496):1181–1182, 2020.

[1245] Seoni Kim, Jiye Kim, Seonghwan Kim, Jaehan Lee, and Jeyong Yoon. Electrochemical lithium recovery and organic pollutant removal from industrial wastewater of a battery recycling plant. *Environmental Science: Water Research & Technology*, 4(2):175–182, 2018.

[1246] Zhongwei Zhao, Xiufen Si, Xuheng Liu, Lihua He, and Xinxing Liang. Li extraction from high mg/li ratio brine with lifepo4/fepo4 as electrode materials. *Hydrometallurgy*, 133:75–83, 2013.

[1247] Lihua He, Wenhua Xu, Yunfeng Song, Yunze Luo, Xuheng Liu, and Zhongwei Zhao. New insights into the application of lithium-ion battery materials: Selective extraction of lithium from brines via a rocking-chair lithium-ion battery system. *Global Challenges*, 2(2):1700079, 2018.

[1248] Xiaoyu Zhao, Haocun Yang, Yanfei Wang, and Zuoliang Sha. Review on the electrochemical extraction of lithium from seawater/brine. *Journal of Electroanalytical Chemistry*, 850:113389, 2019.

[1249] Xiao Su, Lev Bromberg, Kai-Jher Tan, Timothy F Jamison, Lokesh P Padhye, and T Alan Hatton. Electrochemically mediated reduction of nitrosamines by hemin-functionalized redox electrodes. *Environmental Science & Technology Letters*, 4(4):161–167, 2017.

[1250] Haley Vapnik, Johannes Elbert, and Xiao Su. Redox-copolymers for the recovery of rare earth elements by electrochemically regenerated ion-exchange. *Journal of Materials Chemistry A*, 9(35):20068–20077, 2021.

[1251] Paola Baldaguez Medina, Stephen Cotty, Kwiyong Kim, Johannes Elbert, and Xiao Su. Emerging investigator series: electrochemically-mediated remediation of genx using redox-copolymers. *Environmental Science: Water Research & Technology*, 7(12):2231–2240, 2021.

[1252] Kai-Jher Tan, Satoshi Morikawa, Katherine R Phillips, Nil Ozbek, and T Alan Hatton. Redox-active magnetic composites for anionic contaminant removal from water. *ACS Applied Materials & Interfaces*, 2022.

[1253] Raylin Chen, Jiangyan Feng, Jemin Jeon, Thomas Sheehan, Christian Rüttiger, Markus Gallei, Diwakar Shukla, and Xiao Su. Structure and potential-dependent selectivity in redox-metallopolymers: Electrochemically mediated multicomponent metal separations. *Advanced Functional Materials*, 31(15):2009307, 2021.

[1254] Adetunji Alabi, Ahmed AlHajaj, Levente Cseri, Gyorgy Szekely, Peter Budd, and Linda Zou. Review of nanomaterials-assisted ion exchange membranes for electromembrane desalination. *npj Clean Water*, 1(1):1–22, 2018.

[1255] Amir Razmjou, Mohsen Asadnia, Ehsan Hosseini, Asghar Habibnejad Korayem, and Vicki Chen. Design principles of ion selective nanostructured membranes for the extraction of lithium ions. *Nature communications*, 10(1):1–15, 2019.

[1256] Ramya H Tunuguntla, Robert Y Henley, Yun-Chiao Yao, Tuan Anh Pham, Meni Wanunu, and Aleksandr Noy. Enhanced water permeability and tunable ion selectivity in subnanometer carbon nanotube porins. *Science*, 357(6353):792–796, 2017.

[1257] Rimeh Daghrir, Patrick Drogui, and Joel Tshibangu. Efficient treatment of domestic wastewater by electrochemical oxidation process using bored doped diamond anode. *Separation and Purification Technology*, 131:79–83, 2014.

[1258] David S Sholl and Ryan P Lively. Exemplar mixtures for studying complex mixture effects in practical chemical separations. *JACS Au*, 2022.

[1259] WT Mook, MH Chakrabarti, MK Aroua, GMA Khan, BS Ali, MS Islam, and MA Abu Hassan. Removal of total ammonia nitrogen (tan), nitrate and total organic carbon (toc) from aquaculture wastewater using electrochemical technology: a review. *Desalination*, 285:1–13, 2012.

[1260] Yanhong Bian, Xi Chen, and Zhiyong Jason Ren. ph dependence of phosphorus speciation and transport in flow-electrode capacitive deionization. *Environmental Science & Technology*, 54(14):9116–9123, 2020.

[1261] Kwiyong Kim, Riccardo Candeago, Guanhe Rim, Darien Raymond, Ah-Hyung Alissa Park, and Xiao Su. Electrochemical approaches for selective recovery of critical elements in hydrometallurgical processes of complex feedstocks. *Iscience*, 24(5):102374, 2021.

[1262] Wei Jin and Yi Zhang. Sustainable electrochemical extraction of metal resources from waste streams: from removal to recovery. *ACS Sustainable Chemistry & Engineering*, 8(12):4693–4707, 2020.

[1263] Kwiyong Kim, Darien Raymond, Riccardo Candeago, and Xiao Su. Selective cobalt and nickel electrodeposition for lithium-ion battery recycling

through integrated electrolyte and interface control. *Nature communications*, 12(1):1–10, 2021.

[1264] Luiz Eduardo Oliveira Carmo Rodrigues and Marcelo Borges Mansur. Hydrometallurgical separation of rare earth elements, cobalt and nickel from spent nickel–metal–hydride batteries. *Journal of power sources*, 195(11):3735–3741, 2010.

[1265] Namra Mir and Yusuf Bicer. Thermodynamic modeling of a combined photo-electrodialysis-chloralkali system for sustainable desalination. *Desalination*, 499:114822, 2021.

[1266] Gowri Mohandass, Taeyoung Kim, and Sitaraman Krishnan. Continuous solar desalination of brackish water via a monolithically integrated redox flow device. *ACS ES&T Engineering*, 1(12):1678–1687, 2021.

[1267] Fuming Chen, R Karthick, Qi Zhang, Jian Wang, Mengjun Liang, Jinhong Dai, Xiaofang Jiang, and Yue Jiang. Exploration of a photo-redox desalination generator. *Journal of Materials Chemistry A*, 7(35):20169–20175, 2019.

[1268] Seonghun Kim, Guangxia Piao, Dong Suk Han, Ho Kyong Shon, and Hyunwoong Park. Solar desalination coupled with water remediation and molecular hydrogen production: a novel solar water-energy nexus. *Energy & Environmental Science*, 11(2):344–353, 2018.

[1269] Anaira Román Santiago, Paola Baldaguez Medina, and Xiao Su. Electrochemical remediation of perfluoroalkyl substances from water. *Electrochimica Acta*, 403:139635, 2022.

[1270] Zonglin Pan, Chengwen Song, Lin Li, Hong Wang, Yanqiu Pan, Chunlei Wang, Jianxin Li, Tonghua Wang, and Xianshe Feng. Membrane technology coupled with electrochemical advanced oxidation processes for organic wastewater treatment: Recent advances and future prospects. *Chemical Engineering Journal*, 376:120909, 2019.

[1271] Kyusik Jo, Youngbin Baek, Seoni Kim, Sung Pil Hong, and Jeyong Yoon. Evaluation of long-term stability in capacitive deionization using activated carbon electrodes coated with ion exchange polymers. *Korean Journal of Chemical Engineering*, 37(7):1199–1205, 2020.

[1272] Feng Duan, Xuan Du, Yuping Li, Hongbin Cao, and Yi Zhang. Desalination stability of capacitive deionization using ordered mesoporous carbon: effect of oxygen-containing surface groups and pore properties. *Desalination*, 376:17–24, 2015.

[1273] Pattarachai Srimuk, Marco Zeiger, Nicolas Jäckel, Aura Tolosa, Benjamin Krüner, Simon Fleischmann, Ingrid Grobelsek, Mesut Aslan, Boris Shvartsev, and Matthew E Suss. Enhanced performance stability of carbon/titania hybrid electrodes during capacitive deionization of oxygen saturated saline water. *Electrochimica Acta*, 224:314–328, 2017.

[1274] Donald Vineyard, Andrea Hicks, KG Karthikeyan, Christy Davidson, and Phillip Barak. Life cycle assessment of electrodialysis for sidestream nitrogen recovery in municipal wastewater treatment. *Cleaner Environmental Systems*, 2:100026, 2021.

[1275] C Fernandez-Gonzalez, A Dominguez-Ramos, R Ibañez, and A Irabien. Sustainability assessment of electrodialysis powered by photovoltaic solar energy for freshwater production. *Renewable and Sustainable Energy Reviews*, 47:604–615, 2015.

Chapter 2

Small-Scale Desalination of Seawater by Shock Electrodialysis

The work reported in this chapter has been published as "Small-Scale Desalination of Seawater by Shock Electrodialysis," by Mohammad A. Alkhadra, Tao Gao, Kameron M. Conforti, Huanhuan Tian, and Martin Z. Bazant. It has been adapted with permission from Elsevier, 2020.

Abstract

Conventional desalination technologies such as distillation and reverse osmosis are well suited for the supply of fresh water at large scale. The expensive infrastructure and high capital, operating, and maintenance costs associated with these technologies, however, limits their application in remote or underdeveloped areas. Here, we show that shock electrodialysis, a recently developed electrokinetic process, can be used to continuously desalinate artificial seawater (3.5 wt%) for small-scale ($\leq 25\,\mathrm{m}^3$/day as a long-term goal), decentralized applications. In two steps, 99.8% of the salt fed was rejected, with selectivity for magnesium ions of which $> 99.99\%$ were removed (based on measurements of concentration by mass spectrometry). We also demonstrate for the first time the viability of using and continuously recycling solutions of sodium citrate buffer to simultaneously reduce waste and inhibit precipitation reactions in the electrode streams. As with conventional electrodialysis, the energy consumed by our technology can be significantly reduced by desalinating sources that are less saline than seawater, such as brackish water and various industrial or municipal process streams. Since the design of the system and choice of materials have yet to be optimized, there remain ample opportunities to further reduce the cost of desalination by shock electrodialysis.

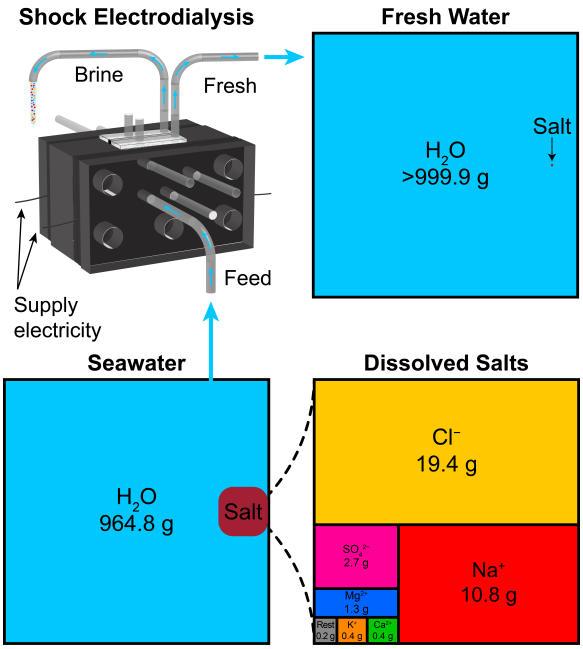

2.1 Introduction and Background

Oceans represent the largest source of surface water and comprise roughly 97% of the total volume of water on Earth. Since these water bodies are salty, seawater is not directly a useful source of drinking water. The average salinity of seawater is approximately 3.5 wt% (i.e., $35\,\mathrm{g\,L^{-1}}$),[1] which means that every kilogram of seawater has about 35 grams of dissolved salts. These salts include mainly sodium (Na^+) and chloride (Cl^-), but also magnesium (Mg^{2+}), calcium (Ca^{2+}), potassium (K^+), and sulfate (SO_4^{2-}). Although a costly endeavor, desalination of seawater is believed to be a promising solution to the globally increasing demand for fresh water. In 2016, the total production of fresh water worldwide via desalination was approximately 38 billion cubic meters, which is more than double the amount of production achieved in 2008.[2] Processes for desalting seawater are typically driven by either thermal (e.g., distillation) or electrical (e.g., osmosis, solar, or wind) power. In this article, we use a nascent electrokinetic method known as shock electrodialysis (SED) to desalinate seawater. A potential advantage of SED over most other methods for continuous desalination is the ability to perform ionic separation, such as selective removal of multivalent ionic solutes. As a result of this selectivity, SED can

be used to capture target species of high value. This technology also operates at ambient conditions and requires only enough pumping for fluidic transport, which precludes the need for high-temperature (distillation) or high-pressure (reverse osmosis, or RO) systems.

Historically, distillation (e.g., multi-stage flash and multiple-effect distillation) has been the method of choice for desalination of seawater, though more than half of the current desalination plants use RO in some capacity.[3] Distillation technologies, which are essentially sequences of heat exchangers, require high capital and energy costs, and are therefore mostly suitable in regions where the necessary fuel is affordable. RO, on the other hand, consumes much less energy and is therefore more efficient (≈ 5 Wh L^{-1}) at desalinating seawater.[4] The governing principle of desalination using RO is to generate large enough pressures to overcome the osmotic pressure of seawater (up to 27 times atmospheric pressure) across a semipermeable membrane. In a sense, RO removes water from the salt, irrespective of its concentration, which makes this technology less practical for decontamination (i.e., removal of trace toxic substances from water). RO also suffers from low water recovery during seawater desalination, such that the larger volumes of brine discharged are associated with high additional costs for disposal as well as environmental damage.

Another technology used for desalination is electrodialysis (ED), in which hydrated ions are forced through their respective ion-selective membranes by electrokinetic action. The advantage of this technology is that it does not involve phase changes (as in distillation) or conversion of energy from electrical to mechanical (as in RO). In electrodialysis, ions are directly transported by applying an electric field from a source of direct current. Once the region between these membranes becomes depleted of salt, however, the low conductivity of the solution will be compensated by an increased electric potential that ultimately drives up the energy requirement. This limitation has made electrodialysis impractical for processing feeds of less than 400 ppm of total dissolved salts.[5]

Table 2.1. Composition of artificial seawater based on the proportions of salt reported in Section 2.3. Concentrations are per unit volume of the solution. This formulation was motivated by data in a technical report published by the US Department of Energy;[1] these data (US DOE) are shown pictorially in the graphical abstract.

	Concentration & Mass/Mole Fraction			
Species	g L^{-1}	[%]	mol L^{-1}	[%]
Sodium (Na^+)	11.178	[29.660]	0.486	[40.132]
Magnesium (Mg^{2+})	1.332	[3.533]	0.055	[4.522]
Calcium (Ca^{2+})	0.700	[1.859]	0.017	[1.433]
Potassium (K^+)	0.822	[2.181]	0.021	[1.735]
Chloride (Cl^-)	21.674	[57.514]	0.611	[50.467]
Sulfate (SO_4^{2-})	1.980	[5.253]	0.021	[1.701]
Total	37.685	[100]	1.211	[100]

A promising feature of SED is that it can continuously produce deionized ($\approx 10\,\mu$M) water, although the concentrations of the feed have only ranged from ~ 1 to ~ 100 mM of salt.[6–8] These previous experiments also involved only a single species of each charge (i.e., one cation and one anion) at a time. The goal of this study is therefore to examine the ability of SED to desalinate artificial seawater, for which we chose to include only the six most abundant components, namely Na^+, Mg^{2+}, Ca^{2+}, and K^+, as well as Cl^- and SO_4^{2-}. The composition of this model seawater is based on a technical report published by the US Department of Energy[1] and is shown in Table 2.1. In our formulation, we excluded debris and large particulates such as sand, dirt, and seaweed to avoid clogging the device. (An SED system would in practice include a pre-filtration step to remove this suspended matter, which does not influence the energy demand of desalination.)

2.2 Theory and Operating Principles

Although technologies for large-scale desalination have been extensively developed, little attention has been paid to the market of small-scale desalination, in which the capacity of water produced is less than 25 m^3 per day. Desalination at small scales, however, is a capability in high demand by industrial facilities, recreational and infrastructural spaces, development projects (both inland and coastal), health care

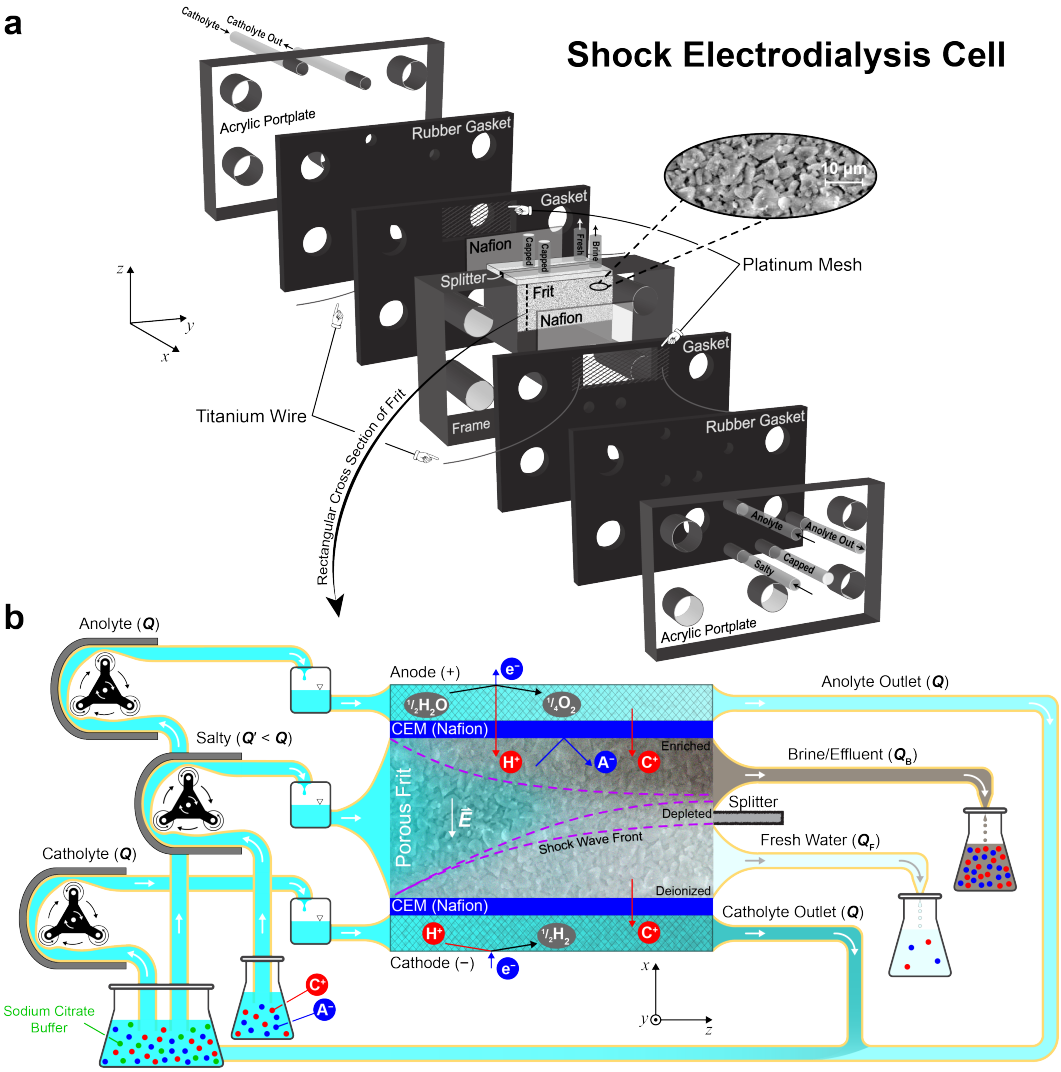

Figure 2-1. Schematic of the SED device that demonstrates both assembly and operating principles. (a) A working device consists of platinum electrodes, titanium wire, and a microporous borosilicate frit sandwiched between identical nafion membranes which permit passage of only cations. The inlet (outlet) streams are labeled *contaminated*, *anolyte* (*anolyte out*), and *catholyte* (*catholyte out*); fluid leaving the top edge of the frit is split into *fresh* and *brine* streams. The close-up image of a glass frit taken by scanning electron microscopy was reproduced with permission from Deng et al. *Langmuir* 2013, 29, 16167–16177. Copyright 2013, American Chemical Society. (b) A rectangular cross section of the frit shows water splitting at the anode and formation of molecular hydrogen at the cathode, which are the primary electrochemical reactions that provide current to the cell. Contaminated water in the frit is then subjected to an external electric field ($\vec{\boldsymbol{E}}$) that transports charged species perpendicular to the flow. In (b), flow rate is denoted by the letter $\boldsymbol{Q}$, and streams are colored based on relative concentration.

and academic institutions, and military vessels.[9] This process, which demands low capital costs, capacities, and flow rates, could also serve isolated communities located in arid or remote regions as well as regions affected by natural disaster and armed conflict.[10] Advantages of desalination at small scales include decentralization of the water supply, low capital and construction costs, and low transportation costs by virtue of operation *in situ*.[9] Moreover, possession of a lightweight and portable device that is adaptable to the available sources of feed water offers flexibility in the types of problems that can be solved based on the unique needs of each sector. SED is a technology that is naturally operated at small scales, so it holds promise as a decentralized, point-of-use desalination system. Our current SED unit is a handheld device ($\sim (3.7\text{ cm})^3$) that weighs 150 g (1/3 lbs, mostly from metal nuts and bolts) and can generate up to 0.5 L per day with little energy needed for fluidic pumping. When scaled up, this device can be designed to have dimensions similar to those of a 10.5-inch tablet computer (e.g., an Apple iPad which has dimensions of $1 \times 20 \times 25\,\text{cm}^3$) and to generate approximately 20 L per day with a pumping requirement similar to that of the current unit. This thin, rectangular geometry will facilitate parallelization of the system—for example by stacking several units on top of one another—to achieve the throughput desired for a small-scale application.

The first system to achieve (batch) deionization by SED in the laboratory was designed, built, tested, and patented by our group.[6,7,11,12] Recent generations of this system[8,13] involve a cross-flow architecture that enables continuous operation, whereby feed flows into a microporous glass frit (a weakly charged medium with small pores) positioned between identical cation exchange membranes, as shown in Figure 2-1. The process of SED requires formation of a sharp gradient—a shock wave—in the concentration of ions in the frit,[14,15] which is accomplished by applying an electric field that drives cations out of the “deionized" region. For the system to maintain bulk electroneutrality, anions leave this region in the opposite direction (toward the anode) because they would be blocked by the ion-selective membrane otherwise. This so-called concentration polarization[14] leads to enrichment of ions

near the anode as well as depletion near the cathode. As ions are depleted in the deionized region, the system will tend to its diffusion limited current at which the rate of ion transport is constrained by how fast analyte can diffuse to or from the electrodes. The weakly charged surfaces of the frit, however, are able to support the electrolyte by providing “overlimiting conductance," which ultimately leads to the separation of ions into enriched and depleted zones.[14] Physically, these zones are separated by a propagating deionization shock wave in the porous medium,[15] similar to the concentration shocks first observed in microfluidic devices.[16–18] This electrokinetic separation can be made continuous by driving flow (through the frit) perpendicular to the applied electric field.[7,8] A physical splitter placed at the outlet is then used to collect each of the enriched and deionized streams.

The primary mechanisms of overlimiting conductance include surface conduction, which dominates in thin channels ($\sim 1\ \mu$m), and surface convection (i.e., electroosmosis), which becomes important in larger channels ($\sim 100\ \mu$m).[14] Surface conduction is driven by excess counterions (in this case cations) that screen the (negative) charge of the wall and amplify the axial electric field in the depleted region, where bulk conductivity is reduced.[15] This amplified electric field then forces coions (in this case anions) out of the depleted region (in the positive x–direction), which sharpens the concentration gradient and concomitantly produces a steady shock wave. As the width of pores is increased, surface convection by electroosmotic flow overpowers surface conduction as the dominant mechanism of overlimiting conductance.[14,18] In our system, electroosmosis also propels the electrolyte in the direction of applied electric field (negative x–direction), such that the fraction of deionized water recovered is automatically increased at high currents.[8]

2.3 Materials and Experimental Methods

The device used here was fabricated according to a design recently published by our group.[13] This continuous, laboratory scale architecture is shown schematically in Figure 2-1. The device comprised 3 inlets and 4 outlets: 2 of the inlets transported fluid to the electrodes and the third delivered contaminated feed; 2

of the outlets transported fluid from the electrodes and the other 2 were generated at the splitter as fresh and brine streams. To eliminate acid dosing of the cathode stream (done in previous studies[13,19] with HCl to inhibit precipitation of metal hydroxides), we used solutions of sodium citrate buffer for both electrode streams which were continuously recycled during the process (closed-loop operation). The electrodes were platinum meshes (Sigma–Aldrich) connected to a Gamry Reference 3000™ potentiostat/galvanostat using titanium wires (Alfa Aesar), the cation exchange membranes were nafion N115 (with dimensions of approximately $127\,\mu\text{m} \times 1\,\text{cm} \times 2\,\text{cm}$), and the porous medium was a borosilicate frit (with dimensions of approximately $3\,\text{mm} \times 1\,\text{cm} \times 2\,\text{cm}$). The frit (Adams & Chittenden Scientific Glass) had ultrafine pores (nominally ranging from 0.9 to $1.4\,\mu$m in size), an internal surface area of $1.75\,\text{m}^2\,\text{g}^{-1}$ based on Brunauer–Emmett–Teller (BET) theory, a mass density of $1.02\,\text{g}\,\text{m}^{-3}$, and a porosity of 0.31. Before assembling the device, the frit was glued onto an acrylic frame using Devcon 2 Ton Epoxy (McMaster-Carr). The splitter, placed midway down the frit for ease of assembly, was made of cast acrylic and was sealed against the top face of the frit using 0.04-inch GORE™ expanded polytetrafluoroethylene (ePTFE) gasket tape. Holes in all of the acrylic slabs and rubber gaskets were created using a laser cutter (Universal Laser Systems) and refined with a drill press (Palmgren 10-inch, 5-speed bench model). These layers were then stacked and held together with nuts, bolts, and washers made of 316 stainless steel.

To prepare artificial seawater with the composition reported in Table 2.1, we added $27.22 \pm 0.01\,\text{g}$ of sodium chloride (NaCl), $3.29 \pm 0.01\,\text{g}$ of sodium sulfate decahydrate ($Na_2SO_4 \cdot 10H_2O$), $11.13 \pm 0.01\,\text{g}$ of magnesium chloride hexahydrate ($MgCl_2 \cdot 6H_2O$), $2.56 \pm 0.01\,\text{g}$ of calcium chloride dihydrate ($CaCl_2 \cdot 2H_2O$), and $1.85 \pm 0.01\,\text{g}$ of potassium sulfate (K_2SO_4) for every liter of deionized water. This solution was fed to the device solely through the stream labeled “salty" (see Figure 2-1) for desalination. The electrode streams, on the other hand, drew from a solution of sodium citrate buffer that was continuously recycled. The purpose of using such a solution (as opposed to acid dosing of the catholyte) was to reduce waste by recy-

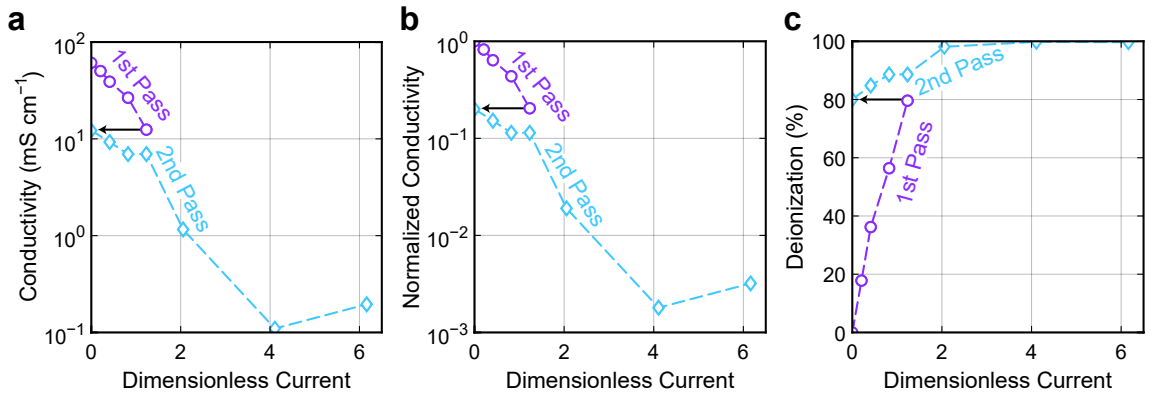

Figure 2-2. Quantitative analysis of (artificial) seawater desalination in a 2-step process. Measurements of (a) absolute and (b) normalized conductivity of the fresh stream; in (b), conductivity is normalized relative to that of the feed to the first pass (composition outlined in Table 2.1). (c) Deionization of the fresh stream calculated based on Equation 2.3. The feed to the second pass ($I_{\text{lim}} = 4.86$ mA) was a 5-fold dilution of the feed to the first ($I_{\text{lim}} = 24.3$ mA).

cling the electrode streams, inhibit precipitation reactions, and prevent undesired side reactions like the evolution of chlorine gas. In this study, we chose sodium citrate because it buffers in the relevant range of pH ($\sim 4-7$) to prevent scaling (i.e., formation of $Mg(OH)_2$ and $CaCO_3$), it does not react with the cations in seawater, and it is stable at the redox potentials in the cell.[19] To prepare the buffer, we first formulated a solution of citric acid ($HOC(COOH)(CH_2COOH)_2$) and its conjugated base sodium citrate dihydrate ($HOC(COONa)(CH_2COONa)_2 \cdot 2H_2O$) with concentrations of 0.5 M each in deionized water. The pH of this mixture was measured to be approximately 4.0 and was adjusted to a final pH of 4.9 by adding an appropriate volume of sodium hydroxide (1 M). (All reagents were purchased from Sigma–Aldrich and used as received.) During operation, the buffer would become slightly more acidic in the anolyte and slightly more alkaline in the catholyte, but as these streams were mixed, the buffer recovered its starting pH and buffering capacity. Moreover, the (anionic) conjugate base of the buffer was confined to the electrode streams because they were separated from the frit by cation exchange membranes. Confinement of the conjugate base to these streams was what allowed the buffer to maintain its pH and buffering capacity under closed-loop operation.

With these solutions prepared, we began experiments by setting the flow rates of

all streams. In this work, all flow rates were held constant: 0.021 ± 0.002 mL min^{-1} for the salty feed and 0.27 ± 0.01 mL min^{-1} for the electrode streams. The cross-sectional area of the frit through which liquid/ flowed had an area of $3\,\text{mm} \times 2\,\text{cm} = 0.6\,\text{cm}^2$, and so the superficial velocity of the salty feed was $5.8 \pm 0.6\,\mu\text{m}\,\text{s}^{-1}$. This flow rate of the feed was chosen to the keep the diffusion limited current (see Section 2.4), and in turn operating voltage, low. The flow rate of the electrode streams was then chosen to be an order of magnitude greater to impose enough pressure on the nafion and prevent salty feed from bypassing the frit. To transport all liquids, we used peristaltic pumps equipped with Tygon® Chemical tubing (Saint-Gobain). With such pumps—and at low speeds of rotation—the flow would be pulsed, though it was made smooth by incorporating hydraulic accumulators just upstream of the device. In our system, the accumulators were capped glass vials that held a small volume of (compressible) air above the (incompressible) liquids being pumped at the bottom to smooth out pulsations. With flow rates set and tubing connected, the accumulators were left to pressurize and the system to equilibrate overnight, after which the Gamry was set to operate galvanostatically. (Air inside the accumulators becomes pressurized over time until the fluidic resistance downstream—such as that created by the porous frit—can be overcome by the pumped liquid.) The measured voltage was allowed to stabilize for at least 1 hour until it reached steady state.

Samples were collected approximately every 3 hours at each dimensionless current directly from the device and stored in conical centrifuge tubes for analysis. Empirical analyses included measurement of volume, conductivity, pH, and concentration of cations. Conductivity and pH were measured using Mettler Toledo analytical instruments (SevenCompact pH/Cond S213), and concentration was determined by inductively coupled plasma mass spectrometry (Agilent 7900 ICP–MS). The plasma in ICP–MS was made from argon gas and was supplemented by helium. To improve the accuracy of our data and subsequent analysis, we incorporated an internal standard that introduced 100 ppb of indium to all samples. Since the output of ICP–MS was in counts per second, quantitative analysis required calibration

of the measurements. A calibration curve was produced by linear regression of reference standards with known concentration. These calibration standards (Na, Mg, Ca, K, and In) were purchased from Sigma–Aldrich and serially diluted to prepare a set of samples that encompassed the concentrations relevant to this study. For concentration to fall within the detection limits of the spectrometer and to avoid damaging the detector, all samples and standard solutions were diluted in nitric acid to a final acid composition of 2 vol%. To calculate the true concentration of a solution, concentrations found from calibration curves were multiplied by the corresponding dilution factor used to prepare the sample.

2.4 Results and Discussion

Propagation of a shock wave across which concentration varies sharply is the key phenomenon that governs deionization in SED. This shock—as well as the depletion zone beneath it—is generated by applying current in excess of the diffusion limited current I_{lim}, which is defined as the rate of advection (i.e., forced convection) of positive charge carriers:

$$I_{\text{lim}} = \sum_j \nu_j C_j F Q' \tag{2.1}$$

where ν is valence (charge), C is molar concentration, F is Faraday's constant, Q' is the volumetric flow rate of the feed, and the sum is taken over all cations j. In the presence of ideal cation exchange membranes, the flux of anions is 0 at steady state (assuming that these species do not participate in chemical reactions). Using the composition of artificial seawater in Table 2.1 and with $Q' = 0.025$ mL min^{-1}, we find that

$$I_{\text{lim}} = 2.43 \times 10^{-2} \text{ A} \tag{2.2}$$

After exceeding I_{lim}, the overlimiting current increases linearly with voltage and effects constant conductance, which is consistent with the governing theory as well as previous experimental observations in negatively charged porous media.[7,14]

Since applying a constant (overlimiting) current facilitates the formation of a stable deionization shock,[8] we operated our SED system galvanostatically. (Poten-

tiostatic operation, on the other hand, may lead to overshoot and oscillation about a desired overlimiting current, which could generate variable or perhaps unstable shocks.[17]) To quantify the performance of SED for desalination of seawater, we measured the conductivity of the fresh stream, as shown in the leftmost panel of Figure 2-2. Based on the observed level of desalination ($\approx 80\%$ in the first pass), we conclude that 2 distinct zones of concentration polarization are established above and below a deionization shock, despite the high ionic strength (≈ 750 mM) of seawater. This high concentration of ions, however, corresponds to a relatively large limiting current, which when multiplied by the steady voltage produces a high power demand. In practice, the energy consumption of common desalination technologies (e.g., distillation and RO) is lowered by using multiple stages serially.[20,21] This approach is particularly suitable for SED because power scales quadratically with current in the overlimiting regime, with voltages on the order of 1 to 10 V. (At voltages a few times the thermal voltage of 26 mV at 300 K, $I \sim V$[14] so that $P = IV \sim I^2$.) Operating the system in a sequence of passes, each at a lower current than for a one-step process, would therefore reduce power consumption, though at the expense of water recovery.

2.4.1 Desalination Performance

We proceeded to desalinate artificial seawater in a 2-step process that we accelerated (to compensate for low throughput) by feeding serially diluted solutions in turn to the same device. A dilution factor of 5 was chosen for the second step based on the reduction of conductivity in the first at 1.2 times the limiting current (arrows in Figure 2-2). In other words, concentrations of the feed to each pass were 35 g L^{-1} (1.1 M; $I_{lim} = 24.3$ mA) and 7 g L^{-1} (0.22 M; $I_{lim} = 4.86$ mA). Our results for desalination of artificial seawater in 2 passes are presented in Figure 2-2, where deionization (the percentage removed of a given species, DI) is defined as

$$DI = 100\% \times \left(1 - \frac{C_{fresh}}{C_{feed}}\right) \tag{2.3}$$

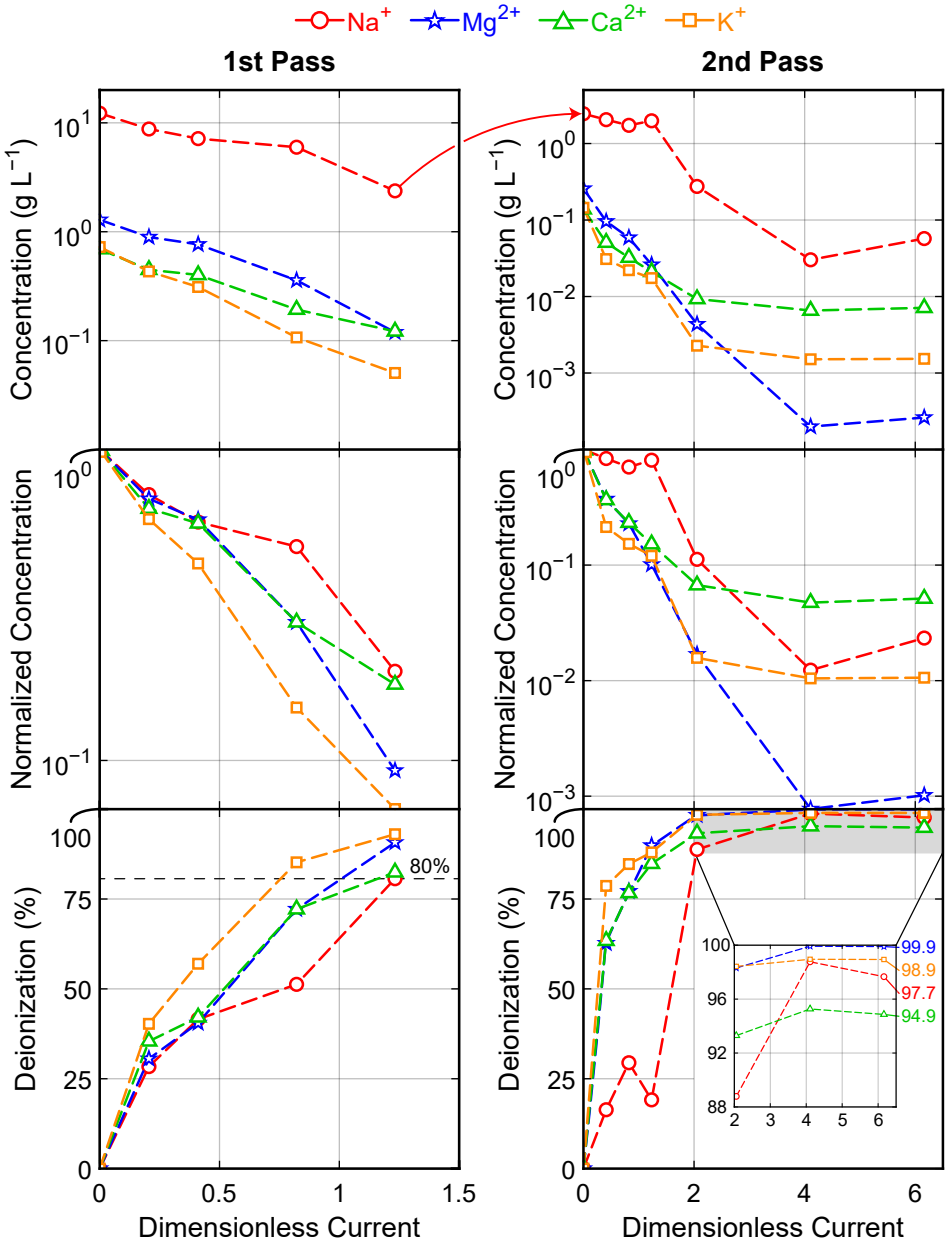

Figure 2-3. Quantitative analysis of (artificial) seawater desalination in the 2-step process using ICP–MS. Measurements of (top) absolute and (middle) normalized concentration of cations in the fresh stream; in the latter, concentration (of each ion) is normalized relative to that of the feed to each respective pass (composition outlined in Table 2.1). (Bottom) Deionization of the fresh stream calculated based on Equation 2.3. Note that the feed to the second pass was a 5-fold dilution of the entire solution, rather than a new solution with one-fifth the composition of each ion.

and dimensionless current as $\widetilde{I} = I/I_{\text{lim}}$. From the middle panel of this figure, SED reduced the conductivity of artificial seawater by 3 orders of magnitude in 2 passes. This reduction in conductivity corresponds to 99.8% desalination under the optimal conditions tested: 79.6% in the first pass with $\widetilde{I} \approx 1.2$, and 99.1% in the second with $\widetilde{I} \approx 4.1$. Purification to this extent brings the artificial seawater to a salinity of 67.8 ppm, well below the recommended upper limit of total dissolved solids in drinking water.[22]

Measurement of desalination by conductivity alone narrows the scope of our analysis because it precludes the ability to examine the fate of individual ions. Moreover, changes in conductivity of the fresh stream are influenced by production (and transport) of hydronium and hydroxide from self-ionization of water. We therefore used ICP–MS as a more precise measure of composition to rigorously characterize deionization. The results of this analysis are presented in Figure 2-3, which demonstrate that the concentration of Na^+ decreased by approximately 80% in the first pass, as indicated by a red arrow in the top row of panels. (The concentrations of the other cations did not match exactly between passes because the feed to the second pass was a 5-fold dilution of the entire solution, rather than a new solution with one-fifth the composition of each ion.) And since Na^+ was the most abundant cation in the electrolyte, we attributed the decrease in conductivity by 80% in the first pass (Figure 2-2) to removal of this species, even though all other cations were removed to a greater extent.

2.4.2 Ionic Selectivity

The other important aspect revealed in Figure 2-3 is selective removal of certain ions over others: in the second pass, Mg^{2+} was preferentially removed relative to all other species by at least one (Mg^{2+}:K^+) and up to nearly two orders of magnitude (Mg^{2+}:Ca^{2+}). For a more quantitative analysis of this observation, we used the data in Figure 2-3 to calculate scaled (retention) selectivity in the fresh stream as a function of dimensionless current between each pair of unique species. In this

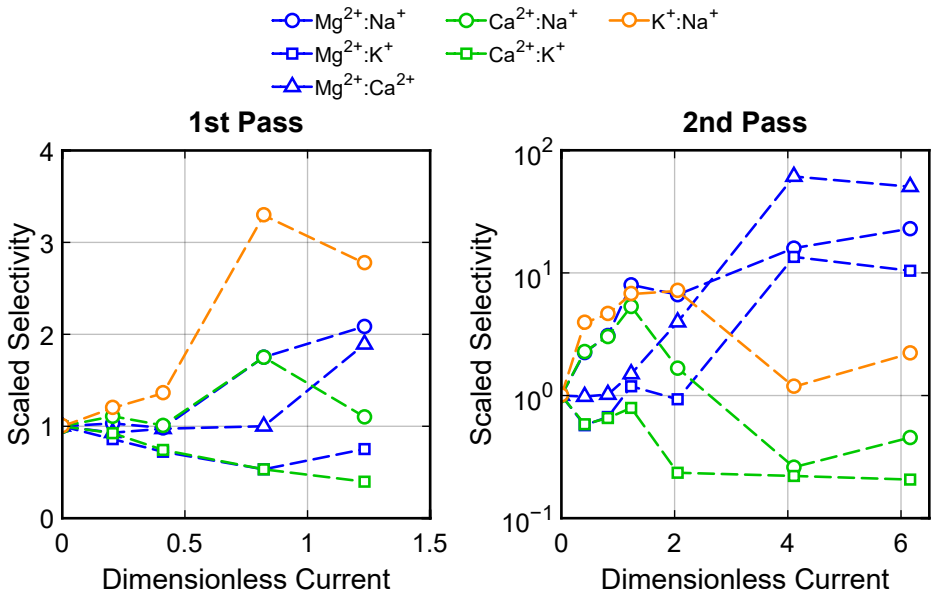

Figure 2-4. Quantification of the selective removal of ions in the 2-step desalination process. Graphs show scaled selectivity ($S_{j:i} \equiv j:i$) for each pair of unique species in the fresh stream as a function of dimensionless current in each pass. Values of $S_{j:i}$ were calculated using Equation 2.4 based on the normalized concentrations in Figure 2-3.

context, scaled selectivity is defined as[13]

$$S_{j:i} \equiv j:i = \frac{C_i/C_j}{C_{i_0}/C_{j_0}} = \frac{C_i/C_{i_0}}{C_j/C_{j_0}} \tag{2.4}$$

which may be interpreted as the ratio of the effluent concentration of species i to that of species j, scaled by the corresponding ratio of feed concentrations (which is also equal to the ratio of normalized effluent concentrations). If $S_{j:i}$ is greater than 1, then species j is selectively removed relative to species i. An experimental paper recently published by our group demonstrated that SED automatically achieves selective removal of the multivalent ion from an electrolyte comprising Na^+ and Mg^{2+} in various proportions. In that article, selectivity based on valence was attributed to differences in ionic mobility across the enriched and deionized regions of the device in the regime of overlimiting current.[13]

In this study, the electrolyte consisted of four primary cations, two of which are monovalent and the other two divalent. The left panel of Figure 2-4 shows that there was only modest selectivity of certain ions relative to others in the first pass.

This behavior was likely because we operated the system at or below the limiting current, which precluded formation of a deionization shock sustained by overlimiting conductance. The right panel of Figure 2-4, on the other hand, indicates that there was significant selectivity of Mg^{2+} relative to all other species in the second pass when overlimiting current was applied. Removal of this ion is an important and desirable capability in the inhibition of magnesium-based (mineral) scale, in which Mg^{2+} forms insoluble salts that precipitate, deposit on surfaces, and impair the performance of desalination units.[23] In this regard, our experiments show that SED has the potential to soften artificial seawater without the need for antiscalants.

Although we expect that multivalent ions should typically be removed more effectively compared to monovalent ions,[13,19] the behavior of Ca^{2+} went against this intuition in the second pass when overlimiting current was applied (in Figure 2-4, Ca^{2+}:Na^{+} and Ca^{2+}:K^{+} are both less than 1 at high current). A possible reason for this lack of selectivity may be reaction of Ca^{2+} to form uncharged species that evade removal by SED. For example, Ca^{2+} can react with bicarbonate[24] (HCO_3^-, which is produced by dissolution of carbon dioxide in water) according to the chemical reaction

$$Ca^{2+}(aq) + 2HCO_3^-(aq) \longrightarrow CaCO_3(s) + CO_2(g) + H_2O(l) \tag{2.5}$$

This reaction more readily occurs under alkaline conditions, which was the case in the second pass at high current (e.g., pH = 9.72 at $\widetilde{I} = 6$, versus pH = 4.65 at $\widetilde{I} = 0.4$). Moreover, since the pH of the desalted stream was only slightly basic, the reaction of Mg^{2+} with hydroxide (OH^-) was negligible, which ensured that magnesium remained charged and amenable to electrokinetic separation. (We estimate that $Mg(OH)_2$ will precipitate from solution when the pH exceeds 10.6 for a concentration of Mg^{2+} of 10^{-3} g L^{-1}, or 0.04 mM, and assuming a solubility product constant of 5.61×10^{-12}.[25]) Practically, it is more desirable to remove Mg^{2+} than Ca^{2+} from seawater because the former is 5 times more abundant (in molar units)[1] and as a result generates more mineral scale.

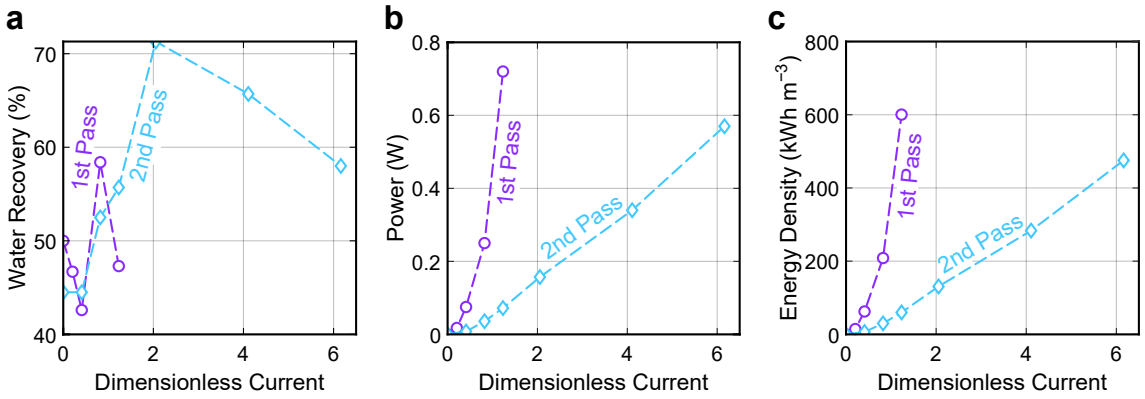

Figure 2-5. Analysis of water recovery and energy demand in the 2-step process of seawater desalination. (a) Water recovery as a function of dimensionless current in each pass. (b) Power and (c) energy density as functions of dimensionless current in each pass.

A subtle feature of Figure 2-4 is the selective removal of all species relative to Na^+ in the second pass at or below the limiting current. This behavior may have been due to inhibited removal of Na^+ from the feed because of the high concentration of this species in the electrode streams (34.5 g L^{-1}, or $\sim$ 1.50 M, in the buffer solution). In other words, it is likely that there existed a driving force—established by gradients in the concentration of Na^+—that balanced the Coulomb force induced at or below the limiting current. This observation would also explain the comparatively poor removal of Na^+ in the second pass at low current in Figure 2-3.

2.4.3 Water Recovery and Energy Demand

Aside from deionization, water recovery and energy efficiency are important metrics in desalination systems, and so we analyze the recovery ability and energy demand of SED when used to desalt artificial seawater. Water recovery (WR), sometimes referred to the recovery ratio, is defined as

$$WR = \frac{Q_F}{Q'} \tag{2.6}$$

where Q_F is the volumetric flow rate of the fresh stream and Q' is the volumetric flow rate of the feed; WR is shown in Figure 2-5a to increase (up to 70% in the second pass) with current. In general, this increase in water recovery is strictly

due to electroosmosis in the direction of applied electric field, which automatically delivers more fluid to the deionized region;[8] the splitter was not repositioned in this experiment. Since the electrode streams were continuously recycled under closed-loop operation, the only waste that was generated by our device (and had to be disposed of) was the concentrated brine stream. And if the system was operated at a dimensionless current of 4, then only 0.5 m^3 of brine was generated for every 1 m^3 of desalinated water in the second pass. In future iterations of our device, water recovery will be increased by adjusting the position of the splitter to favor a larger flow rate of the fresh stream.

Analysis of the electrical power needed for deionization is reported in Figure 2-5b-c; power is calculated as the product of applied current and (steady) voltage, and energy density as power divided by the volumetric flow rate of the feed. In desalinating seawater, power (and thus energy density) increased quadratically with current in agreement with the governing theory.[14] Moreover, Figure 2-5b-c reveal that the overall energy demand of SED is higher than that of more established desalination technologies like RO[26] and ED.[27] This comparison indicates that SED is still in its early stage of development and may not be the preferred method of desalination. Figure 2-5b-c also show, however, that the energy requirement drops significantly as the solution fed becomes more dilute. These observations (supported by the dependence of limiting current on concentration in Equation 2.1) imply that the energy consumption of SED can be significantly reduced by desalinating sources that are less saline than seawater, such as brackish water. (Although energy consumption is reduced in general by treating dilute feeds—even for physical methods such as distillation and RO—this effect is more prominent in the dilute limit for electrochemical methods such as SED,[7,8] ED, or capacitive deionization[28] because ions are removed rather than the water.) We also note that the cost of fluidic pumping in our current laboratory scale system was negligible compared to the cost of electrical energy. (The power needed for pumping was $P_{\text{pump}} = Q\Delta p$, where Δp is pressure drop and was approximately 2 psi across the frit and 1 psi across each electrode.) The cost of pumping will become important at larger scales,

however, and it will increase according to the desired level of throughput.

To lower the energy requirement and improve efficiency, our SED technology can be optimized most directly by modulating the geometry of the frit. By simple scaling arguments, power is calculated as $P = IV$ and Ohm's law states that $V = IR$, so $P = I^2R \sim Q^2L/A$ (L is the length of the resistive material and A is its cross-sectional area) for fixed dimensionless current ($I_{\text{lim}} \sim Q$) and assuming fixed resistivity of the electrolyte. Energy density is then $\hat{E} = P/Q \sim QL/A$ and may therefore be reduced by increasing the cross-sectional area of the frit, which in Figure 2-1 corresponds to the y– and z–dimensions. The only disadvantage of increasing the z–dimension—the direction of fluid flow—would be larger hydrodynamic resistance and in turn greater cost of pumping, although the magnitude of this cost would remain small. Otherwise, increasing cross-sectional area will enable more throughput as well as parallelization of the system, for instance by stacking several units on top of one another. Scaling up the system in this way will also improve the performance of SED by increasing the distance over which the shock wave propagates (in the z–dimension) and, in turn, requiring a smaller overlimiting current to achieve the same degree of desalination.

2.5 Conclusion

Although technologies for large-scale desalination have been extensively studied and optimized, specialized systems for small-scale desalination are underexplored. Motivated to address this shortcoming, we used SED to continuously desalinate artificial seawater and observed selective removal of Mg^{2+} relative to all other cations present. In 2-steps, 99.8% of the salt fed was rejected, with more than 99.99% of Mg^{2+} removed. SED has several unique and attractive features that make it suitable for small-scale and decentralized desalination. In particular, our system is robust, lightweight, and portable, and it may be redesigned in such a way that will facilitate scale-up and parallelization for greater throughput. Moreover, we have shown by scaling arguments that scale-up can reduce power consumption while retaining the high performance demonstrated in this article. Finally, we reported for the first

time use of sodium citrate buffer under closed-loop operation as a robust electrolyte for the electrode streams that also eliminated the waste they would otherwise have generated.

2.6 Acknowledgments

This research was supported by a grant from Mitsubishi Heavy Industries Limited. The authors thank the Center for Environmental Health Sciences (CEHS) for use of ICP–MS. MAA also acknowledges Dr. Hannes Grobe at the Alfred Wegener Institute in Germany for permitting adaptation of part of the graphical abstract.

2.7 References

[1] Andrew G Dickson and Catherine Goyet. Handbook of methods for the analysis of the various parameters of the carbon dioxide system in sea water. version 2. Technical report, Oak Ridge National Lab., TN (United States), 1994.

[2] Quirin Schiermeier. Water: purification with a pinch of salt, 2008.

[3] Huanting Wang. Low-energy desalination. *Nature nanotechnology*, 13(4):273, 2018.

[4] Mark A Shannon, Paul W Bohn, Menachem Elimelech, John G Georgiadis, Benito J Marinas, and Anne M Mayes. Science and technology for water purification in the coming decades. In *Nanoscience and technology: a collection of reviews from nature Journals*, pages 337–346. World Scientific, 2010.

[5] Soteris A Kalogirou. Seawater desalination using renewable energy sources. *Progress in energy and combustion science*, 31(3):242–281, 2005.

[6] Daosheng Deng, Wassim Aouad, William A Braff, Sven Schlumpberger, Matthew E Suss, and Martin Z Bazant. Water purification by shock electrodialysis: Deionization, filtration, separation, and disinfection. *Desalination*, 357:77–83, 2015.

[7] Daosheng Deng, E Victoria Dydek, Ji-Hyung Han, Sven Schlumpberger, Ali Mani, Boris Zaltzman, and Martin Z Bazant. Overlimiting current and shock electrodialysis in porous media. *Langmuir*, 29(52):16167–16177, 2013.

[8] Sven Schlumpberger, Nancy B Lu, Matthew E Suss, and Martin Z Bazant. Scalable and continuous water deionization by shock electrodialysis. *Environmental Science & Technology Letters*, 2(12):367–372, 2015.

[9] Jie Song, Tian Li, Lucía Wright-Contreras, and Adrian Wing-Keung Law. A review of the current status of small-scale seawater reverse osmosis desalination. *Water international*, 42(5):618–631, 2017.

[10] J Ayoub and R Alward. Water requirements and remote arid areas: the need for small-scale desalination. *Desalination*, 107(2):131–147, 1996.

[11] Martin Zdenek Bazant, EthelMae Victoria Dydek, Daosheng Deng, and Ali Mani. Method and apparatus for desalination and purification, August 12 2014. US Patent 8,801,910.

[12] Martin Zdenek Bazant, EthelMae Victoria Dydek, Daosheng Deng, and Ali Mani. Desalination and purification system, April 7 2015. US Patent 8,999,132.

[13] Kameron M Conforti and Martin Z Bazant. Continuous ion-selective separations by shock electrodialysis. *AIChE Journal*, 66(1):e16751, 2020.

[14] E Victoria Dydek, Boris Zaltzman, Isaak Rubinstein, DS Deng, Ali Mani, and Martin Z Bazant. Overlimiting current in a microchannel. *Physical review letters*, 107(11):118301, 2011.

[15] Ali Mani and Martin Z Bazant. Deionization shocks in microstructures. *Physical Review E*, 84(6):061504, 2011.

[16] Ali Mani, Thomas A Zangle, and Juan G Santiago. On the propagation of concentration polarization from microchannel- nanochannel interfaces part i: analytical model and characteristic analysis. *Langmuir*, 25(6):3898–3908, 2009.

[17] Thomas A Zangle, Ali Mani, and Juan G Santiago. On the propagation of concentration polarization from microchannel- nanochannel interfaces part ii: numerical and experimental study. *Langmuir*, 25(6):3909–3916, 2009.

[18] Sungmin Nam, Inhee Cho, Joonseong Heo, Geunbae Lim, Martin Z Bazant, Dustin Jaesuk Moon, Gun Yong Sung, and Sung Jae Kim. Experimental verification of overlimiting current by surface conduction and electro-osmotic flow in microchannels. *Physical review letters*, 114(11):114501, 2015.

[19] Kameron M. Conforti. *Continuous Ion-selective Separation by Shock Electrodialysis*. PhD thesis, Massachusetts Institute of Technology, February 2019.

[20] M Göktuğ Ahunbay, S Birgül Tantekin-Ersolmaz, and William B Krantz. Energy optimization of a multistage reverse osmosis process for seawater desalination. *Desalination*, 429:1–11, 2018.

[21] Aihua Zhu, Panagiotis D Christofides, and Yoram Cohen. Minimization of energy consumption for a two-pass membrane desalination: effect of energy recovery, membrane rejection and retentate recycling. *Journal of Membrane Science*, 339(1-2):126–137, 2009.

[22] Arik Azoulay, Philippe Garzon, and Mark J Eisenberg. Comparison of the mineral content of tap water and bottled waters. *Journal of general internal medicine*, 16(3):168–175, 2001.

[23] Hai-Yan Li, Wei Ma, Lu Wang, Ru Liu, Lin-Sen Wei, and Qiang Wang. Inhibition of calcium and magnesium-containing scale by a new antiscalant polymer in laboratory tests and a field trial. *Desalination*, 196(1-3):237–247, 2006.

[24] Theodore L Brown, Harold E LeMay, Bruce E Bursten, Catherine J Murphy, and Patrick M Woodward. *Chemistry: the central science*. Pearson Education, 12 edition, 2012.

[25] David R Lide. *CRC handbook of chemistry and physics*. CRC press, 85 edition, 2004.

[26] MA Alghoul, P Poovanaesvaran, Kamaruzzaman Sopian, and MY Sulaiman. Review of brackish water reverse osmosis (bwro) system designs. *Renewable and Sustainable Energy Reviews*, 13(9):2661–2667, 2009.

[27] Natasha C Wright. Justification for community-scale photovoltaic-powered electrodialysis desalination systems for inland rural villages in india. *Desalination*, 352:82–91, 2014.

[28] R Zhao, S Porada, PM Biesheuvel, and A Van der Wal. Energy consumption in membrane capacitive deionization for different water recoveries and flow rates, and comparison with reverse osmosis. *Desalination*, 330:35–41, 2013.

Chapter 3

Continuous separation of radionuclides from contaminated water by shock electrodialysis

The work reported in this chapter has been published as "Continuous separation of radionuclides from contaminated water by shock electrodialysis," by Mohammad A. Alkhadra, Kameron M. Conforti, Tao Gao, Huanhuan Tian, and Martin Z. Bazant. It has been adapted with permission from the American Chemical Society, 2019.

Abstract

The increasing popularity of nuclear energy necessitates development of new methods to treat water that becomes contaminated with radioactive substances. Because this polluted water comprises several dissolved species (not all of which are radioactive), selective accumulation of the radionuclides is desirable to minimize the volume of nuclear waste and to facilitate its containment or disposal. In this article, we use shock electrodialysis to selectively, continuously, and efficiently remove cobalt and cesium from a feed of dissolved lithium, cobalt, cesium, and boric acid. This formulation models the contaminated water commonly found in light-water reactors and in other nuclear processes. In a three-pass process, a consistent trade-off is observed between the recovery of decontaminated water and the percentage of cobalt removed, which offers flexibility in operating the system. For example, 99.5% of cobalt can be removed with a water recovery of 43%, but up to 66% of the water can be recovered if deionization of cobalt is allowed to drop to 98.3%. In general, the energy consumed during this process (ranging between 1.76 and $4.8\,\mathrm{kWh\,m^{-3}}$) is low because only charged species are targeted and virtually no en-

ergy is expended removing boric acid, the most abundant species in solution.

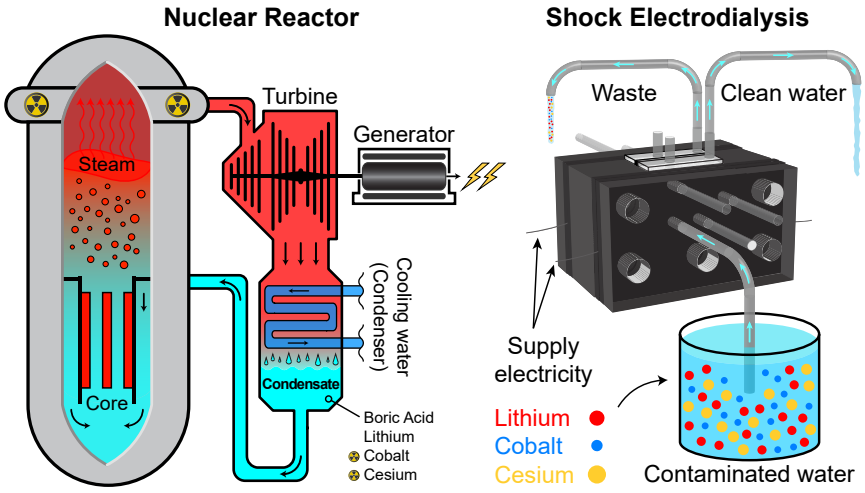

3.1 Introduction

Nuclear waste is matter that undergoes radioactive decay, a spontaneous process by which an unstable atomic nucleus emits radiation and concomitantly transforms into smaller daughter nuclei.[1] Although radioactive decay is stochastic at the level of individual nuclei, the expected rate of decay for a collection of radionuclides can be characterized in terms of an observable decay constant such as the half life.[1] Radioactive waste is often a byproduct in the industrial generation of nuclear power and is hazardous to the environment and to nearly all forms of life. Indeed, high-energy radiation can ionize atoms or even generate free radicals (e.g., hydroxyl from radiolysis of water) that react with the cellular components of an organism, which may cause aberration of chromosomes, mutation of nucleic acids, or death of cells.[2,3] Given the harmful nature of such radiation, the scientific community has sought to develop methods to isolate, manage, and dispose of nuclear waste. In this article, we adapt an emerging electrokinetic deionization method known as shock electrodialysis[4–8] (SED) to continuously treat water contaminated with radioactive ions. This study focuses on the basic physics and design principles needed to selectively remove cobalt (^{59}Co) and cesium (^{133}Cs), while recovering a reasonable fraction of the water fed and minimizing the energy cost of the process. Since SED is an electrokinetic method, separation of ions is based primarily on charge and is

insensitive to mass,[4,5] which implies that our results should also be applicable to radioactive isotopes of cobalt and cesium. The principal aim of our methodology is to concentrate nuclear waste in a contained discharge stream and, in turn, minimize the volume of waste that would need management, recycling, or disposal in subsequent processes.

Our strategy for separation is based on the phenomenon of deionization shock waves[9] by which a sharp gradient in the concentration of salt propagates near an ion selective surface, such as a cation exchange membrane[4,5] or metal electrodeposit.[10,11] Moreover, our system comprises a weakly charged porous medium to sustain overlimiting current—at which transport of ions is faster than by diffusion alone—as the conductivity of the solution diminishes near this surface.[5,10,12,13] The shock wave splits the system into a region that is concentrated and another that is deionized. These regions are then continuously separated by driving flow perpendicular to the applied electric field.[4] This system can therefore achieve electrically tunable and "membraneless" separation within the porous material without any physical barriers in the direction of flow. In contrast to conventional electrodialysis in which overlimiting current is often sustained by chemical or hydrodynamic instabilities,[14] overlimiting current in SED is sustained by electrokinetic phenomena at the scale of pores, namely surface conduction and electroosmosis.[5,12,13,15] Experimentally, concentration polarization was first observed in glass microchannels emanating from nanoscopic junctions[16–18] or membranes.[15] SED, however, relies on the propagation of macroscopic shock waves across a network of charged pores, which is necessary for flow fractionation,[5,7] scale-up to practical flow rates,[4], and improvement of both desalination[5,13] and water recovery[4] by leveraging electroosmotic flow.

The first laboratory scale prototype to successfully demonstrate SED was designed, built, tested, and patented by our group.[5–8] To achieve continuous operation, subsequent iterations of this system introduced a novel cross-flow architecture, in which the feed flows into a porous glass frit placed between identical cation exchange membranes, as shown in Figure 3-1.[4] The frit was made of sintered borosil-

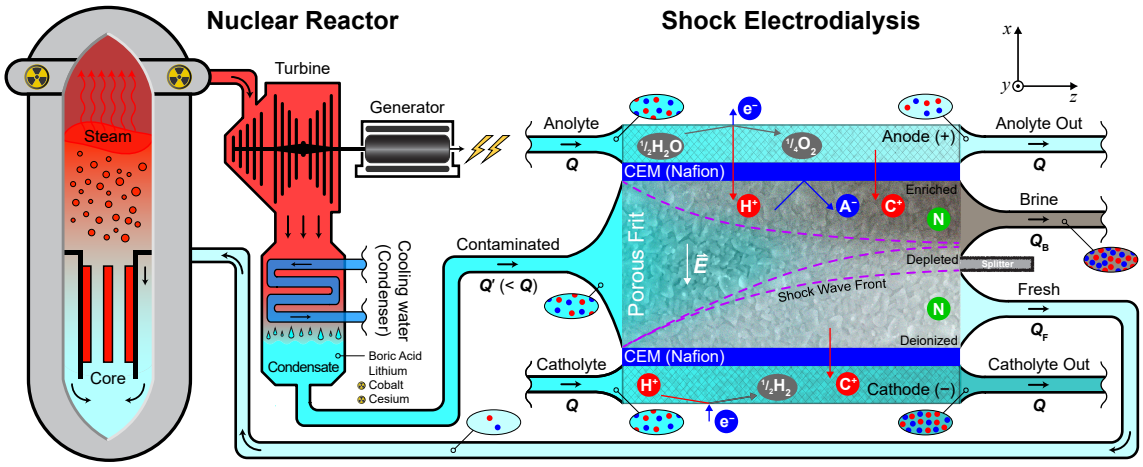

Figure 3-1. Operating principles of a light-water nuclear reactor and the SED device used for decontamination. (left) Simplified schematic of a boiling water reactor (a type of light-water reactor) used to generate electrical power by heating water that turns into steam and drives a turbine. Several radionuclides are present in this water and contaminate the reactor components outside the core; refer to 3.2 for details. (right) A rectangular cross section of the SED device shows water splitting at the anode and formation of molecular hydrogen at the cathode (maintained under acidic conditions to prevent precipitation of metal hydroxides), which are the primary electrochemical reactions that provide current to the cell. Contaminated water in the frit is then subjected to an electric field ($\vec{\boldsymbol{E}}$) that transports charged species (labeled C^+ for cations and A^- for anions) perpendicular to the flow. Anions are blocked by cation exchange membranes (CEMs), and neutral species (labeled N) are unaffected by the electric field. Here, flow rate is denoted by the letter $\boldsymbol{Q}$, and streams are colored based on relative concentration of ions.

icate glass, a porous material with negative charges bound to the surfaces of its pores, which were nominally 1 micron in size. By placing a splitter downstream of the frit, the exiting fluid was separated into enriched and deionized streams on the anodic and cathodic sides of the shock wave, respectively. Previous work showed that SED can continuously deionize electrolytes comprising monovalent cations, including NaCl, KCl, KNO_3, and Na_2SO_4.[4] (These measurements were made by quantifying changes in electrical conductivity of the solution.) This work also revealed that water recovery (defined as the fraction of fluid recovered as desalinated water from the concentrated feed) can be increased to over 80% by increasing the applied current and without repositioning the splitter. Improved water recovery was attributed to electroosmotic flow perpendicular to the imposed flow, which conveniently delivered more fluid to the depleted region.

The present study is motivated by the recently discovered capability of SED to separate specific ions from multicomponent electrolytes. In particular, recent work demonstrated selective removal of magnesium—a divalent cation—from an aqueous mixture of NaCl and $MgCl_2$ with (retention) selectivity of up to 200:1 in the extreme case.[19] Since many radionuclides and harmful products of corrosion are dissolved in water as multivalent ions, this result suggests that SED can be used to purify water contaminated with radioactive ions and byproducts of various nuclear processes.

3.2 Background and Experimental Design

In treating radioactive water, the goal is often to separate the fluid into two streams. The first of these has low enough activity for safe discharge into the environment, and the second (with the smallest possible volume) is concentrated in radionuclides for further management. Existing methods for treatment can be broadly categorized into physical methods, which focus on extracting uncontaminated water, and chemical methods, which focus on extracting radionuclides. Physical methods include evaporation, reverse osmosis, nanofiltration, ultrafiltration, and microfiltration.[20–23] In these methods, water is driven across an interface (either a membrane,

or a gas–liquid interface in the case of evaporation) that retains dissolved species in a concentrated brine. The inclusion of an excess of boric acid (commonly done in the process water of various nuclear reactors for neutron poisoning[24,25]) complicates the use of several physical methods and makes them more energy intensive. This radioactively inert salt increases the osmotic pressure in membrane technologies such as reverse osmosis and is highly corrosive[26] when concentrated. For these reasons, selective removal is preferable to indiscriminately concentrating all dissolved species.[27]

Chemical methods, which are typically (but not always) selective in molecular separations, include solvent extraction (using liquid phase compounds), precipitation, chelation, ion exchange, and electrodeionization (EDI, sometimes called hybrid ion-exchange electrodialysis).[21,22] These methods target ions based on chemical reactivity (adsorption, chelation, precipitation),[28,29] solubility and partition coefficient (solvent extraction),[30] affinity for charged or functionalized surfaces (ion exchange, EDI),[31–33] or response to electric fields in solution (EDI).[32] Apart from SED, EDI is the only technology that involves electrochemistry, and is the only chemical method that can operate continuously without the need for additives or solvents.[32] The remaining methods require the use of sacrificial chemicals, such as carriers or additives (adsorption, chelation, precipitation), non-aqueous solvents (solvent extraction), or ion-exchange resins with regenerating acids and salts (ion exchange), the disposal of which has been deemed challenging.[31,34]

In light-water reactors (LWRs, see Figure 3-1 for a simplified schematic), the most common and active byproducts include cobalt-60 and cesium-137.[35,36] Cobalt-60 is the main contributor to high levels of radiation because it has a short half life (5.3 years) and emits high-energy gamma rays (1.17 and 1.33 MeV).[35] Cesium-137, on the other hand, has a longer half life (30 years) and is not as active as cobalt-60, but it is one of most abundant radionuclides produced from fission of uranium-235.[36,37] Moreover, this species poses long-term risks because, like cobalt-60, it produces high-energy beta particles and gamma rays.[38] Cesium in general is an alkaline metal that becomes a monovalent ion in solution and is chemically similar to

Table 3.1. Concentrations of Prevalent Species in Practical Water, the Non-Radioactive Analog of Contaminated Process Water in Nuclear Reactors

Species	Concentration (ppm [mM])	Role
Boron	4,000 [370]	Present in boric acid; boron-10 serves as neutron poison[24]
Lithium-7	2.2 [0.32]	Used (as LiOH) to stabilize pH and control corrosion[39]
Cobalt-59	20 [0.34]	Cobalt-60 is the main contributor to high levels of radiation[35]
Cesium-133	100 [0.75]	Cesium-137 is one of most abundant fission byproducts[36]

sodium and potassium. Radioactive cesium is therefore readily taken up by biological organisms, in which it can deposit on soft tissue and, over time, induce thyroid cancer.[36] Compared to other radionuclides, cesium-137 has been deemed difficult to remove because of its small radius of hydration and high (mass) diffusivity.[36]

In this study, we prepared model radioactive water (referred to hereafter as "practical water") with the composition outlined in Table 3.1, as proposed by our sponsor, Mitsubishi Heavy Industries. This solution includes non-radioactive isotopes of the ions most abundant and active in the process water of LWRs, namely cobalt and cesium.[35,36] Boric acid is included abundantly as it is often used as neutron poison in these reactors because boron-10 can reduce the likelihood of thermal fission by absorbing neutrons.[24] Lastly, lithium-7 is used (in the form of LiOH) as an additive to control water chemistry and minimize the corrosive effects of boric acid.[39,40] During operation, small amounts of hazardous corrosion and fission byproducts (e.g., cobalt and cesium) are released into the process water, such that non-radioactive species may undergo radioactivation near the hot reactor core.[36,41–43] (For example, cobalt-60 is produced when its precursor, cobalt-59, is bombarded with thermal neutrons; cobalt-59 is the naturally occurring isotope of cobalt with 100% abundance, and it is used in alloys that are required to possess thermal and mechanical resilience.[44]) These species are then able to settle onto surfaces of the cooling system and recirculation pipes, and the quantity of undesired

deposits of radionuclides increases with time.[41,45] Accumulation of radioactive matter in the structural portions of nuclear reactors is thus an occupational hazard to those who work in the vicinity of these systems and are exposed to such radiation. We note, however, that demineralization of process water in LWRs is only one possible application of SED, and the study of selective removal of cobalt and cesium is generally relevant to treatment of nuclear (waste)water.[20,21,46,47]

3.3 Materials and Experimental Methods

The device used here was based on a design recently published by our group.[19] This continuous, laboratory scale architecture is illustrated in Figure 3-2. Our device included 3 inlets, 2 to transport fluid to the electrodes and a third to deliver contaminated feed, as well as 4 outlets, 2 to transport fluid from the electrodes and the other 2 to generate fresh and brine streams at the splitter. All fluids were transported through 1/8$^{\text{th}}$-inch Tygon® tubing (Saint-Gobain) glued onto portplates made of cast acrylic. These portplates were used to seal liquids inside the device and to support the rubber tubing in which fluid flows. Moreover, four 1/16$^{\text{th}}$-inch Viton® rubber gaskets (DuPont) were used to conformally seal the device and simultaneously provide channels for the electrode solutions (catholyte and anolyte). The electrodes in this device were platinum meshes (Sigma–Aldrich) that were connected to a Gamry Reference 3000™ potentiostat/galvanostat using titanium wires (Alfa Aesar). The electrodes and wires were secured in place by compressible Viton® gaskets. Cation exchange membranes (Nafion N115, Ion Power) with a thickness of approximately $130\,\mu$m served as fluidic barriers between the electrode channels and the porous medium, which in this study was a borosilicate frit (Adams & Chittenden Scientific Glass) with ultrafine pores (nominally ranging from 0.9 to $1.4\,\mu$m in size), an internal surface area of $1.75\,\mathrm{m^2\,g^{-1}}$ based on Brunauer–Emmett–Teller (BET) theory, a mass density of $1.02\,\mathrm{g\,m^{-3}}$, a porosity of 0.31, and dimensions of $0.9\,\mathrm{cm} \times 2\,\mathrm{cm} \times 1\,\mathrm{cm}$. Prior to assembly, the frit was glued onto an acrylic frame using Devcon 2 Ton Epoxy (McMaster-Carr). The splitter (placed midway down the frit for ease of assembly) was made of cast acrylic and was sealed against the top

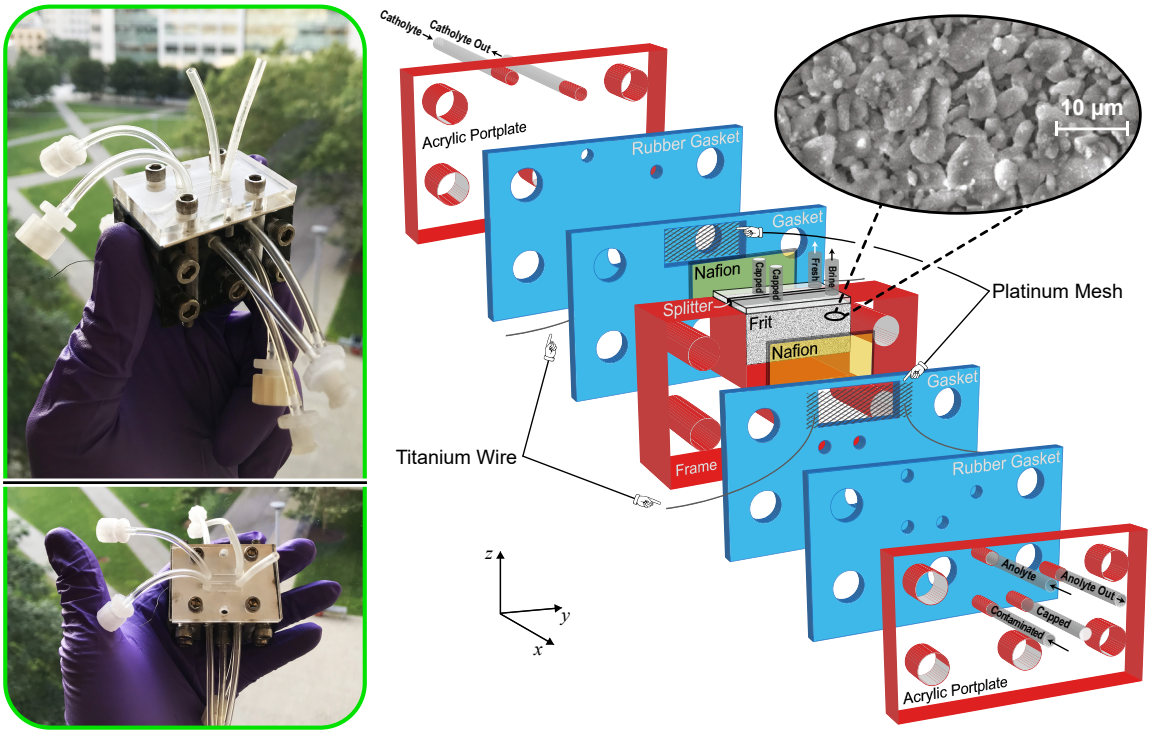

Figure 3-2. Photographs and 3D illustration of the SED device that shows assembly. A working device consists of platinum electrodes, titanium wire, and a microporous borosilicate frit sandwiched between identical Nafion membranes which permit passage of only cations. The inlet (outlet) streams are labeled *contaminated*, *anolyte* (*anolyte out*), and *catholyte* (*catholyte out*); fluid leaving the top edge of the frit is split into *fresh* and *brine* streams. The close-up image of a glass frit was taken by scanning electron microscopy.

face of the frit using 0.04-inch GORE™ expanded polytetrafluoroethylene (ePTFE) gasket tape. Holes in all of the acrylic slabs and rubber gaskets were formed using a laser cutter (Universal Laser Systems) and refined with a drill press (Palmgren 10-inch, 5-speed bench model). These layers were then stacked and held together with nuts, bolts, and washers made of 316 stainless steel.

To prepare practical water with the composition shown in Table 3.1, we formulated stock solutions with 1000 times the target concentrations made from lithium hydroxide monohydrate ($LiOH \cdot H_2O$), cobalt chloride hexahydrate ($CoCl_2 \cdot 6H_2O$), and cesium chloride (CsCl). Appropriate volumes of these solutions were then diluted in deionized water, followed by the addition of solid boric acid (H_3BO_3) to achieve a concentration of 370 mM. (All reagents were purchased from Sigma–Aldrich and used as received.) We note that H_3BO_3 is a weak acid with a first

pK_a of 9.24 in pure water at room temperature; with the following equation for dissociation equilibrium,

$$H_3BO_3 \rightleftharpoons H^+ + H_2BO_3{}^- \tag{3.1}$$

we determined the concentration of $H_2BO_3{}^-$ to be approximately $0.015\,\mathrm{mM}$ in solution. This weak dissociation implied that virtually all of the boron was present as electrically neutral boric acid and thus was not separated by SED. We recognized, however, that H_3BO_3 could have influenced the pH of practical water, the dynamics of proton transport, and the extent of ionic separation. The pH of practical water (assumed here to be an ideal solution) was indeed calculated assuming partial dissociation of H_3BO_3 as well as complete dissociation of LiOH. By definition of the equilibrium constant K_a, we obtained

$$\frac{[H^+][H_2BO_3{}^-]}{[H_3BO_3]} = K_a = 10^{-pK_a} \implies \frac{[H^+]([LiOH]_0 + [H^+])}{[H_3BO_3]_0 - [LiOH]_0 - [H^+]} = 10^{-pK_a} \tag{3.2}$$

where brackets denote concentration (molarity), $[H_3BO_3]_0 = 0.37\,\mathrm{M}$, $[LiOH]_0 = 0.32\,\mathrm{mM}$, and $pK_a = 9.24$. Solving this algebraic equation gave

$$[H^+] = 6.6 \times 10^{-7}\,\mathrm{M} \implies \mathrm{pH} = -\log([H^+]) = 6.2 \tag{3.3}$$

In preparing practical water, the anolyte and contaminated feed were identical in composition, whereas the catholyte included an additional dose of hydrochloric acid (HCl) with a concentration of $10\,\mathrm{mM}$. This dose of HCl was deliberately added to prevent precipitation of cobalt hydroxide that could have formed as a result of hydrogen evolution in the otherwise basic catholyte.

With these solutions prepared, experiments began by setting the flow rates of all streams. In this report, all flow rates were held constant: $0.21 \pm 0.01\,\mathrm{mL\,min^{-1}}$ for the electrode streams (anolyte and catholyte) and $0.065 \pm 0.003\,\mathrm{mL\,min^{-1}}$ for the contaminated feed. To transport these streams to the SED device, we used peristaltic pumps equipped with Tygon® Chemical tubing (Saint-Gobain). With such

pumps—and at low speeds of rotation—the flow would be pulsed, though it was made smooth by incorporating a small buffering tank known commonly as a hydraulic accumulator (or capacitor) just upstream of the device. In our deign, the accumulators were capped glass vials that held a small volume of (compressible) air above the (incompressible) liquids being pumped at the bottom to smooth out pulsations. With flow rates set and tubing connected, the accumulators were left to pressurize and the system to equilibrate overnight, after which the Gamry was set to operate in galvanostatic mode. (Air inside the accumulators became pressurized over time until the fluidic resistance downstream—such as that created by the porous frit—was overcome by the pumped liquid.) The measured voltage was allowed to stabilize for at least 1 hour until it reached steady state.

Samples were collected directly from the device in graduated cylinders and stored in conical centrifuge tubes for analysis, which included measurement of volume, conductivity, pH, and composition of cations. Conductivity and pH were measured using Mettler Toledo analytical instruments (SevenCompact pH/Cond S213), and composition was determined using inductively coupled plasma mass spectrometry (Agilent 7900 ICP–MS). The plasma in ICP–MS was made from argon gas and was supplemented by helium, which is normally needed to analyze elements with high ionization energies (e.g., Co) for which argon plasma alone is not a sufficient source of ionization.[48] To improve the accuracy of our data and subsequent analysis, we incorporated an internal standard that introduced 100 ppb of indium to all of our samples. Since the output of ICP–MS was numerical (in counts per second), quantitative analysis required calibration of the measurements, which was achieved by processing a set of reference standards and producing a calibration curve, an example of which is shown in Figure A-1 (Appendix A). These standards (Li, Co, Cs, and In) were purchased from Sigma–Aldrich and serially diluted to prepare a set of samples encompassing the concentrations relevant to this study. All samples and standard solutions were diluted in 2 vol% nitric acid prior to analysis by ICP–MS.

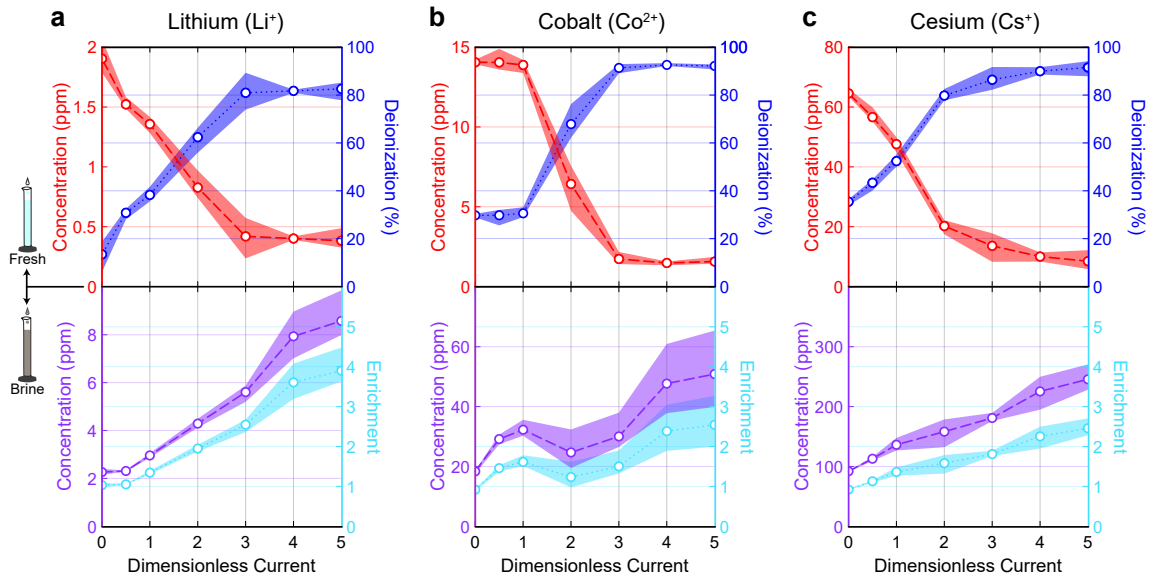

Figure 3-3. Quantitative analysis of the deionization of (a) lithium, (b) cobalt, and (c) cesium in practical water. The upper (lower) half of each panel shows measured concentration and calculated deionization (enrichment) in the fresh (brine) stream as functions of dimensionless current. The concentration of ions in the feed was 1.41 mM, with compositions outlined in Table 3.1. Each data point represents the arithmetic mean of 4 samples, and the shaded areas correspond to the range of those samples.

3.4 Results and Discussion

3.4.1 Principles and Performance of Shock Electrodialysis

The key phenomenon that governs deionization in SED is propagation of a shock wave across which concentration varies drastically and a depletion zone is formed. This shock is generated by providing the system with an overlimiting current, which is current in excess of the flow-limited current (I_{lim}) defined as

$$I_{\text{lim}} = \sum_k \nu_k C_k F Q' \tag{3.4}$$

where ν is valence (charge), C is molar concentration, F is Faraday's constant, Q' is the volumetric flow rate of the feed, and the sum is taken over all cations k. This definition of I_{lim} can be interpreted as the rate of forced convection of positive charge carriers into the device, and it was assumed that the flux of anions is 0 at steady state in the presence of ideal cation exchange membranes. Using the com-

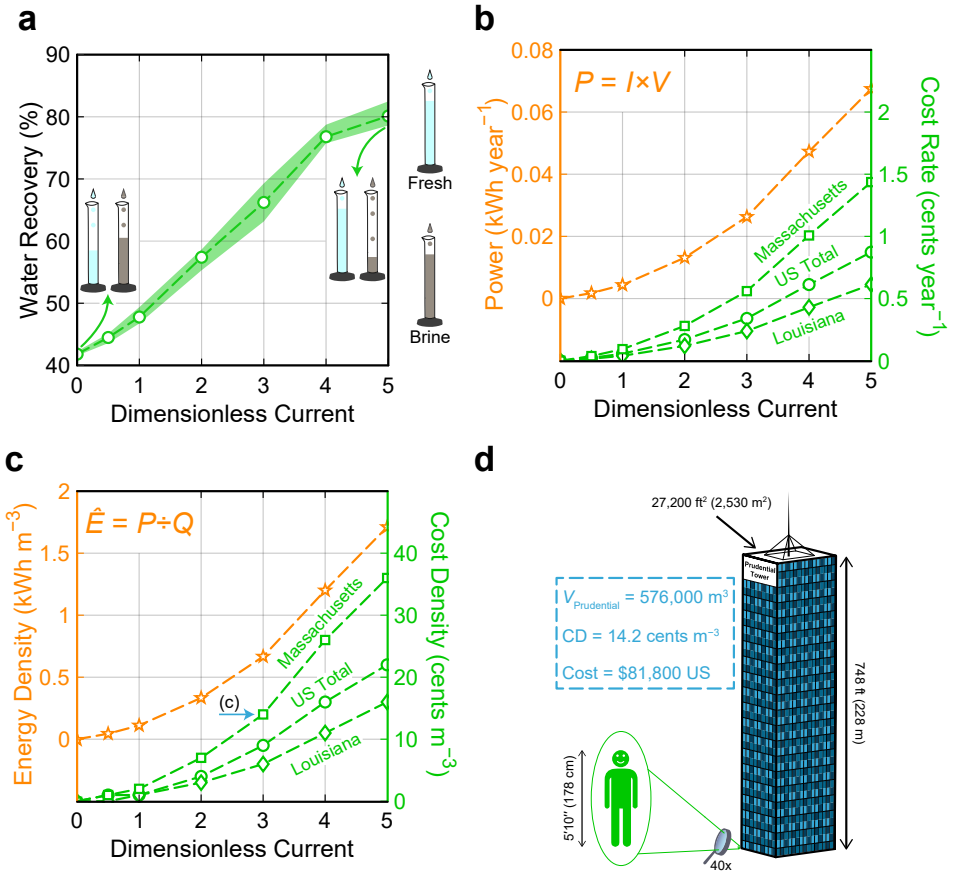

Figure 3-4. Quantitative analysis of the water recovery and energy demand/cost corresponding to the results shown in Figure 3-3. (a) Water recovery as a function of dimensionless current; graduated cylinders portray relative proportions of the fresh and brine products, and each data point represents the arithmetic mean of 4 samples with the shaded area corresponding to the range of those samples. (b) Power and cost rate as well as (c) energy density and cost density as functions of dimensionless current; cost rate (cost density) is equal to power (energy density) multiplied by the residential cost of electricity, which varies between states in the US. (d) Cartoon schematic to aid with visualization of the cost needed to apply 3 times the dimensionless current to a body of water with volume equal to that of the Prudential Tower in Boston, MA; CD is cost density from (c).

position of practical water in Table 3.1 and with $Q' = 0.065\,\mathrm{mL\,min^{-1}}$, we found that $I_{\mathrm{lim}} = 180\,\mu\mathrm{A}$. We verified this value experimentally by performing a conventional voltage sweep from 0 to 10 V and measuring the current, as shown by the *I*–*V* curve in Figure A-2 (Appendix A). After exceeding I_{lim}, the (overlimiting) current increased linearly with voltage and effected constant conductance, which was consistent with the governing theory as well as previous experimental observations in negatively charged porous media.[4,12]

Based on a previous study by our group, we operated our SED system in galvanostatic mode (see Figure A-3 in Appendix A) because it facilitates the formation of a stable deionization shock wave when supplying overlimiting current.[4] (Potentiostatic operation, on the other hand, tends to result in overshoot and oscillation about a desired overlimiting current and is associated with variability in the shock wave.[17]) Our results for treatment of practical water are presented in Figure 3-3, where deionization (the percentage removed of a given species, DI) is defined as

$$DI = 100\% \times \left(1 - \frac{C_{\text{fresh}}}{C_{\text{feed}}}\right) \tag{3.5}$$

enrichment factor (EF) as

$$EF = \frac{C_{\text{brine}}}{C_{\text{feed}}} \tag{3.6}$$

and dimensionless current ($\widetilde{I}$) as $\widetilde{I} = I/I_{\text{lim}}$. The upper half of this figure illustrates that the concentration of cations (Li^+, Co^{2+}, and Cs^+) in the fresh stream decreased—by up to 92% for both Co^{2+}, and Cs^+—with current. Moreover, the lower half shows that the concentration of cations in the brine stream increased with current. Deionization that occurred with no applied current was most likely due to exchange of H^+ (abundant in the cathode) with cations in practical water across the lower membrane.

3.4.2 Water Recovery and Energy Cost

Given the importance of water recovery and energy efficiency in desalination systems, we analyzed the recovery ability and energy demand of SED when used to treat practical water. Water recovery (WR), sometimes referred to the recovery ratio, is defined as

$$WR = \frac{Q_{\text{F}}}{Q'} \tag{3.7}$$

where Q_{F} is the volumetric flow rate of the fresh stream, and it is shown in Figure 3-4a to increase (up to 80%) with current. This increase in water recovery is predominantly due to electroosmotic flow (see Figure 3d and the Supporting Information in ref 4); the position of the splitter was not changed in this study, although

it could be adjusted in future designs for improved water recovery. Analysis of the electrical energy needed for deionization is shown in Figure 3-4b-c, where power P is the product of applied current and (steady) voltage, and energy density $\hat{E}$ is power divided by the volumetric flow rate of the feed. Although electrical power is the more natural measure of energy transport, it is extensive and does not scale with the size of a system (particularly with flow rate). Energy density is therefore of greater value in quantifying the energy efficiency of SED. In treating practical water, the energy density increases quadratically with current, though it was on the order of $1\,\mathrm{kW\,h\,m^{-3}}$ for dimensionless currents between 3 and 5. Moreover, the cost of fluidic pumping in our laboratory scale system was negligible compared to the cost of electrical energy:

$$\begin{aligned} P_{\text{pump}} &= N\left[Q'\Delta p_{\text{frit}} + Q\left(\Delta p_{\text{anoylte}} + \Delta p_{\text{catholyte}}\right)\right] \\ &= 2.0\times10^{-3}\,\mathrm{kW\,h\,year^{-1}} \\ \hat{E}_{\text{pump}} &= N\left[\hat{E}_{\text{frit}} + \hat{E}_{\text{anolyte}} + \hat{E}_{\text{catholyte}}\right] \\ &= 4.2\times10^{-2}\,\mathrm{kW\,h\,m^{-3}} \end{aligned} \tag{3.8}$$

where N is the number of passes (3 here), Δp is pressure drop (6.1 psi across the frit and 0.67 psi across each of the electrodes), and $Q = 0.21\,\mathrm{mL\,min^{-1}}$ is the volumetric flow rate of the electrode streams. At commercial scales, however, we expect that the cost of pumping will become important and will increase according to the desired level of throughput.

A more intuitive way of understanding the energy efficiency of SED is to consider cost rate (Figure 3-4b) or cost density (Figure 3-4c), which are equal to power or energy density, respectively, multiplied by the cost of residential electricity per kilowatt hour. We present average electricity data for a state in which electricity is expensive (MA, $\$0.21\,\mathrm{kWh^{-1}}$) and in the other cheap (LA, $\$0.09\,\mathrm{kWh^{-1}}$) relative to the US total ($\$0.13\,\mathrm{kWh^{-1}}$); costs are based on 2018 data gathered from the US Energy

Information Administration (EIA).[49] Figure 3-4d is a cartoon that helps visualize the cost needed to apply 3 times the dimensionless current (enough to remove 82% of Li^+, 91% of Co^{2+}, and 85% of Cs^+) to a body of water with a volume equal to that of the Prudential Tower in Boston, MA. For comparison, a nuclear reactor with an electrical power output of 1.7 GWe, such as the US Advanced Pressurized Water Reactor, requires coolant at a flow rate of approximately $28\,m^3\,s^{-1}$.[50] This flow rate corresponds to $8.8\times10^8\,m^3$ ($>$ 1500 times the volume of the Prudential Tower) of water that passes through the reactor core annually. The simple economic analysis introduced here will be useful when SED is being scaled up for use at commercial scale.

3.4.3 Implementation of a Multi-Step Process

For common desalination technologies, performance is improved and energy consumption is reduced by using multiple units or stages of the technology in series, and by operating each stage at lower power.[51,52] Such an approach is especially suitable for SED because power increases quadratically with current (Figure 3-4), even though deionization eventually plateaus (Figure 3-3).[53] To demonstrate this claim, we developed a new configuration for our system that involved a 3-step process for deionization of practical water. Because the throughput of our laboratory scale device was low, we accelerated experimentation with this process by feeding serially diluted solutions in turn to the same device. A dilution factor of 5 was chosen for the second step and 25 for the third based on deionization of the target species in the first 2 steps for a dimensionless current of 5. In other words, concentrations of the feed to each pass were 1.41, 0.282, and 0.0564 mM, neglecting boric acid. In Figure 3-5a, we present two-dimensional arrays of deionization for each species as a function of dimensionless current in each pass. In these experiments, dimensionless current ranged from 1 to 20, though deionization typically plateaued at some moderate value. To examine the performance of our system at one such value, we report deionization per pass and cumulative deionization for each species at a dimensionless current of 5, as shown in Figure 3-5b. In the first

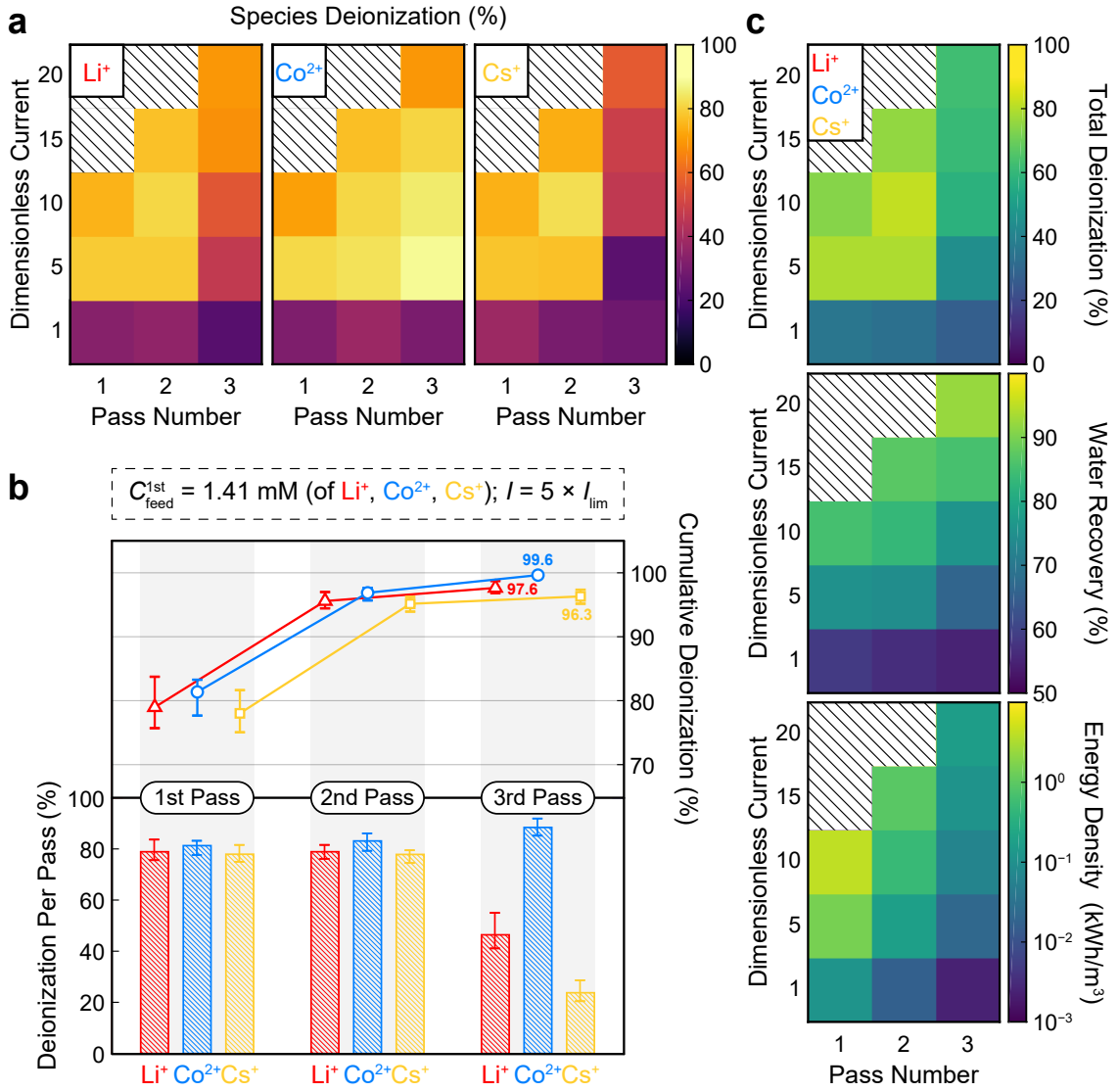

Figure 3-5. Simulation of a 3-step process for deionization of practical water by feeding serially diluted solutions in turn to the same device; neglecting boric acid, concentrations of the feed to each pass are 1.41 mM ($I_{\text{lim}} = 180\,\mu\text{A}$), 0.282 mM (5× dilution, $I_{\text{lim}} = 36\,\mu\text{A}$), and 0.0564 mM (25× dilution, $I_{\text{lim}} = 7.2\,\mu\text{A}$), respectively. (a) Two-dimensional array of deionization as a function of dimensionless current in each pass. (b) Deionization per pass (bottom) and cumulative deionization (top) for each species with a dimensionless current of 5; each data point represents the arithmetic mean of 3 samples with errors bars corresponding to the range of those samples. (c) Two-dimensional arrays of total deionization (top) for the 3 target species, water recovery (middle), and energy density (bottom) as functions of dimensionless current in each pass. Zones of diagonal black stripes in (a) and (c) correspond to parameters that were not tested.

and second passes, all 3 species were removed in nearly equal proportions, whereas in the third pass, Co^{2+} was preferentially removed (see Figure A-4 in Appendix A for discussion of this observation). This selective separation of the divalent ion agreed with a previous experimental study by our group, in which magnesium was selectively removed from an aqueous mixture of NaCl and $MgCl_2$.[19] Figure 3-5b also shows that our 3-step process led to a high cumulative deionization for each species, ranging from 96.3% for Cs^+ to 99.6% for Co^{2+}. Based on its ability to remove target ions from practical water, SED could function as a novel method for treatment of radioactive waste.

In addition to removal of target ions, effective methods for decontamination of water must also optimize total deionization, water recovery, and energy density. These quantities are shown for our 3-step process in Figure 3-5c and are consistent with previously observed trends: total deionization often plateaus at some moderate value of dimensionless current, whereas water recovery and energy density increase monotonically with current. It is striking to learn that our device can sustain water recovery at over 92% ($\widetilde{I} = 20$) only by electroosmotic flow[4] and even though the splitter is positioned midway along the width of the frit. Moreover, successive steps in this process contribute little energy in addition to that consumed in the first step (see Figure A-3 in Appendix A), which implies that a contaminated feed can be repeatedly passed through the device for greater deionization at a reduced cost. This proportionality between energy demand and concentration of the feed—even in the dilute limit—gives SED an advantage over conventional purification techniques, which typically require an input of energy that is bounded from below as the feed becomes more dilute. As with other desalination methods, removal of more ions by multi-step SED comes at the expense of water recovery, which diminishes in every pass. We will address this challenge in future generations of our device by introducing a recycle scheme that feeds the brine stream from a later pass back to an earlier pass in which the original feed is of comparable concentration.

So far, we quantified the ability of SED to remove target species from practical water and identified general rules to optimize the design of a real system that can

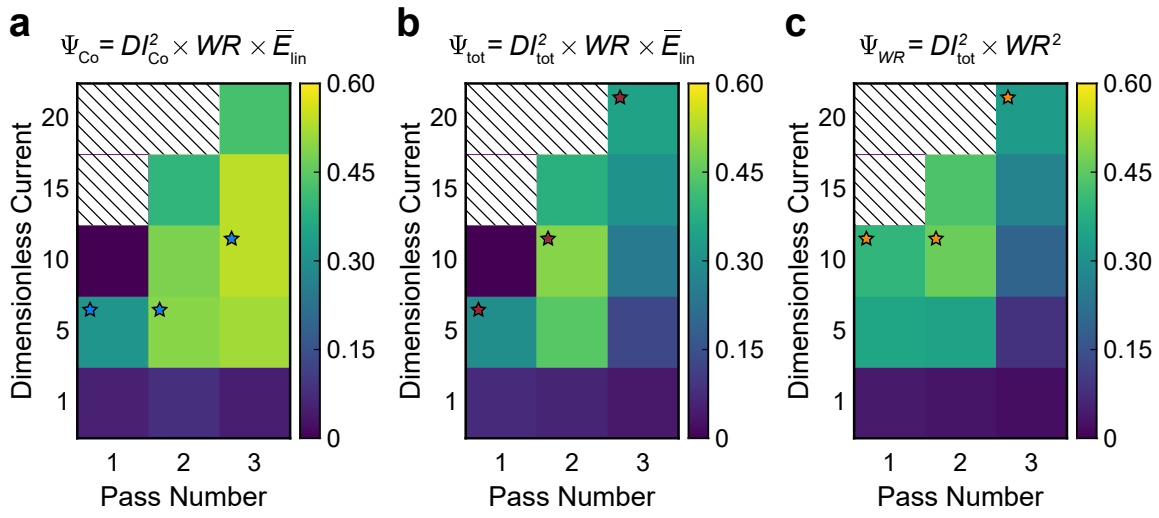

Figure 3-6. Quantitative characterization of the performance of the 3-step process shown in Figure 3-5. Figure of merit Ψ (as defined in Equation 3.9) based on (a) deionization of cobalt only DI_{Co}, (b) total deionization DI_{tot}, and (c) water recovery WR (weighted quadratically, and with no penalty on energy demand) as functions of dimensionless current in each pass; light blue (a), dark red (b), and orange (c) stars indicate which steps in the sequence of passes maximize Ψ (see Table 3.2). Zones of diagonal black stripes in the upper left corners correspond to parameters that were not tested.

treat nuclear waste. In particular, we inferred a complex coupling between the extent of deionization—convoluted by the selective nature of separation by SED (Figure A-4 in Appendix A)—water recovery, and energy demand. The relationship between these parameters is nonlinear, and indeed we observe quadratic growth in energy density with applied current (Figure 3-4b-c and Figure 3-5c). Moreover, deionization varies between species and is not monotonic, and water recovery appears to increase sublinearly with applied current (Figure 3-4a and Figure 3-5c). These results suggest that there is an inherent trade-off between deionization, water recovery, and energy efficiency, which poses a significant challenge to satisfactorily treat nuclear waste while minimizing the demand for power. We addressed this challenge from the perspective of systems engineering by introducing a new figure of merit (Ψ) defined as

$$\Psi = DI^2 \times WR^n \times f(\hat{E}) \tag{3.9}$$

where DI is deionization (squared to emphasize this metric), WR is water recovery, n is a positive integer (either 1 or 2 here), and $f(\hat{E})$ is a dimensionless function of

energy density that ranges from 0 to 1. This function may be constant:

$$f(\hat{E}) = 1 \quad \text{(no penalty on energy demand)} \tag{3.10}$$

linear:

$$f(\hat{E}) = \overline{E}_{\text{lin}} \equiv 1 - \frac{\hat{E}}{\max \hat{E}} \tag{3.11}$$

or nonlinear with respect to $\hat{E}$:

$$f(\hat{E}) = \overline{E}_{\text{quad}} \equiv \sqrt{\frac{1 - \hat{E}/\max \hat{E}}{1 - \min \hat{E}/\max \hat{E}}} \tag{3.12}$$

where "min" and "max" operate on the entire array of energy densities in Figure 3-5c. Although we only considered Equation 3.10 and Equation 3.11 in this study, a nonlinear function such as Equation 3.12 could be used to detract from the merit of steps that operate at high power, such that this penalty would become increasingly severe as $\hat{E}$ approaches $\max \hat{E}$. In any case, all terms in the expression for Ψ (and hence Ψ itself) would range from 0 to 1.

Introducing a figure of merit allows us to quantitatively decide which operating conditions in each pass maximize deionization in our system. Characterization of the performance of our 3-step process is shown in Figure 3-6 based on several variations of Ψ. For example, Ψ may be based on deionization of cobalt only (Figure 3-6a) or total deionization (Figure 3-6b). These variations of Ψ, both with $n = 1$, suggest the same value of dimensionless current in only the first pass ($\widetilde{I} = 5$), but suggest different values in the second and third passes (as designated by the colored stars). This difference can be rationalized by the fact that deionization of Co^{2+} (and not of Li^{+} or Cs^{+}) is often greatest at low to moderate dimensionless current (Figure 3-5a).

To select the most suitable operating conditions, we compared total (and individual) deionization, water recovery, and energy density, all of which are summarized in Table 3.2, for the sequence of passes that maximizes the corresponding variation of Ψ. The sequence that maximizes Ψ_{Co} in each step, for instance, leads

to relatively low water recovery, but the energy density it consumes is also the least. In comparison, the sequence that maximizes Ψ_{tot} in each step gives water recovery of 58%, and it maintains almost 99% deionization of Co^{2+} with little additional demand for energy. This level of water recovery is similar to those achieved by conventional purification technologies, though it can be increased by selecting an alternate sequence in our process. To make a quantitatively motivated selection, more weight is given to water recovery by setting $n = 2$ and $f(\hat{E}) = 1$ in our definition of Ψ, as shown in Figure 3-6c. With this modification, the sequence that maximizes Ψ_{WR} in each step gives a water recovery of 66%. In response, however, consumption of energy increases considerably. It then seems that water recovery can be improved in return for higher energy consumption (or lower deionization, by repositioning the splitter) depending on the targets set by the operator.

3.4.4 Process Intensification for Lithium Recovery

For all cases shown in Table 3.2, total deionization is approximately 98%, and deionization of Co^{2+} is even greater in our 3-step process. Another practical result is the high deionization of Li^{+}, which is used (as LiOH) in nuclear reactors for corrosion control by alkalizing the process water.[39] For this application, LiOH is isotopically enriched in lithium-7 which does not interfere with nuclear reactions (unlike lithium-6), and it is sometimes used in demineralizers (also known as ion exchangers) to remove radioactive contaminants from the process water.[54] Lithium can be selectively captured and recycled in our system (or reused elsewhere) by integrating capacitive deionization (CDI) with intercalation materials[55,56] as a second operation following SED. This process intensification can in principle be achieved in two steps, as illustrated in Figure 3-7. In the first step, SED is used to concentrate

Table 3.2. Summary of Total (and Individual) Deionization *DI*, Water Recovery *WR*, and Energy Density $\hat{E}$ For the Sequence of Passes That Maximizes the Figure of Merit Ψ in Figure 3-6 (Designated by Light Blue (a), Dark Red (b), and Orange (c) Stars)

	DI_{tot} (%)	DI_{Li} (%)	DI_{Co} (%)	DI_{Cs} (%)	WR (%)	$\hat{E}$ (kWh m^{-3})
Optimal for Ψ_{Co}	98.1±0.2	98.0±0.2	99.5±0.1	97.3±0.5	43±2	1.76±0.04
Optimal for Ψ_{tot}	98.6±0.1	98.8±0.2	98.9±0.3	98.3±0.2	58±2	2.18±0.05
Optimal for Ψ_{WR}	98.2±0.2	98.5±0.3	98.3±0.4	98.1±0.2	66±2	4.8±0.2

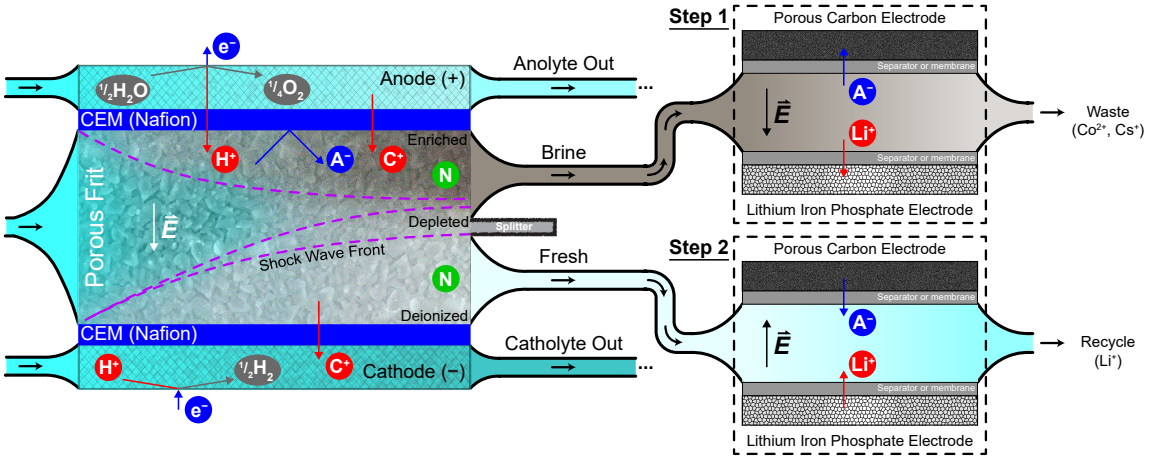

Figure 3-7. Process intensification of SED by using CDI to recycle Li^+ in 2 steps. The first step involves selective capture of Li^+ in the CDI unit from the brine stream discharged by SED. Selectivity is achieved by intercalation of Li^+ into an iron phosphate electrode, which becomes lithium iron phosphate (Li_xFePO_4) upon insertion of Li^+. The second step involves release of Li^+ into the fresh stream exiting the SED device by reversing the direction of electric field.

waste in the brine stream, from which Li^+ is selectively captured in the CDI unit by intercalation into an appropriate electrode such as iron phosphate[57] ($Fe(III)PO_4$, often prepared by deintercalation of Li^+ from $LiFe(II)PO_4$) or lithium manganese oxide[58] ($LiMn_2O_4$). During this process, all cations are driven towards the intercalation electrode, but only Li^+ can be inserted into its crystal lattice because Cs^+ is too large and Co^{2+} will exhibit strong Coulomb repulsion (vacancies in $FePO_4$ are fitted for small monovalent cations[57]). Moreover, the anions are inserted into a porous carbon electrode where they are electrostatically trapped by the applied potential. Fluid leaving the device in this first step will therefore be depleted of lithium and its counterion(s). In the second step, the fresh stream produced by SED is passed through the CDI unit. By reversing the direction of electric field, lithium and its counterion(s) are released from the electrodes back into solution and are recovered for later use.

3.5 Acknowledgments

This research was supported by a grant from Mitsubishi Heavy Industries Limited. The authors thank the Center for Environmental Health Sciences (CEHS) at MIT for

use of ICP–MS.

3.6 References

[1] Douglas C Giancolli. *Physics: principles with applications*. Prentice Hall, 6 edition, 2005.

[2] Shirley Lehnert. *Biomolecular action of ionizing radiation*. CRC Press, 2007.

[3] Wei Han and KN Yu. Ionizing radiation, dna double strand break and mutation. *Advances in Genetics research*, 4:197–210, 2010.

[4] Sven Schlumpberger, Nancy B Lu, Matthew E Suss, and Martin Z Bazant. Scalable and continuous water deionization by shock electrodialysis. *Environmental Science & Technology Letters*, 2(12):367–372, 2015.

[5] Daosheng Deng, E Victoria Dydek, Ji-Hyung Han, Sven Schlumpberger, Ali Mani, Boris Zaltzman, and Martin Z Bazant. Overlimiting current and shock electrodialysis in porous media. *Langmuir*, 29(52):16167–16177, 2013.

[6] Daosheng Deng, Wassim Aouad, William A Braff, Sven Schlumpberger, Matthew E Suss, and Martin Z Bazant. Water purification by shock electrodialysis: Deionization, filtration, separation, and disinfection. *Desalination*, 357:77–83, 2015.

[7] Martin Zdenek Bazant, EthelMae Victoria Dydek, Daosheng Deng, and Ali Mani. Method and apparatus for desalination and purification, August 12 2014. US Patent 8,801,910.

[8] Martin Zdenek Bazant, EthelMae Victoria Dydek, Daosheng Deng, and Ali Mani. Desalination and purification system, April 7 2015. US Patent 8,999,132.

[9] Ali Mani and Martin Z Bazant. Deionization shocks in microstructures. *Physical Review E*, 84(6):061504, 2011.

[10] Ji-Hyung Han, Edwin Khoo, Peng Bai, and Martin Z Bazant. Over-limiting current and control of dendritic growth by surface conduction in nanopores. *Scientific reports*, 4:7056, 2014.

[11] Ji-Hyung Han, Miao Wang, Peng Bai, Fikile R Brushett, and Martin Z Bazant. Dendrite suppression by shock electrodeposition in charged porous media. *Scientific reports*, 6:28054, 2016.

[12] E Victoria Dydek, Boris Zaltzman, Isaak Rubinstein, DS Deng, Ali Mani, and Martin Z Bazant. Overlimiting current in a microchannel. *Physical review letters*, 107(11):118301, 2011.

[13] Shima Alizadeh, Martin Z Bazant, and Ali Mani. Impact of network heterogeneity on electrokinetic transport in porous media. *Journal of colloid and interface science*, 553:451–464, 2019.

[14] Victor V Nikonenko, Anna V Kovalenko, Mahamet K Urtenov, Natalia D Pismenskaya, Jongyoon Han, Philippe Sistat, and Gérald Pourcelly. Desalination at overlimiting currents: State-of-the-art and perspectives. *Desalination*, 342:85–106, 2014.

[15] Sungmin Nam, Inhee Cho, Joonseong Heo, Geunbae Lim, Martin Z Bazant, Dustin Jaesuk Moon, Gun Yong Sung, and Sung Jae Kim. Experimental verification of overlimiting current by surface conduction and electro-osmotic flow in microchannels. *Physical review letters*, 114(11):114501, 2015.

[16] Ali Mani, Thomas A Zangle, and Juan G Santiago. On the propagation of concentration polarization from microchannel- nanochannel interfaces part i: analytical model and characteristic analysis. *Langmuir*, 25(6):3898–3908, 2009.

[17] Thomas A Zangle, Ali Mani, and Juan G Santiago. On the propagation of concentration polarization from microchannel- nanochannel interfaces part ii: numerical and experimental study. *Langmuir*, 25(6):3909–3916, 2009.

[18] Thomas A Zangle, Ali Mani, and Juan G Santiago. Theory and experiments of concentration polarization and ion focusing at microchannel and nanochannel interfaces. *Chemical Society Reviews*, 39(3):1014–1035, 2010.

[19] Kameron M. Conforti and Martin Z. Bazant. Continuous ion-selective separations by shock electrodialysis. *AIChE Journal*, page e16751, 2019.

[20] D Rana, T Matsuura, MA Kassim, and AF Ismail. Radioactive decontamination of water by membrane processes–a review. *Desalination*, 321:77–92, 2013.

[21] Maninder Kaur, Huijin Zhang, Leigh Martin, Terry Todd, and You Qiang. Conjugates of magnetic nanoparticle–actinide specific chelator for radioactive waste separation. *Environmental science & technology*, 47(21):11942–11959, 2013.

[22] RO Rahman, Haneen A Ibrahium, and Yung-Tse Hung. Liquid radioactive wastes treatment: a review. *Water*, 3(2):551–565, 2011.

[23] Wei Luo, Gao Xiao, Fan Tian, Joseph J. Richardson, Yaping Wang, Jianfei Zhou, Junling Guo, Xuepin Liao, and Bi Shi. Engineering robust metal-phenolic network membranes for uranium extraction from seawater. *Energy Environ. Sci.*, 12:607–614, 2019.

[24] S K Sengupta, E Hooper, and E Dubost. Processing of nuclear power plant waste streams containing boric acid. *International Atomic Energy Agency (Technical Report)*, 49.

[25] Karl-Heinz Neeb. *The radiochemistry of nuclear power plants with light water reactors*. Walter de Gruyter, 2011.

[26] JH Park, OK Chopra, K Natesan, WJ Shack, and WH Cullen Jr. Boric acid corrosion of light water reactor pressure vessel materials. In *Proceedings of the 12th International Conference on Environmental Degradation of Materials in Nuclear Power System-Water Reactors*, pages 459–468, 2005.

[27] Kwang-Ho Choo, Dae-Joong Kwon, Kwang-Won Lee, and Sang-June Choi. Selective removal of cobalt species using nanofiltration membranes. *Environmental science & technology*, 36(6):1330–1336, 2002.

[28] Nicholas V Ashley and Daniel JW Roach. Review of biotechnology applications to nuclear waste treatment. *Journal of Chemical Technology & Biotechnology*, 49(4):381–394, 1990.

[29] Tung Cao Thanh Pham, Son Docao, In Chul Hwang, Mee Kyung Song, Do Young Choi, Dohyun Moon, Peter Oleynikov, and Kyung Byung Yoon. Capture of iodine and organic iodides using silica zeolites and the semiconductor behaviour of iodine in a silica zeolite. *Energy Environ. Sci.*, 9:1050–1062, 2016.

[30] Terry A Todd. Solvent extraction research and development in the us fuel cycle program. Technical report, Idaho National Laboratory (INL), 2011.

[31] Junfeng Li and Jianlong Wang. Advances in cement solidification technology for waste radioactive ion exchange resins: A review. *Journal of hazardous materials*, 135(1-3):443–448, 2006.

[32] Özgür Arar, Ümran Yüksel, Nalan Kabay, and Mithat Yüksel. Various applications of electrodeionization (edi) method for water treatment–a short review. *Desalination*, 342:16–22, 2014.

[33] Shuvo Jit Datta, Peter Oleynikov, Won Kyung Moon, Yanhang Ma, Alvaro Mayoral, Hyuncheol Kim, Catherine Dejoie, Mee Kyung Song, Osamu Terasaki, and Kyung Byung Yoon. Removal of 90sr from highly Na^+-rich liquid nuclear waste with a layered vanadosilicate. *Energy Environ. Sci.*, 12:1857–1865, 2019.

[34] Joseph AN Otte and Dennis Liebman. Method for removing cesium from an aqueous liquid and purifying the reactor coolant in boiling water and pressurized water reactors, April 14 1987. US Patent 4,657,731.

[35] M Kikuchi, E Ga, K Funabashi, H Yusa, S Uchida, and K Fujita. Removal of radioactive cobalt ion in high temperature water using titanium oxide. *Nuclear Engineering and Design*, 53(3):387–392, 1979.

[36] Xiaojing Liu, Jinling Wu, and Jianlong Wang. Removal of cs (i) from simulated radioactive wastewater by three forward osmosis membranes. *Chemical Engineering Journal*, 344:353–362, 2018.

[37] R. W. Stoenner and Manny Hillman. Search for radiochemical evidence for ternary fission of ^{235}U by thermal neutrons. *Phys. Rev.*, 142:716–719, Feb 1966.

[38] Debajit Sarma, Christos D. Malliakas, K. S. Subrahmanyam, Saiful M. Islam, and Mercouri G. Kanatzidis. $K_{2x}Sn_{4-x}S_{8-x}$ $(x = 0.65 - 1)$: a new metal sulfide for rapid and selective removal of Cs^+, Sr^{2+}, and $UO_2{}^{2+}$ ions. *Chemical Science*, 7(2):1121–1132, 2016.

[39] B Cox and C Wu. Transient effects of lithium hydroxide and boric acid on zircaloy corrosion. *Journal of nuclear materials*, 224(2):169–178, 1995.

[40] Chul Song Min and Jai Lee Kun. A study on the generation of radioactive corrosion product at pwr for extended fuel cycle. Technical report, 2001.

[41] D. H. Lister. The transport of radioactive corrosion products in high-temperature water ii. the activation of isothermal steel surfaces. *Nuclear Science and Engineering*, 59(4):406–426, 1976.

[42] Takashi Honda, Akira Minato, Katsumi Ohsumi, and Hideo Matsubayashi. Radioactive contamination of carbon steel in a boiling water reactor. *Nuclear Technology*, 65(3):438–443, 1984.

[43] Kálmán Varga, Gábor Hirschberg, Zoltán Németh, Gerrit Myburg, János Schunk, and Péter Tilky. Accumulation of radioactive corrosion products on steel surfaces of vver-type nuclear reactors. ii. 60co. *Journal of Nuclear Materials*, 298(3):231–238, 2001.

[44] Howard Ocken. Reducing the cobalt inventory in light water reactors. *Nuclear Technology*, 68(1):18–28, 1985.

[45] Takashi Honda, Masakiyo Izumiya, Akira Minato, Katsumi Ohsumi, and Hideo Matsubayashi. Radiation buildup on stainless steel in a boiling water reactor environment. *Nuclear Technology*, 64(1):35–42, 1984.

[46] M Khayet, JI Mengual, and G Zakrzewska-Trznadel. Direct contact membrane distillation for nuclear desalination, part ii: experiments with radioactive solutions. *International journal of nuclear desalination*, 2(1):56–73, 2006.

[47] Se-Moon Park, Jong-Kil Park, Jong-Bin Kim, Sang-Woon Shin, and Myung-Chan Lee. Development of the pilot system for radioactive laundry waste treatment using uv photo-oxidation process and reverse osmosis membrane. *Nuclear Engineering and Technology*, 31(5):506–511, 1999.

[48] Sang Ho Nam, Wellington RL Masamba, and Akbar Montaser. Investigation of helium inductively coupled plasma-mass spectrometry for the detection of metals and nonmetals in aqueous solutions. *Analytical Chemistry*, 65(20):2784–2790, 1993.

[49] U.S. Energy Information Administration. Average Price of Electricity to Ultimate Customers by End-Use Sector. https://www.eia.gov/electricity/monthly/epm_table_grapher.php?t=epmt_5_6_a, 2019.

[50] Mitsubishi Heavy Industries, Ltd. Us-apwr design description, 2006.

[51] M Göktuğ Ahunbay, S Birgül Tantekin-Ersolmaz, and William B Krantz. Energy optimization of a multistage reverse osmosis process for seawater desalination. *Desalination*, 429:1–11, 2018.

[52] Aihua Zhu, Panagiotis D Christofides, and Yoram Cohen. Minimization of energy consumption for a two-pass membrane desalination: effect of energy recovery, membrane rejection and retentate recycling. *Journal of Membrane Science*, 339(1-2):126–137, 2009.

[53] Mohammad A Alkhadra, Tao Gao, Kameron M Conforti, Huanhuan Tian, and Martin Z Bazant. Small-scale desalination of seawater by shock electrodialysis. *Desalination*, 476:114219, 2020.

[54] U.S. Government Accountability Office. Managing critical isotopes: Stewardship of lithium-7 is needed to ensure a stable supply. http://www.gao.gov/products/gao-13-716, 2013.

[55] K Singh, HJM Bouwmeester, LCPM de Smet, MZ Bazant, and PM Biesheuvel. Theory of water desalination with intercalation materials. *Physical Review Applied*, 9(6):064036, 2018.

[56] Changyong Zhang, Di He, Jinxing Ma, Wangwang Tang, and T David Waite. Faradaic reactions in capacitive deionization (cdi)-problems and possibilities: A review. *Water research*, 128:314–330, 2018.

[57] Lihua He, Wenhua Xu, Yunfeng Song, Yunze Luo, Xuheng Liu, and Zhongwei Zhao. New insights into the application of lithium-ion battery materials: Selective extraction of lithium from brines via a rocking-chair lithium-ion battery system. *Global Challenges*, 2(2):1700079, 2018.

[58] Dong-Hee Lee, Taegong Ryu, Junho Shin, Jae Chun Ryu, Kang-Sup Chung, and Young Ho Kim. Selective lithium recovery from aqueous solution using a modified membrane capacitive deionization system. *Hydrometallurgy*, 173:283–288, 2017.

Chapter 4

Selective and chemical-free removal of toxic heavy metal cations from water using shock ion extraction

The work reported in this chapter has been submitted as "Selective and chemical-free removal of toxic heavy metal cations from water using shock ion extraction," by Mohammad A. Alkhadra, Matthew L. Jordan, Huanhuan Tian, Christopher G. Arges, and Martin Z. Bazant.

Abstract

Electrochemical methods are known to have attractive features and capabilities when used for ion separations and water purification. In this study, we developed a new process called shock ion extraction (shock IX) for selective and chemical-free removal of toxic heavy metals from water. Shock IX is a hybrid process that combines shock electrodialysis (shock ED) and ion exchange using an ion exchange resin wafer (IERW), and this method can be thought of functionally as an electrochemically assisted variation of traditional ion exchange. In particular, shock IX exhibits greater ion removal and selectivity, and for longer periods of time, compared to the use of ion exchange alone. The use of an IERW in shock ED also increases multivalent ion selectivity, reduces energy consumption, and improves the hydrodynamics and scalability of the system.

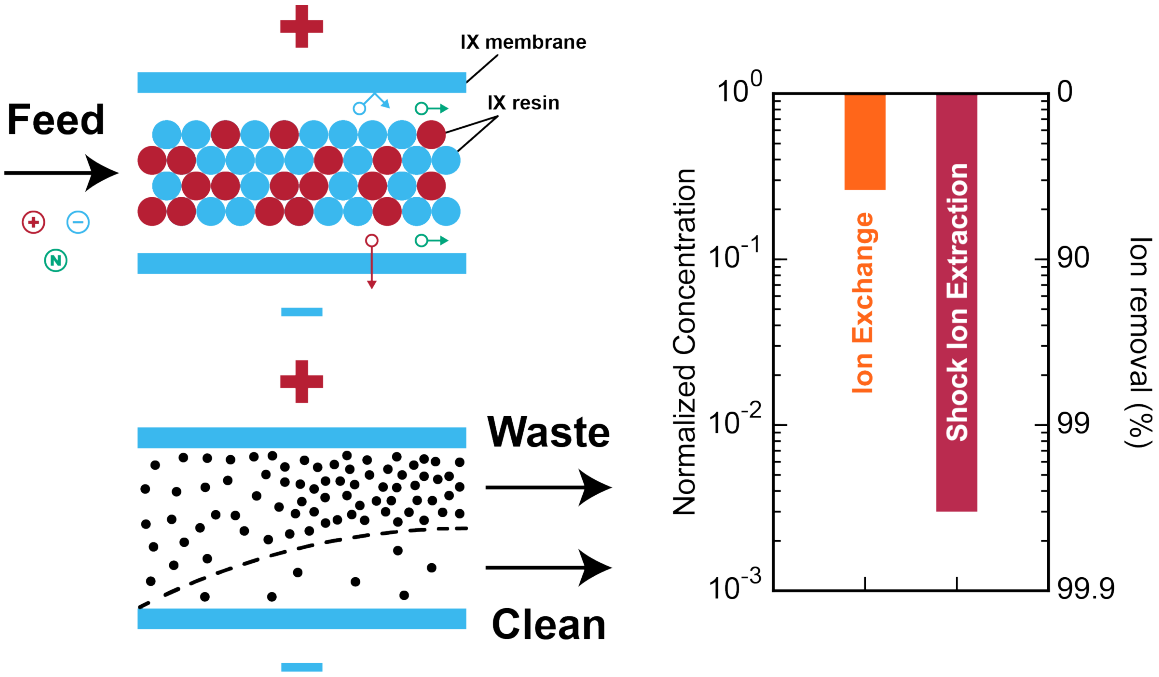

4.1 Introduction

Toxic heavy metal contaminants in water represent a significant hazard to human and animal health as well as to environmental safety. Heavy metal pollution and its concomitant challenges are exacerbated by the large number of candidate pollutants, many of which are extremely toxic and difficult to selectively remove from water. These species contaminate water by various means, such as erosion or leaching of natural deposits (e.g., cadmium, selenium, radium), corrosion of plumbing materials (e.g., copper, zinc, nickel), and discharge from refineries and heavy industries (e.g., chromium, arsenic, mercury, cobalt, antimony). Common methods for removal of heavy metals—often present in trace quantities—from water include adsorption,[1,2] coagulation,[3,4] filtration,[5–7] and ion exchange,[8–12] though these systems are costly and require either regular chemical regeneration or frequent replacement of materials.[1,4,13] In this article, we adapt an emerging chemical-free method for electrokinetic deionization known as shock electrodialysis (or shock ED)[14–17] and for the first time incorporate ion exchange resin wafers (IERWs)—a recent innovation[18–20] in the materials science of ion exchange—to selectively remove heavy metal cations from contaminated water. We call this new method

"shock ion extraction" (shock IX) since it is a hybrid process that combines shock ED and ion exchange. We demonstrated in previous experimental[16,17,21] and theoretical[22,23] work that shock ED is intrinsically selective toward multivalent ions, and we show here that the use of an IERW—composed of strong acid cation exchange resin and strong base anion exchange resin—further increases this selectivity. Moreover, the use of an IERW reduces energy consumption and improves the hydrodynamics of the system by providing regions of high fluidic permeability in a hierarchical pore structure. Shock IX is similar in certain ways to the established method of electrodeionization (EDI),[24] which is a continuous process used to deionize and polish feeds that are typically dilute to begin with. Unlike shock IX, however, EDI displays limited multivalent selectivity despite the presence of selective ion exchange resins,[25–27] which makes it more appropriate when the goal is to remove all dissolved species.

Separation of multivalent ions by shock ED, irrespective of the kind of porous material used, relies on the action of a deionization shock wave,[28] which produces a sharp concentration gradient near an ion selective surface such as a cation exchange membrane[14,29] or a metal electrodeposits.[30,31] This shock wave is generated when overlimiting current is applied (i.e., when transport of ions is faster than by diffusion alone), and it is sustained in the system due to the presence of a charged porous material.[29,32,33] While overlimiting current in conventional ED can be achieved by a chemical process or by hydrodynamic instabilities,[34] surface conduction and electroosmosis are the two dominant mechanisms that enable overlimiting current in shock ED.[29,32,35] By promoting these pathways for charge transfer, IERWs are more ionically conductive and thus reduce the electrical resistance across the device compared to borosilicate glass.[36,37] In dilute solutions, ion exchange resins generally prefer the ion with the highest charge and lowest degree of hydration,[38] which makes these materials suitable for applications that require multivalent selectivity. As shown in Figure 4-1, the deionization shock in shock IX splits the contaminated feed into depleted and enriched product streams, which are continuously separated by driving a flow perpendicular to the applied electric field.[14,39,40]

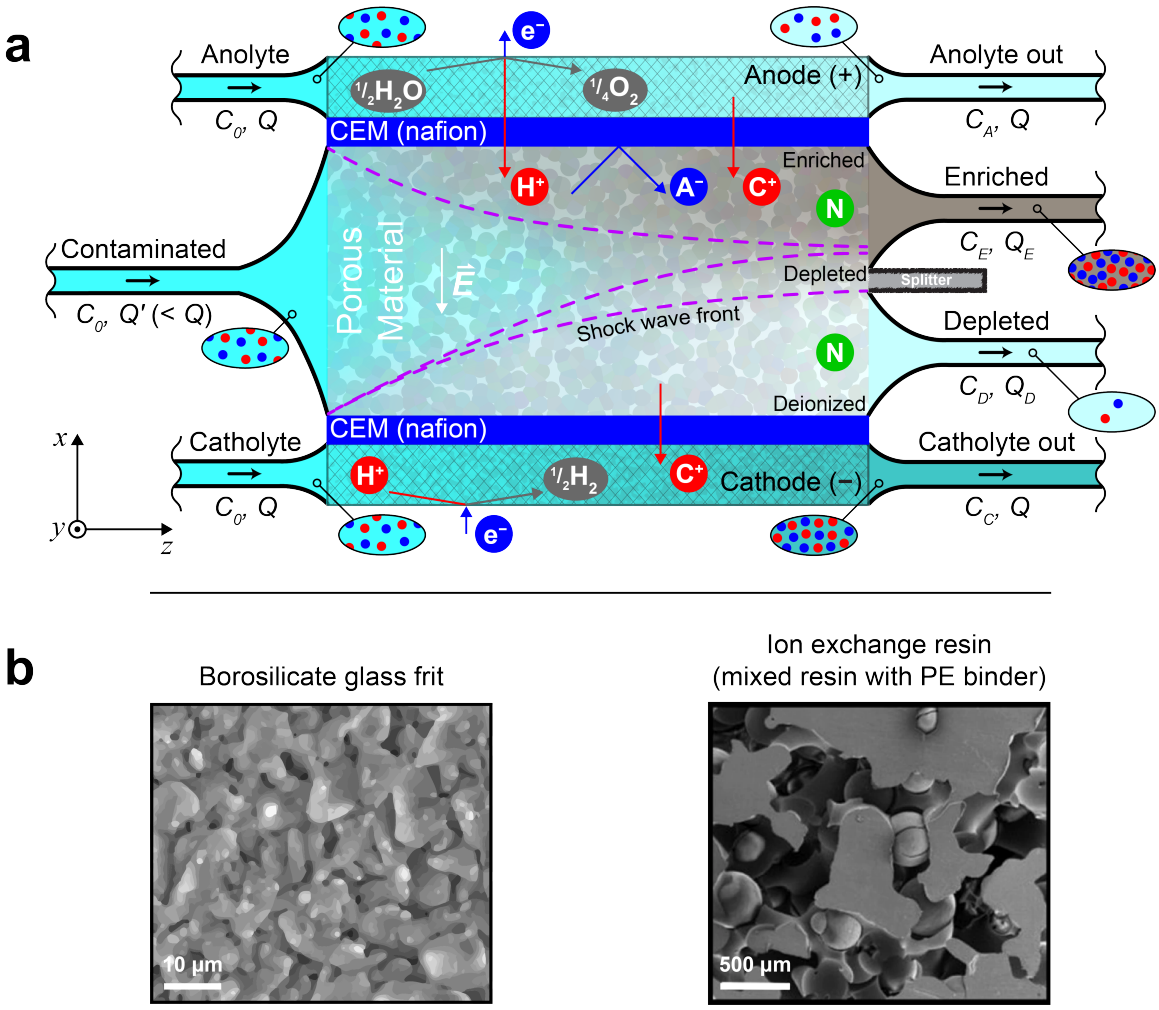

Figure 4-1. Schematic of the governing principles of shock ED and shock IX. (a) A rectangular cross section of the device shows water splitting at the anode and formation of molecular hydrogen at the cathode (maintained under acidic conditions to prevent precipitation of metal hydroxides), which are the primary electrochemical reactions that provide current to the cell. Contaminated water in the porous material is then subjected to an electric field ($\vec{E}$) that transports charged species (labeled C^+ for cations and A^- for anions) perpendicular to the flow. Anions are blocked by cation exchange membranes, and neutral species (labeled N) are unaffected by the electric field. For each stream, flow rate is denoted by the letter Q and concentration by the letter C; streams are colored based on relative concentration of ions. (b) Scanning electron microscopy images of the two porous materials used in this study, one of which is a borosilicate glass frit (shock ED) and the other is an IERW (shock IX). Image of the IERW is adapted from Palakkal et al.[19]

4.2 Materials and Experimental Methods

Device design and fabrication

The two devices used here (one for shock ED and the other for shock IX), shown schematically in Figure 4-1a, are based on a design previously published by our group.[15,21] The only difference between the two devices is the type of porous material used (Figure 4-1b). Both devices consist of three inlets (two to transport the electrode streams and a third to deliver contaminated feed) and four outlets (two to transport the electrode streams and two to generate depleted and enriched product streams at the splitter). All fluids are transported through $1/8^{\text{th}}$-inch Tygon tubing (Saint-Gobain) glued onto portplates made of cast acrylic. These portplates seal liquids inside the device and support the rubber tubing through which fluid flows. Moreover, four $1/16^{\text{th}}$-inch Viton rubber gaskets (DuPont) are used to seal the device and simultaneously provide channels for the electrode streams. The electrodes are made of platinum meshes (Sigma–Aldrich), which are connected to a Gamry Reference 3000 potentiostat/galvanostat using titanium wires (Alfa Aesar). The electrodes and wires are secured in place by compressible Viton gaskets. Cation exchange membranes (Nafion N115, Ion Power) with a thickness of approximately $130\,\mu$m and an area of $1.0\,\text{cm}^2$ are used as fluidic barriers between the electrode channels and the porous material. The porous materials are glued onto acrylic frames using Devcon 2 Ton Epoxy (McMaster-Carr). The splitter (placed midway down the outlet for ease of assembly) is made of cast acrylic and is sealed against the top face of the porous material using 0.04-inch GORE expanded polytetrafluoroethylene (PTFE) gasket tape. During assembly, holes in all of the acrylic slabs and rubber gaskets are formed using a laser cutter (Universal Laser Systems) and refined with a drill press (Palmgren ten-inch, five-speed bench model). These layers are then stacked and held together with nuts, bolts, and washers made of 316 stainless steel.

Porous materials

The first porous material used in this study is a borosilicate frit (Adams & Chittenden Scientific Glass) with ultrafine pores (nominally ranging from 0.9 to $1.4\,\mu$m in size), an internal surface area of $1.75\,\mathrm{m^2\,g^{-1}}$ based on Brunauer–Emmett–Teller theory, a mass density of $1.02\,\mathrm{g\,m^{-3}}$, a porosity of 0.31, and approximate dimensions of $0.5\,\mathrm{cm} \times 1.8\,\mathrm{cm} \times 0.6\,\mathrm{cm}$ ($x \times y \times z$). The other material is an IERW, specifically a conventional polyethylene resin wafer, synthesized by mixing polyethylene binder (Microthene MN71120), ion exchange resin, and sodium chloride in a ratio of $2 : 1 : 0.5$ by mass. The ion exchange resin blend is produced using cation exchange resin (Purolite PFC 100E, which is sulfonated sodium polystyrene crosslinked with divinylbenzene; capacity is $1.9\,\mathrm{Eq\,L^{-1}}$ and density is $1.27\,\mathrm{g\,cm^{-3}}$) and anion exchange resin (Purolite PFA400, which is quaternary benzyl trimethylammonium chloride polystyrene crosslinked with divinylbenzene; capacity is $1.3\,\mathrm{Eq\,L^{-1}}$ and density is $1.07\,\mathrm{g\,cm^{-3}}$) in a ratio of $1 : 1.3$. The mixture is packed into a foil-lined mold and hot pressed to $> 109\,^\circ\mathrm{C}$ with two metric tons of force for one hour. The resin wafer is cooled to room temperature under load and then immersed in deionized (DI) water three times for twenty minutes to dissolve the sodium chloride porosigen. This IERW has a capacity of $0.93\,\mathrm{Eq\,L^{-1}}$, a porosity of 0.27, and the same dimensions as the borosilicate frit.

Preparation of feed and electrode solutions

To prepare the artificial wastewater with the composition shown in Table 4.2, we formulate stock solutions with 1000 times the target concentrations made from cobalt sulfate heptahydrate ($CoSO_4 \cdot 7H_2O$), copper sulfate pentahydrate ($CuSO_4 \cdot 5H_2O$), zinc sulfate heptahydrate ($ZnSO_4 \cdot 7H_2O$), mercury chloride ($HgCl_2$), cadmium chloride ($CdCl_2$), nickel sulfate heptahydrate ($NiSO_4 \cdot 7H_2O$), manganese sulfate monohydrate ($MnSO_4 \cdot H_2O$), and sodium sulfate decahydrate ($Na_2SO_4 \cdot 10H_2O$). (All reagents were obtained from Sigma–Aldrich.) Appropriate volumes of these solutions are then diluted in DI water. In preparing the artificial wastewater, the contaminated feed and anolyte are identical in composition, whereas the

catholyte includes an additional dose of hydrochloric acid with a concentration of 10 mM. This dose of acid is added to prevent precipitation of metal hydroxides that could form as a result of hydrogen evolution in the otherwise basic catholyte.

Experimental procedure

Experiments begin by setting the flow rates of all streams: $n \times 0.21\,\mathrm{mL\,min^{-1}}$ for the electrode streams and $n \times 0.065\,\mathrm{mL\,min^{-1}}$ for the contaminated feed, where $n = 1, 3, 6, \text{or } 9$. These streams are transported using peristaltic pumps equipped with Tygon Chemical tubing (Saint-Gobain), and the flows are made smooth by incorporating hydraulic accumulators (i.e., glass vials). The accumulators are left to pressurize and the system to equilibrate overnight, after which the Gamry is set to operate in galvanostatic mode with periodic polarity reversal (see Section B.1). The measured voltage is allowed to stabilize for at least one hour until it reaches steady state. Samples are collected directly from the device in graduated cylinders and stored in centrifuge tubes for analysis, which include measurement of volume, conductivity, pH, and composition of cations. Conductivity and pH are measured using Mettler Toledo analytical instruments (SevenCompact pH/Cond S213), and composition is determined using inductively coupled plasma mass spectrometry (Agilent 7900 ICP–MS). The plasma in ICP–MS is made from argon gas and is supplemented by helium, and we add an indium internal standard at 100 ppb to all of our samples. Quantitative analysis requires calibration of the measurements, which is achieved by processing a set of reference standards and producing a calibration curve. (All standard solutions were obtained from Sigma–Aldrich.) Samples and standard solutions are diluted in 2 vol% nitric acid prior to analysis by ICP–MS.

Static ionic conductivity of porous materials

Electrochemical impedance spectroscopy (EIS) measurements are conducted on a Nuvant Systems EZstat Pro operated in galvanostatic mode. A two-point probe method is used with a cell consisting of two platinum foil working electrodes adhered to two adjustable stainless steel collectors in a PTFE housing. A stainless

Table 4.1. Summary of results obtained from static ionic conductivity measurements

	Conductivity ($\mathrm{mS\,cm^{-1}}$)	
Spacer Material	DI Water	$0.5\,\mathrm{g\,L^{-1}}$ NaCl
Borosilicate Frit	0.42 ± 0.03	8.4 ± 0.2
IERW	0.56 ± 0.06	8.7 ± 0.8
Solution Only	$(0.81 \pm 0.02) \times 10^{-3}$	0.946 ± 0.001

steel screw is used to adjust the distance between the electrodes to the thickness of the material. EIS is performed with a perturbation of 1 mA in the frequency range of 100 kHz to 1 Hz. The high-frequency resistance from the Nyquist plot is used to calculate the (ionic) conductivity κ as

$$\kappa = \frac{t}{AR} \tag{4.1}$$

where t is material thickness, A is material surface area, and R is the measured resistance. Conductivity is measured in DI water with a $0.5\,\mathrm{g\,L^{-1}}$ solution of NaCl as the supporting electrolyte. The results of these measurements are summarized in Table 4.1.

4.3 Results and Discussion

To compare the performance of the original shock ED method (with borosilicate glass) with that of the new shock IX process, we used an artificial multicomponent mixture comprising seven divalent heavy metal cations and one monovalent cation as the feed. Table 4.2 shows the composition of this mixture as well as the potential health effects from ingestion and sources of each contaminant. (We note that the speciation of mercury(II), which includes $Hg(OH)_2$, $HgOH^+$, and Hg^{2+} as prominent species, depends on its concentration and on pH.) In all experiments, we operated the system at constant current because it facilitates the formation of a stable deionization shock wave at overlimiting current.[15] (In contrast, operating at constant voltage can cause overshoot and oscillation about a desired overlimiting current and is associated with variability in the shock wave[41]). As explained in Sec-

tion B.1, we employed polarity reversal in all experiments in this study to reduce the formation of metal hydroxides and deposits at the electrodes. Our results for selective separation of heavy metals from this multicomponent mixture are presented in Figure 4-2, where normalized concentration of species j in the depleted stream is defined as

$$\widetilde{C}_D^{(j)} = \frac{C_D^{(j)}}{C_0^{(j)}} \tag{4.2}$$

total mass balance as

$$\mu = \frac{\sum_j \left[C_D^{(j)} Q'\gamma + C_E^{(j)} Q'(1-\gamma) + \left(C_C^{(j)} + C_A^{(j)}\right) Q\right]}{\sum_j C_0^{(j)} (Q' + 2Q)}, \gamma = \frac{Q_D}{Q'} \tag{4.3}$$

(γ is water recovery), and dimensionless current as

$$\widetilde{I} = \frac{I}{I_{\text{lim}}} \tag{4.4}$$

Values of $C_0^{(j)}$ are provided in Table 4.2; values of $C_D^{(j)}$, $C_E^{(j)}$, $C_C^{(j)}$, and $C_A^{(j)}$ are measured experimentally. In Equation 4.4, I is applied current and I_{lim} is flow-limited current:

$$I_{\text{lim}} = \sum_j \frac{\nu^{(j)} C_0^{(j)} F Q'}{M^{(j)}} \tag{4.5}$$

where where ν is valence (charge), C is mass concentration, F is Faraday's constant, Q' is the volumetric flow rate of the feed, M is molar mass, and the sum is taken over all cations j. This definition of limiting current can be interpreted as the rate of forced convection of positive charge carriers into the device, and it is assumed that the flux of anions is zero at steady state in the presence of ideal cation exchange membranes.

Figure 4-2a shows that the concentration of ions in the depleted stream decreases with increasing current when using the borosilicate frit. (Ion removal that occurs when no current is applied is due to exchange of H^+ in the catholyte with cations in the feed channel across the bottom membrane.) This material, however, provides only limited selectivity toward the multivalent ions relative to sodium

Table 4.2. Composition of Artificial Wastewater Comprising Seven Divalent Heavy Metal Cations and One Monovalent Cation (This Mixture is Used as Feed, Anolyte, and Catholyte)

Species, j	Concentration, $C_0^{(j)}$ (mg L^{-1})	Potential Health Effects From Ingestion[42–45]	Sources of Contaminant[42–45]
Cobalt (Co^{2+})	12.97	Nausea and vomiting	Coal-fired power plants, mining, erosion of natural deposits
Copper (Cu^{2+})	11.17	Gastrointestinal distress, liver and kidney damage	Corrosion of pipes, erosion of natural deposits
Zinc (Zn^{2+})	10.95	Damage to nervous system, dermatitis	Refineries, electroplating, metals manufacturing
Mercury (Hg(II))	9.61	Damage to nervous system, toxic to kidneys	Batteries, paper industry, erosion of natural deposits
Cadmium (Cd^{2+})	9.78	Renal dysfunction, lung disease, bone defects	Welding, electroplating, pesticides
Nickel (Ni^{2+})	11.82	Dermatitis, allergic reaction	Corrosion of pipes, erosion of natural deposits
Manganese (Mn^{2+})	10.62	Damage to nervous system, toxic	Welding, chemicals manufacturing, erosion of natural deposits
Sodium (Na^{+})	35.39	-	-

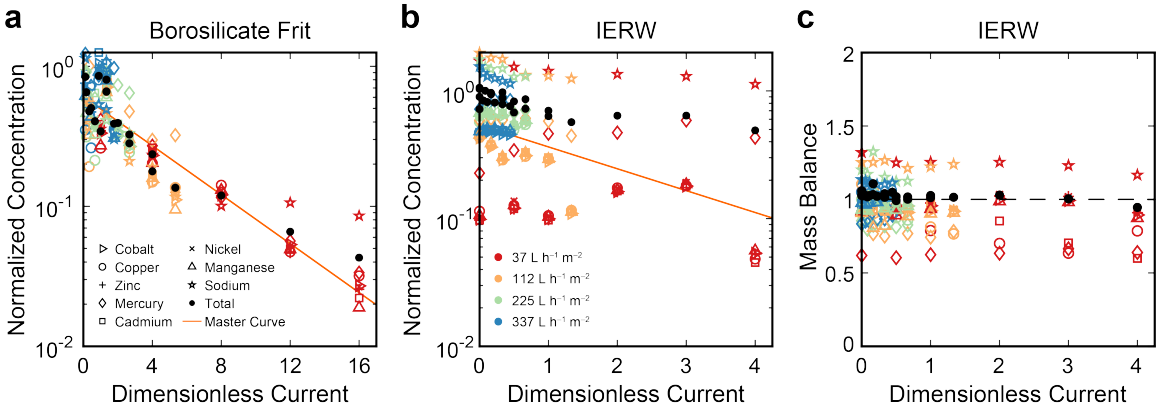

Figure 4-2. Quantitative analysis of selective ion removal using shock ED and shock IX. Normalized concentration of the cations in the depleted stream (Equation 4.2) versus dimensionless current (Equation 4.4) using (a) the borosilicate frit and (b) the IERW. Markers are used to designate different species and colors to designate different productivities (feed flow rate, Q', per unit projected active area). Black circles represent the normalized (total) concentration of all dissolved cations, and the solid lines are guides to the eye. (c) Total mass balance (black circles, Equation 4.3) and mass balances of individual species (colored markers, obtained by omitting the summations in Equation 4.3) versus dimensionless current using the IERW. Total and species mass balances in each of the product streams are shown in Figure B-4. A value of one for the mass balance implies no accumulation. Water recovery and energy demand are analyzed in Section B.2.

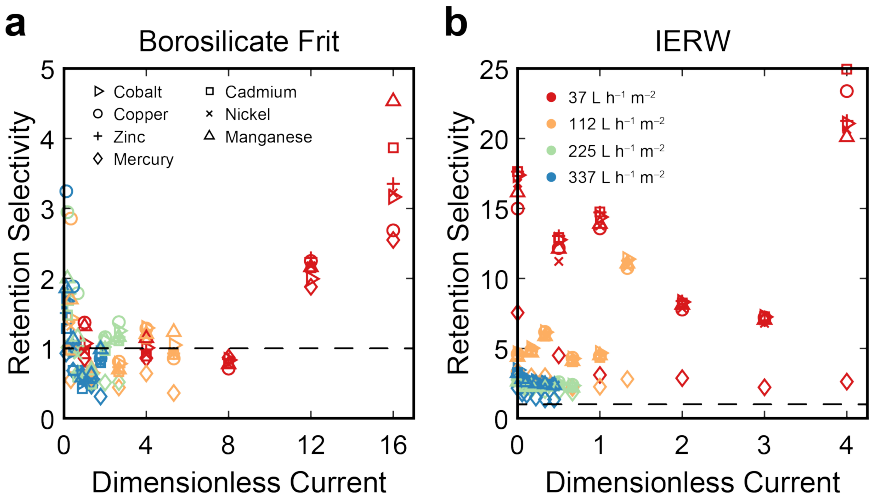

Figure 4-3. Comparison of multivalent ion selectivity (Equation 4.6, with species k taken to be sodium) versus dimensionless current using (a) shock ED and (b) shock IX. Markers are used to designate different species and colors to designate different productivities.

(Figure 4-3a), where selectivity becomes prominent at high current. In this study, (retention) selectivity is defined as

$$S_{j:k} = \frac{C_D^{(k)}/C_D^{(j)}}{C_0^{(k)}/C_0^{(j)}} = \frac{C_D^{(k)}/C_0^{(k)}}{C_D^{(j)}/C_0^{(j)}} = \frac{\widetilde{C}_D^{(k)}}{\widetilde{C}_D^{(j)}} \tag{4.6}$$

which may be interpreted as the ratio of the concentration of species k to that of species j in the depleted stream, scaled by the corresponding ratio of feed concentrations (if $S_{j:k} > 1$, then species j is selectively removed relative to species k). Figure 4-2b again shows that the concentration of ions in the depleted stream decreases with increasing current when using the IERW, though, in contrast to the borosilicate frit, the IERW provides massive selectivity toward the multivalent ions (Figure 4-3b), where little to no sodium is removed in the process. The overall mass balance in Figure 4-3c indicates that the system was operated at steady state, with no accumulation of mass in the device ($\mu = 1$). We note, however, that there may be accumulation of individual species (primarily the multivalent ions, $\mu^{(j)} < 1$) due to their exchange with other, previously adsorbed species (primarily sodium, $\mu^{(\mathrm{Na})} > 1$).

Multivalent ion selectivity in shock ED was observed in our previous experimen-

tal work,[16,17,21] and its mechanisms were examined in our subsequent theoretical studies.[22,23] In this paper, we demonstrate for the first time that multivalent ion selectivity in shock ED (or shock IX when using an IERW) can be significantly boosted by using a class of porous material with known selective properties. Figure 4-3a shows that retention selectivity is small (near one), except at high currents, when using the borosilicate frit, even though the fraction of ions removed is large (Figure 4-2a). On the other hand, Figure 4-3b shows that retention selectivity is large, especially at low flow rates, when using the IERW. A lower flow rate increases the contact time between solution and resin, which likely leads to more favorable ion exchange kinetics (e.g., diffusion of ions toward and within resin beads, adsorption of ions) and greater transport of divalent species by surface conduction in the direction of applied current. The selectivity we obtained using shock IX is large even when compared to specialized capacitive deionization (CDI) systems that use intercalation electrodes, such as Prussian Blue Analogues. For example, Singh et al. developed a CDI system with two identical nickel hexacyanoferrate (NiHCF) electrodes to selectively separate sodium (monovalent) from magnesium and calcium (divalent).[46] In one experiment, the concentration of sodium was reduced from 20 mM to approximately 12 mM and the concentrations of magnesium and calcium were reduced from 20 mM to approximately 19.6 mM,[46] which corresponds to a retention selectivity of $S_{\mathrm{Na:Mg}} \approx S_{\mathrm{Na:Ca}} = 1.6$. In another example, Singh et al. developed a CDI system with two identical vanadium hexacyanoferrate (VHCF) electrodes to selectively remove divalent cations from water.[47] In one experiment, the concentration of sodium was reduced from 10 mM to approximately 7.2 mM and the concentration of calcium was reduced from 10 mM to approximately 5.1 mM,[47] which corresponds to a retention selectivity of $S_{\mathrm{Ca:Na}} = 1.4$. These results are representative of the extent of cation retention selectivity that can be achieved using CDI and intercalation technologies.[48,49] And while multivalent selectivity by shock IX is comparatively large, the values shown in Figure 4-3 can be increased further for instance by using advanced electrodes to drive current by divalent ion intercalation.[49–51]

Since ion exchange resins have inherent loading capacities and ion affinity orders, we expect there to be non-steady substitution of adsorbed ions on the IERW, as suggested by Figure 4-2c. In particular, the overall mass balance shows that more sodium exits the system than is fed, whereas all divalent cations exhibit the opposite trend. It is known in the EDI literature that ion exchange resins are at least partially regenerated by the action of H^+ and OH^- produced via water splitting at bipolar junctions,[52–54] and we expect this to be the case in shock IX as well. To study the dynamics and time dependence of ion separation by shock IX in greater detail, we performed a continuous experiment spanning one week, and the results are shown in Figure 4-4. We began the experiment by feeding a $0.1\,\mathrm{M}$ NaCl solution at $111\,\mathrm{L\,h^{-1}\,m^{-2}}$ ($\widetilde{I}=0$) for two hours to preload the cation exchange resin with sodium. After that, the multicomponent mixture in Table 4.2 was fed at $37\,\mathrm{L\,h^{-1}\,m^{-2}}$ for six days (with either $\widetilde{I}=0$ or $\widetilde{I}=2$), and samples were collected periodically to quantify performance. When no current was applied, we observed ion exchange with replacement of the preloaded sodium with divalent cations, as shown in Figure 4-4a. We note that the hydrochloric acid in the catholyte (see Section 4.2) partly contributes to transport of ions out of the feed when no current is applied. To further quantify the extent of ion removal by ion exchange alone, we repeated the experiment in Figure 4-4 but without applying current, as explained in Section B.3. Figure B-3a shows that ion removal by ion exchange was in the range of 60-75% for the divalent cations, and breakthrough (or resin exhaustion) was reached at approximately 500 bed volumes.

Figure 4-4a and b show that the applied current significantly increased both ion removal and retention selectivity—with over 99% removal of four out of the seven divalent cations—and delayed the onset of breakthrough compared to ion exchange alone. However, both ion removal and selectivity decreased to steady values over time, which suggests that the electroregeneration of resin surfaces by protons produced at the anode may not be sufficient to operate the system continuously over long periods of time. These results imply that stable, long-term operation can be achieved either by optimizing the rate at which protons are produced via electrol-

ysis or by introducing a brief, periodic cleaning step using a benign solution such as 0.1 M NaCl (regions colored green in Figure 4-4).[55,56] In mixed-ion exchange resin beds and wafers, it is known that hydroxide is generated via water splitting in regions of ion depletion at the interfaces between oppositely charged surfaces (e.g., cation exchange membrane and anion exchange resin).[57,58] The results in Figure 4-4c show accumulation ($\mu < 1$) of species in the device, which may be explained by the fact that heavy metal cations react with these hydroxide ions to produce insoluble metal hydroxides.[57] This observation is supported by the measured increase in hydrodynamic resistance (and, in turn, pressure drop) in our device, and it implies that the metal hydroxides form films[59] on the resin beads and physically plug the compartments of the wafer. This phenomenon also occurs in EDI systems when used to remove heavy metal cations from water,[57–59] and one proposed solution is to design a vertically layered bed of cation, anion, and mixed-ion exchange resins to better manage ion removal and prevent precipitation reactions.[57,60] This kind of system requires complex stack design and operation, whereas shock IX can potentially achieve the same device durability by using a homogeneous cation exchange resin wafer with cation exchange membranes. Future work will thus focus on designing homogeneous and layered IERWs to reduce water splitting and prevent precipitation of metal hydroxides in shock IX.

4.4 Environmental Implications

Metals and metalloids exist in virtually all ecosystems, and their natural concentrations vary depending on the local geology. Occurrences such as a land disturbance in metal-rich areas can lead to erosion and mobilization of these elements into nearby water streams. Similarly, human and industrial activity may redistribute and concentrate metals in areas that are not naturally enriched in these species, and often there is no visible evidence of water contamination. While some metals are essential as nutrients (e.g., iron), all metals are toxic above a certain level, and in fact some are toxic even in trace quantities (e.g., lead, mercury, cadmium). In this study, we demonstrated that systems based on deionization shock waves can

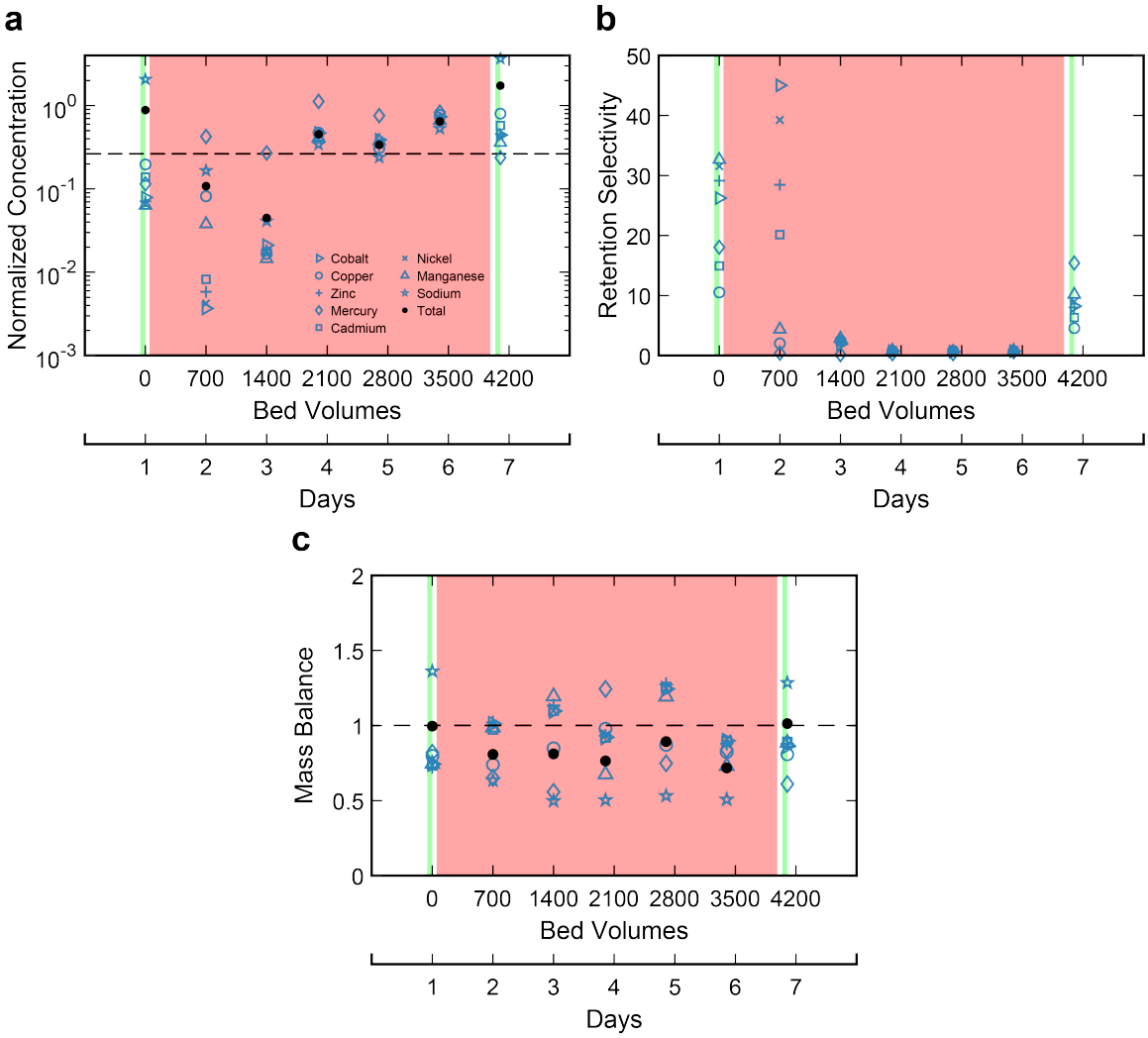

Figure 4-4. Quantitative analysis of the dynamics and time dependence of ion removal by shock IX. (a) Normalized concentration and (b) retention selectivity (relative to sodium) of the cations in the depleted stream versus time. The dashed line in (a) represents the maximum ion removal achieved by ion exchange alone ($\widetilde{I} = 0$; see Figure B-3). (c) Total mass balance and mass balances of individual species versus time; balances in each of the product streams are shown in Figure B-5. One bed volume equals the total volume of the porous IERW multiplied by its porosity (see Section 4.2). Markers are used to designate different species, and black circles represent the normalized (total) concentration of all dissolved cations. Regions colored green correspond to a feed of 0.1 M NaCl ($\widetilde{I} = 0$ and $Q' = 111\,\mathrm{L\,h^{-1}\,m^{-2}}$), and the region colored red corresponds to the feed in Table 4.2 ($\widetilde{I} = 2$ and $Q' = 37\,\mathrm{L\,h^{-1}\,m^{-2}}$).

efficiently and selectively remove toxic metal cations from dilute feeds. We also showed that the use of shock IX with an IERW is a viable approach to electrify traditional ion exchange and eliminate the need for frequent regeneration using strong acids. The hybrid shock IX method exhibits greater ion removal and selectivity, and for longer periods of time, compared to the use of ion exchange alone. Shock IX also displays greater multivalent ion selectivity compared to other electrochemical methods, such as EDI (which actually comprises selective ion exchange resins) and CDI with intercalation electrodes. These attractive properties make shock IX a viable method for tackling heavy metal pollution and a suitable technology in general for selective ion separations.

4.5 Acknowledgements

The authors thank the Center for Environmental Health Sciences (CEHS) at MIT for use of ICP–MS.

4.6 References

[1] Fenglian Fu and Qi Wang. Removal of heavy metal ions from wastewaters: a review. *Journal of environmental management*, 92(3):407–418, 2011.

[2] Dimple Lakherwal. Adsorption of heavy metals: a review. *International journal of environmental research and development*, 4(1):41–48, 2014.

[3] Md Juned K Ahmed and M Ahmaruzzaman. A review on potential usage of industrial waste materials for binding heavy metal ions from aqueous solutions. *Journal of Water Process Engineering*, 10:39–47, 2016.

[4] C Femina Carolin, P Senthil Kumar, A Saravanan, G Janet Joshiba, and Mu Naushad. Efficient techniques for the removal of toxic heavy metals from aquatic environment: A review. *Journal of environmental chemical engineering*, 5(3):2782–2799, 2017.

[5] Rakesh Chandra Vaishya and Sudhir Kumar Gupta. Coated sand filtration: an emerging technology for water treatment. *Journal of Water Supply: Research and Technology—AQUA*, 52(4):299–306, 2003.

[6] Jamaleddin Esalah and Maen M Husein. Removal of heavy metals from aqueous solutions by precipitation-filtration using novel organo-phosphorus ligands. *Separation Science and Technology*, 43(13):3461–3475, 2008.

[7] Yilmaz Yurekli, Mehmet Yildirim, Levent Aydin, and Melih Savran. Filtration and removal performances of membrane adsorbers. *Journal of hazardous materials*, 332:33–41, 2017.

[8] Sultan Ahmed, Shiraz Chughtai, and Mark A Keane. The removal of cadmium and lead from aqueous solution by ion exchange with na–y zeolite. *Separation and purification technology*, 13(1):57–64, 1998.

[9] J Paul Chen and Lin Wang. Characterization of a ca-alginate based ion-exchange resin and its applications in lead, copper, and zinc removal. *Separation science and technology*, 36(16):3617–3637, 2001.

[10] Roman Petrus and Jolanta K Warchoł. Heavy metal removal by clinoptilolite. an equilibrium study in multi-component systems. *Water Research*, 39(5):819–830, 2005.

[11] Tonni Agustiono Kurniawan, Gilbert YS Chan, Wai-Hung Lo, and Sandhya Babel. Physico–chemical treatment techniques for wastewater laden with heavy metals. *Chemical engineering journal*, 118(1-2):83–98, 2006.

[12] Wei Qiu and Ying Zheng. Removal of lead, copper, nickel, cobalt, and zinc from water by a cancrinite-type zeolite synthesized from fly ash. *Chemical Engineering Journal*, 145(3):483–488, 2009.

[13] Frank N Kemmer and John McCallion. *The NALCO water handbook*. McGraw-Hill New York, 1979.

[14] S. Schlumpberger, N. B. Lu, M. E. Suss, and M. Z. Bazant. Scalable and continuous water deionization by shock electrodialysis. *Environmental Science & Technology Letters*, 2(12):367–372, 2015.

[15] Mohammad A Alkhadra, Kameron M Conforti, Tao Gao, Huanhuan Tian, and Martin Z Bazant. Continuous separation of radionuclides from contaminated water by shock electrodialysis. *Environmental Science & Technology*, 54(1):527–536, 2019.

[16] Mohammad A Alkhadra, Tao Gao, Kameron M Conforti, Huanhuan Tian, and Martin Z Bazant. Small-scale desalination of seawater by shock electrodialysis. *Desalination*, 476:114219, 2020.

[17] Kameron M Conforti and Martin Z Bazant. Continuous ion-selective separations by shock electrodialysis. *AIChE Journal*, 66(1):e16751, 2020.

[18] Shu-Yuan Pan, Seth W Snyder, Hwong-Wen Ma, Yupo J Lin, and Pen-Chi Chiang. Development of a resin wafer electrodeionization process for impaired water desalination with high energy efficiency and productivity. *ACS Sustainable Chemistry & Engineering*, 5(4):2942–2948, 2017.

[19] Varada Menon Palakkal, Lauren Valentino, Qi Lei, Subarna Kole, Yupo J Lin, and Christopher G Arges. Advancing electrodeionization with conductive ionomer binders that immobilize ion-exchange resin particles into porous wafer substrates. *npj Clean Water*, 3(1):1–10, 2020.

[20] Matthew L Jordan, Lauren Valentino, Nargiza Nazyrynbekova, Varada Menon Palakkal, Subarna Kole, Deepra Bhattacharya, Yupo J Lin, and Christopher G Arges. Promoting water-splitting in janus bipolar ion-exchange resin wafers for electrodeionization. *Molecular Systems Design & Engineering*, 5(5):922–935, 2020.

[21] Huanhuan Tian, Mohammad A Alkhadra, Kameron M Conforti, and Martin Z Bazant. Continuous and selective removal of lead from drinking water by shock electrodialysis. *ACS ES&T Water*, 1(10):2269–2274, 2021.

[22] Huanhuan Tian, Mohammad A Alkhadra, and Martin Z Bazant. Theory of shock electrodialysis i: Water dissociation and electrosmotic vortices. *Journal of Colloid and Interface Science*, 589:605–615, 2021.

[23] Huanhuan Tian, Mohammad A Alkhadra, and Martin Z Bazant. Theory of shock electrodialysis ii: Mechanisms of selective ion removal. *Journal of Colloid and Interface Science*, 589:616–621, 2021.

[24] Mohammad A et al. Alkhadra. Electrochemical methods for water purification, ion separations, and energy conversion. *Chemical Reviews*, 2022.

[25] Zhaoyang Zhang and Aicheng Chen. Simultaneous removal of nitrate and hardness ions from groundwater using electrodeionization. *Separation and purification technology*, 164:107–113, 2016.

[26] Brigitte Rodgers. *Electrodeionization Versus electrodialysis: A Clean-Up of Produced Water in Hydraulic Fracturing*. PhD thesis, University of Arkansas, 2016.

[27] Humeyra B Ulusoy Erol, Christa N Hestekin, and Jamie A Hestekin. Effects of resin chemistries on the selective removal of industrially relevant metal ions using wafer-enhanced electrodeionization. *Membranes*, 11(1):45, 2021.

[28] Ali Mani and Martin Z Bazant. Deionization shocks in microstructures. *Physical Review E*, 84(6):061504, 2011.

[29] Daosheng Deng, E Victoria Dydek, Ji-Hyung Han, Sven Schlumpberger, Ali Mani, Boris Zaltzman, and Martin Z Bazant. Overlimiting current and shock electrodialysis in porous media. *Langmuir*, 29(52):16167–16177, 2013.

[30] Ji-Hyung Han, Edwin Khoo, Peng Bai, and Martin Z Bazant. Over-limiting current and control of dendritic growth by surface conduction in nanopores. *Scientific reports*, 4:7056, 2014.

[31] Ji-Hyung Han, Miao Wang, Peng Bai, Fikile R Brushett, and Martin Z Bazant. Dendrite suppression by shock electrodeposition in charged porous media. *Scientific reports*, 6:28054, 2016.

[32] E Victoria Dydek, Boris Zaltzman, Isaak Rubinstein, DS Deng, Ali Mani, and Martin Z Bazant. Overlimiting current in a microchannel. *Physical review letters*, 107(11):118301, 2011.

[33] Shima Alizadeh, Martin Z Bazant, and Ali Mani. Impact of network heterogeneity on electrokinetic transport in porous media. *Journal of colloid and interface science*, 553:451–464, 2019.

[34] Victor V Nikonenko, Anna V Kovalenko, Mahamet K Urtenov, Natalia D Pismenskaya, Jongyoon Han, Philippe Sistat, and Gérald Pourcelly. Desalination at overlimiting currents: State-of-the-art and perspectives. *Desalination*, 342:85–106, 2014.

[35] Sungmin Nam, Inhee Cho, Joonseong Heo, Geunbae Lim, Martin Z Bazant, Dustin Jaesuk Moon, Gun Yong Sung, and Sung Jae Kim. Experimental verification of overlimiting current by surface conduction and electro-osmotic flow in microchannels. *Physical review letters*, 114(11):114501, 2015.

[36] Jin-Woo Lee, Kyeong-Ho Yeon, Jung-Hoon Song, and Seung-Hyeon Moon. Characterization of electroregeneration and determination of optimal current density in continuous electrodeionization. *Desalination*, 207(1-3):276–285, 2007.

[37] IG Wenten, K Khoiruddin, Mohammad A Alkhadra, Huanhuan Tian, and Martin Z Bazant. Novel ionic separation mechanisms in electrically driven membrane processes. *Advances in Colloid and Interface Science*, page 102269, 2020.

[38] Dennis A Clifford. *Ion exchange and inorganic adsorption*. McGraw-Hill, Inc., 1990.

[39] E Victoria Dydek and Martin Z Bazant. Nonlinear dynamics of ion concentration polarization in porous media: The leaky membrane model. *AIChE Journal*, 59(9):3539–3555, 2013.

[40] Martin Zdenek Bazant, EthelMae Victoria Dydek, Daosheng Deng, and Ali Mani. Method and apparatus for desalination and purification, 2014. US Patent 8,801,910.

[41] Thomas A Zangle, Ali Mani, and Juan G Santiago. On the propagation of concentration polarization from microchannel- nanochannel interfaces part ii: numerical and experimental study. *Langmuir*, 25(6):3909–3916, 2009.

[42] Sanjay K Sharma. *Heavy metals in water: presence, removal and safety*. Royal Society of Chemistry, 2014.

[43] Mihaela-Cristina Anton, MM Baltazar Rojas, Alina Aluculesei, R Marguba, and Dana Dorohoi. Study regarding the water pollution in romania and spain. *Rom. Journ. Phys*, 53(1-2):157–163, 2008.

[44] Reena Singh, Neetu Gautam, Anurag Mishra, and Rajiv Gupta. Heavy metals and living systems: An overview. *Indian journal of pharmacology*, 43(3):246, 2011.

[45] Shohreh Fahimirad and Mehrnaz Hatami. Heavy metal-mediated changes in growth and phytochemicals of edible and medicinal plants. In *Medicinal plants and environmental challenges*, pages 189–214. Springer, 2017.

[46] Kaustub Singh, Zexin Qian, PM Biesheuvel, Han Zuilhof, Slawomir Porada, and Louis CPM de Smet. Nickel hexacyanoferrate electrodes for high mono/divalent ion-selectivity in capacitive deionization. *Desalination*, 481:114346, 2020.

[47] Kaustub Singh, Guanna Li, Juhan Lee, Han Zuilhof, B Layla Mehdi, Rafael L Zornitta, and Louis CPM de Smet. Divalent ion selectivity in capacitive deionization with vanadium hexacyanoferrate: Experiments and quantum-chemical computations. *Advanced Functional Materials*, 31(41):2105203, 2021.

[48] JG Gamaethiralalage, K Singh, S Sahin, J Yoon, M Elimelech, ME Suss, P Liang, PM Biesheuvel, R Linzmeyer Zornitta, and LCPM De Smet. Recent advances in ion selectivity with capacitive deionization. *Energy & Environmental Science*, 14(3):1095–1120, 2021.

[49] Rana Uwayid, Eric N. Guyes, Amit N. Shocron, Jack Gilron, Menachem Elimelech, and Matthew E. Suss. Perfect divalent cation selectivity with capacitive deionization. *Water Research*, 210:117959, feb 2022.

[50] Pattarachai Srimuk, Juhan Lee, Simon Fleischmann, Mesut Aslan, Choonsoo Kim, and Volker Presser. Potential-dependent, switchable ion selectivity in aqueous media using titanium disulfide. *ChemSusChem*, 11(13):2091–2100, 2018.

[51] Kaustub Singh, Guanna Li, Juhan Lee, Han Zuilhof, Beata L Mehdi, Rafael L Zornitta, and Louis CPM de Smet. Divalent ion selectivity in capacitive deionization with vanadium hexacyanoferrate: Experiments and quantum-chemical computations. *Advanced Functional Materials*, page 2105203, 2021.

[52] Hong Meng, Changsheng Peng, Shaoxian Song, and Dayao Deng. Electro-regeneration mechanism of ion-exchange resins in electrodeionization. *Surface Review and Letters*, 11(06):599–605, 2004.

[53] Jung-Hoon Song, Kyeong-Ho Yeon, and Seung-Hyeon Moon. Transport characteristics of Co^{2+} through an ion exchange textile in a continuous electrodeionization (cedi) system under electro-regeneration. *Separation science and technology*, 39(15):3601–3619, 2005.

[54] Jun Lu, Yu-Xin Wang, Yao-Yao Lu, Guang-Le Wang, Long Kong, and Jia Zhu. Numerical simulation of the electrodeionization (edi) process for producing ultrapure water. *Electrochimica acta*, 55(24):7188–7198, 2010.

[55] VI Fedorenko. Ultrapure water production using continuous electrodeionization. *Pharmaceutical Chemistry Journal*, 37(3):157–160, 2003.

[56] Xiao Feng, Zucheng Wu, and Xuefen Chen. Removal of metal ions from electroplating effluent by edi process and recycle of purified water. *Separation and purification Technology*, 57(2):257–263, 2007.

[57] Kyeong-Ho Yeon, Jung-Hoon Song, and Seung-Hyeon Moon. A study on stack configuration of continuous electrodeionization for removal of heavy metal ions from the primary coolant of a nuclear power plant. *Water research*, 38(7):1911–1921, 2004.

[58] Huixia Lu, Yuzhen Wang, and Jianyou Wang. Removal and recovery of ni2+ from electroplating rinse water using electrodeionization reversal. *Desalination*, 348:74–81, 2014.

[59] Bei Jiang, Fuzhi Li, and Xuan Zhao. Removal of trace cs (i), sr (ii), and co (ii) in aqueous solutions using continuous electrodeionization (cedi). *Desalin. Water Treat*, 155:175–182, 2019.

[60] Kyeong-Ho Yeon and Seung-Hyeon Moon. A study on removal of cobalt from a primary coolant by continuous electrodeionization with various conducting spacers. *Separation science and technology*, 38(10):2347–2371, 2003.

Chapter 5

Continuous and selective separation of heavy metals using shock electrodialysis

The work reported in this chapter has been submitted as "Continuous and selective separation of heavy metals using shock electrodialysis," by Mohammad A. Alkhadra and Martin Z. Bazant.

Abstract

Selective separations of chemically and physically similar heavy metals is an important capability in extractive metallurgy and minerals processing. Metals with complex water chemistries present a fundamental challenge for selective hydrometallurgy, which often necessitates the implementation of complicated, many-step, and reagent-intensive processing techniques to achieve these separations. In this article, we use shock electrodialysis to continuously and selectively separate heavy metals, including cobalt, nickel, vanadium, molybdenum, and tungsten, from an artificial leach liquor in a two-step process. In the first step, cobalt and nickel are separated from the other metals by selectively enriching these multivalent cations in the catholyte. In the second step, vanadium, molybdenum, and tungsten are separated from one another by adjusting the feed pH to control the speciation of these metals. Our results demonstrate for the first time the utility of speciation control for selective ion separations by deionization shock waves.

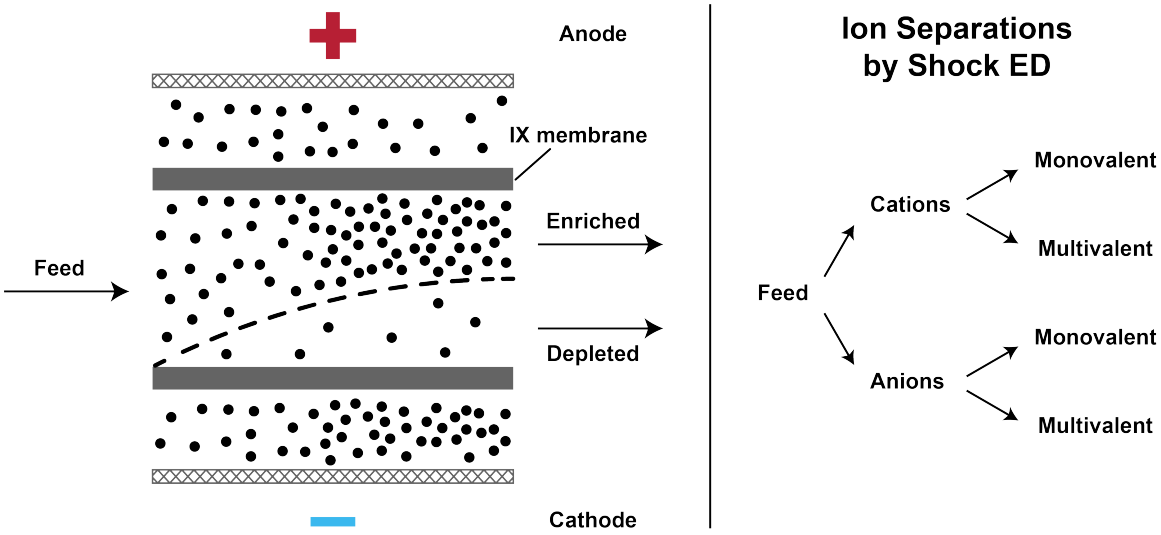

5.1 Introduction

Heavy metals are characterized as metallic elements of relatively high density or atomic weight.[1] Most heavy metals also have the capacity to exist as ions in different oxidation states, as these species can readily lose or gain electrons in their partially filled d or f atomic orbitals. In solution, many heavy metals form water-stable cations, though the majority of simple, water-stable ions formed by the heavier d-block elements are oxyanions.[2] Vanadium, molybdenum, and tungsten are examples of heavy metals with many oxidation states and that form extensive families of oxyanions in water. These species are used in many modern technologies and have a wide range of uses in alloy and steel manufacturing, catalysis, and electronics. Since primary resources of vanadium, molybdenum, and tungsten are insufficient to meet demand in the manufacture of advanced materials, extraction of these metals from secondary resources, such as ores (e.g., nickel–molybdenum ores) and spent catalysts (e.g., molybdenum–vanadium mixed oxides), has become increasingly important.[3] Moreover, efficient recovery of critical minerals in spent catalysts has great economic benefits, and it abates the environmental pollution associated with the disposal of these materials. Many physical and metallurgical processes have been reported in the literature for separation and recovery of these elements, along with other valuable metals, from ores and spent catalysts.[3–6] In general, pyrometallurgy

produces hazardous gases and leads to large losses of the metals, and biometallurgy requires complex process designs and high maintenance costs.[6] Hydrometallurgy, including precipitation,[7,8] adsorption,[9,10] ion exchange,[11,12] and solvent extraction,[3,13–18] is therefore widely used for the recovery of metals from various resources, typically after roasting and leaching the spent catalysts or ores.[3,4]

Since vanadium, molybdenum, and tungsten have similar chemical properties, the extraction and separation of these metals is difficult. In the literature, solvent extraction is often regarded as the best method for recovery of these metals from leach liquors.[3,5,6] However, solvent extraction exhibits low yields, requires large amounts of toxic organic solvents, and operates over long extraction times. Ion exchange is another common method for separation of heavy metals, though it requires use of specialty ion exchange resins and consumes larges volumes of concentrated acids and bases. In this paper, we adapt the emerging chemical-free method known as shock electrodialysis (or shock ED)[19–25] to electrokinetically separate vanadium, molybdenum, and tungsten. Shock ED has previously been used to remove toxic metal contaminants (usually multivalent cations) from water by transporting these species across a cation exchange membrane into the catholyte (see Figure 5-1).[24] Here, we demonstrate for the first time that dissolved oxyanions can be continuously fractionated based on electric charge into two product streams without the need for these species to pass though an ion exchange membrane. In fact, fractionation can be achieved as long as overlimiting current[24,26] is sustained across the device via the transport of a mobile cation (e.g., sodium, hydronium) through an ion selective surface (e.g., cation exchange membrane,[19,27] metal electrodeposit[28,29]). Our results reinforce the fact that separation of differently charged ions by shock ED relies on the action of a deionization shock wave (i.e., a sharp concentration gradient) in weakly charged porous media.[24,27,30] As shown in Figure 5-1, the deionization shock splits the feed of dissolved metals into two product streams, which are continuously separated by driving a flow perpendicular to the applied electric field.[19,31,32]

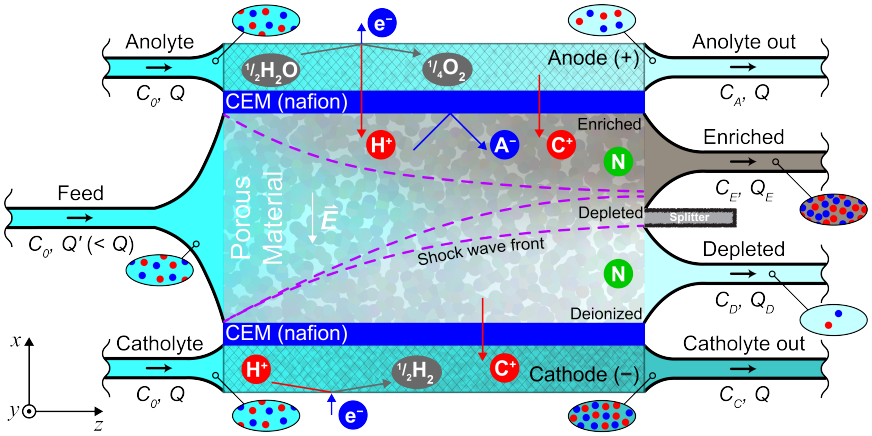

Figure 5-1. Schematic of the governing principles of shock ED. A rectangular cross section of the device shows water splitting at the anode and formation of molecular hydrogen at the cathode (maintained under acidic conditions), which are the primary electrochemical reactions that provide current to the cell. The feed is then subjected to an electric field ($\vec{E}$) that transports charged species (labeled C^+ for cations and A^- for anions) perpendicular to the flow. Anions are blocked by cation exchange membranes, and neutral species (labeled N) are unaffected by the electric field. For each stream, flow rate is denoted by the letter Q and concentration by the letter C; streams are colored based on relative concentration of ions.

5.2 Materials and Experimental Methods

Thermodynamic simulation of chemical equilibria

The distribution diagrams shown in Figure 5-2 were generated using the open-source thermodynamics software DATABASE and graphical user interface SPANA. The chemical reactions and equilibrium constants of all species considered in the simulations are preloaded in the DATABASE package and are reproduced in Table 5.1. (The parameters in DATABASE are obtained from the NIST Critically Selected Stability Constants of Metal Complexes database[33] and other sources.[34,35]) This program solves the mass balance equations for the components in an aqueous mixture using these chemical reactions and equilibrium constants.

Device design and fabrication

The device used here, shown schematically in Figure 5-1, is based on a design previously published by our group.[20,23,25] The device consists of three inlets (two

Table 5.1. Chemical Reactions and Equilibrium Constants at 25 °C

Chemical Reaction			Equilibrium Constant, $\log K$
$H^+ + VO(OH)_3$	$\rightleftharpoons$	$VO_2^+ + 2H_2O$	4.2
$2H^+ + VO_2(OH)_2^-$	$\rightleftharpoons$	$VO_2^+ + 2H_2O$	6.8
$3H^+ + VO_3OH^{2-}$	$\rightleftharpoons$	$VO_2^+ + 2H_2O$	15.6
$4H^+ + VO_4^{3-}$	$\rightleftharpoons$	$VO_2^+ + 2H_2O$	29.5
$4H^+ + H_2V_2O_7^{2-}$	$\rightleftharpoons$	$2VO_2^+ + 3H_2O$	11.3
$5H^+ + HV_2O_7^{3-}$	$\rightleftharpoons$	$2VO_2^+ + 3H_2O$	20.9
$6H^+ + V_2O_7^{4-}$	$\rightleftharpoons$	$2VO_2^+ + 3H_2O$	32.2
$8H^+ + V_4O_{12}^{4-}$	$\rightleftharpoons$	$4VO_2^+ + 4H_2O$	19.6
$13H^+ + H_3V_{10}O_{28}^{3-}$	$\rightleftharpoons$	$10VO_2^+ + 8H_2O$	5.1
$14H^+ + H_2V_{10}O_{28}^{4-}$	$\rightleftharpoons$	$10VO_2^+ + 8H_2O$	9.8
$15H^+ + HV_{10}O_{28}^{5-}$	$\rightleftharpoons$	$10VO_2^+ + 8H_2O$	14.0
$16H^+ + V_{10}O_{28}^{6-}$	$\rightleftharpoons$	$10VO_2^+ + 8H_2O$	21.5
$H^+ + MoO_4^{2-}$	$\rightleftharpoons$	$HMoO_4^-$	4.2
$2H^+ + MoO_4^{2-}$	$\rightleftharpoons$	H_2MoO_4	8.2
$3H^+ + MoO_4^{2-}$	$\rightleftharpoons$	$H_2O + MoO_2OH^+$	9.5
$5H^+ + 2MoO_4^{2-}$	$\rightleftharpoons$	$2H_2O + Mo_2O_5OH^+$	18.8
$6H^+ + 2MoO_4^{2-}$	$\rightleftharpoons$	$3H_2O + Mo_2O_5^{2+}$	20.3
$7H^+ + 2MoO_4^{2-}$	$\rightleftharpoons$	$3H_2O + HMo_2O_5^{3+}$	20.1
$8H^+ + 7MoO_4^{2-}$	$\rightleftharpoons$	$4H_2O + Mo_7O_{24}^{6-}$	54.3
$9H^+ + 7MoO_4^{2-}$	$\rightleftharpoons$	$4H_2O + HMo_7O_{24}^{5-}$	60.7
$10H^+ + 7MoO_4^{2-}$	$\rightleftharpoons$	$4H_2O + H_2Mo_7O_{24}^{4-}$	65.5
$11H^+ + 7MoO_4^{2-}$	$\rightleftharpoons$	$4H_2O + H_3Mo_7O_{24}^{3-}$	69.5
$H^+ + WO_4^{2-}$	$\rightleftharpoons$	HWO_4^-	3.6
$2H^+ + WO_4^{2-}$	$\rightleftharpoons$	H_2WO_4	5.8
$3H^+ + WO_4^{2-}$	$\rightleftharpoons$	$H_3WO_4^+$	7.2
$6H^+ + 6WO_4^{2-}$	$\rightleftharpoons$	$3H_2O + W_6O_{21}^{6-}$	47.0
$8H^+ + 7WO_4^{2-}$	$\rightleftharpoons$	$4H_2O + W_7O_{24}^{6-}$	54.1
$9H^+ + 7WO_4^{2-}$	$\rightleftharpoons$	$4H_2O + HW_7O_{24}^{5-}$	71.3
$14H^+ + 12WO_4^{2-}$	$\rightleftharpoons$	$7H_2O + W_{12}O_{41}^{10-}$	105.7
H_2O	$\rightleftharpoons$	$H^+ + OH^-$	-14.0

to transport the electrode streams and a third to deliver the feed) and four outlets (two to transport the electrode streams and two to generate depleted and enriched product streams at the splitter). All fluids are transported through $1/8^{\text{th}}$-inch Tygon tubing (Saint-Gobain) glued onto portplates made of cast acrylic. These portplates seal liquids inside the device and support the rubber tubing through which fluid flows. Moreover, four $1/16^{\text{th}}$-inch Viton rubber gaskets (DuPont) are used to seal the device and simultaneously provide channels for the electrode streams. The electrodes are made of platinum meshes (Sigma–Aldrich), which are connected to a Gamry Reference 3000 potentiostat/galvanostat using titanium wires (Alfa Aesar). The electrodes and wires are secured in place by compressible Viton gaskets. Cation exchange membranes (Nafion N115, Ion Power) with a thickness of approximately $130\,\mu\text{m}$ and an area of $1.0\,\text{cm}^2$ are used as fluidic barriers between the electrode channels and the porous material.

The porous material is a borosilicate frit (Adams & Chittenden Scientific Glass) with ultrafine pores (nominally ranging from 0.9 to $1.4\,\mu\text{m}$ in size), an internal surface area of $1.75\,\text{m}^2\,\text{g}^{-1}$ based on Brunauer–Emmett–Teller theory, a mass density of $1.02\,\text{g}\,\text{m}^{-3}$, a porosity of 0.31, and approximate dimensions of $0.5\,\text{cm} \times 1.8\,\text{cm} \times 0.6\,\text{cm}$ ($x \times y \times z$). The frit is glued onto acrylic frames using Devcon 2 Ton Epoxy (McMaster-Carr). The splitter (placed midway down the outlet for ease of assembly) is made of cast acrylic and is sealed against the top face of the porous material using 0.04-inch GORE expanded polytetrafluoroethylene (PTFE) gasket tape. During assembly, holes in all of the acrylic slabs and rubber gaskets are formed using a laser cutter (Universal Laser Systems) and refined with a drill press (Palmgren ten-inch, five-speed bench model). These layers are then stacked and held together with nuts, bolts, and washers made of 316 stainless steel.

Preparation of feed and electrode solutions

To prepare the aqueous mixture with the composition in Table 5.2, we formulated stock solutions with concentrations of $1000\,\text{mg}\,\text{L}^{-1}$ made from sodium orthovanadate (Na_3VO_4), sodium molybdate (Na_2MoO_4), and sodium tungstate dihy-

drate ($Na_2WO_4 \cdot 2H_2O$). We also formulated stock solutions with concentrations of $1000\,mg\,L^{-1}$ made from cobalt sulfate heptahydrate ($CoSO_4 \cdot 7H_2O$) and nickel sulfate heptahydrate ($NiSO_4 \cdot 7H_2O$) to prepare the artificial leach liquor. Appropriate volumes of these solutions were then diluted in deionized water, and the pH of these mixtures was adjusted using hydrochloric acid (HCl). All reagents were obtained from Sigma–Aldrich. The anolyte and catholyte were prepared by diluting a $1000\,mg\,L^{-1}$ stock solution of sodium chloride (NaCl) to $40\,mg\,L^{-1}$, and these streams were recirculated to a single reservoir during operation.

Experimental procedure

Experiments began by setting the flow rates of all streams: $0.2\,mL\,min^{-1}$ for the feed and $1.0\,mL\,min^{-1}$ for the electrode streams. These streams were transported using peristaltic pumps equipped with Tygon Chemical tubing (Saint-Gobain), and the flows were made smooth by incorporating hydraulic accumulators. The accumulators were left to pressurize and the system to equilibrate overnight, after which the Gamry was set to operate at constant current. The measured voltage was allowed to stabilize for at least one hour until it reached steady state. Samples were collected directly from the device in graduated cylinders and stored in centrifuge tubes for analysis, which included measurements of volume, pH, conductivity, and composition of all dissolved species. Conductivity and pH were measured using Mettler Toledo analytical instruments (SevenCompact pH/Cond S213), and composition was determined using inductively coupled plasma mass spectrometry (Agilent 7900 ICP–MS). The plasma in ICP–MS was made from argon gas and was supplemented by helium, and we added an indium internal standard at $100\,\mu g\,L^{-1}$ to all samples. Quantitative analysis required calibration of the measurements, which was achieved by processing a set of reference standards and producing a calibration curve. (All standard solutions were obtained from Sigma–Aldrich.) Samples and standard solutions were diluted in 2 vol% nitric acid (HNO_3) prior to analysis by ICP–MS.

5.3 Results and Discussion

To assess the ability of shock ED to separate dissolved vanadium, molybdenum, and tungsten, we used a synthetic mixture comprising these species and varied pH. The composition of this mixture is shown in Table 5.2. In solution, these metals form many complexes whose distribution depends on concentration and fluid properties (e.g., pH, temperature). To define and understand possible separation schemes, we studied the speciation of vanadium, molybdenum, and tungsten using the open-source thermodynamics software DATABASE (which contains chemical reactions and equilibrium constants) and graphical user interface SPANA. With these tools, we produced chemical equilibrium diagrams of the relevant metal species in solution, as shown in Figure 5-2. According to these distribution diagrams, vanadium, molybdenum, and tungsten exist primarily as anionic species down to pH values of 4 (or 0 in the case of tungsten). In moderately acidic solutions ($2 < \text{pH} < 6$) and at the concentrations tested, the anionic species of vanadium include $VO_2(OH)_2^-$, $H_3V_{10}O_{28}^{3-}$, $H_2V_{10}O_{28}^{4-}$, and $HV_{10}O_{28}^{5-}$; the anionic species of molybdenum include $HMoO_4^-$, MoO_4^{2-}, $H_3Mo_7O_{24}^{3-}$, $H_2Mo_7O_{24}^{4-}$, and $HMo_7O_{24}^{5-}$; the anionic species of tungsten include WO_4^{2-} and $HW_7O_{24}^{5-}$. In strongly acidic solutions ($\text{pH} < 2$), cationic species vanadium, molybdenum, and tungsten appear and are stable: VO_2^+, MoO_2OH^+, and $H_3WO_4^+$, respectively. The distribution diagrams suggest that tungsten could be separated from vanadium and molybdenum at $\text{pH} \leq 2$ because the dominant species of the latter two metals are either neutral or cationic. Moreover, the diagrams suggest that vanadium could be separated from molybdenum at $\text{pH} \gtrsim 2$ because the dominant species of vanadium is cationic while that of molybdenum is neutral.

In all shock ED experiments, we operated the system at constant current because it facilitates the formation of a stable deionization shock wave at overlimiting current.[20] (In contrast, operating at constant voltage can cause overshoot and oscillation about a desired overlimiting current and is associated with variability in the shock wave[36]). Our results for selective separation of vanadium, molybdenum, and

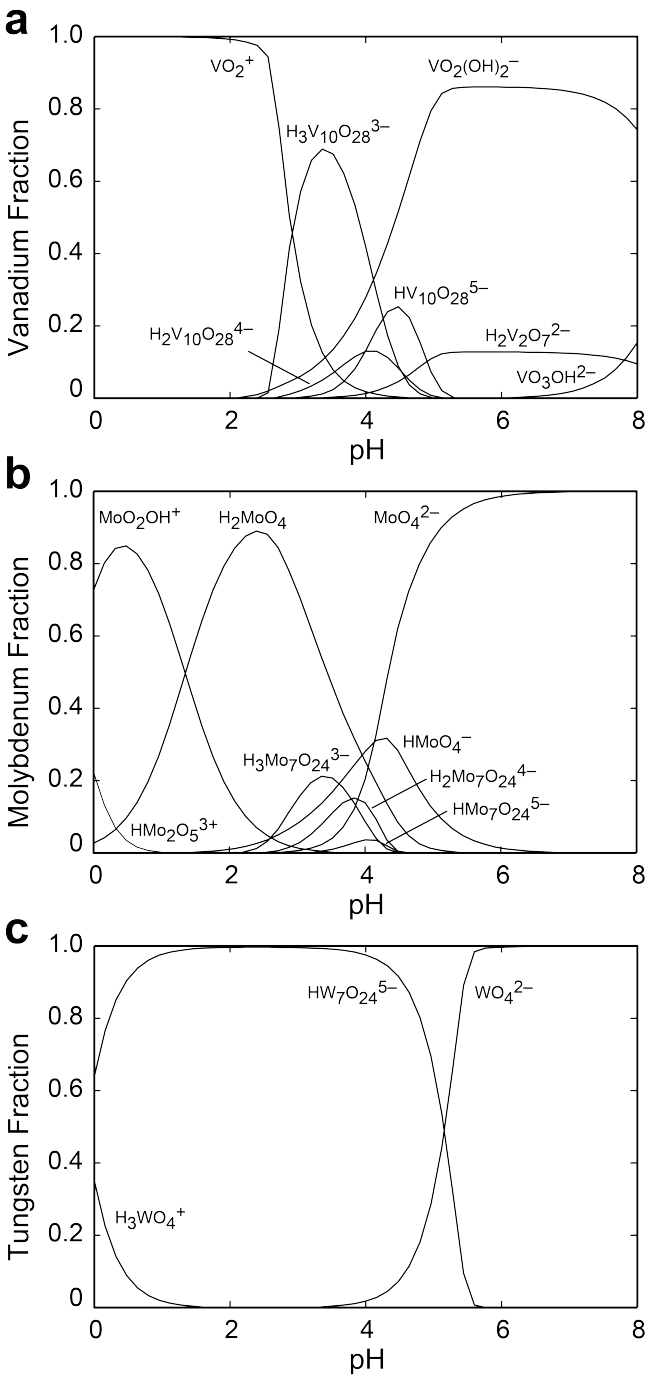

Figure 5-2. Distribution diagrams of (a) vanadium, (b) molybdenum, and (c) tungsten versus pH for the concentrations in Table 5.2 and at 25 °C. These data were obtained using the open-source thermodynamics software DATABASE. Ionic strength was calculated in these simulations, and the chemical reactions and equilibrium constants of all species considered in the simulations are reported in Table 5.1.

Table 5.2. Composition of Feed Mixture Tested in This Study

Species, j	Concentration, $C_0^{(j)}$	
	$\mathrm{mg\,L^{-1}}$	$\mathrm{mmol\,L^{-1}}$
Vanadium	20	0.39
Molybdenum	20	0.21
Tungsten	20	0.11
Sodium	42	1.8
Hydronium	variable	

tungsten are presented in Figure 5-3. Here, ion removal of species j in the depleted stream is defined as

$$D^{(j)} = 1 - \frac{C_D^{(j)}}{C_0^{(j)}} \tag{5.1}$$

enrichment of species j in the enriched stream as

$$E^{(j)} = \frac{C_E^{(j)}}{C_0^{(j)}} \tag{5.2}$$

dimensionless current as

$$\widetilde{I} = \frac{I}{I_{\mathrm{lim}}} \tag{5.3}$$

water recovery as

$$\gamma = \frac{Q_D}{Q'} \tag{5.4}$$

energy density as

$$\varepsilon = \frac{IV}{Q'} \tag{5.5}$$

where V is (steady) voltage, and the separation factor as

$$S^{(j:k)} = \frac{1 - C_D^{(j)}/C_0^{(j)}}{1 - C_D^{(k)}/C_0^{(k)}} = \frac{D^{(j)}}{D^{(k)}} \tag{5.6}$$

where a value of $S^(j:k) > 1$ suggests that species j is selectively removed relative to species k. Values of $C_0^{(j)}$ are provided in Table 5.2; values of $C_D^{(j)}$, $C_E^{(j)}$, $C_C^{(j)}$, and $C_A^{(j)}$ are measured experimentally. In Equation 5.3, I is applied current and I_{lim} is

flow-limited current:

$$I_{\text{lim}} = \sum_j \frac{\nu^{(j)} C_0^{(j)} F Q'}{M^{(j)}} \tag{5.7}$$

where where ν is valence (charge), C is mass concentration, F is Faraday's constant, Q' is the volumetric flow rate of the feed, M is molar mass, and the sum is taken over all cations j (primarily sodium and hydronium). This definition of limiting current can be interpreted as the rate of forced convection of positive charge carriers into the device, and it is assumed that the flux of anions is zero at steady state in the presence of ideal cation exchange membranes.

Figure 5-3 shows that ion removal in the depleted stream (Equation 5.1) generally increases with both pH and applied current, up to 99.5% at pH $= 6$ and $I = 2.3\,\text{mA}$ ($\widetilde{I} = 4$). We note that dimensionless current (Equation 5.3)—a proxy for the extent of development of the deionization shock wave—depends on pH, particularly in strongly acidic solutions, as the major contributor to the limiting current (Equation 5.7) at low pH is hydronium. For example, the concentration of hydronium at pH $= 2$ is $10\,\text{mmol}\,\text{L}^{-1}$, which is much greater than the concentration of sodium in our feed mixture. Moreover, a low pH reduces the magnitude of the zeta potential—a measure of the effective electric surface charge—of borosilicate glass,[37,38] which in turn decreases the extent of development of the deionization shock wave in our system.[19,27] Figure 5-3 also shows that the separation factor decreases with increasing pH, which reflects the fact that vanadium, molybdenum, and tungsten exist exclusively as anionic species at moderate to high pH values (see Figure 5-2). As a result, we expect these species to be removed to a similar extent that depends on the dimensionless current. At low pH, however, we observe selective separation of tungsten relative to vanadium and, to a lesser extent, molybdenum. This separation factor increases with applied current, which we attribute to the formation of a more developed deionization shock that promotes the mechanisms of ion selectivity in shock ED.[39] We note that pH may be decreased further to achieve greater ion separation, for example by transporting vanadium and molybdenum cations to the catholyte and accumulating tungsten oxyanions in the

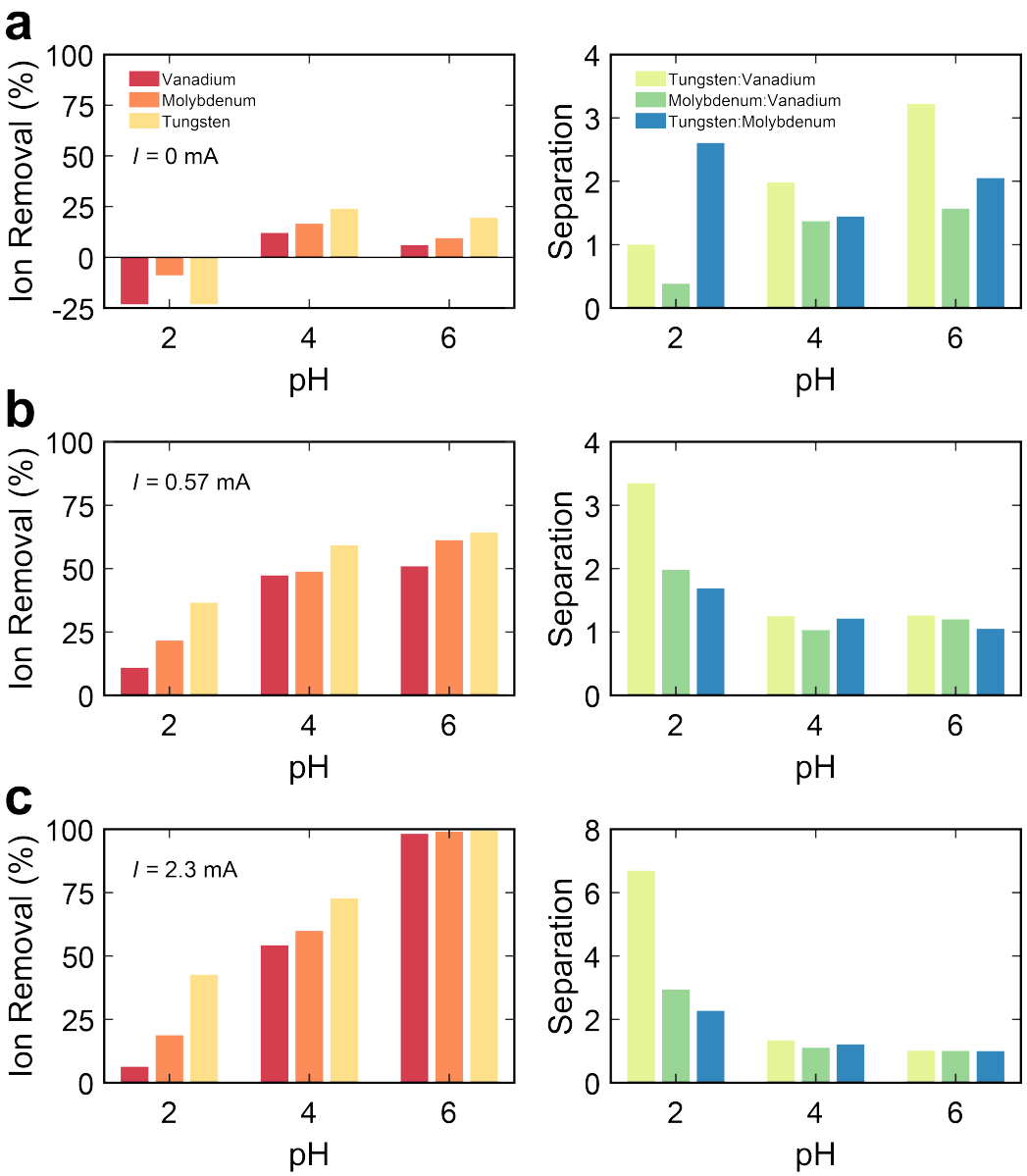

Figure 5-3. Quantitative analysis of selective separation of vanadium, molybdenum, and tungsten using shock ED. Ion removal (left) and separation factor (right) of the metals versus pH at applied currents of (a) 0 mA, (b) 0.57 mA, and (c) 2.3 mA.

Table 5.3. Energy Consumption and Water Recovery Data

$I = 0\,\mathrm{mA}$				
pH	I_{lim} (mA)	Voltage (V)	Energy Density ($\mathrm{kW\,h\,m^{-3}}$)	Water Recovery (%)
2	3.7	0	0	49
4	0.60	0	0	51
6	0.57	0	0	52
$I = 0.57\,\mathrm{mA}$				
pH	I_{lim} (mA)	Voltage (V)	Energy Density ($\mathrm{kW\,h\,m^{-3}}$)	Water Recovery (%)
2	3.7	2.6	0.13	52
4	0.60	8.5	0.41	50
6	0.57	9.1	0.44	60
$I = 2.3\,\mathrm{mA}$				
pH	I_{lim} (mA)	Voltage (V)	Energy Density ($\mathrm{kW\,h\,m^{-3}}$)	Water Recovery (%)
2	3.7	5.6	1.1	51
4	0.60	13.8	2.7	56
6	0.57	19.4	3.8	84

enriched product stream. If the system is to be operated near or above limiting current, however, the high concentration of hydronium at low pH would lower overall ion removal and significantly increase electrical energy consumption, as shown in Table 5.3 (we note that $I_{\mathrm{lim}} = 32\,\mathrm{mA}$ at $\mathrm{pH} = 1$). In practice, it may be possible to achieve greater separation of a specific species at favorable conditions (i.e., high ion removal, high water recovery, low energy consumption) by using a multistage shock ED process, as we demonstrated in previous work for continuous separation of radionuclides from contaminated water.[20]

In practice, leach liquors produced from spent catalysts typically comprise several heavy metals other than vanadium, molybdenum, and tungsten. Examples of these metals include cobalt and nickel, both of which form water-stable divalent cations in acidic media. Here, we test the applicability of shock ED to first extract and then separate vanadium, molybdenum, and tungsten from an artificial leach liquor (Table 5.2) that contains cobalt and nickel as well, both present at $20\,\mathrm{mg\,L^{-1}}$ (or $0.34\,\mathrm{mmol\,L^{-1}}$). In this experiment, the solution was held at $\mathrm{pH} = 6$ to ensure that vanadium, molybdenum, and tungsten were present as oxyanions that could be

separated from the cations. Moreover, the anolyte and catholyte were recirculated to separate reservoirs during operation, where the catholyte was held at pH = 3. Figure 5-4a shows increasing removal of all species in the depleted stream as a function of current, with the greatest preference for the divalent cations, followed by sodium and then the oxyanions. In shock ED, multivalent cations tend to accumulate in the catholyte,[23,39] whereas anions accumulate in the enriched stream near the cation exchange membrane. This fractionation of oppositely charged species is captured by the mass balance in Figure 5-4b, which is defined as the fraction of ions fed that are retained in the main compartment of the device:

$$\mu^{(j)} = \gamma \frac{C_D^{(j)}}{C_0^{(j)}} + (1-\gamma)\frac{C_E^{(j)}}{C_0^{(j)}} \tag{5.8}$$

These results, particularly at a dimensionless current of four, show that cobalt and nickel can be separated almost entirely in a first extraction step from vanadium, molybdenum, and tungsten, which can subsequently be separated from one another in a second purification step. In practice, cobalt and nickel can be further refined starting with the enriched catholyte produced by shock ED and using a chelating agent for speciation control, or alternatively these metals can be co-precipitated using sodium hydroxide (NaOH) to directly produce active cathode materials for batteries.

5.4 Conclusions

In summary, we successfully demonstrated the ability of shock ED, with speciation control, to continuously and selectively separate heavy metals from a multicomponent mixture that resembles the leach liquor of spent catalysts. Operation at or near neutral pH allows heavy metals such as vanadium, molybdenum, and tungsten to exist primarily as multivalent oxyanions, while other elements such as cobalt and nickel exist primarily as divalent cations. Under these conditions, the oxyanions can be separated almost entirely from the cations by selectively enriching the latter in the catholyte. Operation at acidic pH causes vanadium, molybdenum, and

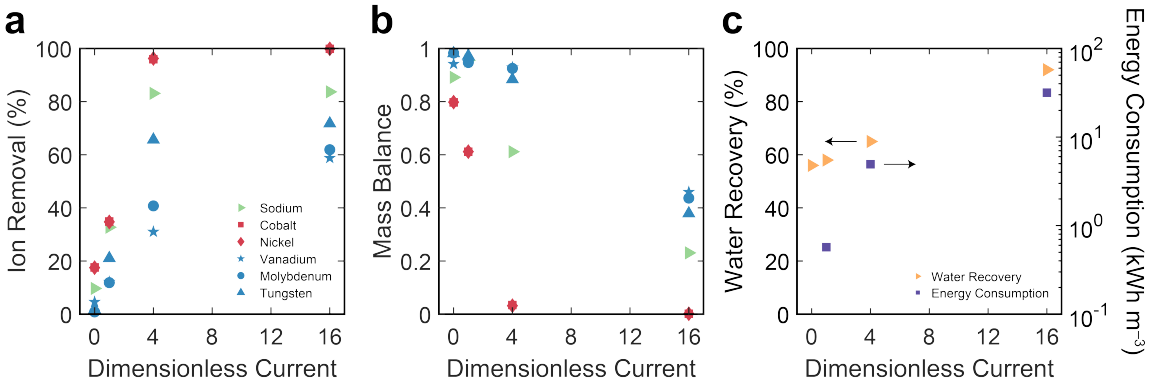

Figure 5-4. Quantitative analysis of selective separation of cations from anions in an artificial leach liquor using shock ED. (a) Ion removal and (b) mass balance of the metals versus dimensionless current. (c) Water recovery and energy consumption versus dimensionless current. The artificial leach liquor is prepared using the composition in Table 5.2 with $20\,\mathrm{mg\,L^{-1}}$ of both cobalt and nickel; this mixture has a limiting current of $1.0\,\mathrm{mA}$ at the tested flow rate.

tungsten to form extensive families of oxyanions, which can then be separated from one another in a second step. We envision that the recovered cobalt and nickel can be further refined, starting with the enriched catholyte produced by shock ED, and then revalorized as precursors for the fabrication of new catalysts or battery-active materials. Similarly, the separated streams of vanadium, molybdenum, and tungsten can be further processed and the metals extracted via chemical precipitation. In the future, we expect our findings on selective ion separations using shock ED to not only enable precision for targeted metal separations, but also offer pathways for process intensification and reduced chemical use.

5.5 Acknowledgements

The authors thank the Center for Environmental Health Sciences (CEHS) at MIT for use of ICP–MS.

5.6 References

[1] John Emsley. *Nature's building blocks: an AZ guide to the elements*. Oxford University Press, 2011.

[2] F Albert Cotton, Geoffrey Wilkinson, Carlos A Murillo, and Manfred

Bochmann. *Advanced inorganic chemistry*. John Wiley and Sons, Inc., 1999.

[3] Thi Hong Nguyen and Man Seung Lee. A review on the separation of molybdenum, tungsten, and vanadium from leach liquors of diverse resources by solvent extraction. *Geosystem Engineering*, 19(5):247–259, 2016.

[4] Li Zeng and Chu Yong Cheng. A literature review of the recovery of molybdenum and vanadium from spent hydrodesulphurisation catalysts: Part i: Metallurgical processes. *Hydrometallurgy*, 98(1-2):1–9, 2009.

[5] Li Zeng and Chu Yong Cheng. A literature review of the recovery of molybdenum and vanadium from spent hydrodesulphurisation catalysts: Part ii: Separation and purification. *Hydrometallurgy*, 98(1-2):10–20, 2009.

[6] Ata Akcil, Francesco Vegliò, Francesco Ferella, Mediha Demet Okudan, and Aysenur Tuncuk. A review of metal recovery from spent petroleum catalysts and ash. *Waste management*, 45:420–433, 2015.

[7] Kyung Ho Park, B Ramachandra Reddy, D Mohapatra, and Chul-Woo Nam. Hydrometallurgical processing and recovery of molybdenum trioxide from spent catalyst. *International Journal of Mineral Processing*, 80(2-4):261–265, 2006.

[8] Alessio Cibati, Ka Yu Cheng, Christina Morris, Maneesha P Ginige, Erkan Sahinkaya, Francesca Pagnanelli, and Anna H Kaksonen. Selective precipitation of metals from synthetic spent refinery catalyst leach liquor with biogenic h2s produced in a lactate-fed anaerobic baffled reactor. *Hydrometallurgy*, 139:154–161, 2013.

[9] EA Sigworth. Potentialities of activated carbon in the metallurgical fi eld. *American Institute of Mining, Metallurgical and Petroleum Engineers*, 1962.

[10] Kyung Ho Park, D Mohapatra, and B Ramachandra Reddy. Selective recovery of molybdenum from spent hds catalyst using oxidative soda ash leach/carbon adsorption method. *Journal of hazardous materials*, 138(2):311–316, 2006.

[11] Patricia Henry and André Van Lierde. Selective separation of vanadium from molybdenum by electrochemical ion exchange. *Hydrometallurgy*, 48(1):73–81, 1998.

[12] Thi Hong Nguyen and Man Seung Lee. Separation of molybdenum and vanadium from acid solutions by ion exchange. *Hydrometallurgy*, 136:65–70, 2013.

[13] MA Olazabal, MM Orive, LA Fernandez, and JM Madariaga. Selective extraction of vanadium (v) from solutions containing molybdenum (vi) by ammonium salts dissolved in toluene. *Solvent Extraction and Ion Exchange*, 10(4):623–635, 1992.

[14] Thi Hong Nguyen and Man Seung Lee. Separation of vanadium and tungsten from sodium molybdate solution by solvent extraction. *Industrial & Engineering Chemistry Research*, 53(20):8608–8614, 2014.

[15] Hoai Thanh Truong, Yong Hwan Kim, and Man Seung Lee. Solvent extraction of tungsten (vi) from moderate hydrochloric acid solutions with lix 63. *Korean Journal of Metals and Materials*, 55(6):405–411, 2017.

[16] Hoai Thanh Truong, Thi Hong Nguyen, and Man Seung Lee. Separation of molybdenum (vi), rhenium (vii), tungsten (vi), and vanadium (v) by solvent extraction. *Hydrometallurgy*, 171:298–305, 2017.

[17] Yajing Pan, Xiao Sun, and Yongqiang Zhang. Separation of vanadium and molybdenum from aqueous solution using peg2000+ sodium sulfate+ water aqueous two-phase system. *SN Applied Sciences*, 1(11):1–9, 2019.

[18] Keisuke Ohto, Hiroaki Furugou, Shintaro Morisada, Hidetaka Kawakita, Kenichi Isono, and Katsutoshi Inoue. Stepwise recovery of molybdenum, vanadium, and tungsten with amino-type "trident" molecule by stripping. *Solvent Extraction and Ion Exchange*, 39(5-6):512–532, 2021.

[19] S. Schlumpberger, N. B. Lu, M. E. Suss, and M. Z. Bazant. Scalable and continuous water deionization by shock electrodialysis. *Environmental Science & Technology Letters*, 2(12):367–372, 2015.

[20] Mohammad A Alkhadra, Kameron M Conforti, Tao Gao, Huanhuan Tian, and Martin Z Bazant. Continuous separation of radionuclides from contaminated water by shock electrodialysis. *Environmental Science & Technology*, 54(1):527–536, 2019.

[21] Mohammad A Alkhadra, Tao Gao, Kameron M Conforti, Huanhuan Tian, and Martin Z Bazant. Small-scale desalination of seawater by shock electrodialysis. *Desalination*, 476:114219, 2020.

[22] Kameron M Conforti and Martin Z Bazant. Continuous ion-selective separations by shock electrodialysis. *AIChE Journal*, 66(1):e16751, 2020.

[23] Huanhuan Tian, Mohammad A Alkhadra, Kameron M Conforti, and Martin Z Bazant. Continuous and selective removal of lead from drinking water by shock electrodialysis. *ACS ES&T Water*, 1(10):2269–2274, 2021.

[24] Mohammad A et al. Alkhadra. Electrochemical methods for water purification, ion separations, and energy conversion. *Chemical Reviews*, 2022.

[25] Mohammad A Alkhadra, Matthew L Jordan, Huanhuan Tian, Christopher G Arges, and Martin Z Bazant. Selective and chemical-free removal of toxic heavy metal cations from water using shock ion extraction. *Under review*, 2022.

[26] E Victoria Dydek, Boris Zaltzman, Isaak Rubinstein, DS Deng, Ali Mani, and Martin Z Bazant. Overlimiting current in a microchannel. *Physical review letters*, 107(11):118301, 2011.

[27] Daosheng Deng, E Victoria Dydek, Ji-Hyung Han, Sven Schlumpberger, Ali Mani, Boris Zaltzman, and Martin Z Bazant. Overlimiting current and shock electrodialysis in porous media. *Langmuir*, 29(52):16167–16177, 2013.

[28] Ji-Hyung Han, Edwin Khoo, Peng Bai, and Martin Z Bazant. Over-limiting current and control of dendritic growth by surface conduction in nanopores. *Scientific reports*, 4:7056, 2014.

[29] Ji-Hyung Han, Miao Wang, Peng Bai, Fikile R Brushett, and Martin Z Bazant. Dendrite suppression by shock electrodeposition in charged porous media. *Scientific reports*, 6:28054, 2016.

[30] Ali Mani and Martin Z Bazant. Deionization shocks in microstructures. *Physical Review E*, 84(6):061504, 2011.

[31] E Victoria Dydek and Martin Z Bazant. Nonlinear dynamics of ion concentration polarization in porous media: The leaky membrane model. *AIChE Journal*, 59(9):3539–3555, 2013.

[32] Martin Zdenek Bazant, EthelMae Victoria Dydek, Daosheng Deng, and Ali Mani. Method and apparatus for desalination and purification, 2014. US Patent 8,801,910.

[33] National Institute of Standards and Technology (NIST). Critically selected stability constants of metal complexes, 2004.

[34] Allen J. Bard, Roger Parsons, and Joseph Jordan. *Standard potentials in aqueous solution*. CRC Press, 1985.

[35] JJ Cruywagen. Protonation, oligomerization, and condensation reactions of vanadate (v), molybdate (vi), and tungstate (vi). In *Advances in inorganic chemistry*, volume 49, pages 127–182. Elsevier, 1999.

[36] Thomas A Zangle, Ali Mani, and Juan G Santiago. On the propagation of concentration polarization from microchannel- nanochannel interfaces part ii: numerical and experimental study. *Langmuir*, 25(6):3909–3916, 2009.

[37] Fernando Soares Lameiras, Aldalberto Leles de Souza, Valéria Alves Rodrigues de Melo, Eduardo Henrique Martins Nunes, and Ivan Dionizio Braga. Measurement of the zeta potential of planar surfaces with a rotating disk. *Materials Research*, 11:217–219, 2008.

[38] Long Liang, Liguang Wang, Anh V Nguyen, and Guangyuan Xie. Heterocoagulation of alumina and quartz studied by zeta potential distribution and particle size distribution measurements. *Powder Technology*, 309:1–12, 2017.

[39] Huanhuan Tian, Mohammad A Alkhadra, and Martin Z Bazant. Theory of shock electrodialysis ii: Mechanisms of selective ion removal. *Journal of Colloid and Interface Science*, 589:616–621, 2021.

Appendix A

Supporting Information: Continuous separation of radionuclides from contaminated water by shock electrodialysis

A.1 Representative Calibration Curve for ICP–MS

Measurement of concentration by inductively coupled plasma mass spectrometry (ICP–MS) involves dilution of the samples in nitric acid to a final acid composition of 2 vol%. Dilution is necessary for concentration to fall within the detection limits of the instrument and to avoid damaging the detector. The data generated for each sample tested by ICP–MS are represented as a signal intensity (in counts), which is subsequently converted into concentration. Intensity data are transformed to concentration using a calibration curve, which is produced by linear regression of calibration standards with known concentration, as shown in Figure A-1. Concentrations determined from a calibration curve are then multiplied by the corresponding dilution factor used to prepare the samples.

A.2 Current and Voltage Data

Before performing any experiments involving shock electrodialysis (SED), the device must be characterized by linear voltammetry (voltage sweeps) to experimentally validate the expected current–voltage (I–V) relationship.[1,2] Figure A-2 presents a typical I–V curve for the SED device for practical water with a concentration of ions of $1.41\,\mathrm{mM}$ (i.e., neglecting boric acid). This curve was obtained by ramping voltage at a fixed rate of $2\,\mathrm{mV\,s^{-1}}$ and measuring the corresponding current generated between working and reference electrodes. Linear sweep voltammetry provided experimental validation for the theoretically calculated limiting current of $180\,\mu\mathrm{A}$ ($=\sum_k \nu_k C_k F Q'$, where Q' is the volumetric flow rate of the feed), above which current increases linearly. This linear relationship between current and voltage is a manifestation of overlimiting current and is what gives rise to the shock wave responsible for deionization in our system. In the regime of overlimiting current, (overlimiting) conductance G is constant and equal to $0.20\,\mathrm{mA\,V^{-1}}$ (or

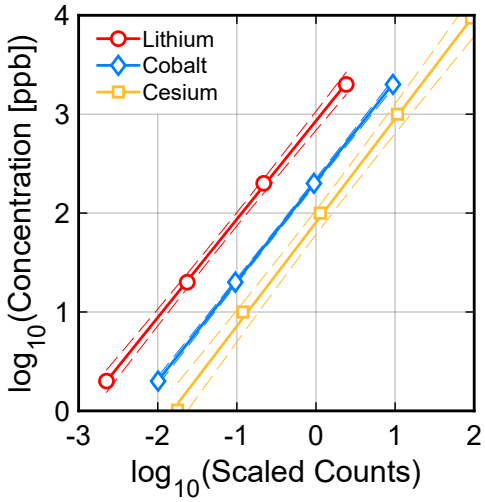

Figure A-1. Representative calibration curve used in the analysis of samples with unknown concentration by ICP–MS. This calibration curve was generated by measuring the analytical signal (in counts) produced by reference standards with known concentration. Moreover, the counts for each of the species of interest were scaled by the counts corresponding to an internal standard of indium. Logarithmic scales were used to better capture the wide range of concentrations, which span several orders of magnitude. Dashed lines represent 95% prediction intervals on each fit (solid lines) and estimate the outcome of future samples based on what has already been observed.

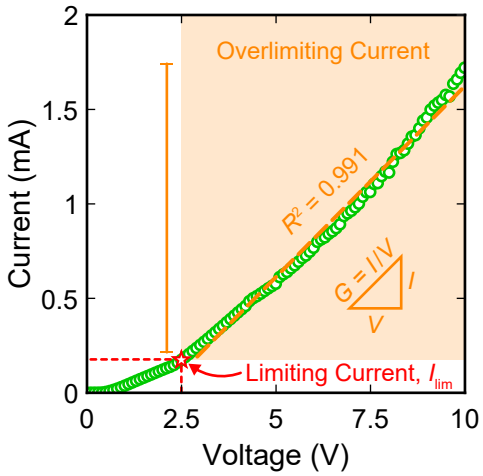

Figure A-2. Linear sweep voltammetry (I–V curve) for the SED device performed at a rate of $2\,\mathrm{mV\,s^{-1}}$ for practical water with a concentration of ions of $1.41\,\mathrm{mM}$. The theoretical limiting current $I_{\mathrm{lim}} = 0.18\,\mathrm{mA} = 180\,\mu\mathrm{A}$ is indicated by the red star. Current increases linearly above I_{lim}, which is a manifestation of what is known as overlimiting current (region shaded in orange), a phenomenon predicted theoretically and observed experimentally by our group in negatively charged porous media. In the regime of overlimiting current, conductance G is constant and equal to $0.20\,\mathrm{mA\,V^{-1}}$ (or $2.0 \times 10^{-4}\,\Omega^{-1}$).

$2.0 \times 10^{-4}\,\Omega^{-1}$).

Although linear sweep voltammetry is an essential component of the initial experimental characterization, SED is normally operated in galvanostatic mode (i.e., by delivering constant current), which facilitates the formation of a stable deionization shock wave when supplying overlimiting current. (The reason this mode of operation is preferred to potentiostatic operation is because the latter has been shown to produce oscillations about a desired overlimiting current, which lead to variable and possibly unstable shocks.[2,3]) Moreover, running the system potentiostatically permits current to fluctuate in the event of electroosmotic instabilities or during formation of bubbles in the electrode channels, both of which could perturb and ultimately destabilize the shock wave.[4,5] To preclude these undesirable effects, we operated the SED device galvanostatically and observe in Figure A-3a the evolution of voltage as a function of time for each of the 3 passes and values of dimensionless current tested in Figure 2-5. In each case, the system was considered to be at steady state within approximately 2 hours of supplying current, and in each pass, the limiting current was reduced by a factor of 5 relative to the previous (5×

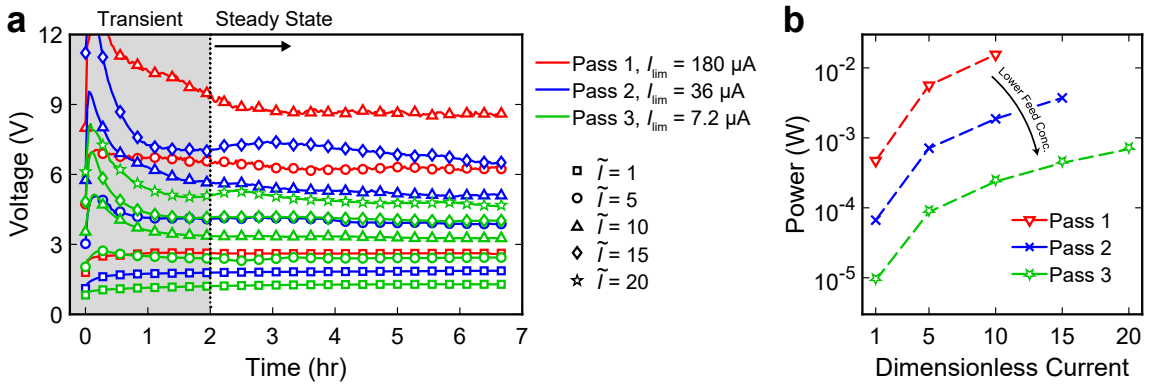

Figure A-3. Evolution of (a) voltage as a function of time and (b) power under galvanostatic operation for each of the 3 passes and values of dimensionless current tested in Figure 2-5. In each case, the SED device was considered to be at steady state within approximately 2 hours of supplying current. In (a), the startup phase in which we observed transient behavior is shaded in gray.

dilutions). We learn from Figure A-3 that successive steps in this process contribute little energy in addition to that needed in the first step. The reason for this behavior is that power (and hence energy density, defined as power divided by volumetric flow rate) decreases as the square of applied current, even though resistivity of the electrolyte increases at lower concentration. This proportionality between energy demand and concentration of the feed at a given dimensionless current makes SED advantageous for targeted removal of trace ions compared to conventional techniques, which usually require an input of energy that is bounded from below as the feed becomes more dilute.

A.3 Analysis of Species Selectivity

A previous experimental paper by our group showed that SED automatically achieves selective removal of the multivalent ion from an aqueous mixture comprising both mono- and divalent cations, namely Na^+ and Mg^{2+}. Selectivity based on valence was attributed to differences in ionic mobility across the enriched and deionized regions of the device when an overlimiting current was applied. In this study, the electrolyte (i.e., practical water) consisted of three primary cations, two of which are monovalent and the third is divalent. Figure A-4a demonstrates selective removal of Co^{2+} from practical water in the third pass of our 3-step process, even

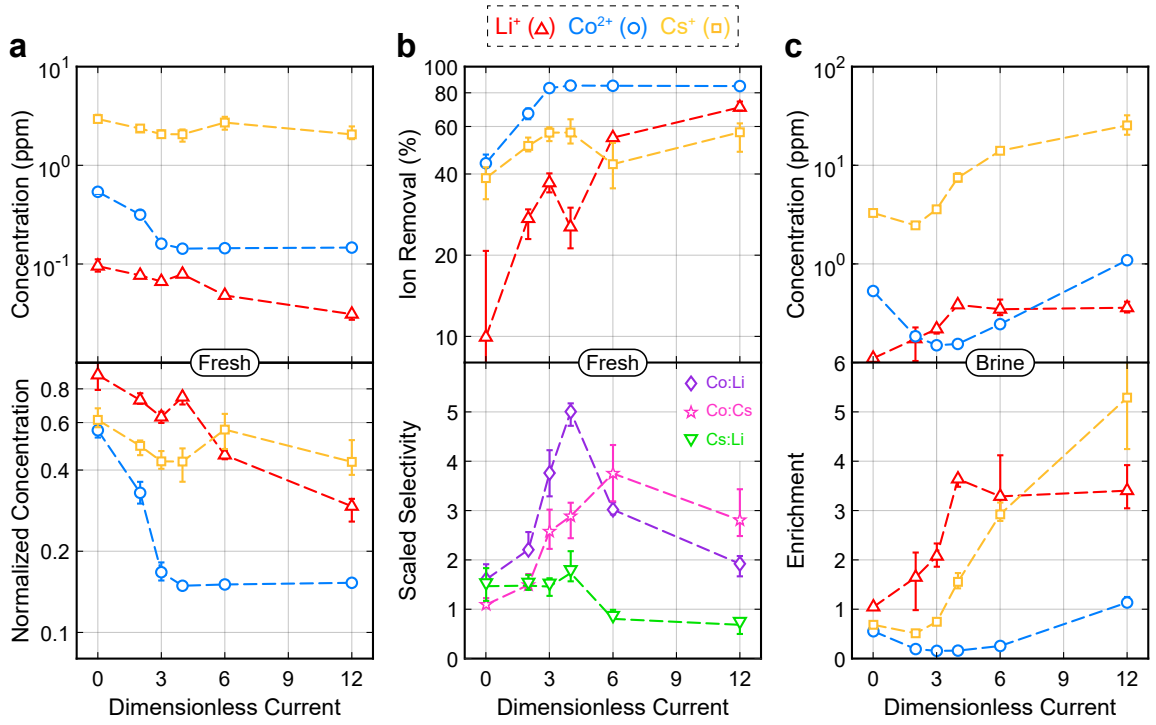

Figure A-4. Analysis of the selective removal of cobalt relative to lithium and cesium in the third pass of the 3-step process shown in Figure 2-5; the feed to this pass is a 25-fold dilution of the feed to the first pass (Table 2.1), and $I_{\text{lim}} = 7.2$ μA. (a) Measured concentration for each species, both absolute (top) and normalized by initial concentration (bottom), in the fresh stream as a function of dimensionless current. (b) Calculated deionization for each species (top) and scaled selectivity for each pair of unique species (bottom) in the fresh stream as functions of dimensionless current. (c) Measured concentration (top) and enrichment (bottom) for each species in the brine stream as functions of dimensionless current. Each data point represents the arithmetic mean of 3 samples, and the error bars correspond to the range of those samples.

though the initial concentration of this species is neither the highest nor the lowest. Moreover, the concentration of Co^{2+} decreases the fastest with dimensionless current and appears to saturate at $\widetilde{I} = 4$. With these data, we calculate scaled (retention) selectivity in the fresh stream as a function of dimensionless current between each pair of unique species, with scaled selectivity ($S_{j:i}$) defined as[6]

$$S_{j:i} \equiv j:i = \frac{C_i/C_j}{C_{i_0}/C_{j_0}} = \frac{C_i/C_{i_0}}{C_j/C_{j_0}} \tag{A.1}$$

This definition of selectivity can be interpreted as the ratio of the effluent concentration of species i to that of species j, scaled by the corresponding ratio of initial

(feed) concentrations, which is equal to the ratio of scaled effluent concentrations. It follows that species j is selectively removed relative to species i if $S_{j:i}$ is greater than 1. Figure A-4b shows that Co^{2+} is selectively removed compared to both Li^{+} and Cs^{+}, and that there is little to no selectivity between the two monovalent cations. Since the three cations are removed in different proportions at each dimensionless current, and the removal of Co^{2+} plateaus at $\widetilde{I} = 4$, the scaled selectivity of Co^{2+} relative to the two monovalent cations diminishes past a critical current. These results prove that, while selective removal of a valuable or target multivalent ion may be advantageous from a practical standpoint, it complicates the design of a low-cost process in which water recovery is high.

A.4 Conductivity and pH Data

Conductivity has normally been used as a rough metric to quickly confirm the proper function of SED. We note, however, that measurements of conductivity alone are not sufficient to rigorously characterize deionization because information regarding the fate of individual ions is lost. Moreover, changes in conductivity of the fresh stream are influenced by crossing of protons from the catholyte (present because of the added HCl), which also establishes a driving force for other ions to leave the fresh stream and preserve electroneutrality. We therefore used ICP–MS as the primary measure of composition (and in turn deionization), with conductivity serving as a complementary measurement. Based on the data shown in Figure A-5a, the conductivity of the fresh (brine) stream decreases (increases) with increasing current in each of the 3 passes. Figure A-5b presents these same data normalized by the conductivity of the feed corresponding to each pass. These data reveal that the conductivity of the fresh stream in the third pass reaches a lower limit (since normalized conductivity > 1), even though Li^{+}, Co^{2+}, and Cs^{+} continue to be removed in this pass (see Figure 2-5). We postulate that this lower bound on conductivity exists in the third pass because of transport of protons (which are highly electromobile in water) from the catholyte, as hinted by the slightly acidic pH shown in Figure A-5c.

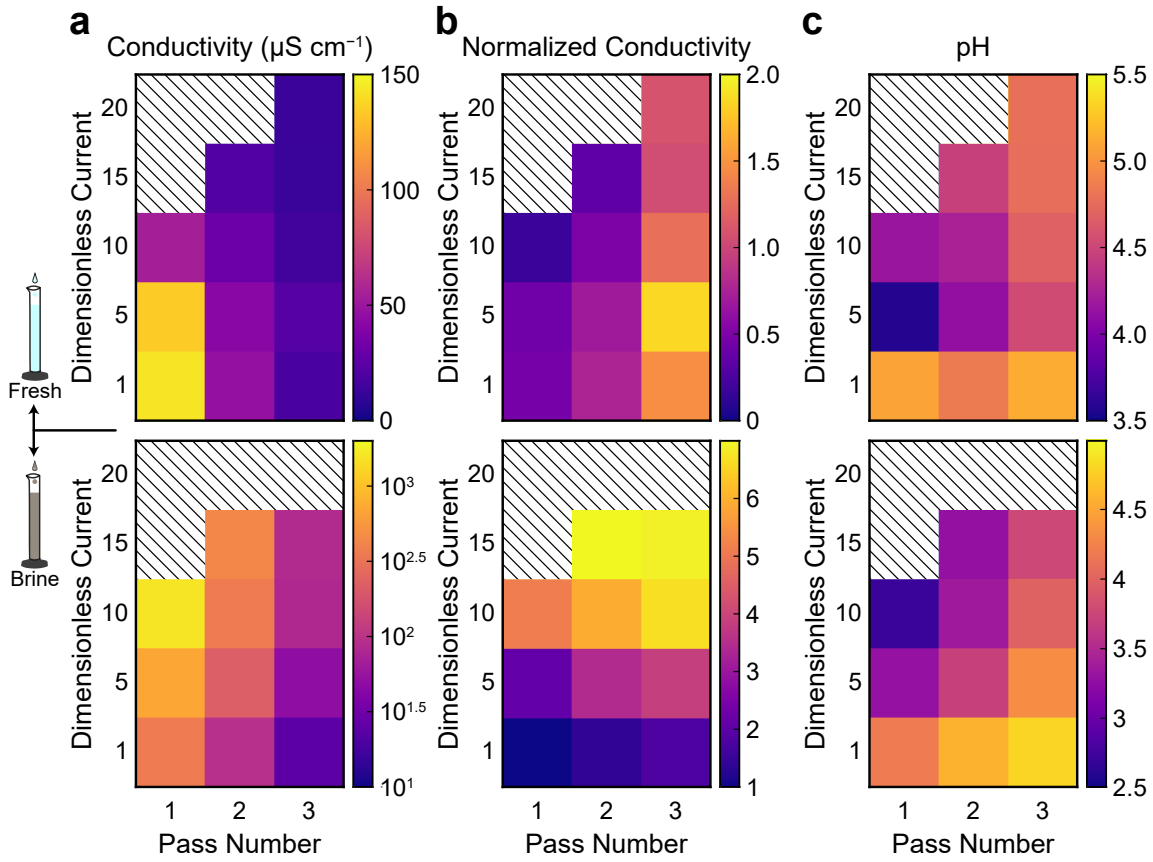

Figure A-5. Measurements of (a) conductivity, (b) normalized conductivity, and (c) pH as functions of dimensionless current in the fresh (top) and brine (bottom) streams of each pass of the 3-step process described in Figure 2-5. The data in (b) are normalized by the conductivity of the feed corresponding to each pass: namely, 305.8, 61.2, and 12.2 $\mu S\,cm^{-1}$. Measurements in the brine stream of the third pass at $\widetilde{I} = 20$ were not obtained because the volumes collected were too small. Otherwise, zones of diagonal black stripes in the upper left corners correspond to parameters that were not tested.

Although we do not entirely understand the role of pH on the performance of SED, we believe that this quantity influences species selectivity. This observation was originally made in a previous study by our group, in which the mechanism responsible for changes in the apparent mobility of divalent cations was thought to be influenced by internal gradients in pH. Since it is difficult to determine these internal gradients, the pH of the outlet stream is measured as a proxy, as shown in Figure A-5c. These data reveal that pH in the fresh stream of the third pass is at a minimum when $\widetilde{I} = 5$, which happens to be near the dimensionless currents that maximize selectivity of Co^{2+} to Li^{+} ($\widetilde{I} = 4$) and Co^{2+} to Cs^{+} ($\widetilde{I} = 6$). This observation suggests

that there may exist operating conditions at which an exchange between protons and divalent cations across the membrane is maximized. From an alternative perspective, we know that local fluctuations in pH influence the zeta potential—and in turn the electroosmotic slip velocity[7,8]—as well as the distribution of charge on surfaces of the frit and membranes, all of which ultimately determine deionization and selectivity.

A.5 References

[1] E Victoria Dydek, Boris Zaltzman, Isaak Rubinstein, DS Deng, Ali Mani, and Martin Z Bazant. Overlimiting current in a microchannel. *Physical review letters*, 107(11):118301, 2011.

[2] Daosheng Deng, E Victoria Dydek, Ji-Hyung Han, Sven Schlumpberger, Ali Mani, Boris Zaltzman, and Martin Z Bazant. Overlimiting current and shock electrodialysis in porous media. *Langmuir*, 29(52):16167–16177, 2013.

[3] Thomas A Zangle, Ali Mani, and Juan G Santiago. On the propagation of concentration polarization from microchannel- nanochannel interfaces part ii: numerical and experimental study. *Langmuir*, 25(6):3909–3916, 2009.

[4] Thomas A Zangle, Ali Mani, and Juan G Santiago. Effects of constant voltage on time evolution of propagating concentration polarization. *Analytical chemistry*, 82(8):3114–3117, 2010.

[5] Sven Schlumpberger, Nancy B Lu, Matthew E Suss, and Martin Z Bazant. Scalable and continuous water deionization by shock electrodialysis. *Environmental Science & Technology Letters*, 2(12):367–372, 2015.

[6] Kameron M. Conforti and Martin Z. Bazant. Continuous ion-selective separations by shock electrodialysis. *AIChE Journal*, page e16751, 2019.

[7] Dominik PJ Barz, Michael J Vogel, and Paul H Steen. Determination of the zeta potential of porous substrates by droplet deflection. i. the influence of ionic strength and ph value of an aqueous electrolyte in contact with a borosilicate surface. *Langmuir*, 25(3):1842–1850, 2009.

[8] SS Dukhin, NA Mishchuk, and PV Takhistov. Electroosmosis of the second kind and unrestricted current increase in the mixed monolayer of an ion-exchanger. *Colloid Journal of the USSR*, 51(3):540–542, 1989.

Appendix B

Supporting Information: Selective and chemical-free removal of toxic heavy metal cations from water using shock ion extraction

B.1 Shock ED with polarity reversal

When present in solution, heavy metals can foul the membranes and electrodes of an ED-type device by generating scalants in the form of metal hydroxides. Several measures can be employed to inhibit the formation of these scalants, such as redesigning the cell configuration, incorporating protective compartments for the electrodes, and controlling the applied voltage and pH in the device.[1,2] In addition to these approaches, periodic polarity reversal is known to effectively reduce the formation of mineral scale in electromembrane processes.[3] We therefore employed polarity reversal for all experiments in this study and demonstrated in Figure B-1 that this approach maintains the performance of shock ED over many cycles and for different applied currents. Practically, polarity reversal in shock ED involves changing the sign of the applied current and leads to periodic switching of the anode and cathode as well as of the enriched and depleted streams at a set interval. In this

demonstration, we chose to reverse polarity every hour, as shown in Figure B-1d. The voltage response exhibited a delay with a transient ramp-up period that lowered performance (Figure B-1a and b, shaded regions) before the device reached steady state. As a result, we extended the duration of polarity reversal to either 6 or 12 hours in all other experiments in this study. Future work will more carefully assess the influence of reversal duration and its dependence on solution chemistry and operating conditions in both shock ED and shock IX.

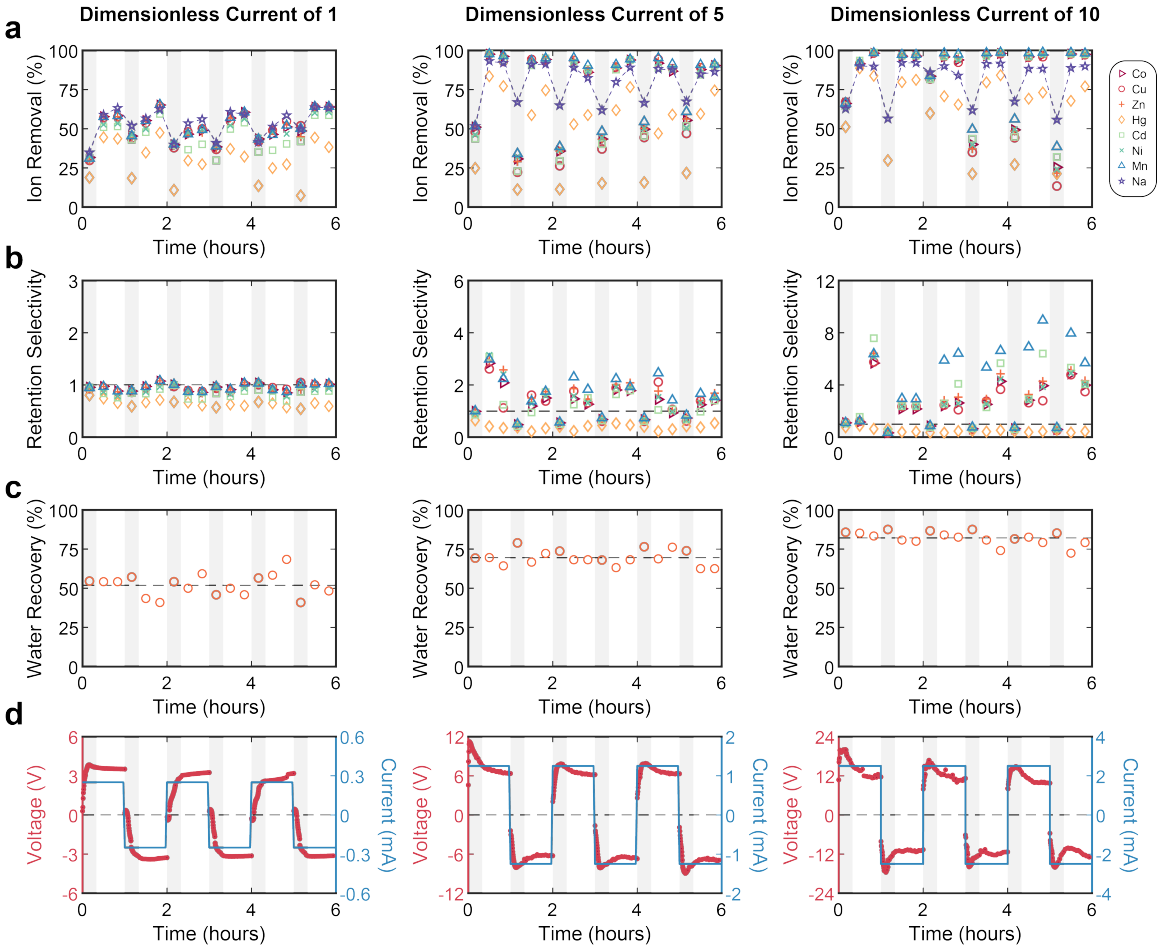

Figure B-1. Quantitative analysis of selective ion removal using shock ED with polarity reversal ($Q' = 111\,\mathrm{L\,h^{-1}\,m^{-2}}$). (a) Ion removal in the depleted stream ($1-\widetilde{C}_D^{(j)}$), (b) retention selectivity (relative to sodium), (c) water recovery (γ in Equation 4.3), and (d) voltage and current versus time for different values of dimensionless current ($\widetilde{I} = 1, 5, 10$). Markers in (a) and (b) are used to designate different species, and the dashed line in (c) represents the mean water recovery. The regions shaded in grey correspond approximately to the transient ramp-up period before the device reaches a steady voltage.

B.2 Analysis of water recovery and energy demand

Water recovery (defined in Equation 4.3), energy consumption, and current efficiency are important metrics in assessing the performance of water purification systems. Energy consumption is defined as

$$E = \frac{IV}{Q'} \tag{B.1}$$

where V is (steady) voltage, and current efficiency is defined as

$$\eta = \sum_j \frac{\nu^{(j)} \left(C_0^{(j)} - C_D^{(j)} \right) F Q_D}{M^{(j)} I} \tag{B.2}$$

where the sum is taken over all cations j. Figure B-2a shows that water recovery increases with current for the borosilicate frit but not for the IERW. We attribute this decrease in water recovery (which corresponds to an increase in the flow of the enriched) at high current to the presence of a larger proportion of anion exchange resin in the wafer, and water recovery is one of several criteria involved in the design of the IERW. In both the borosilicate frit and IERW, the deviation of water recovery from 50% is primarily due to electroosmotic flow. The position of the splitter was not changed in this study, although it could be adjusted in future designs for improved water recovery. The electrical energy needed for ion removal is shown in Figure B-2b, and it increases with current for both systems. We observe, however, that the IERW lowers the energy consumption for every value of current tested by 50-80%, which we attribute to the greater conductivity of the IERW in the dilute limit (see Table 4.1). Although the energy required for fluid pumping in our laboratory system is negligible compared to the electrical energy demand, the IERW provides regions of high fluidic permeability in its hierarchical pore structure, which significantly reduces the hydraulic resistance in the device. Figure B-2c shows that the IERW also slightly increases the current efficiency of ion removal at low productivities, although both systems exhibit rapid decay in efficiency at high current.

This result suggests that a significant fraction of the applied current is carried by protons instead of the metal cations across the depleted region.

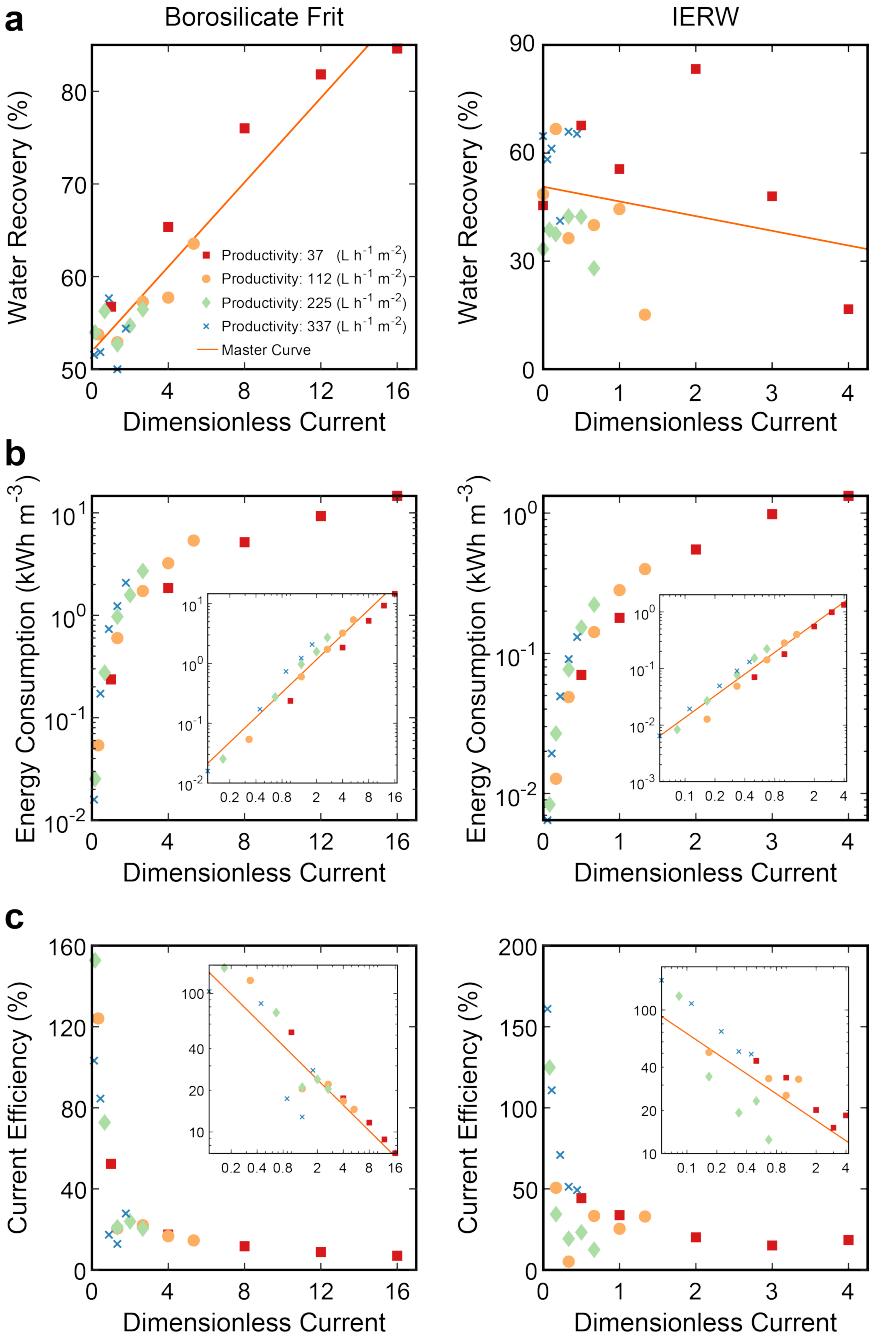

Figure B-2. Comparison of (a) water recovery, (b) energy consumption, and (c) current efficiency versus dimensionless current using shock ED (left) and shock IX (right). Colored markers are used to designate different productivities. The insets in (b) and (c) are log–log plots.

B.3 Ion removal with no applied current

To assess the role of the electric field in the hybrid shock IX process, we repeated the time-dependent experiment presented in Figure 4-4 but without applying current. In particular, the experiment was preceded by feeding a 0.1 M NaCl solution at $111\,\mathrm{L\,h^{-1}\,m^{-2}}$ ($\widetilde{I}=0$) for 24 hours to preload the cation exchange resin with sodium, as is done in an ordinary ion exchange process. The multicomponent mixture in Table 4.2 was then fed at $111\,\mathrm{L\,h^{-1}\,m^{-2}}$ ($\widetilde{I}=0$), and samples were collected periodically to quantify performance. To completely isolate the role of ion exchange in this experiment, no acid was used in the catholyte, except in the region colored gray in Figure B-3. The results in Figure B-3a show a trend that resembles a breakthrough curve in ion exchange: heavy metal cations are exchanged with sodium until normalized concentration (and retention selectivity, Figure B-3b) reaches a value of one. Normally, this criterion would indicate exhaustion of the resin, but we observe an extended region of ion removal (between 400 and 500 bed volumes) by exchange of mercury with other heavy metals. As expected, we also observe resumption of ion exchange at 500 bed volumes when hydrochloric acid is added to the catholyte.

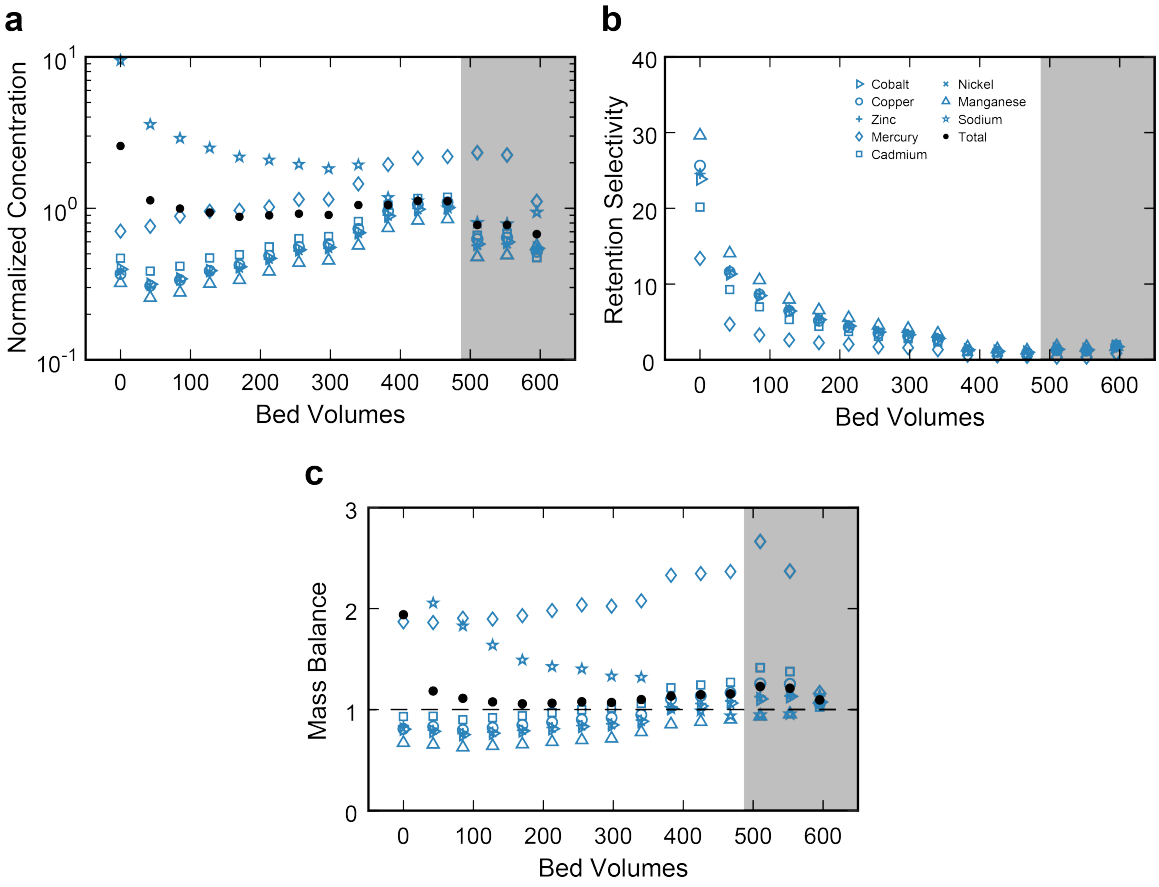

Figure B-3. Quantitative analysis of the dynamics and time dependence of ion removal by ion exchange ($\widetilde{I} = 0$ and $Q' = Q = 111\,\mathrm{L\,h^{-1}\,m^{-2}}$). (a) Normalized concentration and (b) retention selectivity (relative to sodium) of the cations in the "depleted" (or "enriched", as $\widetilde{I} = 0$) stream versus time. (c) Total mass balance and mass balances of individual species versus time; balances in each of the product streams are shown in Figure B-6. Markers are used to designate different species, and black circles represent the normalized (total) concentration of all dissolved cations. In this experiment, no acid was used in the catholyte except in the region colored gray.

B.4 Auxiliary mass balance data

Figures B-4–B-6 show the total and species mass balances in each of the product streams for steady shock IX (Figure 4-2), transient shock IX (Figure 4-4), and ion exchange ($\widetilde{I} = 0$; Figure B-3).

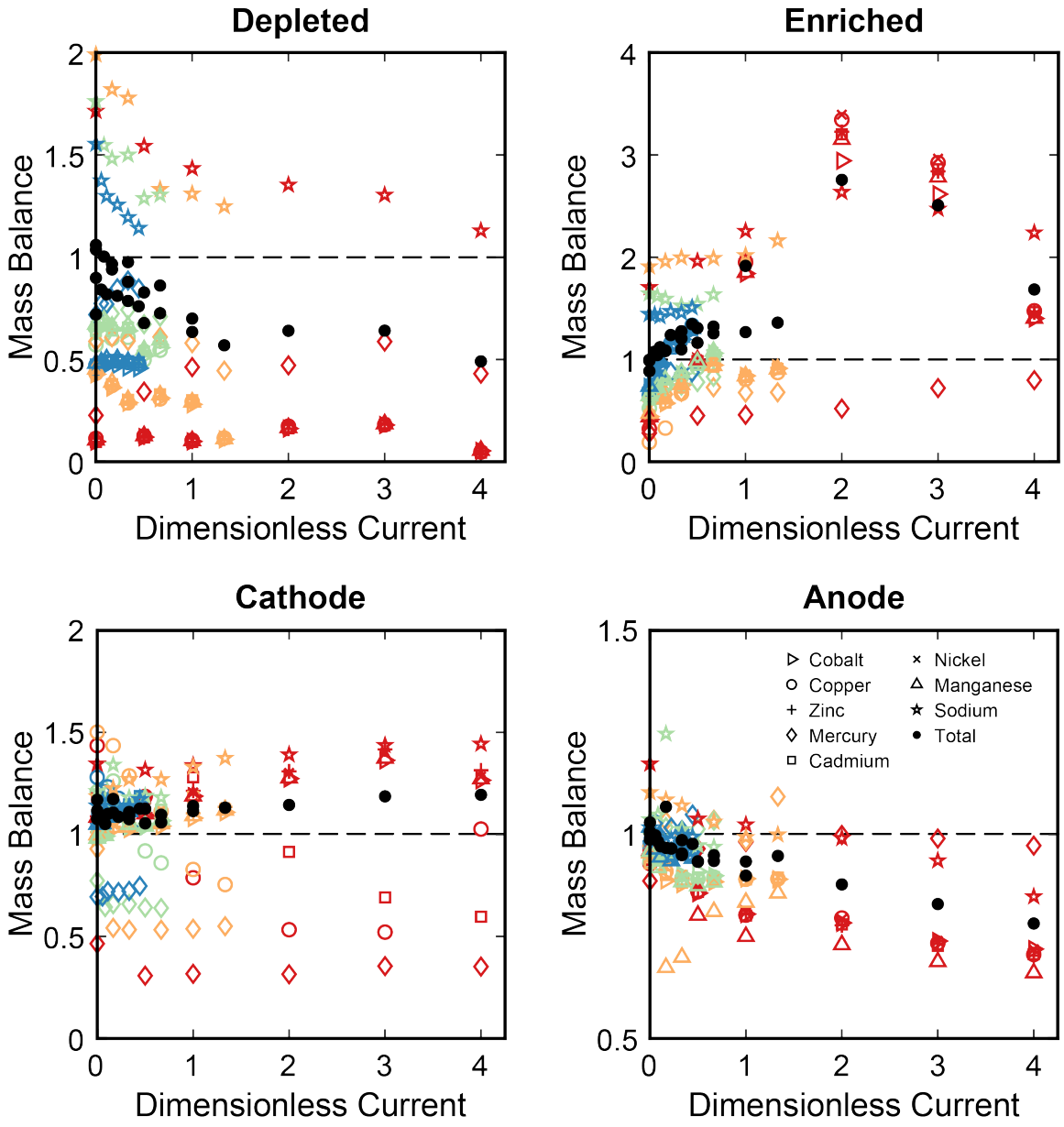

Figure B-4. Total mass balance (black circles) and mass balances of individual species (colored markers) versus dimensionless current in each of the product streams obtained using shock IX (system mass balances are shown in Figure 4-2c).

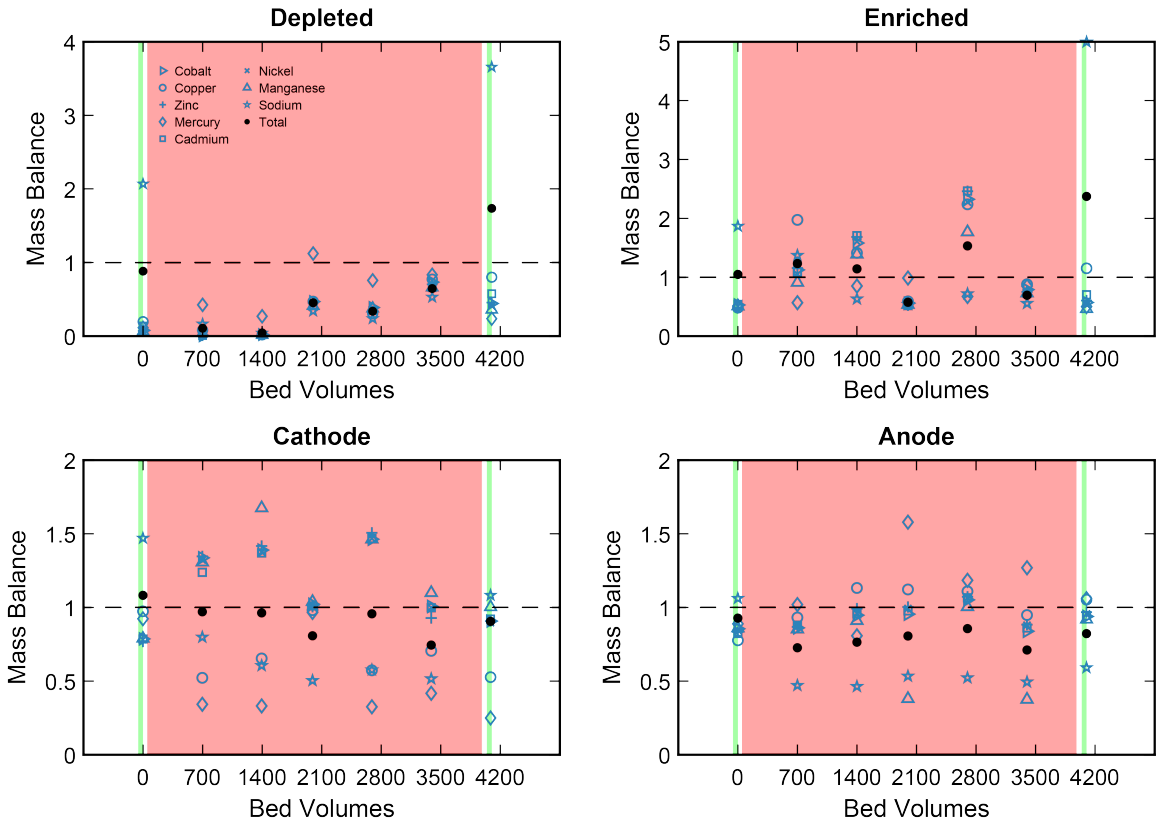

Figure B-5. Total mass balance and mass balances of individual species versus time in each of the product streams in shock IX (system mass balances are shown in Figure 4-4c). Regions colored green correspond to a feed of 0.1 M NaCl ($\widetilde{I} = 0$ and $Q' = 111\,\mathrm{L\,h^{-1}\,m^{-2}}$), and the region colored red corresponds to the feed in Table 4.2 ($\widetilde{I} = 2$ and $Q' = 37\,\mathrm{L\,h^{-1}\,m^{-2}}$).

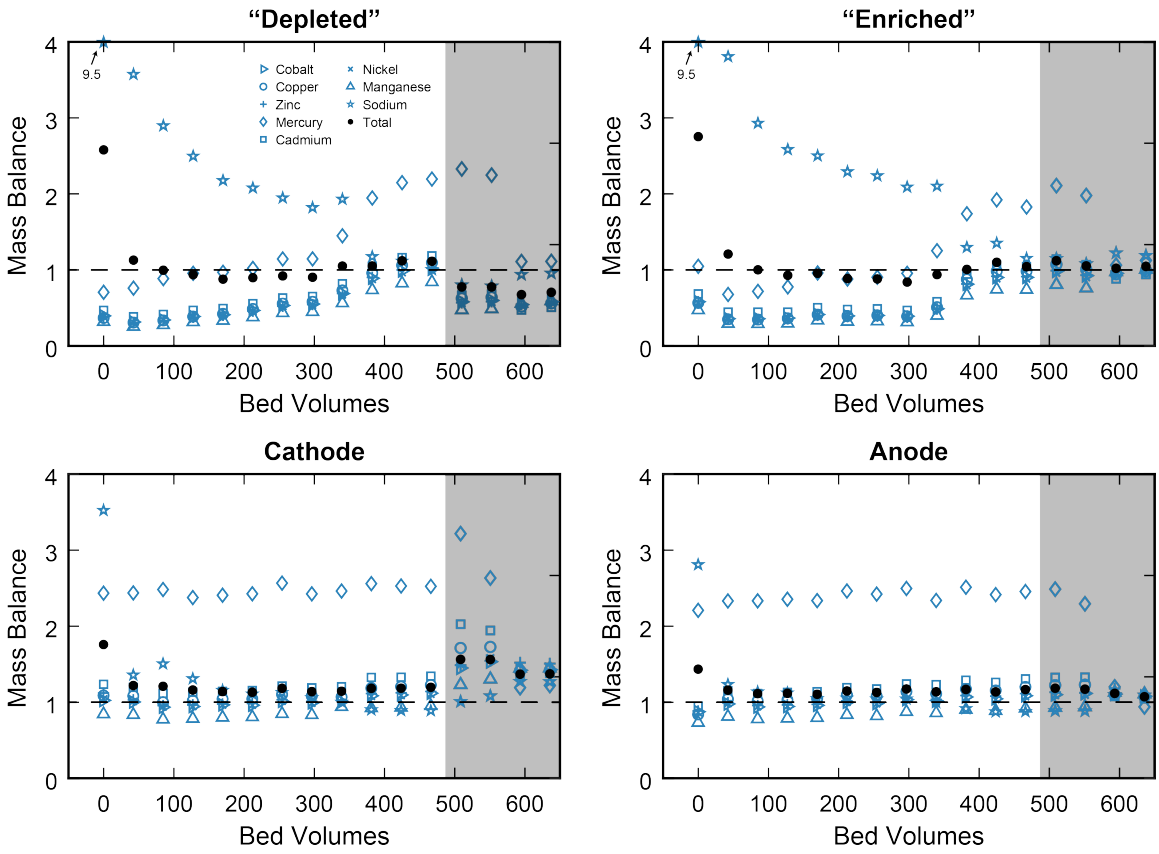

Figure B-6. Total mass balance and mass balances of individual species versus time in each of the product streams in ion exchange ($\widetilde{I} = 0$ and $Q' = Q = 111\,\mathrm{L\,h^{-1}\,m^{-2}}$; system mass balances are shown in Figure B-3c). In this experiment, no acid was used in the catholyte except in the region colored gray.

B.5 References

[1] Yu-Mei Chao and TM Liang. A feasibility study of industrial wastewater recovery using electrodialysis reversal. *Desalination*, 221(1-3):433–439, 2008.

[2] Huixia Lu, Yuzhen Wang, and Jianyou Wang. Removal and recovery of ni2+ from electroplating rinse water using electrodeionization reversal. *Desalination*, 348:74–81, 2014.

[3] Mohammad A et al. Alkhadra. Electrochemical methods for water purification, ion separations, and energy conversion. *Chemical Reviews*, 2022.